

ASTROPHYSICS AND SPACE SCIENCE LIBRARY

EARTH'S MAGNETOSPHERIC PROCESSES

Edited by B. M. McCormac



D. REIDEL PUBLISHING COMPANY

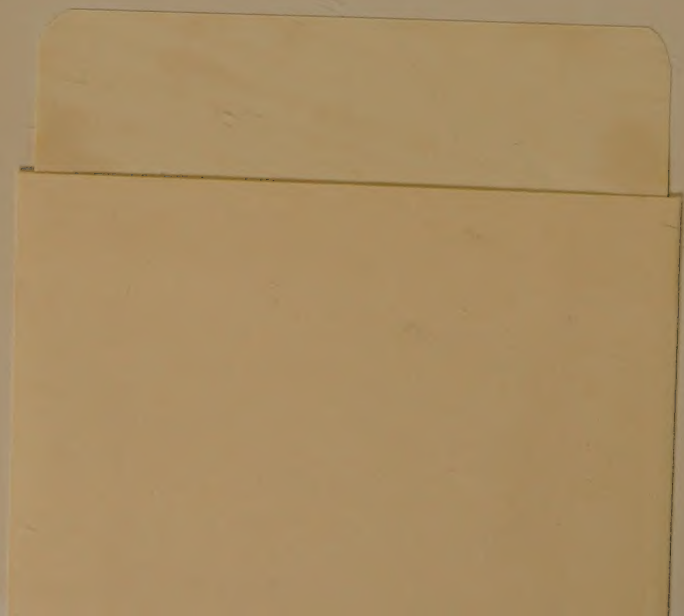
DORDRECHT-HOLLAND



MICHIGAN STATE UNIVERSITY
LIBRARY
Michigan State University
JUL 2017

WITHDRAWN

QC
809
.M35
N38
1971



[REDACTED] LIBRARY

**MICHIGAN STATE UNIVERSITY
LIBRARY**

THIS BOOK READY

FOR ISSUE SEP 10 1973 **JUN 15 2017**

WITHDRAWN

EARTH'S MAGNETOSPHERIC PROCESSES

ASTROPHYSICS AND SPACE SCIENCE LIBRARY

A SERIES OF BOOKS ON THE RECENT DEVELOPMENTS
OF SPACE SCIENCE AND OF GENERAL GEOPHYSICS AND ASTROPHYSICS
PUBLISHED IN CONNECTION WITH THE JOURNAL
SPACE SCIENCE REVIEWS

Editorial Board

- J. E. BLAMONT, *Laboratoire d'Aéronomie, Verrières, France*
R. L. F. BOYD, *University College, London, England*
L. GOLDBERG, *Harvard College Observatory, Cambridge, Mass., U.S.A.*
C. DE JAGER, *University of Utrecht, Holland*
Z. KOPAL, *University of Manchester, Manchester, England*
G. H. LUDWIG, *NASA, Goddard Space Flight Center, Greenbelt, Md., U.S.A.*
R. LÜST, *Institut für Extraterrestrische Physik, Garching-München, Germany*
B. M. MCCORMAC, *Lockheed Palo Alto Research Laboratory, Palo Alto, Calif., U.S.A.*
H. E. NEWELL, *NASA, Washington, D.C., U.S.A.*
L. I. SEDOV, *Academy of Sciences of the U.S.S.R., Moscow, U.S.S.R.*
Z. ŠVESTKA, *Freiburg im Breisgau, Germany*

Secretary of the Editorial Board

- W. DE GRAAFF, *Sterrewacht 'Sonnenborgh', University of Utrecht, Utrecht, Holland*

VOLUME 32

EARTH'S MAGNETOSPHERIC PROCESSES

PROCEEDINGS OF A SYMPOSIUM ORGANIZED
BY THE SUMMER ADVANCED STUDY INSTITUTE
AND NINTH ESRO SUMMER SCHOOL,
HELD IN CORTINA, ITALY,
AUGUST 30-SEPTEMBER 10, 1971

Edited by

B. M. McCORMAC

Lockheed Palo Alto Research Laboratory, Palo Alto, Calif., U.S.A.



D. REIDEL PUBLISHING COMPANY

DORDRECHT-HOLLAND

Library of Congress Catalog Card Number 70-188007

ISBN 90 277 0231 4

All Rights Reserved

Copyright © 1972 by D. Reidel Publishing Company, Dordrecht, Holland
No part of this book may be reproduced in any form, by print, photoprint, microfilm,
or any other means, without written permission from the publisher

Printed in The Netherlands by D. Reidel, Dordrecht

PREFACE

This book contains the lectures presented at the Summer Advanced Institute and Ninth ESRO Summer School which was held in Cortina, Italy, during the period August 30 through September 10, 1971. One hundred seventy-nine persons from eighteen different countries attended.

The authors and the publisher have made a special effort for rapid publication of an up-to-date status of the particles, fields, and processes in the earth's magnetosphere, which is an ever changing area. Special thanks are due to the lecturers for their diligent preparation and excellent presentations. The individual lectures and the published papers were deliberately limited; the author's cooperation in conforming to these specifications is greatly appreciated. The contents of the book are organized by subject area rather than in the order in which papers were presented during the Institute/School. Many thanks are due to Drs J. Ronald Burrows, James W. Dungey, Harry Elliot, Roger Gendrin, Edward W. Hones, Jr., Reimar Lüst, and J. Ortner who served as session chairmen during the Institute and contributed greatly to its success by skillfully directing the discussion period in a stimulating manner after each lecture.

Many persons contributed to the success of the Institute/School. The co-chairman, Dr Reimar Lüst, was most helpful during all phases of the preparation and planning. Drs J. Ronald Burrows, Harry Elliot, Carl-Gunne Fälthammar, M. Giorgi, J. Ortner, J. R. U. Page, Alois Schardt, James A. Van Allen, and Martin Walt were especially helpful in preparing the technical program.

Mr J. R. U. Page, assisted by Mr Claude Jovart and Suzan Garrad, handled the ESRO arrangements and provided much needed funds for many lecturers and students. Dr Giovanni Gregori played a most important and difficult role in arranging the facilities in Cortina and in providing the visual aids, recording equipment, office support, and projectionists. Dr Gregori was ably assisted by Dr Carlos Valenti, our favorite cartoonist, and Michelangelo Pangia. Mr. Sandro Righetti, manager of the Cristallo Palace Hotel, which was the site of the Institute/School, endeavored far beyond the call of duty to provide the best possible service. The assistant editor, Mrs Diana McCormac, checked the manuscripts and proofs and worked hard to achieve a uniform style in this book.

Direct financial support was provided the Institute/School by the European Space Research Organization, Italian National Research Council, Lockheed Palo Alto Research Laboratory, Advanced Research Projects Agency, Defense Nuclear Agency, and the Office of Naval Research. The National Aeronautics and Space Administration also was a sponsor.

BILLY M. MCCORMAC

Palo Alto, March 1972

TABLE OF CONTENTS

PREFACE

v

PART I: MAGNETOSPHERIC STRUCTURE AND PROCESSES

L. D. KAVANAGH, JR. / Magnetospheric Structure	3
C.-G. FÄLTHAMMAR / Magnetospheric Processes	16
V. M. VASYLIUNAS / The Interrelationship of Magnetospheric Processes	29
C. T. RUSSELL / Magnetic and Electric Waves in Space	39

PART II: MAGNETOSPHERIC PARTICLES

J. I. VETTE / Magnetospheric Particle Populations	53
J. D. WINNINGHAM / Characteristics of Magnetosheath Plasma Observed at Low Altitudes in the Dayside Magnetospheric Cusps	68
G. P. HASKELL and R. J. HYNDIS / Mechanisms for the Injection of Protons into the Magnetosphere	81
J. ENGELMANN / Solar Particle Injection at Medium Energies ($25 < E < 250$ MeV)	95
A. C. DURNEY and G. E. MORFILL / Entry of Energetic Solar Protons into the Tail	101
D. E. PAGE and V. DOMINGO / New Results in Particle Arrival at the Polar Caps	107
D. HOVESTADT, E. ACHTERMANN, B. EBEL, B. HÄUSLER, and G. PASCHMANN / New Observations of the Proton Population of the Radiation Belt between 1.5 and 104 MeV	115
F. SØRAAS / ESRO IA/B Observations at High Latitudes of Trapped and Precipitating Protons with Energies above 100 keV	120
W. RIEDLER / Auroral Particle Precipitation Patterns	133
D. A. BRYANT, G. M. COURTIER, and G. BENNETT / Electron Intensities over Auroral Arcs	141
L. ROSSBERG / The Pre-Midnight Asymmetry in the 40 keV Electron Flux Profiles and Its Relation to Magnetospheric Substorms	147
J. R. BURROWS, I. B. MCDIARMID, and M. D. WILSON / Pitch Angles and Spectra of Particles in the Outer Zone near Noon	153
G. PASCHMANN / Angular Distributions of Precipitating Electrons	168
D. E. PAGE and M. L. SHAW / Some Parameters Affecting the Poleward Boundary of Trapped Electrons	175
S. B. MENDE and R. H. EATHER / Photometric Auroral Particle Measurements	179

PART III: MAGNETIC FIELDS AND CURRENTS

N. F. NESS / Review of Magnetic Field Observations	189
K. SCHINDLER / A Self-Consistent Theory of the Tail of the Magnetosphere	200
J. W. DUNGEY / Theory of Neutral Sheets	210

PART IV: ELECTRIC FIELDS AND PLASMA CONVECTION

U. V. FAHLESON / Critical Review of Electric Field Measurements	223
D. A. GURNETT / INJUN 5 Observations of Magnetospheric Electric Fields and Plasma Convection	233
G. HAERENDEL / Plasma Drifts in the Auroral Ionosphere Derived from Barium Releases	246
L. P. BLOCK / Acceleration of Auroral Particles by Electric Double Layers	258
C. E. MCILWAIN / Plasma Convections in the Vicinity of the Geosynchronous Orbit	268
C. R. CHAPPELL / Thermal Ions in the Magnetosphere	280

PART V: ACCELERATION AND DIFFUSION

M. WALT and T. A. FARLEY / High Energy Proton Model for the Inner Radiation Belt	293
D. J. SOUTHWOOD / Magnetic Field Variations at Micropulsation Frequencies	302
R. GENDRIN / Changes in the Distribution Function of Magnetospheric Particles Associated with Gyroresonant Interactions	311
F. L. SCARF and R. W. FREDRICKS / Electrostatic Waves in the Magnetosphere	329
T. R. KAISER / VLF Phenomena	340
G. E. PERONA / A Theory on the Latitude and Local Time Distribution of Precipitating Electrons During a Sudden Commencement	351

PART VI: MAGNETOSPHERIC SUBSTORMS

M. P. AUBRY / A Short Review of Magnetospheric Substorms	357
E. W. HONES, JR. / Substorm Behavior of Plasma Sheet Particles	365
G. ROSTOKER / Interpretation of Magnetic Field Variations During Substorms	379
G. R. PILKINGTON / X-Ray Observations and Interpretations	391
A. NISHIDA / Excitation of Polar Substorms by Northward Interplanetary Magnetic Field	400

PART VII: SUMMARY AND CONCLUSIONS

B. M. MCCORMAC / Summary and Conclusions	409
GLOSSARY	412
INDEX OF SUBJECTS	415

PART I

MAGNETOSPHERIC STRUCTURE AND PROCESSES

MAGNETOSPHERIC STRUCTURE

LAWRENCE D. KAVANAGH, JR.

NASA Headquarters, Washington, D.C., U.S.A.

1. Introduction

This paper attempts to summarize many of the more significant results which have been achieved in the study of the earth's magnetosphere during 1969–1971. It concentrates on studies of the bow shock, magnetosheath, magnetopause, polar cusp, convection-driving electric fields, and the composition of trapped particles of charge greater than one. Whenever possible, particle or field observations are related to the overall question of the magnetosphere: namely, where do the particles come from, where do they go, and what sustains the entire system in equilibrium.

2. Bow Shock

When the supersonic solar wind encounters the earth, the magnetosphere becomes greatly distorted from the simple shape of a dipole magnetic field. Figure 1 is a general picture of the average shape of the magnetosphere as seen in the noon-midnight meridian plane, illustrating many of the observed and expected features.

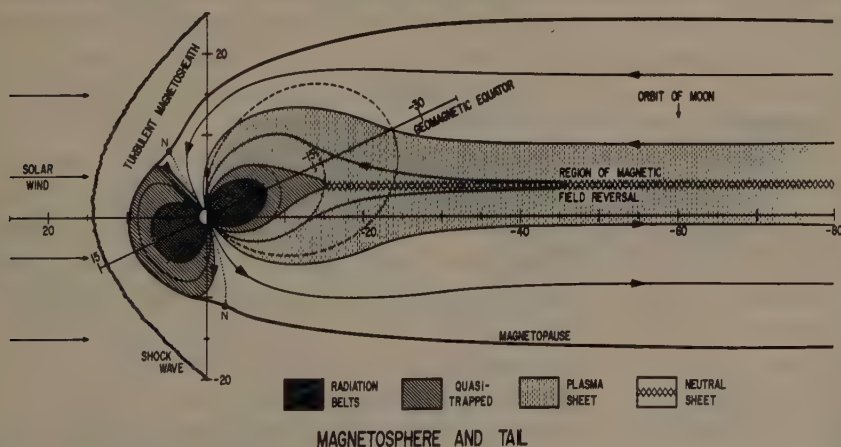


Fig. 1. Magnetic field and particle configuration of the earth's magnetosphere (coordinates shown are in units of R_E) (Courtesy of Dr N. F. Ness).

The interface between the free-streaming solar wind and the magnetosphere is a large bow shock, as illustrated. Since the scale size of individual particle motions in the solar wind is quite small (proton, electron cyclotron radii = 50, 1.5 km; Debye length = 10 m) compared to the dimensions of the magnetosphere, the solar wind acts like an

aerodynamic fluid of Mach number 5 to 10 encountering a large blunt object; the general shape of the bow shock and its associated Mach cone are about what one would calculate from fluid mechanics. The major distinction from fluid mechanics is that the bow shock is formed from collisionless plasma instead of from a Maxwellian gas, and so the thickness of the shock cannot be related to collisional mean free paths. Therefore, the heating of particles on passage through the shock must be explained in terms of damping of plasma waves rather than collisional processes.

The first high resolution measurements near the shock were made by Heppner *et al.* (1967) with a magnetometer on board the OGO 1 satellite. More recently, excellent shock information has been obtained with instruments on OGO 5. A combination of high frequency E and B field information from the plasma wave experiment, low frequency magnetic field information from the fluxgate magnetometer, and proton information from the light ion spectrometer has been assembled to give an extremely detailed picture of shock crossings. One shock that has been analyzed very carefully is that encountered by the spacecraft on March 12, 1968. This crossing has been dis-

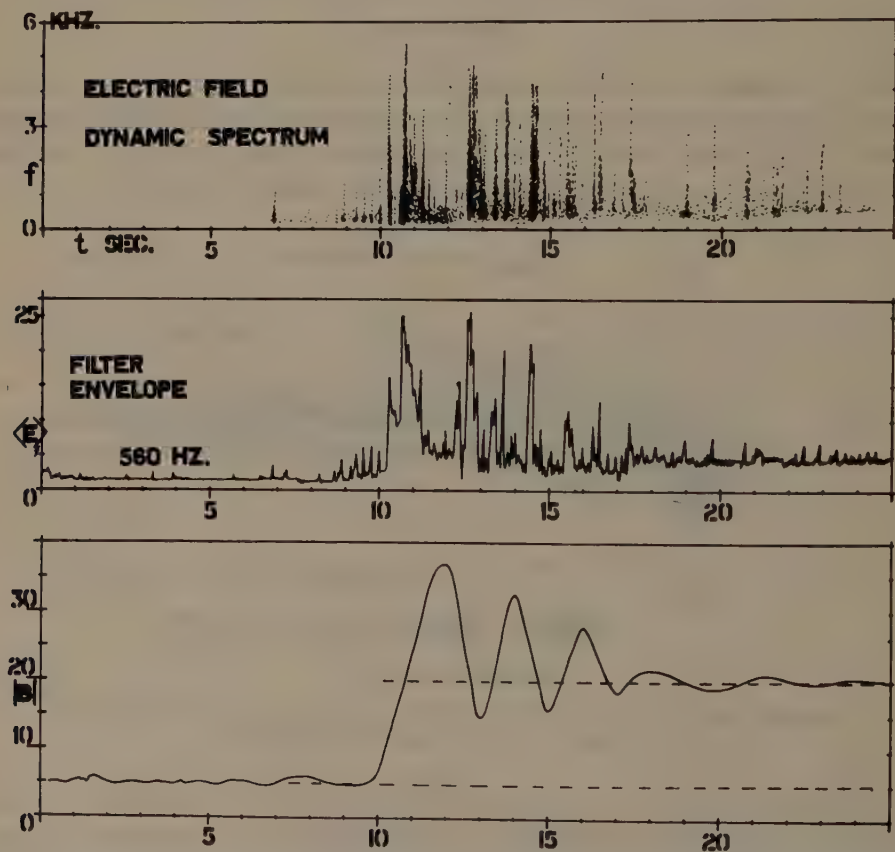


Fig. 2. An idealized sketch of the characteristics of the nearly laminar compressional shock observed by OGO 5 on March 12, 1968 (Fredricks and Coleman, 1969).

cussed by Fredricks and Coleman (1969), Fredricks *et al.* (1970), and Scarf *et al.* (1970a). The key features of the observations are indicated in Figure 2, which has been somewhat idealized for the sake of clarity.

Using arguments to the effect that the shock was nearly stationary at the time of observation, Fredricks and Coleman (1969) inferred the shock thickness to be equal to spacecraft velocity (1.8 km s^{-1}) \times characteristic time of the B field wavetrain (3 s, from bottom graph in Figure 3) or about 5 km. Taking into account uncertainties in the shock velocity, the authors set an upper limit to the shock thickness of about 24 km. These thicknesses correspond to a few times the electron inertial length c/ω_{pe} in the upstream plasma medium; that is, the wavelength of an electromagnetic wave traveling at the electron plasma frequency (30 kHz) in the solar wind. Thus, the main shock structure as determined from the B field wavetrain would seem to correspond to an MHD pulse structure (possibly a standing Alfvén wave), triggered by a resonance at the solar wind electron plasma frequency, and with wavelength determined by the solar wind electron inertial length.

Along with the B field MHD structure, there are bursts of higher frequency (0.1 to 6 kHz) electrostatic waves which seem to be most numerous in regions where grad B is large (top of Figure 2). These have been interpreted as ion waves produced by a current-driven plasma instability, possibly a two-stream instability. Here, electrons inside the shock moving tangent to the shock surface (forming the current required to produce a gradient in B) act as the fast stream, and the ambient ions inside the shock act as the slow stream. That the disturbances seen are electrostatic rather than electromagnetic (e.g., whistlers) is attested by the fact that a search coil magnetometer operating simultaneously at the same frequencies did not detect any comparable activity. Thus, the existence of a current-driven ion instability appears to be confirmed, and this provides the dissipation mechanism required for the shock. Observations of other, more complex shock structures have also been observed and reported by Fredricks and Coleman (1969) and Scarf *et al.* (1970b).

The earth's bow shock apparently also triggers hydromagnetic waves which propagate back into the upstream solar wind. Fairfield (1969) has reported frequent observations of these waves (0.01 to 0.05 Hz) in the interplanetary medium near earth; the observations nearly always occurred at times when interplanetary magnetic field lines at the spacecraft (Explorer 34) also intersected the bow shock. Energetic electrons and protons are also frequently seen in the solar wind just outside the bow shock, apparently traveling along magnetic field lines that are connected to the magnetosheath. Recent observations of these phenomena have been made by Anderson (1968) and Asbridge *et al.* (1968).

3. Magnetosheath

After the solar wind crosses the bow shock it becomes more dense, subsonic, and acquires a much higher temperature. Gas-dynamic calculations carried out by Spreiter *et al.* (1966), assuming that the solar wind behaves like an ideal gas of Mach number 8, show that at the subsolar point the temperature of the solar plasma rises by a factor

of about 20 across the shock, while its flow velocity decreases by about a factor of 4. However, as this plasma is deviated around the magnetosphere by the geomagnetic field, it re-acquires a more directed flow and a lower temperature. By the time it reaches the dawn (or dusk) meridian, a sufficient exchange of energy from thermal to directed flow has occurred so that the plasma has regained a directed flow velocity of about 75% of solar wind velocity (i.e. it has become supersonic again).

Using gasdynamic solutions of the distribution and characteristics of plasma in the

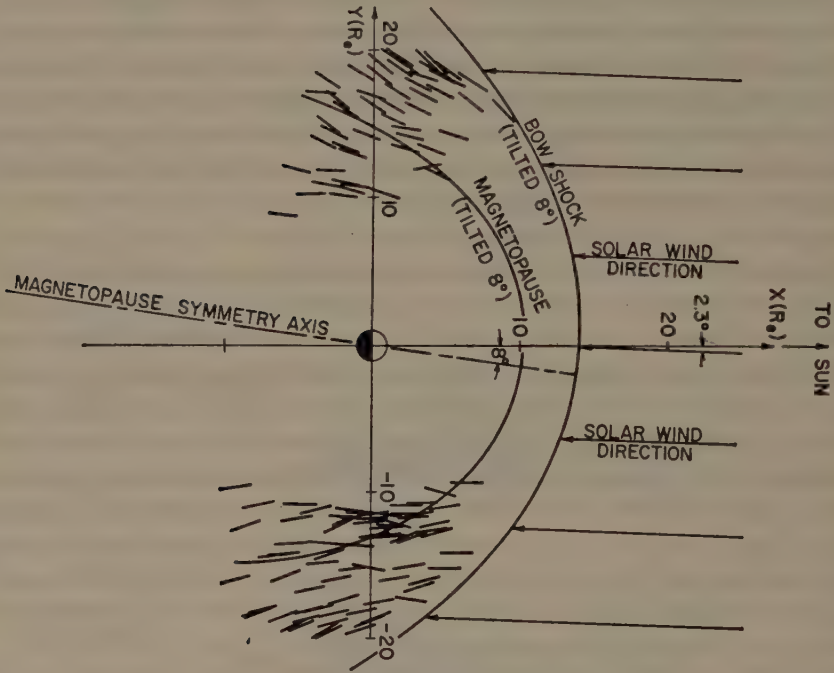


Fig. 3. A possible magnetosheath configuration suggested by Vela 3 observations. Viewed in a frame of reference moving with the earth, the average direction of incident solar wind flow is from 2.3° west of the sun. The magnetosheath flow pattern is symmetric about a line tilted at 8° from the sun-earth line. A hypothetical bow shock and magnetopause also tilted by 8° are shown (Hundhausen *et al.*, 1969).

magnetosheath, and making the assumption that this highly conducting plasma is tied to the interplanetary magnetic field through frozen-in flux, it is relatively straightforward to calculate what the magnetic field configuration of the magnetosheath should be. These calculations have been performed by Alksne (1967) for a variety of solar wind conditions and relative orientations of the interplanetary magnetic field.

Alksne's (1967) theoretical calculations are in general borne out by satellite measurements. A multi-satellite study by Behannon and Fairfield (1969), utilizing more than 1600 hr of magnetometer data from four of the IMP spacecraft, taken when one satellite was in the magnetosheath while at least one other was in the solar wind, has

revealed the following consistencies with theory: (a) the ratio B/B_0 (magnetosheath field/interplanetary field) is about 4 near the subsolar point and declines asymptotically behind the earth, frequently becoming less than one beyond about $40 R_E$; (b) when the interplanetary field is aligned near the spiral angle, fields measured in the dusk hemisphere are much more ordered and are larger in magnitude than those measured in the dawn hemisphere; (c) when the interplanetary field is aligned at about 90° to the solar wind flow, the magnetosheath field directions in both the dawn and dusk hemispheres are consistent with an appearance of 'draping' of field lines around the magnetosheath.

Plasma flow in the magnetosheath has been directly and systematically observed over the course of several years by the VELA satellites. Hundhausen *et al.* (1969), using ion data obtained near the dawn/dusk meridians over a 5 mo period in 1967 with VELA 3A and 3B, have reported a number of general features. A significant finding is the observation that the magnetosheath flow pattern is asymmetric with the solar wind. As illustrated in Figure 3, this flow pattern appears to be aligned around an axis of symmetry which is tilted about 8° from the earth-sun line (or about 6° from the solar wind flow direction). This slight tilting of the flow may be explained by a suggestion made several years ago by Walters (1964). The suggestion was that the entire magnetosphere should be tilted relative to the solar wind direction, because of the asymmetry introduced by the 'garden-hose' angle of the interplanetary magnetic field. Although the energy density of the interplanetary field is small compared to the solar wind or magnetosheath bulk flow (β about 65), it is nevertheless sufficient for Walters' theory to predict a deviation from symmetry about the solar wind of approximately 5° , which is very close to that observed.

4. Magnetopause

The boundary around which the magnetosheath flow is deviated has been termed the magnetopause, and its general shape in the noon-midnight meridian plane is as illustrated in Figure 1. This overall morphology has been confirmed by numerous satellite observations (Sugiura, 1969). The observed position of the magnetopause is fully consistent with its function as the pressure-balance surface between the magnetosheath (i.e., shocked solar wind) plasma and the geomagnetic field.

With regard to the nature of this boundary, considerable attention has been focused on whether it is a rotational discontinuity (i.e., a large amplitude standing Alfvén or whistler wave), or a tangential discontinuity (i.e., an equipotential current sheet with unequal particle pressures on either side). If it is a rotational discontinuity, then there can be a component of magnetic field normal to the boundary surface, and plasma can flow through the boundary at a speed equal to the Alfvén wave speed based on that normal component of field. If it is a tangential discontinuity, then no such plasma flow through the boundary is possible, and there can be no interconnection of magnetic field lines between the magnetosphere and magnetosheath.

Sonnerup and Cahill (1967, 1968) have investigated 91 magnetopause crossings of

Explorer 12, using that satellite's magnetometer data. Applying various statistical tests to the data, they concluded that about one-third of the observed boundaries were more likely to be rotational than tangential. Also, the likely rotational discontinuities all seemed to be associated with high magnetic field values just inside the magnetopause, indicating an association with magnetic storms or large-scale inward motions of the boundary.

Although it would be tempting to conclude on the basis of the Explorer 12 study that every time the boundary moves inward its nature changes to that of a rotational discontinuity, there is contrary evidence furnished by the magnetometer on ATS 1. On January 14, 1967, the magnetopause moved inward to less than $6.6 R_E$ geocentric distance at the subsolar point and crossed the orbit of the synchronous satellite ATS 1 several times. An extensive study of satellite magnetometer data by Cummings and Coleman (1968), using an analysis of variance technique, indicated that none of the observed boundaries could be clearly called a rotational discontinuity, although there were some that clearly appeared to be tangential discontinuities. Thus, the true nature of the magnetopause and the circumstances which can cause it to change remain a subject for exploration.

Another fruitful approach to the study of the boundary is a consideration of its associated electric fields. Parker (1967) has considered, from an individual particle point of view, what are the consequences of a sudden surge in intensity of the solar wind when it reaches the magnetopause. The analysis begins with an electron and proton traveling parallel through the magnetosheath and striking the magnetopause with equal velocity. Considering the magnetic field to be parallel to the magnetopause, and considering no other particles to be present in the near vicinity, both particles will attempt to execute cyclotron motion inside the magnetosphere. The proton, because of its greater momentum, would ordinarily have a much larger cyclotron radius; however, a charge-separation electric field will necessarily be produced and it prevents the proton from penetrating deeper into the magnetosphere than the electron. The direction of this electric field will maintain itself near the boundary until thermal ions and electrons from the ionosphere or deeper in the magnetosphere can rise along magnetic field lines to cancel it, possibly seconds or minutes. Only after this period will the incident solar wind particles begin to move independent of each other in the magnetosphere. (The resulting deeper penetration of the protons will then introduce a magnetic field perturbation, but this will not be discussed here; however, Su and Sonnerup (1971) have questioned Parker's model on the basis of it.)

As long as the strong electric field exists (i.e., while the solar wind intensity is rapidly increasing, or, equivalently, while the magnetopause is moving inward), it should be possible to look for its effects on magnetospheric particles near the boundary. Such an observation has been made recently by Bogott and Mozer (1971), utilizing an energetic electron and proton instrument on the synchronous satellite ATS 5. A deep penetration of the boundary, again inside $6.6 R_E$, occurred on September 29, 1969. Energetic electrons were seen to drop precipitously in counting rate about 8 s before the boundary was reached, while a corresponding drop in the proton flux was not seen until

about 8 s after the boundary had crossed the satellite. The situation is illustrated in Figure 4. This observation has been interpreted to be the result of a strong electric field directed towards the boundary, giving rise to an $\mathbf{E} \times \mathbf{B}$ drift velocity which is opposite in sense to the gradient drift for electrons and enhances the gradient drift for protons. As a result, electrons are swept away from the boundary and protons are not.

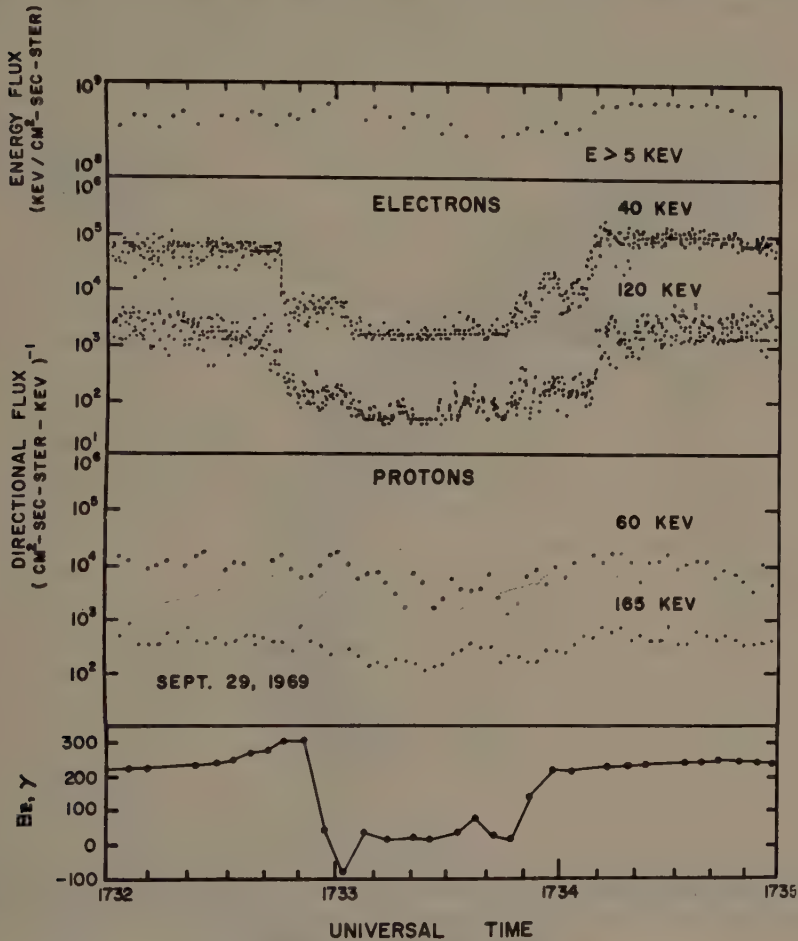


Fig. 4. High time resolution data for the ATS 5 magnetopause crossing near 1733 UT on September 29, 1969. The spacecraft z-axis is parallel to the earth's spin axis (Bogott and Mozer, 1971).

5. Particle Entry Ways into the Magnetosphere

A. THE POLAR CUSP

In the illustration of the magnetosphere previously shown in Figure 1, it can be seen that there are two regions in the dayside magnetosphere, one in the northern and one in the southern hemisphere, in which magnetic field lines lead up from the earth and

appear to touch the magnetopause. These two points of contact at the magnetopause are generally referred to as the neutral points, since in any mathematical field model the total magnetic field goes to zero there. Of course, in reality, nature would not permit such an extreme point singularity to exist; but it is a requirement of the field line geometry that the immediate vicinity of these points (and along a line running east and west of them) must be characterized by extremely low magnetic field. Thus, the pressure balance at the magnetopause is extremely tenuous near these points, and any

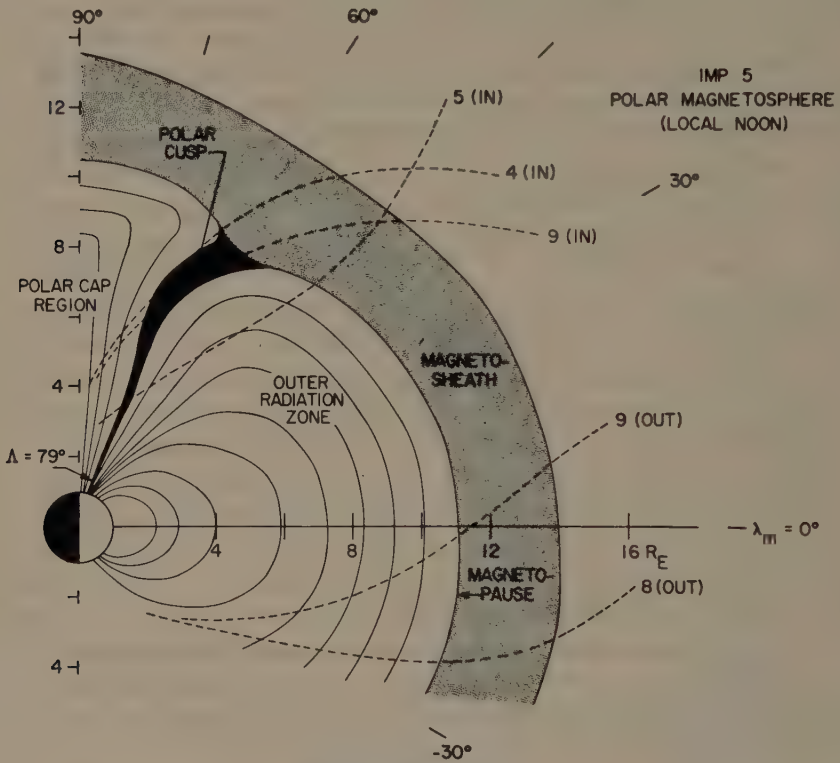


Fig. 5. A diagram showing the geometry and location of the polar cusp within the polar magnetosphere in the noon meridional plane during periods of relative magnetic quiescence. The polar cusp intersects the auroral zone at 79° . Several sample trajectories of IMP 5 through the dayside magnetosphere are also shown (Frank, 1971a).

small irregularities in the magnetosheath flow will result in plasma streaming through the magnetopause down into the dayside auroral regions of the earth.

Verification that this phenomenon actually does occur has come very recently from two sources: one, a direct observation of both electrons and protons streaming down high-latitude magnetic field lines at radial distances between about 4 and $7 R_E$ and magnetic latitudes between 65 and 75° , reported by Frank (1971a, b) from IMP 5 data; and two, similar observations at magnetic latitudes as low as 43° recorded by several

instruments on OGO 5 during a large magnetic storm and reported by Russell *et al.* (1971).

Frank's observations with IMP 5, obtained during July through August 1969, are summarized in Figure 5. This figure shows three separate inbound trajectories of IMP 5 on which the phenomenon was observed, with dark shading to indicate the extent of the region. The figure also gives a name to this region: the polar cusp, a designation which will be used hereafter in this paper. The fact that charged particles enter the polar cusp directly from the magnetosheath appears to be incontestable, especially when the energy spectra of particles from these two regions are compared. In cases where the IMP 5 orbit crossed the polar cusp and magnetosheath within 2 or 3 hr of each other, both the shape of the spectra and the magnitude of the particle fluxes were virtually identical.

B. THE PLASMA SHEET AND MAGNETOTAIL

Although it has not been firmly established whether particles arrive at the geomagnetic tail and plasma sheet via the polar cusp or via direct field line connection between the distant magnetotail and the solar wind, it is nevertheless a fact that there are particles in these regions; and this can be used as a starting point for discussing convection electric fields within the magnetosphere.

The geomagnetic tail has been observed to extend downstream of the earth as far as $500 R_E$ (Mariani and Ness, 1969) and possibly as far as $1000 R_E$ (Ness *et al.*, 1967; Intriligator *et al.*, 1969). However, plasma sheet particles have been observed only as far as about $40 R_E$ (Meng and Anderson, 1971). These particles are both electrons and protons in the energy range 100 eV to 10 KeV, with a peak in the energy distribution at about 1 keV for electrons, and between 1 and 5 keV for protons. The energy density of particles in the plasma sheet is roughly comparable to the energy density of the magnetic field in which they reside. The plasma sheet has a sharp cutoff near earth at a distance of about $10 R_E$ (Vasyliunas, 1968), which has been alternately termed the 'inner edge of the plasma sheet' or the 'Alfvén layer.' The latter designation is in recognition of early work on electric fields in the magnetosphere performed by Alfvén (1939). As was noted in a paper by Kavanagh *et al.* (1968), if a uniform electric field of about 0.3 mVm^{-1} , directed from dawn to dusk exists across the magnetosphere, then the observed position of the Alfvén layer corresponds very closely to the position where the combined effects of electric field drift and gradient drift establish a forbidden zone for 1 keV electrons.

The plasma sheet is presumed to be a source for many of the particles seen deeper in the magnetosphere, including the ring current particles and outer zone trapped particles (which are themselves, in turn, presumed to be the source for inner zone particles via radial diffusion processes). The mechanism by which these plasma sheet particles enter the magnetosphere is a large scale electric field which must exist across the magnetosphere cavity, directed from dawn to dusk. Although many mechanisms have been proposed to explain the formation of the magnetosphere, almost all contain an acknowledgment of this electric field (see, for example, the recent review by Axford

(1969). Although a uniform steady convection electric field would prevent particles above a few keV energy from penetrating the magnetosphere deeper than 8 to 10 R_E , this electric field must certainly be fluctuating, since its origin is related to the solar wind. Therefore, on occasions when the electric field becomes very strong for short periods of time, we can expect that clouds of plasma sheet particles will be driven deep into the magnetosphere and will be observable there.

Such observations have been made most recently and in greatest detail by DeForest and McIlwain (1971), with an instrument aboard the geosynchronous ATS 5 satellite.

When a cloud of plasma is injected from the tail into the magnetosphere, three major forces are at work: The gradient in the magnetic field, which causes electrons to drift towards dawn and protons to drift towards dusk at a speed proportional to the particle energy; The rotation of the earth, which produces an electric field that makes all particles tend to drift towards dawn; and the convection electric field, which gives a component of velocity to all particles in the direction towards the sun. The net result is that the plasma cloud disperses itself around the magnetosphere, but at any given location along the drift paths, particles of different energies arrive at different times. ATS 5 (orbiting earth at 6.6 R_E , circular, in the equatorial plane) is an ideal platform from which to observe these plasma clouds, since it is far enough out in the magnetosphere that the main components will pass through its orbit, and since it is moving in a frame of reference in which the particle drift due to rotation of the earth may be neglected.

A sample of detailed time and energy spectra of plasma clouds seen by ATS 5 over the course of several hours is presented in Figure 7 of the paper by McIlwain (1972). Differences in arrival times for particles of various energies can be clearly seen here, as well as fluctuations in the characteristics of the cloud itself. From information such as this, it is possible to put together a model of the strength and shape of the convection electric field required to produce this particular pattern of arrival times, assuming that the plasma originates as single clouds injected somewhere near midnight. Of course, the model electric field inferred will necessarily be somewhat different for each discrete set of observations, since the convection is certainly not steady. Nevertheless, from a study of many sets of observations, McIlwain (1971) has formulated a general field pattern which appears to represent reasonably well the majority of the observations. Equal potential contours for this field pattern in the equatorial plane are shown in Figure 2 of the paper by McIlwain (1972). These contours, which include the effect of the electric field produced by rotation of the earth, are also coincident with the drift paths of low energy plasma through the magnetosphere (i.e., plasma for which gradient drift can be neglected).

On the above referenced figure it must be noted that the electric field pattern is derived only from particle trajectories which pass through the synchronous orbit. Therefore, strictly speaking, the model has validity only within 2 or 3 R_E of 6.6 R_E . In particular, the fact that the electric potential lines are allowed to strike the magnetopause instead of being bent back into the tail there (to make the magnetopause itself an equipotential surface), is not based on data and should not be considered a discovery of the experiment.

6. Composition of the Trapped Radiation

The stably trapped components of energetic particle radiation, consisting of energetic electrons and protons in the outer and inner magnetosphere, have been mapped extensively by a large number of satellites. Detailed models of the trapped radiation environment have been catalogued and are generally available (Vette, 1966; Vette *et al.*, 1966; King, 1967; Vette and Lucero, 1967, Lavine and Vette, 1969). Rather than attempting to summarize this great bulk of information, this section will concentrate on observations of a rare class of trapped particles, the alphas and heavier nuclei. Study of these particles is motivated primarily by a desire to use them as tracers of source mechanisms which supply particles to the regions deep in the magnetosphere.

Trapped α -particles have been detected by instruments aboard a number of satellites, including Injun 4 and 5, OGO 4, 1966-70A, and 1968-26B, and the results are available in the literature (see, for example, Fritz and Krimigis, 1969; Krimigis, 1970; and Van Allen and Randall, 1971). The energy spectra of the trapped alphas normally peak at about 0.3 to 0.5 MeV/nucleon and the distribution is normally centered at about $L = 3$. The ratio of trapped alpha/proton fluxes is normally quite small, about 2×10^{-6} . This may be compared to the alpha/proton ratio in the solar wind of about 0.04.

Three sources have been suggested to explain the presence of energetic trapped α -particles (Krimigis, 1970), and two of these have received serious consideration. These are:

(a) Capture of α -particles from the solar wind into the outer regions of the magnetosphere with subsequent radial diffusion across L shells and betatron acceleration.

(b) Direct magnetospheric capture of energetic α -particles in the interplanetary medium associated with solar particle events.

For the first suggested source, it is possible to predict the alpha/proton ratio at various energies deep in the magnetosphere, if proper account is taken of the effect on α -particles of crossing the earth's bow shock and of loss mechanisms during the time that the radial diffusion process is operative. As discussed by Krimigis (1970), these theoretical predictions have not yet been able to match the experimentally measured alpha/proton ratio. However, it is suspected that the calculations have not taken into full account all the relevant loss processes, and that a more complete calculation will yield more acceptable results.

The second suggested source has received considerable impetus from a report by Van Allen and Randall (1971) of α -particle observations from the Injun 5 and Explorer 35 satellites during 8 mo in 1968 and 1969. From October 29 to November 1, 1968, a dramatic rise in intensity of trapped α -particles occurred, with flux levels rising by about a factor of 40. This rise was coincident with a very large magnetic storm and with an available large source of α -particles in the interplanetary medium. Although there were other magnetic storms during this 8 mo period, and other occasions when large fluxes of alphas were available in the interplanetary medium, the simultaneity of the two events was unique. Thus, the supposition is that these α -particles were directly injected into $L = 3$ during this event. The absolute magnitude of the α -particle fluxes seen in the interplanetary medium and in the magnetosphere

during this event were about equal, lending added credence to this supposition.

Energetic C, N, and oxygen nuclei have also recently been observed trapped in the radiation zone (Krimigis *et al.*, 1970; Van Allen *et al.*, 1970). These particles also appear to have a distribution centered about $L = 3$. A statistically significant number of counts at energies greater than 0.3 MeV/nucleon was obtained with Injun 5. The ratio of intensities of C, N, O/alphas is observed to be about 3×10^{-3} , which may be compared to the solar wind C, N, O/alpha ratio of about 0.01 to 0.04 (Bame *et al.*, 1968). Thus, both the alpha/proton and the C, N, O/alpha flux ratios are considerably lower in the trapped radiation than in the solar wind. This suggests that if the solar wind is indeed the source of these particles, then the transport mechanism must be either less effective for higher Z nuclei, or the loss mechanisms in the magnetosphere must be more effective for higher Z .

7. Conclusions

The study of the magnetosphere becomes more difficult as our bank of data increases. It no longer suffices to send a satellite anywhere above the atmosphere, armed with any type of particle or field detector, and expect any result to be scientifically significant. In general, any measurement taken now must be tied in with other measurements, either taken simultaneously on the same satellite, or taken by another satellite at a different location. In short, we have moved from an era of exploration to an era of understanding. There are still some fundamental single-point measurements to be made, such as a direct measurement of the convection electric field in the outer magnetosphere and a detailed exploration of the neutral point regions, but the bulk of the exploratory work is now in hand. We should now be in a position to exploit the magnetosphere for what may prove to be its greatest value: a laboratory in which a great many types of plasma phenomena can be isolated and studied each in its turn.

References

- Alfvén, H.: 1939, *Kungl. Sv. Vet-Akademiens Handl.* **3**, 18(3).
 Alksne, A. Y.: 1967, *Planetary Space Sci.* **15**, 239.
 Anderson, K.: 1968, *J. Geophys. Res.* **73**, 2387.
 Asbridge, J. R., Bame, S. J., and Strong, I. B.: 1968, *J. Geophys. Res.* **73**, 5777.
 Axford, W. I.: 1969, *Rev. Geophys.* **7**, 421.
 Bame, S. J., Hundhausen, A. J., Asbridge, J. R., and Strong, I. B.: 1968, *Phys. Rev. Letters* **20**, 393.
 Behannon, K. W. and Fairfield, D. H.: 1969, GSFC preprint X-616-69-61.
 Bogott, F. H. and Mozer, F. S.: 1971, *J. Geophys. Res.* **76**, 892.
 Cummings, W. D. and Coleman, P. J.: 1968, *J. Geophys. Res.* **73**, 5699.
 DeForest, S. E. and McIlwain, C. E.: 1971, *J. Geophys. Res.* **76**, 3587.
 Fairfield, D. H.: 1969, *J. Geophys. Res.* **74**, 3541.
 Frank, L. A.: 1971a, *J. Geophys. Res.* **76**, 5202.
 Frank, L. A.: 1971b, *J. Geophys. Res.* **76**, 2512.
 Fredricks, R. W. and Coleman, P. J.: 1969, *Proc. International Conference on Plasma Instabilities in Astrophysics*, Gordon and Breach, New York.
 Fredricks, R. W., Crook, G. M., Kennel, C. F., Green, I. M., Scarf, F. L., Coleman, P. J., and Russell, C. T.: 1970, *J. Geophys. Res.* **75**, 3751.

- Fritz, T. A. and Krimigis, S. M.: 1969, *J. Geophys. Res.* **74**, 5132.
- Heppner, J. P., Sugiura, M., Skillman, T. L., Ledley, B. G., and Campbell, M.: 1967, *J. Geophysics. Res.* **72**, 5417.
- Hundhausen, A. J., Bame, S. J., and Asbridge, J. R.: 1969, *J. Geophys. Res.* **74**, 2799.
- Intriligator, D. S., Wolfe, J. H., McKibbin, D. D., and Collard, H. R.: 1969, *Planetary Space. Sci.* **17**, 321.
- Kavanagh, L. D., Jr., Freeman, J. W., Jr., and Chen, A. J.: 1968, *J. Geophys. Res.* **73**, 5511.
- King, J. H.: 1967, NASA SP-3024, **4**.
- Krimigis, S. M.: 1970, in B. M. McCormac (ed.), *Particles and Fields in the Magnetosphere*, D. Reidel Publishing Company, Dordrecht, Holland, p. 364.
- Krimigis, S. M., Verzariu, P., Van Allen, J. A., Armstrong, T. P., Fritz, T. A., and Randall, B. A.: 1970, *J. Geophys. Res.* **75**, 4210.
- Lavine, J. P. and Vette, J. I.: 1969, NASA SP-3024, **5**.
- Mariani, F. and Ness, N. F.: 1969, *J. Geophys. Res.* **74**, 5633.
- McIlwain, C. E.: 1971, *EOS (AGU Transactions)* **52**, 328.
- McIlwain, C. E.: 1972, this volume, p. 268.
- Meng, C. and Anderson, K. A.: 1971, *J. Geophys. Res.*, **76**, 873.
- Ness, N. F., Searce, C. S. and Canterano, S. C.: 1967, *J. Geophys. Res.* **72**, 3769.
- Parker, E. N.: 1967, *J. Geophys. Res.* **72**, 4365.
- Russell, C. T., Chappell, C. R., Montgomery, M. D., Neugebauer, M., and Scarf, F. L.: 1971, *J. Geophys. Res.* **76**, 6743.
- Scarf, F. L., Fredricks, R. W., and Kennel, C. F.: 1970a, in B. M. McCormac (ed.), *Particles and Fields in the Magnetosphere*, D. Reidel Publishing Company, Dordrecht-Holland, p. 102.
- Scarf, F. L., Coleman, P. J., Fredricks, R. W., Kennel, C. F., and Russell, C. T.: 1970b, in V. Manno and D. E. Page (eds.), *Intercorrelated Satellite Observations Related to Solar Events*, D. Reidel Publishing Company, Dordrecht-Holland, p. 181.
- Sonnerup, B. U. O. and Cahill, L. J.: 1967, *J. Geophys. Res.* **72**, 171.
- Sonnerup, B. U. O. and Cahill, L. J.: 1968, *J. Geophys. Res.* **73**, 1757.
- Spreiter, J. R., Alksne, A. Y., and Abraham-Shrauner, B.: 1966, *Planetary Space Sci.* **14**, 1207.
- Su, S. Y. and Sonnerup, B. U. O.: 1971, *J. Geophys. Res.* **76**, 5181.
- Sugiura, M.: 1969, GSFC Preprint X-612-69-12.
- Van Allen, J. A. and Randall, B. A.: 1971, *J. Geophys. Res.* **76**, 1830.
- Van Allen, J. A., Randall, B. A., and Krimigis, S. M.: 1970, *J. Geophys. Res.* **75**, 6085.
- Vasyliunas, V. M.: 1968, *J. Geophys. Res.* **73**, 2839.
- Vette, J. I.: 1966, NASA SP-3024, **1**.
- Vette, J. I. and Lucero, A. G.: 1967, NASA SP-3024, **3**.
- Vette, J. I., Lucero, A. B., and Wright, J. A.: 1966, NASA SP-3024, **2**.
- Walters, G. K.: 1964, *J. Geophys. Res.* **69**, 1769.

MAGNETOSPHERIC PROCESSES

CARL-GUNNE FÄLTHAMMAR

Department of Plasma Physics, Royal Institute of Technology, S-100 44 Stockholm, Sweden

1. Introduction

Not so long ago the region of space that we now call the magnetosphere used to be considered a very simple part of our environment from a physical point of view: essentially a vacuum penetrated by a magnetic field.

After it was realized that interplanetary plasma would deform the geomagnetic field and create what came to be called the magnetosphere, this domain of space became much more interesting. Still, however, it was a widely held view that this system was in principle a rather simple magnetohydrodynamic system, although, of course, the complicated geometrical configuration made most quantitative calculations a matter of great mathematical difficulty.

Since then the amount of observational knowledge has increased very much and a more refined picture of the physical structure of the magnetosphere has evolved. The present state of knowledge in this respect has been summarized in the previous paper (Kavanagh, 1972). However, the observations have also revealed numerous interesting plasma phenomena, many of which are of a little known or entirely unknown character.

One may consider the magnetospheric research effort as consisting of two different and partly overlapping phases. The first is the *exploratory phase* in which the magnetosphere's spatial and temporal structure and the distribution and properties of its content of matter are recorded. This phase still continues to accomplish a number of remaining tasks. Presently, we are in the beginning of a second phase, which we may call the *physics phase*, which is characterized by conscious attempts to clarify the plasma physical phenomena discovered in the exploratory phase.

Many of these phenomena involve matter in an extreme state (the low density plasma state (Section 3)) whose properties are very poorly known because this state has only recently, and only within very limited parameter ranges, been subject to experimental study. Investigation of such phenomena may therefore contribute valuable new substance to our knowledge of physics.

Among many different plasma populations, the magnetosphere also contains plasma in a state which very much resembles the state that will be typical of the fuel in future thermonuclear fusion reactors. Progress in the understanding of the plasmas of the magnetosphere may therefore widen the basis for the fusion research effort. At the same time much of the experience gained in fusion experiments and other laboratory plasma experiments can be a greatly helpful input in space plasma research. The mutual benefits of close contact between plasma research in space and in the laboratory seem to be underestimated and will be further discussed in Section 7.

Finally, the magnetosphere may also serve as a planetary-scale laboratory for active

plasma experiments, which will also improve the understanding of naturally occurring magnetospheric phenomena.

2. Brief Phenomenological Survey

The present section will give a brief outline of magnetospheric processes on a phenomenological basis. The subsequent discussion of the physical processes behind them will concentrate on a few of these phenomena.

The interaction between solar wind and the magnetosphere involves several mutually interrelated processes:

The *confinement of the magnetic field* involves processes that determine the size of the magnetosphere, especially the *stand-off distance* of the magnetopause, the *length of the tail*, and the magnetic *topology*. The processes determining the magnetic field may alternatively be discussed in terms of the corresponding current system, and this is sometimes advantageous (Alfvén, 1968a, b; Alfvén and Fälthammar, 1971).

The *exchange of matter* between the solar wind and the magnetosphere is a process of key importance in maintaining the internal structure of the magnetospheric plasma population, such as the *plasma sheet*, the *ring current* and the *radiation belts*. This exchange of plasma is intimately related with the topology of the geomagnetic field. The open topology alternative allows plasma penetration through the frontside reconnection region into polar cap magnetic field lines. Another possibility is *plasma entry* via the dayside *polar cusp regions*. The latter alternative has become an issue of great interest as a consequence of recent satellite experiments in which the particle population in these formerly little known regions has been directly measured (Heikkilä and Winningham, 1971). The *transport* of the plasma after it has gained access to the inside of the magnetopause is also a poorly known process. One possibility is that the quasi-trapping regions of the magnetosphere (Roederer, 1967, 1970) play a role by allowing particles to enter by *gradient and centrifugal drift*. (As gradient and centrifugal drift are so intimately connected, we shall for brevity use the term gradient drift for both.) Electric field drift (convection) generally in combination with gradient drift is also a most important process. Its role was emphasized long ago (Alfvén, 1939) in the electric field theory of the aurora (for a review of recent observational knowledge, see Fahleson, 1972; Gurnett, 1972; McIlwain, 1972). *Inertia drift* other than the centrifugal drift is generally small but can still be of decisive importance indirectly by way of the charge separation it can cause (Section 5).

For the geomagnetically trapped particles, the gradient drift dominates so as to prevent convective transport by electric fields. The latter will only cause perturbations in the drift orbits. However, as the electric fields fluctuate with time, so do the orbit perturbations, and this leads to an effective *radial transport process of a diffusion-like kind*. Recent reviews have been given by Fälthammar (1972) and Walt (1971). However, the transport of trapped radiation does not have to take place by diffusion all the way from the magnetopause. The discovery of frequent injection events at the geostationary orbit reveals that substorms are associated with transient electric fields strong

enough to convect even particles of several keV energy deep into magnetosphere (Lezniak and Winckler, 1970; De Forest and McIlwain, 1971). The location of the source of the further inward diffusion therefore is where the particles from the injection events are deposited.

The *exchange of energy* between the solar wind and the magnetosphere is a particularly intriguing phenomenon. Energy can be fed into the magnetosphere in various ways. Waves generated in the magnetosheath or magnetopause may propagate into the magnetosphere and dissipate there. Compressions of the geomagnetic field as a whole (in other words, increases in the magnetopause surface current) will temporarily increase the internal magnetic energy at the same time heating the magnetospheric particle population adiabatically. Because non-adiabatic processes are also present, irreversible energization becomes possible. This is of some importance for the radiation-belt particles. By far the most important energy input, however, is the one associated with the establishment of large scale internal electric potential fields and current systems penetrating the magnetosphere. This seems to be the energy input that leads to the conditions required for the release of *magnetospheric substorms*. It is also intimately connected with the *convection of plasma* in the magnetosphere, *formation of the plasma sheet*, and the *shaping of the plasmapause*. The transverse plasma convection may also be coupled in part to the field-aligned plasma flux of the *polar wind* (Banks and Holzer, 1968; Donahue, 1971; Holzer *et al.*, 1971). Part of the polar wind may, through *reconnection in the 'magnetic neutral sheet'* of the *geomagnetic tail*, be fed into closed magnetic flux tubes. This possible recycling of polar wind particles has attracted attention in connection with the question of the origin of auroral and radiation belt particles, a problem that has been reviewed by Axford (1970). He found that no definite conclusion could be drawn regarding the question whether they are all of direct solar wind origin or could be in part of ionospheric origin. Recent measurements have added evidence in favor of direct solar wind origin (Whalen *et al.*, 1971).

The *substorm phenomenon* (reviewed by Akasofu, 1968; Aubry, 1972) seems to be the syndrome of an instability leading to a major restructuring of the magnetospheric system, causing a number of plasma processes to be excited. In terms of magnetic field structure it represents a relaxation from an 'inflated' state with drawn out magnetic field lines on the nightside, even as close as at the geostationary orbit. This state, which corresponds to a large magnetic energy, has been built up during a period previous to the substorm. The state to which the system relaxes is generally reported to be characterized by a more 'dipole-like shape' (lower magnetic energy) at the geostationary orbit. The question of what particular instability is responsible for the onset of substorm that attracts intense interest but remains unsolved.

At ground level the magnetic manifestation of the substorm is a large negative change (often hundreds of gammas) in the horizontal component at auroral latitudes, caused by an overhead westward electrojet, carrying a total current of the order of 1 Mamp. At lower latitudes there is instead an increase in the horizontal component. The electric currents causing most of the ground level magnetic changes are not con-

fined to the ionosphere but connected with the outer magnetosphere by currents coming down and going out along geomagnetic field lines. As the current conduction in the ionosphere depends on both the Pedersen and Hall conductivities, the coupling between the ionosphere and the magnetosphere will contain both 'line currents' connecting at the ends of the jet and 'sheet currents' at the edges of the jet i.e., a combination of Boström's (1964, 1968) two models (cf., also Atkinson (1970)). In terms of current circuit restructuring the substorm-associated magnetic field changes correspond to having part of the nightside dawn to dusk current rerouted via the ionosphere.

The substorm appears to consist of a *growth phase* during which the magnetic field disturbance grows at a moderate rate (during a time interval of the order of 1 hr), and an *explosive phase* (characterized by a rapid field change, reaching a maximum within 10 min or less). However, there remains some controversy regarding to what extent a growth phase can always be distinguished.

Concurrent with the polar magnetic substorm is the *auroral substorm* (Akasofu, 1968). Here we may only note the two main features of this intricate phenomenon: equatorward movement of auroral arcs previous to the explosive phase of the substorm during which the auroras brighten, move rapidly poleward, and break-up.

The many facets of the substorm process also include *drastic changes* in the *magnetotail plasma*. According to the most recent summary by Hones *et al.* (1971) and Hones (1971) the major features are the following. Coincident (within minutes) with the onset of negative magnetic disturbances in the auroral zone the tail plasma region starts becoming thinner in terms of spatial extent. Generally it also becomes thinner in terms of particle content except for an occasional transient increase at the beginning. At a later phase, typically by the time the poleward-moving auroras reach a magnetic latitude of 74° , the tail plasma region widens again.

Some further remarks on the substorm will be given in Section 4. The complex of processes that constitutes the magnetospheric substorm seems to be a very important guide to understanding the dynamics of the magnetospheric system as a whole.

3. Classes of Plasmas and Plasma Phenomena

The magnetospheric plasma (including the ionosphere) covers a wide range of parameters (e.g., densities ranging from more than 10^6 cm^{-3} in the F region to much less than 1 cm^{-3} for energetic trapped particles, thermal energies from less than an eV in the ionosphere to many MeV in the radiation belts). The phenomena that take place in these various plasma populations are correspondingly different. A classification based on the value of the mean free path relative to the gyroradius and the characteristic dimension of the plasma will reflect basic differences in their properties (Alfvén and Fälthammar, 1963). We consider three main classes of plasmas:

- (a) High density plasmas: mean free paths much shorter than gyroradii.
- (b) Medium density plasma: mean free paths much greater than gyroradii but shorter than characteristic lengths.

(c) Low density plasma: mean free paths much larger than characteristic lengths. (Sometimes a finer gradation is needed in transition regions where differences in mean free path and gyroradii between different particle species are important. An example is the 90 to 120 km altitude region in the ionosphere.)

Inside the magnetosphere, high density plasmas are found only in the lower ionosphere (D and lower E region). Medium density plasmas constitute the rest of the ionosphere (except at high latitudes) and the plasmasphere. The rest of the magnetosphere contains low density plasmas in the above sense.

High and medium density plasmas behave in a comparatively 'classical' (but not necessarily simple) way. For example, a fluid like macroscopic behavior requires that the particles occupying a volume element stay together for a certain amount of time. In high density plasmas this is achieved by collisions. In medium density plasmas the particles of a volume element are held together along the magnetic field by collisions and transverse to it by gyration. In low density plasmas only the transverse confinement remains. Mathematically, single or multiple fluid models, so useful in high end medium density plasma, cannot be applied except in special configurations. Instead we have to resort to formalisms involving the distribution function.

Whereas in high and medium density plasma electric field and current density are related by more or less sophisticated forms of the generalized Ohm's law, they need have no relation of this kind at all in a low density plasma (Alfvén and Fälthammar, 1963; cf., Persson, 1963, 1966).

Physically, the low density plasma exhibits the most complicated behavior. The study of it only has barely begun. Some of the technological facilities required for its study in the laboratory have recently been developed in connection with the thermonuclear effort. In the space physics context, low density plasma is of particular interest because it constitutes the matter that fills most of the magnetosphere, and it plays a key role in generating the more spectacular magnetospheric phenomena such as auroras and magnetic storms.

4. Ionosphere – Magnetosphere Interaction

The ionosphere constitutes a boundary region of the magnetosphere, which greatly influences the dynamics of the latter. The interaction between the two regions is quite different at low and high magnetic latitudes.

At *low and middle latitude* (the domain of the plasmasphere) the interaction is largely characterized by approximate *diffusive equilibrium* (Bauer, 1969) and good *thermal contact*. The densities are comparatively high – of the order of 10^1 – 10^2 cm⁻³ at the lowest density (Chappell *et al.*, 1970, 1971) and the temperatures are comparable to those in the ionosphere (of the order of an eV). The plasma in the plasmasphere, being of medium density (Section 3) is in good *electrical contact* with the ionosphere, which means that the magnetic field lines are equipotentials and an electric field distribution is established which keeps the plasma essentially in corotation with the ionosphere. It may be noticed that the corotational electric field is not divergence-

free but corresponds to a certain distribution of net charge throughout the plasmasphere.

Within the plasmasphere there may be certain less 'classical' processes going on, namely instabilities leading to rapid precipitation of ring current higher energy protons brought into the same region of space. The protons precipitated in this way may be the cause of the proton auroras referred to as SAR (Cornwall *et al.*, 1970, 1971; cf., also Eather and Carovillano, 1971). The contact between plasmasphere and ring current protons can be established either by the ring current being moved into the plasmasphere or by the expansion of the plasmasphere (by buildup from the ionosphere) into regions occupied by the ring current. The experimental observations of Chappel *et al.* (1971) seem to support the connection between the plasmopause and the SAR.

At high magnetic latitudes (in the auroral oval and polar cap) the conditions are entirely different. Along the open magnetic field lines ionospheric plasma can escape from the earth. According to the *polar wind theory* (Banks and Holzer, 1968; Holzer *et al.*, 1971) this occurs by a supersonic expansion analogous to the expansion of the solar corona to form the solar wind, although the physical conditions are even more complicated in the ionosphere.

The ionosphere, rotating with the earth in the presence of the geomagnetic field, acts as a unipolar dynamo with an e.m.f. of nearly 100 kV, whose external circuit is the magnetospheric plasma. At low and moderate latitudes where the plasma is of medium density, the external load is brought to at least approximate corotation, so that the dynamo current ceases, except for a small trickle needed to maintain the corotation. At high latitudes the conditions are different in two respects:

(a) The configuration of the high latitude field lines is such that the plasma on them cannot easily be brought into corotation; therefore, the unipolar e.m.f. remains active.

(b) The load is a low density plasma which does not respond in a simple way to the applied e.m.f. The part of the e.m.f. that is applied to the polar cap plasma (polewards of the auroral zones) is as large as about 10 kV. Precisely how the plasma does respond to an applied electric field is an interesting but still essentially unsolved problem. For example, it is likely to be able to support electric fields along magnetic field lines. In fact, this is a necessary condition for 'cutting the field lines,' i.e., for decoupling the plasma on polar cap magnetic field lines from moving with the ionosphere. As such decoupling seems almost inevitable it means that somewhere there are electric fields along magnetic field lines above the polar caps. The electrical conditions have been discussed by Fälthammar and Block (1971).

The electric fields, which may or may not be concentrated to sheaths, will accelerate particles upwards and downwards depending on their sign (Block, 1971a, b, 1972).

Although the earth's rotational energy has been suggested as a possible energy source for geophysical phenomena such as radiation belts and auroras (McIlwain, 1969) it has attracted comparatively little interest. However, in view of the conditions above the high latitude ionosphere, the unipolar-dynamo e.m.f. applied over that region may be far from uninteresting.

Another important aspect of the electrical coupling between ionosphere and magnetosphere is the linkage between them via electric currents. In agreement with early predictions by Birkeland but contrary to widespread belief during several decades there are electric currents flowing along magnetic field lines between the ionosphere and magnetosphere. According to measurements by magnetometers on polar orbiting satellites current sheaths are a frequently occurring feature (Cummings and Dessler, 1967; Zmuda *et al.*, 1967; 1970; Armstrong and Zmuda, 1970). Such currents have also been detected by rocket measurements (Cloutier *et al.*, 1970) and by combined ground-based and space observations (Haerendel *et al.*, 1971). Current densities of the order of 10^{-5} amp m^{-2} have been detected (Armstrong and Zmuda, 1970). The field-aligned currents may have an influence on the density distribution of the topside ionosphere and in particular according to Block and Fälthammar (1968), it may be the cause of local field aligned density depletions discovered by topside sounders (Herzberg and Nelms, 1969).

If the current density becomes large, as during magnetic substorms, it may lead to the formation of large magnetic field aligned electric potential drops, perhaps concentrated to space charge sheaths. Although the conductivity along magnetic field lines was often considered practically infinite, this view has been challenged on several grounds. In a low density plasma in an inhomogeneous magnetic field, the concept of conductivity ceases to be valid in its ordinary sense (Alfvén and Fälthammar, 1963). Several authors have invoked various instabilities expected to lead to a state of anomalous resistivity (Swift, 1965; Sagdeev and Galeev, 1966; Ossakow, 1968; Coroniti, 1969).

In laboratory plasma physics, space charge sheaths are known to occur in gas discharges not only at walls and electrodes but also at detached positions in the body of a gas discharge. Among the conditions that favor the occurrence of such free space charge sheaths are, in particular, those where a discharge current connects two regions of plasmas with different temperatures and densities.

The possibility that free space charge sheaths may also occur in or above the ionosphere and be responsible for acceleration of auroral particles was proposed long ago by Alfvén (1958). Unfortunately, at that time there was prevalent belief in the purely ionospheric current systems without connection with the space above, and little or no attention was paid to the idea. The modern *in situ* observations however, have changed the picture entirely. Satellite borne magnetometers have proven the validity of the Alfvén-Birkeland type of current system that connects the ionosphere and the magnetosphere, especially in the high latitude regions. It has further been found that in these regions the electric currents flow between a magnetospheric plasma which is very thin and very hot, and a dense and cool ionospheric plasma. Thus some of the typical conditions for sheath formations are present. More importantly, however, there are indications that space charge sheaths do indeed occur during the auroras. Early satellite observations prompted cautions speculation of electric field acceleration as a hypothetical possibility. More direct indications came later from the observations by Albert (1967), Evans (1968), and recently by Heikkila (1970) of very

narrow peaks sometimes occurring in the energy spectra of precipitating electrons.

Other rocket borne particle measurements have been interpreted in terms of multiple sheaths, each with a potential drop in the hundreds of volts range (Albert and Lindstrom, 1970). The evidence was an intensity distribution with energy and pitch angle of a kind expected for particles moving between a set of electric potential barriers above and a magnetic mirror below. In this case too, the electric field was directed upward. Field aligned electron bursts, observed by Hoffman and Evans (1968) at high latitudes also indicate electric field acceleration along the magnetic field.

Corresponding measurements for low energy protons have only recently become available. Reme and Bosqued (1971) have reported rocket borne measurements of 0.5 to 5 keV protons with angular distribution and energy spectra indicating a downward electric field (potential 1 to 2 kV) as responsible for the acceleration. Comprehensive satellite measurements of precipitating protons below 10 keV have been reported by Hultqvist *et al.* (1971). They show that precipitating 6 keV protons are frequently very strongly magnetic-field aligned; flux ratios at 10 and 80° pitch angle can be as large as 50 or more. The phenomenon may prevail over large areas (comparable in size with the polar cap) and last for hours. Hultqvist (1970) has also given a theoretical discussion of the formation of sheaths (cf. Block, 1972).

A space charge sheath above a region of auroral precipitation may reveal itself through typical patterns of motion of the visual aurora (opposite streaming in neighboring regions). From analyzing of cinematographic recordings of aurora, Carlqvist and Boström (1970) have discovered such motions and thereby brought further support that space-charge sheaths exist in or above the ionosphere.

Certain observed features have been thought to be incompatible with electric field acceleration (O'Brien, 1970). Examples quoted include simultaneous precipitation of electrons and protons, and the precipitation of low energy electrons together with the energetically spiked electrons in the several keV range. However, closer examination indicates (Block, 1972) that the difficulties so far suggested are only apparent and that some of them are in support rather than in conflict with the hypothesis of electric acceleration.

5. Electric Fields and Convection

There is now general agreement that large scale electric fields and corresponding plasma convections throughout the major part of the outer magnetosphere are a key feature of the magnetosphere under auroral and magnetic storm conditions. In addition there is the corotational field (i.e., electric field corresponding to plasma corotation) within the plasmasphere.

Different models vary in their details. We shall not discuss these details but only some questions of a general kind relating to the electric field and the convection.

In early models of the magnetosphere the electric fields were rarely discussed explicitly but instead hidden in the concept of convecting magnetic flux tubes. Common assumptions were that the magnetosphere was filled by a 'cool background plasma' and that the electrical conductivity along magnetic field lines (σ_{\parallel}) could be considered

infinite. Under such conditions the convection of magnetic flux tubes is a valid and utterly convenient concept.

In the magnetosphere, as we now know it, the situation is much more complicated. The magnetospheric particle population outside the plasmapause is not dominated everywhere by a cool plasma (ATS measurements indicate a characteristic energy of several keV), which means that gradient and centrifugal drifts are not negligible. The conductivity along magnetic field lines cannot be trusted to be large enough to make magnetic field lines electrical equipotentials. On the contrary, under the very conditions where the electric field (and plasma convection) is strong (namely substorms), there may be considerable voltage drops of the order of several kV along magnetic field lines.

The circumstances just mentioned have a rather profound influence on the character of the convection.

Consider first the role of the particle energy, and for simplicity, let the particles involved be limited to the equatorial plane, thus performing a two dimensional motion. As the particles approach the earth, the gradient drift will sooner or later become large enough to prevent further approach. There is a forbidden region (Alfvén, 1939; Karlson, 1963, 1971; Block, 1966; Kavanagh *et al.*, 1968) of finite width (which shrinks to zero in the case of cold plasma).

As a consequence of the high thermal energy of the plasma, the drift motion also causes a charge separation. In a steady state, self-consistency requires that the net-charge distribution associated with the flow be identical with the source distribution required to sustain the electric field that causes part of the drift. To find the steady state one should consider simultaneously the field equations and the equations of motion and continuity and find a self-consistent configuration. This problem is extremely difficult and has not been solved except under very idealized assumptions.

We may notice that although in any given steady state, there is a well defined electric field $E(\mathbf{r})$ at any point \mathbf{r} in space, there is no corresponding unique drift velocity since particles of different charge, energy, or pitch angle will have different drift velocity vectors at any given point.

Looking next at the full three dimensional problem we notice that even if σ_{\parallel} was infinite, the flux tube motion would not be unique for the reason just mentioned. One could still introduce a separate flux tube velocity for particles of each sign, energy, and equatorial pitch angle which would be inconvenient. One might make a convention of taking the average velocity of the particles in a flux tube to be the flux tube velocity. This would however, greatly reduce the physical significance of the concept (since the particles in the flux tube would subsequently follow different paths). Furthermore, when $\sigma_{\parallel} \neq 0$, a possibility which seems very likely to exist under disturbed conditions, the situation is further complicated by the fact that the frozen field line condition may be violated so that not even different parts of the same flux tube would 'move' in a coherent way.

The concept of magnetic field line motion (although meaningless in itself and definable only as a convention) can be a convenient concept when the appropriate

conditions are fulfilled. In the magnetosphere however it can be very misleading. It would seem advisable in discussions of the magnetospheric dynamics, therefore, to dispense with it altogether and adhere to the corresponding physically measurable quantity, which is the electric field.

6. Response of the Magnetosphere to Interplanetary Conditions

The magnetosphere is continually immersed in the solar wind flow. The energy flux over a surface as large as the magnetospheric cross section is at any time more than sufficient to maintain a high level of magnetic activity. However, it is only occasionally that an appreciable fraction of this energy enters the magnetosphere to drive magnetic and auroral substorms and all the phenomena associated with them. The 'key to the magnetosphere', i.e., the interplanetary conditions for energy release has been a favorite and controversial subject for some time. A review of early work has been given by Hirshberg and Colburn (1969). Substantial progress has been made by Nishida (1971a, b) and Nishida and Maezawa (1971a, b). These authors distinguish between different modes of interaction, each requiring different conditions.

One mode is manifested geomagnetically as so-called magnetic impulses. These correlate very well with the dynamic pressure of the solar wind and can be understood in terms of a 'compression' of the geomagnetic field.

Another mode is represented by the magnetic field variations called DP2 (Nishida, 1968). They show no correlation with the dynamic pressure of the solar wind, nor with the dynamic pressure of the solar wind, nor with density or velocity, but they do show a strikingly detailed correlation with the southward component of the interplanetary magnetic field. For the substorm disturbance (DP1), too, the southward component of interplanetary magnetic field plays a key role, although in a less direct way. Typically, a substorm is preceded by a period of the order of 1 hr (although varying within very wide limits), with a southward interplanetary field and a corresponding disturbance at ground level correlating well with the southward interplanetary magnetic field.

Very recently Arnoldy (1971) has presented further strong evidence for the southward magnetic field component being of singular importance.

Nishida's interpretation is that the DP2 disturbance is due to currents driven by the interplanetary electric field penetrating directly into the outer parts of the magnetosphere. On the basis of Dungey's magnetospheric model this seems plausible on general grounds (cf., Alfvén and Fälthammar, 1971) and as well in line with laboratory experience of the interaction of plasmas with magnetic obstacles (Danielsson and Lindberg, 1964) (cf. Section 7).

7. Remarks on Laboratory Experiments

Although the main sources of empirical information about the magnetosphere are space experiments and ground based observations, there is also a third source,

namely laboratory plasma experiments. Their role in the process of understanding the physics of the magnetosphere is too often undervalued, perhaps because a correct scaling of cosmical phenomena to laboratory size is in general impossible.

Even with perfect scaling being impossible, suitably chosen scaling compromises may still allow certain aspects of interest to be studied. Reviews of model experiments have been given by Schindler (1969) and Podgorny and Sagdeev (1970). An example of interest is the terrella experiments by Lindberg and his group (Danielsson and Lindberg, 1964). In these experiments the interaction between a streaming magnetized plasma and a magnetic dipole field was studied. The experiments showed very clearly the role of the magnetic field direction in the plasma in agreement with what has been theoretically expected and later confirmed by space experiments.

However, the virtue of laboratory experiments as a potential contributor of insight into magnetospheric phenomena has a deeper foundation. This is because they act as a check on theoretical idealizations by revealing theoretically unexpected behavior of real plasmas. Furthermore, laboratory experiments can be very helpful in stimulating new ideas on the interpretation of space measurements.

It is interesting to notice that it was Birkeland, guided by discharge experiments, who several decades ago first proposed that auroral current systems are closed by field aligned currents. This concept was kept alive only among a few heretics used to thinking in terms of laboratory plasma behavior. Even when a satellite magnetometer first detected the local magnetic effects of the field aligned currents their true nature was not immediately recognized. Now the Birkeland currents have been subject to extensive measurements and are recognized as an important feature of the electrodynamics of the magnetosphere.

Similarly, the concept of electric fields along geomagnetic field lines was introduced more than a decade ago by Alfvén (1958), who was thinking in terms of a gas-discharge analogy (the earth as a probe in a cosmical plasma). This concept, too, was received unfavorably until recently, when rocket and satellite borne measurements caused numerous experimenters to invoke such fields to explain their data. As a consequence of this development the more recent experiments on sheath formation in discharges (Babic *et al.*, 1971) may be of great interest in magnetospheric physics.

Although the two examples mentioned represent contributions by exceptionally outstanding scientists it may often be so that close contacts with laboratory plasma physics can be useful as a guide to recognizing essential space plasma processes, even in cases where the plasma parameters involved are very different in the laboratory and space.

References

- Akasofu, S.-I.: 1968, *Polar and Magnetic Substorms*, D. Reidel Publishing Company, Dordrecht-Holland.
- Albert, R. D.: 1967, *J. Geophys. Res.* **72**, 5811.
- Albert, R. D. and Lindstrom, P. J.: 1970, *Science* **170**, 1398.
- Alfvén, H.: 1939, *Kungl. Svenska Vetenskapsakademiens Handlingar* **18**, 1.
- Alfvén, H.: 1958, *Tellus* **10**, 104.
- Alfvén, H.: 1968a, *Ann. Geophys.* **24**, 1.

- Alfvén, H.: 1968b, *J. Geophys. Res.* **73**, 4379.
- Alfvén, H. and Fälthammar, C.-G.: 1963, *Cosmical Electrodynamics, Fundamental Principles*, Clarendon Press, Oxford.
- Alfvén, H. and Fälthammar, C.-G.: 1971, *Cosmic Electrodyn.* **2**, 78.
- Armstrong, J. C. and Zmuda, A. J.: 1970, *J. Geophys. Res.* **75**, 7122.
- Arnoldy, R. L.: 1971, *J. Geophys. Res.* **76**, 5189.
- Atkinson, G.: 1970, *J. Geophys. Res.* **75**, 4746.
- Aubry, M.: 1972, this volume, p. 357.
- Axford, W. J.: 1970, in B. M. McCormac (ed.), *Particles and Fields in the Magnetosphere*, D. Reidel Publishing Company, Dordrecht-Holland, p. 46.
- Babic, M., Sandahl, S., and Torvén, S.: 1971, Paper presented at the Tenth Internat. Conference on Phenomena in Ionized Gases, Oxford, Sept. 1971.
- Banks, P. M. and Holzer, T. E.: 1968, *J. Geophys. Res.* **73**, 6846.
- Bauer, S. J.: 1969, *Proc. IEEE* **57**, 1114.
- Block, L. P.: 1966, *J. Geophys. Res.* **71**, 855.
- Block, L. P.: 1971a, *Proc. IXth Internat. Conf. on Phenomena in Ionized Gases*, in press.
- Block, L. P.: 1971b, to be published.
- Block, L. P.: 1972, this volume, p. 258.
- Block, L. P. and Fälthammar, C.-G.: 1968, *J. Geophys. Res.* **73**, 4807.
- Boström, R.: 1964, *J. Geophys. Res.* **69**, 9983.
- Boström, R.: 1968, *Ann. Geophys.* **24**, 1.
- Carlqvist, P. and Boström, R.: 1970, *J. Geophys. Res.* **75**, 7140.
- Chappell, C. R., Harris, K. K., and Sharp, G. W.: 1970, *J. Geophys. Res.* **75**, 50.
- Chappell, C. R., Harris, K. K., and Sharp, G. W.: 1971, *J. Geophys. Res.* **76**, 2357.
- Cloutier, P. A., Anderson, H. R., Parks, Vondrak, R. R., Spiger, R. J., and Sandel, B. R.: 1970, *J. Geophys. Res.* **75**, 2595.
- Cornwall, J. M., Coroniti, F. V., and Thorne, R. M.: 1970, *J. Geophys. Res.* **75**, 4699.
- Cornwall, J. M., Coroniti, F. V., and Thorne, R. M.: 1971, *J. Geophys. Res.* **76**, 4498.
- Coroniti, F. V.: 1969, in S. C. Coroniti and J. Hughes (eds.), *Planetary Electrodynamics*, Gordon and Breach, p. 309.
- Cummings, W. D. and Dessler, A. J.: 1967, *J. Geophys. Res.* **72**, 1007.
- Danielsson, L. and Lindberg, L.: 1964, *Arkiv Fysik* **28**, 1.
- De Forest, S. E. and McIlwain, C. E.: 1971, *J. Geophys. Res.* **76**, 3587.
- Donahue, T. M.: 1971, *Rev. Geophys. Space Phys.* **9**, 1.
- Eather, R. H. and Carovillano, R. L.: 1971, *Cosmic Electrodyn.* **2**, 105.
- Evans, D. S.: 1968, *J. Geophys. Res.* **73**, 2315.
- Fahleson, U.: 1972, this volume, p. 223.
- Fälthammar, C.-G.: 1972, in Dyer (General ed.), *Solar Terrestrial Physics/1970; Part III*, D. Reidel Publishing Company, Dordrecht-Holland, p. 270.
- Fälthammar, C.-G. and Block, L. P.: 1971, *Proc. ESRO Colloquium on Wave Particle Interactions in the Magnetosphere*, ESRO SP-72, p. 147.
- Gurnett, D.: 1972, this volume, p. 233.
- Haerendel, G., Hedgecock, P. C., and Akasofu, S.-I.: 1971, *J. Geophys. Res.* **76**, 2382.
- Heikkilä, W. J.: 1970, *Nature* **225**, 369.
- Heikkilä, W. J. and Winningham, J. P.: 1971, *J. Geophys. Res.* **76**, 803.
- Herzberg, L. and Nelms, G. L.: 1969, *Ann. IQSY* **3**, 426.
- Hirshberg, J. and Colburn, D. S.: 1969, *Planetary Space Sci.* **17**, 1183.
- Hoffman, R. A. and Evans, D. S.: 1968, *J. Geophys. Res.* **73**, 6201.
- Holzer, T. E., Fedder, J. A., and Banks, P. M.: 1971, *J. Geophys. Res.* **76**, 2453.
- Hones, E. W., Jr.: 1971, Los Alamos Scientific Laboratory, preprint.
- Hones, E. W., Jr., Singer, S., Lanzerotti, L. J., Pierson, J. D., and Rosenberg, T. J.: 1971, *J. Geophys. Res.* **76**, 2977.
- Hultqvist, B.: 1970, Kiruna Geophysical Observatory, preprint.
- Hultqvist, B., Borg, H., Riedler, W., and Christophersen, P.: 1971, *Planetary Space Sci.* **19**, 279.
- Karlson, E. T.: 1963, *Phys. Fluids* **6**, 708.
- Karlson, E. T.: 1971, *Cosmic Electrodynamics* **1**, 474.
- Kavanagh, L. D.: 1972, this volume, p. 3.

- Kavanagh, L. D., Jr., Freeman, J. W., and Chen, A. J.: 1968, *J. Geophys. Res.* **73**, 5511.
- Lezniak, T. W. and Winckler, J. R.: 1970, *J. Geophys. Res.* **75**, 7075.
- McIlwain, C. E.: 1969, *Ann. OQSY* **4**, 302.
- McIlwain, C. E.: 1972, this volume, p. 268.
- Nishida, A.: 1968, *J. Geophys. Res.* **73**, 1795.
- Nishida, A.: 1971a, *Planetary Space Sci.* **19**, 205.
- Nishida, A.: 1971b, Invited paper presented at IAEA Symposium 'Electric Fields in Space and their Connection with Atmospheric Effects', Moscow, August, 1971.
- Nishida, A. and Maezawa, K.: 1971a, *J. Geophys. Res.* **76**, 2254.
- Nishida, A. and Maezawa, K.: 1971b, Institute of Space and Aeronautical Science, Univ. of Tokyo, preprint.
- O'Brien, B. J.: 1970, *Planetary Space Sci.* **18**, 1821.
- Ossakow, S. L.: 1968, *J. Geophys. Res.* **73**, 6366.
- Persson, H.: 1963, *Phys. Fluids* **6**, 1756.
- Persson, H.: 1966, *Phys. Fluids* **9**, 1090.
- Podgorny, I. M. and Sagdeev, R. Z.: 1970, *Soviet Phys. USPEKHI* **98** (No. 3 and 4) English transl. Jan.-Febr., p. 445.
- Reme, H. and Bosqued, J. M.: 1971, *J. Geophys. Res.*, **76**, 7683.
- Roederer, J. G.: 1967, *J. Geophys. Res.* **72**, 981.
- Roederer, J. G.: 1970, *Dynamics of Geomagnetically Trapped Radiation*, Springer-Verlag, Berlin, p. 66.
- Sagdeev, F. L. and Galeev, A. A.: 1966, International Centre for Theoretical Physics, Trieste, Report IC/66/64.
- Schindler, K.: 1969, *Rev. Geophys.* **7**, 51.
- Swift, D. W.: 1965, *J. Geophys. Res.* **70**, 3061.
- Walt, M.: 1971, *Space Sci. Rev.* **12**, 446.
- Whalen, B. A., Miller, J. R., and McDiarmid, J. B.: 1971, *J. Geophys. Res.* **76**, 2406.
- Zmuda, A. J., Jr., Heuring, F. T., and Martin, J. H.: 1967, *J. Geophys. Res.* **72**, 1115.
- Zmuda, A. J., Armstrong, J. C., and Heuring, F. T.: 1970, *J. Geophys. Res.* **75**, 4757.

THE INTERRELATIONSHIP OF MAGNETOSPHERIC PROCESSES

VYTENIS M. VASYLIUNAS

*Dept. of Physics and Center for Space Research, Massachusetts Institute of Technology,
Cambridge, Mass., U.S.A.*

"One Ring to rule them all . . ."

J. R. R. TOLKIEN

1. Introduction

Convection of plasma in the magnetosphere is one of the major aspects of magnetospheric dynamics. Attempts during the past 10 yr to understand this complicated phenomenon have led to a sequence of theoretical models of constantly increasing sophistication (see, for example, Axford (1969)). Most of these models have been formulated in qualitative terms. But although such qualitative models are very useful, and indeed indispensable, it is also necessary to construct the corresponding quantitative models: to write down the physical equations implied by the qualitative ideas, and solve them. Quantitative models, although of necessity greatly simplified and schematic, serve to test whether our qualitative models really behave as we think they do.

In a previous paper (Vasyliunas, 1970; hereafter referred to as Paper I) I described a systematic approach to the calculation of magnetospheric convection, in the form of a self-consistent chain of equations: the electric field in the magnetosphere determines the plasma pressure gradient, which determines the perpendicular electric current, which flows into the ionosphere and determines the ionospheric electric field, which maps along magnetic field lines into the magnetosphere. Then I solved the equations for the extremely simplified case where the plasma pressure inside the magnetosphere was assumed negligible and only the field aligned currents resulting from the processes that drive the convection (viscous drag or magnetic merging) were considered. (The same calculation, with more realistic magnetic field and ionospheric conductivity, was done independently by Wolf (1970).) The resulting configuration of convective flow looked exactly like the conventional two-cell pattern that had always been drawn on qualitative grounds. The calculation thus showed that the basic ideas of magnetospheric convection can be derived from the interplay between the driving processes and the ionosphere, without involving in any crucial way the energetic plasma within the magnetosphere.

Nevertheless, there can be no doubt that plasma pressure inside the magnetosphere is very much non-negligible. The purpose of this paper is to examine some of the ways in which this plasma pressure modifies magnetospheric convection. The approach is the same as in Paper I: simplify the problem by retaining only the essential physical features, and then seek quantitative solutions of the governing equations. Only some

of the basic ideas and results are presented here; the full calculation will be published elsewhere.

The dominant contributor to the total plasma pressure is the proton population of the plasma sheet and the ring current (the two really form one continuous region, as discussed by Frank (1971) and Vasyliunas (1972); I shall call this entire population simply the ring current. The contribution of other particles to the plasma pressure is here assumed to be negligible. The transport of ring current protons is treated as adiabatic, in a broad sense of that term: local sources and losses are assumed negligible. For simplicity, the magnetic field is assumed to be dipolar, neglecting in particular the inflation of the field by the ring current itself. (The ring current affects convection primarily by producing field-aligned currents; the inflation of the magnetic field complicates the geometry but is not expected to introduce any qualitatively new features into the convective flow pattern.)

2. Effect of the Ring Current on Magnetospheric Convection

The ring current gives rise to field aligned currents whenever the plasma pressure has an azimuthal gradient (or, more precisely, a gradient in the direction of the $\mathbf{B} \times \nabla B$ drift; cf., Equations (4), (5), and (6) of Paper I*). Such azimuthal gradients can result from ionospheric dynamo or corotational electric fields (Fejer, 1964), or from LT dependent non-adiabatic sources or losses (Swift, 1967). However, here I will consider only the azimuthal gradients produced by the convection electric field itself, since it is the simplest cause and one that is always present whenever there is magnetospheric convection.

Let $\Phi(\lambda, \varphi)$ be the electric potential as a function of the latitude and LT of the intersection of magnetic field lines with the ionosphere. (Field lines are assumed to be equipotentials and throughout this paper all quantities will be mapped to the ionosphere.) The magnetospheric electric current perpendicular to the magnetic field and averaged along a magnetic flux tube can be written as

$$\mathbf{I}_m = [eN(\mathbf{V}_B + \mathbf{V}_d)] - eN\mathbf{V}_B + \mathbf{I}_M, \quad (1)$$

where N is the number of protons in a flux tube of unit cross sectional area, $\mathbf{V}_B \equiv c\mathbf{E} \times \mathbf{B}_i/B_i^2 = c\mathbf{B}_i \times \nabla\Phi/B_i^2$, \mathbf{B}_i is the magnetic field in the ionosphere, \mathbf{V}_d is the proton gradient and curvative drift averaged along the flux tube, and \mathbf{I}_M is the (divergence-free) magnetization current. The term in brackets is the contribution from the proton drift; the next term is the contribution of the electron drift (neglecting the electron pressure is equivalent to neglecting the electron gradient-curvature drift). The field aligned current density flowing into the ionosphere is given by the negative divergence of the magnetospheric current

$$J_{\parallel} \sin \chi = -\nabla \cdot \mathbf{I}_m, \quad (2)$$

where χ is the inclination of the magnetic field. But the assumed adiabatic behavior of

* Note two misprints in Paper I: Equations (4) and (5) should have minus signs.

protons implies a continuity equation for the tube content of protons

$$\partial N / \partial t + \nabla \cdot N (\mathbf{V}_B + \mathbf{V}_d) = 0. \quad (3)$$

Combining Equation (1), (2), and (3), and assuming a steady state yields an expression for the field aligned current density resulting from the interaction of the ring current with an electric field:

$$J_{\parallel} \sin \chi = \nabla \cdot e N \mathbf{V}_B. \quad (4)$$

(An equivalent result was obtained by Fejer (1964)). This can be rewritten in a form analogous to the divergence of a Hall current

$$J_{\parallel} \sin \chi = - \nabla \cdot \Sigma^* \mathbf{B}_i \times \mathbf{E} / B_i \quad (5)$$

where, with n the proton number density,

$$\Sigma^* \equiv N e c / B_i = \int dl (n e c / B). \quad (6)$$

Equation (4) or (5) can also be derived directly from the equations relating J_{\parallel} and the pressure, given in Paper I, making use of the fact that the adiabatic motion of protons follows the contours of constant total energy.

Thus the modification of the convection electric field by the ring current is the same as if the ring current were replaced by a region of enhanced Hall conductivity proportional to its proton content. The effect of the ring current will be important or unimportant depending on whether the parameter Σ^* is large or small compared to the ionospheric Hall conductivity Σ_H . Inserting numbers into Equation (6) and assuming that n is constant along a field line (as required by the observed isotropy of the ring current protons; cf. Frank (1967)) yields for a dipole field

$$\Sigma^* = \frac{n}{1 \text{ cm}^{-3}} \left(\frac{L}{10} \right)^4 308 \text{ mho}.$$

Since $n \sim 1 \text{ cm}^{-3}$ at $L = 10$, Σ^* is much larger than Σ_H and the ring current may be expected to modify drastically the convective flow pattern. (Note that inflation of the magnetic field increases the volume of a flux tube and hence would make Σ^* even larger.)

3. Models of Steady Magnetospheric Convection with a Ring Current

The electrical potential associated with magnetospheric convection can be calculated from the continuity of current in the ionosphere

$$\nabla \cdot \Sigma \cdot \mathbf{E} = J_{\parallel} \sin \chi, \quad (7)$$

where Σ is the height integrated ionospheric conductivity tensor. As in Paper I, the driving field (representing the effect of magnetic merging or viscous drag) is introduced as a boundary condition on the potential at the edge of the polar cap (modeled as a

circle of 72° latitude): $\Phi(\lambda, \varphi) = \Phi_0 \sin \varphi$ at $\lambda = 72^\circ$. At latitudes below the polar cap, the only field aligned currents are assumed to be due to the ring current and are given by Equation (5).

Observations of the ring current (Frank, 1967) show that with decreasing L the proton pressure increases smoothly from the plasma sheet values (in a manner not grossly inconsistent with adiabatic radial transport and hence constant tube content), until one reaches a fairly well defined inner edge at which the proton pressure drops very steeply. Hence Σ^* is approximated as constant from the polar cap down to the (invariant) latitude λ_{RC} of the inner edge of the ring current and zero elsewhere. (The actual inner edge cannot, of course be a circle of constant latitude but must be deformed by the electric field; indeed, it is this deformation that results in the field aligned currents described by Equation (5). However, once these currents have been taken into account through the use of Equation (5), the remaining effects of the deformation are small and may be neglected, a procedure equivalent to a first-order expansion of the problem in the ratio Φ_{RC}/K_{RC} , with K_{RC} the proton kinetic energy per charge and Φ_{RC} the electric potential, both at λ_{RC} .)

Solutions of Equations (5) and (7) were calculated for various values of the two model parameters, the latitude λ_{RC} and the ratio Σ^*/Σ_H . (The third parameter, the polar cap potential Φ_0 , merely determines the scale factor of the solution.) As in Paper I, the conductivity model of Fejer (1964) was used, with constant Pedersen and Hall conductivities and $\Sigma_H/\Sigma_P = 3.5$. As an example, Figure 1 shows the calculated equipotentials for the case $\lambda_{RC} = 60^\circ$ and $\Sigma^*/\Sigma_H = 2$, and for comparison also the case $\Sigma^* = 0$, i.e., negligible ring current effect. As can be seen, at latitudes below the inner edge of the ring current the electric field has been greatly reduced and rotated in LT; within the ring current region, the N-S component of the electric field (E-W component of the flow) has been enhanced.

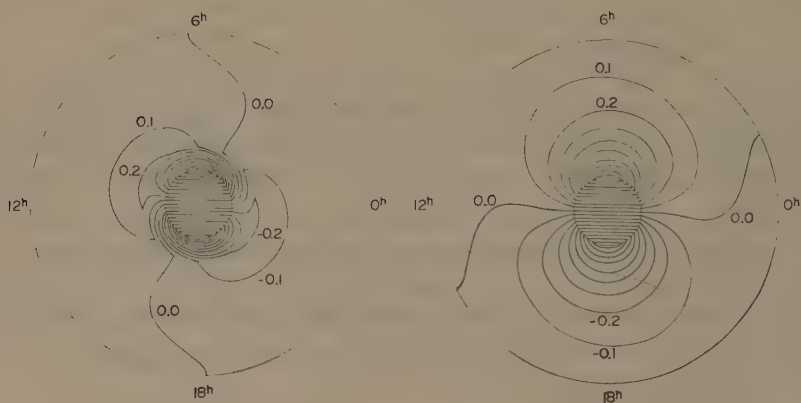


Fig. 1. Latitude-LT plot of calculated equipotential contours in the ionosphere, labeled by values in units of Φ_0 . The innermost circle is $\lambda = 72^\circ$; the outermost is the equator. Left: model with $\Sigma^*/\Sigma_H = 2$ and the ring current between 72° and 60° . Right: model with $\Sigma^* = 0$ (except for presentation, identical with the model of Figure 2 in Paper I).

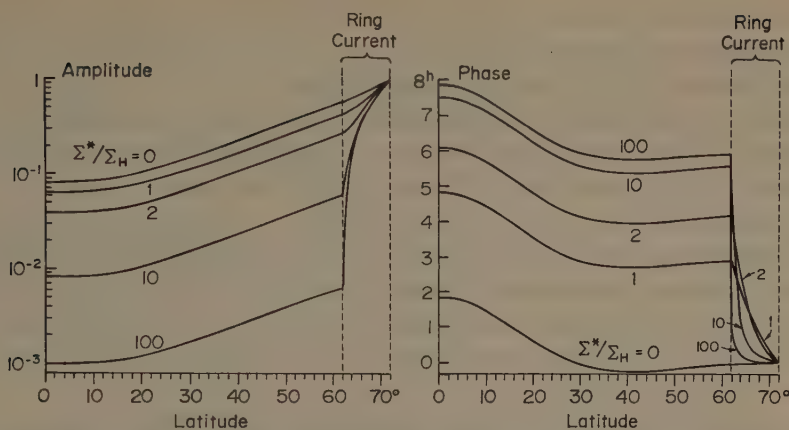


Fig. 2. Calculated amplitude (in units of Φ_0) and phase (LT where potential changes from $-$ to $+$) of the potential for convection models of varying ring current strength.

The calculated potential is a sinusoidal function of LT with latitude-dependent amplitude and phase. Hence, although a presentation like Figure 1 gives a ready visual impression of the convection pattern, a more succinct but still complete presentation is to plot the amplitude and phase as functions of latitude. Such a plot is given in Figure 2 for a sequence of models with fixed $\lambda_{RC} = 62^\circ$ and various values of Σ^*/Σ_H (in the actual magnetosphere, Σ^*/Σ_H is probably within the range 10 to 100). For large values of Σ^*/Σ_H , the convection electric field at latitudes below λ_{RC} is greatly reduced (roughly Σ_H/Σ^* times the field for the case of no ring current) and the rotation

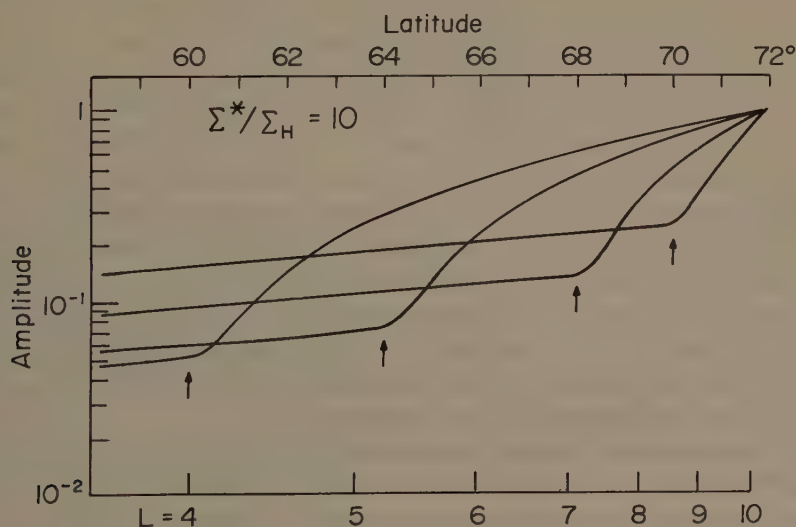


Fig. 3. Calculated amplitude of the potential for models of varying ring current extent. The arrow under each curve marks the inner edge of the ring current.

of its phase approaches 90° . In effect, magnetospheric convection is very nearly terminated with the ring current.

Figure 3 shows a plot of the amplitude of the potential for a sequence of models with fixed $\Sigma^*/\Sigma_H = 10$ and various values of λ_{RC} . Deeper penetration of the ring current is associated with somewhat greater reduction of the electric field at low latitudes, but the reduction is large even if $\lambda_{RC} = 70^\circ$ (corresponding to a ring current with its inner edge at $L = 8.6$).

It is easy to understand in physical terms why convection is almost confined to the ring current region. The tangential electric field E_t at the inner boundary of the ring current deforms the boundary and creates field aligned currents, of order of magnitude $\Sigma^* E_t$. Since $\Sigma^* \gg \Sigma_H$, if the electric field at the boundary were of the same order of magnitude as the field elsewhere, the resulting field aligned currents would be much larger than ionospheric currents and therefore could not close through the ionosphere. Hence the electric field must be reduced to values of the order of Σ_H/Σ^* at the inner edge of the ring current; but it is thereby reduced at all lower latitudes, since the driving field comes from high latitudes.

4. Self-Consistent Ring Current Formed by Convection

So far I have treated the spatial extent of the ring current as an adjustable parameter. In a self-consistent model the proton distribution ought to result from proton motion in the electric and magnetic fields of the model. It is necessary now to make some assumption about the transport processes that form the ring current. I shall assume, following Kavanagh *et al.* (1968), that the ring current protons are simply convected inward from the tail of the magnetosphere and that the inner edge of the ring current is an 'Alfvén layer', i.e., it is the boundary of the forbidden zone into which protons from the tail cannot penetrate because of the opposing effect of their gradient curvature drift. For simplicity, the protons are treated here as having a monoenergetic energy spectrum (but it will be apparent that the results are not sensitive to the shape of the assumed spectrum) and the drift velocity is averaged over a flux tube assuming an isotropic pitch angle distribution. The proton kinetic energy then varies as $L^{-8/3}$, and its value per unit charge at $L = 10$ is taken as the energy parameter of the model.

The problem of obtaining a self-consistent model for a given value of Σ^*/Σ_H can be formulated as follows: given λ_{RC} , the electric field is determined; is it then possible to find a value of K/Φ_0 , the ratio of proton kinetic energy per charge at $L = 10$ to the polar cap potential, such that the boundary of the forbidden zone for protons occurs at latitude λ_{RC} ? (The forbidden zone will be approximately circular under the same approximations as the inner edge of the ring current.)

The boundary of the forbidden zone passes through the stagnation point in the proton flow, where $\mathbf{V}_B + \mathbf{V}_d = 0$. At that point the E-W component of the electric field equals zero and the N-S component equals $V_d B_i / c$. Figure 4a is a plot of the N-S component of \mathbf{E} , as a function of latitude, at the particular (latitude dependent) LT at which the E-W component vanishes, for a sequence of models with various λ_{RC} and

with $\Sigma^*/\Sigma_H = 10$ (plus the model with $\Sigma^* = 0$ for comparison). Figure 4b is a similar plot for models with $\Sigma^*/\Sigma_H = 100$. Also shown is the curve $V_d B_i/c$, which scales with the value of K/Φ_0 . The procedure for finding the self-consistent models is now clear: for a given value of λ_{RC} , vary K/Φ_0 until the $V_d B_i/c$ curve and the E_{NS} curve intersect at (or very near) the latitude λ_{RC} .

From inspection of Figure 4 it is apparent that, because of the sharp 'knee' in E_{NS} particularly for very large Σ^*/Σ_H , the desired intersection can be obtained, for any value of λ_{RC} , with a whole range of values of K/Φ_0 . The largest value of K/Φ_0 for which self-consistent models can be obtained with large Σ^*/Σ_H is shown as a function of λ_{RC}

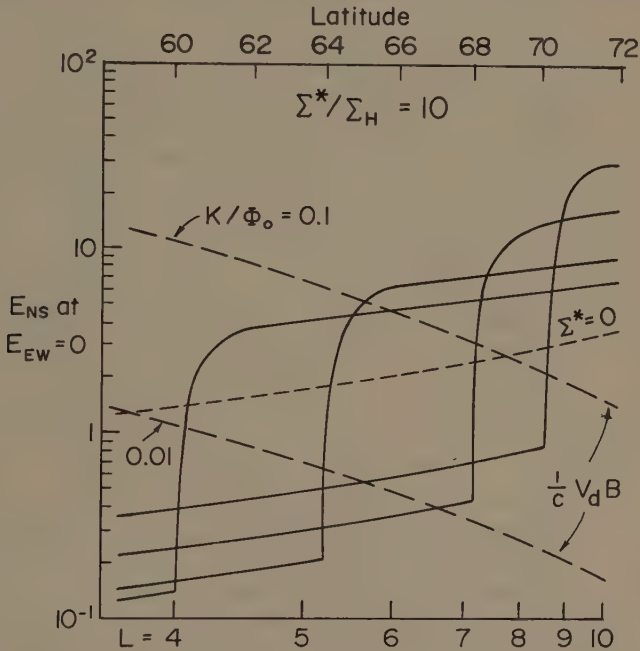


Fig. 4a.

in Figure 5. Thus all the models discussed in Section 3 are self-consistent provided the proton energy is below a certain limit; conversely, given a proton energy, there is a minimum value of λ_{RC} such that all models with larger λ_{RC} are self-consistent.

A simple physical reason for this result can be given. As discussed in Section 3, the effect of the ring current is to reduce the electric field to very low values for $\lambda < \lambda_{RC}$, but to enhance the N-S component of the field throughout the ring current region. Therefore, at all latitudes between λ_{RC} and the polar cap, the E-W component of the convective flow is large and able to overcome the gradient curvature drift (unless the proton energy is too high); but as soon as one crosses λ_{RC} , the convective flow at once becomes very small and the gradient curvature drift becomes dominant. Hence the boundary of the forbidden zone is always near λ_{RC} (wherever λ_{RC} is), except for protons of very high energies.

If the proton drift velocity V_d is replaced by the corotation velocity, the same calculation yields the forbidden zone for very low energy plasma, which conventionally has been identified with the plasmasphere (e.g., Nishida, 1966; Brice, 1967). Hence in these models the plasmopause is nearly circular and coincident with the inner edge of the ring current.

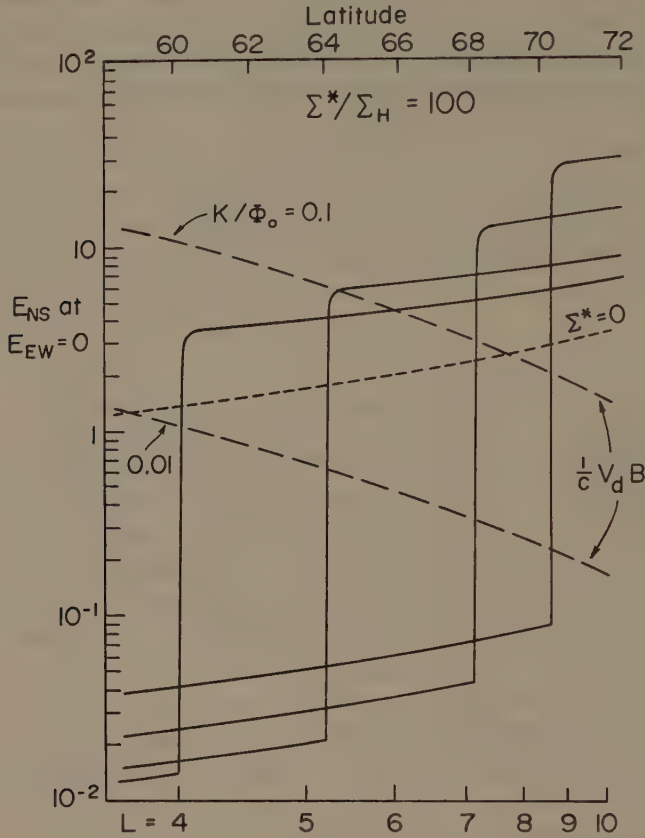


Fig. 4b.

Fig. 4. (a) N-S component of electric field and $V_d B_l / c$ for models of varying position of the inner edge of the ring current (at the sharp break near the bottom of each curve) and $\Sigma^*/\Sigma_H = 10$. See text for description. (b) Same as (a), for $\Sigma^*/\Sigma_H = 100$.

5. Discussion

The quantitative treatment of steady state magnetospheric convection with a ring current has revealed several features of the models that might not have been apparent from a purely qualitative description:

(a) The particle content of the observed ring current is so high that the ring current is the dominant factor in determining the convection pattern, rather than a small correction as sometimes supposed.

(b) The effect of the ring current is to virtually exclude convection from the low latitude region bounded by it, creating a nearly circular convection-free zone similar to that originally proposed by Axford and Hines (1961).

(c) The position of the inner edge of the ring current does not depend on the strength of the driving convection field, but is an arbitrary parameter (within limits). Hence there is no basis in the models for the common view that enhanced convection is associated with deeper penetration of the ring current.

Inclusion of nonadiabatic effects, such as rapid loss of ring currents protons inside the plasmasphere as suggested by Cornwall *et al.* (1970), is not likely to modify these conclusions greatly. First, if the idea of Cornwall *et al.* is pushed to its limit and the

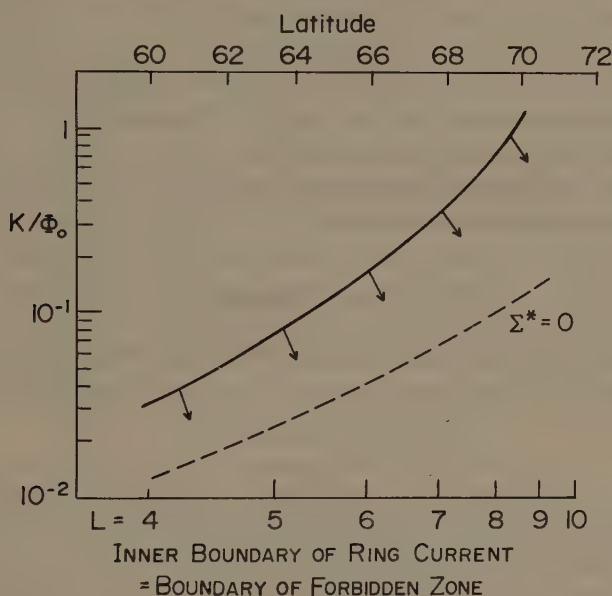


Fig. 5. Upper limit on ratio of proton energy/charge to polar cap potential required to place the forbidden zone boundary at the inner edge of the ring current, for large Σ^*/Σ_H (solid curve). Also shown is that ratio as a function of forbidden zone boundary for the case of $\Sigma^* = 0$ (dashed curve).

proton pressure assumed to have its adiabatic value outside the plasmasphere and zero inside, then the proton pressure follows contours of constant electric potential instead of constant total energy, and it can be shown that Equation (5) is still valid but Σ^* is now negative (and has a slightly different value); but, since $|\Sigma^*| \gg \Sigma_H$, changing the sign of Σ^* simply changes all solutions to their mirror images. Second, a LT dependent nonadiabatic source or loss will create its own convection system, as described by Swift (1967), and may lead to secondary flows at low latitudes, but it will not prevent the ring current boundary from terminating an externally driven convection.

In fact, however, there is considerable evidence that, at least for time varying phenomena, magnetospheric convection does penetrate to low latitudes; for example, the

observation of DP2 variations at the equator (Nishida, 1968), and the dynamical behavior of the plasmasphere (Chappell, 1972). Hence the magnetospheric convection not only cannot be treated as steady (which has always been obvious), but neither can it be treated (as has often been done) as quasi-steady, i.e. allowing the driving field to vary but assuming the convection at any time to be approximately the steady configuration appropriate to the present value of the driving field. The time constants of magnetospheric processes must play an important role.

When the driving field changes with time, three time constants must be considered: the times required to (a) establish the new electric field throughout the ionosphere (τ_1), (b) propagate the electric field along the magnetic flux tubes (τ_2), and (c) bring the ring current into equilibrium with the new driving field (τ_3). τ_1 is the induction time constant of the ionosphere and can be shown to be of the order of seconds; τ_2 is essentially the travel time of an Alfvén wave along a field line (minutes); τ_3 can be shown to be of the order of Σ_H/Σ^* times the proton gradient curvature drift period (hours). The models presented here are valid for variations with time scale $t \gg \tau_3$. If $t \lesssim \tau_3$, convection may penetrate to low latitudes.

Construction of quantitative time-dependent models is the next major challenge to the theory of magnetospheric convection.

Acknowledgments

I am grateful to A. Nishida for a discussion of DP2 in relation to the models. This work was supported by the National Aeronautics and Space Administration under grant NGL 22-009-015.

References

- Axford, W. I.: 1969, *Rev. Geophys.* **7**, 421.
 Axford, W. I. and Hines, C. O.: 1961, *Can. J. Phys.* **39**, 1433.
 Brice, N. M.: 1967, *J. Geophys. Res.* **72**, 5193.
 Chappell, C. R.: 1972, this volume, p. 280.
 Cornwall, J. M., Coroniti, F. V., and Thorne, R. M.: 1970, *J. Geophys. Res.* **75**, 4699.
 Fejer, J. A.: 1964, *J. Geophys. Res.* **69**, 123.
 Frank, L. A.: 1967, *J. Geophys. Res.* **72**, 3753.
 Frank, L. A.: 1971, *J. Geophys. Res.* **76**, 2265.
 Kavanagh, L. D., Freeman, J. W., and Chen, A. J.: 1968, *J. Geophys. Res.* **73**, 5511.
 Nishida, A.: 1966, *J. Geophys. Res.* **71**, 5669.
 Nishida, A.: 1968, *J. Geophys. Res.* **73**, 5549.
 Swift, D. W.: 1967, *Planetary Space Sci.* **15**, 835.
 Vasyliunas, V. M.: 1970, in B. M. McCormac (ed.), *Particles and Fields in the Magnetosphere*, D. Reidel Publishing Company, Dordrecht-Holland, p. 60.
 Vasyliunas, V. M.: 1972, in Dyer (General ed.), *Solar Terrestrial Physics/1970, Part III*, D. Reidel Publishing Company, Dordrecht-Holland, p. 192.
 Wolf, R. A.: 1970, *J. Geophys. Res.* **75**, 4677.

MAGNETIC AND ELECTRIC WAVES IN SPACE

CHRISTOPHER T. RUSSELL

*Institute of Geophysics and Planetary Physics,
University of California, Los Angeles, Calif., U.S.A.*

Abstract. Waves play a fundamental role in many processes occurring in the solar wind and in the magnetosphere. These waves have been observed by a variety of experiments on many different spacecraft and analyzed with an increasing number of different techniques. In this review, we examine a number of the recent observations of waves in space, discussing the role of waves in the various regions and their characteristics, and illustrating some of their techniques used in their analysis.

1. Introduction

In this review, we shall attempt first, to demonstrate the importance of waves in the physical processes occurring in the interplanetary medium and in the magnetosphere; second, to illustrate the variety of wave phenomena observed and their characteristics; and third, to present examples of the various techniques that are used to analyze waves. Consequently, we will be discussing a wide range of varied and seemingly unrelated phenomena. Furthermore, each topic can only be treated very briefly. We shall attempt to provide some thread of coherence by following an element of the solar plasma as it makes its way from the solar surface into the magnetosphere.

2. The Photosphere and Corona

The solar wind begins to expand supersonically in the solar corona. The energy for this expansion against the solar gravitational field is derived from the thermal energy of the corona. It is generally believed that waves generated in the photosphere and damped in the corona provide the energy source for the corona. A mechanism for the generation of such waves has been proposed by Hollweg (1971). In this mechanism, the super granular motions of the highly conducting photosphere move the feet of the field lines back and forth creating Alfvén waves. Although super granular motions are readily observed, at the present time we have no means to check on the existence of such waves in the corona. However, large amplitude Alfvén waves have been identified in the solar wind.

3. The Distant Solar Wind

Figure 1 shows an example of Alfvén waves detected by the magnetometer and solar wind probe on Mariner 5 (Belcher and Davis, 1971). The upper three sets of double traces are the three vector components of the solar wind velocity and the magnetic field. The scales of the field and the velocity have been chosen so that the relative variation of the traces would be equal for an Alfvén wave. We see that the traces are virtually indistinguishable. The bottom two traces, giving the field strength and plasma

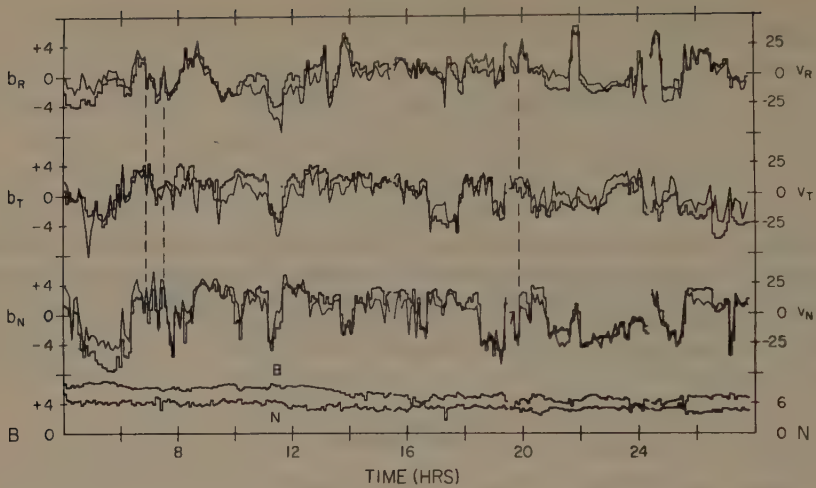


Fig. 1. 24 hr of magnetic field and plasma data obtained by Mariner 5 which demonstrate the existence of nearly pure Alfvén waves. The data have been averaged over 5.04 min. The velocity data have been sketched as histograms while the magnetic field data have been connected with straight lines. The components R , T , and N are radially outwards, parallel to the solar equator in the direction of planetary motion and normal to the RT plane northwards, respectively (Belcher and Davis, 1971).

density, show very little variation as expected for an Alfvén wave. This display illustrates the first technique for analyzing waves, that is, the cross correlation of parameters affected by the wave.

These waves, of course, are being convected outwards by the solar wind. However, the phase of the correlation indicates that they may be the remnants of Alfvén waves created by the super granular motions. The existence of these waves in the supersonic solar wind can cause additional heating and further acceleration of the solar wind.

Besides magnetic fluctuations with periods less than 1 s only primitive measurements of the VLF electric field at a limited number of frequencies have been obtained (Sarf *et al.*, 1971b; Siscoe *et al.*, 1971). These measurements reveal some VLF waves at discontinuities and shocks. This paucity of measurements is indeed unfortunate because such wave studies provide information on the coupling processes between the solar wind constituents (Sarf, 1970; Forslund, 1971; Parker, 1971).

4. Upstream Waves

As the solar wind approaches the earth's bow shock a new set of wave phenomena appears in the solar wind. These are all generally thought to be associated with particles backstreaming along field lines from the shock front. Figure 2 shows a times series plot of the waves in this region. We see there is an irregular low frequency background of wave activity plus several discrete wave packets at higher frequencies (Russell *et al.*, 1971a). In addition to generation by reflected particles, it has been proposed that these

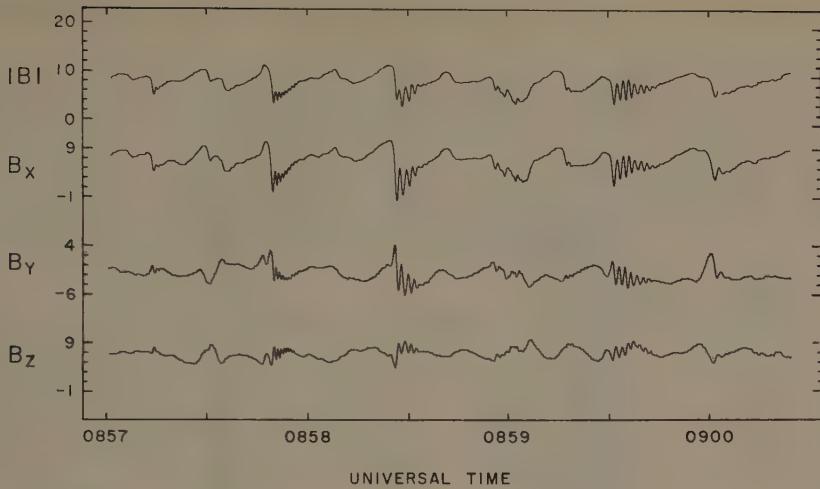


Fig. 2. Discrete wave packets occurring in association with irregular low frequency waves on March 10, 1968, while the satellite was at $19.1 R_E$ and at a sun-earth-satellite angle of 67.5° . The X , Y , and Z components are in the spacecraft coordinate system (Russell *et al.*, 1971a).

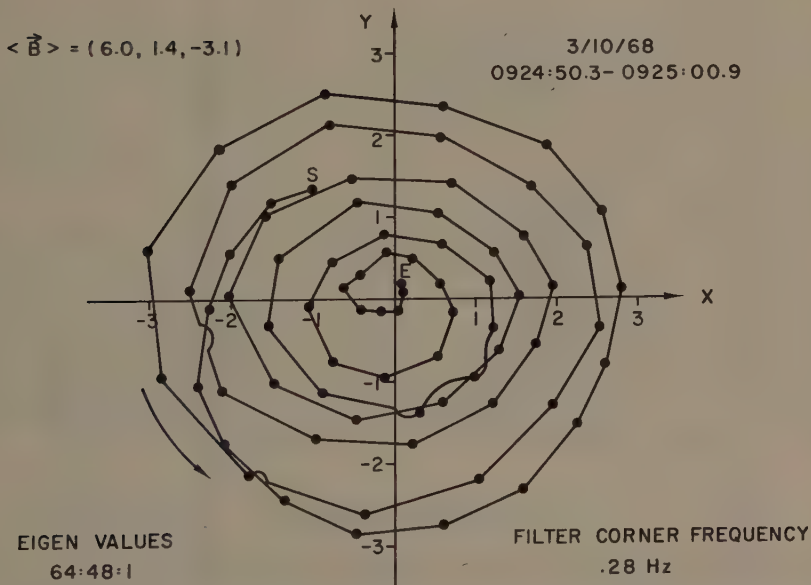


Fig. 3. A hodogram of the oscillating field due to a discrete wave packet in the principal axis system. The low frequency fluctuations and background magnetic field have been removed with a high pass filter. The average magnetic field in this system averaged over the duration of the wave packet and the ratio of the eigen values obtained in the analysis of the variance matrix are given in the figure. The satellite was at a radial distance of $19.3 R_E$ and at a sun-earth-satellite angle of 67.1° (Russell *et al.*, 1971a).

waves packets are created by the breakup of the low frequency waves (Hasegawa, 1972) and by the plasma echo mechanism (Wu, 1972).

This brings us to another technique of wave analysis, the principal axis technique. Since the perturbations of the magnetic field caused by a plane wave lie in the wave-front, we can solve an eigenvector problem on the variance matrix of the perturbation to obtain the direction of minimum perturbation. This direction is along the wave normal, e.g., the direction of the phase velocity. This technique will only achieve unambiguous results when it is possible to isolate the contribution from one wave. This is obviously possible here.

Figure 3 shows a hodogram of a discrete wave packet in the principal axis system. From this diagram we can see the buildup and decay of the wave, that it is almost circularly polarized, and that it is rotating in a left-handed sense about the magnetic field.

Very low frequency electric oscillations are also seen in this region (Fredricks *et al.*, 1971a, b; Scarf *et al.*, 1971b). These are observed in conjunction with backstreaming electrons.

5. The Bow Shock

The earth's bow shock contains perhaps the most complicated interplay of wave-particle interactions found in nature. Two common features of the bow shock are a precursor wave upstream at high frequencies which decays with distance from the shocks and a regular low frequency large amplitude wave train downstream. Features such as these appear quite readily using dynamic spectral analysis. Figure 4 shows such a display for a series of multiple shock crossings (Simmons and Coleman, 1969). The upper trace is the filtered wave form and the lower panel contains contours of constant power density as a function of time and frequency. This shows the high frequency precursor wave at each shock crossing merging with the low frequency wave train in the magnetosheath.

Figure 5 shows relative locations of wave and particle events at a shock crossing. First, the protons decelerate (Neugebauer, 1970). (Corresponding electron acceleration has been observed in this region at other shock crossings (Neugebauer *et al.*, 1971).) Then VLF electrostatic noise appears (Fredricks *et al.*, 1970), possibly as a result of an instability of the accelerated electrons. At the strong field gradient ELF magnetic waves begin to appear, also probably as a result of an instability of the electrons. Finally the protons are deflected and thermalized (Ossakow *et al.*, 1970).

6. The Magnetosheath

The amplitude of waves in the magnetosheath is greater than in any other region of space near the earth. However, it is also the most difficult region in which to study waves, both experimentally due to the frequent changes in field direction and because the medium is moving, and theoretically, because of the high temperatures and large wave amplitudes. We expect that the magnetosheath plasma is at marginal stability for many emission processes because of its passage through the shock.

UCLA FLUXGATE MAGNETOMETER, OGO-5
MARCH 7, 1968
BOW SHOCK CROSSINGS

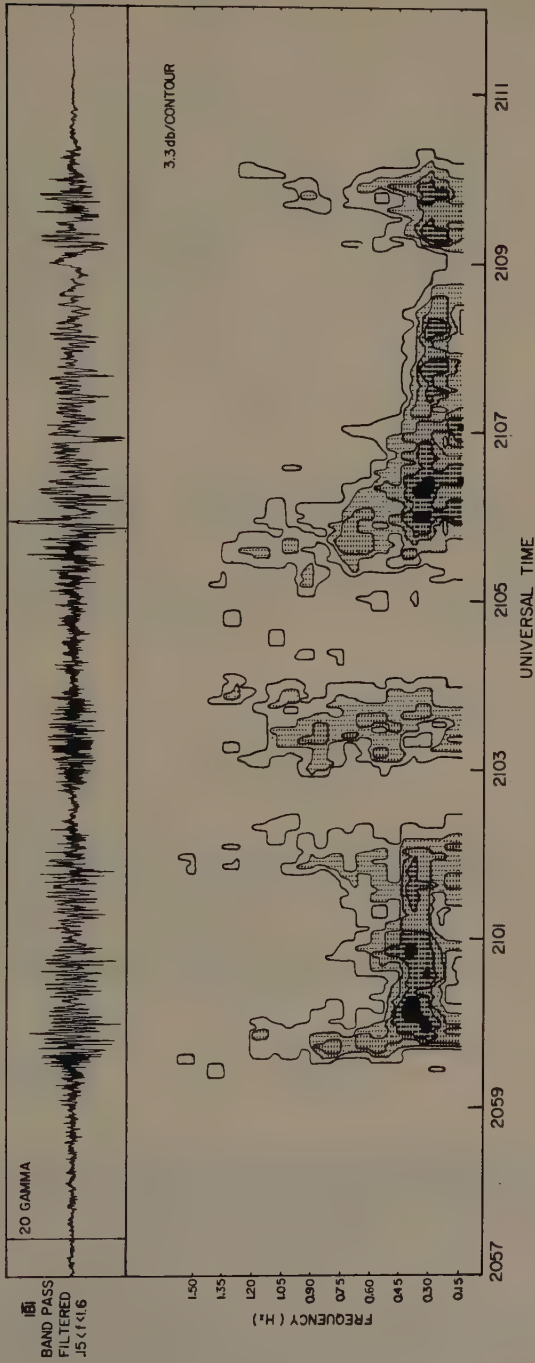


Fig. 4. Digital sonogram of one component of the magnetic field across five bow shock crossings observed by OGO 5. The top trace shows the wave form of this component bandpassed in the frequency range from 0.15 to 1.6 Hz (Simmons and Coleman, 1969).

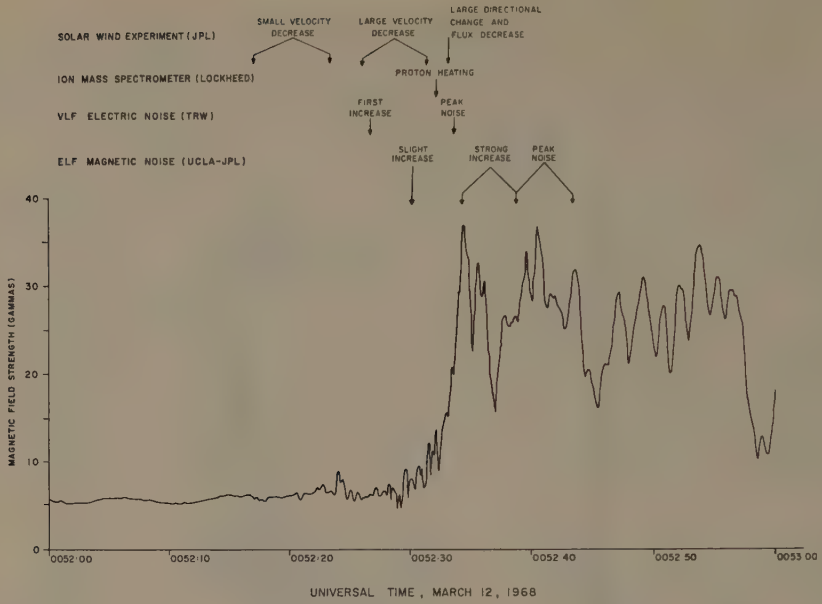


Fig. 5. The location of wave and particle events relative to the steep gradient in the magnetic field at a bow shock crossing encountered by OGO 5 (Russell *et al.*, 1969).

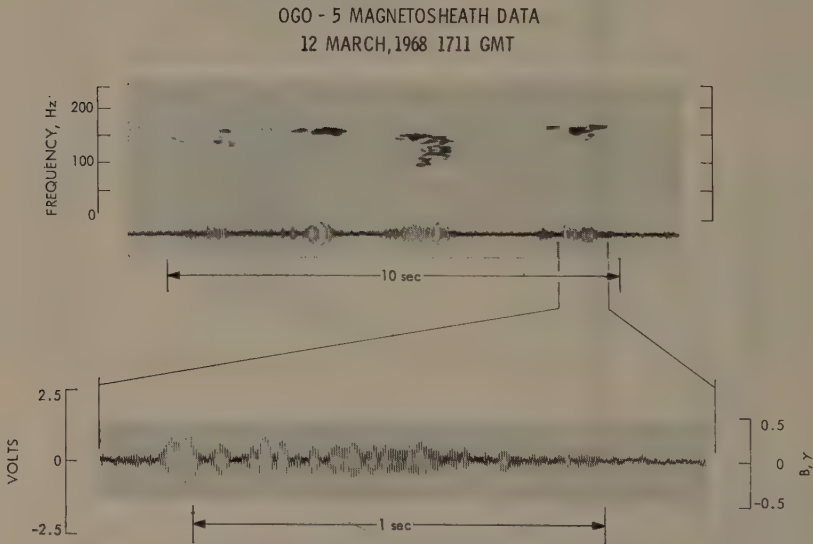


Fig. 6. An analogue sonogram of one component of the derivative of the magnetic field observed by the OGO 5 search coil magnetometer in the magnetosheath. An expansion of the wave form of one of the emissions is shown in the bottom trace. These emissions have been called 'lion roars' (Smith *et al.*, 1969).

Waves in the magnetosheath at frequencies lower than those shown in Figure 4 have been studied by Siscoe *et al.*, (1967), Mariani *et al.* (1970), Fairfield and Ness (1970a), Kaufmann *et al.* (1970), and McLeod (1971). ELF waves have been studied by Smith *et al.* (1967, 1969). One of the interesting phenomena at the ELF frequencies has been called 'lion roars'. A frequency time display of several 'lion roars' is shown in Figure 6. This display has been created by analogue techniques rather than the digital computer method used in constructing Figure 4. Here the darkness is proportional to the intensity. This analogue data may be digitized in the laboratory and the principal axis coordinate system found as was done for a discrete wave packet in Figure 3. When this is done, the 'lion roars' are found to be right-handed circularly polarized with respect to the field. They almost certainly are in cyclotron resonance with magnetosheath electrons (Russell *et al.*, 1969).

7. Boundary Motions

As seen in Figure 4, the position of the shock front exhibits periodic motion. Other magnetospheric boundaries also exhibit periodic motion: the magnetopause (Holzer *et al.*, 1966; Heppner *et al.*, 1967; Anderson *et al.*, 1968; Kaufmann and Konradi,

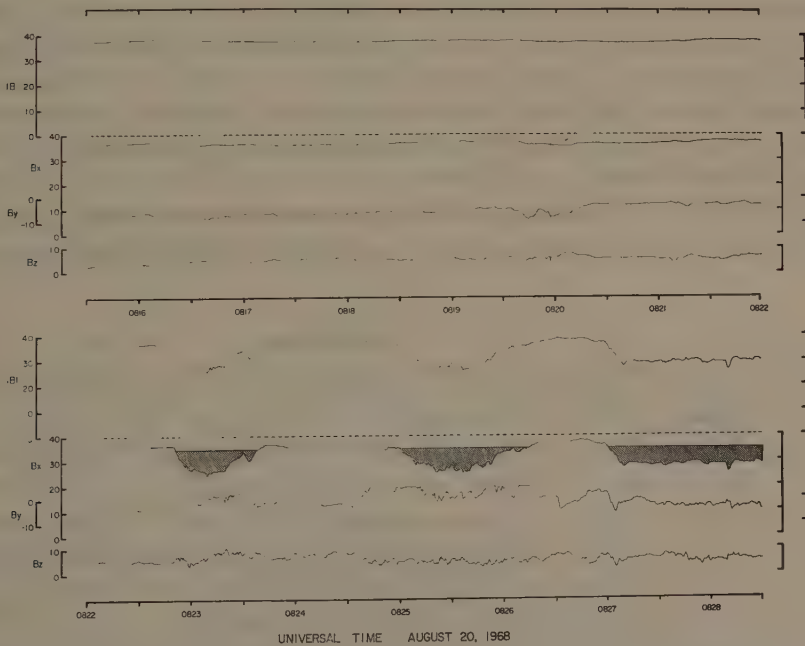


Fig. 7. The three solar magnetosphere vector components and total magnetic field observed by the UCLA OGO 5 fluxgate magnetometer in the tail at a multiple crossing of the boundary of the plasma sheet. OGO 5 was $12.5 R_E$ behind the earth within $2 R_E$ of the midnight meridian and $2 R_E$ above the expected neutral sheet position. The depressions in the X components of the field during the plasma sheet encounters have been shaded to emphasize the periodic nature of the encounters (Russell *et al.*, 1971b).

1969; Aubry *et al.*, 1971) the neutral sheet, (Mihalov *et al.*, 1970), and the plasma sheet (Russell *et al.*, 1971b). The amplitudes of the waves in the magnetic field in the regions adjacent to the boundary which are associated with these motions may be quite small. However, whenever the displacement of the boundaries is much greater than the thickness of the boundary and the satellite is near the boundary these small amplitude waves can have dramatic effects.

Figure 7 shows a multiple crossing of the plasma sheet boundary observed by the UCLA magnetometer on OGO 5. Here the boundary is oscillating with a period of almost 2 min. This figure also shows that the magnetic field in the plasma sheet is very noisy compared to the field in the lobes. Since the major fraction of the solar wind energy, transferred to the magnetosphere, is for a time stored in the tail, it is generally believed that some solar wind particles can gain access to the magnetosphere via the tail. Thus it is important to examine this region for waves that can cause scattering of particles and affect the rate of supply or loss of particles from the plasma sheet.

8. The Tail

Table I lists the various contributors to the study of both electric and magnetic noise in the tail in the different frequency ranges. For periods of hours the magnetic variations are due primarily to expansions and contractions of the plasma sheet. For periods of minutes the presence of waves has been deduced from the boundary motions described above. The electric field measurements of Mozer (1971) are actually measurements made at balloon altitudes, and those of Carpenter (1971) are of whistler duct motion, but they do reflect to some extent the long period changes in the cross tail electric field.

The ELF magnetic measurements of Brody (1970) and the VLF electric measurements of Scarf (1971a) reveal little or no noise in the tail. The only measurements at

TABLE I
Observations of electric and magnetic noise in the earth's magnetotail

Frequency Range	Observations	
	Magnetic	Electric
15 min to 10 hr	Hruska and Hruskova (1969, 1970) Behannon (1970) Fairfield and Ness (1970b) Russell <i>et al.</i> (1971c) Aubry and McPherron (1971) Meng <i>et al.</i> (1971)	Mozer (1971) Carpenter (1971)
30 s to 15 min	Mihalov <i>et al.</i> (1970) Russell <i>et al.</i> (1971b)	none
0.03–3 Hz	Russell <i>et al.</i> (1971b)	none
3–800 Hz	Brody (1970)	none
0.8–70 kHz	none	Scarf (1971)

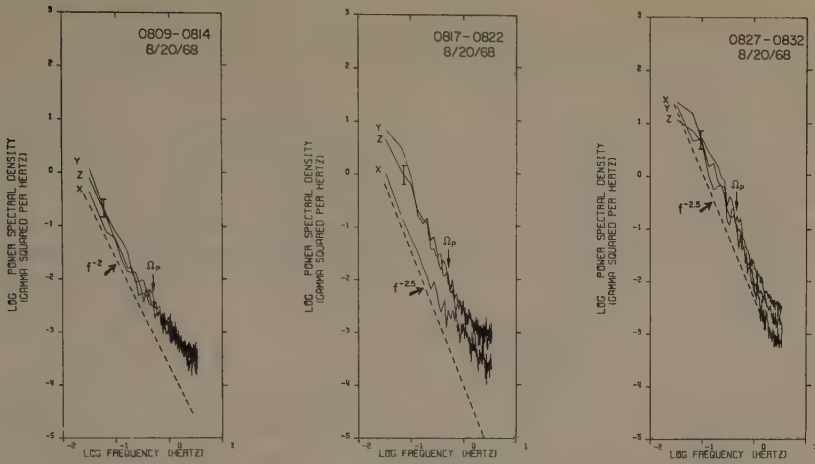


Fig. 8. Power spectra of the three solar magnetospheric components of the magnetic field at and near the plasma sheet crossings shown in Figure 7 (Russell *et al.*, 1971b).

ULF frequencies have been made with magnetometers. The amplitude of waves with periods < 15 s is enhanced only during plasma sheet expansions (Russell *et al.*, 1971b). If the plasma sheet is stationary or thinning little noise is observed even at the neutral sheet.

Power spectra computed from data obtained 10 min before and just after the entry into the plasma sheet shown in Figure 7 are displayed in Figure 8. The spectra are featureless with roughly an inverse square frequency dependence. Since the flow velocities in the plasma sheet are expected to be small, these spectra should not be seriously affected by doppler shifting.

9. The Polar Cusp

The other region of particle entry into the magnetosphere is the dayside polar cusp (Frank, 1971; Heikkila and Winningham, 1971; Russell *et al.*, 1971d). OGO 5 measurements show that this region can be very turbulent at ULF, ELF, and VLF frequencies. Figure 9 shows power spectra computed at four separate times in the polar cusp. In this region the transverse power is greater than the power in the fluctuations parallel to the field but their ratio can vary over a wide range. The lower right hand spectra exhibit a cutoff at the proton gyrofrequency. This is a strong indication that these waves are interacting with protons. Examination of the bursts of noise in the cusp where the spectra exhibited this cutoff confirms this (Russell *et al.*, 1970).

10. The Magnetosphere

The magnetosphere proper, the region of closed field lines and trapped particle orbits,

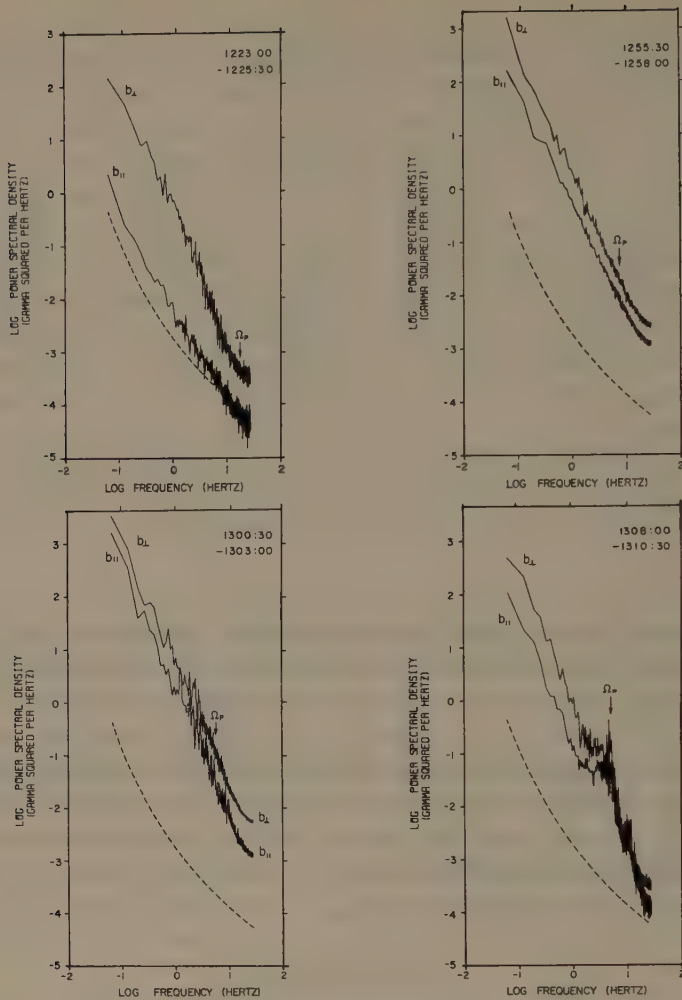


Fig. 9. Power spectra of the compressional (b_{\perp}) and transverse (b_{\parallel}) components of the magnetic field observed by OGO 5 in the polar cusp on November 1, 1968. Ω_p is the local proton gyrofrequency. The dashed line is the spectrum outside the polar cusp in this same region of space. The data were detrended before the power spectra were computed (Russell *et al.*, 1971d).

contains even more wave phenomena than we have described so far. Most of these waves interact with some part of the distribution of Van Allen belt particles causing them to diffuse radially and/or in pitch angles. Not only do the waves, thus, affect the transport of particles in the Van Allen belts and, therefore, determine their spatial distribution, but waves can also transport energy from one region of space to another and from one particle species to another. A mechanism of this type has been used to explain the SAR arcs (Cornwall *et al.*, 1971). Further, waves may be simultaneously resonant with more than one particle species. If the protons were unstable to the

emission of waves while electrons were stable, the waves would be emitted and affect both the protons and electrons. Such a mechanism has been proposed to explain the disappearance of highly relativistic electrons at the peak of the ring current during storms (Thorne and Kennel, 1971).

(For a discussion of wave observations in the magnetosphere, the interested reader is referred to Russell and Holzer (1970) and the more extensive and current reviews of ELF and VLF electromagnetic waves by Russell *et al.* (1972), of ELF and VLF electrostatic waves by Scarf and Fredricks (1972), and of ULF waves by McPherron *et al.* (1972).)

11. Conclusions

There are very few regions of space from the photosphere of the sun to the ionosphere of the earth in which waves do not play an important or even critical role. Many of these waves have been extensively studied but many have not. Notably lacking in the interplanetary medium are ELF and VLF magnetic measurements and electric field measurements at almost all frequencies. Nearer the earth, at the shock, in the magnetosheath and in the tail, the primary lack is low frequency electric field observations. The techniques for examining waves have been improving over the years. Now, not only do we examine time series and create power spectra, but also we create dynamic spectra, perform principal axis computations, and perform cross correlation analyses. Still further refinements are in the offing.

Acknowledgments

The correlative studies of the OGO 5 data discussed in this paper would not have been possible without the cooperative spirit of many of the OGO 5 experimenters whose results have been quoted. I also wish to acknowledge many fruitful discussions of waves with R. L. McPherron and his pioneering work on the digital sonogram technique. The analysis of the data from the UCLA OGO 5 fluxgate magnetometer presented here was supported by NASA contract NAS 5-9098.

References

- Anderson, K. A., Binsack, J. H., and Fairfield, D. H.: 1968, *J. Geophys. Res.* **73**, 2371.
- Aubry, M. P. and McPherron, R. L.: 1971, *J. Geophys. Res.* **76**, 4381.
- Aubry, M. P., Kivelson, M. G., and Russell, C. T.: 1971, *J. Geophys. Res.* **76**, 1673.
- Behannon, K. W.: 1970, *J. Geophys. Res.* **75**, 743.
- Belcher, J. W., and Davis, L., Jr.: 1971, *J. Geophys. Res.* **76**, 3534.
- Brody, K. I.: 1970, Ph.D. Thesis, University of California, Los Angeles.
- Carpenter, D. L.: 1971, (title only), *EOS Trans. Amer. Geophys. Union* **52**, 328.
- Cornwall, J. M., Coroniti, F. V., and Thorne, R. M.: 1971, *J. Geophys. Res.* **76**, 4428.
- Fairfield, D. H. and Ness, N. F.: 1970a, *J. Geophys. Res.* **75**, 6050.
- Fairfield, D. H. and Ness, N. F.: 1970b, *J. Geophys. Res.* **75**, 7032.
- Forslund, D. W.: 1971, *Proc. Solar Wind Conf.* Asilomar, Pacific Grove, Calif., March 22-26, in press.
- Frank, L. A.: 1971, *J. Geophys. Res.* **76**, 5202.

- Fredricks, R. L., Crook, G. M., Kennel, C. F., Green, I. M., Scarf, F. L., Coleman, P. J., Jr., and Russell, C. T.: 1970, *J. Geophys. Res.* **75**, 3751.
- Fredricks, R. W., Scarf, F. L., and Frank, L. A.: 1971a, *J. Geophys. Res.* **76**, 6691.
- Fredricks, R. W., Scarf, F. L., and Green, I. M.: 1971b, *J. Geophys. Res.* **76**, submitted.
- Hasegawa, A.: 1972, *J. Geophys. Res.* **77**, 84.
- Heikkila, W. J. and Winningham, J. D.: 1971, *J. Geophys. Res.* **76**, 883.
- Heppner, J. P., Sugiura, M., Skillman, T. L., Ledley, B. G., and Campbell, J.: 1967, *J. Geophys. Res.* **72**, 5417.
- Hollweg, J.: 1971, in *Proc. Solar Wind. Conf.* Asilomar, Calif., March 22–26, in press.
- Holzer, R. E., McLeod, M. G., and Smith, E. J.: 1966, *J. Geophys. Res.* **71**, 1481.
- Hruska, A. and Hruskova, J.: 1969, *Planetary Space Sci.* **17**, 1497.
- Hruska, A. and Hruskova, J.: 1970, *J. Geophys. Res.* **75**, 2249.
- Kaufmann, R. L. and Konradi, A.: 1969, *J. Geophys. Res.* **74**, 3609.
- Kaufmann, R. L., Horng, J.-T., and Wolfe, A.: 1970, *J. Geophys. Res.* **75**, 4666.
- Mariani, F., Bavassano, B., and Ness, N.F.: 1970, *J. Geophys. Res.* **75**, 6037.
- McLeod, M. G.: 1971, Ph.D. Thesis, Univ. of Calif., Los Angeles.
- McPherron, R. L., Russell, C. T., and Coleman, P. J., Jr.: 1972, *Space Science Rev.*, in press.
- Meng, C.-I., Akasofu, S.-I., Hones, E. W., and Kawasaki, K.: 1971, *J. Geophys. Res.* **76**, 7584.
- Mihalov, J. D., Sonett, C. P., and Colburn, D. S.: 1970, *Cosmic Electrodyn.* **1**, 178.
- Mozer, F. S.: 1971, *J. Geophys. Res.* **76**, 3651.
- Neugebauer, M.: 1970, *J. Geophys. Res.* **75**, 717.
- Neugebauer, M., Russell, C. T., and Olson, J. V.: 1971, *J. Geophys. Res.* **76**, 4366.
- Ossakow, S. L., Sharp, G. W., and Harris, K. K.: 1970, *J. Geophys. Res.* **75**, 6024.
- Parker, E. N.: 1971, in *Proc. Solar Wind. Conf.*, Asilomar, Pacific Grove, Calif., March 22–26, in press.
- Russell, C. T. and Holzer, R. E.: 1970, in B. M. McCormac (ed), *Particles and Fields in the Magnetosphere*, D. Reidel Publishing Company, Dordrecht, Holland, p. 195.
- Russell, C. T., Olson, J. V., Coleman, P. J., Jr., and Holzer, R. E.: 1969, *Microscale Interactions at the Earth's Bow Shock*, Presented at the IAGA General Assembly, Madrid, Spain, Sept. 1969.
- Russell, C. T., McPherron, R. L., and Coleman, P. J., Jr.: 1970, *Instabilities in the outer magnetosphere*, presented at the International Symposium on Solar-Terrestrial Physics, Leningrad, U.S.S.R., May, 1970.
- Russell, C. T., Childers, D. D., and Coleman, P. J., Jr.: 1971a, *J. Geophys. Res.* **76**, 845.
- Russell, C. T., McPherron, R. L., and Coleman, P. J., Jr.: 1971b, (abstract) *EOS Trans. Amer. Geophys. Union*, **52**, 332.
- Russell, C. T., McPherron, R. L., and Coleman, P. J., Jr.: 1971c, *J. Geophys. Res.* **76**, 1823.
- Russell, C. T., Chappell, C. R., Montgomery, M. D., Neugebauer, M., and Scarf, F. L.: 1971d, *J. Geophys. Res.* **76**, 6743.
- Russell, C. T., McPherron, R. L., and Coleman, P. J., Jr.: 1972, *Space Science Rev.*, **12**, 810.
- Scarf, F. L.: 1970, *Space Sci. Rev.* **11**, 234.
- Scarf, F. L.: 1971, private communication.
- Scarf, F. L. and Fredricks, R. W.: 1972, this volume, p. 329.
- Scarf, F. L., Fredricks, R. W. and Green, I. M.: 1971a, in *Proc. Solar Wind Conf.*, Asilomar, Pacific Grove, Calif., in press.
- Scarf, F. L., Fredricks, R. W., Frank, L. A., and Neugebauer, M.: 1971b, *J. Geophys. Res.* **76**, 5162.
- Simmons, L. L. and Coleman, P. J., Jr.: 1969, 'The Bow Shock and Related Wave Phenomena Observed with the UCLA Magnetometer on OGO 5', presented at the 50th annual American Geophysical Union meeting, Washington, D.C.
- Siscoe, G. L., Davis, L., Jr., Coleman, P. J., Jr., Smith, E. J., and Jones, D. E.: 1967, *J. Geophys. Res.* **72**, 5524.
- Siscoe, G. L., Scarf, F. L., Green, I. M., Binsack, J. H., and Bridge, H. S.: 1971, *J. Geophys. Res.* **76**, 828.
- Smith, E. J., Holzer, R. E., McLeod, M. G., and Russell, C. T.: 1967, *J. Geophys. Res.* **72**, 4803.
- Smith, E. J., Holzer, R. E., and Russell, C. T.: 1969, *J. Geophys. Res.* **74**, 3027.
- Thorne, R. M. and Kennel, C. F.: 1971, *J. Geophys. Res.* **76**, 4446.
- Wu, C. S.: 1972, *J. Geophys. Res.* **77**, 575.

PART II

MAGNETOSPHERIC PARTICLES

MAGNETOSPHERIC PARTICLE POPULATIONS

JAMES I. VETTE

NASA – National Space Science Data Center, Greenbelt, Md., U.S.A.

1. Introduction

The present picture of the magnetosphere as seen from charged particle distributions will be presented. Since it is not practical to give a complete review, the results of measurements presented in the past 2 yr which give new information will be emphasized. The various magnetospheric regions are shown schematically in the noon-midnight meridian plane in Figure 1, and some features in the equatorial plane are shown in Figure 2. Each of these regions will be treated in a detailed fashion by other papers in this volume, and many of the dynamical effects will be discussed there. The primary purpose here will be to give a broad overview showing the relationships between these regions and indicating the particle populations.

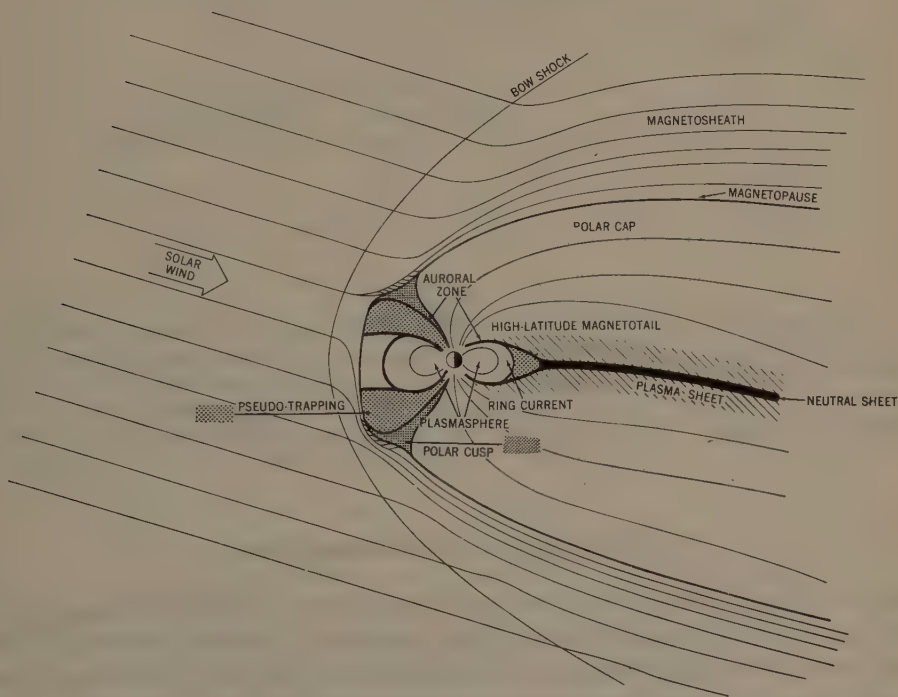


Fig. 1. Regions of the magnetosphere shown in the noon-midnight meridian plane. The thin lines in the solar wind and magnetosheath are a schematic representation of plasma flow lines. The concentrations at the polar cusp are meant to show leakage of plasma from the magnetosheath to the magnetosphere. The thin lines within the magnetosphere represent magnetic field lines.

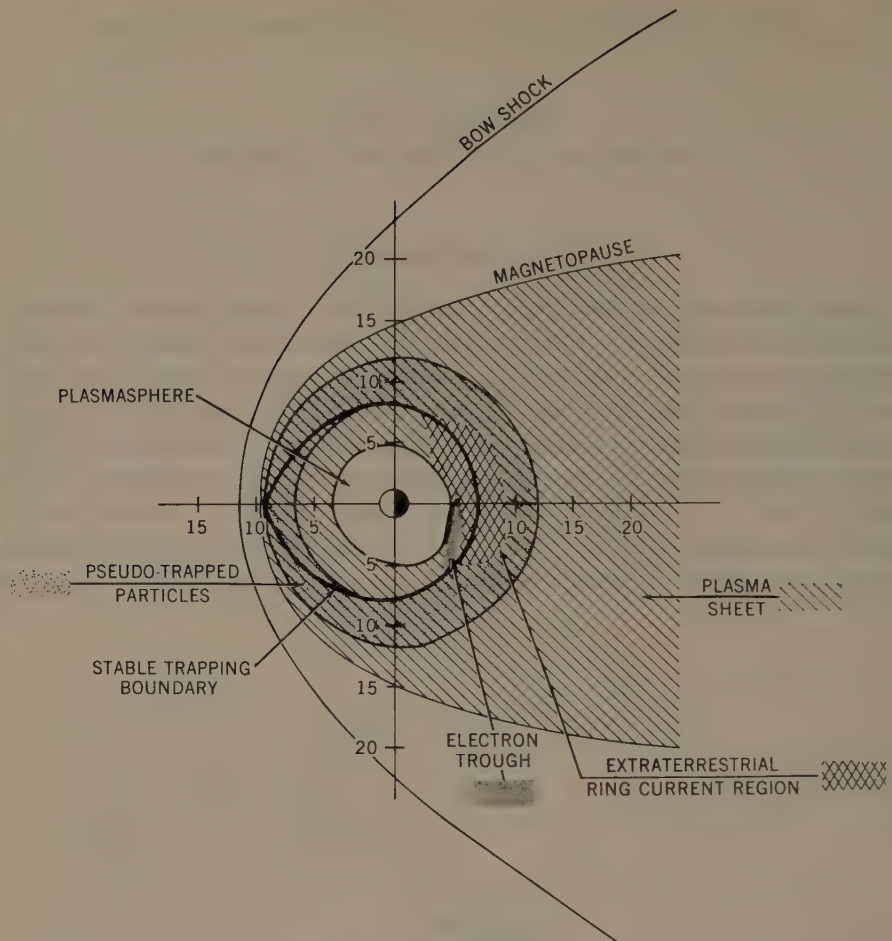


Fig. 2. Regions of the magnetosphere shown in the equatorial plane. The stable trapping boundary is shown for energetic electrons. The pseudo-trapping region represents the projection of high latitude boundaries into the equatorial plane. There are in fact other pseudo-trapped particles that pass through the equatorial plane both inside and outside of the boundaries shown. The extra-terrestrial ring current and electron trough geometries are taken from Frank (1971b). The region of the symmetric ring current is not shown.

2. Distant Regions of the Magnetosphere

Since the early discovery of energetic particles within the magnetosphere, one of the first sources postulated was the solar wind. However, the detailed manner in which particles could flow into the cavity and subsequently be accelerated has been somewhat obscure. Recent ideas and measurements have clarified the picture greatly, and the particles found in the interplanetary medium now seem to constitute the source for many but not all of the regions of the magnetosphere.

As shown in Figure 1, the solar wind flow is diverted around the magnetopause and

fills the magnetosheath region. Hundhausen (1970) has summarized the plasma parameters under quiet conditions for both the interplanetary medium and for the magnetosheath near the dawn-dusk meridian. The solar wind, consisting mainly of protons and electrons with an α -particle component of 5 to 20%, has a particle density of $n \sim 5 \text{ cm}^{-3}$, a flow speed of $v \sim 320 \text{ km s}^{-1}$ nearly radial from the sun; the random motion of the electrons and protons can be represented by temperatures $T_e \sim 1.5 \times 10^5 \text{ K}$ and $T_p \sim 5 \times 10^4 \text{ K}$. In the magnetosheath region, part of the directed flow energy is converted into a heating of the plasma, and typical parameters are $n \sim 15 \text{ cm}^{-3}$, $v \sim 250 \text{ km s}^{-1}$, $T_e \sim 5 \times 10^5 \text{ K}$, and $T_p \sim 10^6 \text{ K}$. Consequently, the magnetosheath electron and proton spectra peak around 150 and 300 eV, respectively.

In addition to the normal solar wind plasma, Frank (1970a) has detected, on occasion, interplanetary protons in the $5 \leq E \leq 50 \text{ KeV}$ region lasting ~ 1 day with peak intensities around $E \sim 20 \text{ keV}$ with $n \sim 10^{-2} \text{ cm}^{-3}$. Frank has noted the similarity of the particles to those of the enhanced ring current during magnetic storms, but Vasyliunas (1971), using Liouville's theorem, has shown that this population cannot contribute to the ring current.

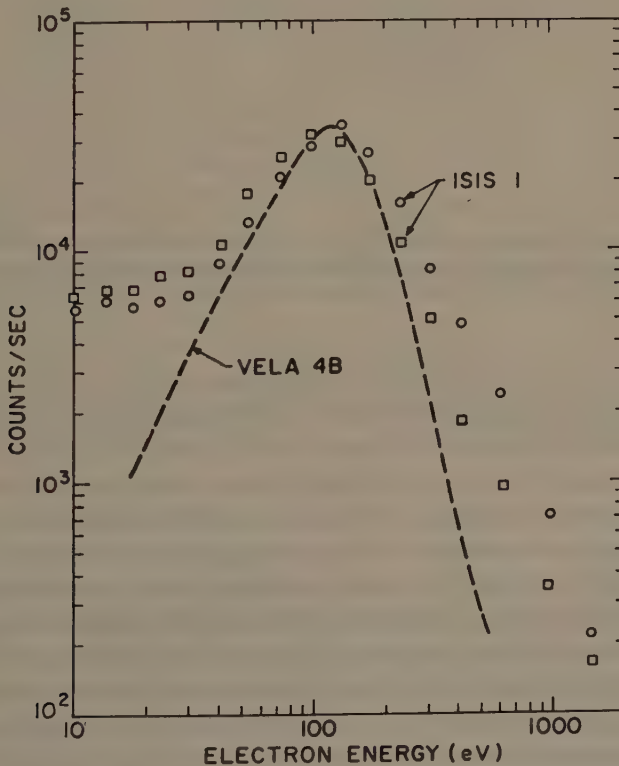


Fig. 3. Comparison of electron spectra in the polar cusp and the magnetosheath. The Vela 4B results were obtained in the magnetosheath and ISIS 1 results in the polar cusp (Heikkila and Winningham, 1971).

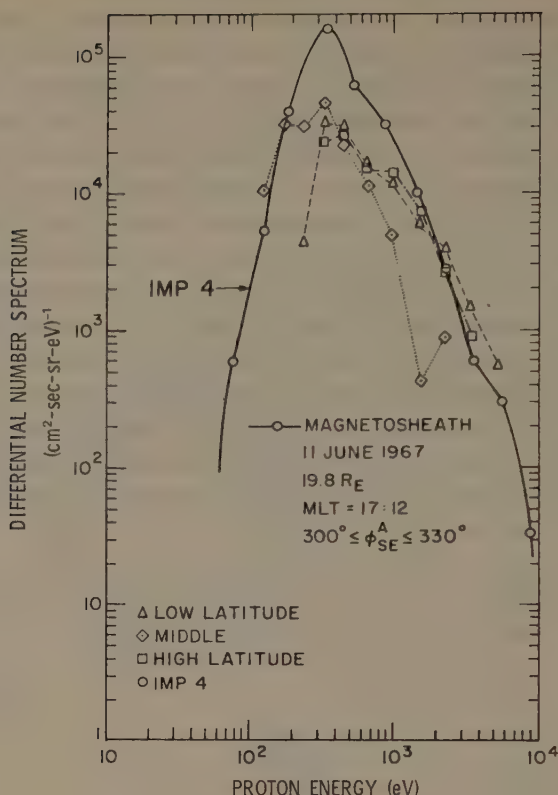


Fig. 4. Comparison of proton spectrum in the polar cusp and the magnetosheath. The IMP 4 results were taken in the magnetosheath while the other results were obtained on ISIS 1 at various positions.

Until recently, it appeared that the magnetopause acted as an effective barrier to any plasma flow from the magnetosheath into the magnetosphere. However, recent measurements by Heikkila and Winningham (1971) and Frank (1971a) have shown that the magnetosheath plasma flows through a region associated with the polar neutral points. This direct flow of plasma, which goes into the dayside auroral oval, is a usual feature of the region and occurs in a band across the magnetosphere rather than in a narrow region of longitude. This region is called the polar cusp in Figure 1, a notation used by Frank (1971a). Comparisons of both electron and proton spectra in the polar cusp and magnetosheath are shown in Figure 3 and 4. As is true of most magnetospheric regions, the spatial location is variable depending on interplanetary conditions. Recently, Russell *et al.* (1971) have reported observing the polar cusp on OGO 5 at magnetic latitudes as low as 43° .

Both Frank (1971a) and Hill and Dessler (1971) have given magnetospheric models in which the particles from the polar cusp flow into the plasma sheet region of the magnetotail. Two characteristic spectra of protons observed by Frank (1970b) in the

magnetotail are shown in Figure 5. These are similar to those obtained by Bame (1968) with the Vela satellites at $18 R_E$. The lower energy spectrum is more characteristic of the high latitude magnetotail while the other is typical of the plasma sheet. The similarity between the magnetosheath and the high latitude magnetotail spectra has been noted by Frank (1971a); however, magnetotail proton densities are lower by a factor of ~ 10 to 100 .

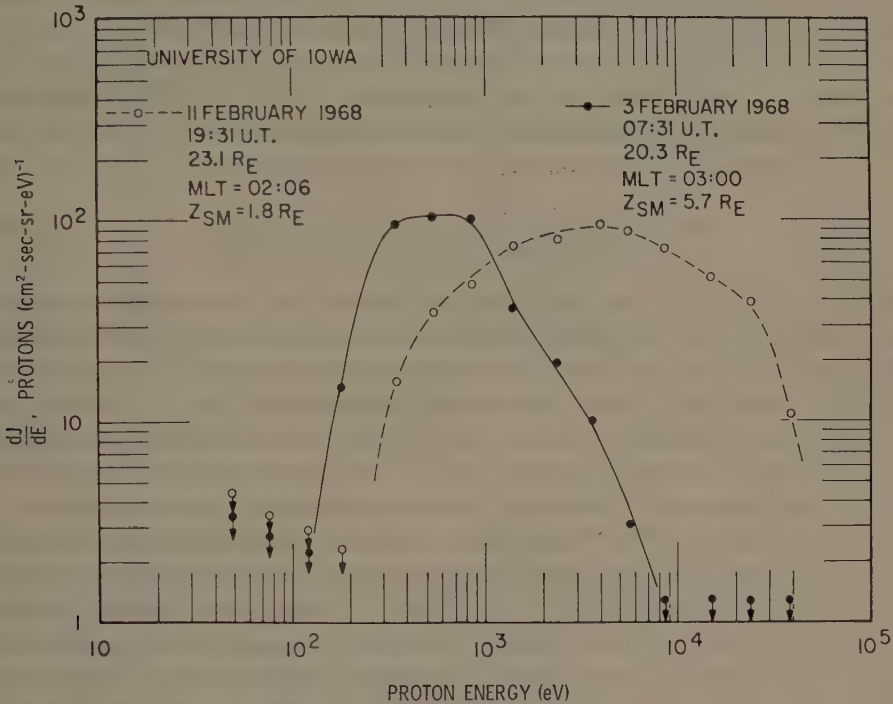


Fig. 5. Characteristic proton spectra seen in the magnetotail. The lower energy spectrum is generally found in the high latitude tail while the other is more characteristic of the plasma sheet (Frank, 1971a).

Within the plasma sheet at $18 R_E$, Hones (1970) and Hones *et al.* (1971a) have summarized the particle population. Electrons and protons have average energies of ~ 1 and ~ 6 keV, respectively, and number densities are $\sim 0.5 \text{ cm}^{-3}$. Angular distributions are usually isotropic. Proton energy densities are about 50% of that of solar wind protons but can reach 100%; electrons have energy densities about 10% of solar wind protons. The plasma sheet pressure responds proportionally within minutes to changes in the dynamic pressure of the solar wind. Electron spectra resemble Maxwellian distributions from energies of 3×10^2 to 3×10^3 eV, frequently becoming power law at higher energies during magnetic activity. In quiet times peak fluxes are $\sim 10^8 \text{ cm}^{-2} \text{ s}^{-1} \text{ sr}^{-1} \text{ keV}^{-1}$ at ~ 300 eV. Following substorms peak fluxes are $\sim 10^7 \text{ cm}^{-2} \text{ s}^{-1} \text{ sr}^{-1} \text{ keV}^{-1}$ at ~ 3 keV. However, energy densities remain ~ 30 eV

$\text{cm}^{-3} \text{sr}^{-1}$ under all conditions. There is a thinning of the plasma sheet during substorms which does represent a net loss of plasma (Hones *et al.*, 1971b).

The general character of the plasma sheet does not seem to change significantly out to $60 R_E$. The high energy tail of plasma sheet particles has continued to be probed by various investigators. Fennell (1970) has reported proton bursts for $E > 0.32 \text{ MeV}$ at $60 R_E$ with spectra E folding energies of 50 to 110 keV and intensities $\sim 300 \text{ cm}^{-2} \text{s}^{-1} \text{sr}^{-1}$. Electron fluxes with $E > 22$ and $> 45 \text{ keV}$ have been mapped by Meng (1971) at $60 R_E$. At flux levels of $\sim 300 \text{ cm}^{-2} \text{s}^{-1} \text{sr}^{-1}$, the distributions resemble those at $18 R_E$ in showing a higher frequency of occurrence near dawn at the equator. Between 20 to $40 R_E$, Meng and Anderson (1971) have measured electron fluxes for $E > 40 \text{ keV}$ between 10^2 and $8 \times 10^5 \text{ cm}^{-2} \text{s}^{-1}$. Our picture of the plasma sheet high energy tail is very similar to that obtained by earlier measurements, and the particle island fluxes are now recognized as the expansion of the plasma sheet.

3. Pseudo-Trapping Region and Vicinity

Recently, Frank (1971b) has presented measurements of electrons and protons between 0.08 and 50 keV near local midnight which greatly clarify the relationship in the equatorial plane between the plasma sheet, ring current, trapping boundary, and the plasmopause. We have shown the spatial positions in Figure 2. The inner edge of the plasma sheet is identified by an exponential decrease of electron energy densities (from a peak of $\sim 3 \times 10^{-9}$ to $10^{-8} \text{ erg cm}^{-3}$) with decreasing radial distance. The ring current protons are evidenced as a broad maximum in the energy density over the region 5.5 to $8.5 R_E$. The plasma sheet protons blend into the ring current protons in a continuous manner with no detectable boundary. Ring current protons extend inside the plasmopause about 0.5 to $1 R_E$ while the plasma sheet electrons terminate at the plasmopause. The stable trapping boundary of energetic electrons lies within the ring current region in the midnight portion of the magnetosphere. In the midnight pseudo-trapping region, the plasma sheet supplies particles for the outer radiation belt and the auroral zone through convection and pitch angle diffusion. Thus, the pseudo-trapping region is not only one where complete drift motion is impossible; it is an injection region during magnetic substorms.

The relationship between the equatorial regions and the auroral zone can probably best be shown using the ϕ contours defined by Fritz (1970) as the ratio of precipitating to local mirroring 40 keV electron fluxes at low altitude. By mapping the $\phi = 0.1$ and 1 boundaries onto the equatorial plane using the average magnetic field configuration given by Fairfield (1968), one obtains the region shown in Figure 2 associated with pseudo-trapped particles.

The auroral precipitation pattern that one observes at low altitude depends on the particle type and the energies observed. Both hard and soft zones depending on the spectrum have been characterized in the past (Sharp and Johnson, 1968), but recent detailed measurements indicate that the phenomenon is too complex for such a simple description. Craven (1970) has given a detailed mapping of auroral zone elec-

trons for $E \geq 5$ keV. He has presented frequency of occurrence for February 1965 to July 1966 as a function of IN Lat and MLT for flux levels ranging from 2.5×10^{-3} to $50 \text{ erg cm}^{-2} \text{ s}^{-1} \text{ sr}^{-1}$. Hoffman and Berko (1971) have presented similar information for $E \sim 0.7$ keV electrons in a burst mode with peak fluxes $\gtrsim 10^8 \text{ e cm}^{-2} \text{ s}^{-1} \text{ sr}^{-1} \text{ keV}^{-1}$ during low magnetic activity. Frequency of occurrence of ~ 60 – 100% is found mainly in the 0500 to 1400 MLT between IN Lat = 75 to 82° . Average values of proton energy fluxes for $E \geq 4$ keV have been given by Sharp *et al.* (1969). Peak fluxes on the nightside of $\sim 0.03 \text{ erg cm}^{-2} \text{ s}^{-1} \text{ sr}^{-1}$ occur around IN Lat = 65° while on the dayside peaks of $\sim 0.02 \text{ erg cm}^{-2} \text{ s}^{-1} \text{ sr}^{-1}$ are observed around IN Lat = 73° . Frank and Ackerson (1971) have presented detailed measurements at low altitude in the energy range $0.005 \leq E \leq 50$ keV in both the late evening and late morning sector. They have developed fully color coded energy time spectrograms to summarize this wealth of data. During precipitation events, electron spectra show a Maxwellian peak around 1 keV rising out of a power law background spectrum.

DeForest and McIlwain (1971), in presenting observations over the range $0.05 \leq E \leq 50$ keV in the equatorial region of $L = 6.6 R_E$, reveal the frequent injection of plasma from the plasma sheet in the vicinity of local midnight during magnetic substorms. Both energy and charge dispersion have been observed, and electric fields have a strong effect on lower energy particles. These workers have also found it necessary to use energy-time spectrograms to display the wealth of detail. Typical values for plasma parameters have been given by DeForest and McIlwain by integrating over energy. Particle densities are $n \sim 1 \text{ cm}^{-3}$, electron energy fluxes are $\sim 2 \text{ erg cm}^{-2} \text{ s}^{-1} \text{ sr}^{-1}$, which is a factor ~ 10 larger than proton fluxes in this range. Although the total energy flux of low energy particles seen at the equator is large enough to account for the outflux into the auroral zone, the spectral shapes are different at high and low altitudes. This suggests some local acceleration along field lines near the ionosphere.

The energetic electrons injected into the midnight region during substorms have been discussed by Winckler and co-workers (Arnoldy and Chan, 1969; Pfizter and Winckler, 1969; Lezniak and Winckler, 1970). They have shown that plasma sheet particles of initial energies 10 to 20 keV are convected inward and energized tenfold.

4. Stable Trapping Region

Since the electron population above 40 keV and protons above 100 keV in this region have been summarized on numerous occasions, the present discussion will be limited to observations published recently and to particles with $Z \geq 2$. An extensive survey of trapped particles including consideration of their sources, losses, and transport has recently been given by Williams (1972). Recent work has extended the energy range and refined the energy resolution of observations as well as solidifying our understanding of the phenomena. Although detailed differential energy spectra now available show interesting new features, the gross particle population characteristics are similar to those previously observed in most cases. It will be most convenient to discuss each particle type separately.

A. PROTONS

The extensive measurements by Frank in the range $0.05 \leq E \leq 50$ keV have provided data on a whole new region of trapped protons including the asymmetric ring current (Frank, 1970c), which represents enhancements of about an order of magnitude during magnetic storms in the ring current region shown in Figure 2. Frank and Owens (1970) have presented detailed L time intensity contour maps at the magnetic equator over this whole range of proton energies during June 10 to July 23, 1966, which show the rich morphology that these particles display.

Cornwall *et al.* (1971) have discussed the precipitation of these particles in terms of enhanced cyclotron wave turbulence, and, recently, they have reported precipitating protons in the range 2.5 to 200 keV with fluxes $\sim 10^7$ to 10^8 $\text{cm}^{-2} \text{s}^{-1}$ that substantiate this theory. In addition, Pizzella and Frank (1971) have shown that the quiet time proton spectrum in this energy range ties naturally into the spectra obtained from earlier measurements on Explorer 12 and 14 and Mariner 4 in the 0.1 to 1 MeV range. The differential energy spectrum shows a peak around 10 keV with a value near $10^2 \text{ cm}^{-2} \text{s}^{-1} \text{sr}^{-1} \text{eV}^{-1}$ in the range $4.5 < L < 6.0 R_E$. From these observations, they suggest that the outer boundary for inwardly diffusing protons lies in the vicinity of the earthward edge of the quiet time extraterrestrial ring current.

Measurements of protons in 12 energy bands between 0.06 and 3.3 MeV at $L = 6.6 R_E$ by Stevens *et al.* (1970) are in general agreement with other data summarized by King (1967) and provide much finer energy resolution. At local noon, an E-W flux difference effect due to a radial gradient of mirror points was observed. Comparison of the observations at local noon with those at local midnight provided excellent confirmation of the Roederer (1967) model of shell splitting in the earth's distorted field. Earlier confirmation of this model had been provided by Pfitzer *et al.* (1969) using correlated electron observations on OGO 3 and ATS 1.

Pizzella and Randall (1971) reported differential energy measurements from Injun 5 mainly covering the energy range 0.3 to 8 MeV. This spectrum shows a peak around 5 MeV in the inner zone with a minimum around 2 MeV. Reasonable agreement with previous measurements above a few MeV was obtained, but at lower energies electron contamination has elevated earlier flux values. Hovestadt (1972) has also made extensive measurements on the AZUR satellite covering the energy range 1.5 to 104 MeV with seven channels. These data also indicate differences from previously measured values in the inner zone. The Injun 5 results may still be affected by electrons.

Two important findings concerning high energy inner zone protons should be cited here. Macy *et al.* (1970) calculated the time dependence of the flux of 55 MeV protons at low altitudes over the period 1961–70 caused by atmospheric loss process, and they obtained good agreement with experimental observations. Earlier, Heckman *et al.* (1971) also reported good agreement between their low altitude observations and similar calculations. In both calculations, an empirical source independent of time has been determined from experimentation. The altitude dependence of this source suggests that a diffusion process may be occurring. By incorporating a radial

diffusion mechanism with a CRAND source and atmospheric losses, Farley *et al.* (1970) have been able for the first time to get good agreement with equatorial proton observations in both intensity and energy spectra in the ranges $20 \leq E \leq 170$ MeV and $1.15 \leq L \leq 1.7 R_E$. The radial diffusion transports protons inward from the outer zone as well as redistributing high magnetic moment CRAND produced protons in both directions. Consequently, both dominant source and loss mechanisms for high energy protons are more clearly established.

B. ELECTRONS

According to the observations of DeForest and McIlwain (1971) cited earlier, as well as those of Winckler and co-workers (Lezniak and Winckler, 1970), the substorm injection of particles from the plasma sheet into the radiation belt through convection processes followed by gradient and curvature drift results in a strong source of outer zone electrons. Recently, Williams (1972) emphasized that 40 keV electrons mirroring at low altitudes in the outer zone are not stably trapped since the pitch angle diffusion mechanisms are strong enough to precipitate these particles before they drift around the earth. McDiarmid and Burrows (1966) had reached this conclusion earlier. Vampola *et al.* (1970) have shown that precipitation of higher energy electrons reaches a maximum at the plasmapause and remains large outside of it. Thus, one expects to find some particle precipitation throughout the stable trapping regions at low altitude caused by wave-particle interactions.

In spite of the numerous dynamical effects that occur with outer zone electrons, it is possible to present a time averaged (over several magnetic storms) outer zone electron flux. Singley and Vette have just completed an empirical model over the L range 2.8 to 11 R_E which includes LT and B dependence. The energy spectra of this model for various L values are shown in Figure 6 for the 1967 time period. The statistical time behavior of the fluxes is represented by a log normal distribution. However, it is clear that solar cycle effects are important even for time averaged outer zone fluxes. This effect is best illustrated in Figure 7 where a comparison of the OGO 1 electron spectrometer data of Pfitzer and Winckler is made with their OGO 3 data. The general average effect is a filling up of the slot region during solar maximum. Average flux levels above $L = 5 R_E$ do not seem to change. Although there must be more injection from the plasma sheet as the frequency of magnetic activity increases, the strong and weak pitch angle diffusion mechanisms maintain a nearly constant average flux level in these regions. Based on ATS 1 observations, this constancy of average flux levels continues on into solar maximum (Paulikas, 1971). A comparison of the local time dependence of data taken prior to 1967 with that of Paulikas and Blake (1971) indicates that there is less diurnal variation during solar maximum conditions; however, this is not yet clearly established.

In the inner radiation belt, the Starfish electrons below 700 keV had decayed to the level where injection events following magnetic storms were seen as early as April 1965 (Bostrom *et al.*, 1970; Winckler, 1970), and once could consider that the natural background levels were reached by mid-1967 for all L values. Stassinopoulos

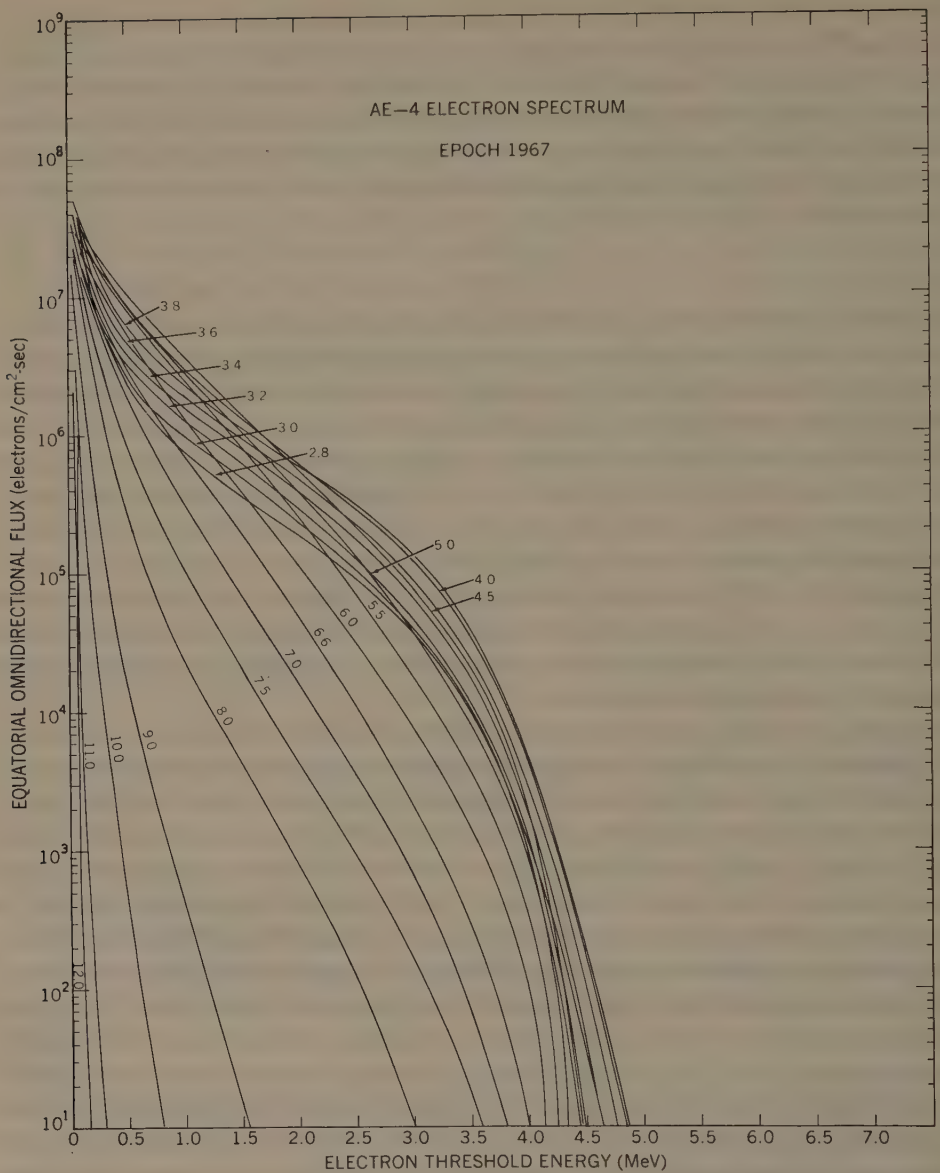


Fig. 6. Electron spectrum for AE4 model environment. The integral spectrum for a local time averaged equatorial flux is shown for various L values ranging from 2.8 to 12 R_E .

and Verzariu (1971) have presented a model for the Starfish decay lifetimes based on the 1963-38C electron measurements over the period October 1963 to July 1965 assuming the natural background is negligible during this time period. This model indicates that τ decreases monotonically with energy for $E > 0.2$ MeV. However, Teague and Vette (1971), using the OGO 1 and 3 data of Winckler, have separated

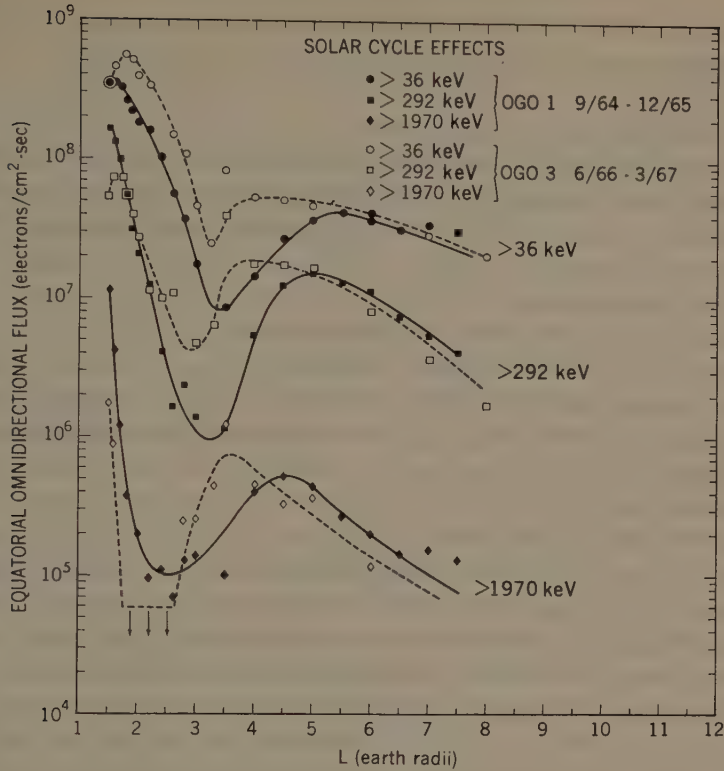


Fig. 7. Long term effects in average electron fluxes. The OGO results are averaged over the time period shown and have been converted to omnidirectional integral fluxes averaged over LT. The two lower energy curves show the slot filling up as solar activity rises. For the highest energy curve, Starfish electrons mask solar cycle effects below $L=2.8 R_E$; however, above this distance behavior similar to the lower energies is noted.

the natural quiet time electron population from the Starfish electrons in order to study both components. They obtained Starfish decay times that were significantly shorter than the model for energies less than 690 keV but in good agreement at higher energies. These latter results indicated that maximum decay times occur for energies around 1 MeV throughout the inner zone. Using these decay times and assuming no natural sources for electrons above 1 MeV, the maximum fluxes >1 MeV that one expects in July 1971 are $10^2 \text{ cm}^{-2} \text{ s}^{-1}$ at $L=1.4 R_E$.

Since it is clear that electrons below 700 keV are injected into the inner zone, one might expect that solar cycle effects would be seen in this region. If one compares the OGO 1 and 3 electron data during magnetically quiet periods, a general increase in the flux levels is seen for the lower energy channels. This increase is greatest in the 292 to 690 keV channel and rises steeply with increasing value until leveling off at $L=1.9 R_E$. The lower energy channels have considerably different L dependence with the largest effect occurring at $L=1.5 R_E$, the lowest value for which comparisons

could be made with these data. A natural inner zone electron model environment will be available soon.

C. ALPHA PARTICLES

There has been considerable interest in the measurement of trapped α -particles since a knowledge of the charge composition of the radiation belts could lead to an increased understanding of the source, loss, and acceleration mechanisms. Three main sources for α -particles are:

- (1) capture of solar wind α -particles,
- (2) ionospheric or plasmaspheric He particles, and
- (3) direct injection of energetic solar α -particles.

For these sources the He/H ratio ranges from $\sim 1-20 \times 10^{-2}$. Of course, acceleration/transport and loss mechanisms can be expected to alter the observed ratios in the trapping region.

The earliest attempts to measure trapped α -particles, which resulted in upper limits, have been summarized by Williams (1972).

The first positive measurements were achieved in the $\gtrsim 0.5$ –1 MeV/nucleon range by the Iowa group using a thin surface barrier detector on Injun 4 (Krimigis and Van Allen, 1967, 1978). Additional measurements extending down to >0.26 MeV/nucleon have been carried out by this group on OGO 4 and Injun 5 as well as one near equatorial pass with Mariner 5 (Fritz and Krimigis, 1969; Krimigis, 1970). The Aerospace group has made confirming measurements in the $\gtrsim 0.5$ to 1 MeV/nucleon range using multi-counter telescopes on satellites 1966–70A and 1968–26B (Paulikas *et al.*, 1968; Blake and Paulikas, 1970). The measurements mainly cover the L range ~ 2 to 4 R_E and B values ~ 0.04 to 21 G; Injun 4 did give coverage down to $L=1.4$.

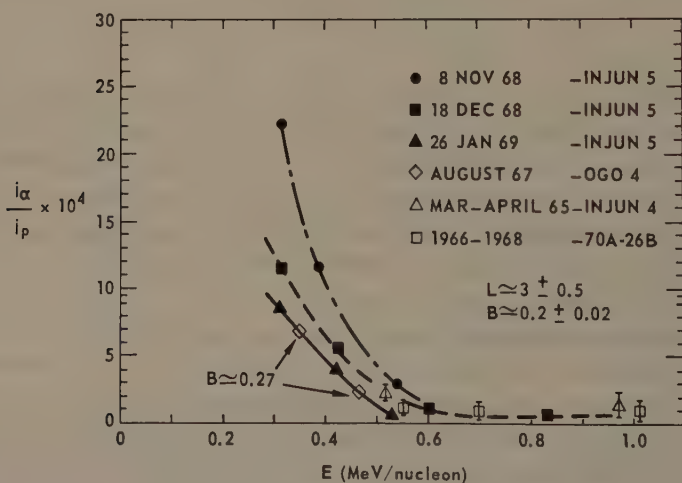


Fig. 8. The alpha to proton flux ratio as a function of energy (Krimigis, 1970). The lowest energy point has continued to decrease with time (Krimigis, 1971).

In the outer zone the α/p ratio at constant energy/nucleon does not change more than a factor of 2 over the B range covered. (The L variation is as much as a factor of 10 for Mariner 5 results.) Above 0.6 MeV/nucleon, the ratio seems fairly stable with time with a value of $\sim 2 \times 10^{-4}$. At lower energies/nucleon, the ratio exhibits changes as large as a factor of 5 following certain magnetic storms. A summary of the j_α/j_p flux ratio for most of the reported measurements has been given by Krimigis (1970) and is shown in Figure 8. The peak in alpha intensity $\gtrsim 0.5$ MeV/nucleon occurs around $L=3 R_E$ with slight changes in position due to some magnetic storms. The fluxes obtained during quiet times with Injun 4 show an L dependence and j_α/j_p flux ratio which led Krimigis and Van Allen (1967) to suggest that the inner zone source for alphas may be different than that for the outer zone.

The energy spectrum has been characterized by both an exponential and power law spectrum. However, the character of the spectrum changes significantly with time. An extensive time history for these particles from early 1968 to mid-1970 has been presented recently by Randall (1971). This is dominated by a 40-fold increase in the flux of 1 to 8 MeV alphas during October 29 to November 1, 1968, as reported by Van Allen and Randall (1971) and thus represents magnetically disturbed conditions. During several separate magnetic disturbances these investigators reported absolute increases in the trapped alpha intensity comparable to the interplanetary fluxes. Since these increases remained for long periods after the interplanetary fluxes, they interpret this as evidence for the direct injection source (3) noted earlier. It should be remarked that there are alpha increases that have been observed during magnetic storms without any interplanetary fluxes being present.

All of the experimenters who have obtained trapped alpha measurements have compared their results with theoretical predictions based on protons and alphas entering the magnetosphere with the same velocity or with the same total energy (Tverskoy, 1965, 1968, 1969; Hess, 1966). The main disagreements have been that the α/p ratio is much smaller than predicted. However, only Coulomb losses have been taken into account, Cornwall (1971) has recently pointed out that when charge exchange and pitch angle scattering losses also are taken into account, proton loss rates at a fixed energy/nucleon are as great or greater than that for either He^+ or He^{++} . Consequently, a transport mechanism which causes charged He to diffuse slower than protons is needed. He points out that electrostatic diffusion does have this property whereas magnetic diffusion does not. Calculations are being carried out to obtain He flux profiles, but no results have been published yet.

D. $Z \geq 3$ PARTICLES

The charge spectroscopy of trapped radiation particles has been extended to the range of medium nuclei, C, N, and O by the Iowa and the Chicago groups. Krimigis *et al.* (1970) and Van Allen *et al.* (1970) have reported on the detection of particles with $Z \geq 3$ with Injun 5 instrumentation and attribute them to the C, N, O group. The measurements cover the range 0.31 to 14 MeV/nucleon. The variation as a function of L for C, N, O is very similar to α -particles over the regions investigated. The peak

flux perpendicular to the magnetic field is $1.1 \text{ cm}^{-2} \text{ s}^{-1} \text{ sr}^{-1}$, and the ratio of medium nuclei to α -particle flux is $\sim 2.8 \times 10^{-3}$. The C, N, O flux was observed to increase by a factor $\sim 10^2$ following the magnetic storms of November 1, 1968, and February 2, 1969. The flux ratio of medium to alpha increased by a factor of 8 during the November event. On the basis of these measurements, one is unable to distinguish between the solar wind or ionized gas in the terrestrial plasmasphere. Mogro-Campero and Simpson (1970) and Mogro-Campero (1970) have measured the trapped fluxes of C, N, and O separately in the 13 to 33 MeV/nucleon range and find the O/C ratio is 0.5 ± 0.4 . Since this ratio in the earth's atmosphere is ~ 670 , a terrestrial origin is definitely ruled out. The C, N, O flux at $L=4$ is $dj/dE = 9.2 \times 10^{-4} \text{ cm}^{-2} \text{ s}^{-1} \text{ sr}^{-1} \text{ MeV}^{-1}$, which is $\sim 10^2$ times the interplanetary C, N, O flux. They report enhancements of this flux of about a factor of 10 during certain solar flares and cannot rule out the possibility of direct trapping since the counting rates are extremely low. However, the average value of the flux is constant over the period of observations, March 3, 1968, to December 31, 1969.

References

- Arnoldy, R. L. and Chan, K. W.: 1969, *J. Geophys. Res.* **74**, 5019.
- Bame, S. J.: 1968, in B. M. McCormac (ed.), *Earth's Particles and Fields*, Reinhold Publishing Corporation, New York, p. 373.
- Blake, J. B. and Paulikas, G. A.: 1970, in B. M. McCormac (ed.), *Particles and Fields in the Magnetosphere*, D. Reidel Publishing Company, Dordrecht, Holland, p. 380.
- Bostrom, C. O., Beall, D. S., and Armstrong, J. C.: 1970, *J. Geophys. Res.* **75**, 1246.
- Cornwall, J. M.: 1971, *J. Geophys. Res.* **76**, 264.
- Cornwall, J. M., Hilton, H. H., and Mizera, P. F.: 1971, *J. Geophys. Res.* **76**, 5220.
- Craven, J. D.: 1970, *J. Geophys. Res.* **75**, 2468.
- DeForest, S. E. and McIlwain, C. E.: 1971, *J. Geophys. Res.* **76**, 3587.
- Fairfield, D. H.: 1968, *J. Geophys. Res.* **73**, 7329.
- Farley, T. A., Tomassian, A. D., and Walt, M.: 1970, *Phys. Rev. Letters* **25**, 47.
- Fennell, J. F.: 1970, *J. Geophys. Res.* **75**, 7048.
- Frank, L. A.: 1970a, *J. Geophys. Res.* **75**, 707.
- Frank, L. A.: 1970b, in B. M. McCormac (ed.), *Particles and Fields in the Magnetosphere*, D. Reidel Publishing Company, Dordrecht, Holland, p. 319.
- Frank, L. A.: 1970c, *J. Geophys. Res.* **75**, 1263.
- Frank, L. A.: 1971a, U. of Iowa 70-55, submitted to *J. Geophys. Res.* **76**, 5202.
- Frank, L. A.: 1971b, *J. Geophys. Res.* **76**, 2265.
- Frank, L. A. and Ackerson, K. L.: 1971, *J. Geophys. Res.* **76**, 3612.
- Frank, L. A. and Owens, H. D.: 1970, *J. Geophys. Res.* **75**, 1269.
- Fritz, T. A.: 1970, *J. Geophys. Res.* **75**, 5387.
- Fritz, T. A. and Krimigis, S. M.: 1969, *J. Geophys. Res.* **74**, 5132.
- Heckman, H. H., Lindstrom, P. J., and Nakano, G. H.: 1971, in NASA SP-3024 Vol. VII, p. 39.
- Heikkila, W. J. and Winningham, J. D.: 1971, *J. Geophys. Res.* **76**, 883.
- Hess, W. N.: 1966, in B. M. McCormac (ed.), *Radiation Trapped in the Earth's Magnetic Field*, D. Reidel Publishing Company, Dordrecht, Holland, p. 352.
- Hill, T. W. and Dessler, A. J.: 1971, *J. Geophys. Res.*, submitted.
- Hoffman, R. A. and Berko, F. W.: 1971, *J. Geophys. Res.* **76**, 2967.
- Hones, E. W., Jr.: 1970, in B. M. McCormac (ed.), *Particles and Fields in the Magnetosphere*, D. Reidel Publishing Company, Dordrecht, Holland, p. 24.
- Hones, E. W., Jr., Asbridge, J. R., Bame, S. J., and Singer, S.: 1971a, *J. Geophys. Res.* **76**, 63.
- Hones, E. W., Jr., Asbridge, J. R., and Bame, S. J.: 1971b, *J. Geophys. Res.* **76**, 4402.

- Hovestadt, D., Achtermann, E., Ebel, B., Häusler, B., and Paschmann, G.: 1972, this volume, p. 115.
- Hundhausen, A. J.: 1970, in V. Manno and D. E. Page (eds.), *Intercorrelated Satellite Observations Related to Solar Events*, D. Reidel Publishing Company, Dordrecht, Holland, p. 155.
- King, J. H.: 1967, NASA SP-3024 Vol. IV.
- Krimigis, S. M.: 1970, in B. M. McCormac (ed.), *Particles and Fields in the Magnetosphere*, D. Reidel Publishing Company, Dordrecht, Holland, p. 364.
- Krimigis, S. M.: 1971, private communication.
- Krimigis, S. M. and Van Allen, J. A.: 1967, *J. Geophys. Res.* **72**, 5779.
- Krimigis, S. M. and Van Allen, J. A.: 1968, in B. M. McCormac (ed.), *Earth's Particles and Fields*, Reinhold Publishing Corporation, New York, p. 127.
- Krimigis, S. M., Verzariu, P., Van Allen, J. A., Armstrong, T. P., Fritz, T. A., and Randall, B. A.: 1970, *J. Geophys. Res.* **75**, 4210.
- Lezniak, T. W. and Winckler, J. R.: 1970, *J. Geophys. Res.* **75**, 7075.
- Macy, W. W., White, R. S., Fitz, R. C., and Holeman, E.: 1970, *J. Geophys. Res.* **75**, 4322.
- McDiarmid, I. B. and Burrows, J. R.: 1966, *Can. J. Phys.* **44**, 669.
- Meng, C. I.: 1971, *J. Geophys. Res.* **76**, 862.
- Meng, C. I., and Anderson, K. A.: 1971, *J. Geophys. Res.* **76**, 873.
- Mogro-Campero, A.: 1970, *Geomagnetically Trapped C, N, and O Nuclei*, Ph.D. Thesis, Univ. of Chicago.
- Mogro-Campero, A. and Simpson, J. A.: 1970, *Phys. Rev. Letters* **25**, 1631.
- Paulikas, G. A.: 1971, private communication.
- Paulikas, G. A. and Blake, J. B.: 1971, NASA SP-3024, Vol. VII, p. 51.
- Paulikas, G. A., Blake, J. B., and Freden, S. C.: 1968, Aerospace Report No. TR-0200 (4260-20)-3.
- Pfitzer, K. A. and Winckler, J. R.: 1969, *J. Geophys. Res.* **74**, 5005.
- Pfitzer, K. A., Lezniak, T. W., and Winckler, J. R.: 1969, *J. Geophys. Res.* **74**, 4687.
- Pizzella, G. and Frank, L. A.: 1971, *J. Geophys. Res.* **76**, 88.
- Pizzella, G. and Randall, B. A.: 1971, *J. Geophys. Res.* **76**, 2306.
- Randall, B. A.: 1971, *Trans. Amer. Geophys. Union* **52**, 321.
- Roederer, J. G.: 1967, *J. Geophys. Res.* **72**, 981.
- Russell, C. T., Chappell, C. R., Montgomery, M. D., Neugebauer, M., and Scarf, F. L.: 1971, *J. Geophys. Res.* **76**, 6743.
- Sharp, R. D. and Johnson, R. G.: 1968, in B. M. McCormac (ed.), *Earth's Particles and Fields*, Reinhold Publishing Corporation, New York, p. 113.
- Sharp, R. D., Carr, D. L., and Johnson, R. G.: 1969, *J. Geophys. Res.* **74**, 4618.
- Stassinopoulos, E. G. and Verzariu, P.: 1971, *J. Geophys. Res.* **76**, 1841.
- Stevens, J. R., Martina, E. F., and White, R. S.: 1970, *J. Geophys. Res.* **75**, 5373.
- Teague, M. J. and Vette, J. I.: 1971, National Space Science Data Center Report 71-11.
- Tverskoy, B. A.: 1965, *Geomagnetiz i Aeronomiya* **5**, 617.
- Tverskoy, B. A.: 1968, *Soviet Phys. JETP* **26**, 821.
- Tverskoy, B. A.: 1969, *Rev. Geophys.* **1**, 219.
- Vampola, A. L., Koons, H. C., and McPherson, D. A.: 1970, Aerospace Corp. Report TR-0059 (9220-02)-5.
- Van Allen, J. A. and Randall, B. A.: 1971, *J. Geophys. Res.* **76**, 1830.
- Van Allen, J. A., Randall, B. A., and Krimigis, S. M.: 1970, *J. Geophys. Res.* **75**, 6085.
- Vasyliunas, V. M.: 1971, *Trans. Amer. Geophys. Union* **52**, 329.
- Williams, D. J.: 1972, in E. R. Dyer (General editor), *Solar-Terrestrial Physics/1970, Part III*, D. Reidel Publishing Company, Dordrecht, Holland, p. 66.
- Winckler, J. R.: 1970, in B. M. McCormac (ed.), *Particles and Fields in the Magnetosphere*, D. Reidel Publishing Company, Dordrecht, Holland, p. 332.

CHARACTERISTICS OF MAGNETOSHEATH PLASMA OBSERVED AT LOW ALTITUDES IN THE DAYSIDE MAGNETOSPHERIC CUSPS

J. DAVID WINNINGHAM

*Atmospheric and Space Sciences Division,
The University of Texas at Dallas, Tex., U.S.A.*

Abstract. Magnetosheath plasma penetrating to low altitudes in the dayside cusp region of the magnetosphere has been observed by the ISIS 1 soft particle spectrometer (SPS). The extent of these particle fluxes in MLT and IN Lat, their variation with magnetic activity, and their pitch angle distribution are given. Comparison between the SPS data and energetic particle data indicates that the boundary between open and closed field lines on the dayside is associated with a sharp drop in the outer zone > 1 keV electron fluxes. It is shown that these newly identified cusp fluxes provide the necessary energy to produce observed dayside auroral oval phenomena.

1. Introduction

Heikkilä *et al.* (1970), Winningham (1970), and Heikkilä and Winningham (1971) gave the first definitive evidence for linking dayside 'soft zone' fluxes with a magnetosheath source via the cusps in the dayside magnetosphere. The existence of magnetosheath plasma penetration to low altitudes had long been postulated by theoreticians and experimentalists alike (the reader is referred to the review in Winningham (1970) and Heikkilä and Winningham (1971)). This paper will extend the dayside results presented in the earlier ISIS 1 papers.

Winningham (1970) identified the IN Lat, denoted by Λ_{CL} , where outer zone fluxes cease and soft fluxes with magnetosheath characteristics begin as the last closed field line on the dayside. He further postulated this boundary to mark the beginning of interconnected terrestrial and interplanetary field lines. The IN Lat, Λ_{CU} , where soft magnetosheath-like proton fluxes end was identified as marking the last merged field line which has free access to magnetosheath plasma. Electron fluxes are often observed above Λ_{CU} but they do not, in general, exhibit magnetosheath characteristics, and no protons are observed in the polar cap region. This terminology and its implied assumptions will be used in the remainder of this paper.

2. Instrumentation

ISIS 1 was launched into a 570 by 3500 km polar orbit (inclination 88.5°) on January 30, 1969. The ISIS 1 SPS simultaneously measures the differential energy spectra of positive and negative particles in the energy range 10 eV to 12 keV per unit charge with a resolution of $\pm 40\%$ (see Heikkilä *et al.*, 1970; Winningham, 1970 for a more detailed description). Results presented in this paper were obtained with a $15^\circ \times 35^\circ$ collimator pointed perpendicular to the satellite spin axis.

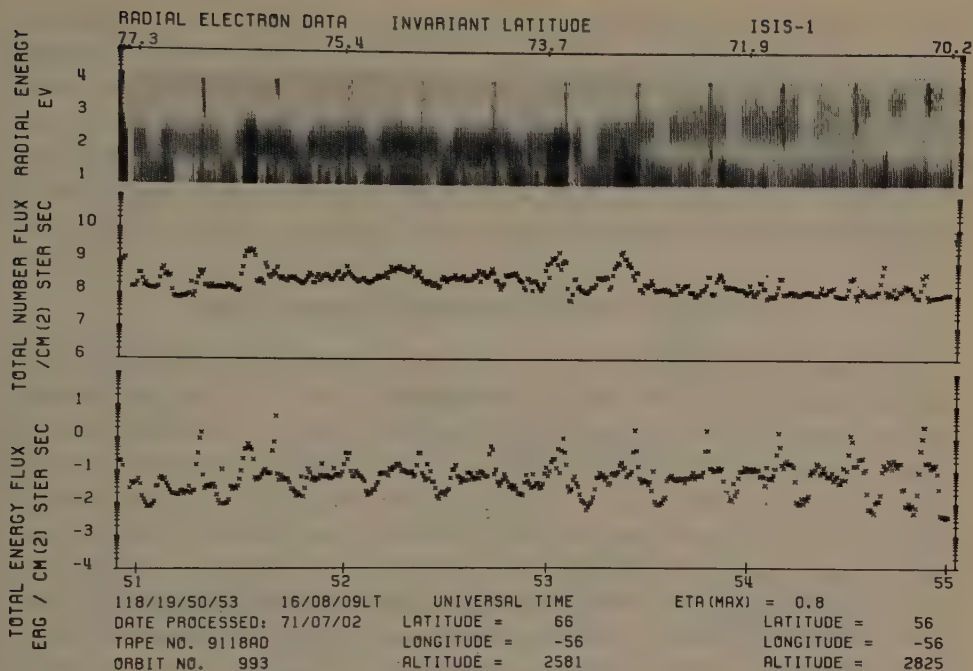


Fig. 1a. Electron spectrogram for April 28, 1969, at 19:50:53 UT.

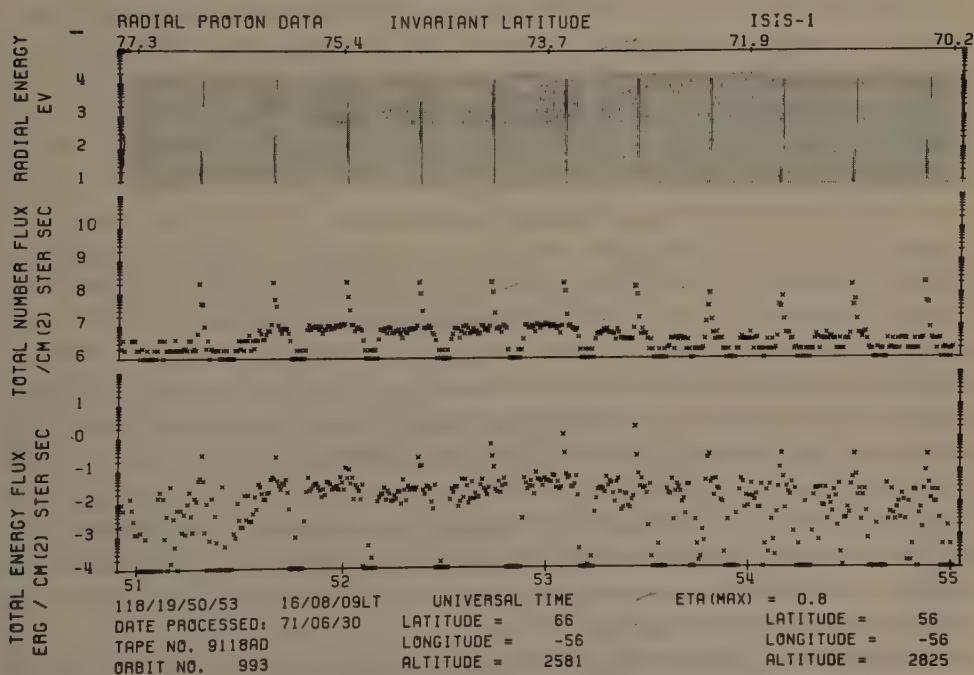


Fig. 1b. Proton spectrogram for April 28, 1969 at 19:50:53 UT.

The results obtained in the swept mode of operation are conveniently displayed as energy-time spectrograms. Each differential energy sweep of the instrument is shown as a separate line in the spectrogram (top portion of Figures 1a and 1b) with the density of the trace being modulated by the counting rate. A readout of 15 or less per sample is inhibited, with accumulation continuing during successive sampling intervals until > 15 counts are accumulated. The middle and lower graphs of the spectrogram give the total number and energy flux over the 10 eV to 12 keV energy range.

3. Observations on the Dayside High Latitude Region

A pair of high resolution spectrograms (one spectrum every $\frac{1}{2}$ sec or 4 km) is reproduced in Figure 1a and b. This pass, which began at 19:50:53 UT on April 28, 1969, occurred during the recovery phase ($K_p = 3^-$) of a storm that commenced at ~ 0300 hr UT on the same day. The MLT was 1645 hr. At the beginning of this pass only low energy electrons are observed in the polar cap region. The vertical bars appearing at 20 s intervals in the spectrogram are due to solar UV contamination. An isotropic flux of protons begins at 19:51:30 UT ($A_{CU} = 76.5^\circ$) and continues to 19:53:26 UT ($A_{CL} = 73^\circ$). Below A_{CL} the proton flux peaks at large pitch angles. Between A_{CL} and A_{CU} an isotropic flux of electrons with a spectral peak at ~ 100 eV is observed. Below A_{CL} the electron average energy increases and the pitch angle distribution becomes anisotropic towards 90° .

It should be noted that electron fluxes for most cusp passes exhibit a greater variability than shown in Figure 1a (see Winningham (1970) for a larger collection of spectrograms). This pass was selected because of the large pitch angle scan and good angular resolution, not because it is 'the typical pass.'

Representative spectra from the cusp data in Figure 1a and b are given in Figure 2. The cusp electron spectrum at a pitch angle (α_p) of 29° is observed to have a peak at 100 eV as do a majority of the cusp spectra observed with ISIS 1 (Figure 3). Below ~ 60 eV a roughly power law component is observed in both cusp and outer zone spectra which is due to atmospheric photoelectrons (Heikkila, 1970) and secondaries. Outer zone electron spectra (Figure 2) gradually harden from an average energy of ~ 500 eV just below A_{CL} to ~ 1 keV when they go below threshold at $A = 68^\circ$. Just below A_{CL} the electron flux is isotropic but rapidly becomes anisotropic towards 90° as the IN Lat decreases. Proton spectra observed in the cusp region peak at ~ 600 eV (Figure 2) with a decrease in intensity towards higher and lower energies. Below A_{CL} the proton flux decreases in intensity, becomes harder, and is peaked at 90° pitch angle.

Rather than compare the spectra in Figure 2 with those in the magnetosheath for different periods as was done by Heikkila and Winningham (1971), comparison will be made in a later section between near concurrent IMP 5 (Frank, 1970) and ISIS 1 spectra recorded on July 11, 1969.

Close inspection of detailed spectral printouts reveals that up to 19:53:26 UT ($A = 73^\circ$) electron spectra are identical to the cusp spectrum in Figure 2, and those

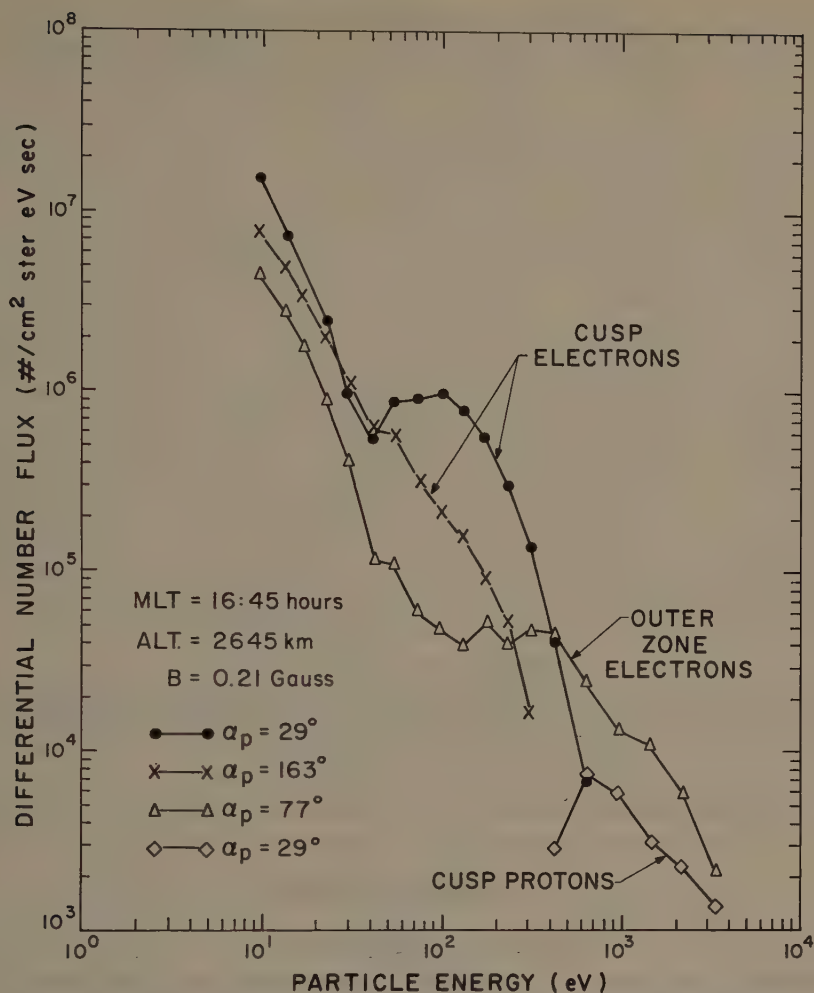


Fig. 2. Electron and proton differential spectra for the data contained in Figures 1a and 1b. Cusp spectra were obtained for the period 19:51:57 to 19:52:07 UT. The outer zone spectrum is for 19:54:01 UT.

after 19:53:36 (below $\lambda = 72.9^\circ$) are similar to the outer zone spectra in Figure 2. In the intervening region (10 seconds) the spectra appear to be an admixture of both. Burrows (1971) indicates that above $\lambda = 71.6^\circ$ the trapped energetic (>20 keV) electron fluxes begin a rapid drop to background. The >20 keV flux reaches 10% of maximum at 72.3° and background at 72.6° . The >200 keV detector (which has a larger geometric factor) reaches background at $\lambda = 72.8^\circ$. It thus appears that on this pass, hard outer zone electron fluxes extend up to the boundary between softer outer zone electrons and magnetosheath electrons. Winningham (1970) compared a larger number of passes and found similar results to the above. However, during very active periods, fluxes of >20 keV electrons can be above background between λ_{CL} and λ_{CU} .

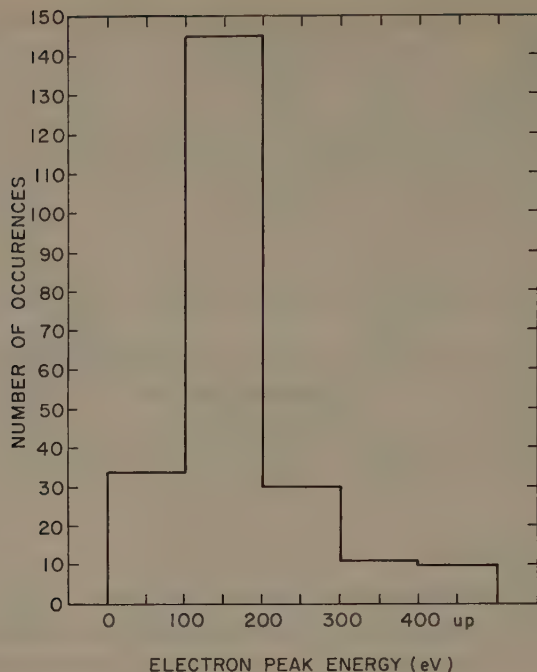


Fig. 3. Frequency of occurrence for the peak energy of the primary electron spectrum in the day-side magnetospheric cusp.

Further intercomparison is being made and the results will be presented in a future paper.

4. Pitch Angle Distribution

In the normal mode of SPS operation (one spectrum every 2 s) only three samples are obtained in one quadrant resulting in a coarse pitch angle distribution. In the all-radial sweep mode approximately 12 samples (one sweep every $\frac{1}{2}$ s) are obtained in one quadrant. Figure 4 illustrates a typical high resolution electron and proton pitch angle distribution for the cusp fluxes shown in Figure 1a and b. As noted earlier soft electron and proton fluxes from the dayside cusp are observed from $\Lambda_{CL}=73^\circ$ to $\Lambda_{CU}=76.5^\circ$. During this period the pitch angle range scanned was $90^\circ \pm 71^\circ$ at $\Lambda=78^\circ$ to $90^\circ \pm 80^\circ$ at $\Lambda=73^\circ$. The large depressions in number and energy fluxes (see Figures 1a and 1b) occur when the instrument scans into the loss cone for upcoming particles (the large regular spikes are sun pulses).

Figure 4 shows that the number and energy flux for the primary electron beam (73 to 420 eV) in the cusp are isotropic up to $\alpha_p \sim 135^\circ$ (α_p is the pitch angle for the normal to the detector aperture). Above 135° both the number and energy flux exhibit the same relative decrease in value. A particle at $\alpha_p=135^\circ$ and 140° (45° and 40° incident angles) will mirror at 700 and 200 km, respectively (see Figure 4 for a graph of mirror heights appropriate to the altitude of the results presented in Figure 4).

Particles incident at angles less than 38° ($>142^\circ$ return angle) will find their mirror points below 100 km. Thus particles observed above $\sim 140^\circ$ cannot be particles that have simply mirrored below the satellite.

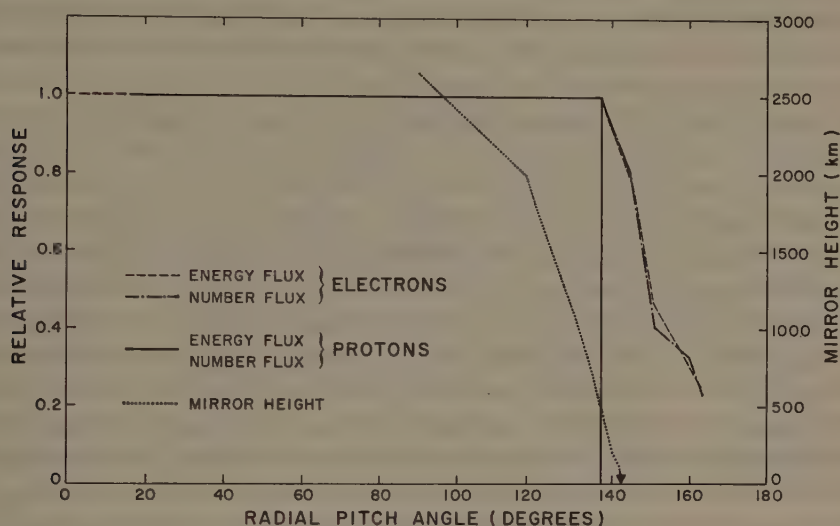


Fig. 4. Normalized proton and electron pitch angle distributions for the energy range 73 to 420 eV. These distributions are for the period 19:51:57 to 19:52:07 UT in Figures 1a and 1b. Unity represents $2.5 \times 10^8 \text{ cm}^{-2} \text{ sr}^{-1} \text{ s}^{-1}$ and $6.0 \times 10^{-2} \text{ erg cm}^{-2} \text{ sr}^{-1} \text{ s}^{-1}$ for electrons; and $1.0 \times 10^7 \text{ cm}^{-2} \text{ sr}^{-1} \text{ s}^{-1}$ and $3.0 \times 10^{-2} \text{ erg cm}^{-2} \text{ sr}^{-1} \text{ s}^{-1}$ for protons.

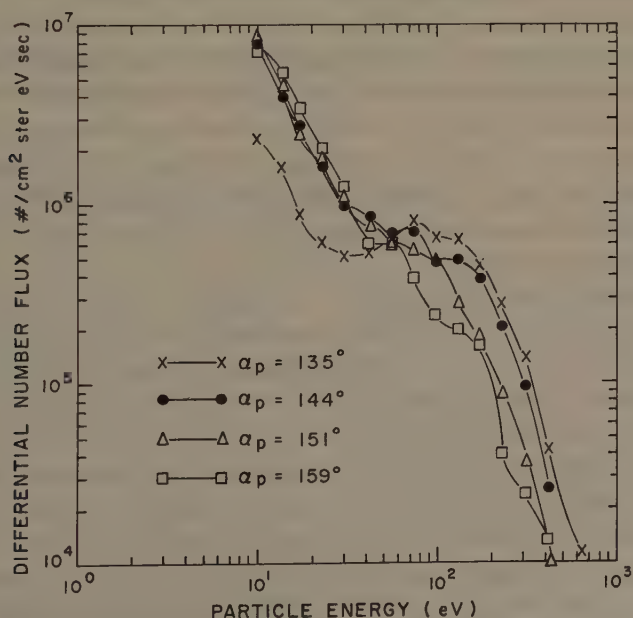


Fig. 5. Electron spectra for the data contained in Figure 4.

Figure 5 gives electron spectra for pitch angles just prior to and after the decrease in Figure 4. The spectra at $\alpha_p = 144^\circ$ and 151° are observed to be similar in shape to the one at 135° but decreased in amplitude. This seems to indicate that a significant amount of elastic scattering exists in the ionosphere below the cusp. As the pitch angle increases, the peak in the > 73 eV range is lost and the spectra appear to be due to backscatter of secondaries and degraded primaries. The return flux for particles inside the loss cone is observed to be much smaller for soft outer zone fluxes (see Figure 1a at 19:53:38 UT). As mentioned earlier the average energy for the soft outer zone spectra is 5 to 10 times that of the cusp spectra. The 500 eV outer zone electrons thus deposit a greater fraction of their incident energy in the ionosphere as compared to the 100 eV cusp electrons. This difference in the fraction of the incident energy flux lost (i.e., different albedos) can probably be explained by the manner in which energy is lost as a function of incident particle energy. The ~ 100 eV cusp electrons begin their energy loss at very high altitudes (~ 600 km) whereas the ~ 500 eV outer zone electrons begin theirs at ~ 400 km (Rees, 1964). If at higher altitudes processes such as coulomb scattering off heavy ions, collisional excitation, or weak wave-particle interaction dominate over ionization then large angular scattering is possible without large energy losses. This would result in a large albedo electron flux with a spectrum similar to the incident spectrum (see Figure 5). As the altitude of the energy loss region decreases (i.e., increasing particle energy) ionization, with its accompanying large incremental energy loss, will probably become the major loss mechanism. If present, the albedo flux would be composed mainly of highly degraded primaries and secondaries bearing little resemblance to the incident spectrum. This is consistent with the differences observed in the cusp and outer zone albedo fluxes in Figure 1a.

An alternative explanation to the above would be an electrostatic double layer in the cusp below the satellite. The parallel electric field of the double layer would raise the mirror heights and thus decrease the energy loss. Assuming a 100 V potential to exist between the satellite (2600 km) and the 100 eV maximum loss region (~ 300 km), a field of $\sim 50 \mu\text{V}/\text{m}^{-1}$ would result. This value is not prohibitively large but has one drawback. Such a field would accelerate ionospheric electrons into the energy range of ISIS 1. No such fluxes are observed on April 28, 1969, or other ISIS 1 passes which scan from 0 to 180° pitch angle.

Figure 4 indicates that the loss process for protons occurs in the altitude range below ~ 700 km ($\alpha_p = 135^\circ$). The albedo proton flux above 135° is observed to be vanishingly small. This is consistent with the usual assumption of loss from the primary proton beam by charge exchange (i.e., conversion to H which is not measured by the SPS even if it is backscattered).

Assuming that both electron and proton angular distributions are isotropic over the upper hemisphere ($0^\circ \leq \alpha_p \leq 90^\circ$) in the cusp region, the fraction of the incident energy that is lost can be calculated. For protons in Figure 1b it is obvious (Figure 4) that all the incident primary energy ($1.0 \times 10^{-1} \text{ erg cm}^{-2} \text{ s}$) is deposited in the ionosphere. Using an average energy of ~ 1 keV and the results of Eather (1967) this energy loss corresponds to $\sim 5 R$ of $\text{H}\beta$ which is in good agreement with recent air-

borne measurements of the dayside aurora (Eather and Mende, 1971a). According to Figure 4 approximately 60% of the incident primary electron energy flux of 2.5×10^{-1} erg cm $^{-2}$ s is deposited in the ionosphere. Again these results are seen to be in quantitative agreement with Eather and Mende's (1971a) inference that particles causing distinct dayside aurora deposit $\sim 1.3 \times 10^{-1}$ erg cm $^{-2}$ s $^{-1}$ into the ionosphere and have an average energy of ~ 100 to 200 eV (see Figure 3).

5. Extent of Magnetosheath Plasma Penetration and its Dependence on K_p

As pointed out earlier Λ_{CL} is defined empirically as the boundary between hard structureless outer zone fluxes and softer structured cusp fluxes. Physically Λ_{CL} is the last closed magnetic field line on which significant bounce motion between hemispheres can be maintained (i.e., closed on the dayside of the magnetosphere). Between Λ_{CL} and Λ_{CU} (the upper limit of cusp proton fluxes) the ISIS 1 data indicates that terrestrial field lines have continuous free access to magnetosheath plasma. Figure 6 illustrates the extent of this region of magnetosheath plasma penetration in MLT (8 to 16 hr). Data for a given hour interval are averaged and plotted at the mid-point of the interval. The largest sampling density is in the forenoon, $K_p \leq 3$ region with less statistical accuracy for other points. The lower limit of penetration, Λ_{CL} , is observed to be largest at local magnetic noon with a decrease before and after midday. Also Λ_{CL} is observed to move progressively equatorward with increasing K_p . The upper limit, Λ_{CU} , of cusp fluxes is observed to be less responsive to changes in K_p (it should be noted, however, that due to orbit parameters the sampling density for Λ_{CU} is much less than Λ_{CL}). Also Λ_{CU} does not exhibit the same statistical magnetic time dependence as Λ_{CL} . For some passes at increased K_p , Λ_{CU} is observed to track Λ_{CL} (i.e., the whole cusp moves equatorward without an appreciable change in width). A comparison with changes in solar wind and interplanetary magnetic conditions would probably be more appropriate.

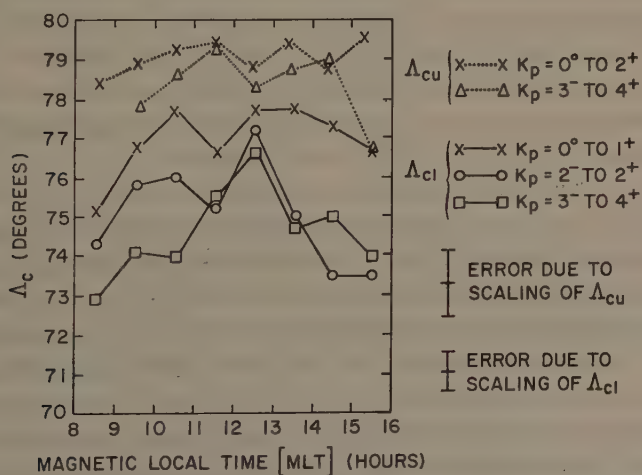


Fig. 6. Extent of magnetosheath plasma penetration in MLT and IN Lat as a function of K_p .

te than the above comparison to K_p . Such a comparison is presently being undertaken and will be reported in a future paper.

The above results do not imply that softer fluxes of electrons and protons do not exist before and after 8 and 16 hr MLT. Significant fluxes of low energy particles are indeed present outside these limits but their spectra peak at higher energies and do not in general exhibit magnetosheath characteristics.

For magnetically quiet periods the boundary (in MLT) of magnetosheath fluxes can be quite sharp. During days when the LT is ~ 7 to 8 (or 16 to 17) hr, the dipole wobble causes a large diurnal variation in MLT. When the dipole tilt results in times inside the 8 to 16 hr MLT interval, magnetosheath fluxes are observed; when MLT is outside this period, non-magnetosheath fluxes are observed. During more disturbed periods magnetosheath fluxes are observed as early as 0500 MLT and as late as 1800 MLT as evidenced by Figure 1.

Using the result of Fairfield (1968) the 8 to 16 hr MLT interval at ISIS 1 altitudes maps into the magnetic equatorial plane at ~ 06 and 18 hr LT (i.e., solar dawn-dusk). Thus if we take these results at face value, magnetosheath plasma has access to the magnetosphere across its entire front side during quiet periods and over a larger extent during disturbed periods. It will be extremely interesting in terms of magnetospheric structure and dynamics if the above results inferred from low-altitude measurements are verified by a comprehensive *in situ* survey.

6. Comparison with Other Observations of Dayside Cusp Fluxes

Winningham (1970) and Heikkila and Winningham (1971) compared their dayside high latitude spectra with earlier magnetosheath spectra and inferred that the magnetosheath is the source for the dayside 'soft zone'. This comparison obviously suffers in that the measurements compared are neither concurrent in time and meridian nor obtained for similar solar wind and geomagnetic conditions. Also Winningham's (1970) and Heikkila and Winningham's (1971) observations were obtained during the recovery phase of a magnetic storm where K_p was 5+ and ΣK_p equalled 41+. These results (mainly the latitudinal width of the cusp) could thus be construed as a transient phenomenon occurring only during large storms. As pointed out earlier in this work and that of Winningham (1970) this is not the case, however.

Figure 7 details a comparison of near coincident electron spectra obtained with the high latitude, high inclination IMP 5 spacecraft (Frank, 1970) and the low altitude ISIS 1 polar satellite on July 11, 1969. These observations were made within ~ 2 hr of UT and LT and during a relatively quiet period with $K_p = 1$, $A_p = 6$, and $\Sigma K_p = 11$. The electron average energy is ~ 60 eV and the electron number and energy fluxes are lower than normal (presumably a result of the quieter solar wind conditions, $V_H = 332$ km s $^{-1}$ and $N_H = 3.7$ cm $^{-3}$). For the region of energy overlap the ISIS 1 cusp spectrum is observed to be in quantitative agreement with the magnetosheath and mid-altitude cusp spectra obtained concurrently by IMP 5. The outer zone electron spectra are also observed to be in quantitative agreement (the outer zone fluxes were

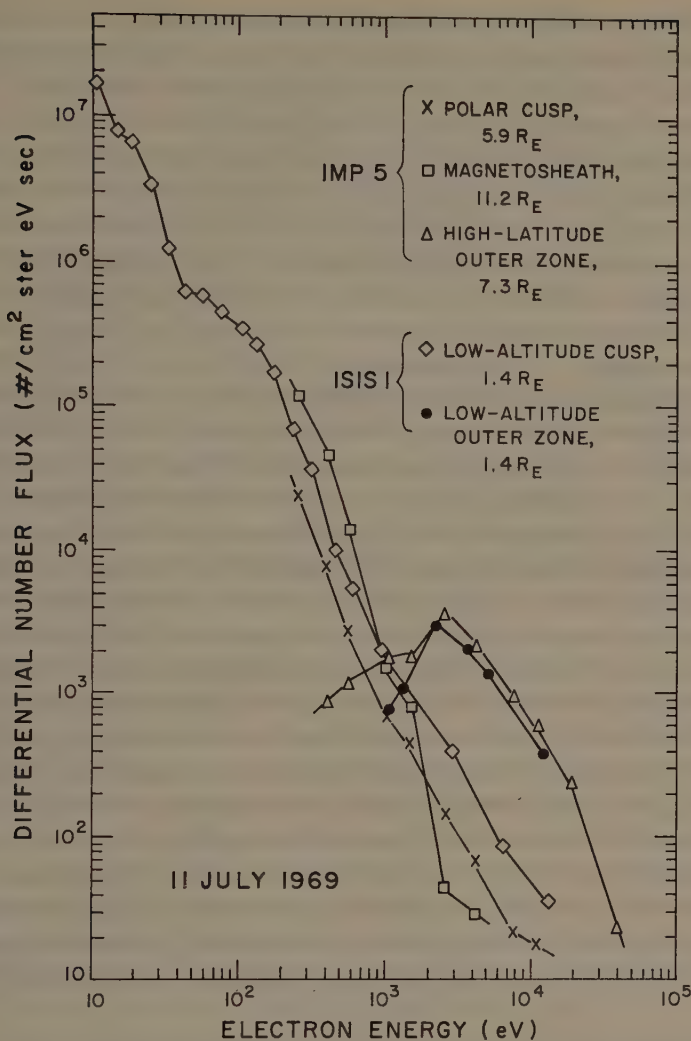


Fig. 7. Comparison of outer zone and cusp spectra obtained within 2 hr LT and UT on July 11, 1969, with ISIS 1 and IMP 5.

also much lower here than during more disturbed periods). The width of the cusp was however at least 2.5° even for these low K_p and solar wind conditions. A_{CU} and the actual width could not be determined because data transmission began within the cusp region. The above results are in agreement with other quiet time ISIS 1 cusp data and indicate the large width to be a permanent feature.

The proton directional number flux ($3 \times 10^6 \text{ cm}^{-2} \text{ sr s}$) was also low for this cusp traversal and the proton average energy was low ($\sim 300 \text{ eV}$). This is also quite likely a result of the quiet solar wind (and presumably magnetosheath) conditions during this period.

As discussed earlier fluxes of protons and electrons with magnetosheath characteristics are observed nearly continuously in a 2 to 3° zone (Figure 6) above the limit of closed field lines (evidenced by a large drop in the outer zone fluxes). Frank and Ackerson (1971) gave two examples of very narrow (20 to 30 km or $\Delta A = 0.2^\circ$) electron spikes obtained with INJUN 5 which they identify as the low altitude signature of the cusp. At $A_{CU} = 76.5^\circ$ (19:51:30 UT) in Figure 1a a large increase in both the number and energy flux is observed, but the average energy and spectral shape are similar to the remainder of the cusp. This feature is 3 s (~ 21 km) wide and is probably similar to the narrow (20 to 30 km) features observed by Frank and Ackerson (1971) (see section 7). Other examples of this narrow feature have been observed in the ISIS 1 data (see Winningham, 1970) and are generally found close to either A_{CL} or A_{CU} .

An apparent discrepancy also exists between the ISIS 1 and IMP 5 results. Frank (1970) observed 690 to 1100 eV protons to lie poleward of 305 to 510 eV electrons in the mid-altitude cusp. In general no such separation is observed in the ISIS data and in particular no such separation is found in the data at 0900 UT on July 11, 1969.

Russell *et al.* (1971) reported a high altitude observation of the northern dayside cusp at 45° geomagnetic latitude during the large storm of October 31 to November 1, 1968. During quiet periods the inclination of OGO 5 does not allow it to traverse the cusp. They concluded the cusp to be moving back and forth at velocities comparable to the satellite in response to changes in geomagnetic and solar wind parameters. During the storm of February 2 to 3, 1969, A_{CL} was observed to move to as low as 67° at 1000 hr LT with ISIS 1. The cusp widths for two passes at $K_p = 6^-$ and 7 and low A_{CL} during this period were no larger than usual indicating the varying response of the cusp to changes in K_p . During a small storm on June 8, 1969, the northern cusp was observed to be 8° (~ 2000 km) wide at 3500 km ($A_{CL} = 75.5^\circ$, $MLT = 0300$ hr) for a time when K_p was 3^- (3^- was also the maximum K_p). This would correspond to ~ 800 km at auroral heights. As mentioned earlier in this paper and in Russell *et al.* (1971) changes in the cusp are probably more intimately related to changes in the solar wind and the interplanetary magnetic field than to changes in geophysical parameters.

7. Discussion

The results presented in this paper and those of Frank (1970), Winningham (1970), Frank and Ackerson (1971), Heikkila and Winningham (1971), and Russell *et al.* (1971) have established the existence of two cusp-like regions in the dayside magnetosphere and the penetration of magnetosheath plasma to low altitudes through them. The main difficulty in reconciling these various measurements lies in the width and structure of the cusp at auroral heights. Frank (1970), using IMP 5 data, indicates the low altitude width should map to 20 to 30 km ($\Delta A = 0.2^\circ$) at the ionosphere, and reports a feature of the INJUN 5 data (Frank and Ackerson, 1971) which would support this. On the other hand the ISIS 1 data indicate a region which is on the average ~ 2 to 3° wide at low altitudes.

The discrepancy between the ISIS 1 data and the projection of the IMP 5 data onto

the ionosphere can be resolved, I believe, in the following way. Frank (1970) indicates the latitudinal width of the cusp to be $\sim 1 R_E$ at its high altitude limit (which lies at $\sim 10 R_E$). If the results presented in this paper are correct, then the cusp will extend over the complete front surface of the magnetosphere. The length of the cusp will thus be $\sim \pi \times 10 R_E = 2 \times 10^5$ km which results in a magnetopause cusp area of $dA_s = 1.3 \times 10^9$ km². Using a value of B at $10 R_E$ of $B_s = 50 \gamma$ (Fairfield, 1971) and $B_1 = 0.5$ G at auroral heights the ratio of B_s/B_1 will be 10^{-3} . Using the conservation of flux, dA_1 (the cusp area at low altitudes) is given by

$$\begin{aligned} dA_1 &= (B_s/B_1) dA_s \\ dA_1 &= 1.3 \times 10^6 \text{ km}^2. \end{aligned}$$

The longitudinal extent of magnetosheath fluxes reported in this paper is ~ 4000 km which results in a latitudinal width of ~ 320 km (3°) at auroral heights which is in good agreement with the ISIS 1 observations. Frank (1970) also indicates that the cusp width does not increase more than a factor of 2 even for disturbed conditions. Everything else being the same, a factor of 2 increase in width at the magnetopause would result in a width of ~ 1900 km at 3500 km. This is also in good agreement with the maximum cusp width of 2000 km observed with ISIS 1 at this altitude on June 8, 1969, as mentioned earlier.

The difference in widths observed at low altitudes by INJUN 5 and ISIS 1 could be the result of different instrumental sensitivities. Another, and more likely, possibility exists in the impression gained from a spectrogram presentation and the inferences made therefrom. Frank and Ackerson (1971) associated the sharp low energy electron burst at 23:31:00 UT (their plate 6a) with the low altitude cusp. This burst was superimposed on a broad lower intensity soft electron flux which was considered not to be a direct part of the low altitude cusp. However, inspection of their proton results (Gurnett, 1971) indicated that the cusp for plate 6A of Frank and Ackerson (1971) instead extended 2° above the sharp 0.2° wide burst. This brings the ISIS 1 and INJUN 5 data into closer agreement and points up the need to define the cusp from both electron and proton results as is done with the ISIS 1 data.

Frank (1971), in a recent letter, has indicated that his original estimate (Frank, 1970) of the low altitude cusp width was much smaller than the average value of 200 km obtained from a larger set of IMP 5 data. This updated width brings the IMP 5 observations into much closer agreement with those observed by ISIS 1 and calculated in this section. However, this larger set of IMP 5 data still indicated two distinct, yet not mutually exclusive, field aligned 'sheets' of proton and electron fluxes (with electrons lying equatorward of protons) at mid-altitudes in the cusp. No evidence of such clear separation can be found in the ISIS 1 data. Protons, if above the instrument threshold, are always coincident with electron fluxes. Electron fluxes in the cusp do have bursts superimposed on a background continuum flux but these electron bursts have no counterpart in the accompanying proton fluxes. Also no evidence for proton precipitation poleward of electron precipitation is observed in airborne photometric data (Eather and Mende, 1971b). If this sheet structure is a permanent

feature of the cusp at mid-altitudes it then appears that 'remixing' of the plasma must occur between 5 and 1.5 R_E . The resolution of this question should be possible by a careful intercomparison of the available ground based and satellite data pertinent to the dayside magnetospheric cusps.

8. Conclusions

From the data presented in this and earlier works by Winningham (1970), and Heikkila and Winningham (1971) the following conclusions are reached:

(a) The long postulated free access of magnetosheath plasma to ionospheric heights does exist.

(b) Access of magnetosheath plasma extends from 0800 to 1600 MLT and is on the average 2 to 3° IN Lat wide at auroral heights.

(c) Using the results of Fairfield (1968) penetration through the dayside magnetospheric cusps occurs over the complete front side of the magnetosphere and during disturbed periods possibly over a larger extent.

(d) The postulated separation of proton and electron fluxes at mid-altitudes in the dayside cusps is not present at heights $\leq 0.5 R_E$.

(e) The dominant effect of increased magnetic activity is an equatorward motion of the boundary between open and closed field lines with the largest cusp width being approximately a factor of 2 greater than the average.

(f) The energy and number flux and particle average energies are sufficient to explain observed dayside auroral phenomena.

(g) Electron spectra observed concurrently at low and mid-altitudes in the cusp and outer zone are similar in shape and magnitude.

References

- Burrows, J. R.: 1971, private communication.
 Eather, R. H.: 1967, *Rev. Geophys.* **5**, 207.
 Eather, R. H. and Mende, S. B.: 1971a, *J. Geophys. Res.* **76**, 1746.
 Eather, R. H. and Mende, S. B.: 1971b, Paper presented at Advanced Study Institute on Magnetosphere-Ionosphere Interactions, Dalseter, Norway.
 Fairfield, D. H.: 1968, *J. Geophys. Res.* **73**, 7329.
 Fairfield, D. H.: 1971, private communication.
 Frank, L. A.: 1970, *U. of Iowa Report*, 70-55.
 Frank, L. A.: 1971, *J. Geophys. Res.* **76**, 2512.
 Frank, L. A. and Ackerson, K. L.: 1971, *J. Geophys. Res.* **76**, 3612.
 Gurnett, D.: 1972, this volume, p. 233.
 Heikkila, W. J.: 1970, *J. Geophys. Res.* **75**, 4877.
 Heikkila, W. J. and Winningham, J. D.: 1971, *J. Geophys. Res.* **76**, 883.
 Heikkila, W. J., Smith, J. B., Tarstrup, J., and Winningham, J. D.: 1970, *Rev. Sci. Instrum.* **41**, 1393.
 Rees, M. H.: 1964, *Planetary Space Sci.* **12**, 722.
 Russell, C. T., Chappell, C. R., Montgomery, M. D., Neugebauer, M., and Scarf, F. L.: 1971, *J. Geophys. Res.*, **76**, 6743.
 Winningham, J. D.: 1970, Dissertation, Texas A & M University.

MECHANISMS FOR THE INJECTION OF PROTONS INTO THE MAGNETOSPHERE

G. P. HASKELL and R. J. HYND S

*Dept. of Physics, Imperial College of Science and Technology,
London S.W. 7, England*

1. Introduction

Energetic solar particles detected at low altitudes over the polar caps can be considered to be 'probes' of large regions of the outer magnetosphere including the magnetotail, and should help us to understand the physical processes occurring in the magnetosphere. Flux profiles of low energy (~ 1 MeV) solar protons over the polar caps have been studied by many workers, beginning with Williams and Bostrom (1967) and Blake *et al.* (1968). In this paper we try to identify some of the processes that lead to structure in the profiles in the region of closed field lines. We also show that the use of a suitable coordinate system improves our insight into the causes of structure observed on open field lines.

The data to be presented were obtained from a proton telescope on the low altitude polar satellite ESRO 2 (Bewick *et al.*, 1970). Protons in the energy range 2 to 17 MeV were measured every 16 sec. Since the satellite was not aligned with the earth's magnetic field, and because the counts were accumulated over several spacecraft spin periods an omni-directional type of measurement was obtained. The data have been corrected for the atmospheric loss cone beneath the satellite at times when the viewing cone of the detector swept through this loss cone. The flux was assumed to be isotropic outside this loss cone for the purpose of this correction.

2. Closed Field Lines

Much of the structure in solar proton profiles has nothing to do with processes occurring in the tail, but is determined by the topology and dynamics of the closed field line region of the magnetosphere. Let us first consider the kind of profile we should expect in a typical field configuration, assuming that the adiabatic invariants of particle motion are conserved for the solar protons, that Liouville's theorem applies, and also that the interplanetary proton flux is isotropic. Near the last closed field lines, the directional flux measured at low altitudes should be equal to the flux in interplanetary space near the earth. This is because the low energy protons follow the field lines fairly closely, and the last closed field lines pass either to the surface of the magnetosphere or to the inner edge of the neutral sheet which we assume to be readily accessible to protons from outside the magnetosphere.

In the pseudo-trapping region, which is the region between the last closed field lines and the last closed drift shell, protons detected at low altitudes can be traced back

through their bounce and drift motions on the closed field lines, either to the surface of the magnetosphere on the dayside or to a region very close to the neutral sheet. The directional flux in the pseudo-trapping region should therefore be equal to the flux at the last closed field line. The omnidirectional flux should be less because particles with small pitch angles are lost into the atmosphere at the first bounce and the loss cone subsequently remains empty.

The above argument is essentially that used by Flindt (1970) to account for the 'edges' in the profiles observed by Injun 4 in the neighborhood of the last closed field lines. If we add the possibility of delayed access of the protons to higher latitudes (Östman and Hynds, 1971), then during the rising phase of an event peaks instead of edges are to be expected near the last closed field lines as shown in Figure 1a.

The adiabatic invariants are not conserved if the magnetic field changes too rapidly in time or in space. Computations in a model field (Morfill, 1971) have shown that

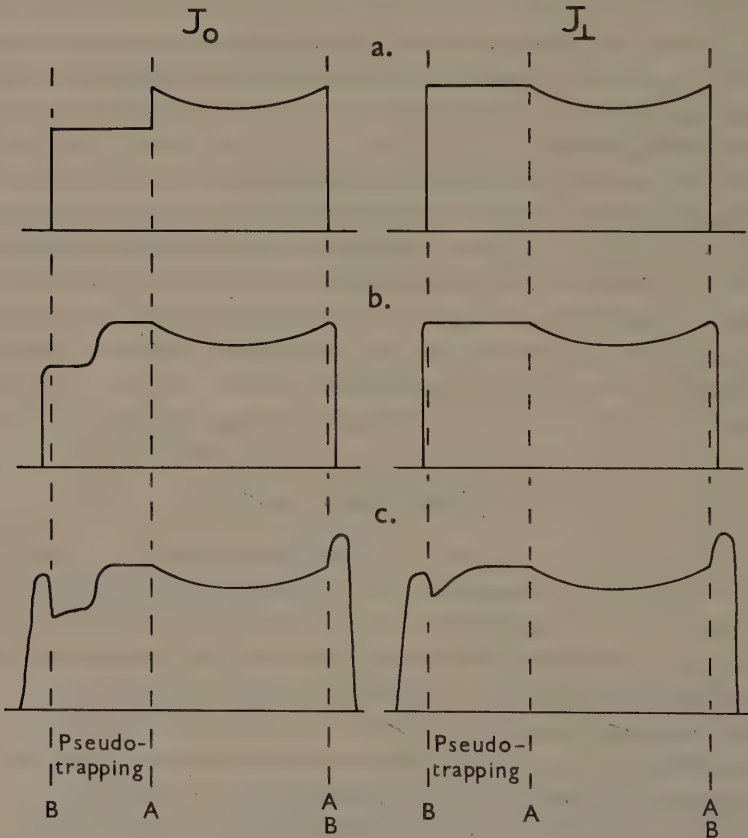


Fig. 1. A schematic diagram showing the flux profiles expected on a noon-midnight low altitude satellite pass under various physical assumptions described in the text. J_0 is omnidirectional flux. J_{\perp} is directional flux measured outside the atmospheric loss cones. The vertical dashed lines mark the last closed field lines (A) and closed drift shell (B). These coincide at midnight but are separated by the pseudo-trapping region at noon.

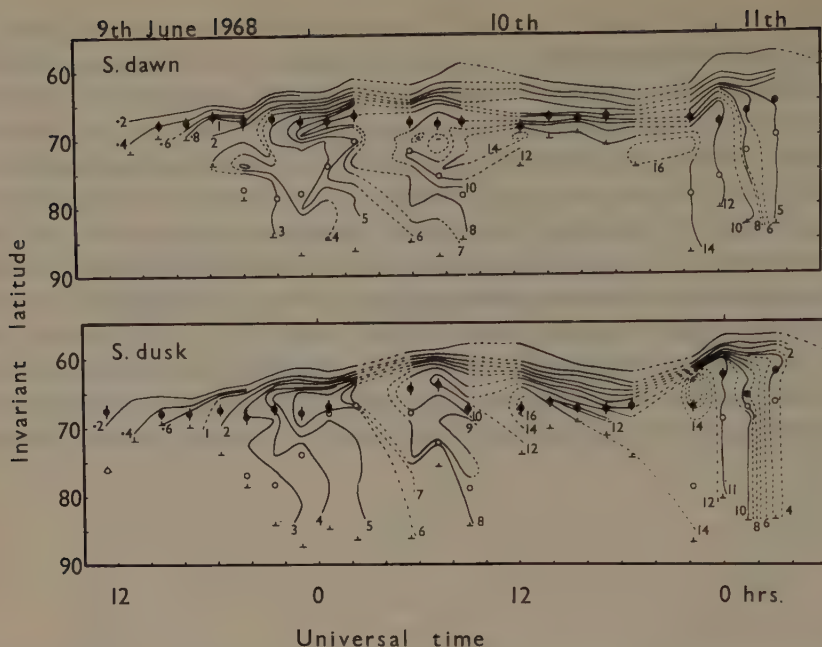


Fig. 3. Data from 22 passes over the southern polar cap are summarized by contours of constant flux of 2–17 MeV protons. Contours are labelled in units of 100 counts/15.875 s. Each satellite pass corresponds to a vertical line through an inverted T symbol which also marks the highest latitude reached by that pass. Solid dots mark the measured boundary of stably trapped electrons of energy > 1.2 MeV (Bewick *et al.*, 1970). Open circles mark the intersection of the orbits with Taylor's (1967) calculated pseudo-trapping boundary.

of strong pitch angle scattering are shown in Figure 2. In the flux profiles, we should expect to find a broad peak centered a little below the last closed field line as shown in Figure 1b. We suggest that the edges measured by Flindt (1970) do not mark the boundary of the pseudo-trapping region determined by the last closed field line, but mark the latitude at which the strong pitch angle scattering ceases. In Figure 3 the open circles show where the orbits cross Taylor's (1967) calculated pseudo-trapping boundary. During the rising phase of the event the high latitude peaks in Figure 3 tend to follow the open circles and we suggest that they are produced in the manner described above.

The above arguments suggest that there should be very little loss of flux during longitudinal drift in the pseudo-trapping region. However, we have measurements (Figure 4) in which substantial loss of flux occurs in the low latitude part of the pseudo-trapping region. This flux loss also occurs in the adjacent stable trapping region. (The boundary of stably trapped electrons $E > 1.2$ MeV is marked by arrows.) This can be explained by weak pitch angle diffusion, presumably resulting from gyro-resonance with hydromagnetic waves, which changes the distribution of equatorial pitch angles. The results suggest that isotropic flux enters on the dusk side and

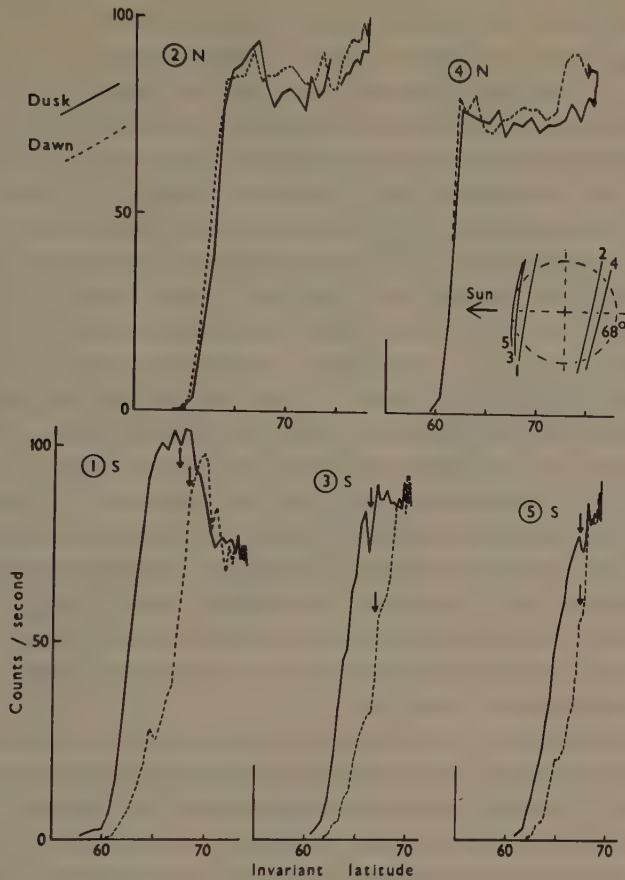


Fig. 4. Five consecutive passes beginning at 12 hr on June 10 alternately from the northern and southern polar caps, showing flux loss during drift from dusk to dawn on the dayside. For the southern passes the detector did not view the loss cone at all, but a significant correction for the loss cone has been applied to the northern data. The arrows mark the measured boundary of stably trapped electrons of energy > 1.2 MeV.

then, as the particles drift to the dawn side, the equatorial pitch angle distribution approaches the 'normal' distribution (Roberts, 1969) with a maximum at 90° . In this way the total number of particles in the flux tube can decrease by a very small fraction while the flux measured within a small range of pitch angles near the edge of the loss cone can decrease by a large fraction. In order to maintain the steady state where the protons are stably trapped the flux must be made isotropic again by strong pitch angle diffusion as the protons drift across the nightside. It is clear from Figure 4 why there is a dawn-dusk asymmetry in cutoff latitudes when the cutoff is defined as the point at which the flux begins to fall (Thomas *et al.*, 1970), whereas there is little or no asymmetry when the cutoff at very low flux values is chosen (Bewick *et al.*, 1970).

Peaks frequently occur near the boundary of stably trapped electrons ($E > 1.2$ MeV) which is marked by the solid dots on Figure 3. When these peaks occur on the night-side (where the solid and open circles are very close), they can be understood in terms of delayed access to open field lines as illustrated in Figure 1b. When these peaks occur on the dayside (where the solid and open circles are far apart or no open circle is plotted), then the foregoing discussion provides no explanation. Because the peaks are associated with the stable trapping boundary, it is tempting to suppose that they are produced by a mechanism that relies on the protons entering the stable trapping region and drifting many times around the earth. There is now a large amount of evidence that solar protons do become stably trapped (Lanzerotti, 1968; Bewick *et al.*, 1970; Lanzerotti *et al.*, 1971). Under these circumstances large scale electric fields across the magnetosphere would be able to accelerate the protons to produce peaks.

L shell diffusion, which implies breakdown of the third invariant, would automatically accompany this acceleration if the first and second invariants were conserved (Fälthammar, 1965; Birmingham, 1969). But we have shown in Figure 4 that the first invariant is not conserved. However, large scale electric fields can still accelerate the protons as they drift around the earth, no matter what their pitch angles, and the pitch angle diffusion itself is capable of producing L shell diffusion if the magnetic field is asymmetric. Therefore the same qualitative result – inward diffusion and acceleration – is still expected even when all three invariants are violated. A quantitative explanation is more difficult (Walt, 1971).

Figure 1c summarizes the main features we expect to see in and near the region of closed field lines as a result of the following physical processes: (a) delayed access to tail field lines, (b) strong pitch angle scattering near the last closed field lines due to large spatial gradients in the magnetic field, (c) weak pitch angle scattering at low latitudes on the dayside, and (d) acceleration and L -shell diffusion on closed drift shells. All the features shown schematically in Figure 1c can be seen in the data shown in Figures 3 and 4.

3. Open Field Lines

Within the space available it is not possible to review the considerable volume of published work on intensity variations observed on so-called 'open' lines of force, and the subsequent discussions of the problem of particle access to the polar cap regions. All we will attempt is a review of recent work done on the problem at Imperial College, and a discussion of it in respect to directly related published work.

A major problem in the study of proton intensity variations over the central polar cap regions is the lack of a satisfactory coordinate system with which to organize the data. At Imperial College we have attempted to deal with the coordinate problem by using a model of the earth's magnetic field to trace back points from the polar cap region, down the tail, and so project the polar cap regions onto a cross section of the tail. However, before we consider this approach we wish to briefly outline our thinking on the basic physics involved.

Our approach to the analysis of the ESRO 2 data has been governed by an attempt

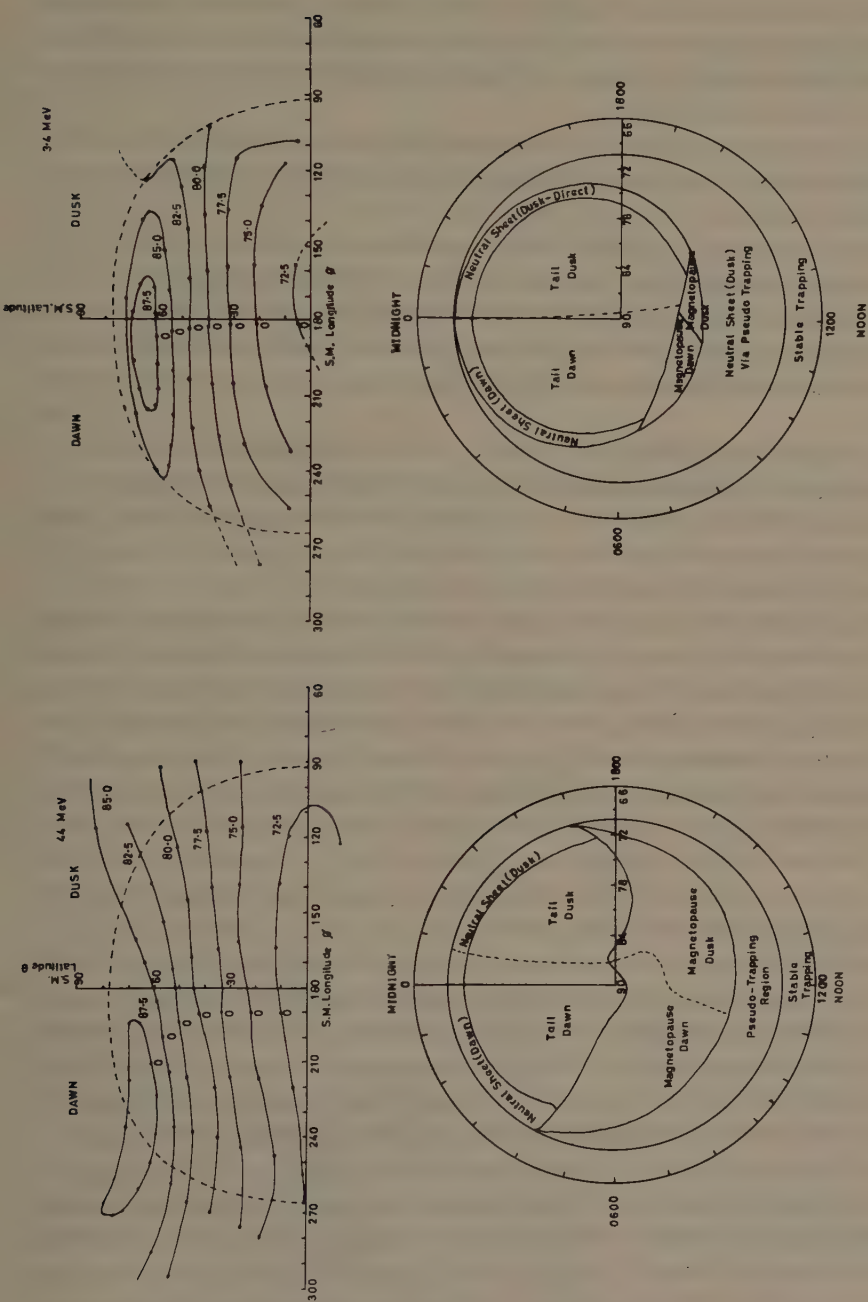


Fig. 5. The upper half of Figure 5a shows contours of IN Lat-MLT. (the dots represent two-hourly intervals of MLT with 0 corresponding to midnight) projected onto a cross section of the magnetospheric tail at a distance of $15 R_E$, plotted as a function of solar magnetospheric (S.M.) latitude and longitude. The contours were derived by trajectory tracing for 44 MeV protons from a height of 100 km with zero pitch angle over the polar cap. The lower half of Figure 5a shows, as a function of IN Lat and MLT, the magnetopause entry points derived from the same 44 MeV proton trajectories. Figure 5b shows similar plots for protons of 3.4 MeV. The Williams and Mead model field parameters used were $R_s = 10 R_E$, $R_t = 10 R_E$, $R_f = 200 R_E$ and $B_T = 12.5 \gamma$.

to resolve the following problem: Are solar proton intensity variations observed on 'open' lines of force a first order effect of anisotropies and inhomogeneities in the solar proton intensity outside the magnetosphere, with a *quasi-static* magnetotail structure playing a second order role, or is the dominant mechanism a dynamical structure for the magnetotail, with the solar proton external anisotropies and inhomogeneities in the second order role?

In the above *quasi-static* is taken to mean a magnetosphere within which Liouville's theorem applies, while *dynamical* is the case when Liouville's theorem breaks down, e.g., scattering occurs.

For protons of energies > 10 MeV there now seems to be good evidence that the magnetotail plays the quasi-static role (Durney *et al.*, 1971; Engelmann *et al.*, 1971; Morfill and Quenby, 1971). Engelmann (1972) deals with this aspect in detail.

At energies below 10 MeV, and in particular around 1 MeV, the situation is less clear. We report in this paper some of the work done at Imperial College on this problem.

Following suggestions (Elliot, 1970; Quenby, 1970) Morfill (Morfill and Quenby, 1971), by using particle trajectory calculations in the Williams and Mead model of the earth's magnetic field, has attempted to construct coordinate systems more suited to the analysis of intensity variations on 'open' lines of force than the commonly used IN Lat-MLT plots. Two such systems have evolved.

In the first, particles with zero pitch angle are traced back from points at a height of 100 km over the polar cap region down the tail for distances of between 15 and 25 R_E . Within this distance the particles either leave the tail via the neutral sheet or the flanks of the magnetopause, or are still wholly contained within the tail. This procedure is applied over the whole polar cap area and a series of contours drawn over the area showing the entry point to the tail, within the given tail distance, of the particles. The resulting plot is shown in the lower parts of Figure 5a and 5b for particles of 44 and 3.4 MeV, respectively. Thus we have a standard IN Lat-MLT coordinate system, with a series of overlaid contours showing where the particles observed at a particular point entered the tail.

In the second system, particles are again traced back down the tail from a height of 100 km over the polar cap. At a fixed distance down the tail (either 15 or 25 R_E) if the particle is still contained within the tail, the originating IN Lat-MLT coordinates are plotted on the cross section of the tail. By repeating this process the IN Lat-MLT plot is projected onto a cross section of the tail. The upper parts of Figure 5a and 5b show the results of such a process for particles of 44 and 3.4 MeV, respectively.

The advantage of these systems of coordinates is that they provide a much clearer physical insight into the access of the particles into the tail. What are the problems associated with their use?

Figure 5a and 5b refer to computations that have traced particles 15 R_E down the tail, using a 12.5 γ tail field strength. This immediately defines the first problem, that of selection of a suitable tail field strength, since this is the most critical variable

parameter in the Williams and Mead field model. In general, an empirical approach is necessary, selecting a tail field strength that provides a reasonable fit to the trapping zone boundary and that is compatible with the recent substorm activity in the tail. The value used in Figure 5a and 5b is rather low and was obtained using this sort of approach to the early stages of the November 18, 1968, event (Durney *et al.*, 1971).

A second problem concerns the distance down the tail necessary to trace the particle trajectories. The difficulty here is curvature of lines of force which causes the particle trajectories to drift for protons to the dawn side of the magnetotail. For particles ~ 1 MeV, this is no longer a problem at $15 R_E$. At higher energies a distance of $20 R_E$ may be more appropriate. Of course any magnetic field gradients across the tail have a similar effect. However, away from the neutral sheet and magnetopause, the gradients out to at least $80 R_E$ are small (Behannon, 1970). Thus, provided caution is exercised over trajectories that pass very close to the neutral sheet or the magnetopause, this is not a problem.

Caution must be applied in the use of such coordinate systems in the sense that they are not absolute systems, i.e., within the time scale of one event the tail field strengths may vary significantly. Thus a change from 12.5 to 40γ can shift the latitudes of the boundary contours by up to 3° . Hence while of considerable help with the physical interpretation they do not really help resolve spatial or temporal variation problems.

As an example of the use of these coordinate systems we have taken some low energy proton data ($2 < E < 17$ MeV) from the February 25, 1969 event. The observations cover 3 northern polar cap passes between 2033 and 2400 UT, about 11 hr after high energy protons were first detected in the vicinity of the earth. At this time a significant particle anisotropy existed outside the magnetosphere for protons of a few MeV, while at energies > 30 MeV the anisotropy had vanished (Engelmann *et al.*, 1971). The low energy proton anisotropy was approximately aligned with the magnetic field direction.

Figure 6 shows the 3 passes in consecutive order. The lower part of each figure shows the satellite trajectory plotted on the polar cap system and the upper half of each figure shows the trajectory plotted on the cross section of the tail system. To represent the proton counting rates we have drawn perpendiculars of length proportional to the counting rates along the path of the trajectories. A tail field strength of 12.5γ was used in the magnetic field model and the trajectories traced a distance of $15 R_E$ down the tail.

The lower part of Figure 6a shows a marked enhancement of counting rate in the region of access from the dawn side neutral sheet, which we consider to be additional evidence that we have selected the correct tail field strength. We also see that particle intensity gradient exists across the open lines of force with a marked dawn-dusk asymmetry across local midnight. The upper half of Figure 6a shows the same data projected onto the tail cross section.

Figures 6b and 6c show the two subsequent passes displayed in a similar fashion, and we see that the intensity gradient across the tail is maintained during these passes.

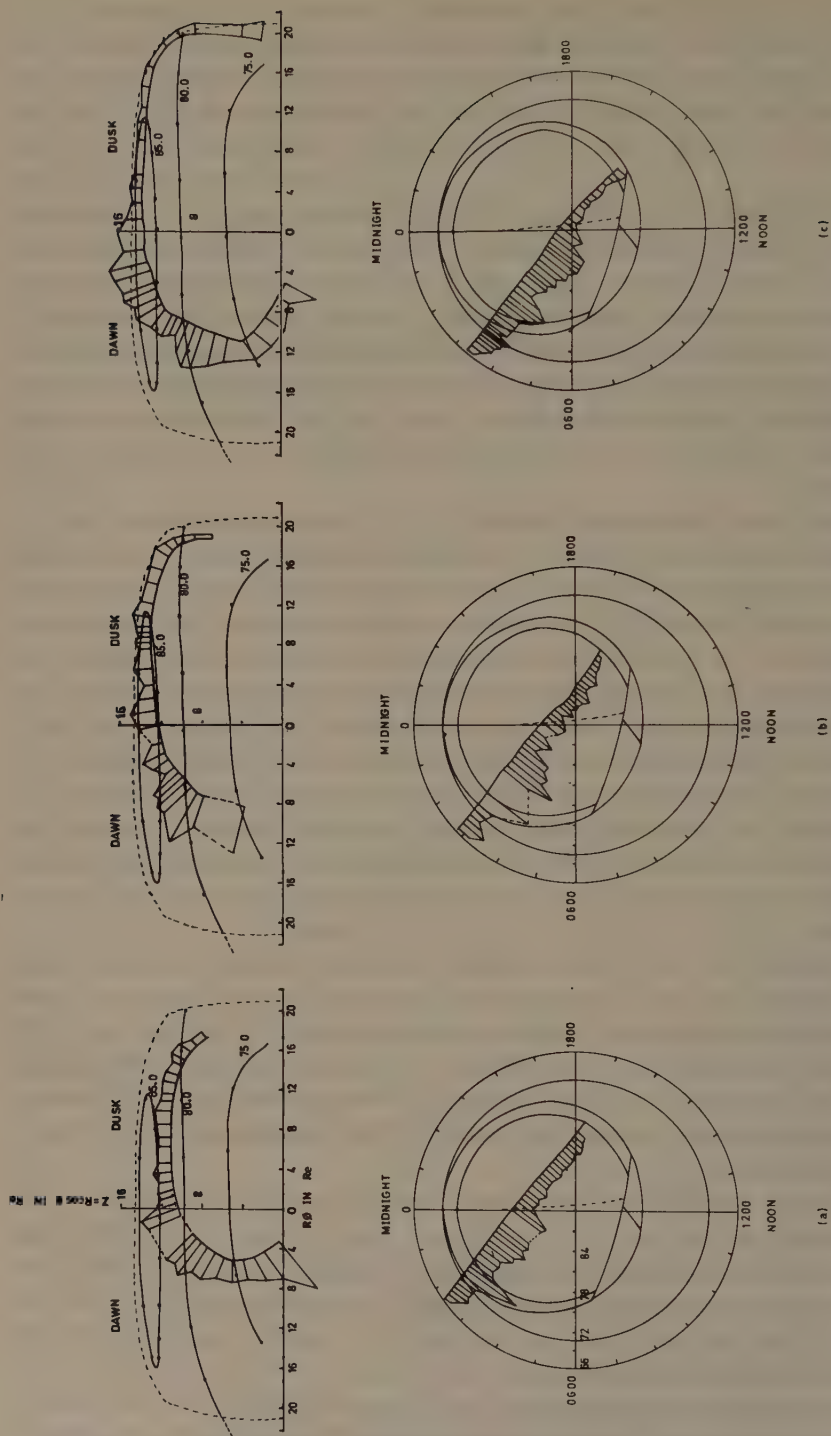


Fig. 6. This figure shows three satellite passes of the ERSO 2 satellite projected onto the coordinate systems shown in Figure 5b. The passes correspond to 2033 to 2047 UT, 2210 to 2225 UT, and 2347 to 2402 UT on Feb. 25, 1968. Perpendiculars to the trajectory paths have been drawn of length proportional to the $2 < E < 17$ MeV proton intensities observed at these times. The coordinates are similar to those of Figure 5 except that the coordinates of the tail projection now give equal areas on the cross section of the tail. $R = 15 R_E$, θ is the colatitude and ϕ is the longitude measured from midnight.

An examination of the upper halves of Figures 6a, b, and c suggests that the whole of the dawn side of the northern tail lobe is more strongly 'illuminated' with protons than the dusk side. Data for protons of $E > 30$ MeV show no significant flux gradient across the tail during this period (Engelmann *et al.*, 1971). Figure 6c has a number of interesting features. The polar cap plot shows that the intensity maximum associated with the dawn side neutral sheet region may have been displaced to a higher latitude. We consider this to be an example of a small drift in the coordinate system due to an increasing magnetic tail field strength as a result of a pre-substorm buildup, with the substorm occurring within 2 hr. From this plot we also see evidence that the dusk side neutral sheet region is depleted of particles relative to the dawn side region. Finally, from the tail cross section projection of Figure 6c we see a very clear example of the dawn side of the northern tail lobe showing a significantly greater intensity of solar protons than observed close inside the magnetopause on the dusk side.

To summarize, we have established that at this stage of the event a marked dawn-dusk particle asymmetry existed across the northern tail lobe, with evidence to suggest that the whole of the dawn side of the lobe was more strongly 'illuminated' with solar protons than the dusk side. Also that the dusk side neutral sheet region was depleted of particles relative to the dawnside region.

We relate this dawn-dusk particle asymmetry to the strong particle anisotropy that existed outside the magnetosphere at this time (Balogh and Hynds, 1970). This anisotropy was from west of the earth-sun line and approximately in the plane of the ecliptic. This interpretation is supported by the absence of an asymmetry across the tail and lack of an external anisotropy for protons of $E > 30$ MeV (Engelmann *et al.*, 1971).

The form of the asymmetry across the tail should provide us with information as to the method of particle access to the tail. We need to consider the problem of relatively good access to the dawn side, and poor access to the dusk side of the tail when a particle anisotropy is incident on the dawn side. There are at least two possibilities. One is diffusion perpendicular to the lines of force with a non-uniform diffusion coefficient across the tail. The second requires a particle coupling mechanism across the magnetopause which acts more efficiently on the dawn side.

We dismiss the first possibility since during the November 18, 1968, event we have data showing a reversal of the tail asymmetry following a change in the external anisotropy direction from west to east of the earth-sun line.

The simplest particle coupling mechanism across the magnetopause is direct connection between the interplanetary and tail field lines (Dungey, 1961). Such a method of particle access has a number of problems associated with it (Durney *et al.*, 1971). We should like to make an additional point. If no external particle gradients exist outside the magnetosphere and the anisotropy is field aligned then direct access via coupled lines of force will produce a radially symmetric gradient in the tail, and *not* a gradient across the tail. Under these conditions, the existence of a gradient across the tail could only be explained in terms of asymmetric reconnection of the

front of the magnetosphere. While such asymmetry might be maintained for short periods, it could not be maintained for a number of hours. Thus this is an additional way of studying possible reconnection models.

A form of particle coupling across the magnetopause which relies on reconnection of field lines plus a diverging magnetic tail, and which overcomes the access problems inherent in the Dungey model, has been suggested by Morfill (Durney *et al.*, 1971; Morfill and Quenby, 1971). This mechanism, which relies on the particle trajectory reversing effects of two sets of inclined magnetic field lines plus the diverging tail field to provide access across the entire polar cap, seems plausible at energies of a few tens of MeV and upwards. However, a particle is required to make multiple crossings of the magnetopause, over a distance of the order of 10 to 100 R_E , to effect a reversal of the particle direction from along the interplanetary field line to moving back towards the earth.

There seems good evidence (Montgomery and Singer, 1969) that the magnetopause has an efficient isotropising effect on low energy protons. If this is due to scattering caused by a magnetopause that appears irregular to protons of these energies, then it seems unlikely that Morfill's proposal would work for low energies, since the particle trajectories could not maintain the required directions in their multiple crossings of the magnetopause. However, it is of interest that such a mechanism could possibly produce a 'well coupled' dawn side and a 'poorly coupled' dusk side for protons of energies of a few tens of MeV, and an anisotropy directed from the west of the earth-sun line.

While the coupling mechanism suggested by Morfill breaks down at low energies it has been suggested (Morfill and Quenby, 1971) that an external anisotropy can still cause a low energy particle gradient across the tail. The reasoning is that the magnetopause isotropises the incoming radiation leading to a particle gradient between the two sides of the tail. The isotropic distribution plus the diverging tail field then provides the required access. Our result of a 'well coupled' dawn side and a 'poorly coupled' dusk side suggests the intensity on each side of the tail to be roughly uniform on that side. Two effects could prevent the above mechanism from accomplishing this. One is the coupling of the two sides via the neutral sheet. As we point out below, there are times when this coupling is poor. The second effect is that of line draping which couples the two sides of the tail and so tends to equalize a gradient. While such coupling may not be effective uniformly over the tail, it would seem to imply rather localized mechanism.

The final point of interest from Figure 6c is the suggestion that the dawn and dusk side regions of the neutral sheet do not show the same intensity during a single satellite pass. That this can occur is confirmed by data from the November 18, 1968, event. This could either be a temporal effect due to changes in the interplanetary flux occurring in the time taken by the satellite to cross the polar region, or more plausibly, due to poor particle coupling across the neutral sheet for protons of a few MeV. The implication of a rather turbulent neutral sheet region is in accordance with evidence from magnetic field measurements (Schindler and Ness, 1971).

4. Conclusions

A reasonably consistent picture of solar proton intensity variation within the pseudo-trapping region is beginning to emerge. The problem area is the boundary between the stable trapping and pseudo-trapping regions, where the transport process that injects solar protons well inside the stable trapping boundary is still undetermined.

A better understanding of the physical features of solar proton intensity variations occurring on open lines of force follows from the use of coordinate systems based on calculations of particle trajectories between the polar caps and the tail. The major problem here is the resolution of spatial and temporal variations, for which field model calculations are little help.

It seems clear that further significant progress can only be made by an integrated type of approach, i.e., by studying the phenomena over a range of energies and of a number of places, simultaneously. This approach has already provided some very useful results (e.g., Williams and Bostrom, 1967; Lanzerotti *et al.*, 1970; Engelmann *et al.*, 1971). Thus geostationary satellite field and particles measurements combined with polar cap and tail particle measurements should help with the problems of injection into the stable trapping region. For phenomena occurring on open lines of force particle measurements over the polar cap and in the tail combined with magnetic field, and directional particle measurements, outside the magnetosphere are essential. In the latter case, data from two spacecraft would greatly assist the problem of determining the particle gradients.

Acknowledgments

We have benefited greatly from discussions with our colleagues in the Cosmic Ray and Space Physics Group, especially H. Elliot, G. E. Morfill and R. P. Rampling.

References

- Balogh, A. and Hynds, R. J.: 1970, in V. Manno and D. E. Page (eds.), *Intercorrelated Satellite Observations Related to Solar Events*, D. Reidel Publishing Company, Dordrecht, Holland, p. 471.
- Behannon, K. W.: 1970, *J. Geophys. Res.* **75**, 743.
- Bewick, A., Haskell, G. P., and Hynds, R. J.: 1970, *J. Geophys. Res.* **75**, 4605.
- Birmingham, T. J.: 1969, *J. Geophys. Res.* **74**, 2169.
- Blake, J. B., Paulikas, G. A., and Freden, S. C.: 1968, *J. Geophys. Res.* **73**, 4927.
- Dungey, J. W.: 1961, *Phys. Rev. Letters* **6**, 47.
- Durney, A. C., Morfill, G. E., and Quenby, J. J.: 1971, to be published.
- Elliot, H.: 1970, private communication.
- Engelmann, J.: 1972, this volume, p. 95.
- Engelmann, J., Hynds, R. J., Morfill, G., Axisa, F., Bewick, A., Durney, A. C., and Koch, L.: 1971, *J. Geophys. Res.* **76**, 4245.
- Fälthammar, C.-G.: 1965, *J. Geophys. Res.* **70**, 2503.
- Flindt, H. R.: 1970, *J. Geophys. Res.* **75**, 39.
- Lanzerotti, L. J.: 1968, *Phys. Rev. Letters* **21**, 929.
- Lanzerotti, L. J., MacLennan, C. G., and Robbins, M. F.: 1971, *J. Geophys. Res.* **76**, 259.
- Lanzerotti, L. J., Montgomery, M. D., and Singer, S.: 1970, *J. Geophys. Res.* **75**, 3729.
- Montgomery, M. D. and Singer, S.: 1969, *J. Geophys. Res.* **73**, 4915.

- Morfill, G. E.: 1971, private communication.
- Morfill, G. E. and Quenby, J. J.: 1971, *Planetary Space Sci.* **19**, 1541.
- Ostman, B. and Hynds, R. J.: 1971, to be published.
- Quenby, J.: 1970, private communication.
- Roberts, C. S.: 1969, *Rev. Geophys.* **7**, 305.
- Schindler, K. and Ness, N. F.: 1971, *J. Geophys. Res.* to be published.
- Taylor, H. E.: 1967, *J. Geophys. Res.* **72**, 4467.
- Thomas, G. R., Dalziel, R., and Donaldson, W.: 1970, in V. Manno and D. E. Page (eds.), *Inter-correlated Satellite Observations Related to Solar Events*, D. Reidel Publishing Company, Dordrecht, Holland, p. 492.
- Walt, M.: 1971, *Rev. Geophys. Space Phys.* **9**, 11.
- Williams, D. J. and Bostrom, C. O.: 1967, *J. Geophys. Res.* **72**, 4497.
- Williams, D. J. and Mead, G. D.: 1965, *J. Geophys. Res.* **70**, 3017.

SOLAR PARTICLE INJECTION AT MEDIUM ENERGIES ($25 < E < 250$ MeV)

J. ENGELMANN

Service d'Electronique Physique, CEN Saclay, France

1. Introduction

Flux structures above the polar caps have been extensively studied during the last few years. Most observations were made at low energies (protons of $E < 10$ MeV and electrons of $E < 1$ MeV) and particular attention has been paid to the flux enhancements frequently observed close to the cutoff latitude, characteristic of the particles (e.g., Williams and Bostrom, 1967, 1969; Blake *et al.*, 1968; McDiarmid and Burrows, 1969; Bostrom, 1970).

At higher energies ($E > 25$ MeV) the auroral flux enhancement was also observed (Engelmann *et al.*, 1971; Durney *et al.*, 1971), but the mechanism does not appear to be directly related to that of the low energy phenomenon. Another enhancement is sometimes observed at high latitudes ($\lambda > 77^\circ.5$) (Durney and Morfill, 1972). When both phenomena occur simultaneously the latitude profile registered by a polar orbiting satellite is three peaked with troughs around 72° .

In this paper we restrict our study to the auroral flux enhancement at medium energies ($25 < E < 250$ MeV). We use mainly data from three experiments aboard the ESRO 2 satellite, namely S72 (protons $26 < E < 400$ MeV), S25 (protons $E > 30$ MeV) and S28 (protons $90 < E < 350$ MeV). The first experiment was flown by the Saclay group, the two others by the Imperial College group.

A. OBSERVATIONS

The ESRO 2 satellite was launched on May 16, 1968, into a sun synchronous orbit, with an inclination of 98° and an apogee of 1100 km. Since launch, 8 high energy proton events were recorded with good time coverage and good statistics. For four of them (June 9, November 4 and 18, 1968, and February 25, 1969), a statistically significant auroral enhancement appeared lasting for a few hours after the flare onset. The latitudes of the peak and the trough are found to be $\sim 67^\circ$ and 72° IN Lat, respectively. When data are available (i.e., the November 18 event), the enhancement is observed on both polar caps. Some characteristics of the 8 flares recorded are given Table I.

From this table, the auroral enhancement seems to appear only when the time delay to flux maximum is shorter than 3.5 hr (i.e., 6 times the curvilinear travel time to earth along the Archimedean spiral, assuming a mean energy of 50 MeV). But the duration of the phenomenon is sometimes greater than this delay. It cannot then be due to a delayed entry of the particles at latitudes corresponding to the trough since, in that case, the phenomenon would reverse its amplitude after the time of maximum.

TABLE I

Date	Time UT (estimated)	Heliographic coordinates	Time delay to flux max. ($26 < E < 400$ MeV)	Duration of the auroral enhance- ment after the flare onset	Interplanetary Sector (+ when field directed out of the sun)
9. 6.68	0900	S14 W08	3.3 h	2.5 h	+
29. 9.68	1620	N16 W52	5.6 h	0	+
31.10.68	0013	S14 W37	14.5 h	0	+
1.11.68	0844	S15 W47	11.6 h	0	—
4.11.68	0542	S15 W90	~ 3.0 h	3 h	+
18.11.68	1030	N21 W87	3.5 h	7.5 h	—
2.12.68	2202	N18 E80	75 h	0	+
25. 2.69	0900	N14 W36	3.5 h	15 h	+

But the short delay to maximum means a good connectivity between the flare site and the earth, therefore resulting in a low scattering of the particles and a high anisotropy of the flux. This short delay is only loosely correlated with the longitude of the parent flare, since it depends not only on the distance to the flare of the field line connecting to the earth, but also on the magnetic regime prevailing at the flare site (Barouch *et al.*, 1971). We study now in more details the February 25, 1969, solar event, since for that event we are able to compare the ESRO 2 observations with those collected by the HEOS A1 Satellite in interplanetary space.

The first 8 ESRO 2 passes after the event onset are displayed Figure 1. The MLT's sampled are between 1700 and 2400 hr during the early passes, extending to 0300 hr in the later passes. Data contaminated by Van Allen electrons have been excluded. From this Figure, and a comparison with interplanetary data collected aboard HEOS A1 (Balogh *et al.*, 1969; Barouch *et al.*, 1970; Engel, 1970; Hedgecock, 1970), we are able to draw the main observational characteristics:

(1) The structure is not due to a pitch angle anisotropy near the auroral zone, as shown by comparison between S25 and S72: both experiments respond nearly to the same energy and see quite similar structures, although S25 is omnidirectional and S72 is looking nearly perpendicularly to the magnetic field line over the auroral zone.

(2) The enhancement is not correlated with the N-S direction of the interplanetary magnetic field: during all passes except the third the field was southward directed; its value was approximately the same during the first and fifth pass, the latter being a pass for which no auroral enhancement is detectable. Thus it does not seem that connection between the earth's field lines and the interplanetary field is favored when the interplanetary field is southward directed, as proposed by Dungey (1961).

(3) The interruption of the auroral enhancement during pass 5 can be correlated with the azimuthal angle of the interplanetary magnetic field. During all passes except the fifth, the field had nearly the garden hose direction; during pass 5 it was at 90° to this direction.

(4) When the comparison could be made (at $E > 90$ MeV), the fluxes in the auroral

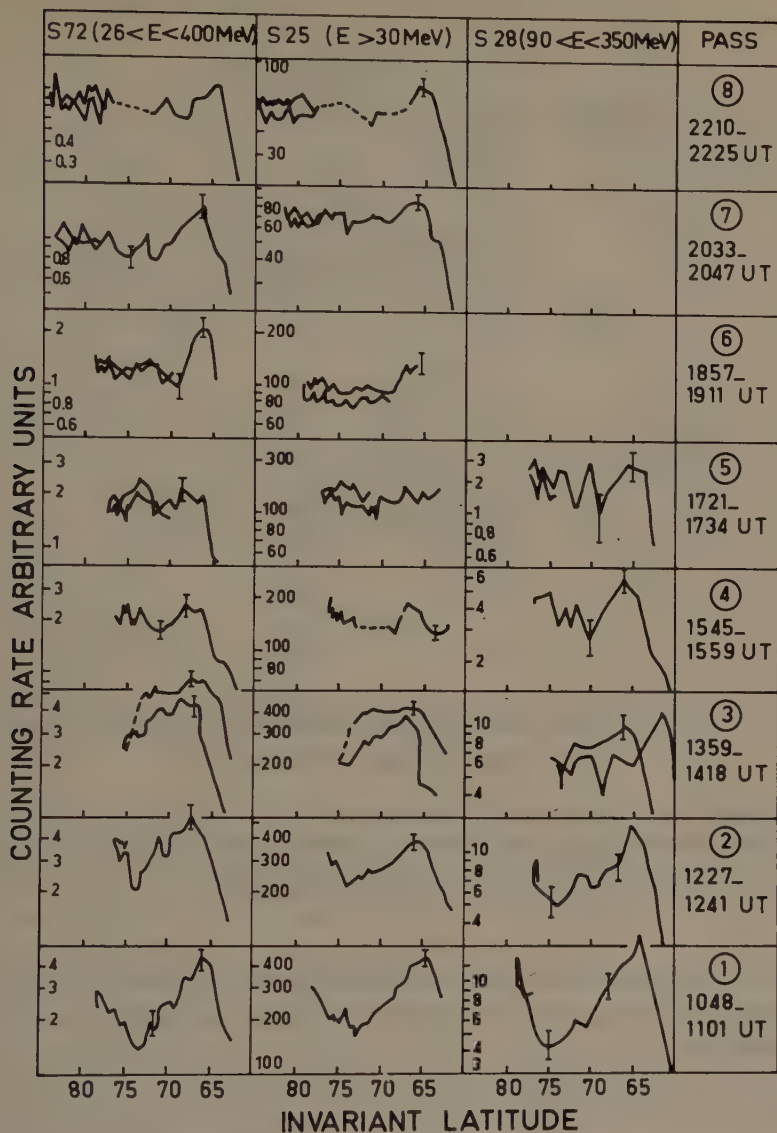


Fig. 1. The counting rates as a function of IN Lat over the northern polar cap for three different detectors on the ESRO 2 satellite. The first 8 passes after the February 25 1969, event are presented.

zone peak and the trough appeared to follow the fluxes observed in interplanetary space antisunwards and sunwards, respectively.

Another observation of interest is the energy limit of the phenomenon. On Figure 2 the peak/trough ratio was plotted at various energies for the first three passes. The points were obtained from the spectral measurements of S72 and from the integral data of S27 (protons $2 < E < 17 \text{ MeV}$), S25, and S28. This figure shows that two

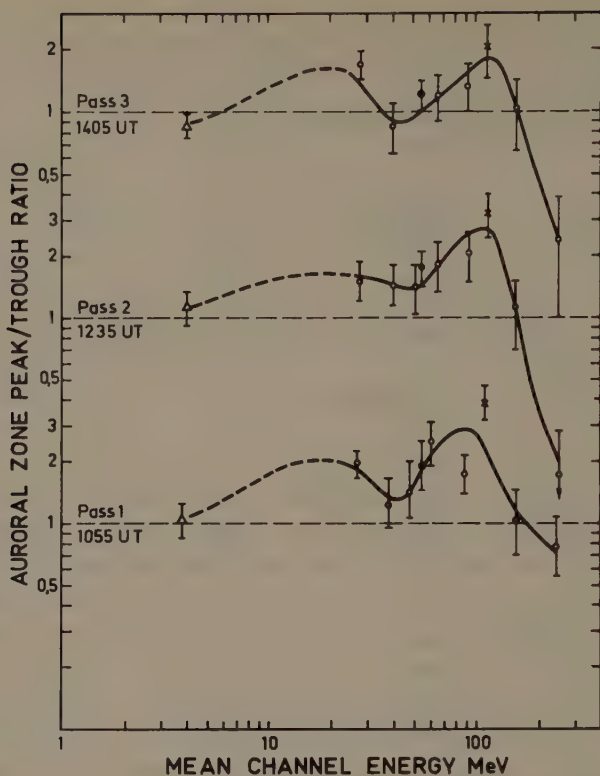


Fig. 2. The ratio of the fluxes measured in the auroral zone peak and in the trough plotted as a function of the energy. The open circles correspond to spectral measurements from S72 ($26 < E < 400$ MeV), the triangle to S27 data ($2 < E < 17$ MeV), the solid circle to S25 data ($E > 30$ MeV), and the cross to S28 data ($90 < E < 350$ MeV).

independent phenomena are acting: one at low energies, the other, which we are discussing, at energies between ~ 40 and 300 MeV. The maximum of the curve occurs at ~ 100 MeV.

B. DISCUSSION

In summary we are dealing with a phenomenon working in a limited range of energies, lasting a few hours after the onset of solar flares magnetically connected to the earth, and seeming well correlated with the interplanetary anisotropy of the particles.

To try to explain this correlation, the Imperial College group computed a large number of particle trajectories, using a refined model of the earth's magnetic field (Morfill and Quenby, 1971). For particles of different energies directed outward from various positions along the ESRO 2 trajectory, the points of intersection of the trajectories with the magnetospheric boundary were computed; the directions of the velocity vectors at these points were also computed. The calculation was terminated at a plane situated at a distance of $25 R_E$ on the nightside if the particle had not

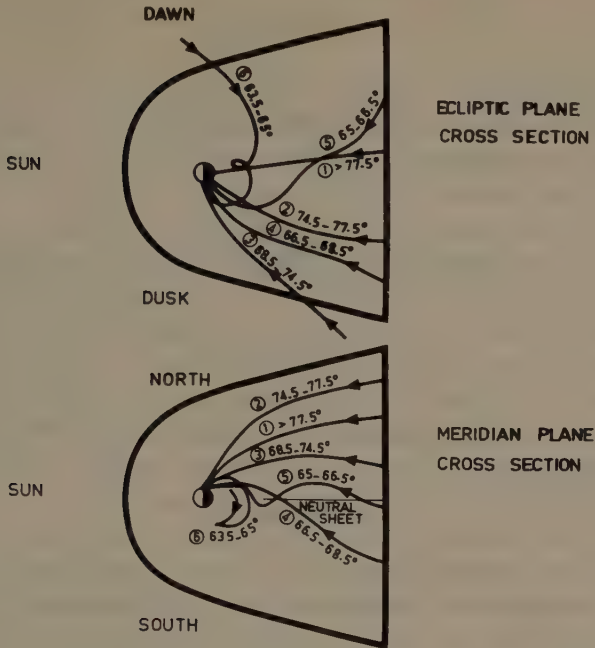


Fig. 3. The results of a trajectory calculation for points along the path of ESRO 2 over the polar cap; each typical trajectory for a certain range of IN Lat is plotted as projections onto the ecliptic and meridional planes of the magnetosphere.

crossed the magnetospheric boundary by then. The results at energies between 90 and 220 MeV may be summarized in Figure 3 where typical trajectories are projected onto cross sections of the magnetosphere. The trajectories could be grouped into 6 categories, depending on the range of IN Lat.

This figure shows that particles arriving at latitudes around 63.5 to 65° , i.e. at auroral latitudes, enter the magnetosphere on the dawn side, nearly from the garden hose direction; we expect the anisotropy vector to lie in this direction since it is generally field aligned at the beginning of an event (McCracken *et al.*, 1967). On the contrary, particles arriving around 68.5 to 74.5° (range of latitudes corresponding to the trough) enter the magnetosphere on the dusk side, from the antigarden hose direction, and we expect a minimum of flux to be sampled at these latitudes. In particular this can explain point 3 of Section 1A. If the anisotropy vector is directed along the magnetic field direction, a change of 90° from its mean direction will cause peak and trough regions to sample approximately equal particle intensities.

Figure 3 is valid at energies >90 MeV. At lower energies ($30 < E < 90$ MeV) trajectories of type 6 still exist, but their position is now between 63.5 and 68.5° and depends on the energy of the particle; this gives rise to a penumbral type of structure. The impact zone effect still holds, but is less effective than at higher energies. This may explain the preferential entry of particles around 100 MeV noted above.

2. Conclusion

Auroral flux enhancements at energies $25 < E < 250$ MeV were observed by detectors aboard the ESRO 2 satellite during the early stages of certain flares. In this range of energies, the phenomenon can be explained by an impact zone effect combined with an anisotropy of the solar proton flux in interplanetary space.

At a given energy, the amplitude of the enhancement is a function of the amplitude and direction of the anisotropy. For a satellite orbiting in a dawn-dusk meridian, the enhancement is highest when the anisotropy vector is directed along the garden hose direction. As observed for the February 25 event, we expect the amplitude and duration of the enhancement to be energy dependent. Near the lower energy limit, the impact zone effect is less effective due to a penumbral type of structure. When the energy increases, the duration of the non-equilibrium anisotropy diminishes and so does the auroral enhancement.

Acknowledgments

This work was made possible through the friendly cooperation with the Imperial College group. A great deal of the work reported here was made by Drs R. J. Hynds and G. Morfill from this group, and we want to express our gratitude to them.

References

- Balogh, A., Durney, A. C., Elliot, H., Engel, A. R., Morfill, G., and Quenby, J. J.: 1969, in *Proc. 11th Int. Conf. on Cosmic Rays, Budapest*.
- Barouch, E., Engelmann, J., Gros, M., Koch, L., and Masse, P.: 1970, in V. Manno and D. E. Page (eds.), *Intercorrelated Satellite Observations Related to Solar Events*, D. Reidel Publishing Company Dordrecht, Holland, p. 448.
- Barouch, E., Gros, M., and Masse, P.: 1971, *Solar Phys.* **19**, 483.
- Blake, J. B., Paulikas, G. A., and Freden, S. C.: 1968, *J. Geophys. Res.* **73**, 4927.
- Bostrom, C. O., 1970 in V. Manno and D. E. Page (eds.), *Intercorrelated Satellite Observations Related to Solar Events*, D. Reidel Publishing Company, Dordrecht, Holland, p. 229.
- Dungey, J. W.: 1961, *Phys. Rev. Letters* **6**, 47.
- Durney, A. C. and Morfill, G. E.: 1972, this volume, p. 101.
- Durney, A. C., Morfill, G., and Quenby, J. J.: 1971, *J. Geophys. Res.*, to be published.
- Engel, A. R.: 1970, in V. Manno and D. E. Page (eds.), *Intercorrelated Satellite Observations Related to Solar Events*, D. Reidel Publishing Company, Dordrecht, Holland, p. 478.
- Engelmann, J., Hynds, R. J., Morfill, G., Axisa, F., Bewick, A., Durney, A. C., and Koch, L.: 1971, *J. Geophys. Res.* **76**, 4245.
- Hedgecock, P. C.: 1970, in V. Manno and D. E. Page (eds.), *Intercorrelated Satellite Observations Related to Solar Events*, D. Reidel Publishing Company, Dordrecht, Holland, p. 419.
- McCracken, K. G., Rao, U. R., and Bukata, R. P.: 1967, *J. Geophys. Res.* **73**, 4159.
- McDiarmid, I. B. and Burrows, J. R.: 1969, *J. Geophys. Res.* **74**, 6329.
- Morfill, G. E. and Quenby, J. J.: 1971, *Planetary Space Sci.* **19**, 1541.
- Williams, D. J. and Bostrom, C. O.: 1967, *J. Geophys. Res.* **72**, 4497.
- Williams, D. J. and Bostrom, C. O.: 1969, *J. Geophys. Res.* **74**, 3019.

ENTRY OF ENERGETIC SOLAR PROTONS INTO THE TAIL

A. C. DURNEY

Space Science Dept. ESTEC, Noordwijk, Holland

and

G. E. MORFILL

Imperial College of Science and Technology, London S.W. 7 England

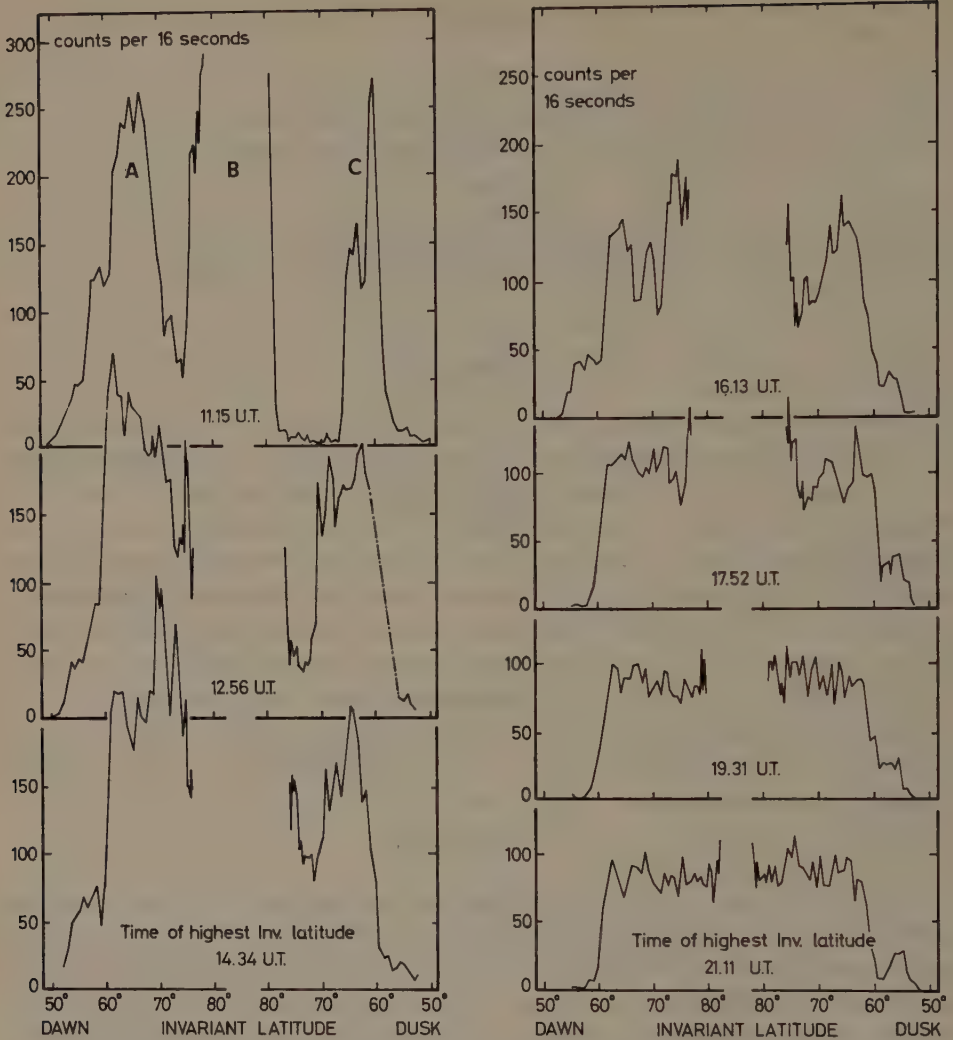
1. Introduction

A number of studies have been made recently of the intensities of particles over the polar caps during solar events in order to investigate properties of the magnetosphere (e.g., Krimigis *et al.*, 1967; Evans and Stone, 1969; Williams and Bostrom, 1969; Van Allen *et al.*, 1971). Most of these investigations have been confined to relatively low energy particles. During the solar events of November 18, 1968, and February 25, 1969, large interplanetary anisotropies were observed in the flux of high energy protons. At the same time a detector of 90 to 360 MeV protons aboard the low altitude polar orbiting satellite ESRO 2 measured heavy structure over the north and south polar caps. The higher energy range of the proton measurements lends itself more readily to investigation by trajectory integration methods, and these have been used here in an attempt to link the structure with the interplanetary anisotropy and hence deduce the penetration mechanisms.

2. Observations

During the November 18 solar event, interplanetary anisotropy measurements and neutron monitor analysis (Durney *et al.*, 1972) showed an interplanetary flux directed entirely away from the sun with no return flux in the energy range between 1 MeV to about 4 GeV. Also during this event, the S.28 detector on ESRO 2 detected structure in the flux of protons over the polar caps in the energy range between 90 and 360 MeV. Figure 1 demonstrates these observations for the first seven northern polar cap passes after the flare which occurred at 10.30 UT. Several of the passes show a clear demonstration of three peaks, in particular, the first pass which also shows a wide trough at only the background counting rate. Passes 4 and 5 show the central peak to have a higher flux than the side peaks; by pass seven the structure had disappeared.

In order to account for this structure an accurate trajectory program was developed, based on a field model using the six term Williams and Mead (1965) expansion (described in Morfill and Quenby (1971)). The trajectories of negative particles were integrated starting vertically from the spacecraft position until they reached a model magnetopause, where their positional coordinates and their direction of motion were noted. This model magnetopause is the same as that used by Gall *et al.* (1968) with



TIME VARIATION OF PROTON INTENSITY STRUCTURE OVER THE NORTHERN POLAR CAP.

Fig. 1. Northern polar cap observations of 90–350 MeV protons made on Nov. 18, 1968, from the low altitude, polar orbiting satellite ESRO 2. The first seven northern polar cap passes after the flare are shown; these passes were made at approximately 100 min intervals. The spacecraft was approximately following the dawn-dusk meridian at this time.

the addition of a tail cross section plane at $25 R_E$ from the earth, completing the surface. The results of the trajectory integrations are displayed in Figure 2. This shows that the spacecraft sampled a large flux of solar protons arriving from the distant tail, giving rise to peak B in the structure (see Figure 1). It is important to notice in Figure 2 that high flux levels are seen arriving from the north dawn quadrant of the tail.

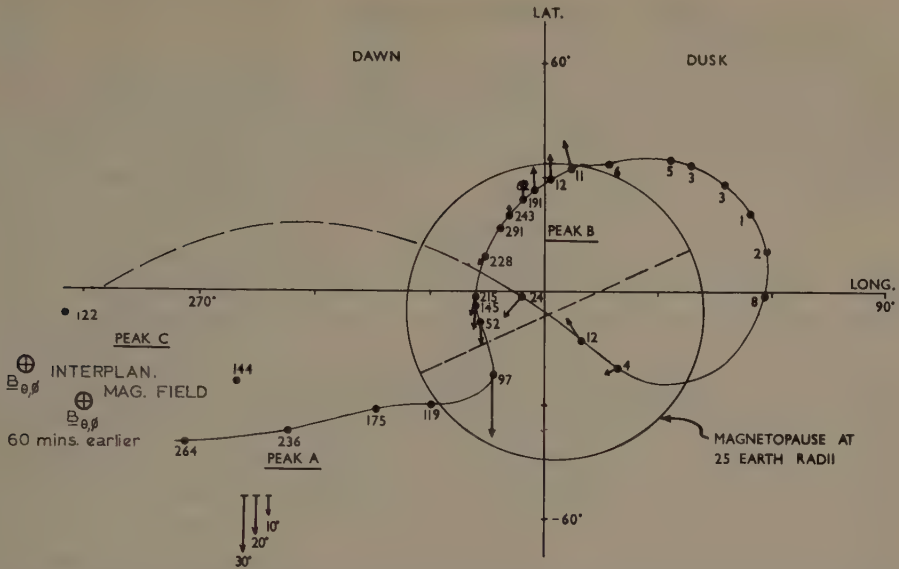


Fig. 2. An entry point diagram, which shows the first northern polar cap pass after the flare projected by means of trajectory calculations onto the magnetopause or onto a tail cross section at $25 R_E$ from the earth. The coordinates here are solar ecliptic with the origin at noon. The circle represents the tail cross section and the dashed line shows the position of the neutral sheet which is tilted in these coordinates because of the earth's tilted axis. The solid circles show the entry points (not the asymptotic directions) of particles at the magnetopause or at the tail cross section and the number by each point represents the corresponding count in the detector. The positions of peaks A, B, and C of Figure 1 are shown. The arrows are an attempt to illustrate the 'blurring' effect of the particle rotation around the field lines; the length of the arrow represents the particle pitch angles at $25 R_E$ in the tail and the direction shows the particle velocity vector projected in the plane perpendicular to the earth-sun line. The directional coordinates of the interplanetary magnetic field are shown by the circles with crosses inside. The directions at the time of the pass and also 1 hr earlier are given to indicate the stability of the field.

Peaks A and C in Figure 1 are the results of direct penetration of the magnetopause by the interplanetary anisotropy following the 'garden hose' direction.

Figure 3 shows the field aligned interplanetary anisotropy and the high flux of particles entering from the tail at a direction making an angle of approximately 130° with the interplanetary field vector. Notice that the intensity of the flux from the tail is similar to that in the forward direction of the anisotropy.

On February 25, 1969, the interplanetary magnetic field conditions were similar to those on November 18, the important difference being that the field was directed away from the sun instead of towards it as in November. Figure 4 shows the entry point diagram for the first northern polar cap pass of ESRO 2 after the flare on this date. Again high flux values are observed arriving from the northern half of the tail. The similarity of this diagram to the one for November 18 emphasizes that this effect was the result of some long lasting feature of the tail and not of some short lived mechanism peculiar to the November 18 event. On February 25 the tail particles

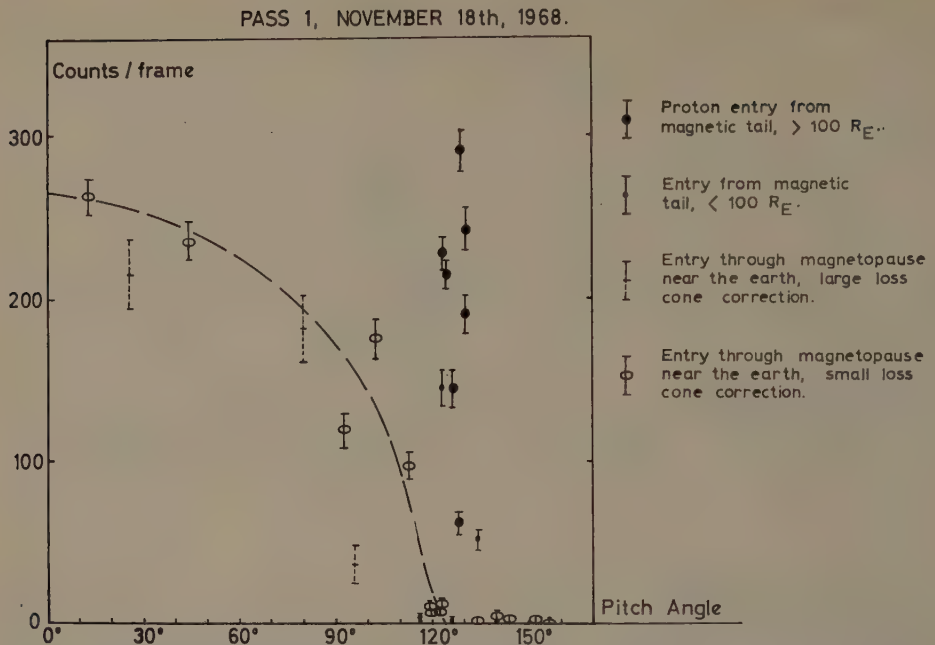


Fig. 3. A pitch angle diagram which shows the angles between the interplanetary field direction and the directions of the particles at the points of entry as a function of counting rate. The dashed curve is drawn for those particles which entered the magnetopause, thus is a measure of interplanetary flux vs. pitch angle, and gives a good demonstration of the completeness of the anisotropy during pass 1 of Nov. 18, when these results were obtained. Notice the anomalous positions for those particles which entered through the tail cross section.

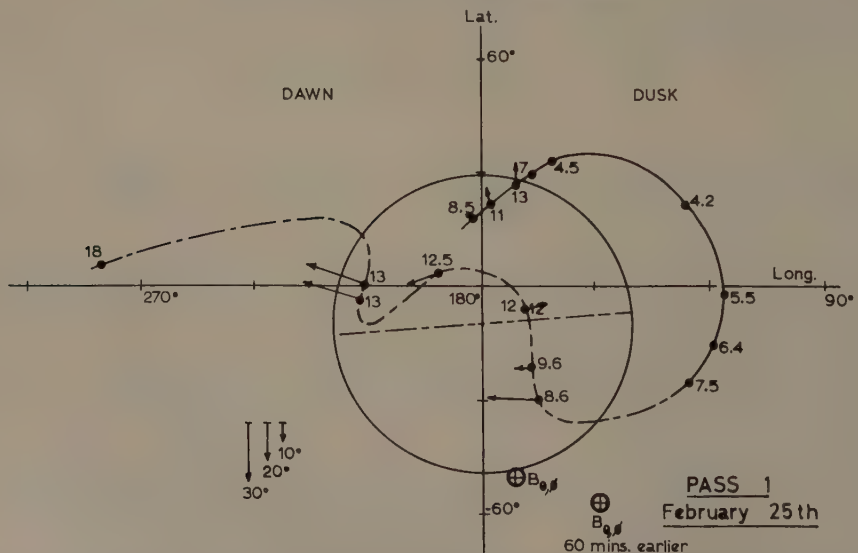


Fig. 4. This diagram is similar to Figure 2 and shows the points of entry for 90-360 MeV solar protons observed during the first northern polar cap pass after the flare on Feb. 25, 1969. The coordinates and legend are the same as for Figure 2.

again arrived from a direction making an angle of approximately 130° with the field vector.

Thus during both events a persistent mechanism exists which injects the forward flux of the interplanetary anisotropy into the northern half of the tail, reversing the flow direction as it does so and directing the particles towards the earth. The question is: 'what is this mechanism?'.

3. Discussion

One can make a detailed investigation of the various tail configurations that may supply such a process. To make a very brief summary, scattering and diffusion processes cannot produce the high flux values observed because they must destroy the anisotropy and would give rise to intensities of about one-quarter of those measured. Magnetic field gradients and electric fields with strengths at the upper limits allowed by present knowledge need several thousands of R_E to drift the particles in sufficiently far, so these are unlikely. Some form of reconnection model seems obvious, especially as the interplanetary fields were directed southwards, for most of the time, on both occasions as required by models of the Dungey (1961) type. In this model the particles follow the field lines adiabatically. However although this simple reconnection model would work for the February 25 event, it would not for November 18 as in this latter event the reversed direction of the interplanetary field would lead to injection of the lowest flux values into the northern half of the tail, which was not the case.

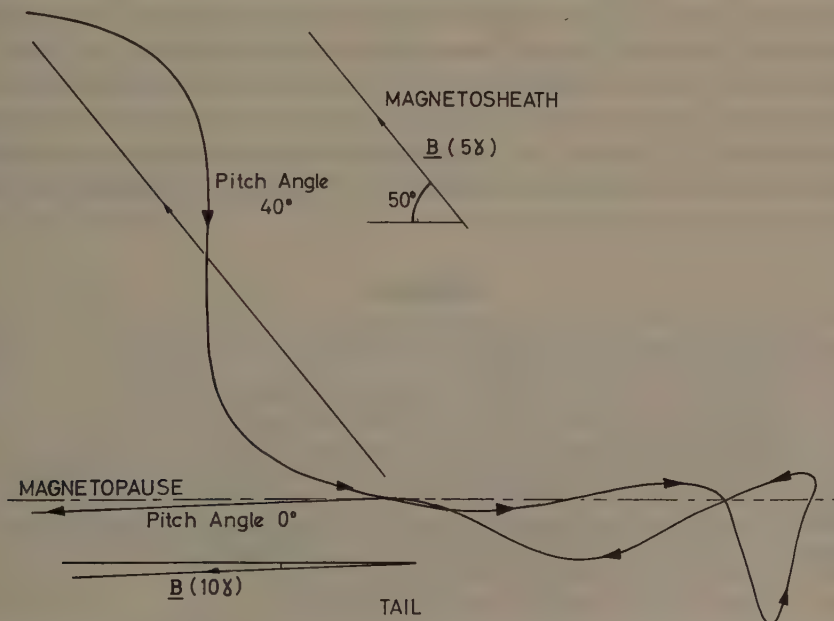


Fig. 5. This diagram shows a projection of a particle transfer trajectory onto a plane tangential to the magnetic field discontinuity. The fields on either side of the discontinuity are similar to those on the north dawn quadrant of the magnetopause on Nov. 18.

Work by Spreiter *et al.* (1966) and Behannon and Fairfield (1969) has shown the presence of field line draping in the magnetosheath. For interplanetary fields at angles of about 35° with the earth-sun line draping is only obvious near to the front of the magnetopause. There is no information as to whether field line draping is important at a distance from the magnetopause equal to the larmor radius of an 0.4 GeV rigidity proton. However, if we take the simple extreme case that the draping is small compared with this larmor radius, then for such a proton the boundary between the interplanetary and tail fields can be considered as a tangential or rotational magnetic discontinuity at any given point. Trajectory integrations across this boundary show that 0.4 to 0.5 GeV particles can cross permanently in the manner shown in Figure 5.

If the motion of a 100 MeV proton in the tail can be considered adiabatic (which seems a reasonable assumption from present knowledge) it has been estimated that the pitch angles of the protons in the peaks observed by ESRO 2 will be less than 5° at $300 R_E$ down the tail. Detailed calculations have shown that if a tail field line divergence of 2° is assumed, particles from the forward part of the anisotropy (taken as interplanetary pitch angles of less than 50° , equivalent to intensities within 10% of the maximum) can penetrate the boundary and will constitute about 100% of the particles traveling towards the earth with pitch angles of 3° or less, and 89% of the particles with pitch angles of 4° or less. Thus the anisotropy can be transferred across the boundary and reversed with little attenuation. The transfer of each particle takes an average of 7 boundary crossings and covers a tail length of about 100 and $200 R_E$. The divergence of the tail field implies that magnetic flux crosses the magnetopause and hence this model falls into the reconnection category, although, of course, the particle transfer motion is not adiabatic. It is impossible to be rigorous about this description of the particle transfer without more detailed knowledge of the magnetosheath flow patterns; however, we put this mechanism forward as a better approximation than reconnection models which rely on adiabatic particle transfer from interplanetary to geomagnetic fields.

References

- Behannon, K. W. and Fairfield, D. H.: 1969, *Planetary Space Sci.* **17**, 1803.
Dungey, J. W.: 1961, *Phys. Rev. Letters* **6**, 47.
Durney, A. C., Morfill, G. E., and Quenby, J. J.: 1972, to be published.
Evans, L. C. and Stone, E. C.: 1969, *J. Geophys. Res.* **74**, 5127.
Gall, R., Jimenez, J., and Camacho, L.: 1968, *J. Geophys. Res.* **73**, 1593.
Krimigis, S. M., Van Allen, J. A., and Armstrong, T. P.: 1967, *Phys. Rev. Letters* **18**, 1204.
Morfill, G. E. and Quenby, J. J.: 1971, *Planetary Space Sci.* **19**, 1541.
Spreiter, J. R., Alksne, A. Y., and Abraham-Shrauner, B.: 1966, *Planetary Space Sci.* **14**, 1207.
Van Allen, J. A., Fennell, J. F., and Ness, N. F.: 1971, *J. Geophys. Res.* **76**, 4262.
Williams, D. J. and Bostrom, C. O.: 1967, *J. Geophys. Res.* **74**, 3019.
Williams, D. J. and Mead, G. D.: 1965, *J. Geophys. Res.* **70**, 3017.

NEW RESULTS ON PARTICLE ARRIVAL AT THE POLAR CAPS

D. E. PAGE and V. DOMINGO

*Space Science Department (ESLAB), European Space Research and Technology Centre,
Noordwijk, The Netherlands*

1. North-South Asymmetry of Solar Particle Fluxes at the Earth

A. INTRODUCTION

Perhaps the first suggestion that solar particles could have a preference for arriving at one of the earth's polar regions came from riometer data (Reid and Sauer, 1967). More recent satellite results have shown that in at least two solar particle events (Evans and Stone, 1969; Van Allen *et al.*, 1971) there were indeed large particle intensity differences between north and south polar regions.

We report our observations around January 24, 1969, and draw conclusions after comparison with the November 2, 1967, event as reported by Evans and Stone (1969).

B. INSTRUMENTATION

An EON 6222 geiger counter responding to electrons above a nominal 40 keV and protons above 500 keV viewed pitch angles between 75 and 105° from the magnetically stabilized polar orbiting ESRO I satellite. Shielding stopping 30 MeV protons produced a geometric factor of $8.3 \times 10^{-3} \text{ cm}^2 \text{ sr}$. Data samples were obtained at 12.8 s intervals via a ratemeter saturating at 4.7×10^3 counts per sec and having a 3 s time constant. Passage over the north pole was at a height around 680 km and over the south pole around 930 km. During the January 24, 1969, event the orbit was on a dawn-dusk meridian.

C. RESULTS

Figure 1 shows the median flux values observed at IN Lat above 78° together with HEOS A interplanetary magnetic field data (Hedgecock, 1971). The error bars represent the FWHM dispersion about the median value.

It can be seen that both poles first recorded a slow rise but at about 1130 UT on January 24 the north pole flux suddenly increased fast while the south pole remained almost constant. At the same time the interplanetary magnetic field switched from north to south pointing while throughout the 'away from the sun' component was maintained. At times the north pole median intensity exceeded the south pole value by a factor of 7.

D. DATA FROM THE NOVEMBER 2 1967, EVENT

In Figure 2 we have redrawn the intensities observed by Evans and Stone (1969) to-

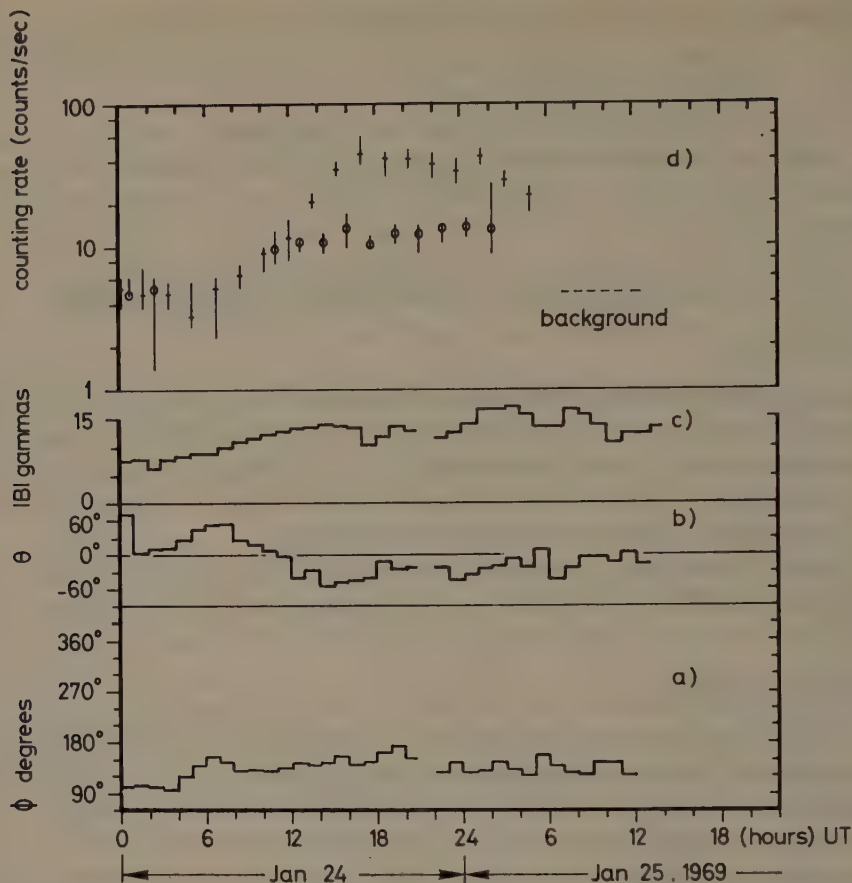


Fig. 1. (a, b, c) Interplanetary magnetic field value measured aboard the HEOS 1 satellite (magnetometer of Imperial College, London). (a) ϕ , angle with the earth-sun direction ($\phi = 0$, vector pointing toward the sun; $\phi = 180$, away from the sun; $\phi = 270$ in the direction of planetary orbital motion). (b) θ , angle with the ecliptic plane ($\theta = +90^\circ$, vector pointing north; $\theta = -90^\circ$ vector pointing south). (c) $|B|$ absolute magnetic field value in gammas. (d) 'plateau level' (IN Lat $> 78^\circ$) of the protons ($E_p > 500$ keV) observed over the polar caps at 90° to earth's magnetic field. ESLAB experiment on ESRO IA satellite.

gether with Explorer 35 Ames magnetometer data kindly made available by Drs C. P. Sonnet, D. S. Colburn, and J. M. Wilcox.

E. INTERPRETATION OF RESULTS

Since the asymmetry polarity reversed from one event to the next, it is natural to attribute the difference to the 'towardness' or 'awayness' of the interplanetary field which on November 2, 1967, was toward the sun and on January 24, 1969, away from the sun. Certain features, however, cannot be explained on this basis alone, particularly if the diffusive entry theory of Michel and Dessler (1970) is to be invoked.

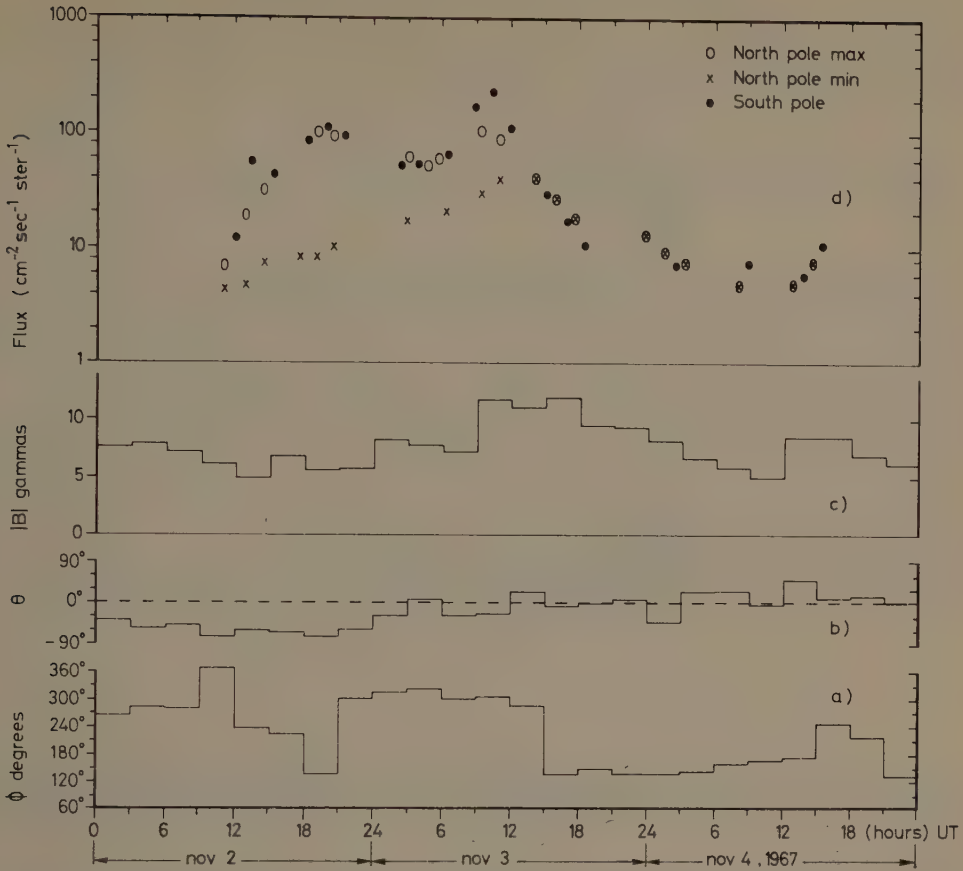


Fig. 2. (a, b, c) Interplanetary magnetic field measured aboard the Explorer 35 satellite (Ames Research Center magnetometer): Same convention as in Fig. 1(a, b, c). (d) Proton fluxes (1.2–40 MeV) measured aboard theOGO 4 satellite over the polar caps; showing southern polar intensity, maximum northern intensity, and minimum northern intensity for a series of orbits (after Figure 2 of Evans and Stone (1969)).

(A) If selective diffusion into the north or south magnetotails was to be controlled by the direction of the surrounding field then it is difficult to understand why we see no appreciable flux gradient across the pole. In addition we cannot see why diffusion from one half of the magnetotail to the other should not remove the asymmetry. It would appear that at least after 11 30 UT on January 24, 1969, access rather than being diffusive was equally easy to all tail field lines rooted in the north polar cap.

(B) If 'towardness' or 'awayness' of the interplanetary field was the only feature controlling N-S asymmetry then the field reversal at about 1400 UT on November 3, 1967, should have led to a reversal of asymmetry polarity rather than to the establishment of isotropy.

It may be significant that in both events asymmetry was accompanied by a southward component in the interplanetary field. Dungey (1961) required this for field

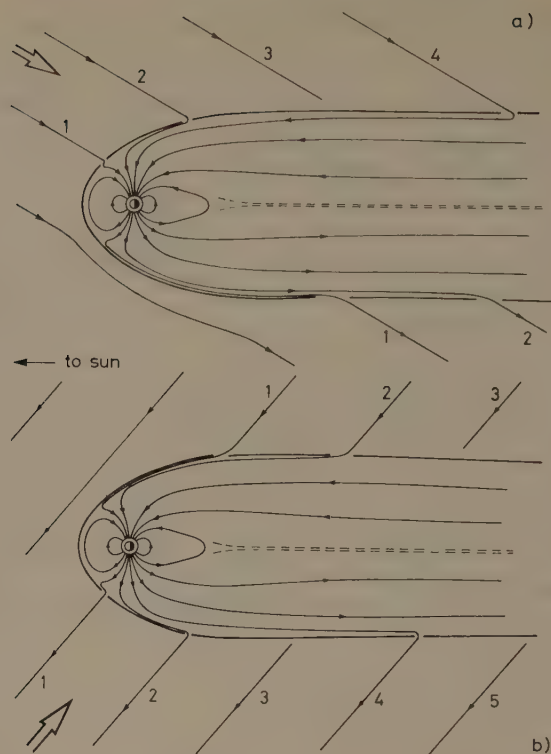


Fig. 3. Proposed magnetic field structure, (a) for the January 24, 1969, and (b) for the November 2, 1967, events. For the sake of simplicity we have omitted the shock wave and other details of the magnetosphere.

merging. The sudden advent of asymmetry at 1130 UT on January 24, 1969, coincided with the arrival of a southward component. At that time direct easy access to the north pole became possible. Evans and Stone (1969) note that asymmetry disappeared around 1400 UT on November 3, 1967, coincident with field reversal from 'toward' to 'away.' We would point out that at roughly the same time the interplanetary field lost its southward component.

In Figure 3 we have illustrated our idea of the configurations for the two events. During January 24, 1969, particle propagation in interplanetary space was very anisotropic (Vernov *et al.*, 1970; Van Allen *et al.*, 1971) and we suggest that anisotropy existed also in November 1967, thus the arrows in Figure 3. The degree of anisotropy will obviously influence the magnitude of the asymmetry seen over the polar caps. Field direction and particle anisotropy cannot be regarded as independent parameters. Taken together as in Figure 3 we think it is evident that one pole of the earth will be favored for particle arrival.

F. CONCLUSION

On the evidence of two events we suggest that the southward component of the inter-

planetary magnetic field 'opened the door' for easy particle access to the magnetosphere. The polarity of the N-S asymmetry was then determined by the 'towardness' or 'awayness' of the field while the magnitude of the asymmetry was further influenced by the degree of particle anisotropy in interplanetary space.

2. Northern Polar Cap Flux Variations Following the November 2, 1969, Event

A. INTRODUCTION

Frequently (for example, Bostrom, 1970; Paulikas *et al.*, 1970) solar particles arriving over a polar cap first filled up the 'quasi-trapping' region in the auroral zone and only after several hours did the polar plateau experience a similar intensity. In fact this result may be the most general one. A study in terms of particle anisotropy in interplanetary space aided by particle trajectory calculations in a model magnetosphere has allowed Engelmann *et al.* (1971) to explain these preferred arrival regions but only for protons above about 30 MeV.

We report on the November 2, 1969, event observed by two polar satellites ESRO IA and ESRO IB at 1000 and 300 km, respectively, over the northern polar cap. The instrumentation as described earlier was the same on both satellites. The orbits were both roughly in the midday-midnight meridian plane.

B. RESULTS

Polar Cap Intensity Structure During Event Rise

On this occasion we were unable to see any auroral zone enhancement. Instead a large intensity spike appeared over the central polar cap and this was maintained for several hours at least. Engelmann *et al.* (1971) reported the simultaneous existence of such a central spike and auroral zone enhancements during the February 25, 1969, event. It would be of interest to know if interplanetary conditions, particularly field direction and particle anisotropy, were on this occasion capable of explaining the existence of the central spike without auroral zone enhancement.

Comparison of the >45 keV electron flux on Explorer 35 (Lin, 1971) and the ESRO I fluxes indicated (Figure 4) that the central polar cap was well connected to interplanetary space and perhaps even exerted a focusing effect on arriving particles. Since the central peak remained during many passes we regard it as a spatial phenomenon.

Coherent Intensity Time Variations

Beside the gross effects described in the previous section there were small but significant fluctuations in the particle count rate over the polar cap plateau region, which were 10 to 20% in magnitude and had time scales of about 1 min. There was no clear evidence of periodicity in the fluctuations but it should be remembered that data samples were available only at 12.8 s intervals.

Usually such variations have been attributed to spatial effects (Hudson and Ander-

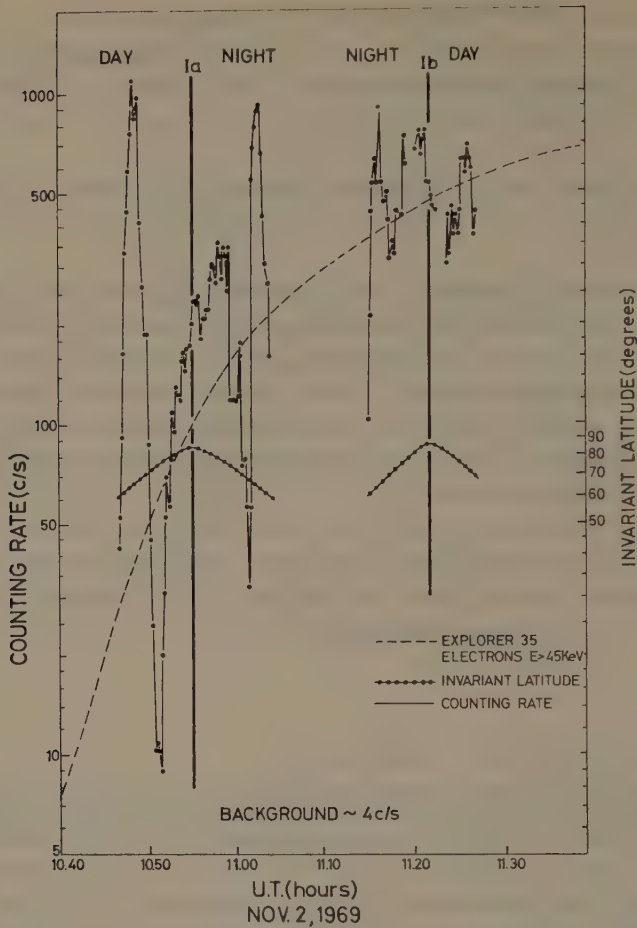


Fig. 4. Protons ($E > 500$ keV) and electrons ($E > 40$ keV) counting rate vs. UT registered over the north polar cap by ESRO IA and ESRO IB on their first passage after the start of the event. For comparison the electron flux ($E > 45$ keV) measured by Explorer 35 outside the magnetosphere is shown on an arbitrary scale.

son, 1969; Page, 1971) i.e., while over the polar region the satellite crossed 'bundles' of magnetic field lines with associated flux variations. Variations of about 1 min would then suggest 'bundle' diameters of a few hundred kilometers.

In the November 1969 event, while the particle flux was high enough to allow the observation of statistically significant short term variations, there was one interval during which we have simultaneous data from both satellites, which at the time were in slightly different regions of the northern central polar cap. The positions are shown in Figure 5. While ESRO IA moved from X' to Y' , ESRO IB moved from X to Y . The UT interval was approximately 1429 until 1433 on November 3 and the count rates observed are shown in Figure 6. It is apparent that these rates follow each other

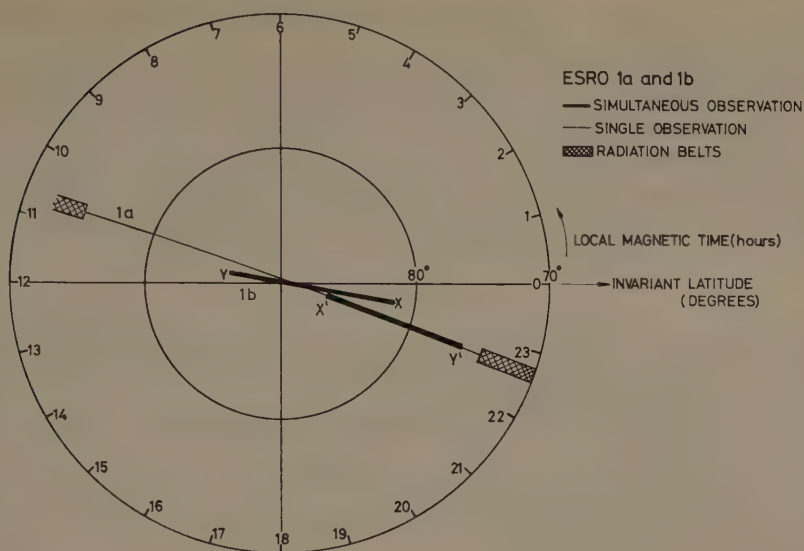


Fig. 5. Spatial position of ESRO 1A and ESRO 1B on an IN Lat vs. MLT map at the time of the existing simultaneous observation.

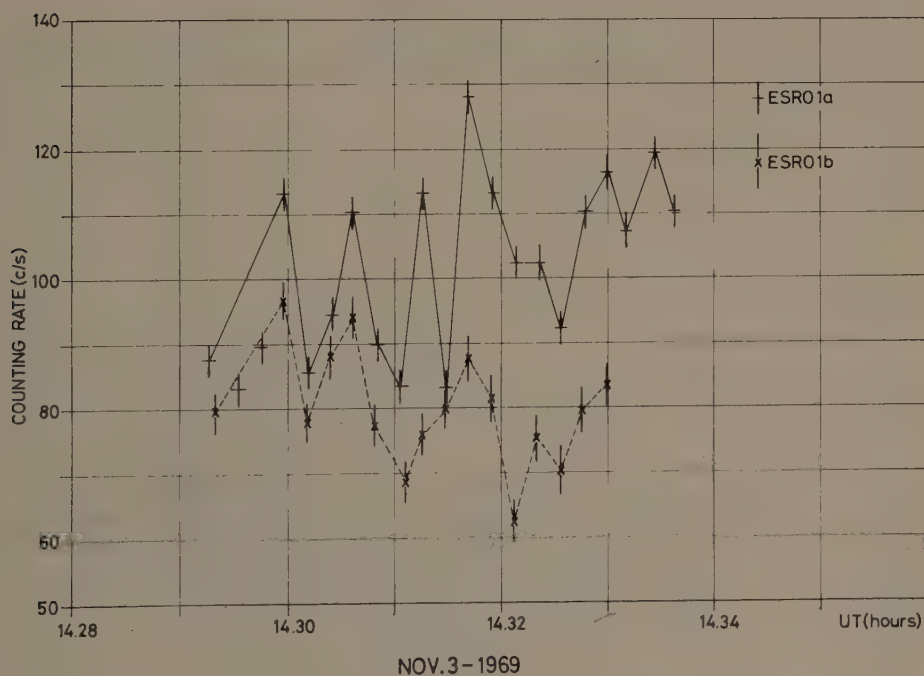


Fig. 6. Counting rate ($E_p > 500$ keV) vs. UT in a simultaneous pass of ESRO 1A and ESRO 1B over the central part of the north polar region.

closely. A simple statistical argument indicates that such a distribution of points has a 3% probability of arising by chance.

The separation of the two satellites above the polar cap is such as to persuade us that these variations are probably of a temporal rather than a spatial nature. It would be of interest to find micropulsation records for this period or riometer records confirming the phenomena on which, on the basis of the present evidence, must be taken as a coherent temporal fluctuation affecting a large area of the polar cap.

References

- Bostrom, C. O.: 1970, in V. Manno and D. E. Page (eds.), *Intercorrelated Satellite Observations Related to Solar Events*, D. Reidel Publishing Company, Dordrecht, Holland, p. 229.
- Dungey, J. W.: 1961, *Phys. Rev. Letters* **6**, 47.
- Engelmann, J., Hynds, R. J., Morfill, G., Axisa, F., Bewick, A., Durney, A. C., and Koch, L.: 1971, *J. Geophys. Res.* **76**, 4245.
- Evans, L. C. and Stone, E. C.: 1969, *J. Geophys. Res.* **74**, 5127.
- Hedgcock, P. C.: 1971, private communication.
- Hudson, P. D. and Anderson, H. R.: 1969, *J. Geophys. Res.* **74**, 2881.
- Lin, R. P.: 1971, private communication.
- Michel, F. C. and Dessler, A. J.: 1970, *J. Geophys. Res.* **75**, 6061.
- Page, D. E.: 1971, in *Space Research XI*, Akademie-Verlag, Berlin, p. 1189.
- Paulikas, G. A., Blake, J. B., and Vampola, A. L.: 1970, in V. Manno and D. E. Page (eds.), *Intercorrelated Satellite Observations Related to Solar Events*, by D. Reidel Publishing Company, Dordrecht, Holland, p. 193.
- Reid, G. C. and Sauer, H. H.: 1967, *J. Geophys. Res.* **72**, 4383.
- Van Allen, J. A., Fennel, J. F., and Ness, N. F.: 1971, *J. Geophys. Res.* **76**, 4262.
- Vernov, S. N., Kontor, N. N., Lyubimov, G. P., Pereslegina, N. V., and Chukov, E. S.: 1970, in *Intercorrelated Satellite Observations Related to Solar Events*, D. Reidel Publishing Company, Dordrecht, Holland, p. 460.

NEW OBSERVATIONS OF THE PROTON POPULATION OF THE RADIATION BELT BETWEEN 1.5 AND 104 MeV

D. HOVESTADT, E. ACHTERMANN, B. EBEL,
B. HÄUSLER, and G. PASCHMANN

*Max-Planck-Institut für Physik und Astrophysik
Institut für extraterrestrische Physik, Garching, Germany*

The identification of the source and loss mechanisms is still the outstanding problem of radiation belt research. Part of the problem encountered in testing theoretical concepts has been the incompleteness of the available data. Several surveys of the trapped proton population have been performed previously (Davis and Williamson, 1963; Freden *et al.*, 1965; Fillius, 1966; Gabbe and Brown, 1966; Mihalov and White, 1966; Vernov *et al.*, 1967; De Forest, 1970; Burns and Krimigis, 1971). Only a few experiments, however, have covered a wide enough energy range to allow the study of systematic spectral variations over a wide spatial region. In the inner belt, measurements of protons with energies below about 10 MeV have been generally scarce due to instrumental problems caused by penetrating protons or by electrons.

In this brief report we present a mapping of the distribution of trapped protons in the energy range 1.5 to 104 MeV performed with an experiment aboard the German satellite AZUR in 1969. The satellite was launched on November 8, 1969, into a 103° inclination polar orbit with apogee at 3145 km and perigee at 383 km and was magnetically stabilized.

The data were obtained with a proton range telescope consisting of a stack of 7 solid state detectors surrounded by an anti-coincidence scintillator. It covers an energy range between 1.5 and 104 MeV in 6 channels. Each channel requires the coincidence of the outputs of two adjacent detectors in anti-coincidence with the outputs of the subsequent detector and the scintillator. This technique ensures a negligible sensitivity of the instrument to penetrating protons and to electrons which are energetic enough to pass a sweep magnet in front of the aperture. The telescope has a geometric factor of approximately 0.06 cm² sr (for isotropic flux), an acceptance cone of 21° half width, and is oriented perpendicular to the geomagnetic field. A detailed description of the instrument and its calibration with proton and electron beams has been published elsewhere (Achtermann *et al.*, 1970).

For the mapping of fluxes in *B-L* space the data acquired between November 11 and December 2, 1969, have been sorted according to *B* and *L* and subsequently averaged. The selected time interval followed a major geomagnetic storm (on November 8), but did not contain large disturbances itself, the highest K_p value observed being 4+. In addition, all disturbed days were excluded from the analysis. The magnetic field model used was the GSFC 12/66 model (Cain *et al.*, 1967) adjusted for December 1969.

Because the instrument measures the fluxes of protons in the pitch angle range be-

tween approximately 70 and 110° the determination of the fluxes of locally mirroring protons requires a correction of the geometric factor, based upon the local pitch-angle distributions. To first order this correction was achieved at any B - L point by using an approximation to the pitch angle distribution which was obtained from the

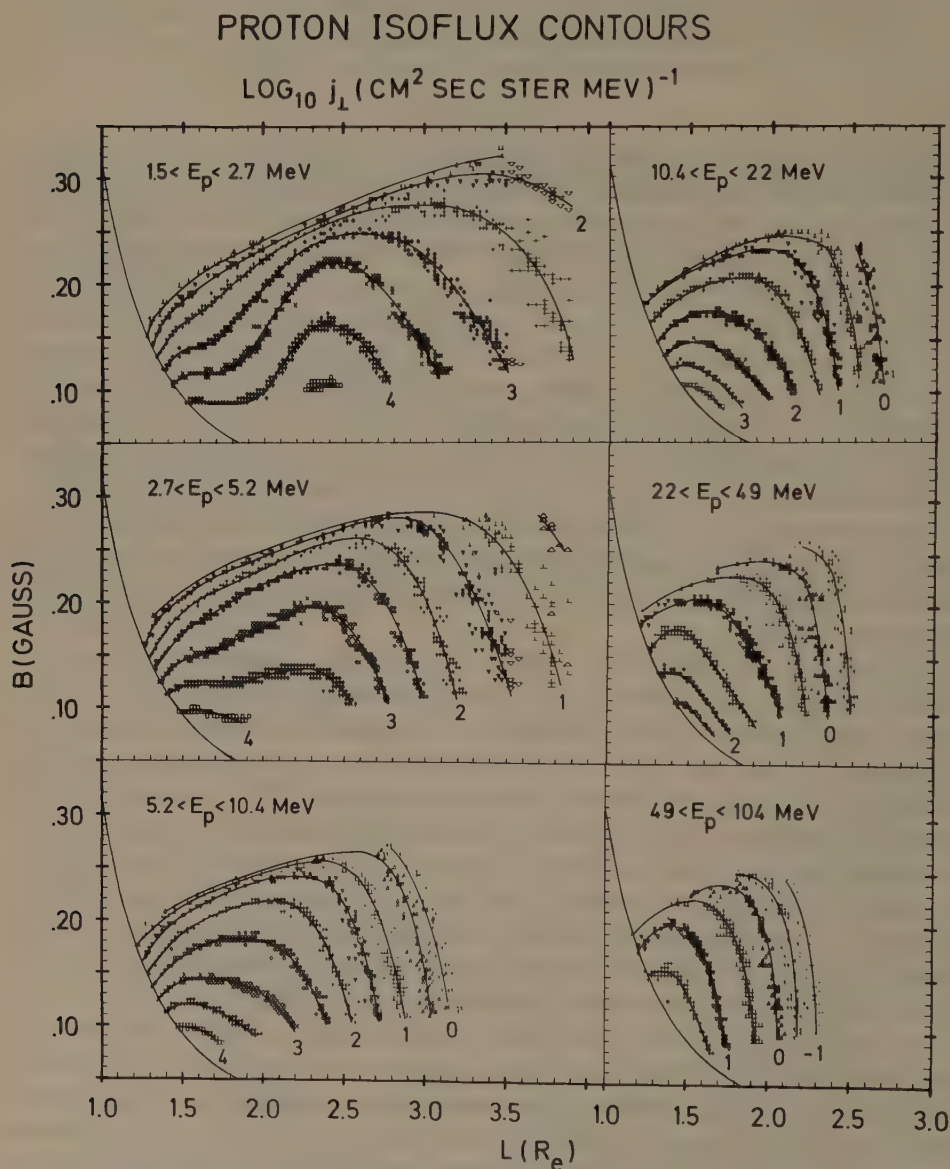


Fig. 1. Corrected iso-flux contour maps in B - L space obtained with the proton range telescope EI 88/1 aboard the GRS-A/AZUR satellite between Nov. 11 and Dec. 2, 1969. Contours not numbered correspond to three times the flux value of the next lower contour. Interval given for plotting iso-flux symbols is $\pm 10\%$ of the selected value.

A comparison of our results with those obtained earlier for protons of similar energies is shown in Figure 2. At L values greater than about 2 there are large discrepancies at all energies shown. However, in this region magnetic storms are known to change the flux profiles significantly over long times. Therefore, a comparison of results obtained at different times is hardly possible for those L values. Where comparisons could be made, agreement is good in the inner belt ($L \leq 2.0$) for the lowest and the highest energy channels of our experiment. For the protons around 4 MeV there are discrepancies in the fluxes which range up to a factor of 20 at $L=1.5$ and $B=0.20$. However, this disagreement can possibly be attributed to background problems of the instrument with which we compared our data (McIlwain, 1971).

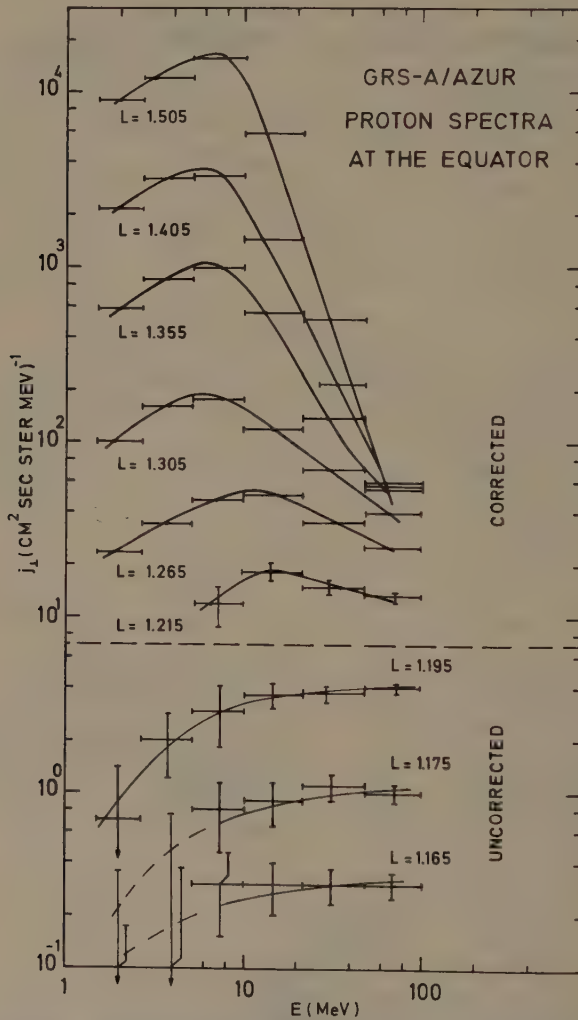


Fig. 3. Equatorial proton spectra between $L=1.165$ and $L=1.505$. Fluxes are corrected for $L > 1.195$ and uncorrected for $L \leq 1.195$. Horizontal bars indicate the widths of the energy channels.

Only a few reliable measurements of the directional proton energy spectra have been reported previously at L values below about 1.5, particularly in the equatorial plane. In Figure 3 we show the equatorial spectra obtained with the present experiment at L values between 1.165 and 1.505. The fluxes shown are averages over the same period used to obtain the iso-intensity contours of Figure 1 and have been corrected with respect to the pitch angle distribution. At L values below 1.215, however, this was not possible because of the lack of information on the angular distribution.

Below $L \approx 1.21$ the spectral shape appears to be constant within the experimental uncertainties and the intensity variation is consistent with a $1/\bar{q}$ dependence as expected for a spatially constant source and atmospheric losses. Beyond $L \approx 1.26$ the fluxes of protons below 10 MeV increase steeper than $1/\bar{q}$. This behavior suggests that the source strength for these protons is not constant but increases with increasing L . At the highest energy 49 to 104 MeV, on the other hand, the flux shows only very little variation with L beyond $L = 1.26$ indicating additional losses and/or a decrease in the source strength with increasing L . From recent work by Walt and Farley (1972) it appears that this behavior might be explained by a combination of a cosmic ray albedo neutron decay source (CRAND) with radial diffusion.

Acknowledgments

The authors would like to thank the technical staff of the Max-Planck-Institut for their assistance in the development and the testing of the instrument. The contribution of Dr S. C. Freden in the early stage of the project is gratefully acknowledged.

This research was supported by the Bundesministerium für wissenschaftliche Forschung under grant WRK 98.

References

- Achtermann, E., Häusler, B., Hovestadt, D., Paschmann, G., Küneth, E., and Laeverenz, P.: 1970, Forschungsbericht W70-67, Bundesministerium für Bildung und Wissenschaft.
- Burns, A. L. and Krimigis, S. M.: 1971, University of Iowa Report 71:8.
- Cain, J. C., Hendricks, S. J., Langel, R. A., and Hudson, W. V.: 1967, *J. Geomagn. Geoelec.* **19**, 335.
- Davis, L. R. and Williamson, J. M.: 1963, in W. Priester (ed.), *Space Research 3*, North-Holland Publishing Company, Amsterdam, Holland, p. 365.
- De Forest, S. E.: 1970, University of California, San Diego, Report SP-70-20.
- Fillius, R. W.: 1966, *J. Geophys. Res.* **71**, 97.
- Freden, S. C., Blake, J. B., and Paulikas, G. A.: 1965, *J. Geophys. Res.* **70**, 3113.
- Gabbe, J. D. and Brown, W. C.: 1966, in B. M. McCormac (ed.), *Radiation Trapped in the Earth's Magnetic Field*, D. Reidel Publishing Company, Dordrecht, Holland, p. 165.
- McIlwain, C. E.: 1971, private communication.
- Mihalov, J. D. and White, R. S.: 1966, *J. Geophys. Res.* **71**, 2207.
- Vernov, S. N., Vakulov, P. V., Kuznetsov, S. N., Logatchev, Yu. I., Nikolaiev, A. G., Sosnovets, E. N., and Stolpovsky, V. G.: 1967, R. L. Smith-Rose (ed.), *Space Research 7*, North-Holland Publishing Company, Amsterdam, Holland, p. 577.
- Walt, M. and Farley, T. A.: 1972, this volume, p. 293.

ESRO IA/B OBSERVATIONS AT HIGH LATITUDES OF TRAPPED AND PRECIPITATING PROTONS WITH ENERGIES ABOVE 100 keV

FINN SØRAAS

Dept. of Physics, University of Bergen, Bergen, Norway

1. Introduction

In more than a decade now, the energetic protons in the earth's magnetosphere have been studied directly by instruments carried aloft by rockets and satellites. The protons trapped by the geomagnetic field have been measured by a great number of satellites, starting with the measurements of Davis and Williamson (1963), who measured the protons at low latitudes in the energy range 100 keV to several MeV. Frank (1967) extended the measurements down to the 1 keV range, and positively identified the low energy protons responsible for the observed depression of the earth's magnetic field during magnetic storms. Dynamics, loss, and replenishment of the trapped particle populations have been reviewed by Williams (1970).

At auroral latitudes proton detectors have been flown on a number of rockets, starting in the late fifties and continuing up to the present time. For a review see Whalen and McDiarmid (1969).

The observations of precipitating protons at high latitudes by satellites were initiated by the Lockheed group (Sharp *et al.*, 1967). Since then many experimenters, from both American and European groups, have measured protons at high latitudes using polar orbiting satellites.

To describe the charged particles observed at high latitudes, various parameters have been introduced. Such parameters may be the width of the precipitation region, the particle intensity, the particle pitch angle distribution, and their energy spectra. All these characteristics vary with geomagnetic activity, magnetic time and latitude. In this paper some of these variations, as they appear in the above 100 keV protons measured by the ESRO IA and B satellites, will be discussed.

2. Instrumentation

The ESRO IA (Aurorae) satellite was launched from the Western Test Range, California, on October 3, 1968, at 2049 UT into a near polar orbit with initial perigee of 258 km and apogee of 1533 km.

The ESRO IB (Boreas) satellite was launched from the same location on October 1, 1969, into a near polar orbit with initial perigee of 281 km and apogee of 378 km. Both satellites were magnetically stabilized by means of permanent magnets.

The proton data were obtained by a joint experiment between the University of

Bergen, Norway, and the Danish Space Research Institute, Denmark. The experiment employs three totally depleted surface barrier detectors. The detectors have the following orientation: D_1 0° , D_2 90° , and D_3 45° with the satellite axis. The directional geometric factor is $0.037 \text{ cm}^2 \text{ sr}$. Transverse magnetic fields in front of the apertures sweep away electrons with energy less than 500 keV. A complete description of the experiment flown onboard ESRO IA is given by Søråas *et al.* (1970). In the ESRO IA satellite the detector D_3 was shielded by 0.3 mm Al. For the ESRO IB satellite this shielding was removed to improve the pitch angle resolution of the experiment for low energy protons.

3. Quiet Geomagnetic Conditions

In Figure 1, the count rates of locally mirroring (150 to 225) keV and precipitated (115 to 180) keV protons are shown plotted vs. IN Lat for a number of ESRO IA passes. Counts can be converted to protons $\text{cm}^{-2} \text{ s}^{-1} \text{ sr}^{-1} \text{ keV}^{-1}$ by multiplying by 1.2. The data refer to 9 nearly consecutive passes from the northern hemisphere. The data are from a magnetically quiet period. To explain the content of this figure, the pass in the center (orbit 216) will be discussed in detail.

Passing north on the nightside the satellite is below the radiation belt and it encounters the outer radiation belt somewhat above 55° of IN Lat. Near the northern trapping boundary located at about 68° IN Lat, there is a sudden change in the proton pitch angle distribution and we get a region of precipitating protons about 2° wide. Over the polar regions no protons are observed. At the dayside the trapping boundary extends up to 71° IN Lat, i.e., about 3° higher than on the nightside. Near this boundary there is some proton precipitation. Well separated from, and poleward to this

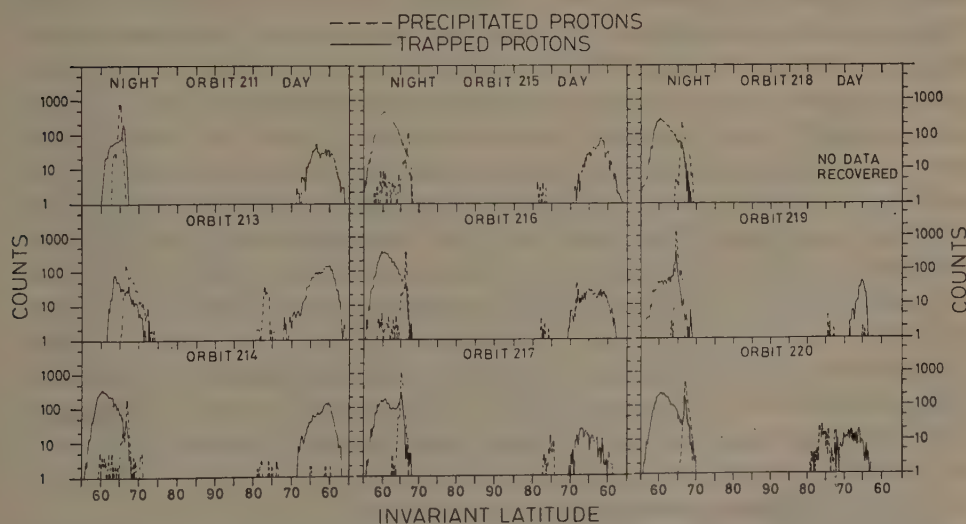


Fig. 1. Trapped and precipitated proton fluxes in the energy bands (150 to 215) keV and (115 to 180) keV plotted vs. IN Lat (Lindalen *et al.*, 1971).

trapping boundary, around 77° of IN Lat, precipitating (115 to 180) keV protons are observed. The reason why no locally mirroring protons in the energy band (150 to 215) keV are observed at these high IN Lat at this particular pass, is due to the low proton intensities and the soft energy spectrum. The pass illustrates some of the main features observed in the proton precipitation pattern in the midnight noon sector during quiet geomagnetic conditions. From the other passes presented in the figure it is seen that the description given for pass 216 more or less holds for all of them. In all 9 passes there is proton precipitation on the nightside located around 68° IN Lat. This confirms the findings of Aarsnes *et al.* (1970) and Eather and Mende (1971) that there always is some proton precipitation around magnetic midnight. In the midnight sector the precipitating protons and the locally mirroring protons extend poleward to the same IN Lat, about 68° during quiet geomagnetic conditions.

On the dayside, the (150 to 215) keV locally mirroring protons extend poleward to 70° IN Lat during quiet conditions. At this boundary a region of precipitating protons in the energy range (115 to 180) keV can be found, but it is most often absent during quiet conditions. Well separated from and poleward to this dayside trapping boundary, around 77° of IN Lat precipitating protons can be found in a region about 2 to 4 wide. The differential intensity is about $10 \text{ protons cm}^{-2} \text{ s}^{-1} \text{ sr}^{-1} \text{ keV}^{-1}$.

4. Substorm Behavior

It is of considerable interest to study the initial phase of the auroral substorm. A detailed study of the different aspects of the substorm and their interrelations could possibly prove useful in giving an answer to the question of how the auroral particles are accelerated and from where they are coming. The time resolution of a polar orbiting satellite is rather limited. It has the advantage, though, that it gives a rapid latitude scan of the precipitation region, and the time for making a complete night-day scan in a hemisphere is smaller than the orbital drift time for most auroral particles.

In an effort to shed some light on the relationship between the polar magnetic substorm and the proton substorm, data from the initial phase of the October 12, 1969 storm are studied in detail. This phase of the storm as viewed in some magnetic recordings is shown in Figure 2. The upper curve gives the hourly Dst values, below it the H-component of the magnetograms from Kiruna, Leirvogur, Godhavn, and College is presented. The lower most curve gives the AE index. This is a preliminary AE index computed by Stauning (1970). Looking at the magnetograms and the AE index, the onset of the magnetic bay is approximately 0040 UT on October 12. Above the time scale, the satellite southpole passes are marked with capital S and the northpole passes with capital N. In Figures 3 and 4 particle data corresponding to these passes will be examined. The count rate in selected energy channels is thus plotted vs. IN Lat for orbits prior to and through the initial phase of the storm in order to see how they respond to the different geomagnetic disturbance levels.

The left hand side of Figures 3 and 4 refers to the northern hemisphere and the right hand side to the southern hemisphere. In the northern hemisphere the count rate

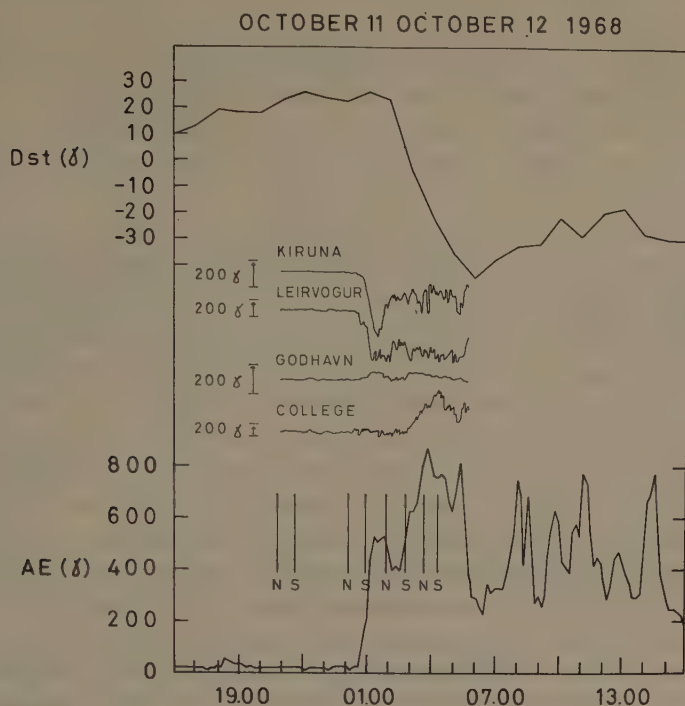


Fig. 2. The hourly Dst values, the H-component of the magnetograms from Kiruna, Leirvogur, Godhavn, and College and the AE index are plotted vs. UT. The southern and northern-hemisphere passes are marked with a capital S and N, respectively.

of locally mirroring and precipitating protons in the energy band (150 to 225) keV and (115 to 180) keV, respectively, is plotted vs. IN Lat. In the southern hemisphere the count rate of locally mirroring protons in the three energy channels (150 to 215) keV, (225 to 360) keV and (500 to 920) keV is plotted vs. IN Lat thus giving spectral information.

The times quoted in the figure are average pass times; the data shown are from a time period of approximately 20 min for each pass.

The north pole pass with center time 2048 UT shows a count rate pattern fairly typical for quiet geomagnetic conditions. The same is true for the southern hemisphere pass at 2136 UT. Protons are observed in both hemisphere around 78° IN Lat on the dayside.

The next northern hemisphere pass from which we have data occurred at 0010 UT. This is approximately half an hour before the onset of the bay. The following can be noticed: The maximum precipitation on the nightside has shifted one latitude degree equatorward and the same is true for the trapping boundary. The maximum intensity has gone up with a factor of 4 compared with the measurements around 2048 UT. This increase in the maximum proton precipitation intensity prior to a magnetic bay has been discussed for a number of magnetic bays by Lindalen *et al.* (1971). Apart

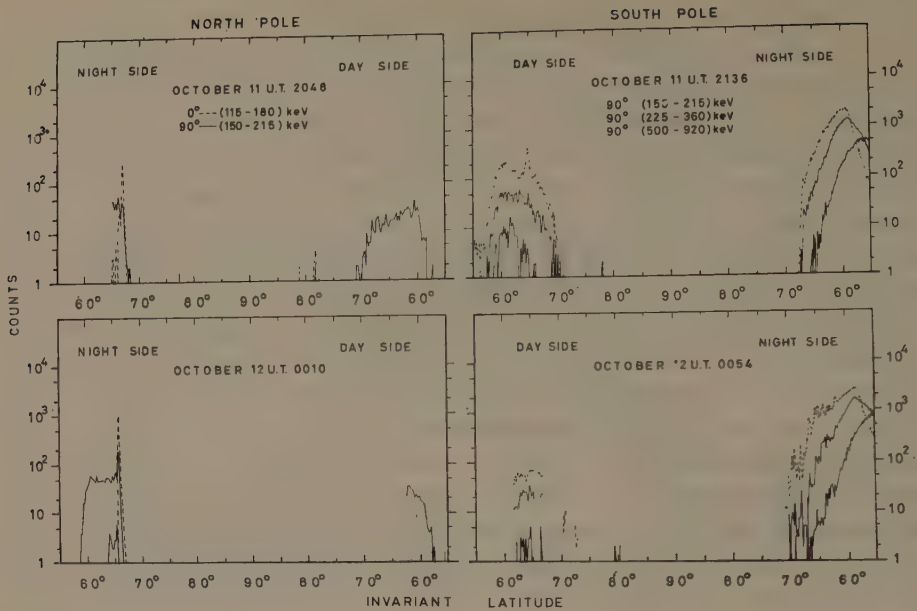


Fig. 3. Left hand side, north pole trapped and precipitated proton fluxes, and right hand side, south pole trapped proton fluxes plotted vs. IN Lat.

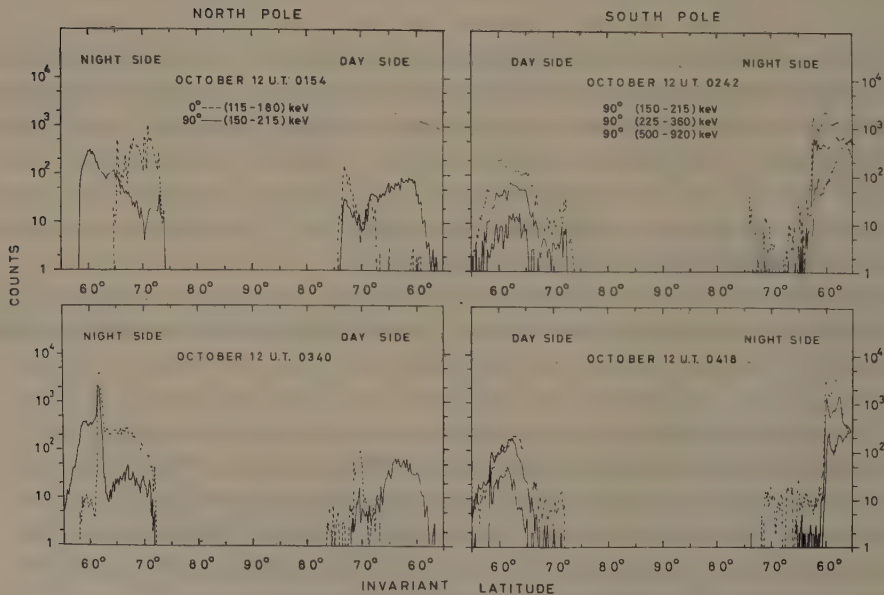


Fig. 4. Same as Figure 3.

from these changes, the precipitation pattern is similar to quiet conditions, there is no increase in the latitudinal extent of the proton precipitation.

The data coverage is poor on both the northern and the southern hemisphere dayside, but it seems as the southern hemisphere trapping boundary has moved poleward up to 73° IN Lat. The time is now 0048 UT and thus 8 min after the bay onset.

The nightside, however, is definitely different from the quiet pattern. There are enhanced fluxes of locally mirroring protons above 63° IN Lat and the trapping boundary has moved poleward; how far is difficult to judge as we do not have complete data coverage. The time is now 0110 UT, 30 min after the bay onset, and it is evident that a major injection of protons has taken place.

The nightside of the northern hemisphere pass around 0150 UT shown in Figure 4 shows an enhanced and poleward expanded region of proton precipitation. The proton precipitation is covering the region from 65 to 74.5° IN Lat. One should notice that there has not been any marked equatorward movement of the precipitation region since the previous pass. The increased count rate in the locally mirroring protons around $\lambda=60^\circ$ is due to a diurnal variation in the flux levels. The dayside pass shows proton precipitation in the latitude interval 67 to 74° . We may note that the equatorward boundary of the precipitation is about 2° farther north than on the nightside.

It is of interest to see how closely the patterns observed in the two dayside hemispheres compare. On the south pole nightside the proton fluxes drop two orders of magnitude in the latitude interval 62 to 63° ; poleward to this drop variable fluxes can be found up to 75° of IN Lat. Such count rate vs. latitude profiles are often observed during disturbed geomagnetic conditions. In his thesis, Berg (1971) suggests that such an abrupt change in the proton intensity at a particular IN Lat may be associated with the sharp gradient in the plasma density at the plasmopause.

In the southern hemisphere nightside around 0418 UT the sharp drop in intensity has moved 2 latitudinal degrees equatorward compared with the previous pass. This corresponds to a movement of $0.6 L$ value in 100 min.

Such equatorward motion of the low latitude boundary of proton precipitation can often be observed in connection with and prior to geomagnetic storms. Prior to the great February 2, 1969, storm, the equatorward boundary of precipitation moved steadily equatorward during 8 satellite orbits, that is 13 hr. Also, on January 31, an equatorward movement associated with increased geomagnetic activity can be observed for approximately 10 hr. In Figure 5 these equatorward movements are plotted in an L time diagram. The speed of the motion decreases with decreasing L value. An exception to this is the rapid movement from $L=5$ to $L=2.9$ in less than 100 min on February 2, associated with an extremely large substorm, -2500γ measured at Kiruna. It is possible that this equatorward movement is driven by fluctuating convection electric fields. Birmingham (1969) has considered the importance of time-dependent convection electric fields as an agent for diffusing trapped magnetospheric radiation in toward the earth. From the inward motion of the proton precipitation one

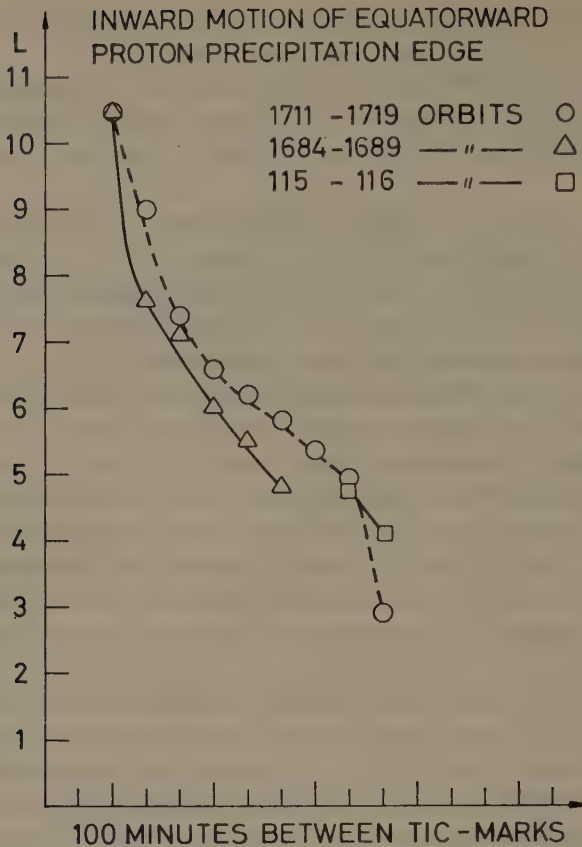


Fig. 5. Equatorward movement of proton precipitation prior to and during magnetic storms.

can derive a rough estimate of the radial diffusion coefficient. In the region $L=6$ to $L=5$ our measurements give a diffusion coefficient of around $1 R_E^2/\text{day}$.

5. Energy Spectra

Since the experiment onboard the ESRO I satellites observes protons in five different energy channels, the differential energy spectrum of precipitated and trapped protons can be obtained. In the auroral zone the proton energy spectra can be highly variable depending upon the degree of magnetic activity. In Figure 6, spectra from the October 12, 1968, storm are shown. The spectra refer to the position of maximum precipitation in the lowest energy channel. Also plotted in the figure is a spectrum from the February 2, 1969, storm (Gustafsson *et al.*, 1971). The proton intensities measured during this storm are among the most intense so far examined in our satellite data. The energy input for protons with energies above 100 keV was $8 \text{ erg cm}^{-2} \text{ s}^{-1}$ and the precipitation covered the region from $L=2.9$ to $L=10$.

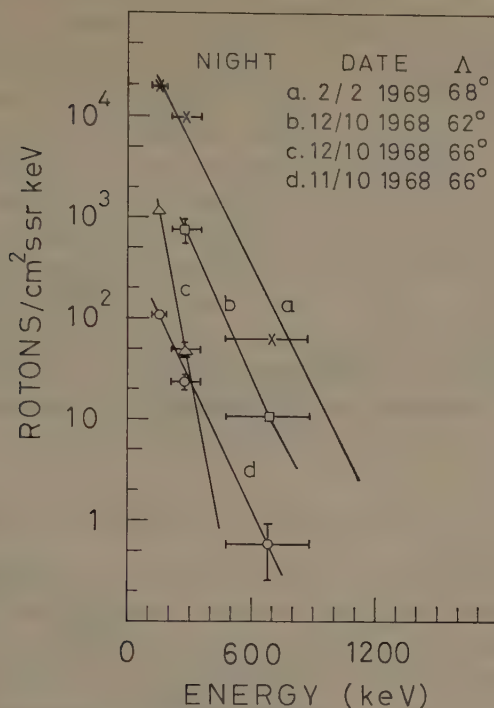


Fig. 6. Nightside proton energy spectra for several passes.

6. Pitch Angle Distribution

From knowledge of the charge particle pitch angle distribution one can extract information on acceleration and loss processes operating in the particles and get information concerning interactions between particles and electromagnetic fields (waves). Knowledge of the pitch angle distribution is essential when one wants quantitatively to understand the processes taking place when energetic charge particles are impinging upon and penetrating the atmosphere. Such information is also helpful when one tries to speculate on where the particles are coming from.

Only a few direct measurements of pitch angle distribution of energetic protons in the ionosphere at higher latitudes have been reported. The evidence is generally indicative of a flux maximum perpendicular to the magnetic field lines or near isotropy over the upper hemisphere.

Amundsen *et al.* (1972) studied the pitch angle distribution of protons above 100 keV using data from the ESRO IB satellite. They used data both from the period when the satellite was tumbling and from the time when it became magnetically stabilized. This enabled them to determine the size of the loss cone for the protons. They found that the experimentally determined loss cone in most of the cases studied by them agrees with what one should expect if the mirror motion of the protons was disrupted when the particle reached the collision-dominated level of the ionosphere.

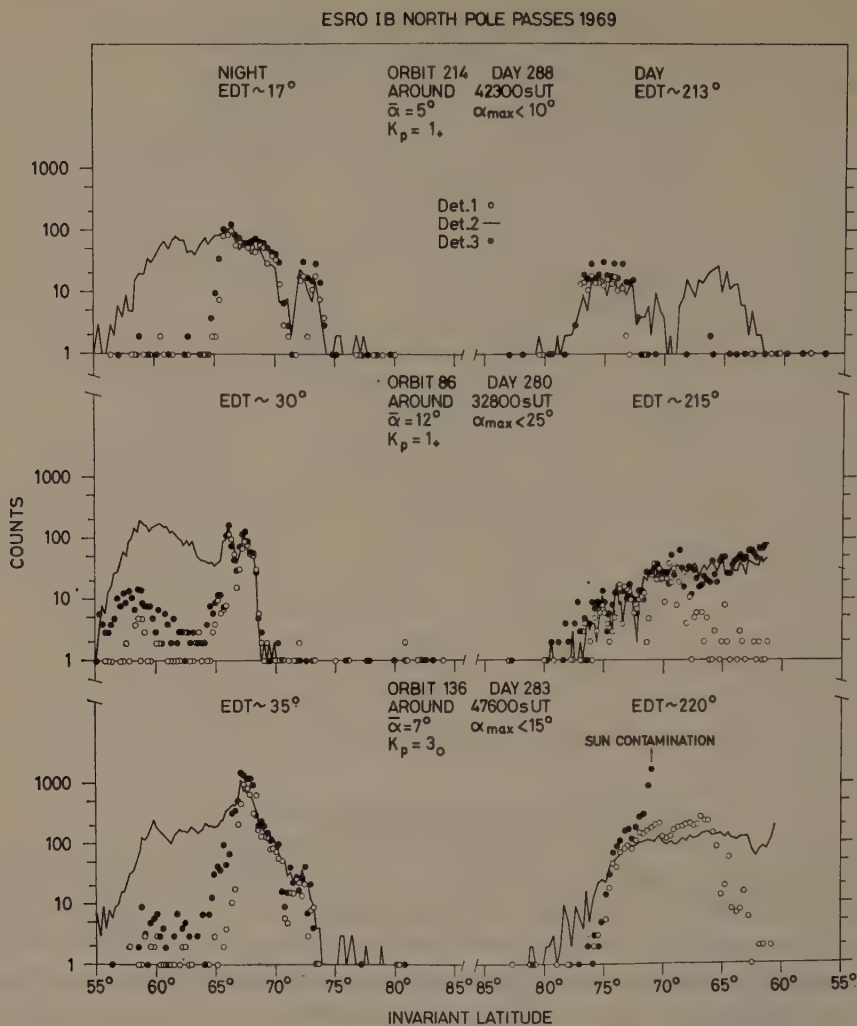


Fig. 7. The detector counts plotted vs. IN Lat for three orbit made during differing magnetic conditions. The mean satellite alignment angle during the pass is given by $\bar{\alpha}$; the upper limit α_{\max} for the misalignment angle is also given. Det. 1 looks along, Det. 2 normal, and Det. 3 45° to the magnetic field (Amundsen *et al.*, 1972).

The proton pitch angle distribution varies with IN Lat, LT, and magnetic activity (Figure 7). In the figure, the particle intensities represented by counts in the three detectors, nominal angles with the magnetic field 0° , 45° and 90° , are plotted as a function of IN Lat, for different degrees of magnetic activity, on the day and the nightside of the earth.

At the equatorward edge of the radiation belt on the nightside, anisotropic fluxes with maximum intensity perpendicular to the magnetic field lines are observed. Then, rather suddenly, the fluxes get isotropic at 66° IN Lat. The pitch angle distribution

stays isotropic until the fluxes drop out at high latitudes. The IN Lat position of this poleward boundary is more fluctuating than the equatorward border of isotropy around 66° IN Lat.

The width of the zone of precipitating protons on the nightside of the earth varies from a very narrow one, during quiet magnetic conditions, to about 10° IN Lat during disturbed conditions. Inside this region the proton pitch angle distribution is isotropic. Compared with the nightside the changes in pitch angle distribution with latitude are more gradual on the dayside. In particular, this is found during disturbed magnetic conditions. The equatorward border of isotropy on the dayside is very sensitive to magnetic conditions, much more than on the nightside. Equatorward of this border the proton fluxes become anisotropic with peak 90° to the magnetic field lines. During relative magnetic quiet, the radiation on the dayside seems to be split into two parts, with the isotropic precipitation concentrated in the poleward part.

7. Relation Between Proton Parameters and Magnetic Activity

As stressed previously, many parameters can be used to describe the particle precipitation at high latitudes. In order to see how these parameters depend on geomagnetic activity, a multiple regression analysis was carried out using a particular parameter as the dependent variable y , and K_p , Dst, and AE as independent variables. The following functional relationship was fitted to the data:

$$y = A_0 + A_1 \cdot K_p + A_2 \cdot D_{st} + A_3 \cdot AE.$$

The Dst and AE indices are in gammas, while the K_p value has been converted to numbers using the relation $0_0 = 0$, $0_+ = 3$, $1_- = 7$, $1_0 = 10 \dots$

Some results are shown in Table I.

TABLE I

y	A_0	A_1	A_2	A_3	r
Equatorward boundary	63.2	-0.046	0.055	-0.0016	0.74
of proton precipitation	1.7	0.019	0.012	0.0019	
Poleward boundary of	70.9	0.0078	-0.022	0.012	0.57
proton precipitation	3.2	0.0400	0.028	0.004	
Precipitation integrated over	248	27	-53	8.4	0.89
latitude arbitrary units	1268	19	12	1.8	

The top number gives the estimates of the regression coefficient and the bottom number its standard deviation. r is the multiple correlation coefficient. The results apply to local midnight, and about 80 data points are used in the analysis.

It can be seen that the equatorward boundary moves to lower latitudes with increasing geomagnetic activity. Its location depends significantly on Dst and to a lesser extent on the K_p index. The location of the equatorward boundary does not

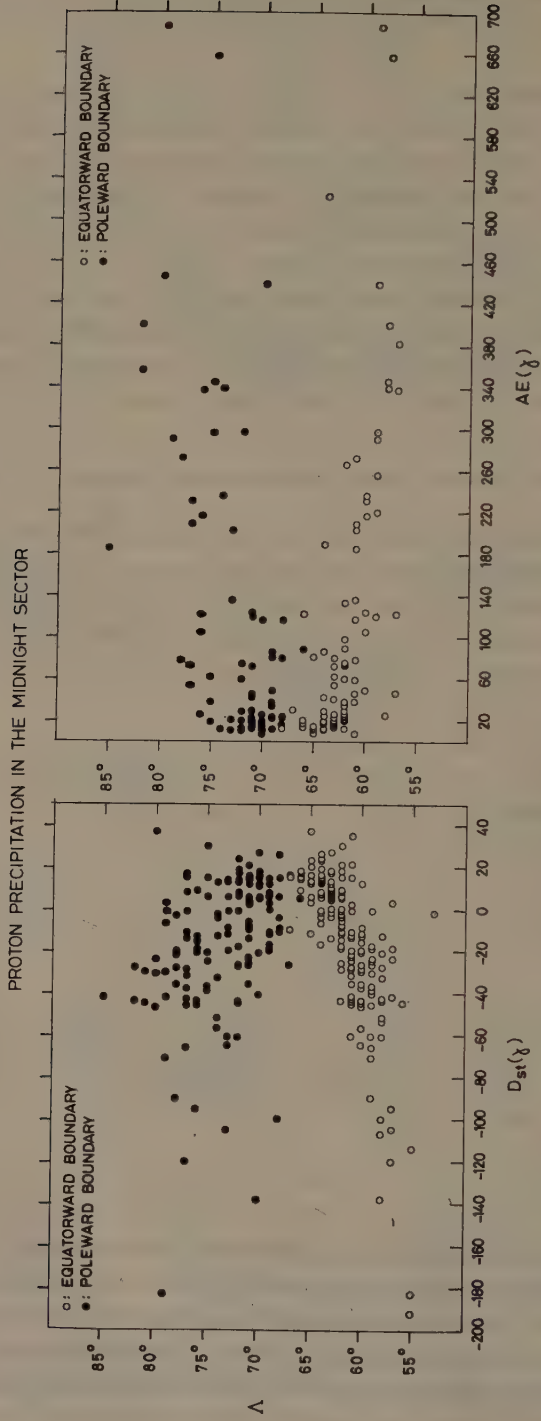


Fig. 8. The IN Lat of the poleward and equatorward proton precipitation boundary plotted vs. the Dst and AE indices.

depend significantly on the AE index, as the error in the regression coefficient exceeds the value of the coefficient itself. The poleward boundary on the other hand seems to depend solely on the AE index. The regression coefficients for both the K_p and Dst terms are not significantly different from zero. The multiple regression coefficient is 0.57, so there is still much scatter in the data not accounted for by the linear regression using K_p , Dst, and AE as independent variables. The total precipitation depends significantly on both Dst and AE. The multiple correlation coefficient is high, suggesting that the total amount of proton precipitation is closely associated with the Dst and AE indices.

In Figure 8 the poleward and the equatorward boundaries of proton precipitation are plotted vs. the Dst and the AE indices. It can be seen that the equatorward boundary moves to lower latitudes with decreasing Dst values. It also looks as there is a clear dependence of this boundary on AE, but when the Dst variation is taken into account, this boundary shows no significant variation with the AE index. There is a general tendency for the poleward boundary to move to higher latitudes with decreasing Dst, but as the statistical analysis has shown, this boundary depends mostly on the AE index. There is an indication in the data that the poleward boundary starts to move equatorward when Dst decreases below -60γ . These statistical results can at best only indicate the general trend. They contain a limited amount of data, mostly from periods with little geomagnetic activity.

8. Summary and Discussion

Many experimenters have established that there always is particle precipitation in the midnight sector even during extremely quiet geomagnetic conditions. This suggests that whatever the exact nature of the energy source it must operate at all times but with varying intensity.

Protons above 100 keV pushed into the midnight sector of the magnetosphere will experience a westward gradient drift. We find that the location of the trapping boundary at midnight and noon (67 and 70° IN Lat) during quiet magnetic conditions is in agreement with calculations performed by Williams and Mead (1965) of the adiabatic motion of electrons in a realistic magnetic field model. The equatorward boundary of precipitation on the nightside can nearly always be found a few degrees lower than on the dayside. This suggests, that these two equatorward boundaries are connected by a proton drift path. If this is the case, one may speculate that the protons precipitating on the dayside below the stable trapping boundary (around $A=70^\circ$) have drifted from the nightside. As they drift they are precipitating due to a pitch angle scattering mechanism. During moderately and quiet magnetic conditions protons with small pitch angles are lost, or their intensities have been reduced below the detector sensitivity before they reach the noon meridian.

Kennel (1969) described the precipitation pattern at the nightside as a competition between radial convective flow and pitch angle scattering. From his Figure 6, which illustrates the flow precipitation coupling, we find an expected precipitation boundary

for 100 keV protons in the midnight meridian for an E-W electric field across the magnetosphere of 30 kV to be at about $L=6$. This agrees with the position of the observed equatorward border of precipitation. By increased electric field strength, expected during disturbed conditions, the border shifts equatorwards in agreement with observations.

On the dayside, two zones of protons have been reported for quiet magnetic conditions (Sharp *et al.*, 1967; Lindalen *et al.*, 1971). The lower zone is probably associated with gradient drifting protons whose origin can be found in the nightside hemisphere. In the poleward zone, at the same latitude in the two hemispheres, the proton fluxes are isotropic, this favoring a local dayside source for these particles (Lindalen *et al.*, 1971). This high latitude dayside particle region is related to penetration of magnetosheath plasma to low altitudes, as observed by Heikkila and Winningham (1971) and Frank (1971). The position of these fluxes coincides with the dayside high latitude cusp in the magnetopause often referred to as the neutral point. The observed high energy protons may constitute the high energy tail of the magnetosheath plasma.

Acknowledgments

I appreciate discussions with my colleagues K. Aarsnes, A. Amundsen and H. R. Lindalen.

This research was financially supported by the Royal Norwegian Research Council for Science and Technology.

References

- Aarsnes, K., Amundsen, R., Lindalen, H. R., and Søråas, F.: 1970, *Physica Norvegica* **4**, 73.
 Amundsen, R., Søråas, F., Lindalen, H. R., and Aarsnes, K.: 1972, *J. Geophys. Res.* **77**, 556.
 Berg, L.: 1971, Cand. real. thesis, Department of Physics, University of Bergen, Norway.
 Birmingham, T. J.: 1969, *J. Geophys. Res.* **74**, 2169.
 Davis, L. R. and Williamson, J. M.: in 1963, *Space Res.* **3**, 365.
 Eather, R. H. and Mende, S. B.: 1971, *J. Geophys. Res.* **76**, 4262.
 Frank, L. A.: 1967, *J. Geophys. Res.* **72**, 3753.
 Frank, L. A.: 1971, *J. Geophys. Res.* **76**, 5202.
 Gustafsson, G., Larsen, T. R., Pettersen, H., Riedler, W., Skovli, G., Søråas, F., and Thomas, G. R.: 1971, Paper presented at Cospar, Seattle, Washington.
 Heikkila, W. J. and Winningham, J. D.: 1971, *J. Geophys. Res.* **76**, 883.
 Kennel, C. F.: 1969, *Rev. Geophys.* **7**, 379.
 Lindalen, H. R., Søråas, F., Aarsnes, K., and Amundsen, R.: 1971, *Planetary Space Sci.* **19**, 1041.
 Sharp, R. D., Johnson, R. G., Shea, M. F., and Shook, G. B.: 1967, *J. Geophys. Res.* **72**, 227.
 Søråas, F., Aarsnes, K., Lindalen, H. R., and Møhl Madsen, M.: 1970, *Årbok, Univ. i Bergen, Norway, Mat.-Nat. rekke*, in press.
 Stauning, P.: 1970, IONLAB R 21, Technical University, DK-2800 Lyngby, Denmark.
 Whalen, B. A. and McDiarmid, I. B.: 1969, in B. M. McCormac (ed.), *Atmospheric Emissions*, Van Nostrand Reinhold Company, New York, p. 93.
 Williams, D. J.: 1970, ESSA Technical Report ERL 180 SDL 16.
 Williams, D. J. and Mead, G. D.: 1965, *J. Geophys. Res.* **70**, 3017.

AUROL PARTICLE PRECIPITATION PATTERNS

WILLI RIEDLER

Institut für Nachrichtentechnik und Wellenausbreitung, Technische Hochschule Graz, Austria

Abstract. Data from a low energy auroral electron and proton experiment are presented which were obtained from October 1968 to June 1970 from the polar-orbit satellite ESRO I A (Aurorae). The results include (a) discontinuities in the precipitation patterns around 5 and 19 hr MLT, (b) 'valleys' in the average flux distributions in the noon/dusk sector, (c) latitudinal cross over of 5.8 keV electron and proton precipitation, and (d) K_p -dependent 5.8 keV proton population at low latitudes, which is presumably connected with the generation of SAR arcs.

1. Introduction

The knowledge of the behavior of electrons and protons in the keV range has increased only recently, contrary to the large amount of data available for auroral particle precipitation characteristics in the >40 keV range. It was mainly after the introduction of the Channel Electron Multiplier that polar-orbiting and other satellites have been instrumented with equipment for particle measurements in the 100 eV to 10 keV range. A review of low energy particle measurements from polar satellites has been given by Sharp and Johnson (1971).

From ground based observations collected during the IGY 1957/58, Feldstein (1963) showed that auroral forms apparently occur in a closed oval shaped region, which was later named the *auroral oval*. The morphological continuity of the auroral oval has been questioned by several authors, however. For example, Russian workers (see e.g. Mishin *et al.*, 1970) pointed out several years ago that a model with two quasi-circular zones, a high-latitude dayside zone, and a lower latitude nightside zone would more adequately describe magnetic observations on the ground. As early as 1963, Lassen (1970) provided evidence that the auroral forms, observed over Greenland, were discontinuous in the morning and evening sectors. The two horseshoe-like patterns would merge for higher geomagnetic activity levels, in agreement with Feldstein's auroral oval, at least for higher K_p values. As to the origin of the particles observed in the different parts of the auroral oval recent ground based work (Eather and Mende, 1971) showed conclusively that in addition to the nightside particle population there must exist a different dayside population.

It has long been speculated that this dayside population has direct access from the magnetosheath to lower altitudes. Recently, this assumption has been fully verified by direct satellite measurements (Frank, 1971; Frank and Ackerson, 1971; Heikkila and Winningham, 1971).

2. Instrumentation

The data presented in this paper have been obtained by a low energy particle spectrometer (S 71-B) designed and built at the Kiruna Geophysical Observatory, Sweden. A

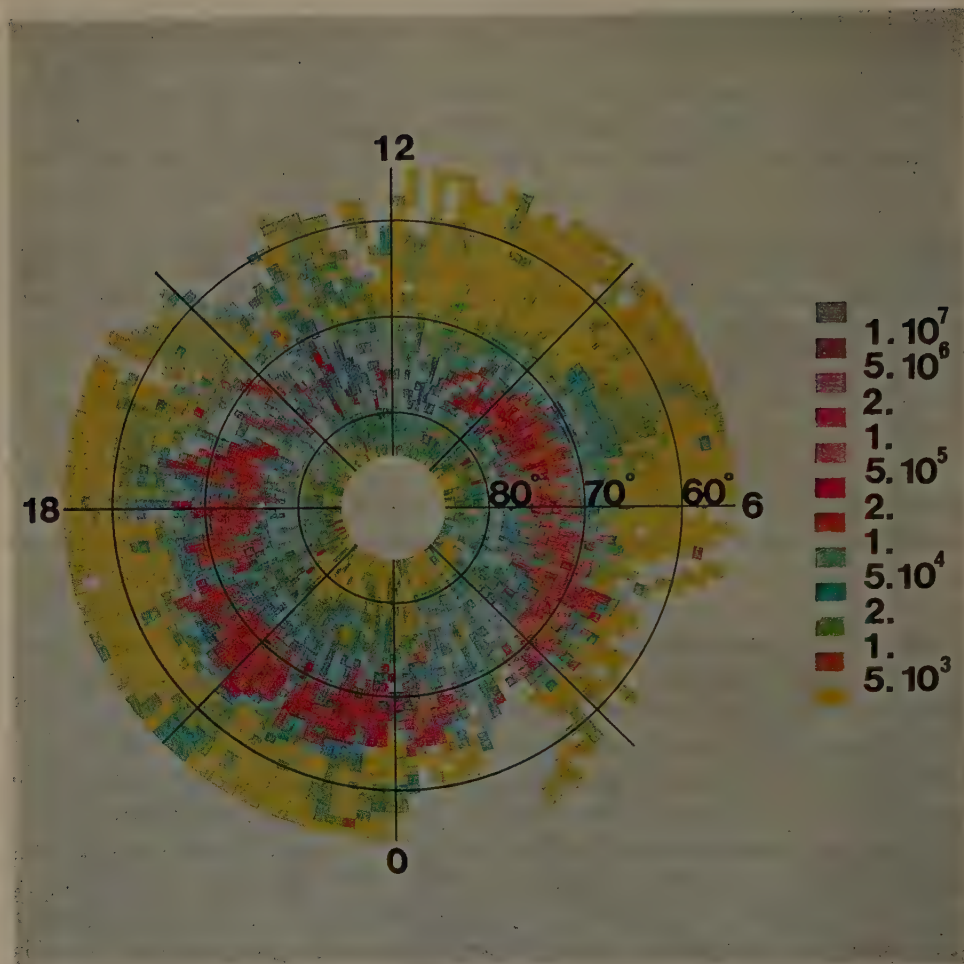


Fig. 1. Precipitation patterns of 5.8 keV protons at $\sim 10^\circ$ pitch angle for low geomagnetic activity ($K_p = 1+$ to 3_0). A : invariant latitude; MLT: magnetic local (eccentric dipole) time.
(For discussion of this figure see Section 3.)

description of this experiment has been given elsewhere (Riedler *et al.*, 1971). In short, altogether 10 sensor units consisting of electrostatic analyzers and Channel Multipliers were arranged at angles of 10° and 80° with the satellite axis. The bandwidths were between 10 and 20%, the acceptance half angles in the order of $\pm 4^\circ$.

The satellite ESRO I A (Aurorae) was launched on October 3, 1968, into a near-polar orbit (inclination 93.8°). The apogee after launch was 1533 km and the perigee 258 km. The satellite decayed on June 26, 1970. The spacecraft was magnetically stabilized, with the S 71-B sensors looking upwards over the northern polar region. Redu (Belgium), Tromsø and Spitsbergen (Norway) and Fairbanks (Alaska) were used as real-time read-out stations for S 71-B. Thus, a good coverage of the northern polar region both in latitude and MLT could be achieved.

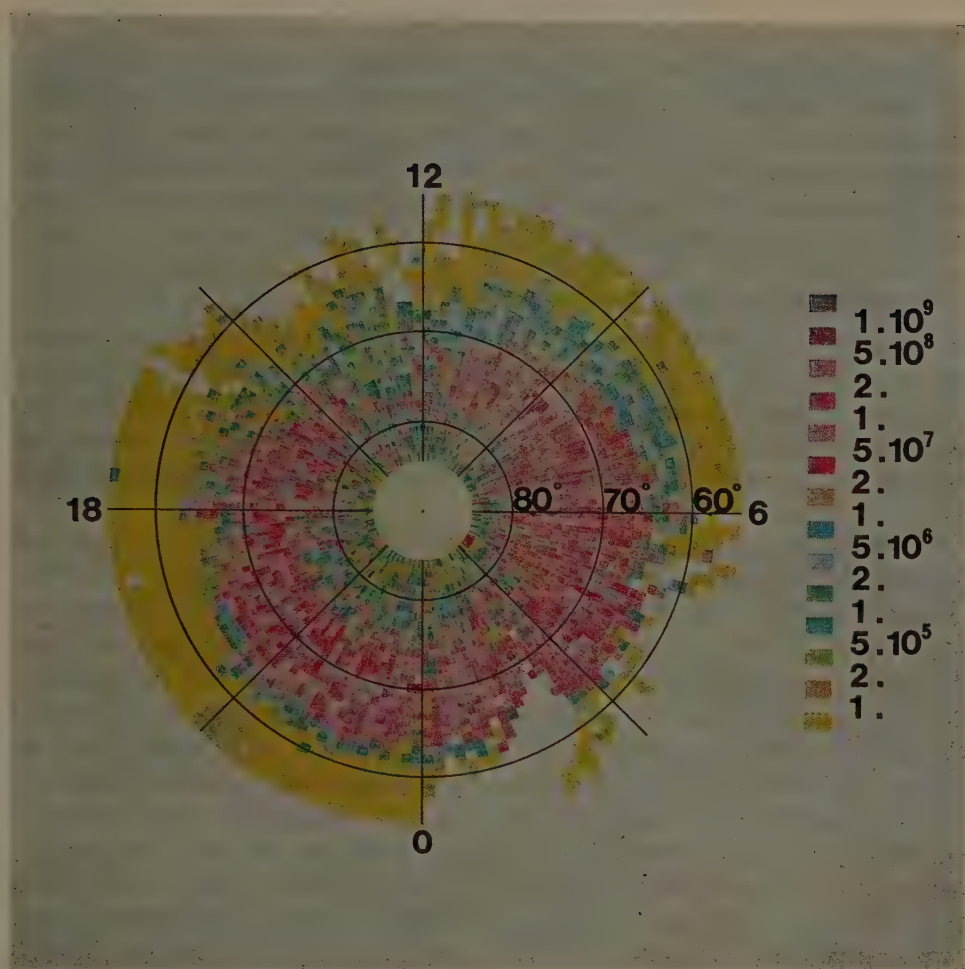


Fig. 2. Precipitation patterns of 1.3 keV electrons at $\sim 10^\circ$ pitch angle for low geomagnetic activity ($K_p = 1_+$ to 3_0). A : invariant latitude; MLT: magnetic local (eccentric dipole) time.
(For discussion of this figure see Section 3.)

3. Results and Discussion

A. GENERAL REMARKS

In the following, data will be discussed which have been collected on approximately 4000 revolutions from October 14, 1969, until June 26, 1970. For this time, average values for the differential flux intensities have been computed. The data have been grouped according to the geomagnetic activity levels into 4 classes: $K_p = 0_0$ to 1_0 ; $K_p = 1_+$ to 3_0 ; $K_p = 3_+$ to 5_0 ; $K_p = 5_+$ to 9_0 . Universal time variations have been taken into account only to the extent that they are represented by K_p . Seasonal effects have been neglected in order to improve the statistical MLT coverage. It should be mentioned, however, that in practically all MLT sectors both sum-

mer and winter data have been obtained at various periods of the satellite's lifetime.

Figure 1 shows an example of the results. The average proton fluxes for 5.8 keV (10° pitch angle) and $K_p = 1_+$ to 3_0 are plotted in a $10' \times 1^\circ$ coordinate system in the MLT - IN Lat plane using a color code. Another example can be seen in Figure 2 (1.3 keV electrons, 10° , $K_p = 1_+$ to 3_0). A series of similar plots for various energies and K_p values, but with lower MLT and intensity resolution, has recently been presented by Riedler and Borg (1971).

B. DISCONTINUITIES IN PRECIPITATION PATTERNS

One of the most striking features of the 5.8 keV proton precipitation patterns is a marked discontinuity at 19 hr MLT and also, but not so pronounced, at ~ 5 hr MLT (Figure 1), for low K_p values. For higher K_p than 3, the two apparent quasi-circular zones merge into one broader region. The same basic behavior can be observed for electrons too, although the apparent shift in latitude is less drastic (Riedler and Borg, 1971).

Instrumental effects or eventual seasonal effects have to be ruled out as a possible cause of the discontinuity, mainly because of the MLT coverage (Section A). Thus, in light of the experimental evidence (Section 1) and due to the lack of any other satisfactory explanation of the apparent discontinuities, the following view is adopted. A nightside particle population, probably injected near the midnight region, is drifting around the earth. The drift paths are determined by various factors: particle charge and energy, magnetospheric magnetic and electric field configuration, including corotation, etc. In addition, a precipitation mechanism, possibly of the Kennel and Petschek (1966) type is acting on the particles, which is also determining the varying intensity regions of precipitation. This drift population, with maximum precipitation on the nightside around $\sim 67^\circ$ IN Lat, is superimposed by a different dayside population at 5° to 10° higher latitude, originating in the direct access of magnetosheath plasma on the dayside. Winningham (1972) has discussed the characteristics of this population. It could be noted, that the maximum average flux values of $\gtrsim 10^5$ protons $\text{cm}^{-2} \text{s}^{-1} \text{sr}^{-1} \text{keV}^{-1}$ (Figure 1) fit the spectra reported by Winningham. This population should then extend in longitude to ~ 5 and ~ 19 hr MLT during considerable portions of time. It is not possible to decide whether the obvious enhancement of the 5.8 keV dayside proton precipitation at dawn and dusk is due to an increase in the overall average flux or whether it is due to the spectral variation caused by some additional acceleration.

It is of interest to note that in the dusk region individual passes have been reported where the 5.8 keV fluxes show two distinct maxima (Riedler and Hultqvist, 1970).

C. NOON DUSK 'VALLEY' IN AVERAGE FLUX DISTRIBUTION

In all electron precipitation patterns (Riedler and Borg, 1971), a "valley" in the average flux distribution is observed. It usually extends from noon towards the dusk region. It is energy dependent, i.e., more pronounced for higher energies (5.8 and 13 keV), and K_p dependent in the sense that its width and depth increase with increasing K_p .

In Figure 2 this "valley" can be seen for 1.3 keV electrons from 12 to 15hr MLT. Apparently, it extends only to latitudes of about 75° . In view of the discussion in Section 2, a more adequate description of the situation is that the 'valley' is bridged by another population of particles centered around 77° IN Lat. This 'bridge' is not present for higher energies in accordance with the soft spectral characteristics of the dayside magnetosheath plasma. For 5.8 keV protons, a similar 'valley' is observed which is centered more around noon. These 'valleys' could be interpreted by the various mechanisms acting on the drift particles. For electrons the drift is eastward, for protons it is predominantly westward. A considerable fraction of the particles is influenced by the existing electric fields in such a way that they cannot complete a full drift path around the earth. For example for electrons the noon/midnight meridian seems to act as an apparent 'barrier' in the 1 to 10 keV range, as evidenced by the 'valley'. Particle trajectories showing the influence of electric fields have been presented by McIlwain (1972) and seem to support this interpretation.

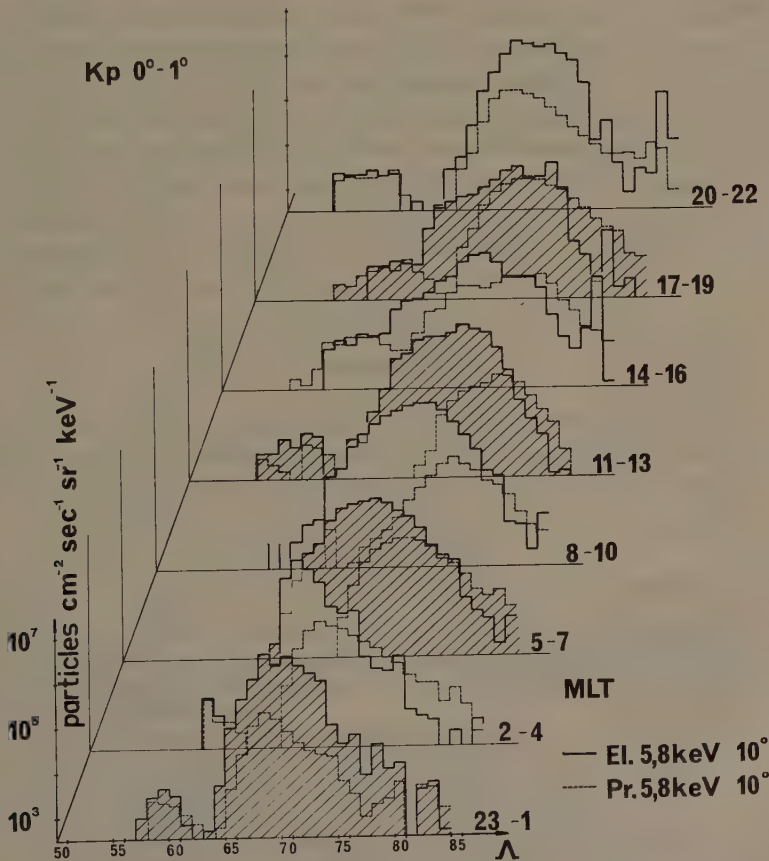


Fig. 3. Relative positions of average proton and electron fluxes at 5.8 keV, $\sim 10^\circ$ pitch angle for magnetically quiet conditions ($K_p = 0_0$ to 1_0). Λ : invariant latitude; MLT: magnetic local (eccentric dipole) time.

D. RELATIVE POSITIONS OF MAXIMUM ELECTRON AND PROTON PRECIPITATION

In the past years the question of a possible cross over of electron and proton auroras in the morning sector has been discussed. This cross over should, of course, be reflected in the particle precipitation patterns. Indeed, as shown in Figure 3 (for magnetically quiet conditions and 5.8 keV electrons and protons) the average proton precipitation maximum is clearly south of the electron maximum in the late evening and midnight sectors and moves poleward during the morning. At noon, the difference is of the order of 5° IN Lat. There is a rather abrupt change from 19 to 21hr, which is connected with the discontinuities (Section B). Thus, the average dayside proton fluxes (5.8 keV) are predominantly observed poleward of the electrons. This is in qualitative agreement with Frank's (1971) observations. For disturbed conditions the situation is not so clear any more.

E. LOW LATITUDE PROTON PRECIPITATION

Figure 4 shows the K_p dependence of the observed average proton fluxes at 10 and

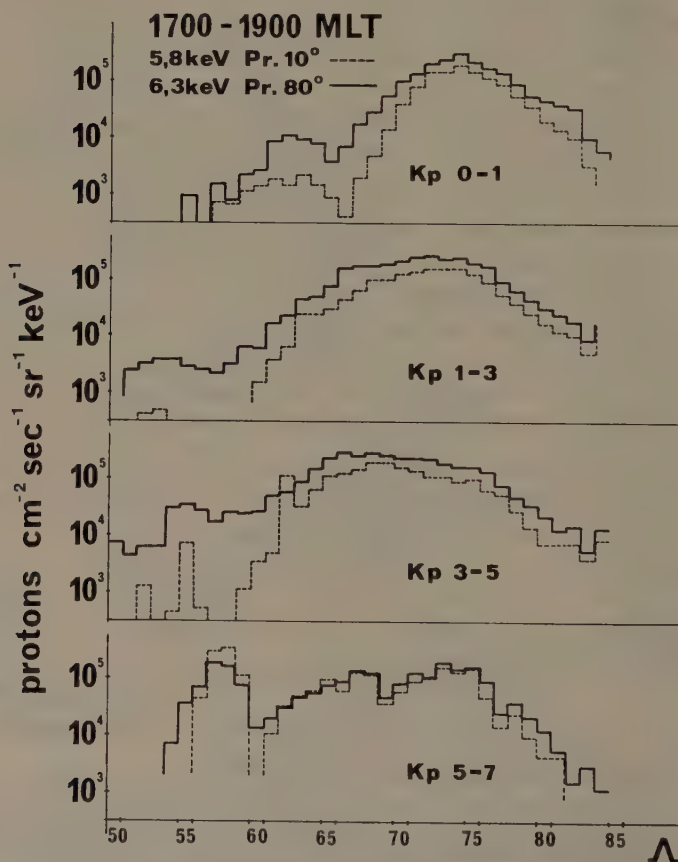


Fig. 4. K_p dependence of average proton fluxes at 17-19 hr MLT.

80° pitch angle with 5.8 and 6.3 keV respectively. As an example, an LT average of 17 to 19hr MLT has been chosen. As can be seen, the maximum values at auroral latitudes remain approximately constant at 10^5 protons $\text{cm}^{-2} \text{s}^{-1} \text{sr}^{-1} \text{keV}^{-1}$. The precipitation is isotropic. The constant difference may be due to the difference in energy or a calibration uncertainty. At lower latitudes (below 60° IN Lat) quite different conditions are observed. The precipitation is pronounced anisotropic, with the 80° fluxes normally considerably higher than at 10°. The maximum flux values increase from 10^3 and below to more than 10^5 protons $\text{cm}^{-2} \text{s}^{-1} \text{sr}^{-1} \text{keV}^{-1}$ with increasing K_p . This could be considered as evidence that at low latitudes a different particle population than at auroral latitudes is observed.

Eather and Carovillano (1971) have shown that the outer edge of the ring current is a likely source for auroral protons. Among other things they discussed the relative constancy of the ring-current population and hence of the proton precipitation during variable magnetic activity levels. Cornwall *et al.* (1971) discussed the possibility of ring current protons as the ultimate cause of SAR arcs. At the inner edge of the ring-current a proton loss should occur due to ion-cyclotron interactions. The observable proton fluxes would be peaked near 90° pitch angle. Also, it is known that SAR arcs are strongly K_p dependent. It can easily be seen that the proton fluxes (Figure 4) fulfill all the above mentioned criteria. Thus, it is postulated that the K_p dependent low latitude fluxes are identical with those predicted by Cornwall *et al.* (1971) in connection with the generation of SAR arcs. For the very high K_p values, the angular distribution seems to have been field aligned in many cases. This effect has been reported earlier (Hultqvist *et al.*, 1971). An investigation of the LT and latitudinal occurrence frequency of this phenomena is under way.

Acknowledgment

The research reported in this paper was sponsored by the Swedish Natural Science Research Council, the Swedish Board for Technical Development and, to a minor extent, by the Space Research Institute of the Austrian Academy of Science.

References

- Cornwall, J. M., Coroniti, F. V., and Thorne, R. M.: 1971, *J. Geophys. Res.* **76**, 4428.
- Eather, R. H. and Carovillano, R. L.: 1971, *Cosmic Electrodyn.* **2**, 105.
- Eather, R. H. and Mende, S. B.: 1971, Paper presented at the Advanced Study Institute on Magnetosphere Interactions, Dalseter, Norway.
- Feldstein, Y. I.: 1963, *Geomagnetizm i Aeronomiya* **3**, 183.
- Frank, L. A.: 1971, *J. Geophys. Res.* **76**, 5202.
- Frank, L. A. and Ackerson, K. L.: 1971, *J. Geophys. Res.* **76**, 3612.
- Heikkila, W. J. and Winningham, J. D.: 1971, *J. Geophys. Res.* **76**, 883.
- Hultqvist, B., Borg, H., Riedler, W., and Christophersen, P.: 1971, *Planetary Space Sci.* **19**, 279.
- Kennel, C. F. and Petschek, H. F.: 1966, *J. Geophys. Res.* **71**, 1.
- Lassen, K.: 1970, *Phys. Norv.* **4**, 171.
- McIlwain, C. E.: 1972, this volume, p. 268.
- Mishin, V. M., Saifudinova, T. I., and Zhulin, I. A.: 1970, *J. Geophys. Res.* **75**, 797.

- Riedler, W. and Hultqvist, B.: 1970, *Space Res.* **10**, North-Holland Publishing Company, Amsterdam, Holland, p. 847.
- Riedler, W. and Borg, H.: 1971, *Space Res.* **12**, Akademie-Verlag, Berlin, in press.
- Riedler, W., Hultqvist, B., and Olsen, S.: 1971, *Arkiv Geofysik* **5**, 619.
- Sharp, R. D. and Johnson, R. G.: 1971, in B. M. McCormac (ed.), *The Radiating Atmosphere*, D. Reidel Publishing Company, Dordrecht, Holland, p. 239.
- Winningham, J. D.: 1972, this volume, p. 68.

ELECTRON INTENSITIES OVER AURORAL ARCS

D. A. BRYANT, G. M. COURTIER and G. BENNETT

*S.R.C., Radio and Space Research Station, Ditton Park,
Slough, SL3 9JX, Bucks., U.K.*

1. Introduction

This report is a summary of measurements of electron intensities made from two sounding rockets flown over auroral arcs. The main conclusion drawn from these measurements is that both the auroral arcs occurred at the boundary between two magnetospheric plasmas. This conclusion is based on the fact that some of the observed changes in electron energy spectrum are unlike the changes to be expected on grounds of continuity from a single source plasma accelerated by different degrees.

The measurements were made on the ESRO Skylark rocket S67/2 launched from Kiruna ($L=5.4$) at 2139:30 UT (approximately geomagnetic midnight) on October 29, 1970, and on the NDRE Nike-Tomahawk rocket F19 launched from Andøya ($L=6$) at 2144:16 UT (also approximately geomagnetic midnight) on October 1, 1968. This brief report deals principally with the results of the S67/2 flight, although the F19 results are introduced in the discussion section.

Electron intensities were measured with channel multipliers and electrostatic analyzers. Each rocket payload contained several such detectors – some with fixed voltages applied to the plates of the electrostatic analyzers, and some with voltages cyclically stepped through eight levels and swept back to the initial level.

2. Flight S67/2

A. FLIGHT CONDITIONS

S67/2 was launched during a magnetic bay at a time of renewed magnetic activity during the recovery of the X-component of the local geomagnetic field from a depression of about 500 γ . A band of multiple arcs reached from the eastern to the western horizon. At the flight time of 100 sec, when measurements began, the rocket was magnetically south of the region where most of the light was produced. By 120 s the rocket was magnetically above the arc region and remained so until about 200 s. The rocket entered the region north of the arc only briefly because by 210 s the arc had begun to move northwards and overtake the rocket. Although these relative positions of the rocket and the arc can be only approximate since the arc was viewed away from the magnetic zenith, they serve as useful references for the various forms of energy spectrum encountered during this flight. Flight F19 was made under very similar magnetic and optical conditions although in this case the rocket sampled the regions from the center of the arc to the north of the arc.

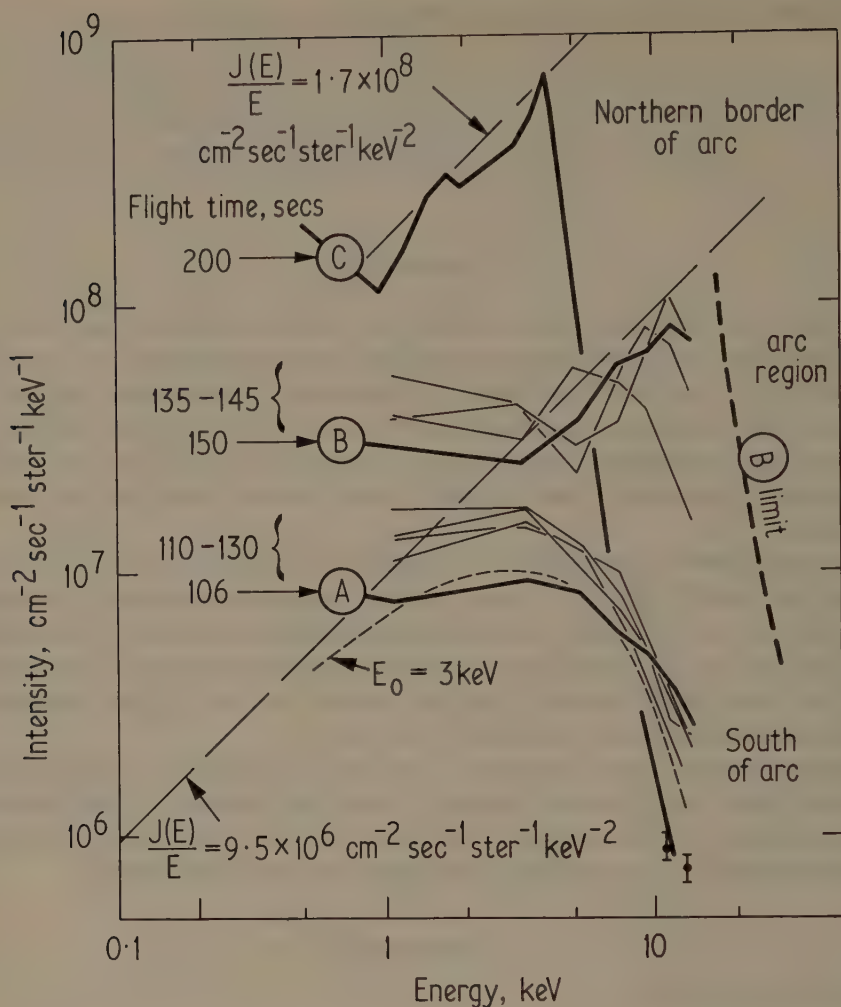


Fig. 1. Electron energy spectra measured on flight S67/2. Spectra A, B, and C were observed south of an auroral arc, within the arc, and at the northern border of the arc, respectively. Energy spectra observed during the transition between A and B are also shown. The other lines are explained in the text.

B. ELECTRON ENERGY SPECTRA

Electron energy spectra typical of the regions through which the rocket passed are shown in Figure 1. These energy spectra are for electrons with pitch angles between 10 and 20° . On both flights the electrons arrived almost isotropically over the upper hemisphere for all observed intensities. Let us examine first the spectra labeled A, B, and C. Spectrum A was observed to the south of the arc region: the peak intensity occurs at about 3 keV, and the shape is approximately that of a Maxwellian distribution with $kT = 3$ keV as shown by the dashed line. Spectrum B within the arc region

has a peak energy of 12 keV or more, and is more sharply peaked than a Maxwellian distribution (a dashed line gives the upper limit to spectrum B set by a measurement of the integral electron intensity). The transition from a spectrum of type B to spectrum C occurred within 1 s at 200 s while the rocket traveled only 200 m relative to the ground. Spectrum C is the first of the energy spectra observed at the northern border of the arc: it differs markedly from spectrum B in that the peak energy is lower and the peak intensity is much higher, and it differs from spectrum A which has approximately the same peak energy in that it is more sharply peaked and has a much higher intensity. Other spectra observed at the northern border of the arc (not shown in Figure 1) are similar to spectrum C in that they have more than one peak, though the energies at which the peak intensities occur exhibit some variability. At about 220 s, when the arc region moved northward and engulfed the rocket again, the energy spectrum reverted in both shape and intensity to type B and remained so for the remaining 200 s of flight.

Let us now consider what relationships exist between these energy spectra and, in particular, whether they could all result from a single source plasma undergoing different degrees of acceleration, or whether more than one source plasma is required. The constraints imposed by continuity are revealing in this respect.

3. Continuity Constraints

Differential intensity measured along a particle trajectory can be expressed (Ray, 1959) as

$$J(E) = \tau p^2, \quad (1)$$

where τ is the density in phase space and p is the momentum.

In the present application one may use the nonrelativistic approximation

$$J(E) = 2m\tau E, \quad (2)$$

where m is the mass and E is the kinetic energy.

Swann (1933) showed that for charged particles moving in an electromagnetic field there is a form of Liouville's theorem which states that along a trajectory the density in phase space remains constant. The theorem does not hold (at least in a simple form) if there is an important degree of scattering or dissipation since these processes would lead in general to a reduction in phase-space density. However we shall explore here only the consequences of a constant phase-space density. In this case we see from Equation (2) that the intensity of a group of particles increases linearly with energy, as pointed out by Rearwin (1971). It follows also that a constraint imposed on the spectrum of electrons accelerated from a given source plasma is

$$[J(E)/E]_{\max} = 2m\tau_{\max}, \quad (3)$$

where τ_{\max} is the maximum phase-space density in the source plasma.

If the source plasma has a Maxwellian distribution

$$J(E) = AEe^{-E/E_0}, \quad (4)$$

where $E_0 (=kT)$ is the peak energy and A is a constant which depends on the electron density N and temperature T , we find from Equations (3) and (4) that the maximum phase-space density occurs in the low-energy tail of the distribution. On substituting the full expression for A we find that

$$[J(E)/E]_{\max} = 1.7 \times 10^8 NE_0^{-3/2} \text{ cm}^{-2} \text{ s}^{-1} \text{ sr}^{-1} \text{ keV}^{-2}. \quad (5)$$

Discussion

Let us suppose at first that the Maxwellian approximation to spectrum A in Figure 1 is the spectrum of electrons in a source plasma. This spectrum imposes the constraint (indicated by a dashed line) that

$$[J(E)/E]_{\max} = 9.5 \times 10^6 \text{ cm}^{-2} \text{ s}^{-1} \text{ sr}^{-1} \text{ keV}^{-2}.$$

We notice that (at least for energies ≥ 2 keV where the effects of atmospheric absorption are negligible) spectrum B and the transition spectra observed between 106 and 150 s lie within this constraint. Furthermore the peak intensities of these spectra lie close to the dashed line. It seems likely therefore that spectrum B and the transition spectra are accelerated versions of spectrum A. Spectrum A is not necessarily the energy spectrum in the source plasma since it may itself be an accelerated version of a lower-temperature plasma with the same maximum phase-space density. Spectrum C, however, has a much higher phase-space density and requires a source plasma with a maximum phase-space density corresponding to at least

$$J(E)/E = 1.7 \times 10^8 \text{ cm}^{-2} \text{ s}^{-1} \text{ sr}^{-1} \text{ keV}^{-2}$$

as indicated in Figure 1. The other energy spectra observed at the northern border of the arc have phase-space densities which are lower but still more than ten times higher than that of the A and B spectra. It seems clear therefore that the electrons observed at the northern border of the arc originated from a different source plasma to those observed south of the arc and within the arc region.

In order to try to identify the source plasmas we make the assumptions that the source plasmas have Maxwellian distributions and that the electrons are isotropic within them. From Equation (5) we see that a given value of maximum phase-space density defines a relationship between the electron density and peak energy in the source plasma. These relationships are indicated by the straight lines of slope 3/2 in Figure 2. Broken lines are used in most cases but solid lines are used where energy spectra were observed over a range of peak energies. The lines are identified by the letters A–C from flight S67/2, and by the numerals 1–4 from flight F19 which has been analyzed in a similar way. The identification is made at the energy where the peak intensity occurred in the energy spectrum from which it was derived. Enclosing circles

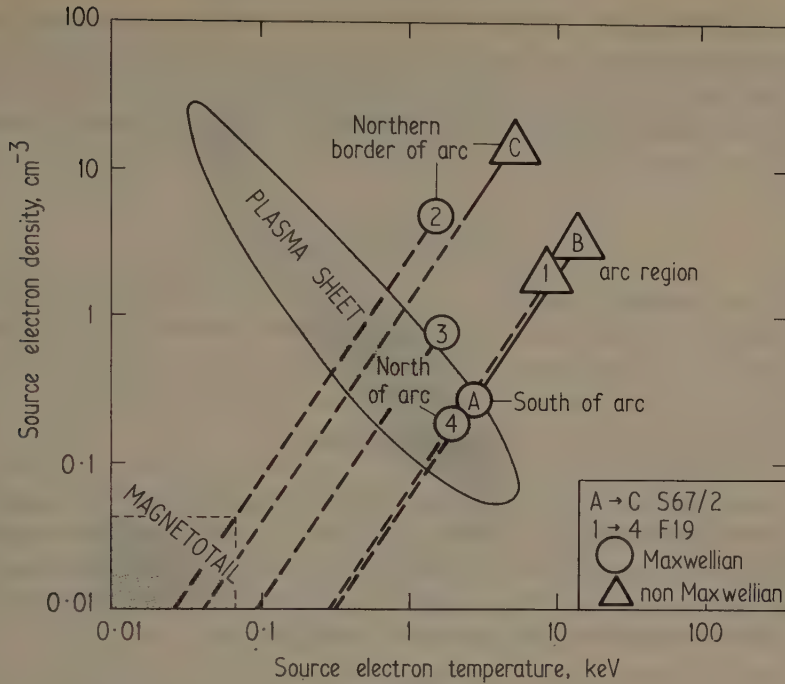


Fig. 2. Electron densities and temperatures of plasmas having the phase-space density required by a source of the observed electrons (solid and broken lines; see text), and densities and temperatures that have been observed at various times in the plasma sheet and high-latitude magnetotail (shaded areas).

indicate that the energy spectra were either observed to be or were consistent with Maxwellian distributions: enclosing triangles indicate that the spectra were more sharply peaked than Maxwellian distributions.

It is unfortunate that we do not have concurrent values of electron densities and temperatures in various magnetospheric plasmas for comparison. However typical values for the plasma sheet and high latitude magnetotail lie within the shaded areas in Figure 2. These are taken from a review by Vasyliunas (1971) and assumed here to have Maxwellian distributions.

Using Figure 2 we may make the following tentative identifications of the source plasmas for the various electrons. To the south of an arc region (spectrum A) the electrons may be unaccelerated plasma-sheet electrons. Within the arc regions (spectra B and 1) the electrons may be plasma-sheet electrons after acceleration. Electrons at the northern borders of the arcs, where the source plasma has a higher phase-space density (spectra C and 2) could originate from the high-latitude magnetotail. The decrease in density at constant temperature observed northward of an arc (spectra 3 and 4) must then be attributed to a gradient in the magnetotail. If the observed rapid transition in phase-space density represents the boundary between the plasma sheet and the high-latitude magnetotail, for the present cases the latter has a higher phase-

space density. This is not always the case as changes of plasma properties observed on particular traversals of this boundary (Hones *et al.*, 1971a,b) may be interpreted as showing that the phase-space density in the high-latitude magnetotail is at times higher, lower or equal to that in the plasma sheet. It would be of interest to establish whether a particular configuration is a requirement for the formation of auroral arcs.

Conclusions

From the above results we conclude that both of the auroral arcs we have investigated occurred at the boundary between two magnetospheric plasmas. It is possible that the two plasmas were the plasma sheet and the high-latitude magnetotail.

Acknowledgments

We are greatly indebted to the European Space Research Organization and to the Norwegian Defence Research Establishment for their cooperation in the preparation and launching of the rockets S67/2 and F19, respectively. The work described in this paper was carried out at the Radio and Space Research Station of the Science Research Council and is published with the permission of the Director.

References

- Hones, E. W., Jr., Asbridge, J. R., and Bame, S. J.: 1971a, *J. Geophys. Res.* **76**, 4402.
Hones, E. W. Jr., Akasofu, S.-I., Bame, S. J., and Singer, S.: 1971b, *J. Geophys. Res.*, **76**, 8241.
Ray, E. C.: 1959, *State University of Iowa Report*, **59-21**.
Rearwin, S. D.: 1971, *J. Geophys. Res.* **76**, 4505.
Swann, W. F. G.: 1933, *Phys. Rev.* **44**, 224.
Vasyliunas, V. M.: 1971, in G. Skovli (ed.), *The Polar Ionosphere and Magnetospheric Processes*, Gordon and Breach, Science Publishers, Inc., New York, p. 25.

THE PRE-MIDNIGHT ASYMMETRY IN THE 40 keV ELECTRON FLUX PROFILES AND ITS RELATION TO MAGNETOSPHERIC SUBSTORMS

L. ROSSBERG

Max-Planck-Institut, Lindau, West Germany

1. Introduction

Passes of the polar orbiting German research satellite AZUR, which are tangential several times per day to the average nightside 40 keV electron flux boundary, often reveal striking asymmetric deviations of the electron flux levels from the average longitudinal or LT distributions. Among these, the most prominent recurrent asymmetric deviation involves an electron flux profile in the dusk-midnight sector which is terminated by a narrow steep spike in the flux of the precipitated and trapped electrons whose location is displaced equatorward from the average boundary (McDiarmid and Burrows, 1968). This phenomenon is probably identical with the 'sharp boundary' described by McDiarmid and Burrows. Adjacent to the east electron fluxes appear highly structured, more or less poleward of the average boundary location and cover a considerable area in longitude and latitude. A phenomenological description of this phenomenon and of the special features of the orbit of AZUR resulting in the tangential passes appears in Rossberg and Theile (1971), Rossberg (1971). This paper deals with the relation of these asymmetric disturbances to geomagnetic activity.

2. Results

Three extremely different electron flux profiles observed during similar tangential traversals of the auroral zone during magnetically quiet days ($K_p < 3_0$) are shown in Figure 1. The scales give the flight time in 1 min intervals, UT, the invariant latitude, IN Lat, and the eccentric dipole time, EDT. The logarithmic ordinate gives the electron flux $\text{cm}^{-2} \text{s}^{-1} \text{sr}^{-1}$ of electrons with energies $> 40 \text{ keV}$ at 90° (heavy line) and 0° (dotted line) pitch angle. The flight direction is from the dawn sector (right) into the dusk sector (left). The insets show the satellite trajectory in EDT and IN Lat coordinates. Figure 1 also illustrates:

- (a) An undisturbed pre-post-midnight profile,
- (b) Fairly symmetric sharp boundaries, most pronounced on the dusk side of the pass, and
- (c) One of the asymmetric cases, with an equatorward displaced boundary terminated by a narrow spike with almost isotropic pitch angle distribution on the dusk side, and eastward of it very structured electron fluxes, extending poleward of the average boundary position.

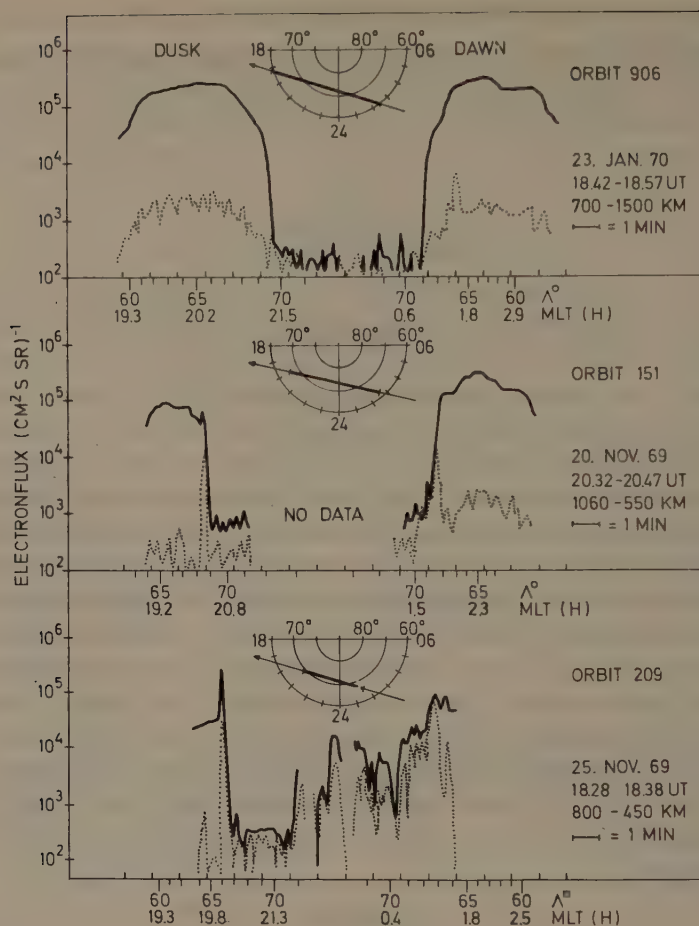


Fig. 1. 40 keV electron fluxes around 90° (heavy line) and 0° pitch angle (broken line), plotted vs. UT. A separate scale is provided for IN Lat and EDT. Shown are three extremely different samples of electron flux profiles observed during similar tangential traversals of the nightside auroral oval under relatively quiet magnetic conditions.

I believe that the sharp boundary is identical with the 35 keV sharp electron boundary reported by McDiarmid and Burrows (1968). An inspection of their Figure 5 shows that the sharp boundaries are located between 68 and 69° IN Lat, 1 or 2° below the average 35 keV background boundary. According to our observations this is another characteristic feature of the sharp boundaries over the whole EDT range of their occurrence. In fact, these boundaries appear compressed equatorward or as if they were sliced or chopped with part of the northern edge of the trapped radiation removed by some unknown mechanism. Consequently I prefer to use the term C boundary for the profile defined here (Rossberg, 1971b). By this new definition sharp boundaries are excluded which occur during disturbed times poleward of the normal position of the boundary.

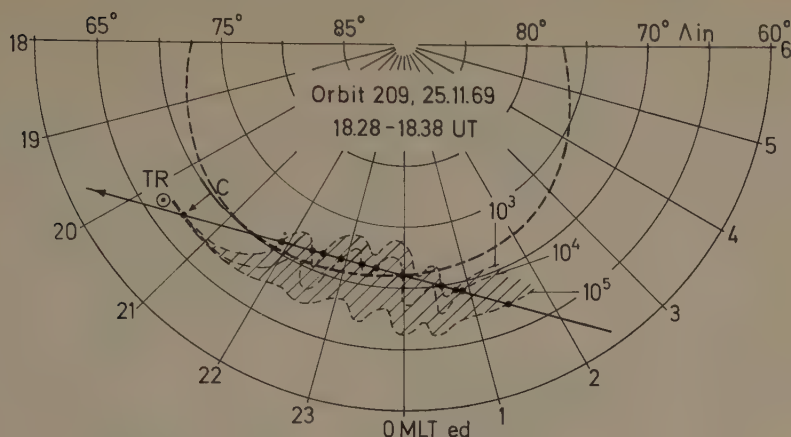


Fig. 2. Polar IN Lat-EDT plot of the trajectory of AZUR during the asymmetric disturbance observation shown in Figure 1. The location of different flux levels is indicated by dots. The broken line represents one possible fit of isoflux lines to the observed points. The equatorward displacement of the C boundary is indicated by an arrow. The heavy broken line gives the average boundary position after McDiarmid and Burrows (1968).

The fluxes adjacent to the C boundary eastward, towards dawn, are highly structured and slowly increasing with decreasing latitude. The boundary is probably also highly structured poleward of the satellite's trajectory. Precipitation extends over a considerably larger area than at the location of the C boundary. This becomes more evident when one plots the traversals of different flux levels along the trajectory of the satellite in a polar IN Lat-EDT diagram (Figure 2). The Alouette 35 keV background boundary is inserted by a dotted line for reference purposes. In order to demonstrate the approximate magnitude and the direction of the deviation, the measured points were tentatively supplemented by dotted lines which represent a possible fit of the isoflux lines to the momentary observations provided that the time scale of temporal variations is smaller than the traversal time. This is probably not the case in the spiky region. However, the sense of the disturbance-asymmetry is independent of temporal variations.

3. Relation to Geomagnetic Activity

The occurrence probability of asymmetric disturbances, including also singly observed C boundaries does not show any significant dependence on K_p between $0^- < K_p < 6_0$. This is surprising because it is generally accepted that the frequency of magnetic substorms increases with K_p . A direct comparison of our observations with magnetograms obtained by stations located in the vicinity of the satellites trajectory revealed that the asymmetric disturbed cases occur predominantly *before* the onset of a negative magnetic bay. Occasionally they occur at the end or between successive bays where the bay onset is determined around the midnight meridian. At the most they are observed 3 hr before the negative bay onset; in one case, they were even recurrent

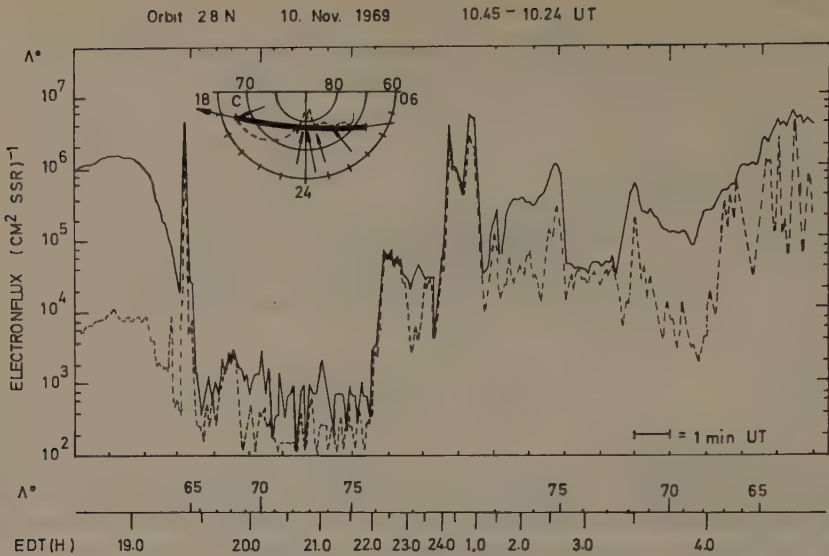


Fig. 3. Electron flux asymmetry across 20–21 EDT observed during a magnetic storm. (For details see caption Figure 1.)

within the 2 hr orbital period (Rossberg, 1971). A sample observed during a magnetic storm, 1.5 hr before the onset of the main magnetic bay, is shown in Figure 3, the trajectory in invariant longitude, UT coordinates together with the magnetograms from College, Sitka, and Meanook are shown in Figure 4. An inset in Figure 3 shows the satellites trajectory in IN Lat-EDT coordinates with arrows indicating the location of the different disturbance phenomena in this polar diagram. The dotted line again indicates the possible instantaneous location of the trapping boundary during that pass. Notice the abrupt termination of an essentially quiet time electron flux profile by the tremendously steep and narrow spike at 65° IN Lat on the dusk side and the highly structured fluxes extending from pre-midnight until morning hours across the highest latitude point reached during that pass. The poleward termination of the electron fluxes around the midnight meridian is located beyond 77° latitude and consequently the latitudinal difference between the midnight location and the dusk location of the boundary is more than 12° . With respect to these high trapped and precipitating electron fluxes it is surprising that this occurs 1.5 hr before the negative bay onset. At times the midnight and dawn precipitation occurs *during* a negative bay in that area, but then the C boundary occurs in the associated positive area towards dusk (Akasofu *et al.*, 1966). There are also cases, however, where the disturbance is not accompanied by any noticeable disturbance or only by a weak positive bay on the magnetograms of the nearby stations. This explains the relatively high occurrence probability at low K_p values. In conclusion, it can be stated that the asymmetric disturbance occurs during all phases of magnetic substorms but predominantly during the development (pre-bay) and recovery phase. Instances where no bay activity

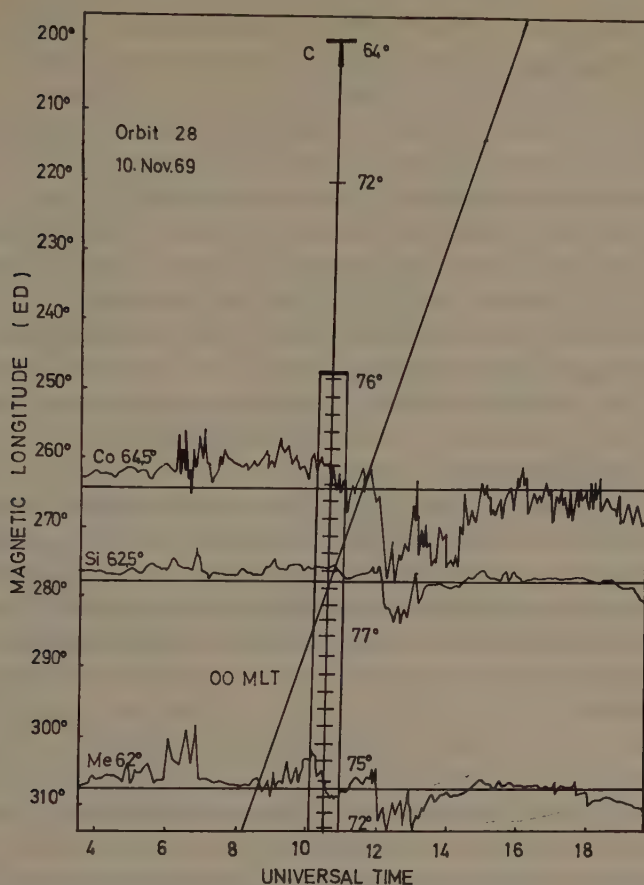


Fig. 4. Supplement to Figure 3, showing the trajectory in UT-IN Long coordinates together with the magnetograms of College, Sitka, and Meanook. Enhanced fluxes are indicated by bars along the trajectory and the boundary by heavy bars. EDT midnight is along the inclined line.

occurs are possibly due to the relatively low latitude ($< 70^\circ$) of most of the observatories.

4. Discussion

There is mounting evidence that enhanced nightside precipitation of energetic particles can start hours before the onset of a negative magnetic bay (Pytte and Trefall, 1971; Pilkington, 1972). Our observations confirm their results. The asymmetric flux distribution across some pre-midnight meridian during these pre-bay events is new. On occasion, however, this phenomenon also occurs also at the end of a magnetic bay or between successive bays; if it occurs at midnight during the time of a bay then the C boundary is observed in the area of an associated positive bay towards dusk. A phenomenon, which shows a similar dependence on various phases of magnetic substorms, is the deviation of magnetic field magnitude and direction from quiet time

values at the synchronous orbit of ATS 1 (Cummings *et al.*, 1968). They observed depressions predominantly in the dusk-midnight quadrant of the magnetic field before, and a sudden recovery of the field to its quiet day configuration at the onset of a negative bay, followed by a renewed depression. They related the depression to the formation of a partial ring current.

Direct evidence for the formation of an asymmetric ring current by low energy protons during magnetic storms was reported by Frank (1970). The location of the C boundary at 68° IN Lat or less can be related to the outer edge of the ring current proton distribution. There the particle energy density approaches that of the magnetic field, resulting in a high β condition (Frank, 1967) and presumably strong pitch angle diffusion for electrons (Kennel, 1969).

These effects may account for the isotropic pitch angle distribution within the spike at the edge of the C boundary. The slight equatorward displacement thus is the result of the total loss of particles further out.

Furthermore, the apparent stability of the spike can be explained by a situation of balance between the eastward moving inner edge of the plasma sheet (Vasyliunas, 1968) and the enhanced magnetic pressure at the outer edge of the ring current. This situation probably terminates then in the vicinity of the midnight meridian where inward convection, acceleration and eastward drift of electrons become dominant (Lezniak and Winckler, 1970), resulting in the observed irregular flux distributions in the auroral zone.

Acknowledgments

The author gratefully acknowledges the encouragement given by Professor G. Pfozter and the late Professor A. Ehmert.

The author also gratefully acknowledges the stimulating discussions with Dr. R. Pilkington and the assistance of Dr. J. Münch, who processed the data discussed in this paper.

This work was supported by contract WRK 64 of the Bundesministerium für Wissenschaftliche Forschung.

References

- Akasofu, S.-I., Meng, C.-I., and Kimball, D. S.: 1966, *J. Atmospheric. Terrestr. Phys.* **28**, 489.
- Cummings, W. D., Barfield, J. N., and Coleman, P. J.: 1968, *J. Geophys. Res.* **21**, 6687.
- Frank, L. A.: 1967, *J. Geophys. Res.* **72**, 185.
- Frank, L. A.: 1970, *J. Geophys. Res.* **75**, 1263.
- Kennel, C. F.: 1969, *Rev. Geophys.* **7**, 379.
- Lezniak, T. W. and Winckler, J. R.: 1970, *J. Geophys. Res.* **75**, 7075.
- McDiarmid, I. B. and Burrows, J. R.: 1968, *Can. J. Phys.* **46**, 49.
- Pilkington, R.: 1972, this volume, p. 391.
- Pytte, Th. and Trefall, H.: 1971, *J. Atmospheric Terrestr. Phys.*, to be published.
- Rossberg, L.: 1971, *J. Geophys. Res.*, to be published.
- Rossberg, L. and Theile, B.: 1971, *Eldo-Cecles/Esro-Cers Scient. Techn. Rev.* **3**, 3.
- Vasyliunas, V. M.: 1968, *J. Geophys. Res.* **73**, 2839.

PITCH ANGLES AND SPECTRA OF PARTICLES IN THE OUTER ZONE NEAR NOON

J. R. BURROWS, I. B. McDIARMID, and MARGARET D. WILSON

Division of Physics, National Research Council of Canada, Ottawa K1A 0R6, Canada

1. Introduction

Precipitation patterns of electrons on the dayside have been studied for many years using ground based evidence and satellite experiments. This article will summarize some of the more recent work, and attempt to extend and refine our understanding of these regions.

Hartz and Brice (1967) made a schematic summary of the experimental evidence in which they emphasized a separation on the dayside between a 'drizzle-type' precipitation peaking at $\sim 65^\circ$ IN Lat at 0800 LT and a splash type precipitation occurring at $\sim 75^\circ$ with increasing latitude separation as noon was approached. They identified the lower latitude region with the mantle aurora. Sharp and Johnson (1968), using polar satellites at ~ 300 km altitude and a detector with a 21 keV energy threshold, distinguished between a 'hard day zone' in the latitude range 64 to 75° near noon and a statistically overlapping 'soft zone' from 66 to 79° defined by the energy flux between 0.08 and 21 keV. A similar distinction was made by Hoffman (1969) using energy bands at 7.3 and 0.7 keV on a polar satellite at ~ 700 km. The lower latitude region was characterized by isotropic radiation not displaying much structure in its latitude profile. Hoffman (1971) identified this region with the 3914 Å mantle aurora emission described by Sandford (1968). Riedler (1972) shows synoptic plots of precipitating electrons at 5.8 and 1.3 keV similar to Hoffman. In contrast to this relatively unstructured 7.3 keV 'band' region, Sharp and Johnson (1968) found that the hard zone ($E > 21$ keV) near noon generally had highly structured precipitation. Since these measurements were made at $\sim 0^\circ$ pitch angle and at low altitude, the nature of the trapped particle flux at higher altitudes was unknown. One of the purposes of this paper is to report such measurements and discuss relevant precipitation mechanisms.

A higher latitude region has been variously described by Burch (1968), Sharp *et al.* (1969), Heikkila and Winningham (1971), and Hoffman and Berko (1971). Hoffman and Berko (1971) found that at 0.7 keV its highest probability of occurrence is between 0500 and 1400 hr MLT and 75 to $82\frac{1}{2}^\circ$ IN Lat when K_p was less than or equal to 2 and the minimum burst flux was taken to be 10^8 electrons $\text{cm}^{-2} \text{sr}^{-1} \text{s}^{-1} \text{keV}^{-1}$. This region is nearly congruent with the region of high probability of discrete auroral emission as recorded on all-sky camera photographs by Stringer and Belon (1967). The energy influx in the more intense electron bursts is sufficient to produce discrete auroral emissions at 3914 and 5577 Å visible in all-sky camera photographs.

The measurements by Heikkila and Winningham (1971) have been made over an energy from 10 eV to 10 keV in the altitude range 500 to 3500 km and over a variety of pitch angles. They distinguish a sharp intensity decrease in the flux of 1 to 10 keV electrons around 75° which presumably would identify with the boundary between the two regions. Primarily poleward of this boundary they observe an electron energy spectrum with a maximum flux at about 100 to 200 eV and with total flux of the order of 10^9 electrons $\text{cm}^{-2} \text{sr}^{-1} \text{s}^{-1}$. There is often considerable structure observed in the energy-time diagrams and it seems probable that the majority of the particle flux in the burst region lies below Hoffman's 0.7 keV band, and produces 6300 Å emissions at altitudes above 150 km as observed by Eather and Mende (1971). Associated with the electron flux there is a much smaller proton flux ($\sim 10^7$ protons $\text{cm}^{-2} \text{sr}^{-1} \text{s}^{-1}$) peaking at a slightly higher energy (~ 300 eV). Heikkila and Winningham (1971) have identified these fluxes with the magnetosheath plasma penetrating through the dayside cusp and propose that at low altitudes they occur on open field lines. From a study of the pitch angle distribution of energetic electrons ($E > 20$ keV) occurring in the same region this article will argue that these fluxes sometimes occur on closed geomagnetic field lines in the dayside magnetosphere.

Frank and Ackerson (1971) have concluded from a study of Injun 5 data that only small practical value is gained from zoning in the manner discussed above.

2. Instrumentation

The data discussed below were acquired by the energetic particle detector (EPD) and soft particle spectrometer (SPS) experiments on the ISIS 1 satellite in near polar orbit (88.7°) with apogee and perigee of 3530 and 600 km, respectively. The SPS experiment has been described by Heikkila *et al.* (1970). The EPD experiment consisted of an electron and a proton spectrometer composed of a number of integral threshold, collimated detectors viewing perpendicular to the satellite spin axis, and two collimated geiger counters viewing along the spin axis. Complete spectra are obtained with a time resolution of 0.267 s and pitch angle scans are obtained by the radially mounted detectors during the 20 sec spin period of the spacecraft. Complete scans (0 to 180°) are obtained when the spacecraft spin axis is perpendicular to the local magnetic field vector. In general, for an angle θz° between the spin axis and the field, a range of $90^\circ \pm \theta z$ is obtained. Electron detectors used in this study range in threshold from 20 to 200 keV, while proton thresholds are from 75 to 600 keV.

3. Data

Figure 1 shows the standard presentation of raw data for selected energy channels of the EPD experiment. Figures 1 to 4 will be discussed in detail as a sample pass. Since $\theta z \sim 90^\circ$, almost a complete pitch angle scan is obtained. The 20 keV detector has a collimator half angle of 5.1° and it measures maximum flux trapped perpendicular to the field twice per spin period. The 200 keV detector has a half angle of 21° ,

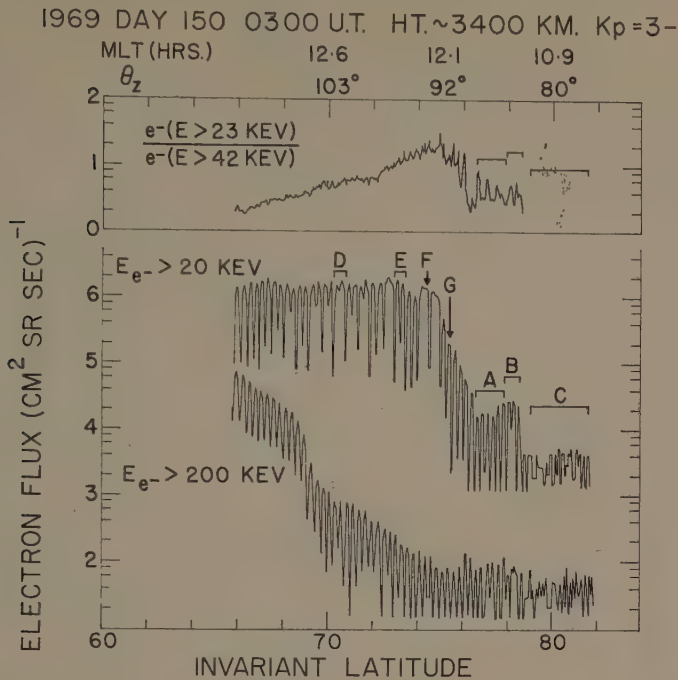


Fig. 1. Electron flux vs. IN Lat. The base 10 is omitted from the ordinate scale, leaving only the indices. The lower panel shows two radial electron detectors modulated at half the spin period. The upper panel shows the spectral ratio of the two axial detectors viewing approximately perpendicular to the spin axis. MLT and the angle between the spin axis and the magnetic field (θ_z) are shown along the top of the graph.

resulting in less resolution of the pitch angle distribution. The spectral ratio from the axial detectors varies from 2 to 20 as one proceeds poleward from 67 to 75° indicating a softening spectrum but it drops abruptly at 76° to about 3, as the low energy component decreases more abruptly than the higher energy flux. A spectral ratio profile of this shape is typical in the morning and early afternoon regions, although the contrast between the softer and harder regions is quite variable and the harder flux is sometimes very weak or absent. Turning to the pitch angle distribution, there is evidently a strong anisotropy and little precipitation below 68°, while between 68 and 75° there are mixed isotropic and anisotropic regions above the 20 keV threshold. Above 200 keV there is relatively little precipitation. This structured precipitation is the most common situation in contrast to the more uniform band region reported for the 7.3 keV energy range at the same latitudes by Hoffman (1969). The 20 keV flux mirroring at the satellite altitude (3400 km) is remarkably uniform and is probably nearly equal to the flux mirroring at the equator. As the flux decreases beyond 75°, it is again clearly anisotropic until it falls to the polar flux level beyond 78.6°. The polar flux is measurable because of a weak solar electron event at this time. The profile of the 200 keV is also typical in that there is usually a sharp decrease near the low

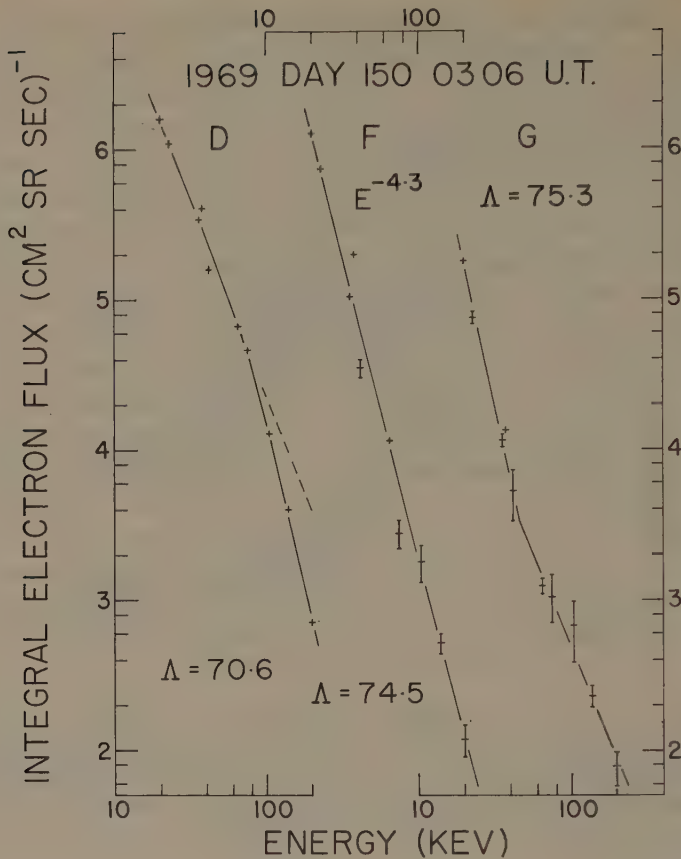


Fig. 2. Integral electron spectra for samples D, F, and G in Figure 1. The relevant energy scales alternate between the bottom and top of the figure and are displaced one decade from each other. The $N^{-1/2}$ error bars due to the counting rate N are indicated. Spectra are plotted for trapped flux with $\theta \sim 90^\circ$.

latitude boundary of the low energy precipitation. This sharpness is in contrast to the gradual softening at lower energies noted above. In the next 3 figures, the spectra and pitch angle distribution are examined in more detail in the intervals A through G and compared to the SPS data from the same pass. First, in Figure 2 spectra are compared at points D, F, and G in the softer zone, for energies from 20 to 200 keV. Sample F is a good power law fit; at D the higher energy particles are relatively depleted while at G they are relatively enhanced. This will be discussed further below.

The pitch angle distribution at D and E forms an interesting comparison since the 20 keV fluxes mirroring at the satellite are equal and the higher latitude sample is more anisotropic. Figure 3 shows the distribution at three energies using collimated detectors with half angles between 5 and 10° . Small intensity fluctuations may occur during the sampling distance of 150 km. At both latitudes there is greater anisotropy

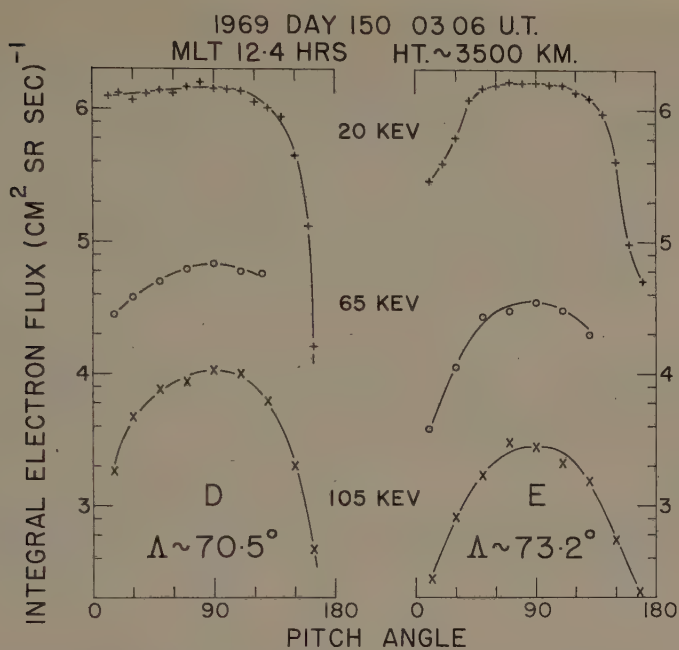


Fig. 3. Pitch angle distributions for samples D and E in Figure 1. 0° is looking up the field line. The half angles of the 20, 65, and 105 keV collimators are 5.1° , 9.2° , and 6.6° , respectively.

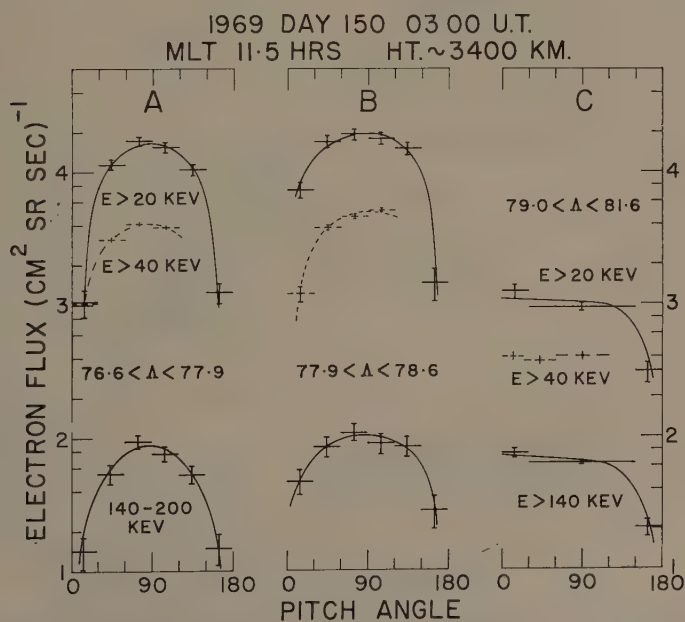


Fig. 4. Pitch angle distributions for samples A, B, and C in Figure 1. A and B are in the dayside cusp associated region on closed dayside field lines. C is in the polar cap on open tail field lines.

at the higher energies, the maximum flux mirrors at the satellite and the precipitating flux at pitch angles less than 30° is greater than the backscattered flux at pitch angles greater than 150° . Even the 20 keV flux in D appears slightly anisotropic with a precipitated/trapped ratio of about 0.9. The flux of $1.5 \times 10^6 \text{ cm}^{-2} \text{ sr}^{-1} \text{ s}^{-1}$ is frequently observed on dayside passes during disturbed conditions and is near the calculated limit of stable trapping for weak cyclotron resonant diffusion described by Kennel and Petschek (1966). However, in a homogeneous medium one would expect the greater anisotropy at the lower latitude, where the magnetic energy density per particle at the equator would be greater (Burton *et al.*, 1970).

Now consider the higher latitude, harder low intensity region sampled in A, B, and C. Figure 4 shows the pitch angle distributions at the 20 and 40 keV integral energies and in the 140 to 200 keV band. The lower count rates make necessary an averaging over larger angular intervals and several spin periods. Region B is less anisotropic than A although both are distinctly anisotropic. Region C by contrast has a much lower flux which is isotropic or perhaps slightly peaked along the field lines. If one interprets the anisotropy as being due to the atmospheric loss cone in both hemispheres, it would appear reasonable to conclude that the polar cusp falls

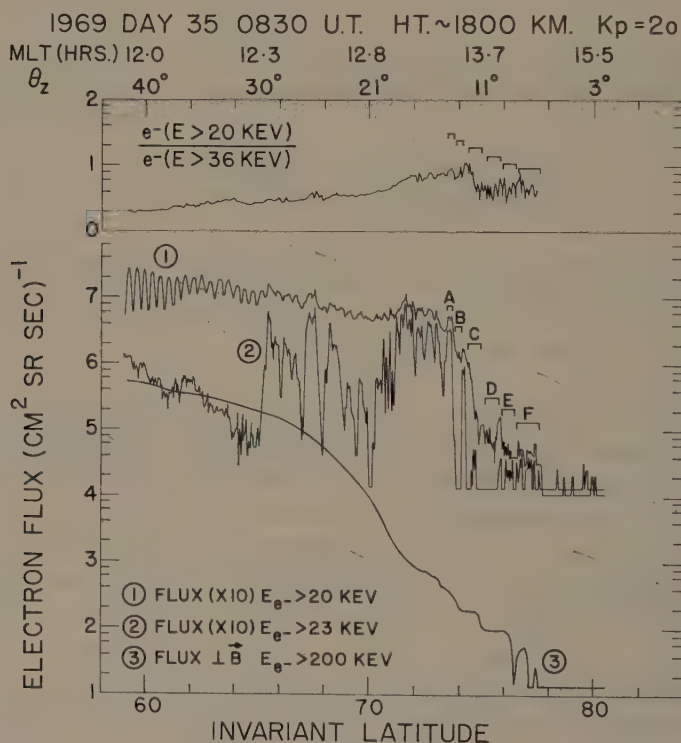


Fig. 5. Electron flux vs. IN Lat from Feb. 4, 1969, at ~0830 hr UT similar to Figure 1. The 20 and 200 keV detectors are radially mounted and view an angular range of $(90 \pm \theta_z)$. The 23 keV detector is axially mounted and views at angle θ_z to the magnetic field.

between B and C at a latitude of $\sim 78.5^\circ$ and that regions A and B are on field lines closed on the dayside while in region C the field lines extend into the magnetotail.

The corresponding data from the SPS radially mounted electron detector for this pass show a rapid decrease in the electron flux between 1 and 10 keV at 76.8° and an intense flux of electrons with mean energy near 100 eV between 77.2 and 78.6° . These are the signatures of electrons of magnetosheath origin (Heikkila and Winningham, 1971). In their interpretation, the magnetic flux from regions A and B is open to the magnetosheath via the dayside polar cusp, whereas for this pass, on the basis of the evidence discussed above, we believe that this flux closes to the southern hemisphere.

Two more passes which show similar features in a different way are described below from day 35 of 1969. The raw data in Figure 5 are obtained at a lower altitude, somewhat lower K_p , and 2 hr later in MLT near the cusp region. The satellite is oriented so that the radial detectors are looking only at trapped particles and the two axial detectors are looking up into the loss cone ($\theta z < 43^\circ$). The spectral ratio for the trapped radiation shows less softening than the previous case and a less marked hardening at 75° IN Lat. The mirroring flux of electrons ($E > 20$ keV) is between 0.5 and 2×10^6 $\text{cm}^{-2} \text{sr}^{-1} \text{s}^{-1}$, close to the stable limit of 1.5×10^6 $\text{cm}^{-2} \text{sr}^{-1} \text{s}^{-1}$ proposed for the previous pass. The flux of precipitating electrons ($E > 23$ keV) is relatively small until the sudden increase at about 65° , with marked structure of a scale size of ~ 100 km.

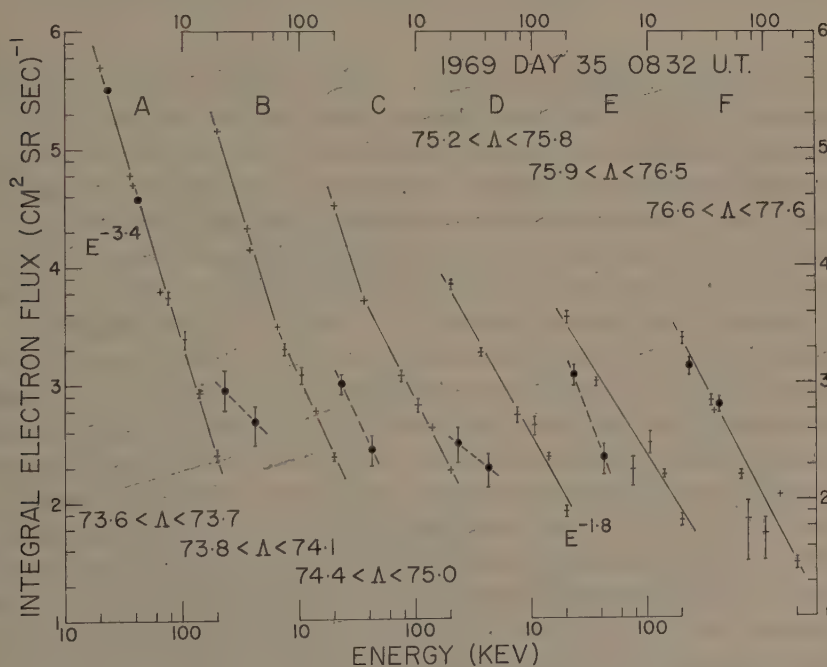


Fig. 6. Six spectra selected from Figure 5. The trapped fluxes are represented by crosses and precipitated fluxes are represented by circles. The scales and error bars are the same as Figure 2.

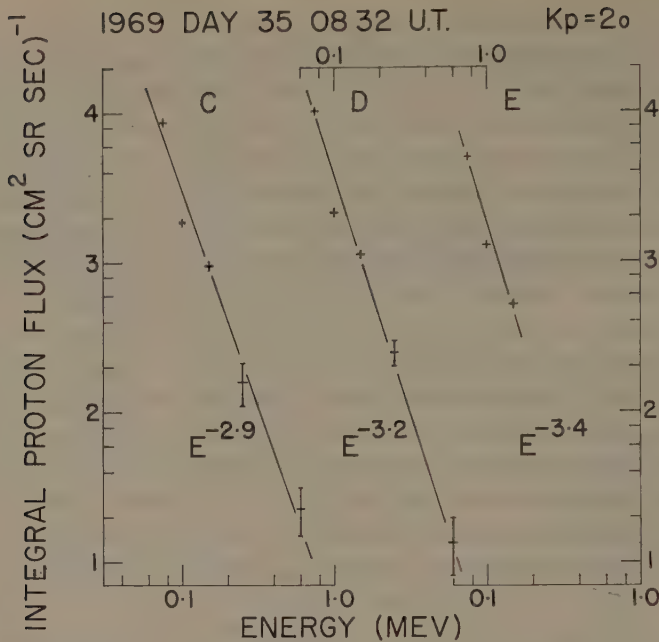


Fig. 7. Proton fluxes occurring coincident with electron fluxes in the polar cusp associated region in Figure 5.

Between 70 and 74°, structure with a diversity of scale sizes exists but the precipitation bursts approach isotropy more closely. Beyond the 20 keV flux decrease at C ($A \sim 75^\circ$) the flux appears harder and anisotropic. The high energy flux ($E > 200$ keV) mirroring at the spacecraft decreases fairly uniformly through four decades and is still measurable at 77°. In Figure 6, we examine the spectrum and anisotropy in the softer (A, B, C) and harder (D, E, F) regions. The trapped fluxes are represented by crosses and the precipitating fluxes measured at 23 and 42 keV thresholds are circles. The spectra show a gradual change from an exponent of -3.4 for A to an exponent of -1.8 for D, E, and F. There seems to be a marginally better fit for B and C using two straight lines rather than a single smooth curve. Considering now the anisotropy, region A appears accurately isotropic while the adjacent region B is very anisotropic. Regions C, D, and E continue to be strongly anisotropic while F is consistent with isotropy.

A somewhat unusual feature of this pass is the proton flux found in regions C, D, and E but not in the softer zone (A and B) or in F. The integral spectra of protons (75 to 600 keV), mirroring at the spacecraft, are shown in Figure 7. The proton fluxes are greater than electron fluxes of the same energy and the spectral exponent of about -3.0 is greater than that of the electrons. Similar fluxes appear in the ESRO 1A data described by Søråas (1972).

The corresponding SPS data in Figure 8 are shown in the standard format (Winningham, 1972). A 1 to 10 keV component ending at region C is recognizable. A

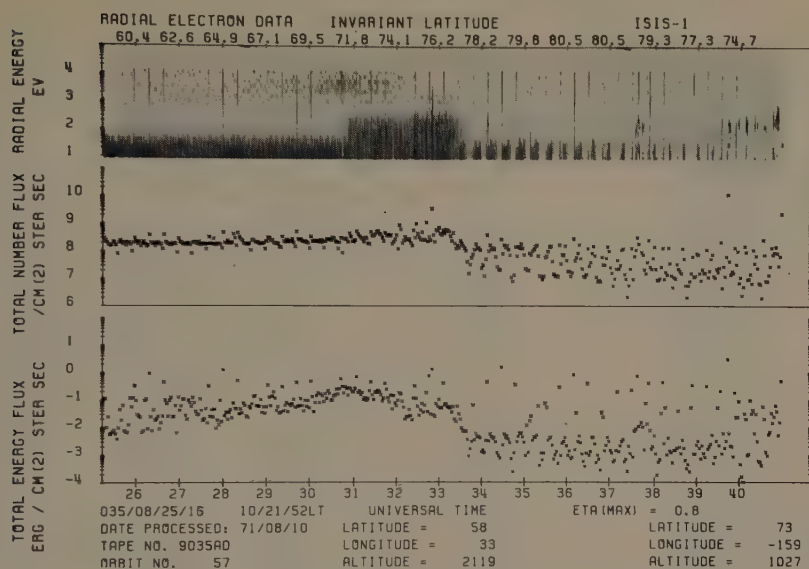


Fig. 8. SPS data corresponding to the pass in Figure 5.

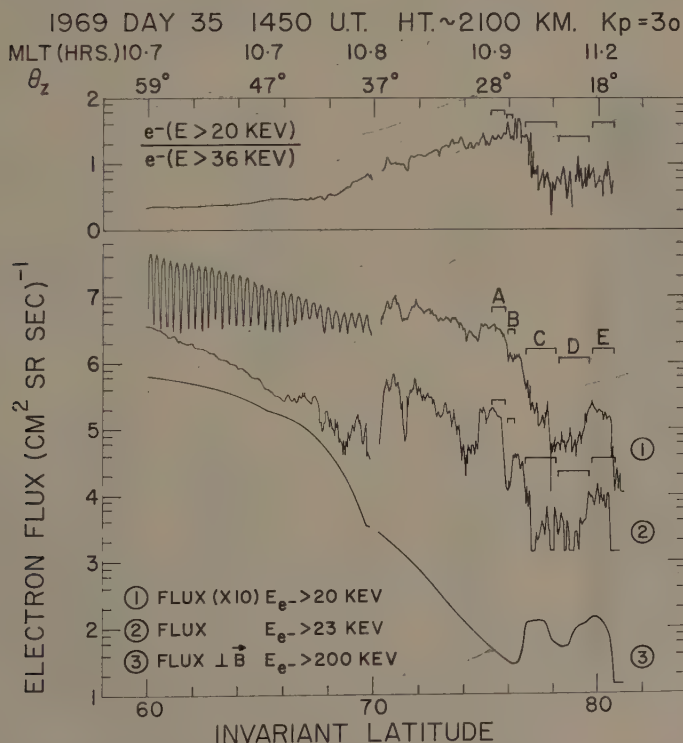


Fig. 9. Electron flux vs. IN Lat from Feb. 4, 1969, at ~1450 hr UT similar to Figure 5.

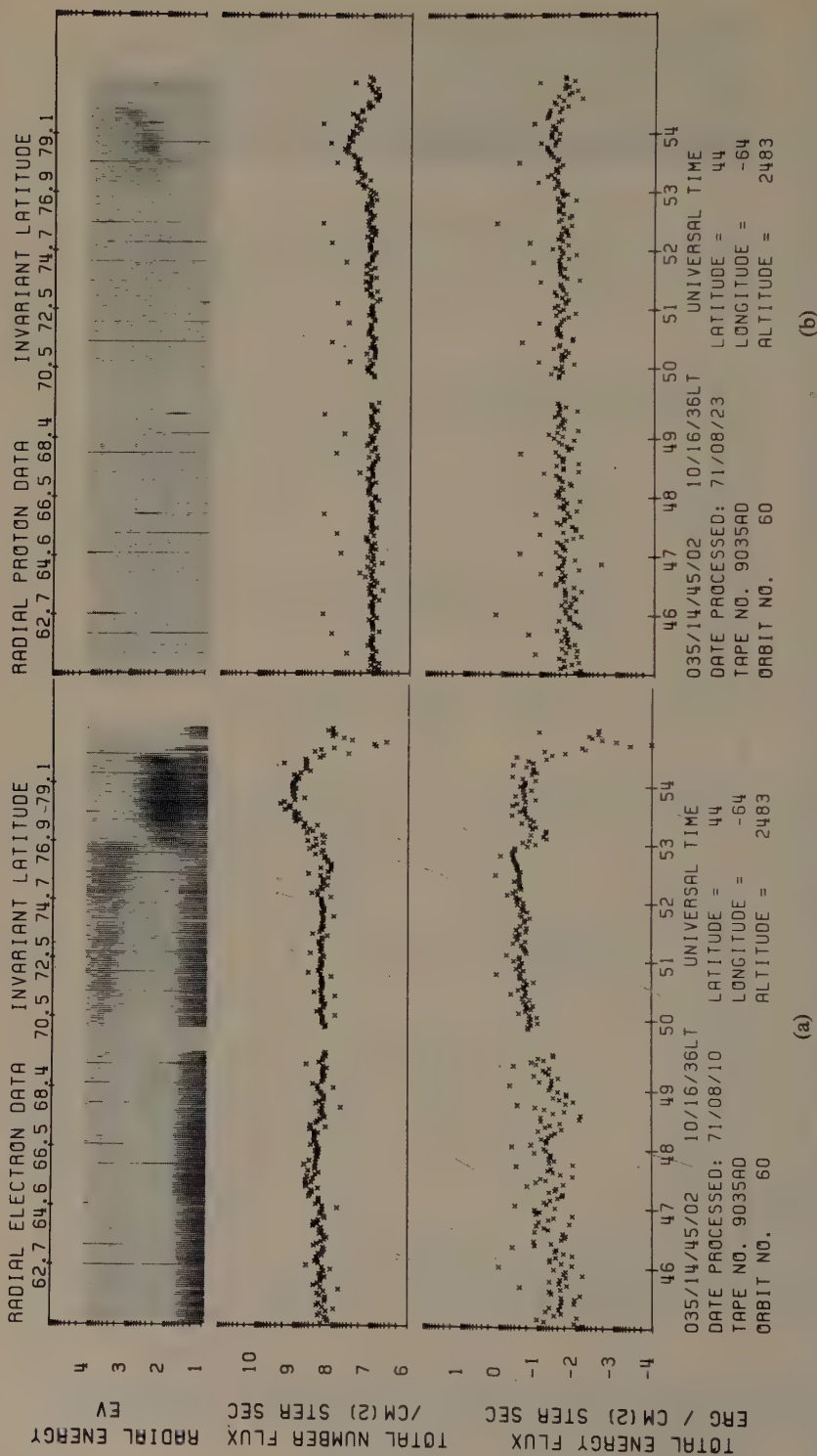


Fig. 10. SPS radial electron and proton data corresponding to the pass in Figure 9. The background count rate on the proton channel is high because of spacecraft outgassing.

~ 100 eV component overlaps it extending down to 71° with considerable structure, but regions C to F have more typical cusp-associated spectra. The ~ 100 eV flux terminates at region F so the evidence suggests that it occurs on closed field lines.

The second pass from day 35 (Figure 9) is at 11 hr MLT, the K_p index is higher, and the spectral index softens progressively from 68 to 77° and then hardens distinctly in region C. Fluxes extend to 81.6° . Detector 2 ($E > 23$ keV) measures precipitated fluxes only beyond about 69° latitude ($\theta z < 38^\circ$). The mirroring flux ($E > 20$ keV) suddenly increases to 1.0×10^6 electrons $\text{cm}^{-2} \text{sr}^{-1} \text{s}^{-1}$ at 70° and extensive bands of nearly isotropic precipitation occur throughout the softer region to 76° . There is weaker structured precipitation between 66 to 70° . It is probable that beyond 70° the 20 keV flux at 2100 km is equal to the mirroring at the equator while below 70° because of the observed anisotropy the flux mirroring at the equator is greater. The 200 keV flux mirroring at the satellite decreases notably at the onset of isotropic precipitation at 70° latitude. It increases at 76.5° , a rather unusual observation, which makes it unlikely that the harder zone near the polar cusp can be explained in terms of fast radial diffusion onto open field lines where no quasi-trapping is possible. Spectra for samples A to E have two slopes which are more prominent than similar spectra shown in Figure 6. A and B were chosen in the softer zone to show isotropic and anisotropic fluxes, respectively. Spectra C and D show the prominent high energy tail and are distinctly anisotropic. Sample E is very nearly isotropic and open field lines presumably start there.

The corresponding SPS data in Figure 10a show a prominent zone of 1 to 10 keV electrons between 70 and 77° , with a well separated zone of 100 eV electrons from 77 to 80° corresponding to zones C, D, and E.

The SPS proton data are also quite distinguishable in this pass (Figure 10b). The flux extends across C, D, and half of E in the same region as the 100 eV electrons. There is a slight suggestion of a V-shape as described by Heikkila and Winningham (1971) but primarily the protons decrease in energy toward lower latitudes.

4. Discussion

A. THE MANTLE AURORAL REGION

On the basis of our present knowledge of the particle population and its associated correlations with optical emission features, it is convenient to call the lower latitude region the 'mantle auroral region'. Some of its particular characteristics observed at an altitude of a few thousand km are summarized below:

(1) The low latitude boundary is marked by the sudden onset of nearly isotropic precipitation in the tens of keV energy range, while the trapped intensity mirroring at the spacecraft remains nearly constant.

(2) The high latitude boundary is marked by a sudden decrease in the mirroring electron flux over a wide energy range from 1 to 50 keV, and a return to anisotropy at higher energies.

(3) The low latitude boundary is often marked in the hundreds of keV energy range by a sudden decrease in the flux mirroring at the satellite.

(4) The spectrum in the 1 to 50 keV range softens with increasing latitude typically from 68 to 75° IN Lat.

(5) Throughout the region there is varying pitch angle anisotropy which is not directly dependent on the intensity of the mirroring flux or the IN Lat.

(6) The flux greater than 20 keV is often near $10^6 \text{ cm}^{-2} \text{ sr}^{-1} \text{ s}^{-1}$ when pitch angle isotropy occurs.

The loss mechanism operating throughout the mantle auroral region is most likely to be weak pitch angle scattering by ELF and VLF whistler mode waves (Kennel and Petschek, 1966). They have shown that the existence of a loss cone maintains an anisotropy in the pitch angle distribution which results in wave growth of whistler mode waves in cyclotron resonance with electrons near the equator. The rate of wave growth depends on the anisotropy and the fraction of electrons which are resonant. The mantle auroral region corresponds to the region of maximum frequency of occurrence of ELF chorus reported by Russell and Holzer (1970) between 0600 and 1200 LT and $7 < L < 12$ in the equatorial plane. Brice and Lucas (1971) have noted that variations in the cold plasma density in the wave growth region will change the fraction of electrons participating in the cyclotron instability since only those having kinetic energy parallel to the magnetic field greater than the magnetic energy per particle in the total plasma will be resonant. Chappell (1972) has reported variations in the thermal ion density which tend to be most common in the late forenoon and afternoon. Such variations would explain the observations in Figures 1 and 3, where 20 keV fluxes of the same intensity were observed to be more anisotropic at the higher latitude. The variations could also affect the length of the growth region by causing partial wave ducting.

The decrease in higher energy electron flux (e.g. $E > 200 \text{ keV}$), which is particularly prominent in Figures 1 and 9 near the equatorward edge of the mantle auroral region, probably results in part from a mapping of the very steep gradient usually found on the nightside at these energies and in part from pitch angle diffusion caused by the ELF power generated by the lower energy electrons. Since there is no source to effectively replenish these higher energy fluxes during a partial drift period, the latitude gradient would develop.

An acceleration mechanism is necessary in order for the mantle auroral region to extend through many morning hours and sometimes past noon. It must be gradual to maintain the fluxes near the weak diffusion limit and it must be widespread in latitude and LT. The convection electric field discussed by many authors (Axford and Hines, 1961; Taylor and Hones, 1965; Nishida, 1966; Brice, 1967; and others) has such characteristics, and is thought to be the principal acceleration mechanism. McDiarmid *et al.* (1969) found by an indirect measurement that the potential difference across the magnetosphere was small at latitudes less than 67° during quiet conditions, while recent measurements of Frank and Gurnett (1971) in the morning and afternoon sectors, show a field corresponding to sunward plasma convection that is

concentrated between 65° and the magnetopause. These measurements are consistent with the location of the mantle auroral region.

The replenishment of the cold plasma on the dayside (Brice and Lucas, 1971) would also be a factor in continuing precipitation toward later hours where the electric field no longer provided acceleration.

B. THE DAYSIDE CUSP REGION

The region poleward of the large relatively abrupt decrease of 1 to 50 keV electron fluxes is associated with the dayside cusp region. In some cases the fluxes fall below the instrumental intensity threshold, but in the cases studied here the flux remains measurable and anisotropic. In such cases the anisotropy is clear evidence that the region lies on closed field lines. Some data from Frank (1971) at mid-altitudes appear to support this view. During the Imp 5 inbound pass on July 11, 1969, the 45 keV electron flux at 35 to 45×10^3 km is much less than the equatorial flux, which is consistent with a pitch angle anisotropy. This occurs where there is a maximum flux of 400 eV electrons and the 895 eV protons are also observed although with intensities reduced from the magnetosheath flux.

The single intense flux of low energy electrons (10 to 30 km wide) observed in Injun 5 data by Frank and Ackerson (1971) and identified by them as the low altitude neutral line, is often not seen as a unique feature in the ISIS 1 SPS data. However, its position, as reported, seems consistent with it occurring at the poleward edge of the dayside cusp region where the fluxes for a short distance again approach isotropy in the tens of keV energy range.

The steep intensity gradient between the mantle auroral region and the dayside cusp region is not clearly understood. However, the following factors may contribute to it and to the anisotropy.

The convection electric field measured by Frank and Gurnett (1971) is largest near the magnetopause, corresponding to sunward convection of plasma at latitudes lower than the polar cusp on the morning side. A 20 mV m^{-1} field extending ~ 500 km N-S at 2000 km altitude would correspond to a potential gradient of 10 kV. It is therefore suggested that some plasma enters from the magnetosheath into the morning side plasma sheet at a position which maps down the magnetic field to 7 to 9 hr MLT and then convects forward on the morning side near the magnetopause without entering the central tail region of substorm activity near midnight. Consequently the plasma returns to the dayside cusp region having spectra similar to the magnetosheath plasma and it is observed to precipitate at low altitudes. Electrons of energy greater than 1 keV, gradient drifting into this morning sector from midnight, will tend to move toward the magnetopause if they mirror near the equator and approximately conserve the first and second adiabatic invariants (Roederer, 1967). However, electrons with energy less than the 10 kV potential gradient will be deflected from the region near the magnetopause, and will tend to form an intensity gradient near the low latitude edge of this strong convection. Higher energy electrons, in particular those mirroring near the equator, would gradient drift out to the magnetopause, and the mirror points

of low altitude mirroring particles will tend to be raised, resulting in more anisotropic fluxes or often no measurable fluxes at ~ 2000 km altitude. The size of the dayside cusp region and the spectral characteristics of electrons in the mantle auroral region will be very dependent on the distribution and velocity of the sunward convecting plasma and the spectrum of the gradient drifting electrons which have been injected by substorm activity on the nightside.

5. Summary

We have deliberately concentrated on a small sample of data in a limited sector of MLT-IN Lat space. Such a selection is necessarily somewhat arbitrary. However, the properties of the regions as interpreted here may be summarized in the following way in terms of the physical processes most important in them.

The mantle auroral region is dominated by a widespread convection electric field which provides a replenishing source of electrons in the approximate energy range of 1 to 50 keV throughout the morning sector. During times of moderate geomagnetic activity, the low energy part of the spectrum reaches the weak diffusion limit set by the cyclotron resonance instability while the higher energy particles receive no significant acceleration and are weakly precipitated by the whistler mode turbulence. Inhomogeneities in the cold plasma density are responsible for the observed spatial structure in the pitch angle anisotropy near 20 keV.

The dayside cusp region falls on the low latitude side of the narrow polar cusp defined by Frank (1971) at mid-altitudes. At low altitudes it is populated predominantly by protons and electrons having spectra similar to the magnetosheath plasma and by a low intensity high energy gradient drifting electron component which has an anisotropic pitch angle distribution and a harder spectrum than the adjacent mantle auroral region. When the convection electric field is sufficiently strong, it appears to prevent gradient drifting electrons of auroral energies from reaching the magnetopause, resulting in a steep intensity gradient at the high latitude edge of the mantle auroral region.

Not all of the points in this model are well established and further work is necessary to confirm or correct our present knowledge.

Acknowledgments

The authors wish to thank Drs W. Heikkila and J. D. Winningham for the opportunity to study and use the soft particle spectrometer data from ISIS 1 prior to publication.

References

- Axford, W. I. and Hines, C. O.: 1961, *Can. J. Phys.* **39**, 1433.
- Brice, N. M.: 1967, *J. Geophys. Res.* **72**, 5193.
- Brice, N. and Lucas, C.: 1971, *J. Geophys. Res.* **76**, 900.
- Burch, J. L.: 1968, *J. Geophys. Res.* **73**, 3585.

- Burton, K., Russell, C. T., and Chappell, C. R.: 1970, *J. Geophys. Res.* **75**, 5582.
- Chappell, C. R.: 1972, this volume, p. 280.
- Eather, R. H. and Mende, S. B.: 1971, *J. Geophys. Res.* **76**, 1746.
- Frank, L. A.: 1971, *J. Geophys. Res.* **76**, 5202.
- Frank, L. A. and Ackerson, K. L.: 1971, *J. Geophys. Res.* **76**, 3612.
- Frank, L. A. and Gurnett, D. A.: 1971, February, Univ. of Iowa Report 71:5.
- Hartz, T. R. and Brice, N. M.: 1967, *Planetary Space Sci.* **15**, 301.
- Heikkila, W. J. and Winningham, J. D.: 1971, *J. Geophys. Res.* **76**, 883.
- Heikkila, W. J., Smith, J. B., Tarstrup, J., and Winningham, J. D.: 1970, *Rev. Sci. Instrum.* **41**, 1393.
- Hoffman, R. A.: 1969, *J. Geophys. Res.* **74**, 2425.
- Hoffman, R. A.: 1971, *J. Geophys. Res.*, to be published.
- Hoffman, R. A. and Berko, F. W.: 1971, *J. Geophys. Res.* **76**, 2967.
- Kennel, C. F. and Petschek, H. E.: 1966, *J. Geophys. Res.* **71**, 1.
- McDiarmid, I. B., Burrows, J. R., and Wilson, M. D.: 1969, *J. Geophys. Res.* **74**, 3554.
- Nishida, A.: 1966, *J. Geophys. Res.* **71**, 5669.
- Riedler, W.: 1972, this volume, p. 133.
- Roederer, J. G.: 1967, *J. Geophys. Res.* **72**, 981.
- Russell, C. T. and Holzer, R. E.: 1970, in B. M. McCormac (ed.), *Particles and Fields in the Magnetosphere*, D. Reidel Publishing Company, Dordrecht, Holland, p. 196.
- Sandford, P. B.: 1968, *J. Atmospheric Terrest. Phys.* **30**, 1921.
- Sharp, R. D. and Johnson, R. G.: 1968, in B. M. McCormac (ed.), *Earth's Particles and Fields*, Reinhold Publishing Corporation, New York, p. 113.
- Sharp, R. D., Carr, D. L., and Johnson, R. D.: 1969, *J. Geophys. Res.* **74**, 4618.
- Söraas, F.: 1972, this volume, p. 120.
- Stringer, W. J. and Belon, A. E.: 1967, *J. Geophys. Res.* **72**, 4415.
- Taylor, H. E. and Hones, E. W.: 1965, *J. Geophys. Res.* **70**, 3605.
- Winningham, J. D.: 1972, this volume, p. 68.

ANGULAR DISTRIBUTIONS OF PRECIPITATING ELECTRONS

G. PASCHMANN

*Max-Planck-Institut für Physik und Astrophysik,
Institut für extraterrestrische Physik,
Garching b. München, Germany*

1. Introduction

For auroral electrons the angular distribution within the loss cone is probably the most sensitive indicator of the mechanism which causes the precipitation. However, in the energy range of a few keV, which generally contains most of the auroral electron flux, only very limited results have been reported to date.

In this paper we briefly present results on the angular distribution of precipitating electrons in the auroral zones, with energies between approximately 0.8 and 16 keV, obtained with the Lockheed experiment on the polar orbiting satellite OV1-18. A more comprehensive report will be published in cooperation with the Lockheed group.

2. Experiment

The satellite was launched on March 18, 1969, into a 99° inclination orbit with apogee at 590 km and perigee at 470 km. Because of a failure of the gravity gradient stabilization the satellite tumbled in a near random fashion. The varying orientation with respect to the geomagnetic field was monitored by an onboard three axis magnetometer.

For the present study the data from three nearly identical spectrometers pointing in different directions were used. The spectrometers consisted of a set of individual detectors measuring electrons in broad and contiguous energy bands centered at 1.2, 2.5, 5.4, and 12.4 keV. The detectors had opening angles of approximately $10 \times 10^\circ$. A more detailed description of the instrument has been presented elsewhere (Shea *et al.*, 1967).

The response functions of the spectrometers were determined experimentally to an accuracy of about 10% (Paschmann *et al.*, 1970). However, several effects of the operating system contribute to inaccuracies in the intercomparison of data from different spectrometers. The analog ratemeters of individual channels were not sampled simultaneously; this, combined with the ratemeter time constants which are comparable with the sampling periods, could lead to relatively large uncertainties in periods of rapid flux changes. Additional inaccuracies are introduced when the energy spectra are steep because the energy response functions were not identical and the spectra were not determined with sufficient resolution to make corrections for this effect practical. Fortunately, the tumbling of the satellite permitted an inflight comparison of detector responses because two or more of the spectrometers were occasionally looking at particles with the same pitch angles. On the average agreement was very good, but

the individual data points showed a scatter resulting from the effects described above with a standard deviation ranging from 25% for the highest energy channel to 40% for the lowest energy channel.

3. Results

The outstanding feature of our angular distribution measurements in the loss cone is a predominance of nearly isotropic distributions at all latitudes and geomagnetic conditions. To demonstrate this quantitatively, a statistical analysis of the data obtained at LT near noon and midnight during approximately 30 orbits was made. These orbits represent the complete range of geomagnetic activity from March to June 1969. As a measure of the angular distribution we chose to compare the fluxes at pitch angles of 20 and 60° within the loss cone which is 65° wide at satellite altitude. Since the satellite tumbled, times had to be selected where the detectors sampled pitch angles in the vicinity of 20 and 60°. The fluxes at exactly 20 and 60° then were obtained from analytical fits to the actual data. Because the deviation from isotropy turned out to be rather small, the type of fit used did not matter significantly. From these data a small but still representative sample was obtained for the analysis by using only the distributions obtained at the time of maximum flux within each portion of the orbit falling in an IN Lat interval of 2° and/or a LT interval of 1 hr. In addition, the integral electron flux was required to be larger than $5 \times 10^6 \text{ cm}^{-2} \text{ s}^{-1} \text{ sr}^{-1}$. No selection concerning LT and latitude has been made. The results are presented in Figure 1.

It is apparent from the figure that at very low intensities the fluxes at pitch angles of 60° on the average exceed the fluxes at 20° for the two highest energy channels. At the lower energies this effect is obscured by the gap at low intensities which is caused by the above mentioned lower limit on the integral fluxes set in this analysis. At intensities above approximately $5 \times 10^6 \text{ cm}^{-2} \text{ s}^{-1} \text{ sr}^{-1} \text{ keV}^{-1}$ fluxes are nearly isotropic. At the 5.4 and 12.4 keV channels the scatter of the data points is consistent with the scatter observed at times when the different spectrometers were looking a equal pitch angle (see Section 2). Therefore, deviations from isotropy are probably not significant at these energies. For the lower energy channels, however, the data points of Figure 1 show a scatter with a standard deviation which is nearly twice the deviation observed for nominally equal fluxes. At these energies there are therefore real deviations from isotropy.

Data points which are located far enough above the diagonal in Figure 1 represent cases where the fluxes maximize at small pitch angles, contrary to the distributions of trapped particles. Observations of this kind have first been reported by Hoffman and Evans (1968). Their experiment, however, only measured the angular distribution at the single energy of 2.3 keV. With the present experiment we are able to study the effect over a wider range of energies. Two examples of our observations are shown in Figure 2. They demonstrate the strong energy dependence of these events. The effect is observed only at energies below 5 keV, usually maximizing in the lowest energy channel, and it occurs only where the energy spectrum is soft.

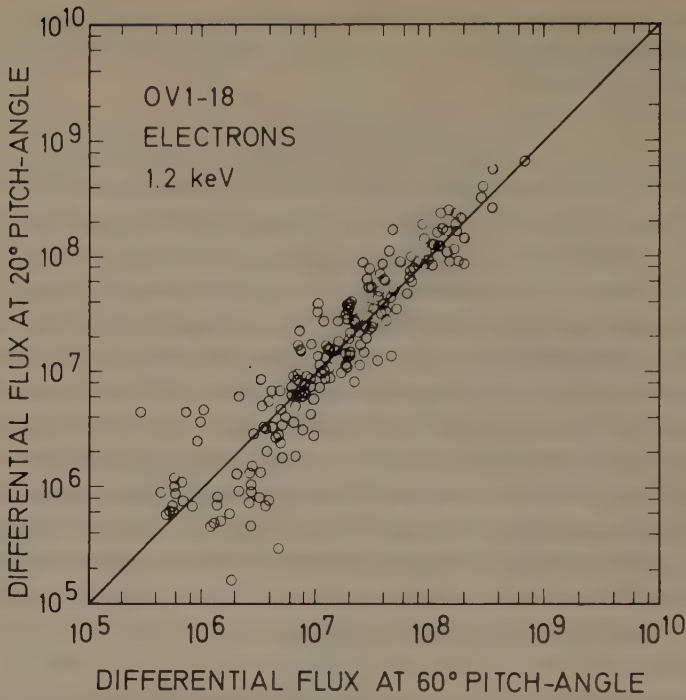


Fig. 1a.

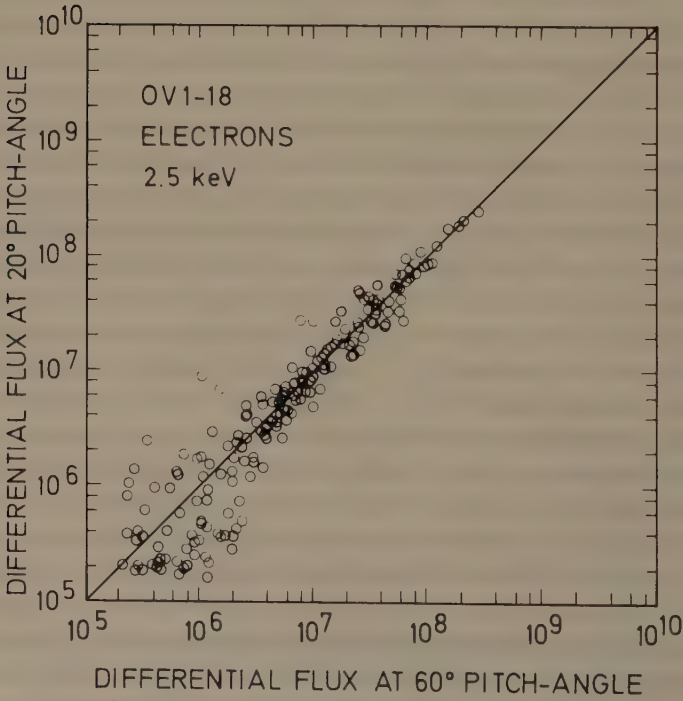


Fig. 1b.

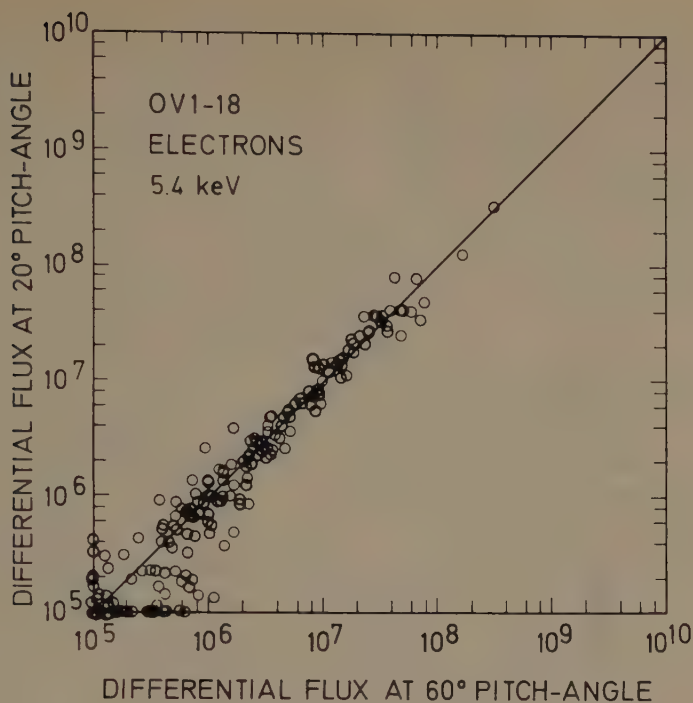


Fig. 1c.

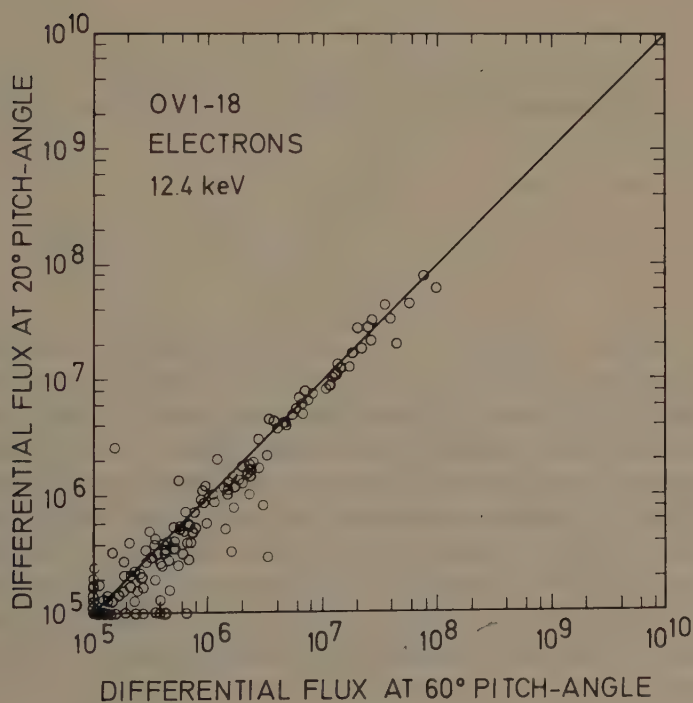


Fig. 1d.

Figs. 1a–d. Scatter plots of electron fluxes $\text{cm}^{-2} \text{s}^{-1} \text{sr}^{-1} \text{keV}^{-1}$ at 20 and 60° pitch angles. The data represent a wide range of geomagnetic activity and all IN Lat's. MLT's are predominantly around noon and midnight. The solid lines indicate isotropic angular distributions.

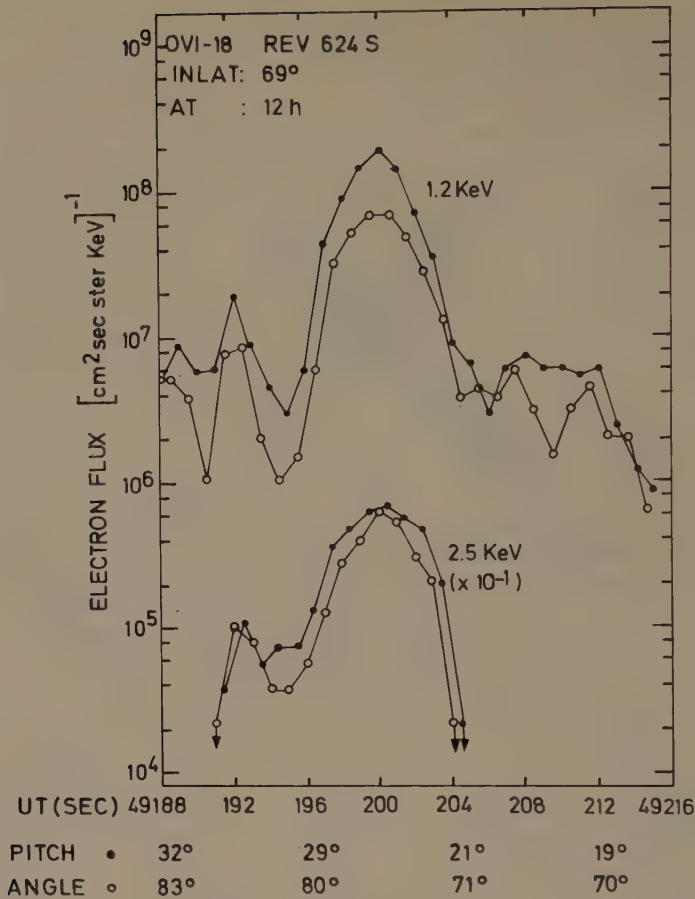


Fig. 2a.

4. Discussion

The results presented in Figure 1 are consistent with the electron precipitation being generally caused by pitch-angle diffusion which reaches the 'strong' diffusion limit (as defined by Kennel, 1969) at intensities in the vicinity of $5 \times 10^6 \text{ cm}^{-2} \text{ s}^{-2} \text{ sr}^{-1} \text{ keV}^{-1}$, whereas it is weaker at lower intensities. Interactions of the particles with waves are generally thought to be the cause of the pitch angle diffusion. The waves which are likely to diffuse the electrons in the 1 to 10 keV range are the electrostatic emissions reported by Kennel *et al.* (1970). These waves are probably generated by the particle distribution itself as is suggested by the observation that the strength of the process depends on the particle intensities. This problem has been discussed recently by Young *et al.* (1971).

The interpretation of the forward peaked angular distributions is much more difficult. Because of the strong pitch angle diffusion generally operating one would expect

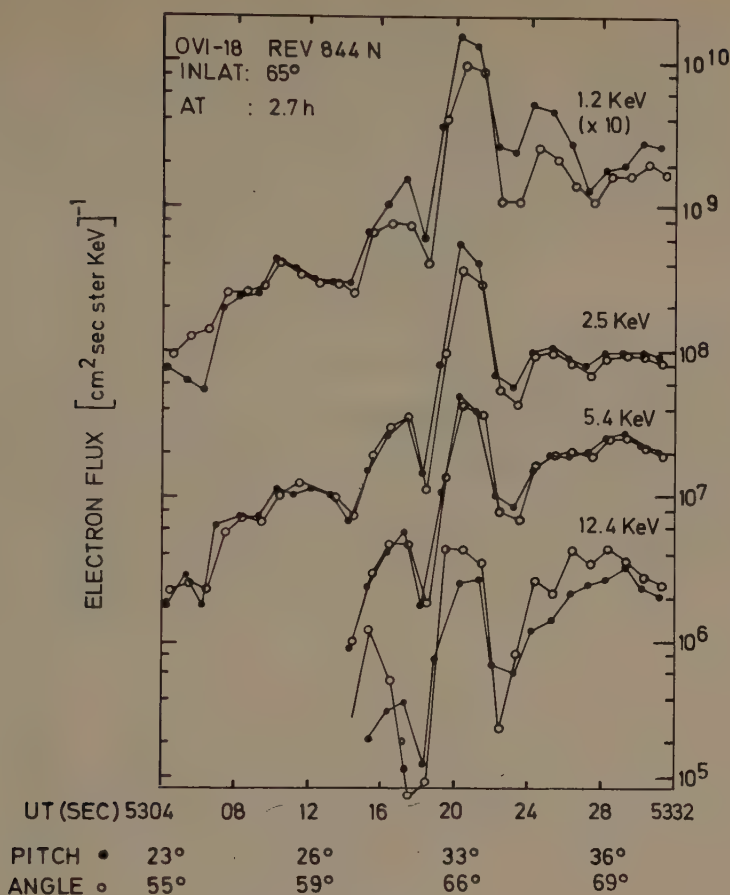


Fig. 2b.

Figs. 2a-b. Examples of anisotropic events measured on April 28 (a) and May 13 (b), 1969.

the phenomenon to be created in the vicinity of the earth. This has prompted the suggestion of electric fields pointing along the geomagnetic field as a mechanism (Hoffman and Evans, 1968). This mechanism is problematic not only because of the difficulties to generate such electric fields for sufficiently long times, but also because it would lead to a flux depletion at pitch angles above a cutoff value depending on the electric field strength, a feature which is in contrast to the observations. Rather than invoking a source of keV electrons within the electric field region for the fluxes at higher pitch angles, as Hoffman and Evans have done, it seems more probable to us that the particle distribution, which is compressed into a narrow peak along the magnetic field lines by the electric field, will fill the larger pitch angles via pitch angle diffusion. In fact, it has been proposed (Haerendel, 1971) that the process creating the electric field might itself lead to an intimate connection between the competing tendencies, i.e., creation of a forward peak through acceleration along the field lines, and creation of an isotropic distribution through pitch angle scattering.

Acknowledgments

The author wishes to thank Drs M. Walt and R. G. Johnson for their hospitality at the Lockheed Palo Alto Research Laboratory and for the permission to use the OV1-18 data. Many valuable discussions with Drs R. G. Johnson, R. D. Sharp, E. G. Shelley, and G. Haerendel are gratefully acknowledged.

References

- Haerendel, G.: 1971, private communication.
Hoffmann, R. A. and Evans, D. S.: 1968, *J. Geophys. Res.* **73**, 6201.
Kennel, C. F.: 1969, *Rev. Geophys.* **7**, 379.
Kennel, C. F., Scarf, F. L., Fredricks, R. W., McGhee, J. H., and Coroniti, F. V.: 1970, *J. Geophys. Res.* **75**, 6136.
Paschmann, G., Shelley, E. G., Chappell, C. R., Sharp, R. D., and Smith, L. F.: 1970, *Rev. Sci. Instr.* **41**, 1706.
Shea, M. F., Shook, G. B., Reagan, J. B., Smith, L. F., and Sanders, T. C.: 1967, *IEEE Trans. Nucl. Sci.* **NS-14**, 96.
Young, T. S. T., Callen, J. D., and McCune, J. E.: 1971, *EOS, Trans. Amer. Geophys. Union* **52**, 329.

SOME PARAMETERS AFFECTING THE POLEWARD BOUNDARY OF TRAPPED ELECTRONS

D. E. PAGE and M. L. SHAW

*Space Science Dept. (ESLAB),
European Space Research and Technology Centre,
Noordwijk, The Netherlands*

1. Introduction

An analysis by McDiarmid and Wilson (1968) has indicated that the poleward boundary of the trapped radiation tends to move lower in invariant latitude λ at the equinoxes, when the angle Φ between the geomagnetic axis and the sun-earth line is near 90° .

We report an attempt to repeat this finding and discuss some interesting effects observed during the investigation.

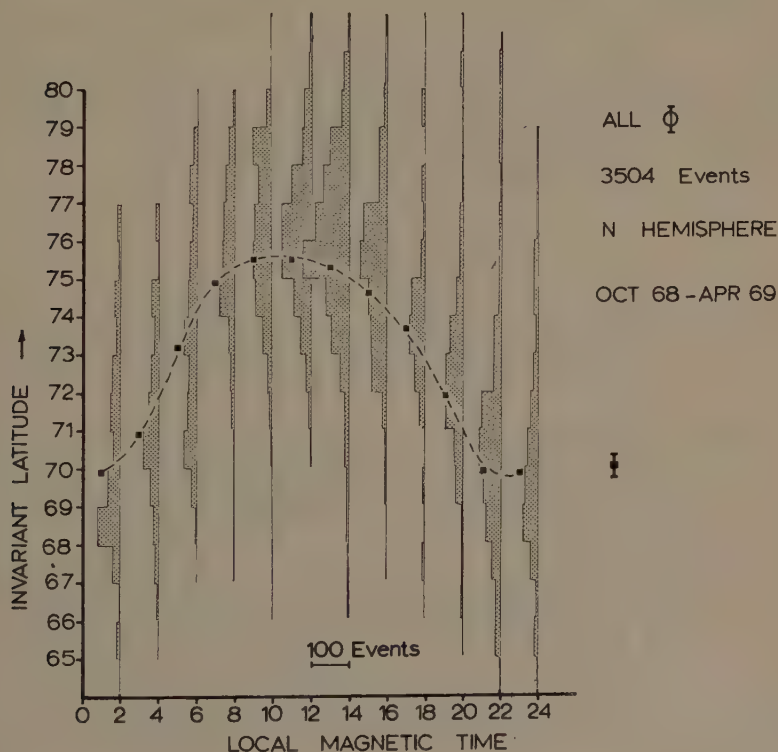


Fig. 1. The average 40 keV trapped electron boundary plotted in IN Lat vs. MLT. The error bar is the standard error of the mean as used by McDiarmid and Wilson (1968).

The data used were taken from about 4000 boundary crossings made by the ESRO satellite between October 1969 and February 1970. The geiger counter and measurement system have been described by Page and Domingo (1972). The background boundary position was defined as by McDiarmid and Wilson (1968).

2. Diurnal Variation

A diurnal variation of the radiation belt boundary was first seen by O'Brien (1963). The result of our investigation on 3500 crossings at altitudes between 350 and 1500 km is shown in Figure 1. The asymmetric diurnal variation is confirmed. One interesting feature is the greater data scatter on the morning side which agrees well with the diurnal distribution of auroras (Feldstein, 1969) and seems consistent with greater particle dumping activity in the morning hours (Parks, 1969). We have no evidence for secondary maxima in the diurnal curve (Fritz, 1970).

3. Seasonal Variations

We have been unable to repeat the McDiarmid and Wilson (1968) result that particularly in the morning hours the boundary is lowest when Φ is near 90° . Other parameters such as UT and K_p index clearly affect the boundary position and it may be that our data are differently biased by these factors.

It could be pointed out for example that to select data in ranges of Φ automatically introduces a UT bias. For example in the northern winter interval, $55 < \Phi < 78$, UT values around 1630 are achievable only precisely at mid-winter.

4. K_p Variations

Figure 2 shows the diurnal variation in trapping boundary position for three ranges of K_p . Since K_p on the average is a maximum at the equinoxes it is easy to see how any seasonal effect might be masked by the K_p distribution in data taken by the satellite.

The similarity of the boundary behavior to that of other magnetic and ionospheric phenomena is striking, with reversals in direction taking place around 1000 and 2220 MLT. As an example we reproduce in Figure 3 Bombay magnetic field records for quiet and disturbed days (Moos, 1910).

We suggest that increased K_p means increased solar wind speed which generates additional electric (and magnetic) fields, causing the particle population to move away from the earth on the morning side and toward the earth in the evening. The diurnal dawn-dusk asymmetry should then tend to disappear at low solar wind speeds, the minimum asymmetry corresponding to solar wind velocities around 300 km s^{-1} . If over short time intervals the relationship between K_p and solar wind velocity was known it should then be possible to calculate in a more quantitative way the convective interaction between the solar wind and the magnetosphere.

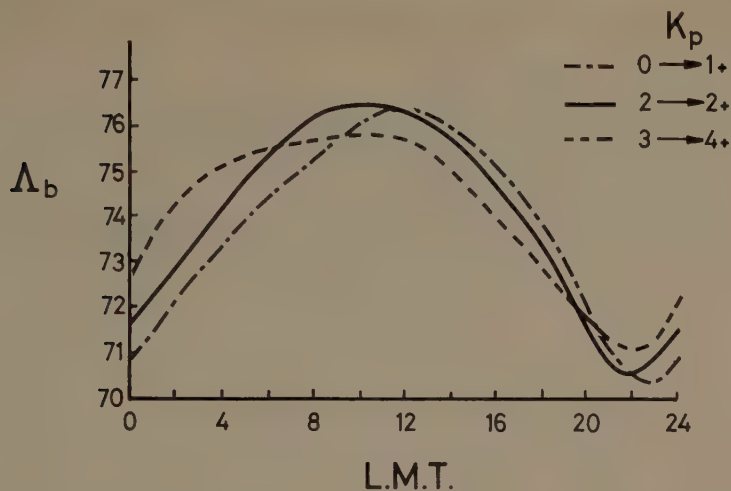


Fig. 2. The average 40 keV trapped boundary for the K_p ranges 0 to 1+; 2- to 2+; 3- to 4+.

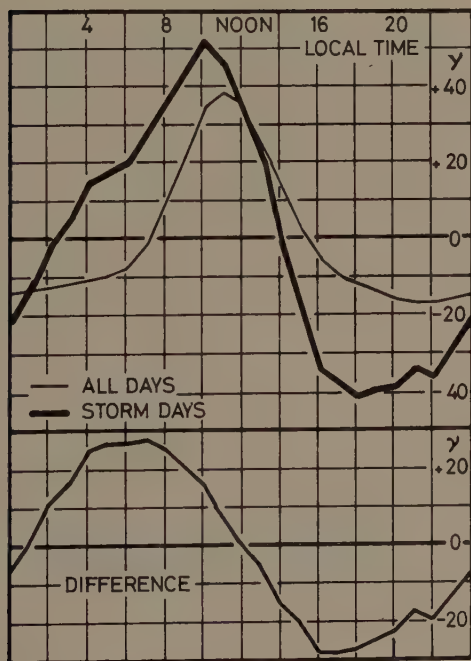


Fig. 3. The solar daily variation of horizontal intensity at Bombay; averages from all days and storm days (Moos, 1910).

References

- Feldstein, Y. I.: 1969, *Rev. Geophys.* **7**, 179.
Fritz, T. A.: 1970, *J. Geophys. Res.* **75**, 5387.
McDiarmid, I. B. and Wilson, M. D.: 1968, *J. Geophys. Res.* **73**, 7237.
Moos, N. A. F.: 1910, in *Colaba Magnetic Data*, Bombay, p. 469.
O'Brien, B. J.: 1963, *J. Geophys. Res.* **68**, 989.
Page, D. E. and Domingo, V.: 1972, this volume, p. 107.
Parks, G. K.: 1970, in V. Manno and D. E. Page (eds.), *Intercorrelated Satellite Observations Related to Solar Events*, D. Reidel Publishing Company, Dordrecht, Holland, p. 351.

PHOTOMETRIC AURORAL PARTICLE MEASUREMENTS

S. B. MENDE

*Lockheed Palo Alto Research Laboratories,
3251 Hanover, Palo Alto, Calif., U.S.A. 94304*

and

R. H. EATHER

*Physics Department, Boston College,
Chestnut Hill, Mass., U.S.A.*

1. The Interpretation of the Photometric Data

Within certain limitations, ground based or airborne measurements of auroral emissions can be used to determine the type, energy, and flux of precipitating particles. The technique uses absolute intensity measurements of total height integrated column emissions in 4861 \AA $H\beta$, 4278 \AA N_2^+ , and 6300 \AA O_I . The data reduction procedure is illustrated schematically in Figure 1. The measured intensities are corrected for atmospheric extinction. The corrected $H\beta$ intensity gives an estimate of the proton flux and the proton contribution to the 4278 \AA N_2^+ and 6300 \AA O_I excitation. The residual 4278 \AA N_2^+ intensity then gives a value of the total energy influx of the precipitating electrons. At times when this residue is zero, airglow corrections can be made to the 6300 \AA O_I intensity. The ratio r of the corrected 6300 \AA O_I emission and the N_2^+ 4278 \AA emission can be used as a parameter related to the mean energy of electron precipitation because soft auroras are generated at higher altitudes where the 6300 \AA O_I quenching is inefficient. The quantity r therefore, can be used to interpret the mean height and mean energy of the precipitating electrons. The mean height provides

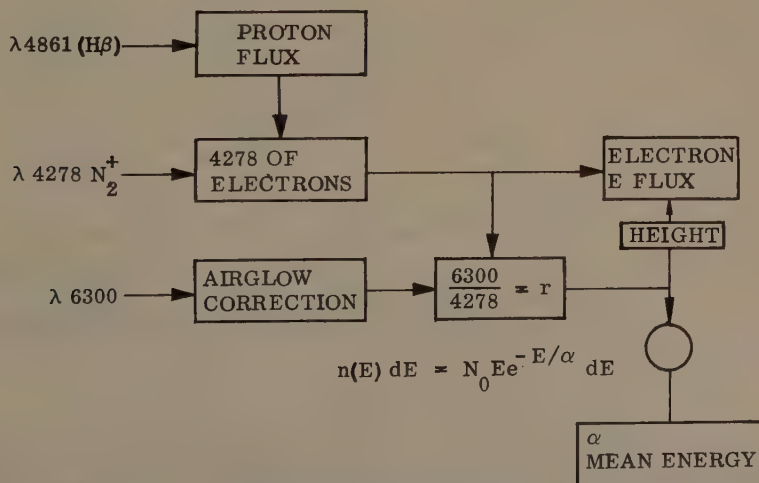


Fig. 1. The data reduction method for the interpretation of photometric data.

a correction for the total electron energy flux as obtained from the 4278 Å emission. The mean energy is obtained by applying a one parameter model of the particle spectrum of the type:

$$N(E) dE = N_0 E e^{-E/\alpha} dE,$$

where the spectral parameter α is half the mean energy and $N(E)$ is the number flux per energy interval. The adopted theoretical dependence of r on 4278 Å intensity and α is shown (Rees, 1971) in Figure 2.

There are uncertainties which must be considered when applying this procedure, such as variations in the extinction correction, temporal airglow fluctuations, lifetime effects, anomalous energy spectra, etc. In any particular case, one can obtain confirming data by measuring additional emissions, such as 3914 Å N_2^+ 5577 Å OI and 5200 Å NI. It is expected that the occurrence of large uncertainties is more the exception than the rule and the technique is satisfactory in the average case. The present discussion will be restricted to average properties of the auroral particles.

The photometer provides very sensitive (5×10^{-3} erg cm $^{-2}$ s $^{-1}$) detection of auroral primary particles and from the photometer data one can obtain three basic quantities related to the primary particles: the proton flux, the electron energy flux, and a mean energy parameter for the electrons.

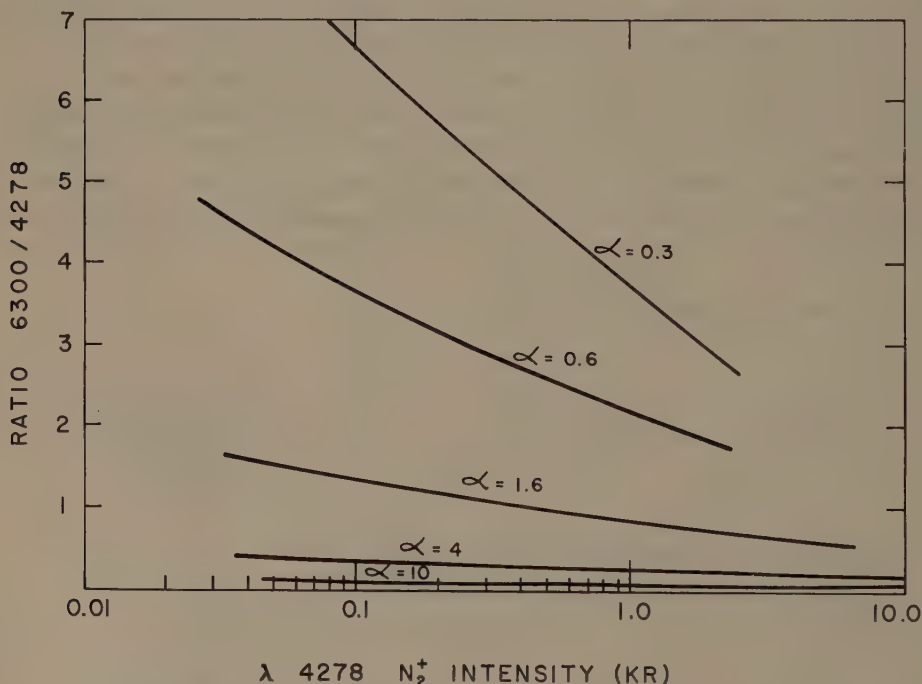


Fig. 2. Theoretical 6300 Å/4278 Å ratios (column integrated) for an assumed form of the electron energy spectrum, with different peak energy spectrum, with different peak energies α , as a function of 4278 Å intensity.

2. New Results

Results from airborne experiments aboard the NASA Convair 990 have been published (Eather, 1969; Eather and Akasofu, 1969; Eather and Mende, 1971a, b). Averaged latitude distributions of the various intensities were published as a function of oval coordinates (Eather and Mende, 1971b).

The previously reported nighttime soft zone (Eather, 1969; Eather and Mende, 1971a) is evident in the peaking of the average $6300 \text{ \AA}/4278 \text{ \AA}$ ratio poleward of the oval position. A new presentation in terms of the average electron energy parameter α

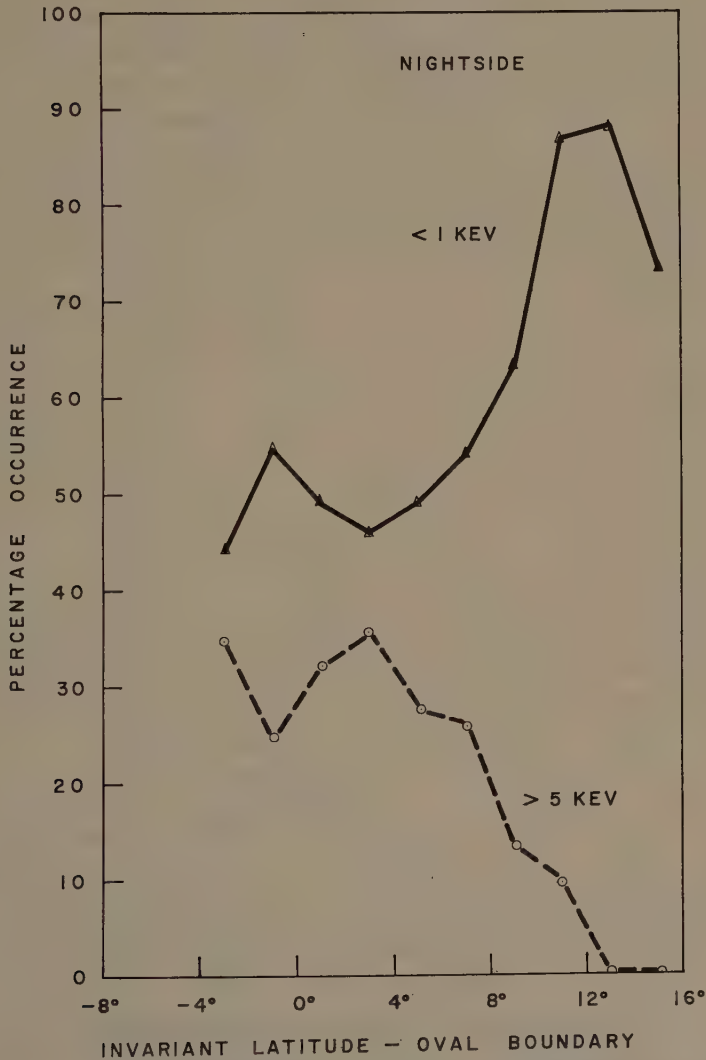


Fig. 3. Percentage occurrence of precipitation with mean electron energy $< 1 \text{ keV}$ and $> 5 \text{ keV}$, as a function of oval coordinates.

(Figure 3) shows the percentage occurrence of energies of <1 keV and >5 keV. The >5 keV precipitation maximizes in the position of the auroral oval, whereas the <1 keV precipitation locates at much higher latitude, in fact, 90% of the occurrences of precipitation in the high-latitude soft zone are of <1 keV electrons. (One hundred percent corresponds to the total number of observations in the latitude interval including airglow.) A plot of percentage occurrence of $4278 \text{ \AA } N_2^+$ exceeding 0.5 and 50 R (Figure 4) shows, by comparison with Figure 3, that the soft precipitation is typically low intensity (<50 R). It is also interesting to note that there is a broad region

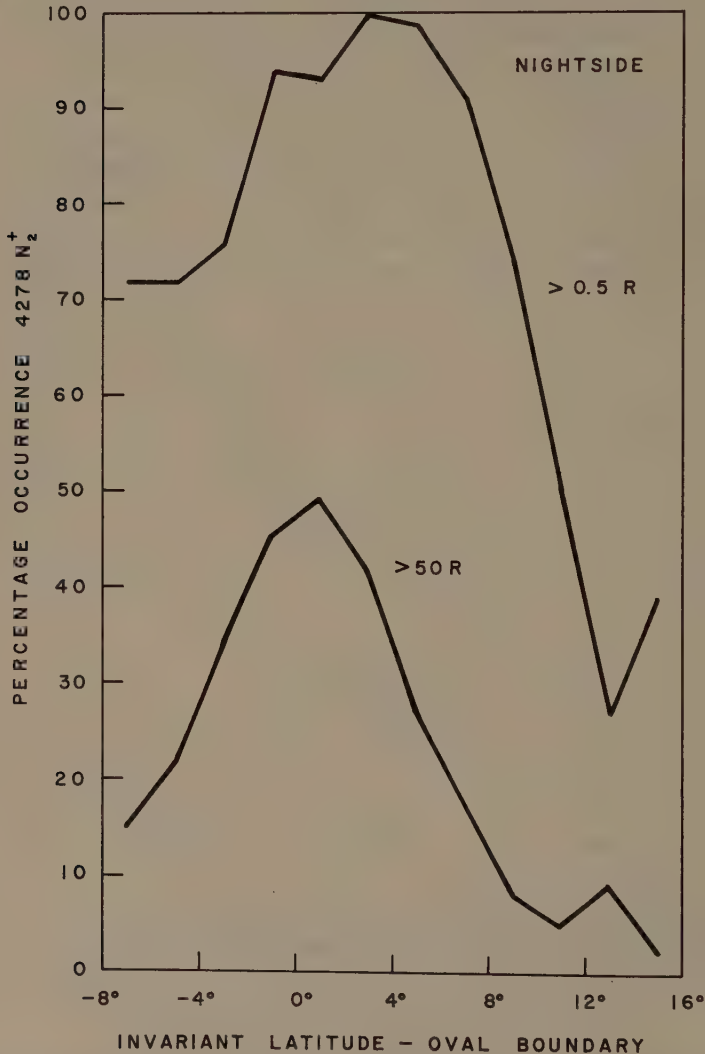


Fig. 4. Percentage occurrence of $4278 \text{ \AA } N_2^+$ exceeding 0.5 R (limit of detection) and 50 R as a function of oval coordinates.

centered on the oval where there is measurable precipitation virtually all of the time.

Various considerations led us to suspect that there may be a systematic relationship between the $6300 \text{ \AA}/4278 \text{ \AA}$ ratio and the 4278 \AA intensity, i.e., between average energy and total energy precipitated. The ratio $6300 \text{ \AA}/4278 \text{ \AA}$ is plotted vs. mean 4278 \AA intensity in Figure 5. The plotted numbers (1→11) represent 4° latitude intervals centered from 8° equatorward of the equatorial boundary of the auroral oval to 12° poleward of that boundary (so, for example, the numeral 6 represents the interval 0° to 2° in oval coordinates, (Eather and Mende, 1971b)). There are no points plotted unless the number of data points in the appropriate latitude intensity box exceeded 5.

We have drawn a division line at an intensity level of 50 R, and note that for $4278 > 50 \text{ R}$, there is a reasonably systematic decrease of the $6300 \text{ \AA}/4278 \text{ \AA}$ ratio with increasing 4278 \AA intensity for all latitudes. For $4278 \text{ \AA} < 50 \text{ R}$, it seems this relation breaks down, but a reasonably systematic increase in the ratio with increasing latitude becomes evident. We interpret these results as follows:

(a) There is a low level ($< 50 \text{ R}$) of precipitation occurring in a very broad region from below the auroral oval position to well poleward of it, such that the average energy of precipitation softens with latitude (from $\sim 1.5 \text{ keV}$ to $\lesssim 500 \text{ eV}$).

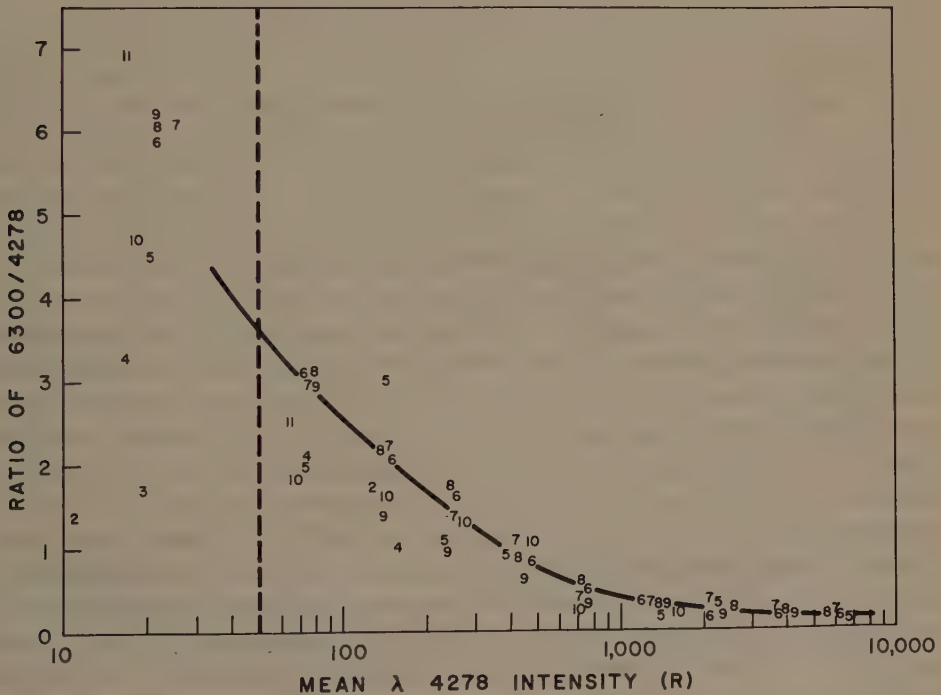


Fig. 5. The mean ratio $6300 \text{ \AA}/4278 \text{ \AA}$ plotted as a function of mean 4278 \AA intensity for 10 latitude intervals. The plotted numbers (1→11) represent 4° intervals centered every 2° from 8° equatorward of the equatorial boundary of the oval to 12° poleward of that boundary (e.g., the numeral 6 represents 0° to 2° in oval coordinates).

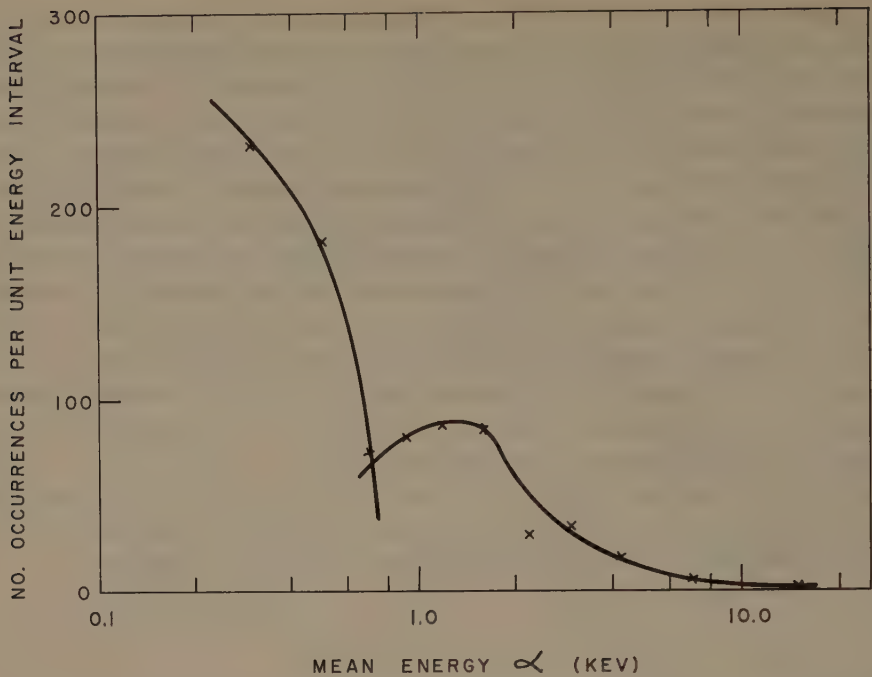


Fig. 6. Number of cases of occurrence of a given α (defined in Figure 2, and is a measure of peak energy for the spectrum), per unit energy interval. Two separate particle distributions are indicated.

(b) Higher intensity precipitation superimposes on this low level precipitation and locates preferentially in the position of the oval. This precipitation is characterized by an increasing average energy as total energy input increases.

We conclude that the so-called 'soft zone' does not just locate poleward of the auroral oval, but extends right across the auroral oval itself. There is a gradual softening with latitude throughout this broad region. Energetic electron precipitation superimposes on the lower-latitude half of the soft zone, and gives rise to the visual auroral forms that make up the auroral oval. As the $4278 \text{ \AA } N_2^+$ intensity in the oval increases from 50 R to up to $\sim 10 \text{ kR}$, there is a systematic hardening of the electron spectrum.

The division of Figure 5 into two intensity division (at 50 R), and our interpretation in terms of two distinct particle observations, is not as arbitrary as it may seem. In Figure 6, we have plotted the occurrence frequency of α , where α is the parameter in the spectrum used in Figure 2, and is a measure of the average energy. It may be seen that there is a definite indication of two separate particle populations, one between $\lesssim 200 \text{ eV}$ and $\sim 700 \text{ eV}$ (our soft particle spectrum), and a wider distribution locating between ~ 1 and $\sim 10 \text{ keV}$. Note that α exceeds 5 keV for only 11% of all cases. However, if we exclude the low α distribution, then for those more energetic electron spectra that excite visual aurora, α exceeds 5 keV some 25% of the time.

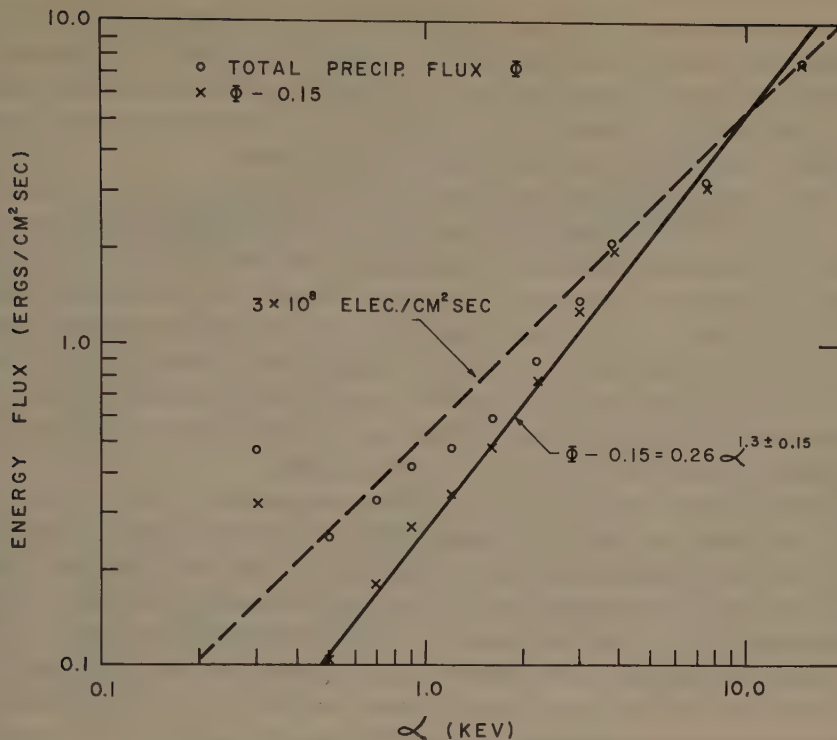


Fig. 7. Total energy precipitated Φ (erg cm⁻² s⁻¹) as a function of energy spectrum parameter α , for nightside data. The relation for a constant number flux of 3×10^8 electrons cm⁻² s is also shown.

The energy spectrum parameter α (Figure 2) and the total energy being precipitated were calculated. The resultant plot of total precipitated energy Φ (erg cm⁻² s⁻¹) vs. the characteristic energy of the spectrum α (keV) is given in Figure 7. (Note that average energy of spectrum = 2α .) The data have been averaged over all latitudes and times for nightside data only.

If these particles had been accelerated by an adiabatic compression process with negligible sources and losses, then Liouville's theorem predicts that Φ vs. α on a log-log plot (as in Figure 7) produces a straight line with a slope of 3. On the other hand, if acceleration was by static electric fields then we would expect a slope of 1.

The plot of total energy precipitated vs. α gives a reasonable straight line, although there seems to be a flattening out at lower energies. In this respect, it is interesting to note that if we subtract a constant $0.15 \text{ erg cm}^{-2} \text{ s}^{-1}$ from Φ , a much better straight line fit results (Figure 7). It is tempting to relate this $0.15 \text{ erg cm}^{-2} \text{ s}^{-1}$ (corresponding to $\sim 40 \text{ R}$ of 4278 \AA N_2^+) with the average contribution of the soft precipitation, and then interpret the remainder as the harder 'auroral' precipitation that superimposes on the soft zone.

Figure 7 shows that for this particle population above about 0.5 keV there is a

quite linear relationship with a slope of 1.3 ± 0.15 . We could argue that this is more consistent with an electric field acceleration mechanism, but other *ad hoc* explanations can explain with such a slope. For example, a combination of electric field acceleration and adiabatic compression with strong losses of the higher energy particles could give a slope in agreement with the experimental results.

In Figure 7, we have also drawn in the Φ vs. α relationship for an electron flux of $3 \times 10^8 \text{ cm}^{-2} \text{ s}^{-1}$. It is interesting to note that our results suggest that the average number flux of precipitating electrons increases by less than 50% for two orders of magnitude increase in the average total energy precipitated. This means that the averaged flux density in a sample of auroras within an intensity range is close to $3 \times 10^8 \text{ cm}^{-2} \text{ s}^{-1}$ regardless of the value of intensity and it does not mean that all auroras are of this flux density. There are times (especially at breakup) when very intense auroras are excited by much higher fluxes of 1 to 10 keV electrons. At those times fluxes in excess of $10^{10} \text{ cm}^{-2} \text{ s}^{-1}$ have been reported.

In summary, there seems to be soft auroral precipitation occurring almost permanently in the auroral zone. The mean energy of this soft precipitation is less than 1 keV. In the equatorward half of the auroral zone harder auroras (of mean energy greater than 1 keV) are superimposed. The poleward softening of the average auroral particle energy (the nightside soft zone) is a result of the gradual decrease in the number of hard precipitation events. Higher intensity electron auroras mostly represent precipitation with higher mean energy rather than the increased flux. Thus, the acceleration mechanism appears to accelerate the auroral electrons to various energies without a large systematic change in the number flux.

References

- Eather, R. H.: 1969, *J. Geophys. Res.* **74**, 153.
Eather, R. H. and Akasofu, S.-I.: 1969, *J. Geophys. Res.* **74**, 4794.
Eather, R. H. and Mende, S. B.: 1971a, *J. Geophys. Res.* **76**, 1746.
Eather, R. H. and Mende S. B.: 1971b, in B. M. McCormac (ed.), *The Radiating Atmosphere*, D. Reidel Publishing Company, Dordrecht, Holland, p. 255.
Rills, M. H.: 1971, private communication.

PART III

MAGNETIC FIELDS AND CURRENTS

REVIEW OF MAGNETIC FIELD OBSERVATIONS

NORMAN F. NESS

*Laboratory for Extraterrestrial Physics, NASA-Goddard Space Flight Center,
Greenbelt, Md., U.S.A.*

Abstract. Detailed magnetic field observations are now routinely conducted on satellites mapping the magnetosphere and its boundaries. Sufficiently comprehensive spatial, temporal, and high time resolution observations have improved the morphological description of the structure of and fluctuations in the magnetosphere, magnetosheath, plasma sheet and bow shock. Large scale distortion of the magnetospheric structure is detectable in the magnetic field data during and following major geomagnetic and substorm disturbances. Recent observations in previously unexplored regions of the magnetosphere, particularly in the polar cusp region, compliment and reinforce emphasis on particle access to the plasma sheet via the polar neutral points. Significant distortions of the geomagnetic field in the polar cusp region suggest field aligned currents at large geocentric distances which can be related to low altitude polar cap phenomena. Studies of the microstructure of the field reversal region of the plasma sheet imbedded in the geomagnetic tail suggest a periodic structure of more complexity than earlier assumed simplified single neutral-line models. No significant solar cycle variation of magnetospheric structure has been detected. This review highlights the salient features of the more recent observations of the magnetic field in the magnetosphere and identifies critical experimental and data areas for further study and theoretical analysis and interpretation.

1. Introduction

Accurate and rapid measurements of magnetic fields in space are now routinely conducted on satellites exploring the inner and outer magnetosphere, distant geomagnetic tail, and the boundaries of the magnetosphere and magnetosheath, the magnetopause and bow shock respectively. Recent reviews of these observations have been published by Heppner (1967a, b), Fairfield (1970), Ness (1967, 1969), Cain (1971), and Sugiura (1971) and the overall geometry and characteristics are now well established describing the earth's plasma field environment in space. It is not the purpose of this review to summarize the well established facts discussed by these earlier authors. Instead this review will concentrate on those recent results of specific interest to:

- (a) Quantitative studies of the solar wind interaction with the earth's magnetic field,
- (b) New regions of measurements near the earth's equator at $R = 2$ to $8 R_E$,
- (c) The polar cusp region of the geomagnetosphere, and
- (d) A new model of the detailed structure of the neutral sheet region in the geomagnetic tail.

2. Observations and Interpretation of Bow Shock and Magnetopause Positions

An extensive set of observations of the earth's bow shock and magnetopause has been obtained by the IMP series of spacecraft since 1963. Fairfield (1971) summarized these observations and derived a quantitative best fit ellipse and hyperbola to the

magnetopause and bow shock on the sunlight hemisphere of the earth. The observations and derived best fit curves are shown in Figures 1 and 2. The data points have been rotated by 4° about the Z_{se} axis to remove the effects of aberration due to the heliocentric motion of the earth. Average geocentric distances to the magnetopause and bow shock at the subsolar point are 11.0 and $14.6 R_E$. In the dawn meridian these distances increase to 15.1 and $22.8 R_E$ while in the dusk meridian they increase further to 15.7 and $27.6 R_E$.

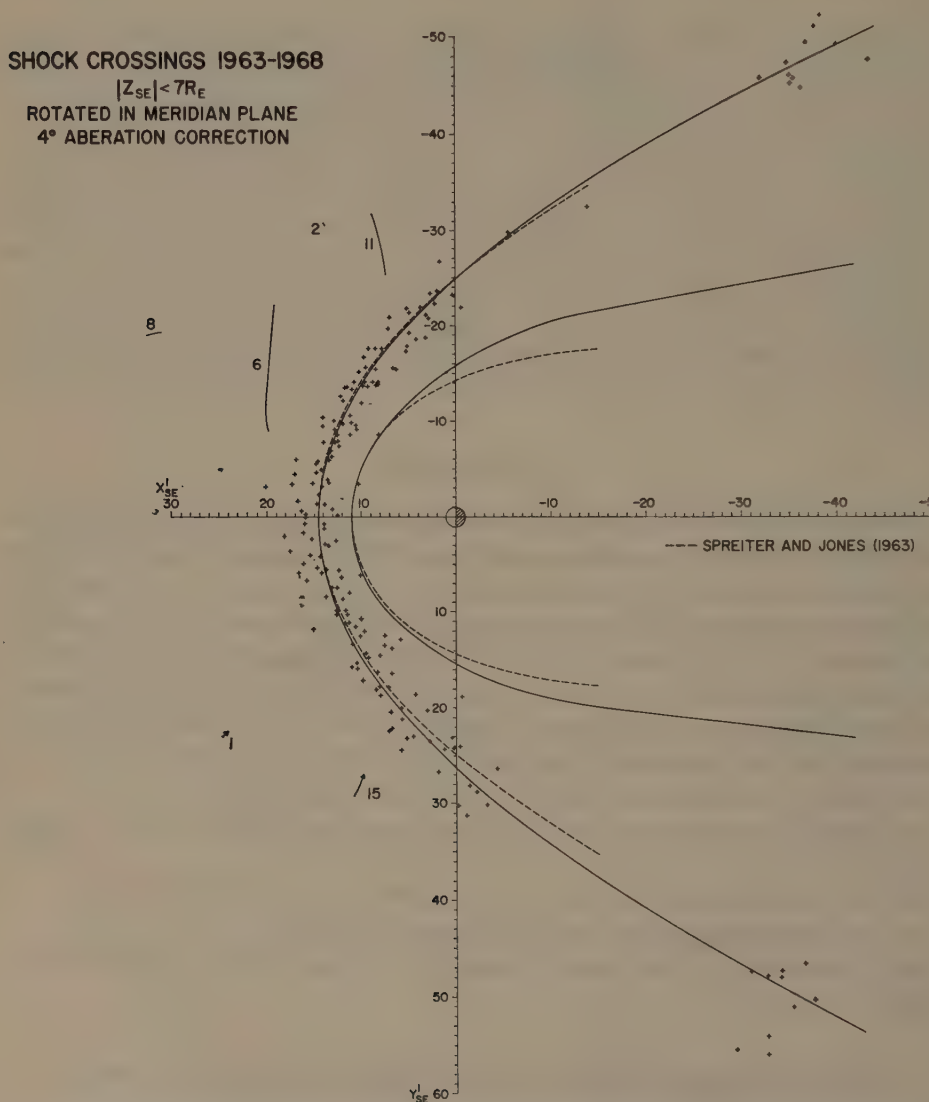


Fig. 1. Projections on ecliptic plane of bow shock observations by IMP spacecraft from 1963-68. Solid line is a best fit hyperbola to those points for which $|Z_{se}|$ less than $7 R_E$. Line segments beyond average shock position represents observations of unusually distant bow shock locations (Fairfield, 1971).

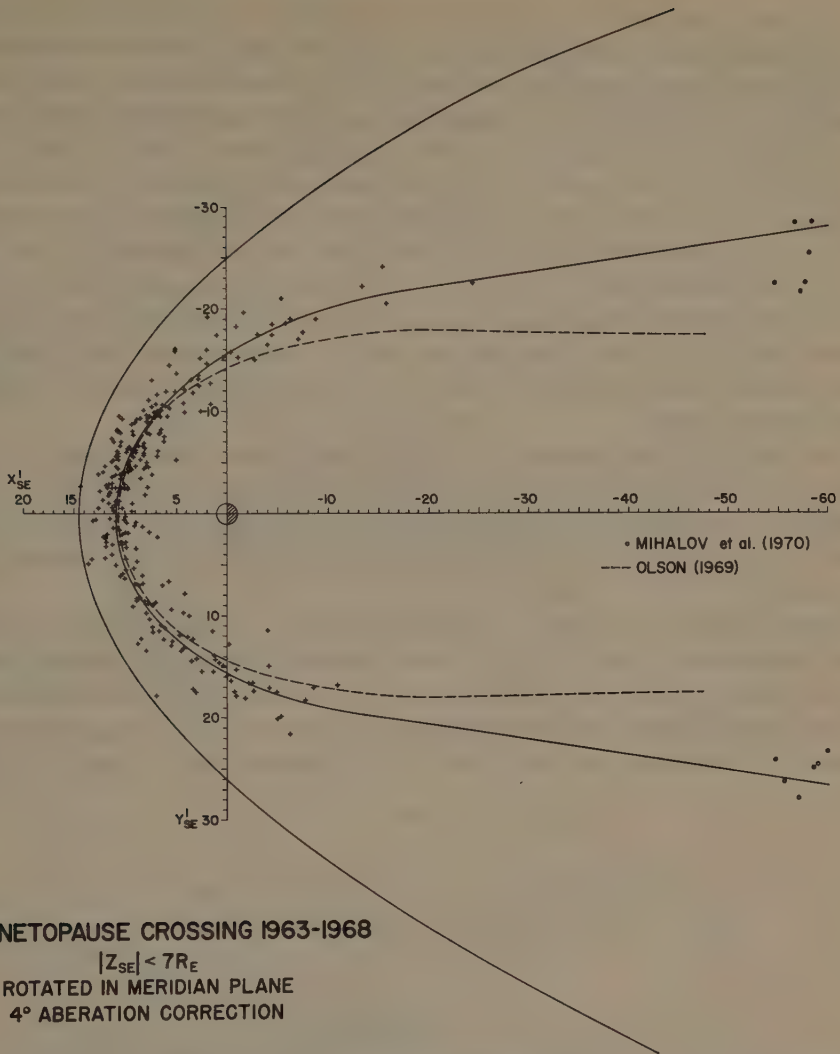


Fig. 2. Projection on ecliptic plane of observations of magnetopause as observed by IMP spacecraft from 1963-68. Solid line ellipse represents the best fit curve to those points for which $|Z_{se}|$ less than $7 R_E$ (Fairfield, 1971).

The dawn-dusk asymmetry is in a direction consistent with that expected when aberration of a radial solar wind flow is considered. The magnetopause observations agree well with theoretical predictions based upon the measured momentum flux of the solar wind near the noon meridian plane but increase to greater distances than the theoretical boundaries in the dawn and dusk meridian plane. All of the observations to date demonstrate that the position of the bow shock (and magnetopause) is time dependent and so the observations reported by Fairfield (1971), as shown in Figure 1 and 2, represent the average position on each orbital pass.

There is no evidence yet available to demonstrate a long term secular variation of the average position of the bow shock and magnetopause. Substantial evidence does exist for short term variations, indicating that the momentum flux, and to a lesser degree the sense of the N-S component of the interplanetary magnetic field, is important in determining the positions of these two boundaries. Figure 3 presents a study of the variation of the position of the magnetopause observed as compared with that predicted on the basis of simple fluid dynamic models in which the momentum flux of the solar wind (unaffected by the earth's bow shock) is balanced by the pressure of the geomagnetic field. The average distance to the magnetopause for the observations would be predicted as $10.3 R_E$ which is to be compared with the observed position of $10.9 R_E$. The discrepancy can easily be accounted for by modification of the measured solar wind number density and is within the experimental accuracy of observations to date.

The very favorable comparison of the frequency distribution shown in Figure 3 has been further investigated by studying explicit time variations on the IMP 4 satellite. It now appears possible to predict the average bow shock and magnetopause position to within $0.5 R_E$ at least 50% of the time and to within $1 R_E$ at least 80% of the time.

An investigation of an effect of the N-S component of the interplanetary magnetic field has shown that when the field is directed northward the average geocentric distance to the magnetopause at the subsolar point is $10.5 R_E$ while it increases to $11.6 R_E$ when the field points to the south. Future studies of the bow shock and magnetopause positions may refine these conclusions but it is not expected that a significant departure

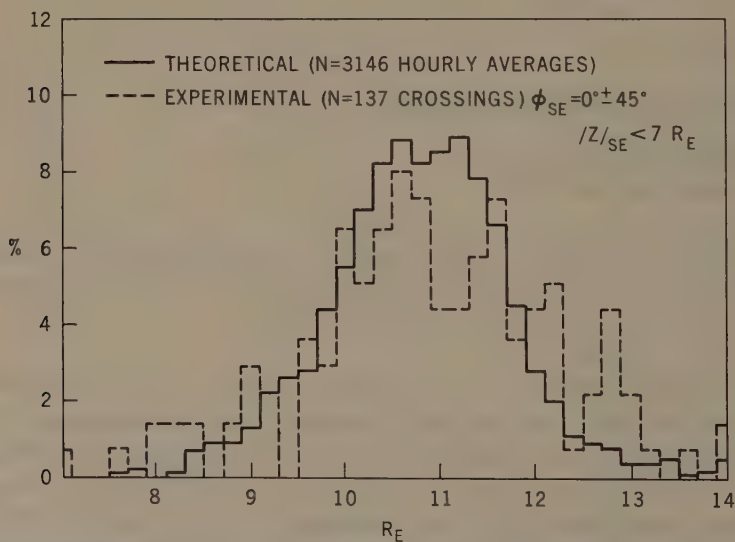


Fig. 3. Frequency distribution of observed (IMP 4: 1967-68), and predicted subsolar magnetopause positions. Note that theoretical positions have been adjusted so they are centered on the observed average position at $10.9 R_E$ (Fairfield, 1971).

from them will arise since the data on which the conclusions are based extend over a substantial time interval under a variety of interplanetary and terrestrial conditions.

It should be noted, however, that on rare occasions the earth's bow shock is observed at extremely distant positions (see Figure 1). Investigation of solar wind

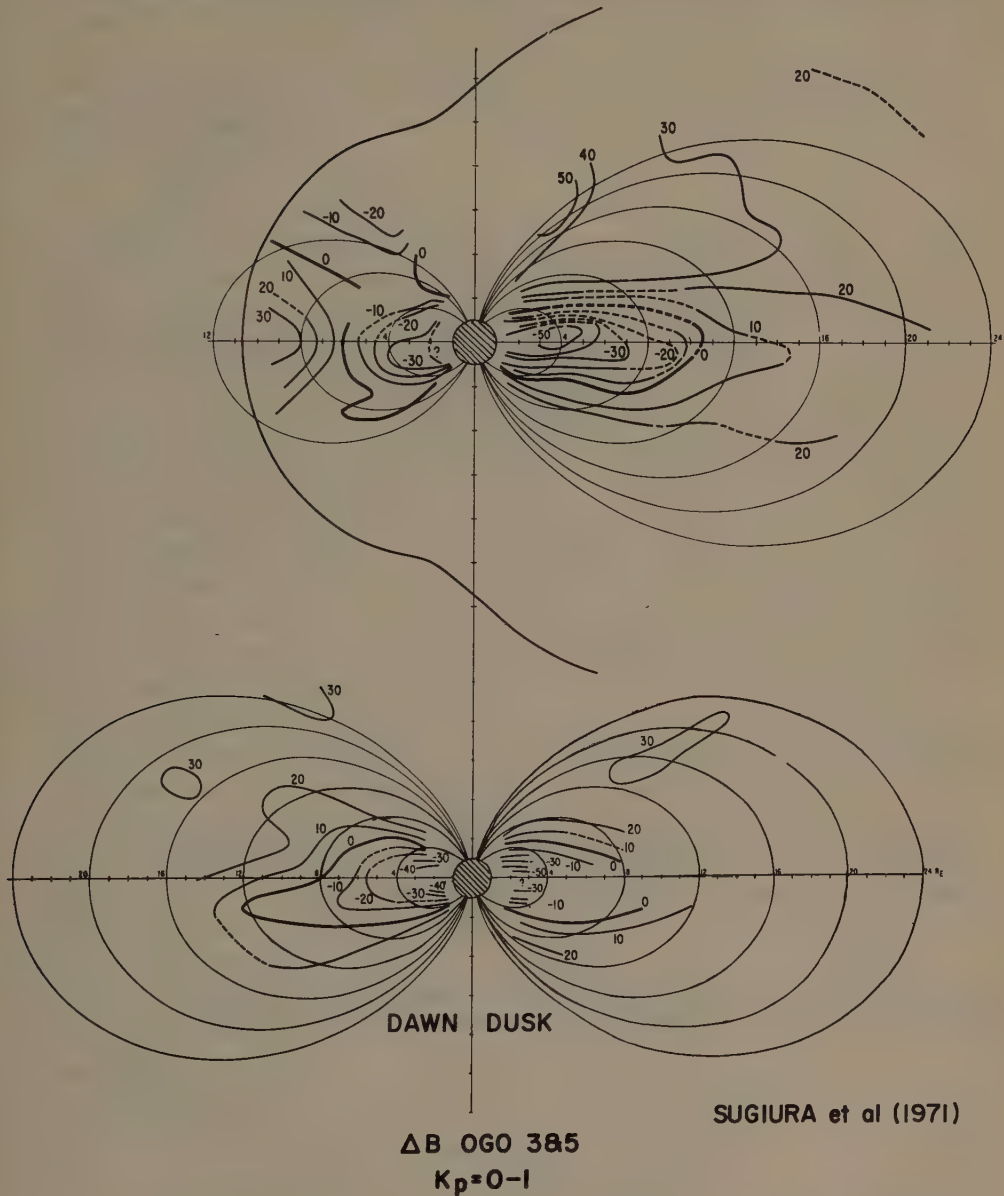


Fig. 4. Contours of isointensity magnetic field magnitude anomaly ΔB in the geomagnetic noon-midnight meridian plane (top) and in the geomagnetic dawn-dusk meridian plane for quiet conditions ($K_p = 0$) in units of gammas (Sugiura *et al.*, 1971).

conditions upstream at this time suggest the possibility that the solar wind flow may not be super-Alfvénic but occasionally sub-Alfvénic so that a Laminar flow pattern develops. Thus far, great success has been achieved in the comparison of continuum fluid models of the collisionless solar wind plasma flow past the geomagnetic field with slight modifications to classical parameters used in continuum approximations.

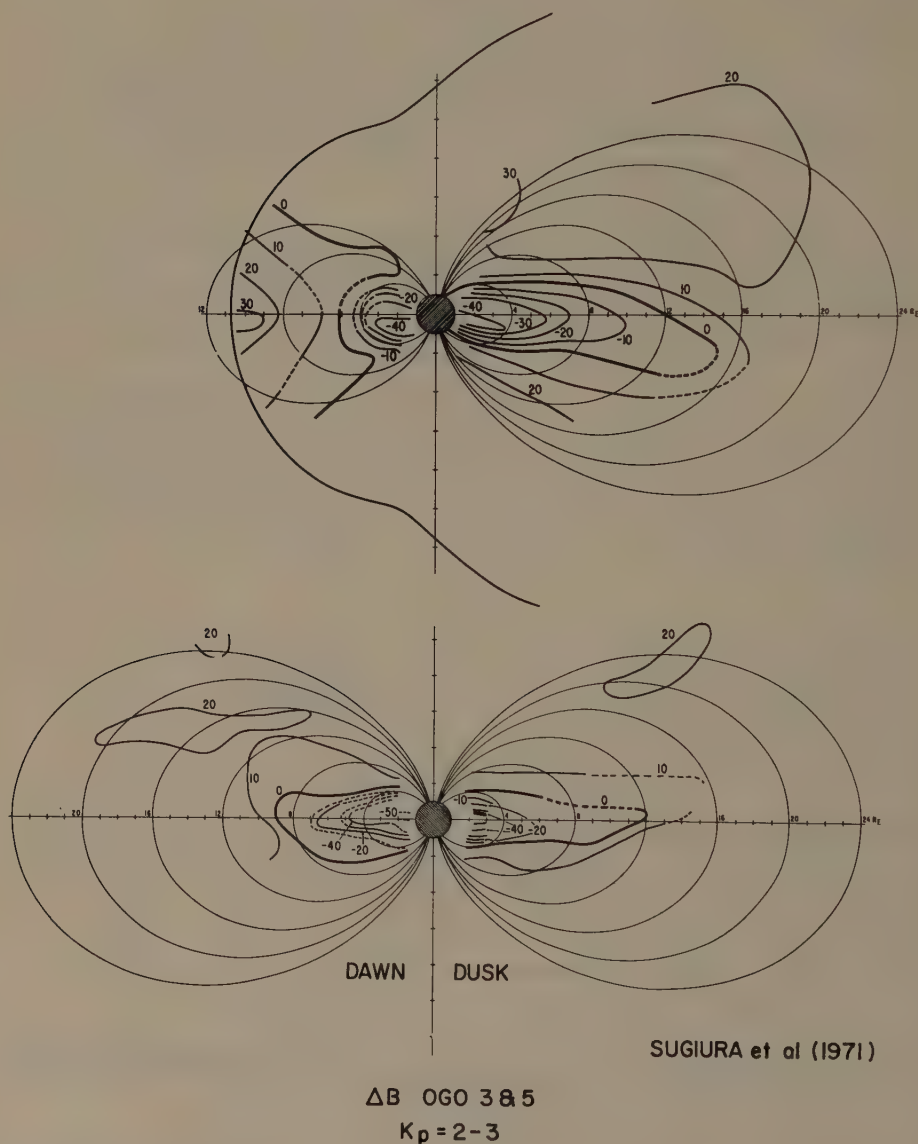


Fig. 5. Contours of isointensity magnetic field magnitude anomaly ΔB in the geomagnetic noon-midnight meridian plane (top) and in the geomagnetic dawn-dusk meridian plane for slightly disturbed conditions ($K_p = 2-3$) in units of gammas (Sugiura *et al.*, 1971).

3. Inflation of the Inner Magnetosphere

The majority of eccentric orbiting satellites has failed to provide measurements *in situ* of the field and plasma characteristics at low geomagnetic latitudes but at moderate distances from the earth, that is geomagnetic latitudes less than 20° and geocentric distances between 2 to $8 R_E$. Recent observations by the ATS 1 and OGO 3 and 5 satellites, however, have contributed significantly to these studies. Sugiura *et al.* (1971) have recently summarized their OGO 3 and 5 magnetic field observations obtained with a Rb vapor magnetometer of high accuracy. For interpretation of data they have utilized the parameter

$$\Delta B = |\mathbf{B}_{\text{obs}}| - |\mathbf{B}_{\text{theory}}|$$

which represents the magnitude difference between observations and theory. Figures 4 and 5 summarize these results for four quadrants of the magnetosphere, according to local magnetic time and for two conditions of magnetic activity: quiet ($K_p=0$ to 1) and moderately disturbed ($K_p=2$ to 3).

Two important results from these observations relate to the classical ring current problem and the recent observations obtained by ATS 1. Computation of the magnetic fields to be expected from ring currents typified by particles observed by Frank and his colleagues (Frank, 1967, 1970, 1971; Frank and Owens, 1970) strongly suggest that the main source of particles responsible for inflation in the magnetosphere has not been measured. The basis for this conclusion by Sugiura *et al.* (1971) is the geometry of the field perturbations observed by OGO 3 and 5 when compared with those obtained from theoretically computed perturbations associated with observed particle flux measurements (Hoffman and Bracken, 1967). Generally, the particle flux measurements have been made at higher geomagnetic latitudes than those required to detect a localized low energy plasma distribution limited near the earth's equator which seems to best fit the disc-like magnetic field anomaly. This currently represents one of the more critical discrepancies in the magnetosphere regarding a need for reconciliation of plasma and magnetic field observations.

It should be noted that the use of a slightly different dipole coefficient for the geomagnetic field will not significantly alter the location of observed magnitude anomaly since the maximum modification (50γ at earth's surface) scales to less than 1γ at the distances of interest (near $5 R_E$).

Another result of this mapping of the inner magnetosphere's magnetic field is summarized in Table I below. Here the average magnitude of the magnetic field in the

TABLE I
OGO 3 and 5

	$K_p=0-1$	2-3	ATS
Moon	120	120	135
Midnight	85	75	105
Diurnal	35	45	30-40

noon-midnight meridian plane at the equator ($R = 6.6 R_E$) is shown for both quiet and moderately disturbed geomagnetic conditions. These values are compared with those derived from ATS 1 observations (Cummings and Coleman, 1968; Cummings *et al.*, 1968; Olson and Cummings, 1970).

The difference between the average fields observed is significant and is no doubt due to an incorrect zero level assumed for the ATS 1 spacecraft magnetic field component parallel to the spin axis (which represents the local horizontal component in the ATS 1 nomenclature). Better models of the distorted magnetosphere are necessary for quantitative comparison with these observations and future work in this area will require substantial improvement and increased sophistication of models used for theoretical studies.

4. Magnetic Field Observations in High Latitude Outer Magnetosphere

Early studies of the problem of solar wind interaction with the geomagnetic field lead to the concept of two neutral points in the polar regions of the magnetosphere which separated field lines which closed on the dayside from those field lines which were stretched back to form the geomagnetic tail. The first good opportunity to make high latitude high altitude measurements began with the IMP 5 satellite in 1969. Early measurements on the plasma flux in the cusp region by Frank (1970) were interpreted in terms of the injection of solar wind plasma from the magnetosheath into the magnetosphere. Corresponding magnetic field measurements have been reported upon by Fairfield and Ness (1972).

Measurements of the magnetic field in the cusp region show a very broad depressed field region in which field strengths are less than 50 to 70% that of the undistorted dipolar field. No well defined magnetopause boundary is observed between the magnetosheath and polar cusp regions. The change from the magnetosheath to the polar cusp is characterized by large amplitude fluctuations of the magnetic field with magnitudes up to 45γ and in directions which are approximately perpendicular to the average field. These magnetic field perturbations are suggestive of field aligned currents such as have been reported from low altitude polar orbiting spacecraft by Zmuda and colleagues.

The general character of the magnetic field in the region of the polar cusp is in good agreement with earlier measurements at low geomagnetic latitudes and theoretical predictions. The orientation of the magnetic field in the polar cusp is suggestive of direct connection with interplanetary magnetic field lines. However, this conclusion is not unique because there exists no well defined boundary to the magnetosheath in this region of space. But no other reasonable alternative to the topology of the magnetic field consistent with the observations has yet to be offered.

5. Microstructure of the Geomagnetic Neutral Sheet

For sometime the existence of a geomagnetic tail with a small magnetic flux crossing

the field reversal region has been an accepted characteristic of the deformed magnetosphere. Experimental observations have not been in perfect agreement, however, on the possible position of a neutral line in the geomagnetic tail since observations of the N-S component have not always revealed only a north component. In an attempt to study the detailed structure of the neutral sheet in the field reversal region, a statistical approach is necessary since it is not possible to uniquely separate space and time variations from each other in observations obtained from a single satellite traversing the field reversal region.

In a study of the detailed observations of the field obtained from IMP 5 by Schindler and Ness (1972), a new configuration for the microstructure was suggested to be consistent with the field reversal region. This new structure consists of a series of neutral lines in the geomagnetic tail and is motivated by theoretical considerations which have been discussed recently by Schindler (1971).

Observations show that for N-S components greater than 1γ the frequency of northward occurring fields is 6 times that of southward occurring fields. If consideration of

TABLE II

Magnitude range	Average field		% Southward field
	North (+)	South (-)	
0-1.25	-0.03		55
1.25-1.875	0.26		39
1.875-2.625	0.81		27
2.625-3.375	1.13		22
3.375-4.125	1.51		18
4.125-5.25	1.83		16
5.25-6.750	2.11		13
6.750-1.50	2.03		17
8.50-10.5	2.26		17

field components greater than 5γ is made, the ratio increases to 20 to 1. The fact that the ratio is magnitude dependent suggests strongly a more detailed structure than the simple one dimensional field reversal region utilizing a single neutral line. The motivation for a statistical study was that relative motion of a relatively fixed spatial structure past the satellite should, providing a sufficiently large number of data are employed, yield statistical characteristics of the field which reflect the spatial structure only and from which the time variations have been removed. Table II above summarizes the statistical distribution of the average N-S component of the field in solar magnetospheric coordinates as a function of field magnitude and the percentage of the time that the N-S component is directed southward.

The nature of this distribution is such that it favors multiple neutral lines over the rather implausible situation of a single neutral line moving rapidly back and forth past the satellite, i.e., towards and away from the earth. Arguments for the choice of interpretation of multiple neutral lines have been presented by Schindler and Ness (1971).

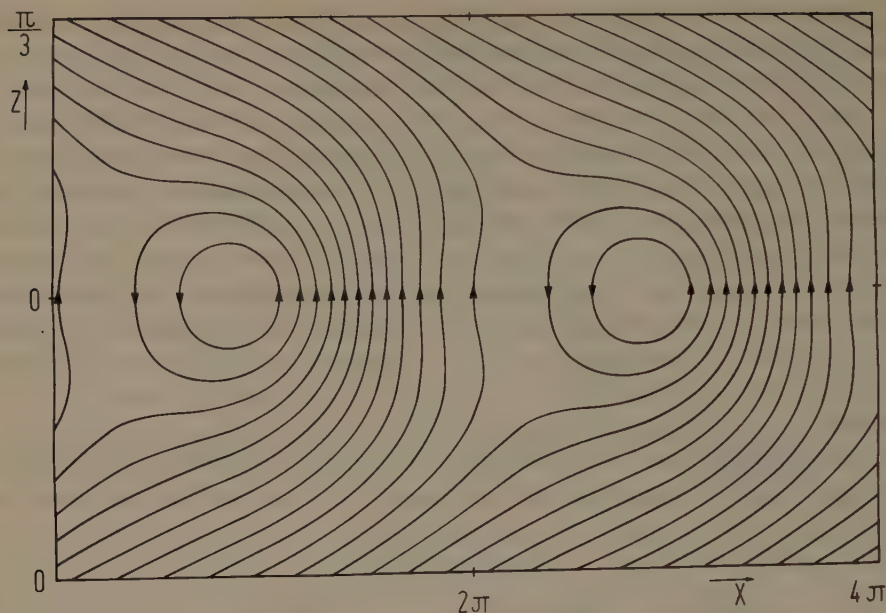


Fig. 6. Topology of magnetic field in model neutral sheet with multiple neutral lines. The two-dimensional structure is replicated along the neutral sheet (Schindler and Ness, 1971).

Figure 6 presents a schematic diagram of the field topology in the midnight meridian plane showing the presence of multiple X and O type neutral points in the geomagnetic neutral sheet on a fine spatial scale.

The merits of this suggestion must be tested by additional studies of satellite measurements at different distances in the geomagnetic tail and an evaluation of the associated theoretical model.

References

- Cain, J. C.: 1971, *Rev. Geophys. Space Phys.* **9**, 259.
 Cummings, W. D. and Coleman, P. J., Jr.: 1968, *Radio Sci.* **3**, 758.
 Cummings, W. D., Barfield, J. N., and Coleman, Jr., P. J.: 1968, *J. Geophys. Res.* **73**, 6687.
 Fairfield, D. H.: 1970, *Inter-Union Commission on Solar Terrestrial Physics Proceedings*, Leningrad, U.S.S.R.
 Fairfield, D. H.: 1971, *J. Geophys. Res.* **76**, 6700.
 Fairfield, D. H. and Ness, N. F.: 1972, *J. Geophys. Res.* **77**, 611.
 Frank, L. A.: 1967, *J. Geophys. Res.* **72**, 3753.
 Frank, L. A.: 1970, *J. Geophys. Res.* **75**, 1263.
 Frank, L. A.: 1971, *J. Geophys. Res.* **76**, 2265.
 Frank, L. A. and Owens, H. D.: 1970, *J. Geophys. Res.* **75**, 1269.
 Heppner, J. P.: 1967a, *Space Sci. Rev.* **7**, 166.
 Heppner, J. P. 1967b, in S. Matsushita and W. H. Campbell (eds.), *Physics of Geomagnetic Phenomena*, Academic Press, New York.
 Hoffman, R. A. and Bracken, P. A.: 1967, *J. Geophys. Res.* **72**, 6039.
 Mihalov, J. D., Colburn, D. S., and Sonett, C. P.: 1970, *Planetary Space Sci.* **18**, 239.
 Ness, N. F.: 1967, in J. W. King and W. S. Newman (eds.), *Solar-Terrestrial Physics*, Academic Press, 57-89.

- Ness, N. F.: 1969, *Rev. Geophys.* **7**, 97.
- Olson, W. P.: 1969, *J. Geophys. Res.* **74**, 5642.
- Olson, W. P. and Cummings, W. D.: 1970, *J. Geophys. Res.* **75**, 7117.
- Schindler, K.: 1971, ESRIN Internal Note 161, August.
- Schindler, K. and Ness, N. F.: 1972, *J. Geophys. Res.* **77**, 91.
- Spreiter, J. R. and Jones, W. P.: 1963, *J. Geophys. Res.* **68**, 3555.
- Sugiura, M.: 1971, A. J. Zmuda (ed.), in *The World Magnetic Survey 1957-1969*, IUGG Publications Office, Paris.
- Sugiura, M., Ledley, B. G., Skillman, T. L., and Heppner, J. P.: 1971, *J. Geophys. Res.* **76**, 7552.

A SELF-CONSISTENT THEORY OF THE TAIL OF THE MAGNETOSPHERE

KARL SCHINDLER

European Space Research Institute (ESRIN), Frascati (Rome), Italy

1. Introduction

The structure of the magnetosphere appears to be so complex that any attempt to theoretically describe the magnetosphere necessarily has to confine itself to specific aspects. In this paper we will be concerned with steady state configurations and to some extent with stability.

In this context it is important that there are regions in the magnetosphere where the kinetic pressure forces are sufficiently large such that they can balance the stresses exerted by the magnetic field. This fact is conventionally expressed in terms of the parameter

$$\beta = \frac{p}{B^2/2\mu_0},$$

where p is a typical particle pressure and B the magnetic field strength. Thus we are interested in regions where $\beta \gtrsim 1$.

This clearly applies to the plasma sheet where β generally exceeds one. Choosing as rough representative values, an ion temperature of 5×10^7 K, a particle number density of 0.5 cm^{-3} (see e.g. Bame, 1968), and a magnetic field of 10γ we obtain $\beta \sim 8$.

To describe equilibria and dynamical phenomena in finite- β regions requires the use of self-consistent models. In the framework of a kinetic model self-consistency means that the currents and space charges as derived from the particle motion have to yield electric and magnetic fields which in turn are consistent with the particle motion. The main consequence of lack of self-consistency in a finite- β situation is an unphysical acceleration force. If for instance the magnetic field in an equilibrium situation deviates from the self-consistent one by a finite amount this acceleration makes the plasma reach the Alfvén velocity in the time an Alfvén wave needs to cross the system.

Although we emphasize the importance of self-consistency for equilibria and dynamical properties, it should be noted that there are other questions of interest which do not critically depend on self-consistency, even if finite- β regions are involved. Examples are models of the overall magnetic field configuration (e.g., Williams and Mead, 1965; for a review, see Roederer, 1969).

So far, self-consistency in finite- β situations has been achieved only under highly simplified conditions. Luckily, for a number of magnetospheric structures such simplifications are reasonably justified. Examples are the magnetopause (e.g. Alpers, 1969) and the plasma sheet with the neutral sheet treated as one-dimensional equilibria

(Schindler and Soop, 1968) or the plasma in strongly inflated radiation belts in spherical symmetry (Lackner, 1970).

In this paper we discuss a self-consistent model of the tail of the magnetosphere which is somewhat more realistic than the previous ones. The new feature is that a slow variation along the tail axis is taken into account.

As the above-mentioned one-dimensional models did, we treat the equilibria as static with an isotropic pressure tensor. The significance of this model is discussed elsewhere (Cole and Schindler, 1972). We only comment here that there are several observations which show that the measured ion fluxes in the plasma sheet are nearly isotropic (Bame, 1968; Frank, 1970). The electrons are unimportant in this context because they are considerably less energetic in the plasma sheet.

This means that pressure anisotropy is probably not important and that directed flow velocities are smaller than the thermal ion speed. In fact, Hones (1968) reported that for $K_p < 2$ the directed ion flow velocities are about 5% of the thermal speed. Our model neglects both effects entirely.

Also, we do not take into account the cross tail dimension parallel to the plasma sheet, and assume the absence of external forces. (For example, a possible friction force exerted by the solar wind will be active only in a region close to the magnetopause, while we are concerned with equilibrium inside the tail.)

It should be emphasized that this model is a rather crude one and we do not expect that it is able to make precise quantitative predictions. We do feel however that it is reasonable to expect some measure of qualitative agreement with the conditions prevailing in the magnetosphere. In any case, based on the observations mentioned above, it seems justified to explore the consequence of such a model. In many ways it is the simplest possible mathematical description and it seems to be the natural starting point for a self-consistent description of the magnetosphere.

The investigation presented in this paper is based on a more general study of equilibria and stability related to the magnetosphere (Soop and Schindler, 1972), where further details of the mathematical procedure and numerical results are given.

2. Smooth Spatial Variation

We shall use a coordinate system where the x -axis points along the tail (away from the earth) and the z -axis along the dipole axis, which is assumed to be perpendicular to the sun-earth line. Variation in the y -direction is neglected. The field lines lie in the x, z -plane.

The plasma is assumed to be quasi-neutral, i.e. number density n is equal for ions and electrons (we assume singly charged ions):

$$\sum nq = 0 \quad (1)$$

(q is the particle charge; the summation is extended over the particle species.) It is important that Equation (1) does not imply the absence of electrostatic fields.

Since we are dealing with a collision-free plasma it seems adequate to use Vlasov's

theory. We prescribe the equilibrium distribution functions of the particle as

$$f_0(x, z, \mathbf{v}) = F_0(H, P_y) \quad (2a)$$

$$\frac{\partial F_0}{\partial H} < 0; \quad (2b)$$

\mathbf{v} is the particle velocity; the Hamiltonian

$$H = \frac{1}{2m} (\mathbf{P} - q\mathbf{A})^2 + e\phi \quad (3)$$

(\mathbf{P} canonical momentum, m particle mass, $\mathbf{A} = (0, A, 0)$ magnetic vector potential, and ϕ electric potential) and the y component of the canonical momentum

$$P_y = mv_y + qA \quad (4)$$

are constants of the motion. Therefore the Liouville part of the Vlasov theory is identically satisfied:

$$\mathbf{v} \cdot \nabla f_0 + \frac{q}{m} (\mathbf{E} + \mathbf{v} \times \mathbf{B}) \cdot \frac{\partial f_0}{\partial \mathbf{v}} = 0. \quad (5)$$

It remains to solve Maxwell's equations, which, in our case, reduce to the quasi-neutrality condition, Equation (1), and

$$\nabla \times \mathbf{B} = \mu_0 \mathbf{j} \quad (6)$$

where $\mathbf{j} = (0, j, 0)$ is the electric current density.

It follows from the form of f_0 as given in Equation (2a) that n and j depend on x and z only via $\phi(x, z)$ and $A(x, z)$. One can use Equation (1) to eliminate ϕ in terms of A and the y -component of Equation (6) then gives

$$AA + J(A) = 0, \quad J = \mu_0 j \quad (7)$$

which is the remaining equation to be solved. Note that this theory gives isotropic pressure, because Equation (2a) is isotropic in the v_x, v_z -plane.

The procedure described above is standard in dealing with one-dimensional equilibria (e.g., Sestero, 1964). We have given a short derivation to show that it also applies to two dimensions.

We shall discuss Equation (7) from the point of view that $j(A)$ can be chosen arbitrarily. This is in fact true to a very large extent, because j follows from $F_0(H, P_y)$ which can be freely chosen for ions and electrons:

$$j = \sum q \int (P_y - qA) F(H, P_y) d^3v. \quad (8)$$

The only condition to be imposed on the choice of $j(A)$ is that the functions $F(H, P_y)$ have to be positive, which usually is easy to satisfy.

Equation (7) is also obtained from a scalar pressure fluid picture of the equilibrium.

The general solution of the momentum equation

$$\nabla p + \mathbf{j} \times \mathbf{B} = 0 \quad (9)$$

is obtained by choosing j as a function of A arbitrarily and the pressure follows as

$$p = \int^A j(A) dA \quad (10)$$

(which also holds in the Vlasov picture). Again, we obtain Equation (7) as the y -component of Equation (6).

If the boundaries are to be field lines, the appropriate boundary condition is to fix a constant value for A at the boundary. This is the boundary condition used in this paper, identifying the boundary with the magnetopause. In dealing with stability we shall assume that the shape of the magnetopause remains unchanged when slow internal perturbations appear. This assumption seems reasonable in view of the fact that in the (realistic) case of a situation which is Kelvin-Helmholtz stable, boundary perturbations will decay rapidly on a time scale not larger than $(kV)^{-1}$, where k is the wave number and V the solar wind velocity outside the magnetopause. The modes of interest for this paper have indeed time constants larger than $(kV)^{-1}$. A final answer requires a detailed study.

We are interested in solving Equation (7) for slow x -dependence. It seems natural to use an expansion of the form

$$A(x_1, z) = \sum_{n=0}^{\infty} \varepsilon^n A_n(x_1, z); \quad x_1 = \varepsilon x, \quad (11)$$

where $0 < \varepsilon \ll 1$ is a measure for the ratio of the characteristic lengths along z and x . Inserting Equation (11) into Equation (7) we obtain in ascending order of ε :

$$\frac{\partial^2 A_0}{\partial z^2} + J(A_0) = 0 \quad (12)$$

$$\frac{\partial^2 A_1}{\partial z^2} + J'(A_0) A_1 = 0 \quad (13)$$

$$\frac{\partial^2 A_2}{\partial z^2} + J'(A_0) A_2 = -\frac{\partial^2 A_0}{\partial x_1^2} - \frac{1}{2} J''(A_0) A_1^2. \quad (14)$$

...

We shall choose

$$J \neq 0. \quad (15)$$

For a comprehensive discussion, a number of different cases would have to be distinguished depending on the shape of the boundaries and whether or not Equation (13) has a non-trivial solution. In this context it is convenient to introduce the eigenvalue problem

$$-\frac{\partial^2 U}{\partial z^2} - J'(A_0) U = \lambda U \quad (16)$$

with $U=0$ at the boundaries. Equation (13) has a non-trivial solution if Equation (16) has an eigen value $\lambda=0$. As discussed in the following section, the sign of the minimum eigen value gives us direct information on the stability of the configuration.

For the present discussion we will exclude some cases which need a separate treatment. We assume that

- (a) none of the eigen values λ of Equation (16) is zero, and
- (b) the tail boundaries are not parallel to the x -axis.

As the discussion in Section 4 will show, (a) is probably satisfied at least for the lowest eigen value, the only one for which there are perhaps reasons to expect that it vanishes non-accidentally. As will also be shown later, (b) seems consistent with observations available for radial distances up to $70 R_E$. Situations where (a) and (b) are not satisfied are discussed elsewhere (Soop and Schindler, 1972).

Because of condition (a) Equation (13) has only the trivial solution $A_n=0$, and it is easy to see that this applies to all A_n with n odd. Equation (14) has a unique solution for any continuous $\partial^2 A_0 / \partial x_1^2$. This again is guaranteed by the absence of a vanishing eigen value of Equation (16). Similarly, all higher A_n with n even are uniquely determined by a sufficiently smooth but otherwise arbitrary choice of $A_0(x, z)$. The main condition on A_0 therefore is that it has to satisfy the boundary conditions.

For the rest of the discussion we will confine ourselves to the zero order term $A_0(x_1, z)$; the subscript 0 will be dropped from here on. We shall address ourselves to the northern half of the tail with the southern half following from the symmetry relation

$$A(x_1, -z) = A(x_1, z). \quad (17)$$

We choose

$$J(A) < 0, \quad B_x < 0. \quad (18)$$

Consequently, B_x varies monotonically from zero ($\partial A / \partial z = 0$ at $z=0$, see Equation (17)) to its boundary value at $z=a(x_1)$. With these assumptions we solve Equation (12) in the following way. (Note that Equation (12) simply has the form of the equation of motion of a mass point with coordinate A in a potential $Q(A) = \mu_0 p(A)$.) Integrating Equation (12) once, we find the local pressure balance (energy conservation of the analogous mass point motion)

$$\frac{1}{2} (\partial A / \partial z)^2 + Q(A) = Q_0; \quad Q(A) = \mu_0 p(A), \quad (19)$$

where

$$Q_0 = Q(A(x_1, 0)). \quad (20)$$

One more integration gives

$$\int_A^{A_b} \frac{dA}{\sqrt{2(Q_0 - Q(A))}} = a(x_1) - z, \quad (21)$$

where A_b is the boundary value of A .

The function $A(x_1, 0)$ follows from choosing $z=0$ in Equation (21):

$$\int_{A(x_1, 0)}^{A_b} \frac{dA}{\sqrt{2(Q_0 - Q(A))}} = a(x_1). \quad (22)$$

It is important to note that we have found a solution without specifying the function $j(A)$. This means that we have treated all possible equilibria together. Therefore our theory contains any configuration which can be observed as a snapshot of a slowly time varying configuration.

Exact numerical solutions of (7) have been obtained by Toichi (1971) and by Soop and Schindler (1972).

A relationship which will prove particularly useful is obtained by differentiating Equation (22) with respect to x (using $x_1 = \varepsilon x$)

$$B_z(x_1, 0) B'_x(x_1, 0) \left[\frac{1}{B_x(x_1, a) B'_x(x_1, a)} + \int_0^{a(x_1)} \frac{B''_x dz}{B_x B'^2_x} \right] = \frac{da}{dx}. \quad (23)$$

Here we have applied a partial integration with respect to z before differentiating, making use of $B'_x \neq 0$ because of Equation (18). B'_x stands for $\partial B_x / \partial z$.

Before applying these results to the magnetosphere we shall briefly turn to stability.

3. Stability

For a comprehensive stability discussion we have to refer to the corresponding literature (see, e.g., the contributions in Schindler, 1968). Here we shall deal with wall stabilization only, which seems of interest for the present discussion.

One general remark however seems appropriate. It can be shown that the only unstable mode which is possible under the present assumption is the tearing mode (Furth, 1963). All other plasma instabilities are excluded by Equation (2b) and by the assumption $\partial/\partial y = 0$ and $\varepsilon \rightarrow 0$. Many of the instabilities which are thereby excluded can be treated separately, for instance if they appear on the scale of the Debye length, which is considerably smaller than any other length involved.

As already mentioned, the stability properties can be described in terms of the eigen value problem in Equation (13). If there is a negative eigen value the configuration is unstable, if not it is stable. Strictly speaking this criterion in this simple form applies only to one-dimensional equilibria. In the framework of the present asymptotic theory it is also valid locally for sufficiently small ε .

As shown by Schindler and Soop (1968) there is always a negative eigen value for a large variety of magnetic field profiles if the walls are sufficiently far away from the axis. The eigen values increase when the walls are moved in from infinity and for a certain wall position, $a=w$, the lowest eigen value vanishes. The wall position w

corresponds to marginal stability. For a given magnetic field profile, w follows from

$$\frac{1}{B_x(x_1, w) B'_x(x_1, w)} + \int_0^w \frac{B''_x}{B_x B_x'^2} dz = 0. \quad (24)$$

In the often used case where the magnetic field varies as $\tanh(z/L)$, w is fairly small, $w \approx 1.2 L$. It seems of interest to investigate under what conditions w is larger (see Section 4).

Clearly, a configuration will be relatively easily stabilized (i.e. with relatively large values of w) if the lowest eigen value is already close to zero for $a \rightarrow \infty$. This case can be realized by choosing the 'Schrödinger potential' $-J'$ in Equation (13) in such a way that it assumes positive values in a sufficiently pronounced way. (For $B_x \sim \tanh(z/L)$ the function $-J'$ is negative everywhere.) A model profile which has the desired feature for instance is the following:

$$\frac{B}{B_\infty} = \begin{cases} b \frac{z}{S}, & 0 \leq \frac{z}{S} \leq 1 \\ bl \tanh \frac{z}{L} + (1 - b - bl) \tanh^3 \frac{z}{L} + b, & \frac{z}{S} > 1, \end{cases} \quad (25)$$

where

$$b = \frac{B(S)}{B_\infty}, \quad l = \frac{L}{S}.$$

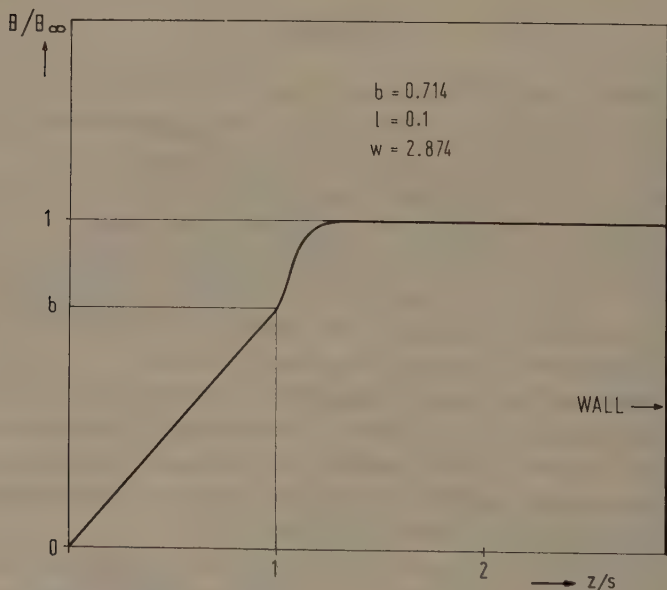


Fig. 1. Model magnetic field profile demonstrating the possibility of achieving marginal stability with the wall being located at a considerable distance from the region of peak field variation. The model is that of Equation (25).

A linearly rising part is followed by a transition to a homogeneous field. Clearly, there is a region where $-J' = B''/B$ is positive. An example ($b=0.714$, $l=0.1$) is given in Figure 1. For that case the marginal wall position is $w=2.87S$, fairly far away from the region of the main field variation. An approximate expression which can be used for sufficiently large values of w is

$$w = 1 + 1/b^2; \quad (26)$$

by reducing b one can make w arbitrarily large.

The geometry of the tearing mode, for instance, can be obtained from the lowest eigenfunction of Equation (13). The dominant feature is the appearance of current concentrations leading to a loop structure of the magnetic field. In the presence of a normal component ($B_z \neq 0$) the loops will be pushed towards the earth (Soop and Schindler, 1972).

4. Discussion

We now apply our results to the magnetosphere and compare the findings with observations.

We first note that our asymptotic theory allows for a remarkably large class of smooth solutions. Somewhat loosely speaking, we can choose freely both the electric current $j(A)$, or equivalently the pressure $p(A)$, and the shape of the boundary. Clearly, this is enough freedom for equilibria of the type realized in the magnetospheric tail to exist. Next we consider Equation (23). It is interesting that it contains an expression which also appears in the condition for marginal stability in Equation (24). Using Equation (24) we can write Equation (23) in the form

$$-B_z(x_1, 0) B'_x(x_1, 0) \int_w^a \frac{dz}{B^2} = \frac{da}{dx}. \quad (27)$$

Assuming that $B_z(0, x_1) > 0$ (Mihalov *et al.*, 1968; Behannon, 1970; Schindler and Ness, 1972) and $B'_x(0, x_1) < 0$ (according to Equation (18), but also suggested by the observations, e.g., Speiser and Ness, 1967) we can discuss four different cases, according to the signs of the integral $I = \int_w^a dz/B^2$ and of da/dx . These signs have immediate physical interpretations: $I > 0$ means that $a > w$ and therefore the configuration is unstable; $I < 0$ means stability. For $da/dx > 0$ the tail diverges (looking from the earth) and for $da/dx < 0$ the tail converges. Equation (27) tells us that only two out of these four combinations can exist: The tail can be either stable and converging or unstable and diverging.

Behannon (1970) has presented evidence for a diverging tail. He concludes that on the average $B_z < 0$ sufficiently close to the magnetopause, and also interprets direct observations of the magnetopause in that sense. Schindler and Ness (1972) have shown that observation suggests an unstable tail, based on the fact that both signs of B_z appear for sufficiently small values of $|\mathbf{B}|$. Similar observations have been reported by Mihalov *et al.* (1968).

We therefore conclude that the tail seems to be in the state of one of the two possibilities admitted by the present theory: Present theory favors a tail which is diverging and unstable, at least for radial distances not exceeding $\sim 70 R_E$. Figure 2 gives a corresponding artistic view. An attempt was made to take into account the fact that the unstable loops are pushed towards the earth.

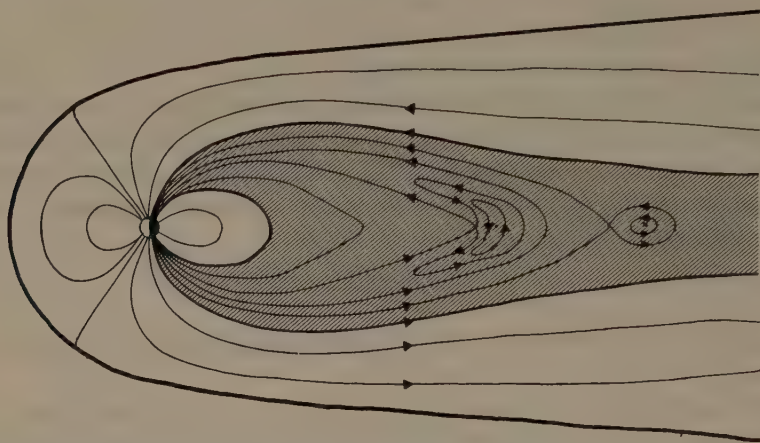


Fig. 2. Schematic drawing of the magnetospheric tail as it appears from present theory. The tail is unstable and diverging. It is indicated that the unstable loops are pushed towards the earth. The shaded area is the plasma sheet.

Using Equation (27) we can estimate how far away the tail boundary is located from its marginal position w . Choosing as typical values $B_z(z=0) \sim 1 \gamma$ (Behannon, 1970; Schindler and Ness, 1972), $B_x(z \rightarrow a)$ as 15γ , $da/dx \sim 3R_E/40R_E = 0.075$ (Behannon, 1970) and $B'_x(z=0)$ between $5 \gamma/R_E$ and $50 \gamma/R_E$ we find $a=w$ ranging from 3 to $0.3 R_E$. This means that the tail, although unstable, is not very far away from its marginal state. The magnetic field profile must therefore be of the type discussed in Section 3, for instance, similar to that of Figure 1. Specifically, a thin depression region would contradict our theory. On the other hand the observed width of the depression region, $\sim 12 R_E$, seems to fit in quite well. A more precise check would require detailed knowledge of the magnetic field profile, which does not seem to be available. In particular, the width of a current sheet cannot be determined safely from one satellite.

In summary, we have described a simple self-consistent model of the magnetospheric tail. A number of consequences have been discussed and they seem to fit the observations related to an average quiet time magnetosphere reasonably well.

In particular, the model allows for a sufficiently large class of slowly x -dependent equilibria. By prescribing only typical values of B_z and B'_x for $z=0$ together with the boundary variation da/dx , the theory predicts that the tail is unstable. Furthermore, we find that the tail must be close to its marginal state which in turn allows us to predict that the tail diameter cannot be larger than a few times the width of the plasma sheet (if it coincides with the magnetic depression region). These results seem to be in

fair agreement with observations. Although future experimental and theoretical studies will more clearly show the limitations of the present simple model, it nevertheless seems to describe reasonably well some essential features of the geomagnetic tail.

References

- Alpers, W.: 1969, *Astrophys. Space Sci.* **5**, 425.
- Bame, S. J.: 1968, in B. M. McCormac (ed.), *Earth's Particles and Fields*, Reinhold Book Corporation, New York, p. 373.
- Behannon, K. W.: 1970, *J. Geophys. Res.* **75**, 743.
- Cole, G. and Schindler, K.: 1972, submitted to *Cosmic Electrodyn.*
- Frank, L. A.: 1970, in B. M. McCormac (ed.), *Particles and Fields in the Magnetosphere*, D. Reidel Publishing Company, Dordrecht, Holland, p. 319.
- Furth, H. P.: 1963, *Nucl. Fusion Suppl.* **Pt. 1**, 169.
- Hones, E. W.: 1968, in B. M. McCormac (ed.), *Earth's Particles and Fields*, Reinhold Book Corporation, New York, p. 403.
- Lackner, K.: 1970, *J. Geophys. Res.* **75**, 3180.
- Mihalov, J. D., Colburn, D. S., Currie, R. G., and Sonett, C. P.: 1968, *J. Geophys. Res.* **73**, 943.
- Roederer, J. G.: 1969, *Rev. Geophys.* **7**, 77.
- Schindler, K. (ed.): 1968, in *The Stability of Plane Plasmas*, European Space Research Organization, Paris, ESRO SP-36.
- Schindler, K. and Ness, N. F.: 1972, *J. Geophys. Res.* **77**, 91.
- Schindler, K. and Soop, M.: 1968, *Phys. Fluids* **11**, 1192.
- Sestero, A.: 1964, *Phys. Fluids* **7**, 44.
- Soop, M. and Schindler, K.: 1972, submitted to *Cosmic Electrodyn.*
- Speiser, T. W. and Ness, N. F.: 1967, *J. Geophys. Res.* **72**, 131.
- Toichi, T. 1971, private communication.
- Williams, D. J. and Mead, G. D.: 1965, *J. Geophys. Res.* **70**, 3017.

THEORY OF NEUTRAL SHEETS

J. W. DUNGEY

Physics Department, Imperial College, London, England

Abstract. The behavior of neutral sheets is important, particularly for understanding substorms. The theory is now developing into an extensive subject as the sheet is decomposed into regions in which different approximations are valid and where different instabilities must be considered. The first breakdown of the sheet is into regions with normal magnetic component B_z in different ranges. The case of negligible B_z has been extensively studied by Cowley (1971a, b). The geometry of the cross section is important and there is a further breakdown into regions with differing behavior. The reconnection is found to be concentrated at the dusk end and effects arise which drive field aligned currents.

Possible electrostatic instabilities are outlined. Our outlook has evolved from instabilities in the y direction, through those in the x direction until now interest is concentrated on those in the z direction.

1. Importance of Neutral Sheets

From the viewpoint of basic plasma physics neutral sheets are interesting because of the inapplicability of standard theoretical treatments. Sheets are very thin, how thin is an important part of the problem, but it is expected that the thickness is comparable to characteristic lengths of the plasma, whose smallness is the basis of much plasma theory. Of great current interest is the neutral sheet in the tail and its role in substorms. Understanding of neutral sheets is also essential to understanding the magnetopause, which is more complicated than the tail neutral sheet. While the tail sheet is symmetrical, the magnetopause has sheath plasma on the outside but not on the inside, which also differs in being connected to the ionosphere. Kelvin-Helmholtz instability is another complication of the magnetopause. Neutral sheets are quite common in the solar wind and these provide useful specimens for observation.

Reconnection at neutral sheets is important in changing the topology of the field, as illustrated in the magnetosphere by the formation of the tail. The tail may be taken to contain open field lines from the polar caps, the northern and southern halves each being bounded by a surface. In the simplest model these surfaces touch at a closed curve ringing the earth and the net rate of reconnection or of interchange between open and closed magnetic flux is $\oint \mathbf{E} \cdot d\mathbf{s}$ around this curve. Typically \mathbf{E} is from dawn to dusk, and dayside reconnection makes the tail while nightside reconnection reduces the tail. The crucial question is the value of \mathbf{E} . This same electric field accelerates particles and its importance as an acceleration mechanism depends crucially on its strength. Apart from acceleration the breakdown of the adiabatic approximation for particle trajectories in the neutral sheet is likely to relate to auroral precipitation.

2. Simple Models

Axes corresponding to solar magnetospheric coordinates for the tail neutral sheet

will be used, but it will be assumed that the axes relate exactly to the sheet as follows: the x axis points in the direction of the field on the northern side of the sheet, the y axis in the direction of the sheet current, and the z axis is normal to the sheet. The indispensable component of the field is $B_x(z)$, which is quite well known from observation. B_x is relatively uniform away from the sheet with opposite signs on opposite sides. The observations show the reversal of direction in a very thin sheet, embedded in a much thicker region of a relatively weak field with fluctuating magnitude, which is almost certainly the plasma sheet. For theoretical purposes, however, B_x is taken to vary smoothly between the two regions of uniformity. The first step is to note the

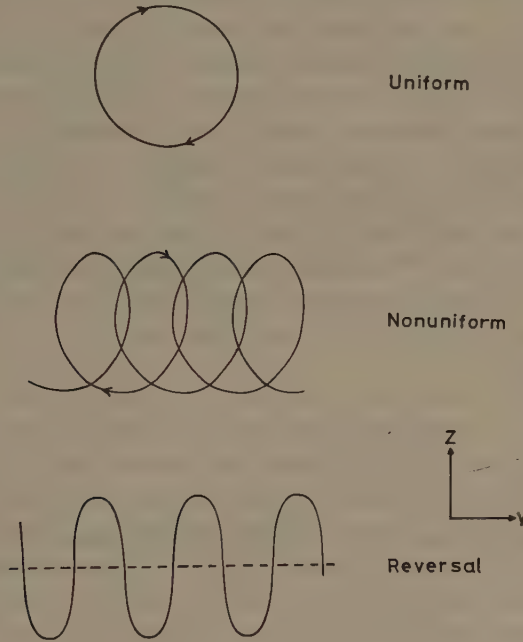


Fig. 1. Particle trajectories.

form of particle trajectories when B_x is the only nonzero component, i.e., B_y , B_z , and $E = 0$, as shown in Figure 1. It is important that particles crossing the reversal plane $z=0$ snake along it with a preferential direction depending on the sign of the charge on the particle, as shown in Figure 1. This direction matches the direction of the current as given by $\text{curl } \mathbf{B}$.

Consider the equations of motion now including $E_z(z)$

$$m\dot{y} = q\dot{z}B_x \quad (1)$$

$$m\ddot{z} = q(E_z - \dot{y}B_x). \quad (2)$$

These equations have integrals of energy and canonical y -momentum

$$\frac{1}{2}m(\dot{y}^2 + \dot{z}^2) + q\phi = H \quad (3)$$

and

$$m\dot{y} + qA = P \quad (4)$$

where

$$\phi = - \int E_z dz$$

and

$$A = - \int B_x dz.$$

Using Equation (4) to obtain \dot{y} in terms of z and noting that A increases linearly in the regions of uniformity, Equation (3) shows that the z motion is oscillatory. If the trajectory does not cross $z=0$, the y motion shows the familiar drifts, while, if it does cross $z=0$, the drift is of the sort shown in Figure 1, though the modification by E_z can be important. Now we can consider the self-consistency problem, which is formulated by requiring distribution functions for electrons and protons satisfying Liouville's theorem and with corresponding charge and current densities agreeing with the field model through Maxwell's equations. Now Liouville's theorem is satisfied by any function of the constants of the motion or in the present case $f(H, P, v_x)$. Given any such functions, the moments of f over velocity space give charge density $\rho(\phi, A)$ and current density $j_y(\phi, A)$. One then obtains the corresponding field model from

$$d^2\phi/dz^2 = -4\pi\rho \quad (5)$$

and

$$\frac{d^2A}{dz^2} = 4\pi j_y. \quad (6)$$

Thus self-consistent models exist, including sensible ones, and the embarrassment

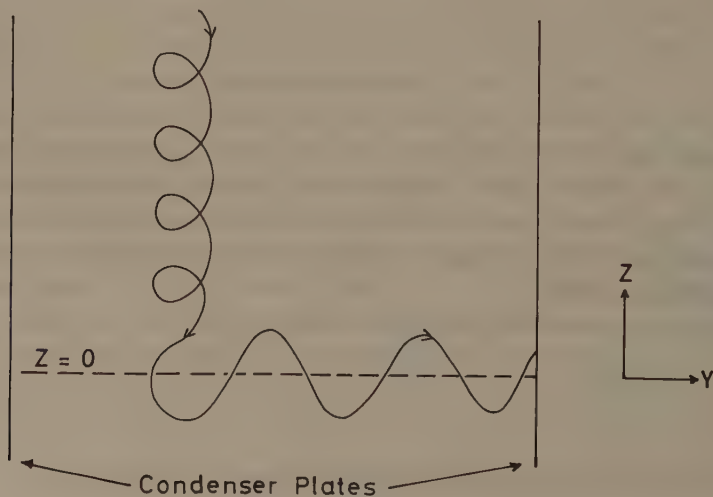


Fig. 2. The Alfvén model.

is the arbitrariness of the distribution functions. It should be noted here that the integrals in Equations (3) and (4) still both exist, if ϕ and A vary with x . Schindler and Soop (1968) have used them to give an elegant treatment of the tearing instability.

If $E_y \neq 0$ the integral in Equation (4) no longer exists (unless a time dependent term is included), but consider the trajectories for small positive E_y as shown in Figure 2. Outside the sheet the electric drift now takes all the particles into the sheet, so that the distribution function in the sheet is related to that outside and is no longer arbitrary. In the sheet the trajectories are qualitatively similar to those in Figure 1, but the motion shown in Figure 1 is already in such a direction that all particles gain energy from the electric field, and the change in energy can be obtained from the electrostatic potential. Because of this gain in energy, further modification and complication of the model is necessary to make it realistic. Otherwise all particles would stay in the sheet and gain energy indefinitely. One realistic modification, first discussed by Alfvén (1968), simply makes the model finite in the y direction, as of course the tail really is, and this will be the subject of Section 3. Another model, first discussed by Speiser (1965), has a small component B_z , in which case the finite geometry is not required for realism. This is discussed by Eastwood (1971).

3. Cowley's Modification of Alfvén's Model

The tremendous virtue of Alfvén's model is that it gives a value for the electric potential across the tail, as will be explained shortly. However, the model is based on an approximation, which should be discussed. This is the neglect of the current due to particles from the magnetosheath at the sides of the tail entering the neutral sheet. The motion of such particles would be affected by E_y , but the current must depend on the number entering and in any case the important question is whether these particles can carry sufficient current with $E_y = 0$. This question has not been treated rigorously, but it is illuminating to ask why the northern and southern halves of the tail are not separated instead of being in contact at the neutral sheet as observed. Viewing this question aerodynamically it seems clear that the pressure of the magnetosheath on the sides opposite to the neutral sheet push the halves together and that the obstruction of the flow by the magnetosphere prevents an equal pressure building up between them. The magnetic field in the magnetosheath would also tend to obstruct any pressure buildup unless it were almost parallel to the neutral sheet. Now the contribution to the current of a subset of particles, such as those of magnetosheath origin, is related to their pressure by $\mathbf{j} \wedge \mathbf{B} = \nabla p$ assuming equilibrium. Consequently, we conclude that the magnetosheath particles are unable to carry the total current of the neutral sheet. It is then sensible to neglect the magnetosheath particles completely and eventually, but not here, to study their entry into the neutral sheet when an adequate field model exists. Following Alfvén then consider the tail to be bounded by 'condenser plates' shown in Figure 2, all the protons ending up on the dusk plate and the electrons on the dawn plate.

Far enough from the neutral sheet it may be assumed that the fields given by B_x and E_y are uniform and all particles drift towards the neutral sheet with speed $c E_y/B_x$. If the potential difference between the plates is Φ , the number of protons or electrons flowing in is $2nc\Phi/B_x$ per unit length of tail, counting both sides. This result is still true even if E_y is nonuniform, provided n and B_x are uniform. Now, since all protons and electrons go to their proper condenser plates, the current per unit length of tail is

$$I = 2nec\Phi/B_x. \quad (7)$$

Now, since the field changes by $2 B_x$ at the neutral sheet, self-consistency requires

$$I = cB_x/2\pi \quad (8)$$

and Equations (7) and (8) give Alfvén's simple value for Φ

$$\Phi = B_x^2/4\pi ne. \quad (9)$$

It is of course sensible that $e\Phi$ is the magnetic energy per proton-electron pair. For $B_x=15 \gamma$, $\Phi \sim n^{-1}$ kV and with the low values of n in the tail, perhaps 10^{-1} cm^{-3} or even less, this voltage is important.

Taking Alfvén's model with uniform E_y and $E_z=0$, Cowley (1971a) pointed out that there must be a large positive charge density in the neutral sheet. The reason is that, whereas the protons and electrons drift in at the same speed until they reach the neutral sheet, when they are accelerated along the sheet the protons are much slower, and so spend more time in the sheet. Cowley therefore considered a modification including E_z , having the same sign as z , corresponding to positive charge, and becoming small far from the sheet. Adding the potential of such an E_z to that of a uniform E_y gives equipotentials like those shown in Figure 3. It is immediately seen that all particles now drift towards the dusk side before entering the sheet and enter

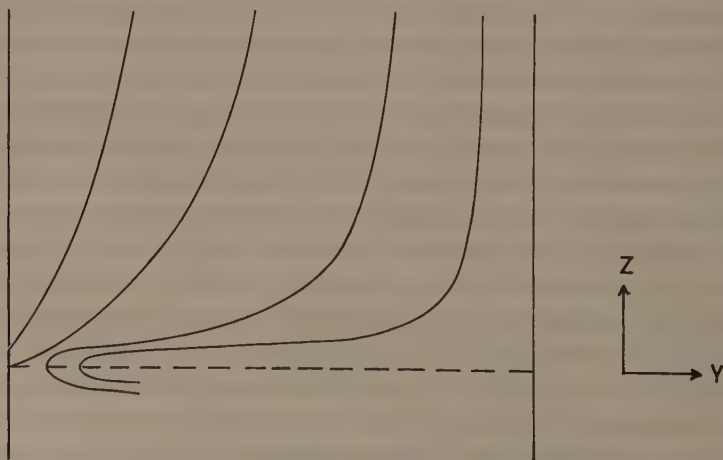


Fig. 3. Equipotentials in the Cowley model.

the sheet nearer the dusk end than in Alfvén's model. Qualitatively this can cure the space charge trouble because the electrons now have more of the sheet to traverse and the protons less. It also implies that the potential change along the sheet is concentrated near the dusk end or that E_y is strong only at the dusk end. Then reconnection is rapid only at the dusk end and should occur mainly on field lines connecting to the auroral oval over a limited range of local time in the evening. This suggests a natural explanation for the westward surge (Akasofu, 1964).

Cowley (1971b) has given an extensive discussion of the conservation of energy and momentum in the plasma flow. The most obvious point is that, since the protons and electrons are ejected with the same energy, the protons have more momentum, and consequently that the ejection of the protons on the dusk side exerts a reaction pushing the tail towards the dawn side. This reaction is taken up by the magnetic field however. The magnetic field is weakened over a width characterizing the neutral sheet and the reduction in magnetic pressure at the dusk end compensates for the proton momentum. From his quantitative investigation Cowley obtains an estimate of the sheet thickness as a function of the local potential ϕ , and at the dusk end it is of the order of the 'proton plasma wavelength' $(m_p c^2 / 4\pi n e^2)^{1/2}$. Taking the dusk end as zero potential the thickness is proportional to $(\Phi - \phi)^{1/2}$ as long as $\Phi - \phi \gg (m_e / m_p) \Phi$. It is possible to give a simple description of the electron trajectories. The electrons move almost adiabatically ($\mathbf{E} + \mathbf{v} \wedge \mathbf{B} = 0$) until they are within a very short distance of the central plane $z = 0$. Once they cross this plane they are rapidly accelerated along the sheet and the amplitude of their oscillations in the z direction is small. The current carried by the accelerated electrons is confined in an inner sheet, which is very thin; the magnitude of this current varies with ϕ , but it is at least a significant fraction of the whole except very near the dusk end. The proton trajectories are more complicated. They cease to move adiabatically much sooner than the electrons, and, when they oscillate, the amplitude in z is larger. Furthermore it is not clear how many protons will oscillate across the central plane and how many will be reflected by E_z before reaching this plane and oscillate on one side of it. Outside the region of proton oscillation, however, a simple formulation is possible.

Remembering that the adiabatic approximation is good for electrons except in a very thin sheet, the electron current outside this thin sheet is simply related to the potential ϕ . Considering a point P outside the sheet and at potential ϕ , electrons entering at potentials less than ϕ pass between P and the plane $z = 0$, and electrons entering at potentials greater than ϕ do not. Thus, if I_t is the total sheet current per unit length of tail, the electron current passing between P and the plane $z = 0$ is $(\phi/\Phi)I_t$. In the region where the adiabatic approximation also holds for protons, the equivalent result for proton current is $(1 - \phi/\Phi)I_t$ and of course negligible current then flows outside the point P. A similar but exact result can be obtained by using the conservation of energy and then the kinetic energy at P is involved. Clearly the kinetic energy of electrons is much smaller than that of protons outside the neutral sheet, and the kinetic energy in the inflow may be neglected even for protons. Then a proton which moves through P must have entered at potential $\phi + m_p v_p^2 / 2e$ where

v_p is its velocity at P. If all protons entering at higher potentials pass between P and the plane $z=0$ and those entering at lower potentials do not, the previous argument can be used giving the current between P and the plane $z=0$ as $(1 - m_p v_p^2 / 2e\Phi) I_t$. Then, using $4\pi I = c \int_0^P \partial B_x / \partial z \, dz$, the magnetic field at P is

$$B = (1 - m_p v_p^2 / 2e\Phi) B_0. \quad (10)$$

The assumption on which this result is based is essentially that the proton trajectories do not cross, and hence it does not extend into the region of proton oscillation. It shows how the field is reduced in the region where the protons begin to speed up and could be used to formulate the flow problem up to the region of proton oscillation, though this region needs to be understood sufficiently to provide boundary conditions. The variation of the density in the region where the adiabatic approximation holds for electrons is simple. The equation $\text{curl}(\mathbf{v}_e \wedge \mathbf{B}) = 0$ can be written $\text{div}(\mathbf{B} \mathbf{v}_e) = 0$, showing that $n_e \propto B$. The plasma approximation is certainly valid and so $\text{div}(\mathbf{B} \mathbf{v}_p) = 0$ and using Equation (10)

$$\nabla \cdot [(1 - m_p v_p^2 / 2e\Phi) \mathbf{v}_p] = 0. \quad (11)$$

It is also easily shown that $\mathbf{v}_p \cdot \nabla(B^{-1} \text{curl } \mathbf{v}_p) = 0$ and then, if the inflow is uniform, $\text{curl } \mathbf{v}_p = 0$. Thus the flow is described by simple equations and the difficulties lie in the neutral sheet. Most of the sheet, however, is probably relatively simple with the electrons carrying the current, while the remaining problem is at the dusk end.

4. Instabilities

Because of the release of magnetic energy in neutral sheets, it is natural to expect instabilities, particularly those which contribute to anomalous resistivity, which would enhance the energy dissipation. The available observations of noise are inadequate, but, such as they are, indicate remarkable quietness. Russell *et al.* (1971) found noise in the period range 1 to 15 s, which is intense only during substorms. In the frequency range 10 to 100 Hz Brody (1970) detected infrequent bursts of noise with amplitudes of $\sim 0.3 \gamma$. Unfortunately electrostatic wave detectors have not passed through the neutral sheet in the tail, but observations on neutral sheets in the solar wind and the magnetosheath are interesting. Scarf (1971), observing the VLF electric field, found cases of both very noisy and very quiet neutral sheets and discovered that the proportion of noisy ones is much higher in the magnetosheath than in the solar wind. It seems plausible that passage through the bow shock can make a previously quiet neutral sheet unstable. The indications are then that neutral sheets can be quiet or unstable, and clearly determination of the stability conditions is an important part of the theoretical problem. The study of quiet models (as described earlier in this paper) is therefore useful for providing actual models when they are stable and is a necessary preliminary for investigating the stability conditions. When discussing the stability of these models, it must be remembered that the geometry is important. Knowledge of instabilities in uniform plasmas is used first as a guide, but,

when the condition for instability is satisfied only in a thin sheet, stability of the whole model must be investigated.

The instability, which comes first to mind as associated with high current densities, is that due to double streaming between electrons and protons. The Cowley model, however, is stable on the double streaming criterion, at least superficially. For instance, over most of the central plane where the electrons carry the current, the electrons are spread over the whole energy range and their distribution is flat down to zero velocity. A more likely cause of instability is that for electrons in this region the energy spread in the motion in the y direction is much larger than the energy in the other two directions; however, on the basis of theory on uniform plasmas this is more likely to lead to electromagnetic instability.

The Speiser trajectories lead to a strange distribution function, which looks unstable. As in Eastwood (1971) let us work in the frame 'moving with the field', so that E_y vanishes and, if E_z is also ignored, the particle energy is constant. Assuming the energy spread of the incoming particles is small compared to the energy associated with the motion of the frame, the velocity distribution is then confined to a thin spherical shell, but Speiser (1968) found that v_z oscillates with small amplitude and v_y is always positive for electrons and negative for protons. Consequently the distribution for either kind of particle is confined in the v_x, v_y plane to a thin semicircular strip, while v_z is also restricted to a range small compared to the radius of the semicircle. Such a distribution is unstable with respect to the double streaming between electrons and protons, but looks even more unstable to the similar electrostatic instability in the x direction. This is seen by integrating the distribution over v_y giving a distribution in v_x with strong peaks at the edges of the semicircle. For a simplified version of the particle motion Tendys (1970) investigated the exchange of energy for electrostatic waves in any direction in the x - y plane. He considered just the semicircular motion described above and studied the integral involved in the expression for the first order change in speed of a particle due to a plane wave, but the qualitative behavior is likely to be of more general applicability. He uses the stationary phase approximation for his integrals and this is usually good, if the typical rate of change of phase is large or, usually, for short enough wavelengths. The condition of stationary phase is simply a generalization of the condition that is usually called resonance between the particle and the wave. An interesting point is that the phase variation of the perturbation f_1 in the distribution function is similar to that in the past history integral for the trajectory, if both are expressed in terms of the angle defining the direction of the velocity. Then, if the stationary phase approximation is good for the trajectory integral, it is also good when integrating f_1 over velocity, as required when calculating the charge or current density. When the stationary phase approximation is valid for two of the integrations, the mathematics is of course greatly simplified, though there may be more than one point of stationary phase. The physical implication of validity of the approximation is that the disturbance f_1 is dominated by the resonant part of the interaction. The consequent validity of the approximation in the velocity integral implies that, when resonance dominates, it is the particles which

have resonated recently that dominate the charge distribution, effects due to earlier resonance being negligible as a result of phase mixing. It appears that this is generally reasonable when the wavelength is small compared to the characteristic scale of a particle trajectory. It is, however, well known that this is not valid in a uniform field, and clearly more care is needed if the undisturbed trajectory is too regular. When this method is applied to a Speiser's distribution function a strong exchange of energy is found, and this can give energy from the particles to the wave because the distribution function is 'hollow'. Thus electrostatic waves in the x - y plane are likely to gain energy in the neutral sheet for any model with Speiser's type of trajectory, but this is not a sufficient condition for instability, because, as already remarked, the geometry must be taken into account. The effect of the geometry will now be outlined.

The importance of the thinness of the sheet is illustrated by considering possible waves radiating from the sides of the sheet. Fourier transformation may be used in the x and y directions, so consider waves described by angular frequency ω , and wave number components k_x and k_y , all of which are independent of z . With a correct model the waves would be described by ordinary differential equations with respect to z , but consider here the limiting behavior outside the neutral sheet, where the waves are described by the dispersion equation for the uniform plasma, which is moreover cold to an adequate approximation. It is important to know whether the waves propagate or evanesce. The simplest case has $k_x = 0$, as in the simple double stream instability, and then the wave normals are perpendicular to the field outside the sheet (neglecting B_z). Further simplifying to illustrate the nature of the problem, consider low frequencies for which the hydromagnetic approximation is valid and the only mode propagating normal to the field is the fast mode. Its dispersion equation gives

$$k_z^2 = \omega^2/A^2 - k_y^2, \quad (12)$$

where A is the phase speed for the fast mode and this is the Alfvén speed to a good approximation in the low β plasma in the tail. Then the waves propagate (i.e., k_z is real), if $\omega > A k_y$, which may be regarded as a Cerenkov condition and is satisfied as long as the phase velocity in the y direction exceeds A . The z component of the Poynting flux, giving the energy flux carried away by the waves, is found to be $4\pi\omega c^2 E_y^2 / k_z A_y^2$ and we can only guess that the electric amplitude E_y for the radiated wave is comparable to the amplitude E_y in the sheet. Consequently energy is radiated at a high rate as soon as the Cerenkov condition is satisfied and for high phase velocities in the y direction, for which Equation (12) gives $k_z \sim \omega/A$, the Poynting flux is $\sim 4\pi e^2 E_y^2 / A$, which is still large. It may well be that the rate of radiation of energy exceeds the rate at which particles energize the wave in the thin sheet, in which case the instability will be quenched for that part of the spectrum which radiates. In the present illustration waves would be restricted to phase velocities in the y direction less than A and quasi-linear diffusion would affect particles only when their velocities satisfied the same restriction. This demonstrates the need to consider the geometry in limiting the spectrum of any noise arising from instability. The more general problem allowing

for any direction of propagation and without restriction to low frequencies is much more complicated even with the cold plasma dispersion equation. The most general account has been given by Gj  en (1971).

The evolution of ideas about instabilities in the neutral sheet progressed, as has been seen, from electrostatic waves in the y direction through those in the x direction. Now greater attention is being paid to electrostatic waves in the z direction although little work has been done on these yet. The problem arises naturally when one considers the self-consistent E_z and also when the problem is viewed as the meeting of the polar winds from the north and south. Even when B_z is so large that the first invariant is valid even for protons, the meeting of the polar winds is expected to set up a pair of shocks, probably involving electrostatic turbulence. Although no work has been done, it now seems that electrostatic noise in the z direction should be considered in every range of B_z . This may be amenable to a computational approach. A very crude consideration of the system with incoming supersonic beams and outgoing thermalized plasma suggests that the growing waves will move towards the neutral sheet and that waves moving outwards will decay. This fits with the quiet observed away from the sheet. In this case a computational experiment should not be sensitive to the artificial boundaries which would have to be imposed and this is crucial for success with computations.

Although the plasma sheet is observed to be quiet, its stability should be considered. Hones *et al.* (1971) found evidence for anisotropy of the electron velocity distribution with the energy of parallel motion exceeding that for perpendicular motion. Such an anisotropy indeed must result from the shortening of field lines as well as from Speiser's mechanism. The anisotropy can cause instability of more than one mode, the simplest being the firehose instability. Schindler and Ness (1972) have found on some occasions rather irregular variations of the magnetic field near the neutral sheet. This may be due to an instability, which is essentially the tearing mode as they suggest, but perhaps also the firehose instability may occasionally occur.

Acknowledgments

This paper owes much to discussions with Mr S. Cowley and Dr T. Holzer. This work was sponsored in part by the Air Force Cambridge Research Laboratories under Contract No. F61052-70-C-0009 through the European Office of Aerospace Research, OAR.

References

- Akasofu, S.-I.: 1964, *Planetary Space Sci.* **12**, 273.
- Alfv  n, H.: 1968, *J. Geophys. Res.* **73**, 4379.
- Brody, K. I.: 1970, Ph.D. Thesis, University of California, Los Angeles.
- Cowley, S. W. H.: 1971a, *Cosmic Electrodyn.* **2**, 90.
- Cowley, S. W. H.: 1971b, *Cosmic Electrodyn.* in press.
- Eastwood, J. W.: 1971, *Planetary Space Sci.*, in press.
- Gj  en, E.: 1971, *Planetary Space Sci.* **19**, 635.
- Hones, E. W. Jr., Asbridge, J. R., Bame, S. J., and Singer, S.: 1971, *J. Geophys. Res.* **76**, 63.

- Russell, C. T., McPherron, R. L., and Coleman Jr., P. J.: 1971, *J. Geophys. Res.* **76**, 1823.
- Scarf, F. L.: 1971, private communication.
- Schindler, K. and Ness, N.: 1972, *J. Geophys. Res.* **77**, 91.
- Schindler, K. and Soop, M.: 1968, *Phys. Fluids* **11**, 1192.
- Speiser, T. W.: 1965, *J. Geophys. Res.* **70**, 4219.
- Speiser, T. W.: 1968, *J. Geophys. Res.* **73**, 1112.
- Tendys, J.: 1970, *Cosmic Electrodyn.* **1**, 328.

PART IV

ELECTRIC FIELDS AND PLASMA CONVECTION

CRITICAL REVIEW OF ELECTRIC FIELD MEASUREMENTS

ULF V. FAHLESON

Division of Plasma Physics, Royal Institute of Technology, Stockholm, Sweden

1. Introduction

Current methods and results of electric field measurements are summarized. An excellent and extensive review covering both experiments and results has been given by Haerendel (1972). The interest in electric fields and electric field measurements has increased enormously during the last year. Therefore it has been necessary to limit this review to cover mainly the new developments since Haerendel's review which was written in 1970. Only dc measurements will be discussed.

2. Methods of Measurement

A. DIRECT MEASUREMENTS

Direct electric field measurements are generally done by the double-probe method by determining the potential difference between two or several identical electrodes sufficiently separated to be undisturbed by each other or the vehicle. The theory of such measurements has been verified in all essential details.

Rocket borne double probe measurements have been reported by four different groups: The Berkeley group (Mozer and Fahleson, 1970; Kelley *et al.*, 1971a, b; Mozer *et al.*, 1971), the Goddard group (Maynard *et al.*, 1970), the New Hampshire group (Potter and Cahill, 1969; Potter, 1970, 1971) and the Stockholm-ESTEC group (Fahleson *et al.*, 1971). Double probe experiments have also been flown on polar satellites OV1-10 and OGO 6 (Maynard and Heppner, 1970), INJUN 5 (Cauffman and Gurnett, 1971), and OV1-17 (Kelley and Mozer, 1970).

Some of these experiments have used spherical probes, others have had cylindrical booms as current collectors. Most experimenters have used probes at floating potential, but the use of probes biased near plasma potential has resulted in improved data quality.

On rocket borne experiments, the choice between spherical probes and long cylindrical booms may be largely a question of technology. If carefully done, both methods can give good measurements.

A complete electric field measurement has to include determination of all three components of the electric field vector, at least in the auroral zone it can *not a priori* be assumed that one of the components is zero. For mechanical reasons, the use of long cylindrical booms implies a virtually non-spinning payload. The necessity of equal orientation of the probes in a pair means that in this case 6 booms are needed for a vector measurement. If spherical probes are used instead, 4 probes will suffice. Further, if the probe carrying booms are sufficiently short and rigid to allow a con-

siderable payload spin and coning, all three electric field components can be determined from ac measurements, whereby dc voltage errors due to work function offsets at the probes can be largely ignored. Even if only 2 probes are used such a spinning and *coning* system can still give accurate time averages of all three field components. The accuracy of the measurement along the spin axis depends upon the coning angle, period of precession and attitude resolution, typically it is about $\pm 5 \text{ mV m}^{-1}$. The uncertainty of this component largely determines the precision with which the magnetic-field aligned electric field component can be measured.

For all types of double probe experiments a careful attitude determination is absolutely necessary. The *complete* attitude has to be determined, meaning that, (except in very special cases) two *independent* attitude sensors have to be used, e.g., an aspect magnetometer and a moon sensor.

It is often hard to judge the quality of published electric field results since even the most fundamental technical information is sometimes omitted in the reports. Flights have been reported without even specifying whether 2 or 6 probes have been used. A graph of a strongly variable electric field *magnitude* together with a statement like 'the field direction stayed approximately constant' does sometimes mean that one or several attitude elements have not been determined.

Measurements from *low flying satellites* are much more difficult because of the high $\mathbf{v} \times \mathbf{B}$ field that has to be subtracted. For absolute measurements the requirement of probe symmetry becomes severe and, if cylindrical probes are used, their alignment and straightness is critical. However, extremely valuable results about electric field variations (Maynard and Heppner, 1970) and high latitude electric fields (Cauffman and Gurnett, 1971) can be obtained also from rather imperfect experiments by in-flight calibration against the $\mathbf{v} \times \mathbf{B}$ field.

Due to the thin plasma, electric field measurements from *high flying satellites* (Fahleson, 1971) and space probes are extremely difficult. Long booms are necessary to get away from satellite induced potentials and photoelectrons. Due to the dominating photo emission and the weak electric field, requirements for equality of probe alignment and photoemissivity become extreme. Spherical probes of special material (vitrous carbon) on long booms seem to be necessary. *Very long* cylindrical booms on a *rapidly rotating* vehicle may be an alternative. No successful experiment of this type has yet been reported, but several are in progress. The requirements on a perfect experiment are extreme. However, a far simpler experiment may successfully measure *variations* of the field.

A large number of *balloon borne measurements* of ionospheric electric fields have been done by Mozer and his collaborators. Further details of the theory and methods of measurement are given by Atkinson *et al.* (1971) and Mozer (1971a, b). The technique is inexpensive and gives averages of the ionospheric field over distances of about 100 km. The measured fields generally show wide fluctuations but there are reasons to believe that the variations are real, reflecting the turbulent state of the ionospheric and magnetospheric plasma. Projected along the magnetic field to the equatorial plane (Mozer, 1970) the measurements are in reasonable agreement with

other measurements and give excellent insight into many features of magnetospheric convection and storm time behavior.

B. INDIRECT MEASUREMENTS

Barium cloud experiments have won a reputation as a reliable and convenient means of measuring ionospheric fields. The main drawback is their inability to measure at times other than twilight. Release altitudes have usually been between 150 and 300 km but other altitudes can be chosen. Experiments at 2000 km altitude within the plasmasphere were successful (Rieger *et al.*, 1970). A cloud released in the outer magnetosphere (Haerendel and Lüst, 1970), however, dispersed before it had reached its final velocity. Further contributions to the theory of Ba cloud motion and diffusion have been done by Giles and Martelli (1971) and Haerendel (1971). A new type of Ba releases involving the production of a very long, field aligned cloud by the explosion of a shaped charge seems to have been first studied by Giles and Martelli (1969) and is now being developed by Haerendel *et al.* (1971a) and Wescott and Murcray (1971).

The analysis of whistler propagation data seems to give reliable electric field information of convection electric fields both inside and outside the plasmasphere. The method suffers from the inability of measuring more than the azimuthal electric field component, but still gives very interesting results (Carpenter, 1970, 1971). There is some possibility to improve the method so that the radial electric field component can also be measured.

Measurements of natural particle fluxes have been used to deduce electric fields. At the geosynchronous orbit Freeman (1968) studied directional fluxes of low energy protons. The low plasma density, however, limits the usefulness of this method to special occasions when the particle densities are enhanced. By calculating particle trajectories using successive approximations for the electric field McIlwain (1971, 1972) has constructed a model of the electric field in the equatorial plane from energy spectra recorded on ATS-5. The field so deduced agrees reasonably with the results of more direct measurements. In the auroral zone differential measurements of low energy proton (Carlson, 1971) and plasma flow (Bering *et al.*, 1970) have been used to deduce electric fields in essential agreement with simultaneous double probe measurements (Mozer *et al.*, 1971).

A wake detection experiment is being developed and tested by Knott *et al.* (1971). The method measures the position of the payload wake which can be used to infer the electric field direction and, hopefully, after a number of calibration flights together with other electric field experiments, also the field strength. Wake effects, however, are extremely complicated depending upon a large number of plasma and vehicle parameters. Methods employing related techniques are studied by Rawer and Spenner (1970).

Accurate measurements of electron or proton energy spectra and pitch angle distributions can be used to draw conclusions about electric fields, especially the component along the magnetic field. The theory and technique of such experiments are outside the scope of this paper, but some results will be referred to below.

Methods based upon the motion of an emitted electron beam seem to offer a good alternative to double probe measurements in low density plasmas. A detector of this kind for ESRO's GEOS satellite is being built at the Max-Planck-Institut, Garching (Melnzer and Völk, 1970).

3. Results

A. LARGE SCALE MAGNETOSPHERIC FIELD

Barium cloud and balloon borne electric field measurements with subsequent projection along the magnetic field lines to the equatorial plane (Haerendel, 1970; Mozer, 1970) as well as whistler measurements (Carpenter, 1970, 1971) and studies of particle trajectories (McIlwain, 1971, 1972) give a large scale magnetospheric electric field indicating a general convection towards the sun except on the afternoon side where the flow seems to turn around approximately corotating with the earth. The field strength associated with this flow is typically 0.5 to 1 mV m^{-1} in the equatorial plane.

None of the satellite electric field experiments yet reported has sufficient accuracy to measure the electric field at latitudes below about 60° IN Lat. Above that latitude they all see a field of the order of 100 mV m^{-1} , above 80° the field is smaller again. The most extensive reports have been published about the INJUN 5 measurements at about 2000 km altitude (Cauffman, 1971; Cauffman and Gurnett, 1971; Frank and Gurnett, 1971). A general sunward convection is found at low latitudes, further north the convection is anti-sunward. The highest velocities are observed near and on both sides of the poleward trapping boundary of $>45 \text{ keV}$ electrons, where an abrupt change in direction takes place over a distance of 50 to a few hundred km. The velocities are higher on the dawnside than the dusk side and the zone of flow reversal agrees roughly with the auroral oval. Integration of the N-S electric field along a satellite pass around 06 LT gave a potential maximum of 40 kV above the auroral zone and at another instant near 03 LT it gave only 4 kV . Simultaneous particle observations may be explained in terms of parallel electric fields or electric double layers as discussed by Carlqvist and Boström (1970). During storms the velocities become higher and the zones move equatorward.

A marginally detectable electric field change of 15 mV m^{-1} was detected at the plasmapause.

Considerable electric fields are also present inside the plasmasphere (Carpenter, 1970, 1971). Drifts of whistler ducts show motions corresponding to up to 0.45 mV m^{-1} , and considerable density fluctuations are also observed (Park and Carpenter, 1970). Studies at balloon altitudes (Mozer, 1971b) have shown electric field variations also on field lines coming from the plasmasphere.

Over the polar caps the INJUN 5 observations show a field generally below the margin of detectability ($\approx 10 \text{ mV m}^{-1}$). Sometimes, however, the field is strong and indicates antisunward convection. Maynard and Heppner (1970), Wescott *et al.* (1970), and Heppner *et al.* (1970) find, from both satellite and Ba measurements, an electric field of about 30 mV m^{-1} directed approximately from dawn to dusk.

From an analysis of the Ba experiments and ground based magnetometers, Heppner

et al. (1971a, b) arrive at a model of field aligned currents to the auroral zone in essential agreement with earlier models by Birkeland (1908) and many others. Also Haerendel *et al.* (1971b) provide experimental verification of such current systems, based on magnetic and electric field measurements.

No reliable measurements have been reported of the electric field in the distant magnetotail. Problems associated with deduction from particle measurements have recently been discussed by Anderson (1970) and Van Allen (1970). The physics of the cross tail electric field and the plasma sheet have been discussed by Dessler (1971) in terms of Alfvén's (1968) theory for a neutral sheet.

For the inner edge of the plasma sheet, Young (1970) deduces a westward-directed electric field of about 0.4 mV m^{-1} from the ATS-1 low energy proton flux detector. Shelley *et al.* (1971) arrive at the same result by studying the electron flux increases at ATS-5 associated with moderate geomagnetic disturbances.

New reports about electric fields in the low latitude ionosphere and the equatorial electrojet have been issued by Woodman (1970), Behnke and Harper (1971), Carpenter and Bowhill (1971), and Subbaraya *et al.* (1971).

B. STRUCTURE OF MAGNETOPOUSE

Two indirect observations from geostationary satellites may be interpreted in terms of electric fields associated with the magnetospheric boundary. Both observations were made during highly disturbed conditions when the magnetopause was pushed inside the geostationary orbit for short times.

Changes in the direction of bulk flow of low energy protons on the ATS-1 satellite measured around 15 LT (Freeman *et al.*, 1968) can be interpreted as due to an electric field of the order of 5 mV m^{-1} shortly inside the magnetopause pointing approximately towards the earth. Outside the magnetopause the flow direction was the same but the magnetic field reversed so the electric field was pointing away from the boundary also on that side.

Shortly before local noon, the flux of 40 keV to 1 MeV electrons measured on the ATS-5 satellite (Bogott and Mozer, 1971) suddenly disappeared several hundred km before the magnetopause was reached. The experimenters interpret their observation in terms of an electric field directed towards the magnetopause so that it turns the gradient-drifting electrons away. For 1 MeV electrons the field has to be at least 65 mV m^{-1} .

The physics of a surface of magnetic field reversal in a plasma is not completely known. Some fundamental properties of such layers have been discussed (Alfvén, 1968; Alfvén and Fälthammar, 1971) but a detailed interpretation of these observations seems rather difficult.

C. STRUCTURE OF MAGNETOSPHERIC PLASMA

The phenomenon of striations has been observed in almost all Ba cloud experiments especially those at high latitudes. In some cases the striations may be explained in terms of plasma instabilities excited during the expansion and drift of the ion cloud.

However, there is growing evidence that in the majority of cases the striations are produced by a general filamentary structure of the ionospheric and magnetospheric plasma, merely rendered visible by the cloud (Reid, 1968; Haerendel, 1971; Völk and Haerendel, 1971).

This view is supported heavily by radar backscatter experiments and topside sounder data (Matuura *et al.*, 1971) that indicate field aligned density structures, and by double probe experiments that have revealed a micro-structure of the electric field, especially in the auroral zones and over the polar caps.

Filamentary structures are often observed in both cosmical and laboratory plasmas. Most commonly they are produced by field aligned currents. Cole (1970) discusses magnetospheric field-aligned structures in terms of current flowing between hemispheres to equalize potential differences at the ionospheric intersections of a field line. Park and Helliwell (1971) consider plasma drift in electric field irregularities and find that potentials from thunder clouds may suffice to produce whistler ducts.

A tentative hypothesis is that the appearance of filamentary plasma structures is a general and sensitive indication of current flow along magnetic field lines.

D. AURORAL ELECTRIC FIELDS

The structure of electric fields in and around auroral forms is largely unknown. Kelley *et al.* (1971c) have compared the N-S motion of auroral arcs with electric fields measured from balloons. In general, the westward electric field component agreed with the product of the magnetic field strength and southward drift velocity, i.e., the aurora seemed to drift together with the ionospheric plasma. During magnetic bays, however, a striking disagreement was that the rapid poleward auroral expansion was not associated with electric field variations. The observation may be interpreted in terms of parallel electric fields between the aurora and its particle source.

From rocket borne double probe measurements Aggson (1969) and Potter (1970) conclude that the electric field is generally directed perpendicular to auroral forms and that it is weaker inside the aurora than outside. This agrees with the auroral electrojet being a Hall current and may explain a rough directional agreement between the electric field and the magnetic disturbance vectors in the auroral zone. On several flights, however, Mozer and his collaborators have found drastic changes in electric field direction and sometimes oscillations at auroral boundaries. Barium experiments have sometimes indicated weaker electric fields near auroral forms (Wescott *et al.*, 1969). Barium clouds have also been seen to drift across auroral arcs, sometimes their motion has changed together with auroras. Barium clouds often get distorted or elongated into draperies, indicating strong electric field gradients, obviously due to large scale turbulence. Also balloon borne double probe experiments (Mozer, 1971b; Mozer and Manka, 1971) indicate such turbulence.

E. PARALLEL ELECTRIC FIELDS

From the laws of 'classical' plasma physics it can be calculated that the magnetic field aligned 'parallel' electric field in the high latitude ionosphere should be of the

order of $10 \mu\text{V m}^{-1}$, hardly ever exceeding $100 \mu\text{V m}^{-1}$. On four different rocket flights in connection with active auroras (Fahleson *et al.*, 1970; Mozer and Fahleson, 1970; Kelley *et al.*, 1971a, b) parallel electric fields have been measured with strengths up to 30 mV m^{-1} , in all cases directed downwards. In a daytime flight (Kelley *et al.*, 1971a) and two nighttime flights during undisturbed and weakly disturbed conditions (Fahleson *et al.*, 1971) no measurable field was found. To the author's knowledge, *no other electric field experiments capable of measuring parallel fields have been flown under appropriate conditions.* A Ba cloud observation (Mende, 1968) has been used as proof against the existence of strong parallel fields. In the analysis of the vertical motion of the cloud, however, Mende neglects to take into account vertical electric currents and anomalous plasma resistivity, thereby excluding all possibilities of describing a situation with a strong parallel field. Consequently he also arrives at a maximum possible field of about $10 \mu\text{V m}^{-1}$. In a theoretical study of the diffusion of Ba clouds, Scholer and Haerendel (1971) conclude that turbulent plasma resistivity should be included in the analysis of the field aligned diffusion. Until this has been done, little can be inferred about parallel electric fields from Ba cloud experiments.

In the latest of the double probe experiments (Kelley *et al.*, 1971b) an electric field detector with four spherical probes was flown during the break up phase of a storm with a 2000 γ magnetic bay. The rocket received a large coning during launch, its attitude varied repeatedly between perpendicular and virtually parallel to the magnetic field thus offering ideal conditions for analysis. The parallel field was determined independently from probe pairs along the rocket axis *and* from the precessional modulation of the perpendicular probe signals with an accuracy of $\pm 3 \text{ mV m}^{-1}$. The perpendicular field was determined with the same accuracy and was in good agreement with the measurements from two Ba clouds released from *the same* rocket. The parallel field was near 30 mV m^{-1} decreasing with time to close to zero at the end. The Ba clouds did not show any obvious anomalous behavior but a special analysis of their motion has been initiated.

There are undisputably large parallel electric currents (Zmuda, 1966) in the auroral zone, strong enough to create instabilities of the two-stream or ion-sound type (Swift, 1965; Kindel and Kennel, 1971). Laboratory plasma measurements (Demidov *et al.*, 1967; Hamberger and Friedman, 1968) and theoretical calculations (Coroniti, 1969; Dupree, 1970) show that such instabilities are capable of increasing the plasma resistivity by several orders of magnitude. The product of measured currents and possible resistivities can very well reach electric field strengths comparable to those measured.

The physics of electric double-layers in or above the auroral ionosphere is discussed in detail by Block (1972). A large number of particle observations as well as the electric field observations on INJUN 5 and laboratory plasma experiments indicate the existence of such sheaths.

The electric field observations and the Ba cloud behavior described in the previous section may be understood in terms of space charge layers, possibly according to models of Carlqvist and Boström (1970) and Block (1971). The double probe

measurements of Aggson and Cahill as well as the Ba releases of Wescott may have been done below the space charge regions in the Hall current associated electric fields, whereas some measurements of Mozer are highly indicative of space charge structures.

A summary of arguments against parallel electric fields has been given by O'Brien (1970). None of the arguments seems severe. For example, protons and electrons may be simultaneously accelerated by two regions with oppositely directed electric fields (Block, 1969; Reme and Bosqued, 1971).

Further information about parallel fields may be gained from Ba jet experiments which will produce a filament of Ba plasma reaching up to several 1000 km. Parallel electric fields producing different plasma drifts at different altitudes will be easily recognized. However, there may be a certain risk that the jet will short circuit the electrical structures that are to be studied.

F. STORM-ASSOCIATED ELECTRIC FIELDS

The electric fields as seen by balloons in the auroral zone during 19 substorms (Mozer, 1971c) have been found to have common features. A certain delay after a reversal of the interplanetary magnetic field from north to south the westward electric field starts to grow. About 1 hr after the onset of this initial phase, the magnetic bay occurs and the aurora surges towards the pole. Simultaneously an equatorward electric field occurs but the westward component remains throughout the storm.

Other electric field observations in connection with storms are the whistler drift observations of Carpenter and Stone (1967) and the observations of Young (1970) and Shelley *et al.* (1971) which also see the westward field. The equatorward displacement of the zones of reversal of Cauffman and Gurnett (1971) can be understood in terms of an inward drift in the westward field.

4. Future Problems and Developments

The interest in electric fields and electric field measurements is presently increasing almost explosively. Hopefully our understanding of magnetospheric physics is increasing at the same rate. Closely related to this development is the shocking discovery that the 'smooth, homogeneous infinitely conducting fluid' now is breaking up into pieces of turbulent matter separated by singular surfaces and electric double layers. The most important objects of study for the next few years obviously are all these new features of 'anomalous' plasma behavior. Electric field measurements and theories containing the electric field as an essential parameter may be the most powerful tools for an easy understanding of these presently very complex phenomena. But first of all, we have to abandon the misleading word *anomalous* and instead start talking of *normal* plasma behavior.

References

- Aggson, T. L.: 1969, in B. M. McCormac (ed.), *Atmospheric Emissions*, Van Nostrand Reinhold Company, New York, p. 305.
Alfvén, H.: 1968, *Ann. Geophys.* **24**, 675.

- Alfvén, H. and Fälthammar, C.-G.: 1971, *Cosmic Electrodyn.* **2**, 78.
- Anderson, K. A.: 1970, *J. Geophys. Res.* **75**, 2591.
- Atkinson, W., Lundquist, S., and Fahleson, U.: 1971, *Pure Appl. Geophys.* **84**, 46.
- Behnke, R. A. and Harper, R. M.: 1971, IAGA Conference, Moscow.
- Bering, E., Kelley, M., and Mozer, F. S.: 1970, *Trans. Amer. Geophys. Union* **51**, 404.
- Birkeland, Kr.: 1908 and 1913, *The Norwegian Aurora Polaris Expedition 1902-1903*, Vol. I, Christiania.
- Block, L. P.: 1969, *Ninth International Conference on Phenomena in Ionized Gases*, Bucharest, Rumania. Preprint: Royal Inst. of Techn. Rep. No. 69-30, Div. of Plasma Physics, Stockholm.
- Block, L. P.: 1971, Royal Inst. of Techn. Rep. TRITA-EPP 71-14, Stockholm.
- Block, L. P.: 1972, this volume, p. 258.
- Bogott, F. H. and Mozer, F. S.: 1971, *J. Geophys. Res.* **76**, 892.
- Carlqvist, P. and Boström, R.: 1970, *J. Geophys. Res.* **75**, 7140.
- Carlson, C. W.: 1971, *Trans. Amer. Geophys. Union* **52**, 329.
- Carpenter, D. L.: 1970, *J. Geophys. Res.* **75**, 3837.
- Carpenter, D. L.: 1971, IAGA Conference, Moscow.
- Carpenter, D. L. and Stone, K.: 1967, *Planetary Space Sci.* **15**, 395.
- Carpenter, L. A. and Bowhill, S. A.: 1971, *Radio Sci.* **6**, 203.
- Cauffman, D. P.: 1971, *Trans. Amer. Geophys. Union* **52**, 328.
- Cauffman, D. P. and Gurnett, D. A.: 1971, *J. Geophys. Res.* **76**, 6014.
- Cole, K. D.: 1970, *J. Atmospheric Terrest. Phys.* **33**, 741.
- Coroniti, F. V.: 1969, in *Planetary Electrodynamics*, Vol. 2 (ed. by S. C. Coroniti and J. Hughes), Gordon and Breach, p. 309.
- Demidov, B. A., Elagin, N. I., and Fanchenko, S. D.: 1967, *Soviet Phys.-Doklady* **12**, 463.
- Dessler, A. J.: 1971, *J. Geophys. Res.* **76**, 3174.
- Dupree, T. H.: 1970, Preprint Internat. Center for Theoretical Physics, Trieste, I. C./70/40.
- Fahleson, U. V.: 1971, in *The ESRO Geostationary Magnetospheric Satellite*. ESRO SP-60, p. 249.
- Fahleson, U. V., Fälthammar, C.-G., Pedersen, A., Knott, K., Brommundt, G., Schumann, G., Haerendel, G., and Rieger, E.: 1971, *Radio Sci.* **6**, 233.
- Fahleson, U. V., Kelley, M. C., and Mozer, F. S.: 1970, *Planetary Space Sci.* **18**, 1551.
- Frank, L. A. and Gurnett, D. A.: 1971, *J. Geophys. Res.* **76**, 6829.
- Freeman, J. W., Jr.: 1968, *J. Geophys. Res.* **73**, 4151.
- Freeman, J. W., Jr., Warren, C. S., and Maguire, J. J.: 1968, *J. Geophys. Res.* **73**, 5719.
- Giles, M. and Martelli, G.: 1969, *Planetary Space Sci.* **17**, 1693.
- Giles, M. and Martelli, G.: 1971, *Planetary Space Sci.* **19**, 1.
- Haerendel, G.: 1971, *Trans. Amer. Geophys. Union* **52**, 298.
- Haerendel, G.: 1972, in E. R. Dyer (ed.) *Solar-Terrestrial Physics/1970, Part IV*, D. Reidel Publ. Co., Dordrecht, Holland, p. 87.
- Haerendel, G. and Lüst, R.: 1970, in B. M. McCormac (ed.), *Particles and Fields in the Magnetosphere*, D. Reidel Publishing Company, Dordrecht, Holland, p. 213.
- Haerendel, G., Föppl, R., Michel, K. W., Neuss, H., Schöning, R., and Stöcker, J.: 1971a, *Trans. Amer. Geophys. Union* **52**, 299.
- Haerendel, G., Hedgecock, P. C., and Akasofu, S.-I.: 1971b, *J. Geophys. Res.* **76**, 2382.
- Hamberger, S. M. and Friedman, M.: 1968, *Phys. Rev. Letters* **21**, 674.
- Heppner, J. P., Stolarik, J. D., and Wescott, E. M.: 1971a, in B. M. McCormac (ed.), *The Radiating Atmosphere*, D. Reidel Publishing Company, Dordrecht, Holland, p. 407.
- Heppner, J. P., Stolarik, J. D., and Wescott, E. M.: 1971b, *J. Geophys. Res.* **76**, 6028.
- Heppner, J. P., Wescott, E. M., and Stolarik, J. D.: 1970, IAGA Conference, Leningrad.
- Kelley, M. C. and Mozer, F. S.: 1970, *Trans. Amer. Geophys. Union* **51**, 812.
- Kelley, M. C., Mozer, F. S., and Fahleson, U. V.: 1971a, *J. Geophys. Res.* **76**, 6054.
- Kelley, M. C., Mozer, F. S., Haerendel, G., Fahleson, U. V., and Kavadas, A.: 1971b, *Trans. Amer. Geophys. Union* **52**, 329.
- Kelley, M. C., Starr, J. A., and Mozer, F. S.: 1971c, *J. Geophys. Res.* **76**, 5269.
- Kindel, J. M. and Kennel, C. F.: 1971, *J. Geophys. Res.* **76**, 3055.
- Knott, K., Brommundt, G., and Schumann, G.: 1971, *Planetary Space Sci.* **19**, 345.
- Matuura, N., Hojo, H., and Nishizaki, R.: 1971, IAGA Conference Moscow.
- Maynard, N. C., Aggson, T. L., and Heppner, J. P.: 1970, *Radio Sci.* **5**, 1049.

- Maynard, N. C. and Heppner, J. P.: 1970, in B. M. McCormac (ed.), *Particles and Fields in the Magnetosphere*, D. Reidel Publishing Company, Dordrecht, Holland, p. 247.
- McIlwain, C. E.: 1971, *Trans. Amer. Geophys. Union* **52**, 328.
- McIlwain, C. E.: 1972, this volume, p. 268.
- Melzner, F. and Völk, H.: 1970, ESRO proposal No. S-329.
- Mende, S. B.: 1968, *J. Geophys. Res.* **73**, 991.
- Mozer, F. S.: 1970, *Planetary Space Sci.* **18**, 259.
- Mozer, F. S.: 1971a, in E. A. Wolff and E. P. Mercanti (eds.), *Geoscience Instrumentation*.
- Mozer, F. S.: 1971b, *J. Geophys. Res.* **76**, 3651.
- Mozer, F. S.: 1971c, *J. Geophys. Res.* **76**, 7595.
- Mozer, F. S. and Fahleson, U. V.: 1970, *Planetary Space Sci.* **18**, 1563.
- Mozer, F. S. and Manka, R. H.: 1971, *J. Geophys. Res.* **76**, 1697.
- Mozer, F. S., Bering, E., Carlson, C. W., and Kelley, M. C.: 1971, *Trans. Amer. Geophys. Union* **52**, 329.
- O'Brien, B. J.: 1970, *Planetary Space Sci.* **18**, 1821.
- Park, C. G. and Carpenter, D. L.: 1970, *J. Geophys. Res.* **75**, 3825.
- Park, C. G. and Helliwell, R. A.: 1971, *Radio Sci.* **6**, 299.
- Potter, W. E.: 1970, *J. Geophys. Res.* **75**, 5415.
- Potter, W. E.: 1971, IAGA Conference, Moscow.
- Potter, W. E. and Cahill, L. J. Jr.: 1969, *J. Geophys. Res.* **74**, 5159.
- Rawer, K. and Spennner, K.: 1970, in *Space Res.* **10**, North-Holland Publ. Co., p. 766.
- Reid, G. C.: 1968, *J. Geophys. Res.* **73**, 1627.
- Reme, H. and Bosqued, J. M.: 1971, *J. Geophys. Res.* **76**, 7683.
- Rieger, E., Neuss, H., Lüst, R., Meyer, B., Haser, L., Loidl, H., Stöcker, J., and Haerendel, G.: 1970, *Ann. Geophys.* **26**, 845.
- Scholer, M. and Haerendel, G.: 1971, *Planetary Space Sci.* **19**, 915.
- Shelley, E. G., Johnson, R. G., and Sharp, R. D.: 1971, *Radio Sci.* **6**, 305.
- Subbaraya, B. H., Sastry, T. S. G., Murali, P., and Prakash, S.: 1971, IAGA Conference, Moscow.
- Swift, D. W.: 1965, *J. Geophys. Res.* **70**, 3061.
- Van Allen, J. A.: 1970, *J. Geophys. Res.* **75**, 29.
- Völk, H. and Haerendel, G.: 1971, B. M. McCormac (ed.), in *The Radiating Atmosphere*, D. Reidel Publishing Company, Dordrecht, Holland, p. 394.
- Wescott, E. M. and Murcray, W. B.: 1971, *Trans. Amer. Geophys. Union* **52**, 295.
- Wescott, E. M., Stolarik, J. D., and Heppner, J. P.: 1969, *J. Geophys. Res.* **74**, 3469.
- Wescott, E. M., Stolarik, J. D., and Heppner, J. P.: 1970, in B. M. McCormac (ed.), *Particles and Fields in the Magnetosphere*, D. Reidel Publishing Company, Dordrecht, Holland, p. 229.
- Woodman, R. F.: 1970, *J. Geophys. Res.* **75**, 6249.
- Young, D. T.: 1970, *Trans. Amer. Geophys. Union* **51**, 811.
- Zmuda, A. J., Martin, J. H., and Heuring, F. T.: 1966, *J. Geophys. Res.* **71**, 5033.

INJUN 5 OBSERVATIONS OF MAGNETOSPHERIC ELECTRIC FIELDS AND PLASMA CONVECTION

DONALD A. GURNETT

Dept. of Physics and Astronomy, The University of Iowa, Iowa City, Iowa, U.S.A.

Abstract. Recent measurements of magnetospheric electric fields with the satellite INJUN 5 have provided a comprehensive global survey of plasma convection at low altitudes in the magnetosphere. A persistent feature of these electric field observations is the occurrence of an abrupt reversal in the convection electric field at auroral zone latitudes. The plasma convection velocities associated with these reversals are generally directed E-W, away from the sun on the poleward side of the reversal, and toward the sun on the equatorward side of the reversal. Convection velocities over the polar cap region are normally less than those observed near the reversal region. The electric field reversal is observed to be coincident with the 'trapping boundary' for electrons with energies $E > 45$ keV. Near local noon the region of anti-sunward convection poleward of the electric field reversal/trapping boundary corresponds to the low altitude extension of the polar cusp plasma. Intense 'inverted V' electron precipitation events associated with auroral arcs are also observed near and poleward of the electric field reversal/trapping boundary. These observations are discussed in terms of a current model of magnetospheric convection.

1. Introduction

Recent measurements of electric fields using the double-probe technique on the low altitude (677 to 2528 km) polar orbiting satellite INJUN 5 have provided the first extensive global survey of electric fields and plasma convection in the magnetosphere. In this paper we summarize the principal observational results from the electric field experiment on this spacecraft.

The electric field experiment on INJUN 5 is of the double-probe type described by Fahleson (1967) and others. The probes used consist of two conducting spheres 20.3 cm in diameter mounted on booms with a center-to-center separation of 2.85 m. The spacecraft is magnetically oriented by a bar magnet within the spacecraft such that the electric antenna axis is maintained approximately perpendicular ($\sim \pm 10^\circ$) to the geomagnetic field. The potential difference between the spheres is obtained from a high input impedance differential amplifier and is recorded, along with other data, by a tape recorder in the satellite so that global surveys of electric fields and other geophysical phenomena can be obtained. Various other parameters such as the antenna impedance and the electron density and temperature are also available to determine if the electric antenna system is operating properly. For further details on the INJUN 5 electric field instrumentation and observations the reader is referred to papers by Gurnett *et al.* (1969), Gurnett (1970), Cauffman and Gurnett (1971, 1972), and Frank and Gurnett (1971).

2. Data Analysis and Instrumental Effects

Electric field measurements obtained for a pass over the northern polar region are shown in Figure 1 to illustrate the technique used in analyzing the INJUN 5 electric

field data. The systematic sinusoidal variation evident in the measured electric field E_m (shown by the light line in the top panel of Figure 1) is caused by the spacecraft rotation in the $\mathbf{V}_s \times \mathbf{B}$ field from the spacecraft motion through the ionosphere. At middle and low latitudes, where the ionospheric plasma is expected to corotate with the earth, the $\mathbf{V}_s \times \mathbf{B}$ field provides a convenient reference for 'calibrating' the overall accuracy of the electric field determination. After all instrumental effects are considered

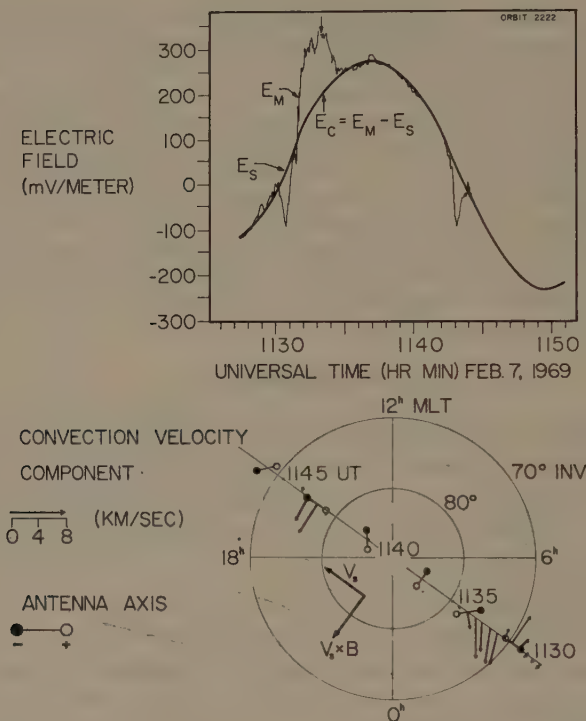


Fig. 1. Method of subtracting the $\mathbf{V}_s \times \mathbf{B}$ electric field, E_s , from the measured electric field, E_m , to determine the convection electric field, $E_c = E_m - E_s$, and a polar plot of the associated convection velocity component.

the overall accuracy of the INJUN 5 electric field measurements, as determined by comparisons with the $\mathbf{V}_s \times \mathbf{B}$ field, is about $\pm 30 \text{ mV m}^{-1}$. This error is primarily caused by unequal photoelectron emission from the two spheres due to asymmetrical sunlight shadowing of the spheres by the supporting booms. For certain orientations and for cases when the spacecraft is rotating very slowly, the effects of this asymmetrical shadowing can be eliminated and the accuracy is increased to about $\pm 10 \text{ mV m}^{-1}$.

To determine naturally occurring convection electric fields it is necessary to subtract the $\mathbf{V}_s \times \mathbf{B}$ field and errors due to shadowing asymmetries from the measured

electric field. The procedure used to determine the subtracted electric field, E_s , is to (a) compute the expected $\mathbf{V}_s \times \mathbf{B}$ field component using the estimated spacecraft orientation (which is sometimes in error by up to 10° in rotation about the geomagnetic field), and then to (b) readjust the amplitude and phase of the sinusoidal $\mathbf{V}_s \times \mathbf{B}$ variations to provide a good fit to the observed $\mathbf{V}_s \times \mathbf{B}$ field at low latitudes where no convection electric fields are expected. The solid dark curve shown in the top panel of Figure 1 is the subtracted electric field, E_s , determined in this manner. The difference between the measured electric field and the subtracted electric field, $E_c = E_m - E_s$, is the best estimate of the actual convection electric field in the ionosphere. Other readily recognizable errors due to sunlight shadowing by the spacecraft body and wake effects must also be eliminated from consideration (see Cauffman and Gurnett (1971) for a discussion of these effects).

The plasma convection velocity \mathbf{V}_c is determined from the convection electric field \mathbf{E}_c using the equation (Axford, 1969)

$$\mathbf{V}_c = \mathbf{E}_c \times \mathbf{B} / B^2.$$

The convection velocity components corresponding to the electric field measurements in the top panel of Figure 1 are shown by the arrows in the IN Lat-MLT polar diagram at the bottom of Figure 1. The direction of the arrow represents the direction of the convection velocity component detected and the length of the arrow is proportional to the magnitude of the convection velocity. Note that the arrows do *not* indicate the vector direction of the convection velocity since only one component is measured.

3. Summary of Observations

The convection observations shown in Figures 2 and 3 have been selected to illustrate some of the general features of the INJUN 5 convection electric field measurements. The most prominent and persistent feature of the INJUN 5 electric field data is the occurrence of an abrupt reversal or discontinuity in the convection electric field at about 70 to 80° IN Lat. An example of such an electric field reversal is shown in Figure 1 at 1132 UT where the convection electric field changes sign, from about -100 to $+125$ mV m^{-1} . The corresponding convection velocity component (shown in the polar diagram at the bottom of Figure 1) shows a reversal from eastward (sunward) flow on the equatorward side of the reversal to westward (anti-sunward) flow on the poleward side of the reversal. The series of successive dawn-dusk polar passes illustrated in Figure 2 also show similar abrupt reversals in the direction of the convection velocity. These reversals are particularly evident in the dawn LT region at about 1724:20, 1925:30, and 2123:30 UT. Smaller reversals are also evident in the dusk region at 1734:00 and 2132:00 UT. In all cases the reversals are consistent with a generally sunward flow on the equatorward side of the reversal and anti-sunward flow on the poleward side of the reversal.

Usually the largest convection velocities are observed near (within 5 to 10° IN Lat) the electric field reversal location. At higher latitudes, in the polar cap region, the

convection velocity is usually less than the $\sim 0.75 \text{ km s}^{-1}$ sensitivity limit imposed by the $\pm 30 \text{ mV m}^{-1}$ uncertainty in the convection electric field determination. Orbit 6909 (Figure 2), however, shows the occurrence of an essentially uniform anti-sunward flow with velocities greater than 1 km s^{-1} along the entire satellite trajectory

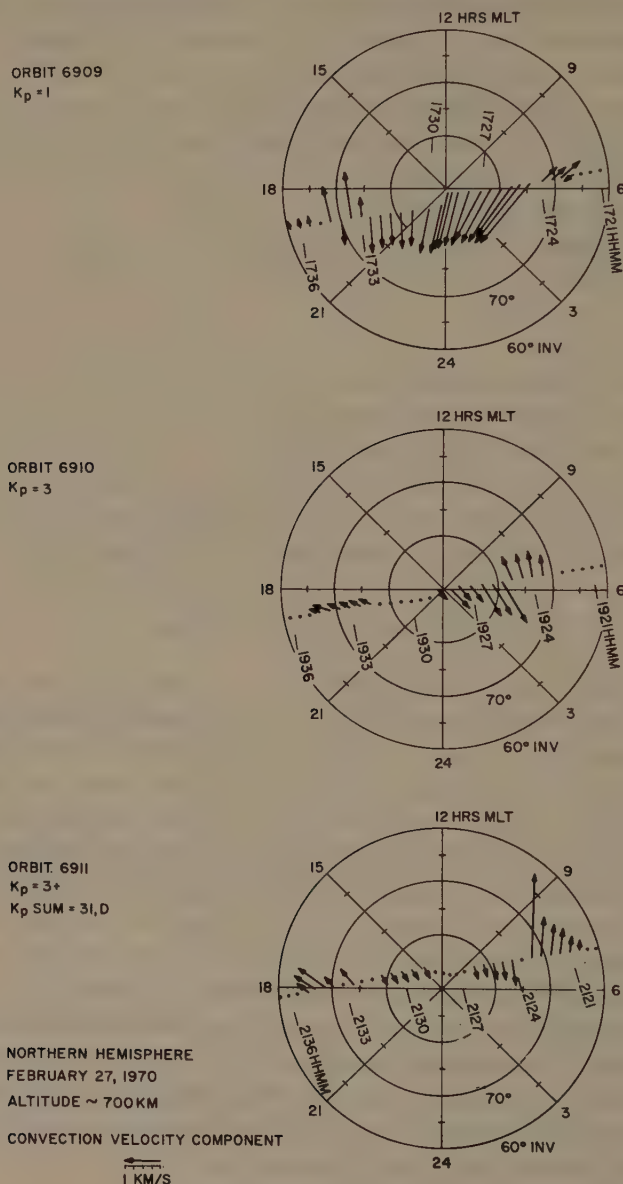


Fig. 2. A series of dawn-dusk orbits showing the persistent occurrence of reversals in the convection electric field in both the dawn and dusk regions, and one case (orbit 6909) having nearly constant antisunward convection along the entire satellite trajectory over the polar cap region.

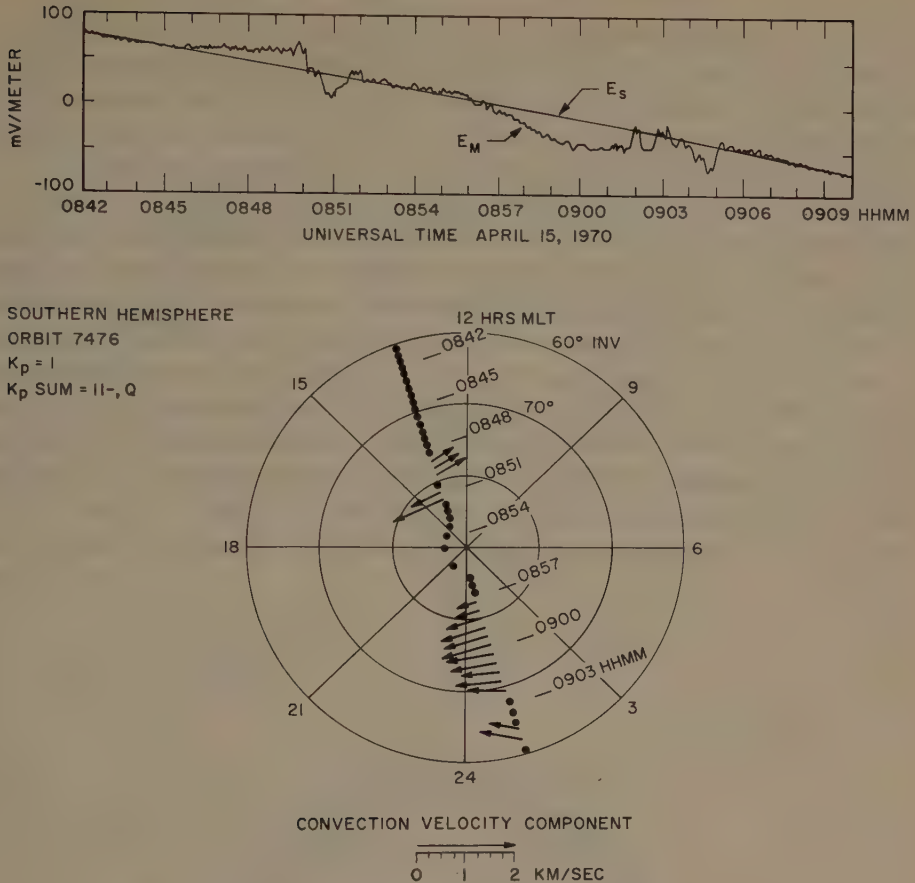


Fig. 3. A noon-midnight pass showing a distinct reversal near local noon at about 80° IN Lat, relatively low convection velocities over the polar cap, and a large zone of westward convection in the local midnight region.

over the polar region from 1724:00 to 1734:00 UT. Examples of relatively uniform transpolar convection, such as might be inferred from cases like orbit 6909, with convection velocities greater than 0.75 km s^{-1} are not commonly observed with INJUN 5.

Figure 3 illustrates the electric field observed for an approximately noon-midnight meridional pass over the southern hemisphere. Near local noon, at about 0852:20 UT and 80° IN Lat, a clearly defined electric field reversal is observed. Over the polar cap region, from about 0852:00 to 0857:00, the convection velocity component detected is very small, less than 0.25 km s^{-1} . The spacecraft orientation and rotation rate for this pass is such that the convection velocity can be determined to within about 0.25 km s^{-1} ($\pm 10 \text{ mV m}^{-1}$). In the local midnight region a large westward (anti-sunward) convection zone is observed from 0857:00 to 0902:00 UT and a variety of more complex variations is observed after 0902:00 UT. In this case, no

discernible electric field reversal is observed in the local midnight region. The INJUN 5 electric field observations through the noon-midnight LT regions generally tend to be more complex and less ordered than in the dawn-dusk regions, particularly near local midnight, with a tendency for multiple zones of convection and more than one electric field reversal or, as in the case shown, no electric field reversal at all.

In order to obtain a general idea of the average or 'typical' high latitude convection pattern a study was performed (Cauffman and Gurnett, 1972) using all of the available INJUN 5 electric field data. Since only one component of the electric field is sensed it is necessary to utilize a large number of observations at different antenna orientations to deduce the general direction of the plasma flow. The method used to determine the general direction of the plasma flow was to analyze all of the observed electric field reversals in terms of either E-W or N-S velocity components on either side of the reversal. Figure 4 shows the results of interpreting all of the observed reversals in terms of E-W convection. Each point represents the position of an electric field reversal. The open circles indicate that the convection velocity is eastward on the poleward side of the reversal and westward on the equatorward side of the reversal.

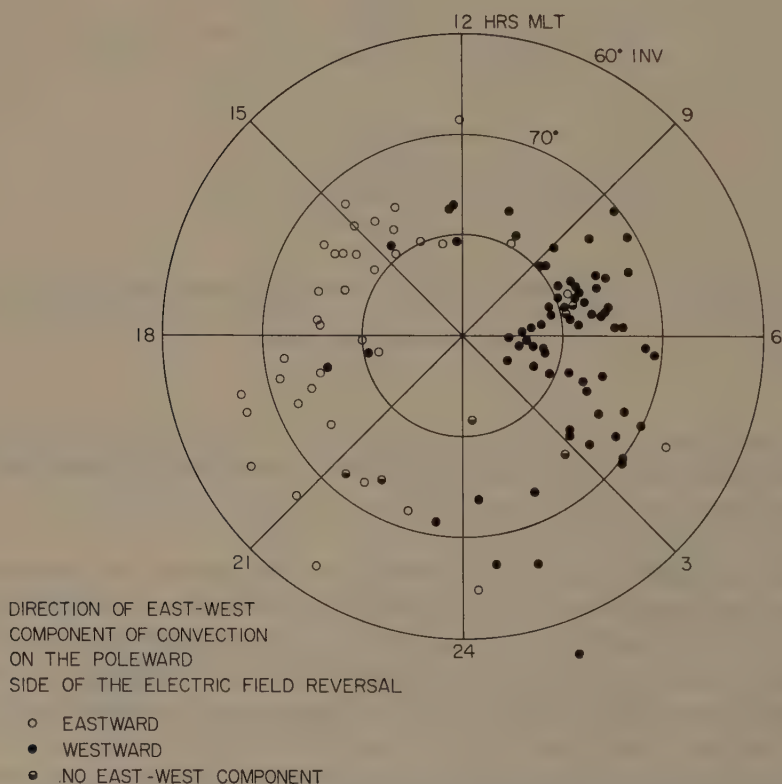


Fig. 4. Locations of reversals observed by INJUN 5, coded to indicate the E-W direction of the convection poleward and equatorward of the reversal.

The dark circles indicate the opposite, westward on the poleward side and eastward on the equatorward side. The half dark circles represent cases where the electric antenna orientation was such that only the N-S component of the convection velocity could be sensed.

From Figure 4 it is seen that for LT's from 0 to 12 hr the convection velocity is generally westward (antisunward) on the poleward side of the reversal and eastward (sunward) on the equatorward side of the reversal. For LT's from 12 to 24 hr the latitudinal variation is just the opposite. A similar scatter plot obtained by analyzing all of the reversals in terms of N-S convection components shows no consistent ordering of the data, thereby indicating that the convection velocities at the reversal boundary are primarily E-W.

The general convection pattern deduced from the INJUN 5 observations is illustrated schematically in Figure 5. This diagram incorporates the results from the statistical study discussed above indicating that near the reversal the plasma flow is

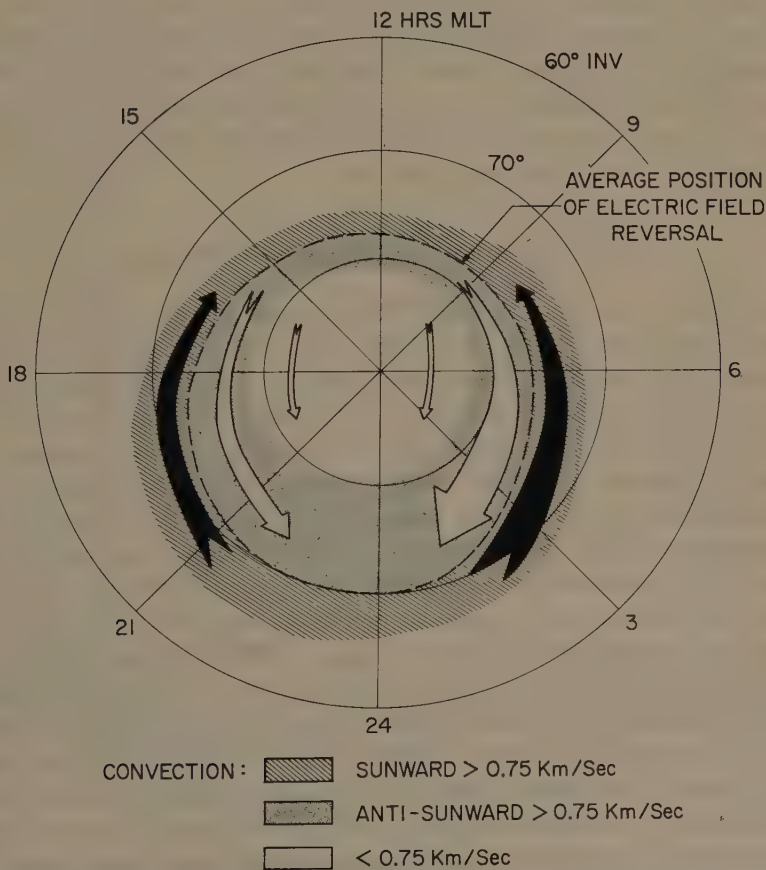


Fig. 5. Qualitative sketch summarizing the 'average' convection pattern obtained from the INJUN 5 electric field measurements.

primarily E-W, away from the sun on the poleward side of the reversal, and toward the sun on the equatorward side of the reversal. The large arrows near the reversal boundary are indicative of the fact that the largest convection velocities are usually observed within about 5 to 10° IN Lat from the reversal boundary. The larger arrows in the dawn region compared to the dusk region are indicative of the fact that the convection velocities are usually largest in the dawn LT region (cf., Figure 2). The narrowing of the arrows toward local noon is indicative of the fact that the latitudinal width of the convection zones tends to be narrower near local noon and wider in the local evening (cf., Figure 3). The smaller arrows over the polar cap region reflect the fact that the convection velocities are generally smaller ($<0.75 \text{ km s}^{-1}$) over the polar cap region than near the reversal boundary. The anti-sunward direction of the convection in the polar cap region is based on the recent electric field measurements by Maynard (1971) with the OGO 6 satellite which reportedly show a general anti-sunward flow over the polar cap region with velocities generally below the 0.75 km s^{-1} sensitivity limit of the INJUN 5 electric field experiment.

It should be emphasized that the convection pattern illustrated in Figure 5 represents a gross average of the convection detected by INJUN 5 and significant departures undoubtedly occur. Since, in many cases, the convection velocity is below the sensitivity limit of the INJUN 5 electric field experiment, the convection pattern in Figure 5 represents conditions of enhanced convection ($>0.75 \text{ km s}^{-1}$) and may not be representative of more quiescent conditions.

4. Association with Charged Particle Observations

Comparisons of the low energy charged particle measurements from the LEPDEA instrumentation on INJUN 5 and the electric field data have shown that the electric field reversal corresponds closely with the position of the 'trapping boundary' for electrons with energies $E > 45 \text{ keV}$ (Frank and Gurnett, 1971). (See Frank and Ackerson (1971) for details of the LEPDEA instrumentation.) An example of this association is illustrated in Figure 6 which shows the electric field and selected charged particle measurements for a dawn-dusk pass over the northern polar region. Because of the favorable antenna orientation and very slow rotation rate on this pass the convection electric field can be determined to an accuracy of about $\pm 10 \text{ mV m}^{-1}$. A clearly defined electric field reversal is observed at about 1443:20 UT in the dawn LT region and a smaller, less distinct, reversal is observed at about 1453:10 UT in the dusk LT region. These electric field reversals are seen to be essentially coincident with the high latitude termination of measurable intensities of electrons with energies $E > 45 \text{ keV}$ (indicated by the dashed vertical lines in Figure 6). This termination is commonly referred to as the 'trapping boundary' and represents a natural coordinate for investigating high latitude magnetospheric phenomena (Frank and Ackerson, 1972). On the basis of these and other measurements, Frank and Gurnett (1971) have interpreted the trapping boundary and associated electric field reversal as delineating the high latitude termination of closed field lines, with the sunward

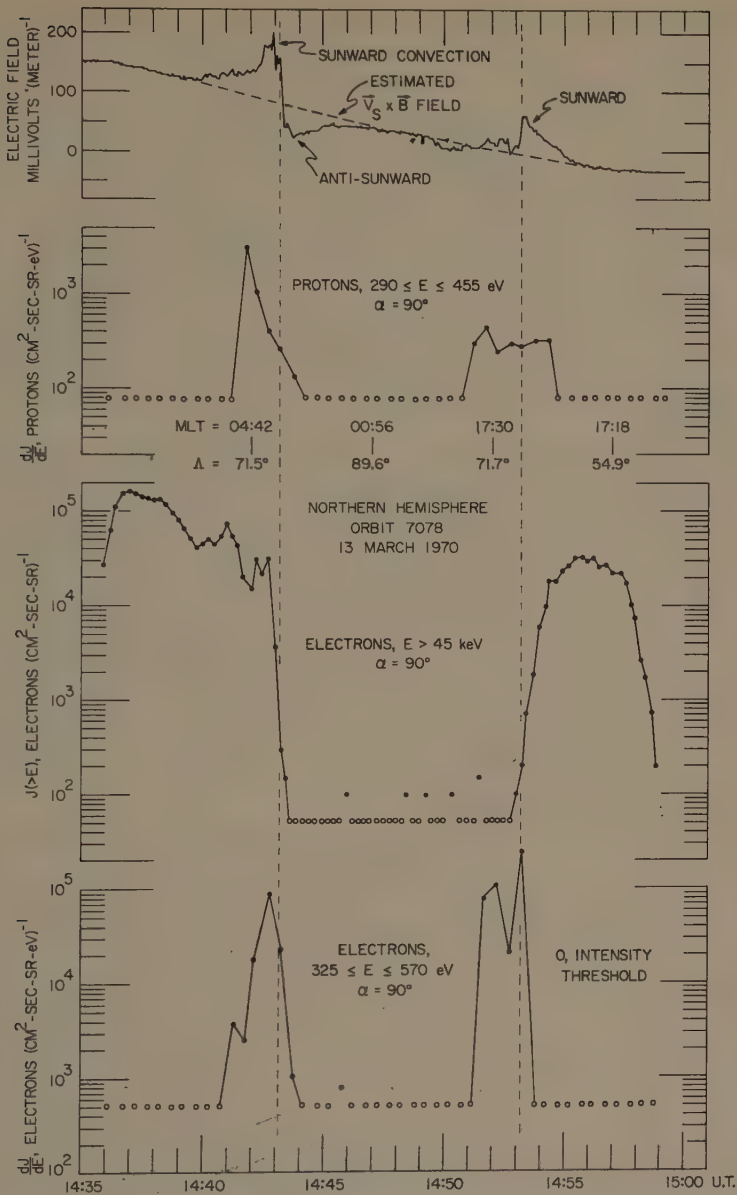


Fig. 6. Simultaneous electric fields and low energy plasma measurements showing the correspondence between the electric field reversal, the $E > 45$ keV trapping boundary, and inverted 'V' electron precipitation events.

plasma flow occurring on closed field lines within the magnetosphere, and the anti-sunward plasma flow occurring on open field lines which connect into the solar wind.

Low energy electron precipitation events associated with auroral arcs are also observed near and sometimes poleward of the trapping boundary/electric field

reversal location. These low energy electron precipitation events often have a characteristic 'inverted V' energy-time signature with the average electron energy increasing from less than 100 eV to a maximum of several keV, or more, subsequently decreasing as the satellite passes through the precipitation region (Frank and Ackerson, 1971a). Inverted 'V' precipitation events have been directly associated with auroral arcs (Ackerson and Frank, 1971). The low energy ($325 \leq E \leq 570$ eV) electron fluxes shown in the bottom panel of Figure 6 provide a coarse indication of the location of inverted 'V' electron precipitation events occurring during this pass. In the local morning region a single inverted 'V' event is observed at approximately 1443 UT, nearly coincident with the trapping boundary/electric field reversal location. In the local evening region two inverted 'V' events are observed, one at about 1453 UT, near the trapping boundary, and the second at about 1452 UT, poleward of the trapping boundary.

The relative locations of the inverted 'V' events and the trapping boundary in this case are consistent with the general survey results of Frank and Ackerson (1972) which show that the inverted 'V' precipitation events occur on open field lines near or poleward of the $E > 45$ trapping boundary and in a region of generally anti-sunward convection (cf., Figure 5). Equatorward of the $E > 45$ keV trapping boundary, in the region of sunward convection, significant electron precipitation and associated auroral light emission are also observed during the local midnight and morning hours. However, the electron precipitation in this region generally has a harder energy spectrum and lower intensity than the inverted 'V' events and is identified by Frank and Ackerson (1971) as originating from plasma sheet electrons injected onto closed field lines in the local midnight region.

Near local noon the convection electric fields observed by INJUN 5 can be directly associated with the entry of magnetosheath plasma into the polar magnetosphere through the dayside polar cusp region identified by Frank (1971a), Frank and Ackerson (1971), and Heikkilä and Winningham (1971). An example of such an observation is shown in Figure 7, from Gurnett and Frank (1972). The intense fluxes of low energy electrons ($325 \leq E \leq 570$ eV) and protons ($290 \leq E \leq 455$ eV) occurring from 1511:30 to 1513:45 UT on this pass, poleward of the $E > 45$ keV trapping boundary, identify this region as the polar cusp. The separation of the polar cusp into an equatorward 'electron sheet' and a poleward 'proton sheet' is directly comparable to Frank's (1971a) IMP 5 observations of the polar cusp at much higher altitudes, $\sim 5 R_E$. The simultaneous observation of broadband VLF hiss generated by the polar cusp plasma (shown in the top panel of Figure 7) provides further evidence of the polar cusp location on this pass. The electric field data for this pass show a negative perturbation from the $V_s \times B$ field of about 30 mV m^{-1} in the polar cusp region. This electric field corresponds to a westward (anti-sunward) convection of about 1 km s^{-1} in the polar cusp region. From this and other similar observations it is concluded that the polar cusp region is directly associated with the region of enhanced anti-sunward convection on the poleward side of the electric field reversal/trapping boundary (cf., Figure 5).

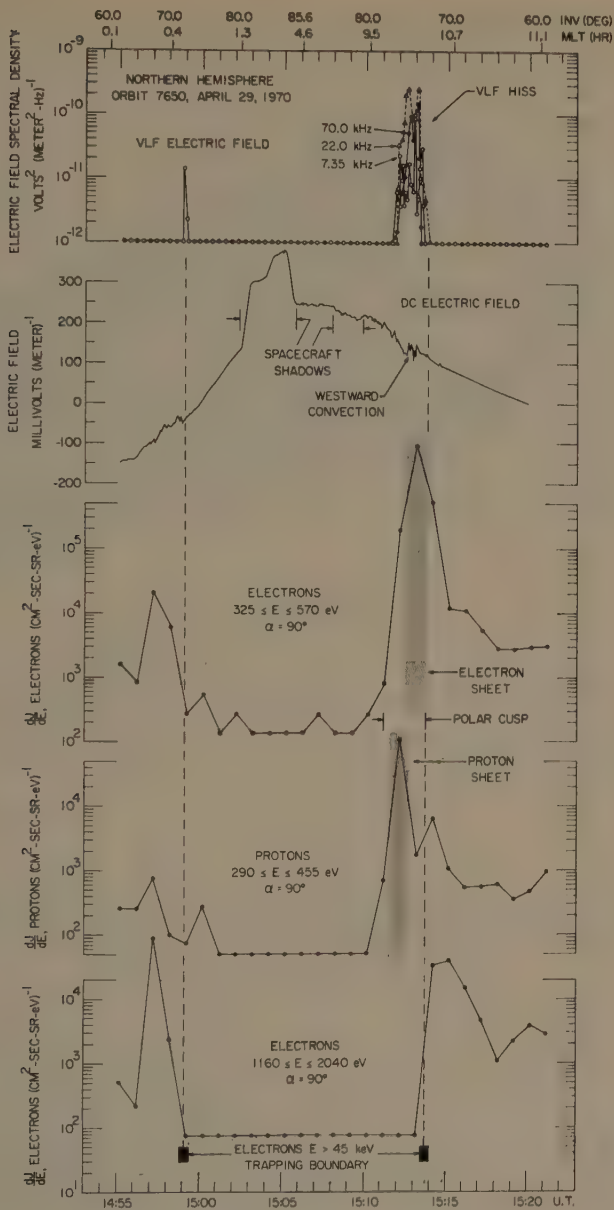


Fig. 7. Simultaneous VLF, electric field, and low energy plasma observations showing the occurrence of anti-sunward (westward in this case) convection in the polar cusp region.

5. Discussion

The general pattern of low altitude convection can be interpreted using the magnetospheric model shown in Figure 8 (Frank and Gurnett, 1971). This model uses the

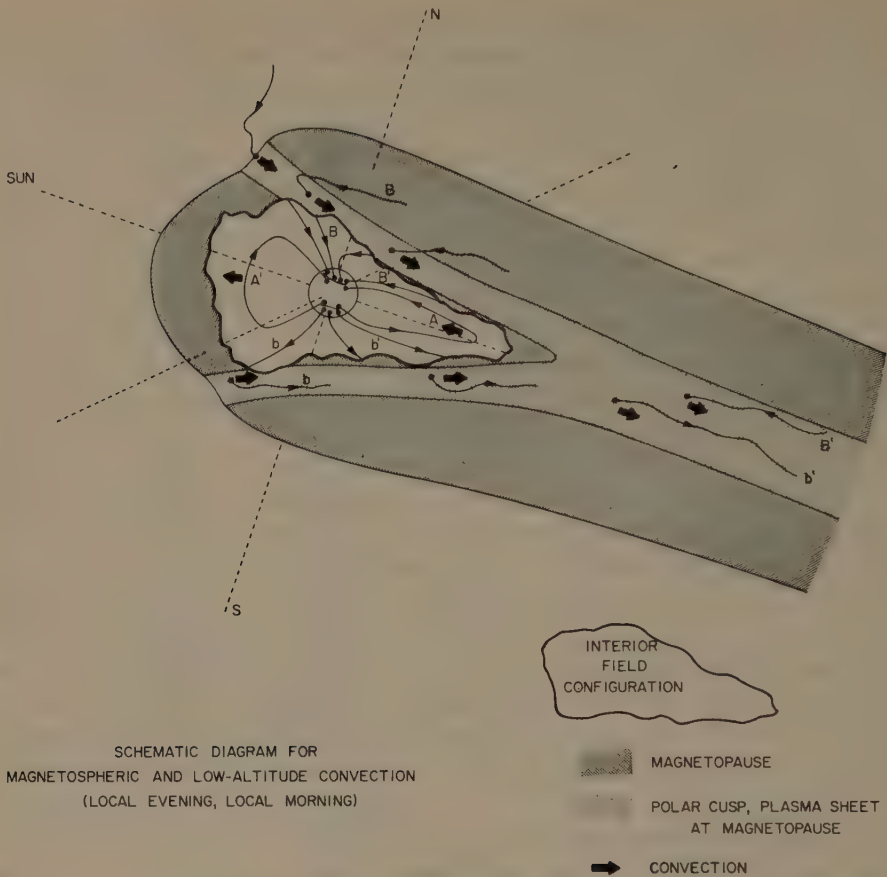


Fig. 8. Schematic diagram showing the proposed model of magnetospheric convection. The electric field reversal and the $E > 45$ keV trapping boundary occur at the boundary between open (B-b and B'-b') and closed (A and A') field lines.

process of merging the geomagnetic field with the solar wind magnetic field proposed by Dungey (1961, 1968), along with the usual 'frozen field' model of plasma flow to explain the coupling of the solar wind convection into a magnetosphere; however, it differs from Dungey's model in the details of the flow over the polar cap region. Magnetic merging along the sunward surface of the magnetosphere allows the direct connection of geomagnetic field lines with the solar wind magnetic field. On the dayside of the magnetosphere, these field lines constitute open field lines through the polar cusp (such as B and b in Figure 8) and provide for the direct entry of magnetosheath plasma to low altitudes within the magnetosphere. Since the plasma convection away from the sun on the dayside of the magnetosphere is usually limited to a relatively narrow zone on the poleward side of the trapping boundary (cf., Figures 3 and 7) the convective flow in the polar cusp region is believed to follow the E-W extension of the polar cusp into the dawn and dusk flanks of the magnetosphere as indicated in

Figure 8. The width of this convection zone, which is initially only a few degrees wide in IN Lat near local noon, increases considerably in the dawn and dusk regions. Subsequent anti-sunward convection carries the field lines into the distant plasma sheet (field lines B' and b') where they again merge to form closed field lines (such as A) in the near earth plasma sheet. (The reader is referred to Frank (1917b) for a discussion of the various plasma regimes involved in this model.) After merging occurs at the neutral sheet the field lines are then convected sunward, toward the front of the magnetosphere (field line A') to complete the flow pattern. This flow pattern for magnetospheric plasma qualitatively accounts for the principal features of the observed convection pattern at low altitudes (cf., Figure 5). It is to be noted that in this model the electric field reversal, which is the boundary between the regions of sunward and anti-sunward flow, occurs on field lines which are in the merging region. Since magnetic merging constitutes a basic process by which energy is dissipated within the magnetosphere, it is understandable that intense electron acceleration and precipitation are associated with the electric field reversals, although the details of these processes remain to be resolved.

Acknowledgments

This research was supported in part by the National Aeronautics and Space Administration under contracts NAS5-10625, NAS1-8141, NAS1-8144(f), NAS1-8150(f), and NGL-16-001-043; and by the Office of Naval Research under Contract N00014-68-A-0196-0003.

References

- Ackerson, K. L. and Frank, L. A.: 1971, *J. Geophys. Res.* to be published.
 Axford, W. I.: 1969, *Rev. Geophys.* **7**, 421.
 Cauffman, D. P. and Gurnett, D. A.: 1971, *J. Geophys. Res.* **76**, 6014.
 Cauffman, D. P. and Gurnett, D. A.: 1972, *Space Sci. Rev.*, submitted.
 Dungey, J. W.: 1961, *Phys. Rev. Letters*, **6**, 47.
 Dungey, J. W.: 1968, in B. M. McCormac (ed.), *Earth's Particles and Fields*, Reinhold Book Corporation, New York, p. 385.
 Fahleson, U. V.: 1967, *Space Sci. Rev.* **7**, 238.
 Frank, L. A.: 1971a, *J. Geophys. Res.* **76**, 5202.
 Frank, L. A.: 1971b, *J. Geophys. Res.* **76**, 2512.
 Frank, L. A. and Ackerson, K. L.: 1971, *J. Geophys. Res.* **76**, 3612.
 Frank, L. A. and Ackerson, K. L.: 1972, *J. Geophys. Res.*, submitted.
 Frank, L. A. and Gurnett, D. A.: 1971, *J. Geophys. Res.* **76**, 6829.
 Gurnett, D. A.: 1970, in B. M. McCormac (ed.), *Particles and Fields in the Magnetosphere*, D. Reidel Publishing Company, Dordrecht, Holland, p. 239.
 Gurnett, D. A. and Frank, L. A.: 1972, *J. Geophys. Res.* **77**, 172.
 Gurnett, D. A., Pfeiffer, G. W., Anderson, R. R., Mosier, S. R., and Cauffman, D. P.: 1969, *J. Geophys. Res.* **74**, 4631.
 Heikkila, W. J. and Winningham, J. D.: 1971, *J. Geophys. Res.* **76**, 883.
 Maynard, N. C.: 1971, *Electric Fields in the Ionosphere and Magnetosphere*, presented at the Advanced Study Institute on Magnetosphere-Ionosphere Interactions, Dalseter, Norway, April 14-23.

PLASMA DRIFTS IN THE AURORAL IONOSPHERE DERIVED FROM BARIUM RELEASES

G. HAERENDEL

*Max-Planck-Institut für Physik und Astrophysik, Institut für extraterr. Physik,
Garching, München, Germany*

Abstract. Barium cloud data on plasma drifts in the auroral ionosphere are reviewed. The convection is directed essentially westward before 2200 MLT and eastward at later night hours; this is opposite to the convection on the polar cap. The west and southward components of the electric field are found to be positively correlated with each other. The correlation is more pronounced in a nonrotating frame of reference. This result and the observed ratios of both field components indicate a dominantly magnetospheric origin of the correlation. Ordering of drift velocities according to typical geomagnetic situations shows the extension of corotation up to the auroral zone during quiet periods. During mildly disturbed periods the typical auroral zone convection pattern shows up with small magnitudes of E_1 (5–15 mV m⁻¹). The growth phase of substorms is characterized by fast westward flows in the evening sector and the region of the westward electrojet by south-easterly motions with speeds of typically 1 km s⁻¹. Close to the evening bulge of the plasmasphere northwestward directed motions were found suggesting a deformation process at work. During a poleward expansion of the auroral oval the plasma drifted southeastward, essentially opposite to the movements of the auroral arcs. This may be understood in terms of the reconnection of magnetic field lines in the tail. Plasma drifts in the westward traveling surge of a substorm are slow and toward the south, but speed up and turn westward after leaving the region of strong auroral precipitation. A model is proposed according to which the westward traveling surge is a result of a reconnection of tail field lines upon which a southeastward directed flow on the polar cap is reversed to a westward one. The existence of strong upward flowing magnetic field aligned currents from the surge is implied.

1. Introduction

The measurement of ionospheric plasma drifts, or equivalently of the transverse component of the electric field

$$\mathbf{E} = -\frac{1}{c}(\mathbf{v} \times \mathbf{B})$$

by means of the Ba plasma cloud technique is possible only during twilight and with a clear sky for the optical observation from groundbased stations. Because of these restrictions this technique is hardly suitable for global applications and for collecting statistical materials. Its main virtue lies in small scale studies of the magnetospheric plasma convection, as it is expressed in the ionosphere. It is instructive, however, to survey the presently available, and fast growing, body of data from many such release experiments in the high latitude ionosphere and order them according to geomagnetic conditions. The seasonal variation of the twilight hours, in particular in northern Scandinavia where the auroral zone is located at relatively high geographic latitudes, allows the coverage of a wide range of local times. In this paper Ba cloud data obtained by the Institut für extraterrestrische Physik will be summarized accordingly. Although the total amount of data is small, distinct differences for dif-

ferent conditions of geomagnetic disturbance become apparent. Some single cases of particular interest will be discussed.

2. Synopsis of Drift Measurements

Figure 1 contains the paths of Ba plasma clouds in a IN Lat (Λ)-MLT plot, i.e., in a nonrotating magnetic coordinate system. It is an updating of a figure presented by Haerendel and Lüst (1970). Numbers were taken from an internal counting system by which the reader can relate the individual paths to dates, places and magnetic conditions with the help of lists and graphs published by Haerendel and Lüst (1970) and, more complete, by Rieger (1971).

A few general conclusions can be drawn from this synopsis, in spite of the great variety of geomagnetic perturbations met during the individual experiments: (a) Drifts are predominantly aximuthal; N-S components are more pronounced near midnight; (b) On the polar cap at $\Lambda = 75$ to 78° , the flow is antisolar towards the midnight sector; in the auroral zone it is reversed; (c) The separation line between west and eastward convection in the auroral zone is found on the average close to 2200 MLT, but varies with latitude and magnetic disturbance; (d) West and northward, and east and southward directed components of the drift appear to be correlated with each other in the auroral zone; and (e) Several occasions of flow reversals have been found, mostly in the sense to turn from a south easterly direction into a generally westward drift.

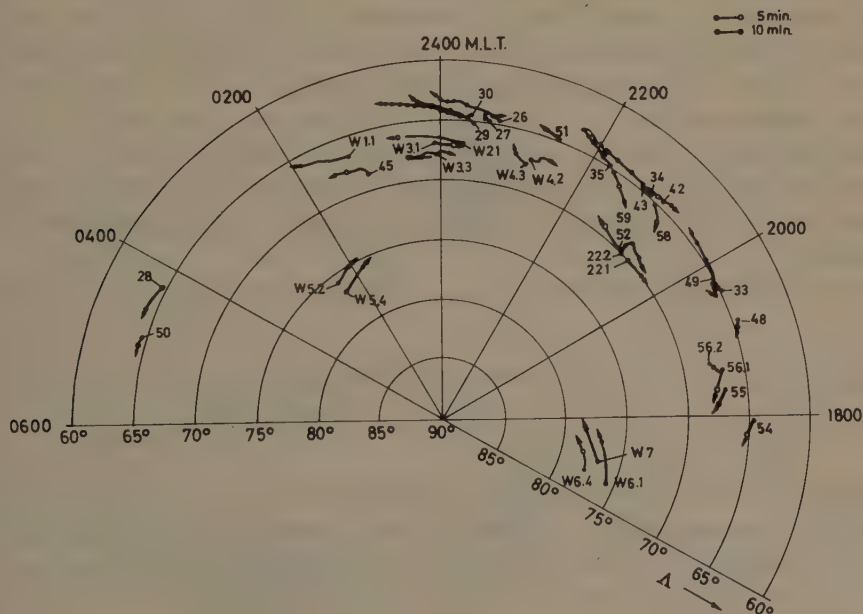


Fig. 1. Paths of Ba clouds in IN Lat-MLT. 5 min intervals end with an open circle, 10 min intervals with a full dot. Numbers preceded with 'W' refer to experiments of Wescott *et al.* (1969, 1970) and Heppner *et al.* (1971).

The flow pattern arising from these data is in agreement with Injun 5 double probe measurements (Cauffman and Gurnett, 1971), with generally higher magnitudes reported by these authors. This need not be due to the higher altitude (700 to 2500 km) of these measurements, but could be a selection effect because of the rather high sensitivity limit of a few tens of mV m^{-1} of the double probe. If the Ba cloud paths are projected along magnetic field lines into the equatorial plane (Haerendel and Lüst, 1970; Haerendel, 1972; Rieger, 1971), some similarity is found with the data inferred from balloon measurements of Mozer and Serlin (1969) and with the electric field model of McIlwain (1972) derived from particle measurements at the geostationary orbit. However, the westward flow of the thermal plasma in the evening sector, which is a prominent feature of our data, does not follow from the latter model.

3. Correlation Between West- and Southward Directed Electric Field Components

The correlation between the meridional and toroidal drift components in the auroral zone (noted in the previous section and reported before by Haerendel and Lüst (1970) and Mozer (1971)) will be inspected a little more closely in order to obtain hints about its origin. Many authors, among them Boström (1964), and more recently Fukushima (1968), Akasofu (1969), Mozer (1971), Aubry (1972), and Fahleson (1972) have suggested an ionospheric origin of the meridional component of the electric field due to polarization effects at inhomogeneities of the conductivity. In these models it is assumed that the primary field is toroidal.

We assume an E-W oriented band of enhanced ionization like the auroral oval as a whole, or individual auroral arcs. The primary field, E_w , drives a Hall current, I_H , in S-N direction. The westward pointing electric fields inside, E_{wi} , and outside, E_{wo} , the high conductivity strip must be equal in an idealized model because of $\text{curl } \mathbf{E} = 0$. But I_{Hi} need not equal I_{Ho} . In order to keep the current divergence-free, a southward Pedersen current, I_p , is set up, driven by a southward oriented polarization field, E_s . In addition magnetic field aligned currents, $I_{||}$, closing in the magnetosphere, may be present.

The continuity of the total current per unit length in E-W direction is expressed by:

$$I_{Hi} - I_{Ho} = I_p + I_{||}.$$

Introducing the height integrated Hall and Pedersen conductivities, $\Sigma_{H,p}$, we obtain:

$$\frac{E_s}{E_w} = \frac{\Sigma_{Hi} - \Sigma_{Ho}}{\Sigma_{Pi}} - \frac{I_{||}}{\Sigma_{Pi} E_w}. \quad (1)$$

In this model the E-W motion is set up in the ionosphere. The ionospheric plasma is dragging the magnetospheric plasma. The force accelerating the magnetospheric plasma is exerted by a transverse current which closes the field aligned currents, $I_{||}$, flowing at the northern and southern borders of the conductivity strip. If there were no dissipation in the magnetosphere, $I_{||}$ would only flow as long as the magnetospheric plasma does not fully participate in the ionospheric convection.

Without looking more closely into the interaction with the magnetosphere, we

derive a simple inequality from Equation (1) by dropping I_{\parallel} as well as Σ_{H_0} (note that Equation (2) considers the inverse of Equation (1)):

$$E_w/E_s > \Sigma_{pi}/\Sigma_{Hi}. \quad (2)$$

The ratios E_w/E_s , as measured with Ba cloud motions, have been plotted in two histograms in Figure 2. West and south are defined with respect to lines of constant λ . The auroral oval, however, has some inclination with respect to these lines in the evening and morning hours. But since most of the data was obtained at late night hours, this should not affect the statistical result seriously. E_w and E_s were derived from averages over the observation period dividing it whenever a reversal occurred. Several clouds released from one rocket were counted once, unless their paths deviated grossly.

If the excess ionization is created by energetic particles we expect $\Sigma_{pi}/\Sigma_{Hi} \gtrsim 0.5$ (Kim and Kim, 1963; Boström, 1964; Föppl *et al.*, 1968). The upper histogram in Figure 2, with E_{\perp} calculated in a rotating frame of reference, does not in general support this expectation, although we have a few such cases.

If instead the correlation were predominantly of magnetospheric origin, we should find a reduced scatter of the data points by calculating E_{\perp} in a nonrotating frame. This is in fact the case as shown in the lower histogram. Although polarization effects in the ionosphere are unavoidable and may be quite appreciable at times, we conclude that the observed correlation is essentially set up in the magnetosphere; or, in other

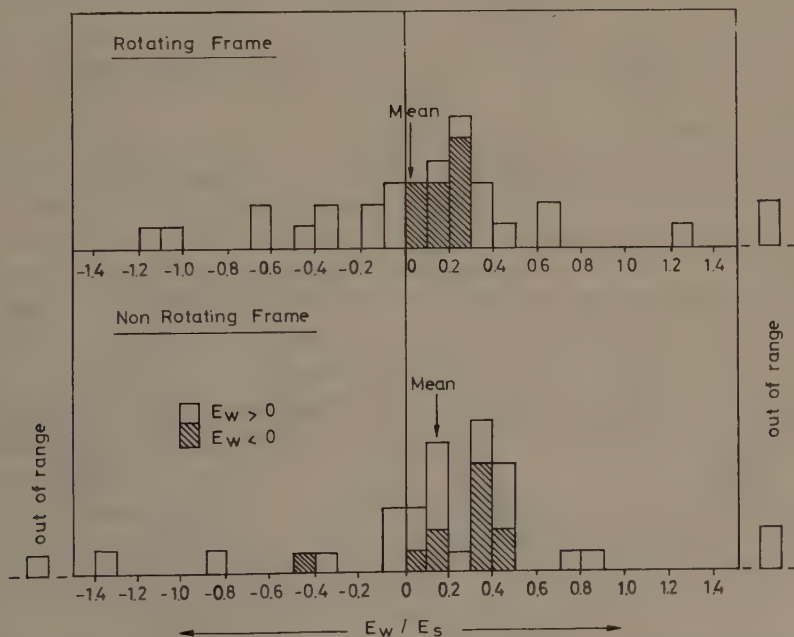


Fig. 2. Distribution of observed ratios E_w/E_s in a frame of reference rotating with the earth (upper histogram) and in a frame stationary with respect to the sun (lower histogram). The electric field components are mean values over intervals of essentially constant orientation.

words, the predominantly toroidal convection in the auroral ionosphere is of magnetospheric origin. One should bear in mind, however, that radial distances in the outer magnetosphere appear rather compressed when projected into the ionosphere, in particular for the nocturnal auroral zone.

4. Drifts During Different Conditions of Magnetic Disturbance

The drift pattern shown in Figure 1 should become somewhat clearer if ordered according to characteristic geomagnetic situations: Four such situations have been

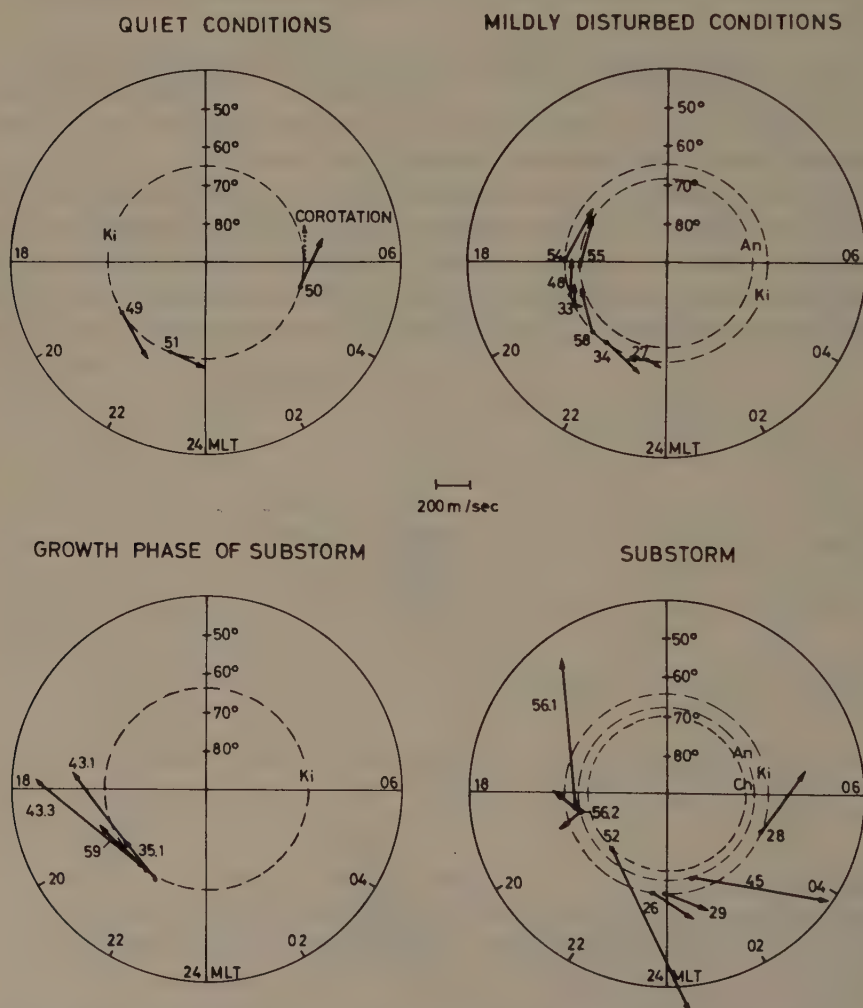


Fig. 3. Mean drift velocity vectors for four different conditions of magnetic perturbation. Corotation speed at the latitude of Kiruna (Ki) is indicated by dotted arrow. Circles labeled with An and Ch refer to Andenes (Norway) and Ft. Churchill (Canada).

chosen: (a) quiet times, (b) mildly disturbed conditions, (c) the growth phase of substorms, and (d) substorms. Events not falling into these categories were omitted. Instead of plotting the drift paths, we indicate the average drift speeds during the observation time by vectors in the four A -MLT diagrams of Figure 3.

(a) Quiet times are defined by magnetic perturbations not exceeding a few tens of gammas for at least 12 hr. Even at the latitude of Kiruna the ionospheric plasma is found to be essentially corotating. During these measurements the plasmopause was most likely located to the north of the clouds. The slight deviations from corotation (dashed arrow) might be impressed by the neutral atmosphere (dynamo effect).

(b) Mildly disturbed conditions are such with perturbations between several tens and about 200 γ not clearly associated with bays. Here we find the typical division of westward convection in the evening auroral zone and eastward convection after about 2200 MLT. Note that the magnitudes range only from about 5 to 15 mV m^{-1} . These data seem to represent the convection outside the plasmasphere between substorm events. As judged from the associated magnetic perturbations it is by no means stationary. It may be identified with the DP 2 field of Nishida (1968a,b) and attain larger amplitudes at somewhat higher latitudes.

(c) The three measurements plotted in the third graph preceded the onset of substorms by a few hours. Characteristic positive perturbations of H were observed at this time at the nearest auroral zone station, whereas the low latitude magnetograms in the evening sector showed the development of a depression of H ending with a recovery during the substorm (Cummings *et al.*, 1968; Akasofu and Meng, 1969; Coleman and McPherron, 1970; McPherron, 1970) and has been called the growth phase (McPherron, 1970). The depression of H found at lower latitudes has been attributed to an asymmetric growth of the ring current (Akasofu and Meng, 1969). The observed velocities are about sufficient to move hot plasma sheet plasma from hours close to midnight to early evening hours. Our few measurements would suggest that the hot plasma piling up in the evening sector prior to the onset of a substorm is not arriving directly from larger radial distances, but approaches the earth at later night hours and is subsequently diverted to the west.

(d) The correlation of south and eastward drift component discussed in Section 3 is very clearly expressed during substorms. This drift direction is associated with the westward electrojet which, according to Akasofu *et al.* (1965), extends to early evening hours at increasing magnetic latitude. The measurements labelled 56 were obtained in and south of a westward traveling surge rather than in the area of the westward electrojet (Section 5c).

It should be noted in this context that the magnitudes of E_{\perp} are not closely correlated with those of ΔH . Apparently, the increase of the transverse conductivity in the E layer by particle impact plays an at least equally important role for the magnitude of ΔH than that of E (Haerendel, 1972; Paschmann, 1971).

The features exhibited by these measurements could well be typical. Large gaps, however, have yet to be filled, not only in local time but also in latitude. In particular the poleward edge of the auroral oval deserves closer inspection.

5. Discussion of Individual Experiments

A. EXPANSION OF THE BULGE OF THE PLASMASPHERE

Three of the experiments plotted under 'mildly disturbed conditions' in Figure 3 were carried out in or at least very close to the evening bulge of the plasmasphere, namely Exp. 48 and 54/55, the latter two being only 1 hr apart. In both cases a positive perturbation of H started between 1600 and 1700 MLT and lasted for about 2 hr. The center of the current was located well north of Kiruna. Nishida (1971) noticed that the cases of asymmetric evening bulges reported by Carpenter (1970a) were accompanied by such positive magnetic perturbations. He suggests that the plasmopause undergoes an unsteady deformation caused by the convection at high latitudes. Our measurements prove the existence of such convective motions.

The paths of four clouds are projected into the equatorial plane in Figure 4 using the model field of Cain *et al.* (1968). The graph shows furthermore Carpenter's (1966) determination of the average position of the plasmopause as well as locations of OGO 5 encounters of steep gradients which are indicative of the evening bulge (Chappell *et al.*, 1970). At the time of Exp. 48 the plasmopause should have been within the drawn brackets according to Injun 4 data of Carpenter (1970b).

In none of these experiments do we have clear information about the relative locations of clouds and plasmopause; but since the positive magnetic perturbation

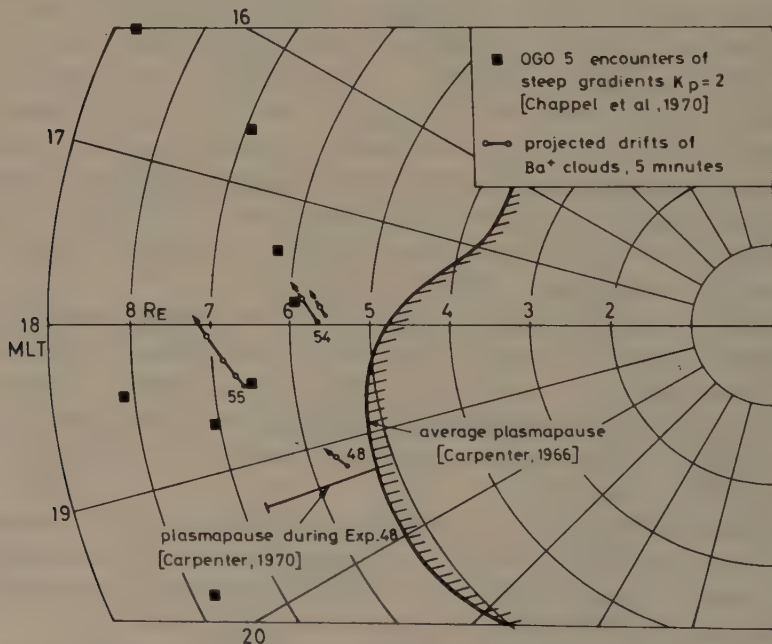


Fig. 4. Barium cloud drifts projected into the equatorial plane. The average position of the bulge of the plasmasphere (Carpenter, 1966), as well as OGO 5 encounters of the bulge (Chappell *et al.*, 1970) are shown. During Exp. 48 the plasmopause was located within the drawn brackets.

was preceded by very quiet fields at Kiruna for several days, K_p being typically 20, it is likely that at least the clouds of Exp. 54 as well as those of Exp. 48 were inside the plasmasphere.

If the outer parts of the plasmasphere were exposed to the observed motions for the period of the magnetic perturbations, deformations of the plasmopause extending several R_E would result. Such deformations or even detachments were inferred from plasma measurements by Carpenter (1970a), Chappell *et al.* (1970), and Chappell (1972).

In Exp. 54 altogether five clouds were released from one rocket. Only two of the paths are shown in Figure 4. A marked gradient of the electric field was found, an increase by a factor of 2 over about 80 km from south to north. If we had a confirmation that these clouds were actually south of the plasmopause, we would interpret this result as showing that the electric field corresponding to the high latitude/low density plasma convection does not penetrate very deeply into the plasmasphere.

B. POLEWARD EXPANSION OF THE AURORAL OVAL

Exp. 52 was carried out during the expansion phase of a substorm. The poleward boundary was just passing the Ft. Churchill area. ΔH was below -2000γ . Figure 5

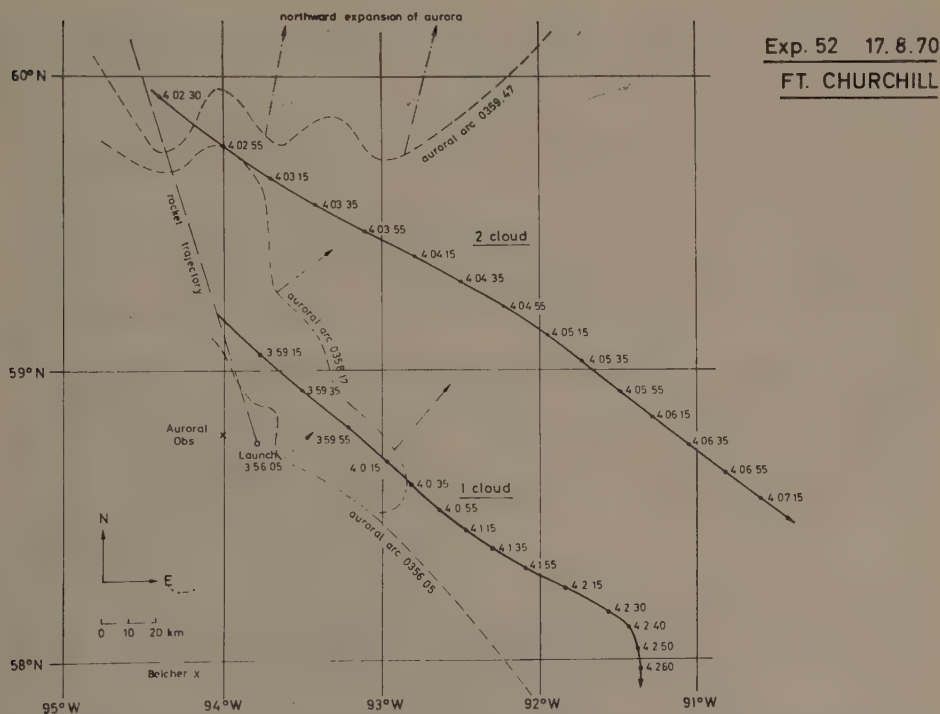


Fig. 5. Paths of two Ba clouds projected to the 100 km level during a poleward expansion of the auroral oval. Three successive positions of the northernmost arc are shown. Times in hours, minutes, seconds UT.

contains the paths of the ion clouds projected along magnetic field lines to the 100 km level, and furthermore three successive positions of the northernmost arc shortly before and after the first release. The most striking feature is the rather steady plasma drift towards southeast, typical of a westward electrojet, in the presence of the northward motion of quite irregular auroral forms. The electric field strength varied between 50 and 80 mV m⁻¹.

Relative motions of ionospheric plasma and auroral forms have been reported before by Wescott *et al.* (1970) and by Kelley *et al.* (1971). A consistent interpretation of this observation can be given in terms of a reconnection process at the neutral sheet (Axford, 1967). The locus of reconnection accompanied by precipitation could involve flux tubes originating at successively higher latitudes while the plasma convection proceeds towards the earth with an eastward component.

C. DRIFTS AND CURRENTS IN THE WESTWARD TRAVELING SURGE

In Exp. 56, 2 Ba clouds were released north of Andenes, just after the arrival of a westward traveling surge which came to a halt in this area. Within 15 min the typical loop structure faded away and reappeared several times with rapidly changing forms. Auroral arcs were crossing several times the position of the northern cloud without noticeably affecting the cloud's motion. One such event is shown in Figure 6 together with the cloud's paths projected to the 100 km level.

The electric field exhibited a strong spatial variation. The westward drift of the first cloud south of the surge corresponds to a northward pointing E_{\perp} of 60 to

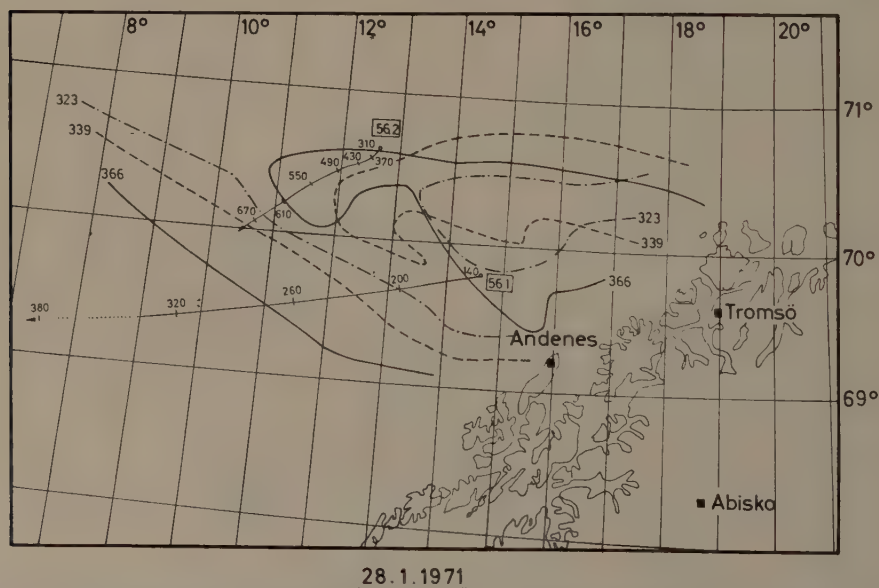


Fig. 6. Three successive positions of auroral arcs belonging to a westward traveling surge and 2 Ba cloud paths projected to the 100 km level. Times in seconds after launch.

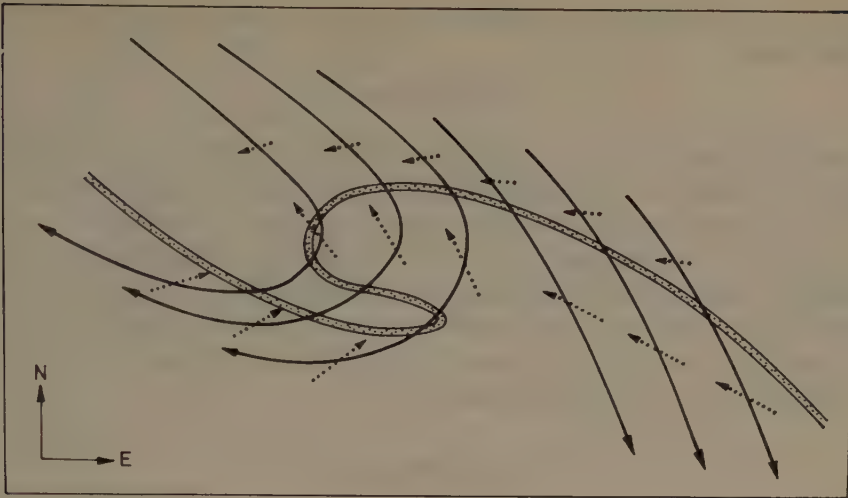


Fig. 7. Suggested plasma convection pattern (solid lines) through a westward traveling surge (dotted band indicates the poleward boundary of the auroral forms). Drift motions are slow when passing through the aurora. Dotted arrows show the direction of the transverse electric currents suggesting field aligned currents to emerge from the surge.

80 mV m^{-1} , whereas the second cloud, just above the loop structure, started to move very slowly southward with a $5 \text{ to } 10 \text{ mV m}^{-1}$ field. As it emerged from the loop region it speeded up reaching later velocities similar to that of the first cloud.

The generally westward drift south of the surge was consistent with the positive ΔH measured in Tromsø, Andenes, and further to the south. The magnetogram of Bear Island ($\approx 400 \text{ km}$ north of Tromsø), however, showed negative ΔH . This is in agreement with the findings of Akasofu *et al.* (1965) that the westward electrojet extends to early evening hours at the poleward side of the westward traveling surge. The southeastward drift motion typical of this current would drive plasma towards the surge.

It is only a small step to derive the complete flow pattern of the plasma, of which the part south of the surge is exhibited by the second cloud. This is qualitatively sketched in Figure 7. The reversal characterized by low velocity and accompanied by strong precipitation may well be set up in a reconnection process converting open tail field lines into closed ones returning towards the sun. The independence of auroral and plasma motions fits into this picture.

The arrows in Figure 7 indicate the general direction of the transverse current assuming about equal Pedersen and Hall conductivities. Although we do not have a measurement of the conductivity distribution, the transverse current pattern is likely to have a positive divergence. Field aligned currents from the surge region into the magnetosphere are postulated in accordance with earlier suggestions of Akasofu and Meng (1969) and Akasofu (1969) and with the positive ΔD observed at low latitude stations south of Tromsø. Akasofu *et al.* (1969) estimated that the flux of pre-

cipitating electrons would be sufficient to carry this field aligned current in the magnetosphere.

6. Conclusions

This survey of plasma drift measurements in the auroral zone throws some light on the convection in characteristic geomagnetic situations. The data generally support ideas derived from other observations, as for instance with regard to the expansive motions of the bulge of the plasmasphere or to the northward expansion of the auroral precipitation pattern opposite to the plasma flow. One of the most urgent tasks to be attempted is the simultaneous measurement of the electric field at the same magnetic flux tubes but at very different altitudes. This affords the development of a good technique applicable in the upper magnetosphere.

Acknowledgments

My sincere thanks belong to all my colleagues who helped making these rocket experiments a success. Figure 5 was taken from a report prepared by Dr H. Kappler.

References

- Akasofu, S.-I.: 1969, *Nature* **221**, 1020.
 Akasofu, S.-I., and Meng, C.-I.: 1969, *J. Geophys. Res.* **74**, 293.
 Akasofu, S.-I., Chapman, S., and Meng, C.-I.: 1965, *J. Atmospheric Terrest. Phys.* **27**, 1275.
 Akasofu, S.-I., Eather, R. H., and Bradbury, J. N.: 1969, *Planetary Space Sci.* **17**, 1409.
 Aubry, M. P.: 1972, this volume, p. 357.
 Axford, W. I.: 1967, B. M. McCormac (ed.), in *Aurora and Airglow*, Reinhold Publishing Corporation, New York, 499.
 Boström, R.: 1964, *J. Geophys. Res.* **69**, 4983.
 Cain, J. C., Hendricks, S., Daniels, W. E., and Jensen, D. C.: 1968, 'Computation of the Main Geomagnetic Field From Spherical Harmonic Expansions', *Data Users' Note* NSSDC 68-11, NASA GSFC, 41.
 Carpenter, D. L.: 1966, *J. Geophys. Res.* **71**, 693.
 Carpenter, D. L.: 1970a, *J. Geophys. Res.* **75**, 3837.
 Carpenter, D. L.: 1970b, private communication.
 Cauffman, D. P. and Gurnett, D. A.: 1971, *J. Geophys. Res.* **76**, 6014.
 Chappell, C. R.: 1972, this volume p. 280.
 Chappell, C. R., Harris, K. K., and Sharp, G. W.: 1970, *J. Geophys. Res.* **75**, 3848.
 Coleman, Jr., P. J. and McPherron, R. L.: 1970, B. M. McCormac (ed.), in *Particles and Fields in the Magnetosphere*, Reidel Publishing Company, Dordrecht, Holland, p. 171.
 Cummings, W. D., Barfield, J. N., and Coleman, Jr., P. J.: 1968, *J. Geophys. Res.* **73**, 6687.
 Fahleson, U. V.: 1972, this volume, p. 223.
 Föppl, H., Haerendel, G., Haser, L., Lüst, R., Melzner, F., Meyer, B., Neuss, H., Rabben, H.-H., Rieger, E., Stöcker, J., and Stoffregen, W.: 1968, *J. Geophys. Res.* **73**, 21.
 Fukushima, N.: 1968, *Rep. Ionosphere Space Res. Japan*, **22**, 173.
 Haerendel, G.: 1972, in E. R. Dyer (General ed.), *Solar-Terrestrial Physics/1970, Part IV*, D. Reidel Publishing Company, Dordrecht, Holland, p. 87.
 Haerendel, G. and Lüst, R.: 1970, in B. M. McCormac (ed.), *Particles and Fields in the Magnetosphere*, D. Reidel Publishing Company, Dordrecht, Holland, p. 213.
 Heppner, J. P., Stolarik, J. D., and Wescott, E. M.: 1971, *J. Geophys. Res.* **76**, 6028.
 Kelley, M. C., Starr, J. A., and Mozer, F. S.: 1971, *J. Geophys. Res.* **76**, 5269.
 Kim, H. Y. and Kim, J. S.: 1963, *J. Atmospheric Terrest. Phys.* **25**, 481.

- McIlwain, C. E.: 1972, this volume, p. 268.
- McPherron, R. L.: 1970, *J. Geophys. Res.* **75**, 5592.
- Mozer, F. S.: 1971, *J. Geophys. Res.* **76**, 7595.
- Mozer, F. S. and Serlin, R.: 1969, *J. Geophys. Res.* **74**, 4739.
- Nishida, A.: 1968a, *J. Geophys. Res.* **73**, 1795.
- Nishida, A.: 1968b, *J. Geophys. Res.* **73**, 5549.
- Nishida, A.: 1971, 'Deformation of the Dusk-side Plasmopause', preprint.
- Paschmann, G.: 1971, private communication.
- Rieger, E.: 1971, *Z. Geophys.* **37**, 795.
- Wescott, E. M., Stolarik, J. D., and Heppner, J. P.: 1969, *J. Geophys. Res.* **74**, 3469.
- Wescott, E. M., Stolarik, J. D., and Heppner, J. P.: 1970, B. M. McCormac (ed.), in *Particles and Fields in the Magnetosphere*, D. Reidel Publishing Company, Dordrecht, Holland, p. 229.

ACCELERATION OF AURORAL PARTICLES BY ELECTRIC DOUBLE LAYERS

LARS P. BLOCK.

Division of Plasma Physics, Royal Institute of Technology, Stockholm, Sweden

Abstract. Recent observations of precipitating particles and motions of auroral forms indicate that auroral particles are accelerated by electric fields directed along the magnetic field. Such electric fields have also been observed. It is argued that large field aligned potential drops should sometimes be concentrated in thin double layers (sheaths). Properties and consequences of such sheaths are reviewed and compared with evidence from several rocket and satellite observations.

It is pointed out that parallel electric fields due to anomalous resistivity may not produce secondary energy distribution peaks, nearly monoenergetic precipitation, and anisotropies since anomalous resistivity is due to scattering processes that should wipe out such peaks. It seems more likely that the acceleration occurs in sheaths, and the velocity distributions may then be partly smoothed out by instabilities.

1. Introduction

The acceleration of auroral particles is still a major problem in magnetospheric physics. The results of measurements on auroral particles have revealed very complex properties, and it seems impossible to account for them by one single acceleration mechanism alone.

The purpose of the present paper is to show that at least sometimes particles may be accelerated in electrostatic double layers. A sheath is an electrostatic structure with a potential drop much larger than kT/e of the plasma existing over a distance smaller than a mean free path, usually of the order of several Debye lengths. Only sheaths with potential drops directed along the magnetic field will be considered here.

2. Observed Properties of Particle Fluxes

Both electrons and ions (usually protons) may cause aurora. Most auroras are due to particles with energies of the order of 100 eV to 10 keV. Their spectra are often rather sharply peaked at a few keV, sometimes even double peaked.

The pitch angle distributions are often anisotropic with most of the flux, sometimes along the magnetic field and sometimes perpendicular to it. In one experiment (Albert and Lindstrom, 1970) multiple peaked pitch angle distributions were observed which were interpreted as due to three sheaths above the rocket. (This will be discussed in Section 7.) Hones *et al.* (1971) have found fluxes of extremely field-aligned protons and electrons in the plasma sheet.

The particles may precipitate in bursts with the fluxes tending towards isotropy, but being peaked 90° from the field between bursts. The rise time of precipitation events may be as short as about 1 s.

For further details of precipitating particle properties see Block (1972), Hones *et al.* (1971), and references therein.

3. Observations of Electric Fields

During the last few years methods have been developed for measuring electric fields in space. Mostly, fields perpendicular to the magnetic field, E_{\perp} , have been measured, but in a few cases E_{\parallel} has also been obtained (Kelley *et al.*, 1970; Mozer and Fahleson, 1970; Kelley, 1971). The following facts are important:

(a) E_{\parallel} has been measured only with double probes. The influence of E_{\parallel} on a Ba cloud is not yet fully understood. In one case $E_{\parallel} \approx 30 \text{ mV m}^{-1}$ was measured with double probes, while these same probes recorded an E_{\perp} in good agreement with simultaneous Ba cloud measurements (Kelley, 1971). No obvious effect of E_{\parallel} was observed on the Ba cloud.

(b) Since sheaths are quite limited spatially, their E_{\parallel} might have escaped experimenter's attention, or been rejected as spurious signals.

(c) So far all observations of E_{\parallel} have been made at F region altitudes and E_{\parallel} was downwards in all cases.

(d) Abrupt reversals in E_{\perp} have been frequently observed by Cauffman and Gurnett (1971) at auroral latitudes in the topside ionosphere (677 to 2528 km altitude). E_{\perp} oscillations (probably spatial with typical scale lengths $\sim 30 \text{ km}$) were observed with much larger amplitudes at the higher altitudes than at the lower, implying potential drops of the order of 1 kV along the magnetic field between 700 and 2500 km.

(e) Mozer and Fahleson (1970) find reversals or oscillations in E_{\perp} near auroral arc boundaries at 300 to 400 km altitude. They may somehow be connected with those seen by Cauffmann and Gurnett at higher altitudes.

4. Possible Causes of E_{\parallel}

Electric fields along the geomagnetic field may occur even if no currents are flowing, provided the electrons and ions have different pitch angle distributions (Alfvén and Fälthammar, 1963; Persson, 1966; Block, 1967). Hultqvist (1970) has drawn attention to the fact that thermo-electric effects occur in collisional plasmas. He suggests that this should give rise to a potential difference between the cold ionosphere and the hot plasma sheet where the temperature is often several keV. Since particle collisions are negligible in this region of space, he assumes that wave-particle interactions play the same role. However, it is questionable if this could explain the observed precipitation characteristics (see Section 8).

It seems likely, however, that E_{\parallel} normally occurs in the presence of field aligned currents. The observed field aligned current densities (10^{-6} – $10^{-4} \text{ amp m}^{-2}$) are sufficient to cause anomalous, turbulent conductivity (Swift, 1965; Kindel and Kennel, 1971).

In all cases mentioned, E_{\parallel} is distributed over large distances. However, it has been shown that the two-stream instability (often assumed to cause anomalous conductivity) may asymptotically develop into laminar sheath-like structures (Armstrong, 1967a, b; Berk and Roberts, 1967; Dawson, 1968). A potential drop along a geomagnetic field line would then be concentrated mainly in sheaths.

5. Properties of Sheaths

Sheaths are frequently observed in laboratory gas discharges when a current flows between two plasma regions with different properties (temperature and density). They should, therefore, occur at field aligned currents between the ionosphere and the magnetosphere.

The simplest structure of a sheath is shown in Figure 1. The z axis is directed along the magnetic field and the sheath is supposed to have a large extent in the x and y directions.

We should first consider the Bohm criterion (Bohm, 1949) which is necessary for the occurrence of a sheath. Consider a thermal plasma to the right of the sheath (in the $+z$ direction). Ions are reflected by the sheath potential. Boltzmann's law gives their density in the sheath

$$n_i = n_0 e^{-(eV/kT_i)} \quad (1)$$

with obvious notations.

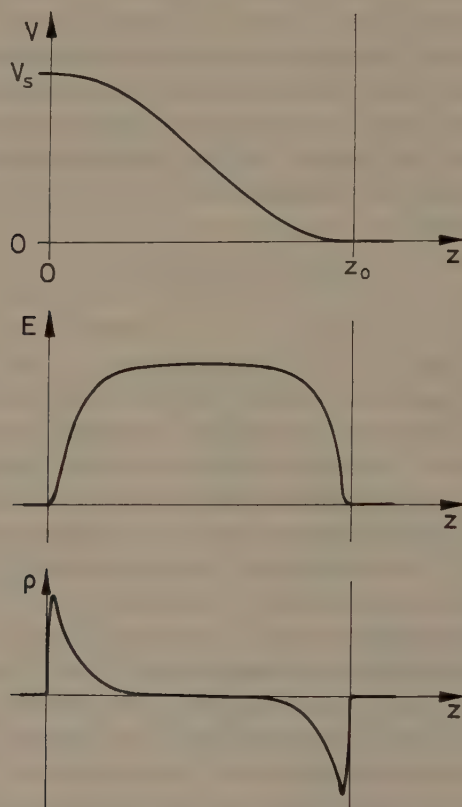


Fig. 1. Potential, V , electric field, E , and space charge, ρ , in a simple sheath. The z axis is supposed to be along the magnetic field.

Electrons from the right are accelerated through the sheath; hence, they have a linear mean velocity in the $-z$ direction. Conservation of their flux gives their density in the sheath (neglecting their temperature)

$$n_e = n_0 v_{e0} \left(v_{e0}^2 + \frac{2eV}{m_e} \right)^{-1/2}. \quad (2)$$

At $V=0$ we have $n_e = n_i = n_0$. At slightly positive V a negative space charge exists in the sheath of Figure 1. A positive space charge would tend to diminish the electric field and counteract the build-up of the sheath. Hence, we require $n_e > n_i$ at small positive V . Differentiating Equations (1) and (2) we find that this requires

$$m_e v_{e0}^2 \geq kT_i \quad (3)$$

at $V=0$. Similarly, at the sheath boundary to the left we must have

$$m_i v_{i0}^2 \geq kT_e. \quad (4)$$

These are the Bohm criteria, implying that a certain preacceleration of the beam particles is necessary before their final acceleration in the sheath.

We may conclude that if field aligned current densities imply supersonic flow of some particle species somewhere along the current path, then a sheath may appear. Numerically, this is about equal to the threshold for various instabilities, supposed to cause anomalous conductivity.

Theoretical analysis of field aligned currents and topside ionospheric properties shows that the most likely sheath altitudes are at a few thousand km where the plasma is 'weakest.' Sheaths may also occur at much lower altitudes provided the current densities are higher there ($\sim 10^{-4}$ amp m^{-2} compared to $\sim 10^{-7}$ at 10000 km). This is analyzed in detail by Block (1972).

The electric field is much stronger in the sheath than outside on both sides, so the net charge integrated through the sheath must be small. Since an electron spends a shorter time than an ion in the sheath the electron flux ϕ_e must be larger than the ion flux ϕ_i . It is easily shown that if no particles are reflected by the sheath

$$\phi_e / \phi_i = (m_i / m_e)^{1/2}. \quad (5)$$

This is called the Langmuir condition (Langmuir, 1929).

Reflected particles may drastically modify this condition, provided their energy is comparable to eV_s where V_s is the total potential drop across the sheath (Block, 1972).

It is important to note that the Langmuir condition applies in the frame of the sheath, i.e., the sheath is at rest. The supply of charged particles to the sheath from both sides may not obey Equation (5) in what might have been defined as the rest frame. However, there always exists some frame in which the condition in Equation (5) is fulfilled. This frame defines the motion of the sheath in the rest frame, where it may be regarded as an electrostatic pulse or wave packet.

6. The Growth of a Sheath

Consider the left half of the sheath in Figure 1. Neglecting thermal energies, beam particles (electrons) from the right (their density being small due to their high speed after acceleration through the right half), as well as reflected particles, the potential distribution is approximately given by Childs law adapted for a hypothetical vacuum 'ion diod' (see e.g., Hemenway *et al.*, 1967).

$$V(z)_+ = V_s - \left(\frac{81 z^4 I_i^2 m_i}{32 e \epsilon_0^2} \right)^{1/3}, \quad (6)$$

where $I_i = e \phi_i$ is the ion current through the sheath. A corresponding analysis of the right half would yield

$$V(z)_- = \left(\frac{81 (z_0 - z)^4 I_e^2 m_e}{32 e \epsilon_0^2} \right)^{1/3} \quad (7)$$

at $z_0/2 < z < z_0$. Because of Langmuir's condition

$$I_i^2 m_i = I_e^2 m_e$$

so that the halves are antisymmetric.

The sheath potential V_s , current I , and thickness z_0 may be functions of time, with Equations (6) and (7) being valid in their respective halves, if the change is small during the time it takes for an ion to traverse the sheath.

Consider a special case. Suppose energetic electrons with nearly 90° pitch angles are injected at a certain fixed altitude in the presence of an ambient plasma with temperature T and density n . Ions from below (and above) are attracted to this region and thermal electrons are repelled. A sheath starts growing with its upper edge, $z = z_0$, at the injection altitude, and the lower edge moving downwards with velocity

$$u = (kT/m_i)^{1/2} \quad (8)$$

so that the Bohm criterion in Equation (4) is satisfied. The frame of Figure 1 is also moving downwards with the same speed. The ion current through the sheath is then

$$I_i = en (kT/m_i)^{1/2} \quad (9)$$

and the sheath thickness is

$$z_0 = I_i t / en, \quad (10)$$

where t is the time from the start of the process. By introducing Equations (9) and (10) into Equation (6) putting $z = z_0/2$ and $V(z)_+ = V_s/2$, we get

$$t^4 = \left(\frac{16 \epsilon_0 m_i}{9 n k T} \right)^2 \frac{V_s^3}{e k T} = 1.65 \times 10^{12} \frac{M^2 V_s^3}{n^2 T^3}, \quad (11)$$

where M is the mass number of the ions.

The electron flux through the sheath may differ from that given by the Langmuir condition, because of the diamagnetism of electrons with near 90° pitch angles.

Sheaths of this kind may serve as pitch angle scatterers, perhaps short lived, appearing and disappearing at random but possibly also stationary.

7. Application to Observations

A. EXPERIMENT BY ALBERT AND LINDSTROM

The only observation directly interpreted in terms of sheaths was reported by Albert and Lindstrom (1970). They utilized a pitch angle resolution as good as about $\frac{1}{2}^\circ$. Below a sheath, accelerating particles downwards, there should be no particles with pitch angles between 90° and some limiting angle, α , that depends on the particle energy. Further down, α should tend closer to 90° as the mirror height of the accelerated particles is approached. Albert and Lindstrom observed such effects due to three simultaneous stable sheaths at altitudes ~ 250 , 270 , and 280 km. The two upper sheaths had potentials of about 160 V each and the lower one 80 V. They accelerated electrons downwards. Electrons scattered into the forbidden pitch angle regions were trapped between the sheaths and the magnetic mirror below. They contributed to the space charges in the sheaths, thus modifying the Langmuir condition.

B. VELA OBSERVATIONS OF FIELD ALIGNED PARTICLE FLUXES

Hones *et al.* (1971) have observed extremely field aligned electron and proton fluxes with energies as high as 45 keV. Within a cone of $\sim 15^\circ$ full angle (possibly much less) along the magnetic field the intensity was 20 to 30 times higher than that perpendicular to the field. VELA was in the plasma sheet at $\sim 18 R_E$. Sheaths with sufficiently high potentials at a few thousand km altitude (the most probable sheath altitude, cf. Section 5) should produce such fluxes away from the earth. Far below the sheath less anisotropic downward fluxes should be observed because of the mirroring effect.

Causes other than sheaths may possibly produce highly field aligned particle fluxes. That will be further discussed in Section 8.

C. TEMPORAL VARIATIONS OF PRECIPITATION

In two rocket experiments (Whalen and McDiarmid, 1970) large temporal variations were observed in energetic particle precipitation. When the northern edge of a series of northward-propagating auroral arcs passed a rocket, electron precipitation increased and the spectrum hardened considerably with a time constant less than about 2 s. Lower energy particles (> 25 keV) arrived about 1 s *before* high energy (> 75 keV) particles.

Although these observations could be due to a number of causes, it is tempting to ascribe them to a growing sheath, as outlined in Section 6. A potential source is moving towards higher L values as indicated by the northward moving arcs. It gives rise to a sheath at lower altitudes in a plasma, that is *not* moving with the same speed (at least not yet). When this plasma suddenly feels the arrival of the potential source a

sheath grows up approximately as described in Equation (11). Reasonable plasma properties give the right order of magnitude for the delay time between 25 and 75 keV electrons. For example, $V_s = 50$ keV, $T = 10^4$ K, and $n = 10^7 \text{ m}^{-3}$ give $t \sim 1$ s. The nearly isotropic fluxes observed on this occasion may be due to several sheaths at different altitudes, with injection of nearly 90° pitch angle particles in-between. The potential drop of each sheath is about equal to the typical perpendicular energy of the particles injected between that sheath and the next higher one.

D. ELECTRIC FIELD REVERSALS

A sheath cannot be infinitely extended perpendicular to the magnetic field. The equipotentials must turn upwards or downwards at the sheath 'boundaries', as originally proposed by Block (1969), and later developed by Carlqvist and Boström (1970). Figure 2 illustrates how this may lead to enhancements and reversals of E_\perp .

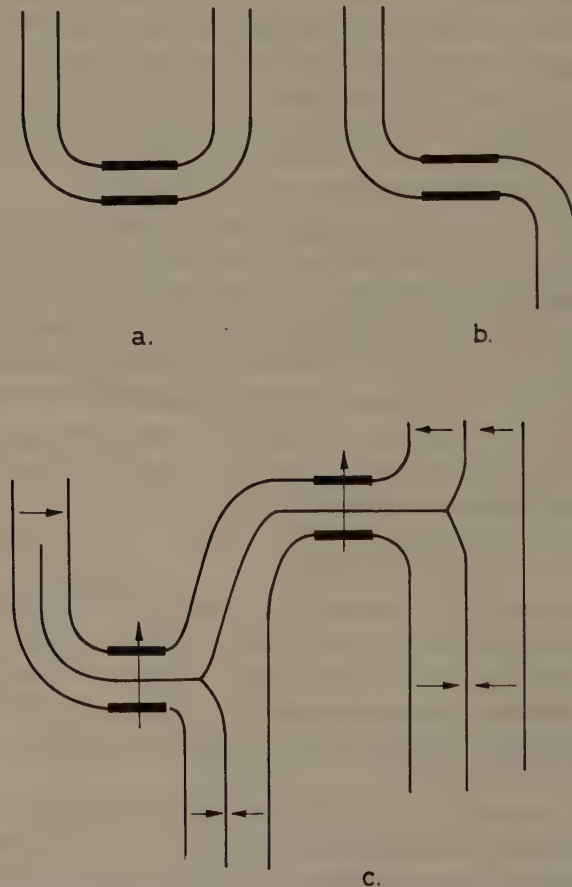


Fig. 2. Qualitative picture of equipotentials in sheaths and their neighborhood. The arrows indicate electric field directions. The heavy lines show the location of the sheaths.

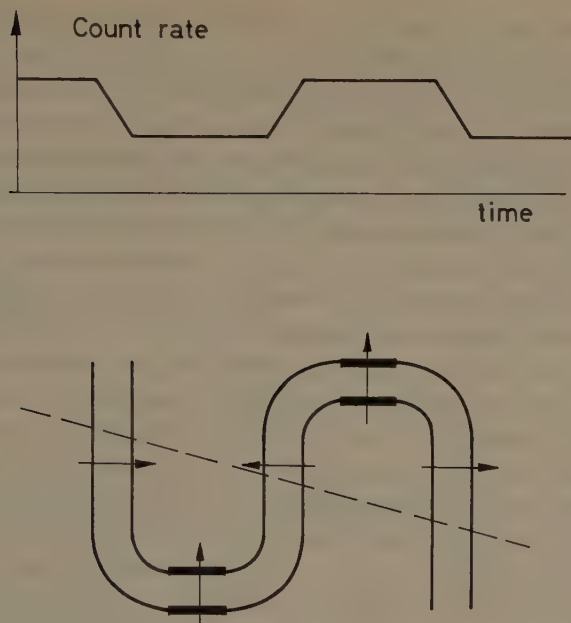


Fig. 3. Qualitative count rate variation for electrons with near 90° pitch angles, as observed on a rocket passing through a region with sheaths below and above the trajectory. The broken line is the trajectory.

above and below the sheaths, as has been observed by Cauffman and Gurnett (1971), and Mozer and Fahleson (1970). The latter authors observed charge oscillations at auroral arc boundaries involving more than one field reversal. Fluxes of 20 keV electrons with nearly 90° pitch angles were found to vary considerably within these oscillations. A qualitative picture of how the equipotentials with associated count rates may show up along a rocket trajectory in a similar situation is given in Figure 3. It should be possible to construct such pictures (perhaps even more complicated) from a detailed analysis of Mozer and Fahleson's raw data. Integration of E_\perp across one half oscillation gives a few hundred V which should appear as E_\parallel in the sheaths. This may be sufficient to account for considerable flux changes of 20 keV, 90° pitch angle electrons (depending on the degree of anisotropy).

8. Discussion

Anomalous or turbulent resistivity has been most frequently discussed as a source for acceleration of auroral particles through the resulting E_\parallel . However, it has never been satisfactorily explained how particles can be accelerated in this way, since *the turbulence is impeding the acceleration*, that would otherwise give rise to abnormally large currents. That is the very mechanism by which anomalous resistivity arises. Thus, extra peaks in the energy distribution cannot be produced in this way. It seems more

likely that monoenergetic fluxes are produced in sheaths, then partly smoothed out, and made more isotropic by instabilities.

It may be possible, of course, that there are two groups of particles, one main group responsible for the turbulence, and another more energetic but less dense group that is unaffected by small scale fields. Ions should also be less affected by turbulence. For example, Reme and Bosqued (1971) have proposed that energetic electron precipitation in the E region drives a return current of cold electrons producing anomalous resistivity. The resulting E_{\parallel} then accelerates protons downwards. This may be a possible mechanism, but *the precise conditions when particles can be accelerated by anomalous resistivity fields should be theoretically clarified.*

It is interesting to note that only downward directed E_{\parallel} has been recorded so far (Section 3). On the other hand, the observations of sheaths by Albert and Lindstrom (1970) indicated an upward electric field in the sheath. Are sheaths stable in the F region for upward electric field only so that downward fields give rise to turbulence instead of sheaths? This is an unsolved theoretical problem, but laboratory experience indicates that this may be the case (Block, 1972). The conditions above the F region are not known, since no measurements of E_{\parallel} have been made there.

The thermo-electric fields suggested by Hultqvist (1970) are directly dependent on 'collisional' effects, not only on cold but also on hot particles, i.e., just those assumed to produce the observed extra peaks of nearly monoenergetic precipitation. Thus, it appears that a temperature gradient, which must necessarily extend over many mean free paths, cannot possibly produce secondary energy distribution peaks or anisotropies. However, a sheath with a thickness much less than a mean free path may serve as a boundary between plasmas with different temperatures, as is frequently observed in laboratory discharges (Torvén, 1968, and references therein).

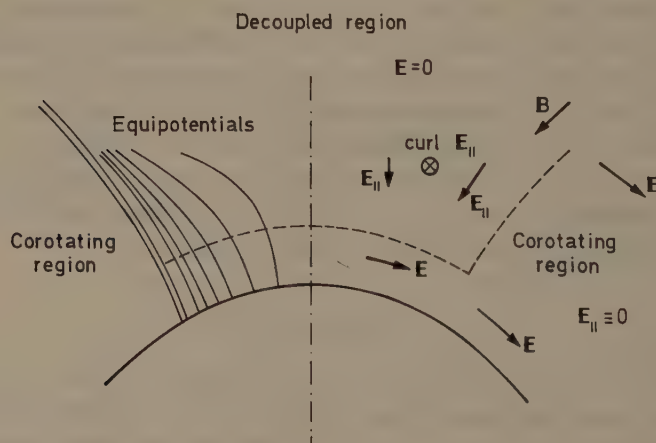


Fig. 4. Decoupling of the plasma on polar cap magnetic field lines from corotation with the lower ionosphere requires that the magnetic field lines are not electric equipotential lines, i.e., $E_{\parallel} = \mathbf{E} \cdot \mathbf{B} / B \neq 0$. The Fig. shows qualitatively the spatial variation of E_{\parallel} in the case of zero field above and smooth transition. If the decoupling occurs via sheaths, there will be sharp knees in the equipotentials.

The field aligned currents and electric fields, whether associated with sheaths or not, are driven by magnetospheric phenomena. For example, the structure of Figure 2b may be the result of a changing magnetospheric convection pattern. If the entire structure is moving towards the left of the Figure the plasma motion is reversed earlier in the magnetosphere and later in the ionosphere, due to field aligned currents that couple the two regions with each other. Figure 4 illustrates another but stationary example namely the interaction between the earth's corotation field in the polar cap ionosphere, and a decoupled convecting plasma at higher altitudes. The result is a field reversal with a large field strength spike on at least one side of the reversal (Fälthammar and Block, 1971). The connection with the field reversals observed by Cauffman and Gurnett (1971) is obvious.

References

- Albert, R. D. and Lindstrom, P. J.: 1970, *Science* **170**, 1398.
- Alfvén, H. and Fälthammar, C.-G.: 1963, in *Cosmical Electrodynamics, Fundamental Principles* (2nd edition), Oxford University Press.
- Armstrong, T. P.: 1967a, *Phys. Fluids* **10**, 1269.
- Armstrong, T. P.: 1967b, *Symposium on Computer Simulation of Plasma and Many-Body Problems*, Williamsburg, Va, NASA, p. 145.
- Berk, H. L. and Roberts, K. V.: 1967, *Phys. Fluids* **10**, 1595.
- Block, L. P.: 1967, *Space Sci. Rev.* **7**, 198.
- Block, L. P.: 1969, *Proc. of the Ninth Internat. Conf. on Phenomena in Ionized Gases*, Bucharest, Rumania, in press.
- Block, L. P.: 1972, *Cosmic Electrodyn.*, to be published.
- Bohm, D.: 1949, in A. Guthrie and R. K. Wakerling (eds.), *The Characteristics of Electrical Discharges in Magnetic Fields*, McGraw-Hill, New-York, p. 77.
- Carlqvist, P. and Boström, R.: 1970, *J. Geophys. Res.* **75**, 7140.
- Cauffman, D. P. and Gurnett, D. A.: 1971, Univ. of Iowa, Rep. 71:4.
- Dawson, J.: 1968, *Third Conf. on Plasma Phys. and Contr. Nucl. Fusion Res.*, CN-24/E-11, Novosibirsk, U.S.S.R.
- Fälthammar, C.-G. and Block, L. P.: 1971, *Proc. ESRO Colloquim on Wave Particle Interactions in the Magnetosphere*, Orléans, France, ESRO SP-72, p. 147.
- Hemenway, C. L., Henry, R. W., and Caulton, M.: 1967, *Physical Electronics* (2nd edition), John Wiley & Sons, USA-Toppan, Japan, p. 109.
- Hones, E. W., Jr., Asbridge, J. R., Bame, S. J., and Singer, S.: 1971, *J. Geophys. Res.* **76**, 63.
- Hultqvist, B.: 1972, in E. R. Dyer (General editor), *Solar Terrestrial Physics/1970, Part IV*, D. Reidel Publishing Company, Dordrecht, Holland, p. 176.
- Kelley, M. C.: 1971, private communication.
- Kelley, M. C., Mozer, F. S., and Fahleson, U. V.: 1970, *Electric Fields in the Nighttime and Daytime Auroral Zone*, Space Sciences Lab. Univ. of Calif., Berkeley, Rep. Sept. 14. 1970.
- Kindel, J. M. and Kennel, C. F.: 1971, *J. Geophys. Res.* **76**, 3055.
- Langmuir, I.: 1929, *Phys. Rev.* **33**, 954.
- Mozer, F. S. and Fahleson, U. V.: 1970, *Planetary Space Sci.* **18**, 1563.
- Persson, H.: 1966, *Phys. Fluids* **9**, 1090.
- Reme, H. and Bosqued, J. M.: 1971, *J. Geophys. Res.* **76**, 7683.
- Swift, D. W.: 1965, *J. Geophys. Res.* **70**, 3061.
- Torvén, S.: 1968, *Arkiv Fysik* **35**, 513.
- Whalen, B. A. and McDiarmid, I. B.: 1970, *J. Geophys. Res.* **75**, 123.

PLASMA CONVECTION IN THE VICINITY OF THE GEOSYNCHRONOUS ORBIT

C. E. McILWAIN

University of California, San Diego La Jolla, Calif., U.S.A.

Abstract. An analytic function representing the quiet time magnetospheric electric field has been constructed with which it is possible to compute complete particle trajectories in a fraction of a second. The function was determined by a trial and error procedure such that it provides reasonable explanations for the characteristics of the plasma observed by the geosynchronous satellite ATS 5. It is believed that the model field is usefully accurate within the region of 5 to 7 R_E on the dawn side of the magnetosphere and 5 to 10 R_E on the dusk side. At a fixed distance of 6.7 R_E , the model field peaks at a value of 1.2 mV m⁻¹ near local midnight and is at a minimum of 0.04 mV m⁻¹ near 19 LT.

1. Introduction

The data being obtained by the four UCSD charged particle spectrometers on the geosynchronous satellite ATS 5 have been used to show that hot plasma is injected during each magnetospheric substorm (DeForest and McIlwain, 1971). It was also shown that there is energy dependent dispersion of the plasma away from an initial location near local midnight.

A prediction of the magnetospheric particle fluxes as functions of position, time, and energy would require knowledge of (a) the particle distributions at some initial time, (b) the magnetic and electric fields everywhere in the vicinity of the earth as a function of time, (c) all sources and sinks of particles, and (d) the pitch angle diffusion rates. Clearly, it will be many years before it is possible to make accurate predictions. One of the key quantities which must be determined is the electric field in the 5 to 10 R_E region. As a first step, a static electric field model for this region has been constructed which seems to predict many characteristics of the particles encountered by the ATS 5 satellite even when drastic simplifications are used in the computation of the particle trajectories.

2. Assumptions, Simplifications, and Limitations

The computational effort was made easier by the following assumptions and simplifications:

- (a) The electric field parallel to \mathbf{B} is zero.
- (b) The electric field is independent of time.
- (c) The magnetic field is independent of time (and thus $\text{curl } \mathcal{E} = 0$).
- (e) The particle motion is adiabatic to the extent that particles not involved in loss processes maintain constant magnetic moments and total energies.
- (d) The treatment of only those particles which mirror at the magnetic equator, i.e., have 90° pitch angles.

The ATS 5 satellite is stationed at about 105° west longitude and is therefore at an average magnetic latitude of about 10° . The magnetic field in the nightside is partially extended to a tail-like shape. The satellite field lines thus meet the magnetic equator at radial distances which can be considerably greater than the $6.62 R_E$ of the satellite. During the winter months, the distortion of the field reduces the average magnetic latitude of the satellite. For simplicity, the particles observed to be mirroring near the satellite in the winter are assumed to be the same as those mirroring at a radial distance of $6.7 R_E$.

For analytic convenience, the model field is extended over almost the entire magnetosphere. Obviously, only that part traversed by particles *before* encountering the synchronous orbit can possibly be determined using only the ATS 5 data. This region lies roughly between 5 and $7 R_E$ on the dawn side and between 5 and $10 R_E$ on the dusk side.

The time independence of the fields is the most drastic simplification. Transient field changes do occur and are of course required to cause the observed particle injections into trapped orbits. The electric field of the present model is static and thus cannot predict transient field effects.

The detailed configuration of the electric fields depends upon the level of magnetic activity. The present model corresponds to K_p values around 1. It should be further noted that even very slow electric field changes can cause large changes in the particles' third invariant of motion, i.e., the particles' total energy may vary even if the field changes are spread out over many hours.

3. Modeling Procedure and Criteria

A. MAGNETIC FIELD

A crude representation of the magnetic field at the magnetic equator (i.e., at the minimum field on the lines of force) was constructed which gives a fair fit to (a) the observed field at $6.6 R_E$ (Cummings *et al.*, 1971), (b) the field just inside the magnetopause (Fairfield, 1968), and (c) a wild guess at the field in the neutral sheet of the magnetotail. This model, labelled M2, is given by the equation

$$B(\gamma) = 6 - 24 \cos(\varphi) + 18 \cos^2(\varphi) / (1 + 1728/R^3) + 31000/R^3 \quad (1)$$

where φ is the local time and R is the radial distance in earth radii. This model is illustrated in Figure 1 along with the equation

$$B_{MP} = 16 - 35 \cos(\varphi) + 12 \cos^2(\varphi) \quad (2)$$

which is used to mark the magnetopause location.

B. ELECTRIC FIELD

Since the electric field is assumed to be curl free and zero along lines of force, it is convenient to represent it by a potential function on the magnetic equatorial surface.

It can be shown that the traces of the trajectories of equatorially mirroring particles are completely determined by the dependence of the electric potential ϕ upon B and local time. The spatial dependence of the fields (as is specified by Model M2) is only required if it is desired to find the speed of the particles along their trajectories (and of course to find actual spatial locations).

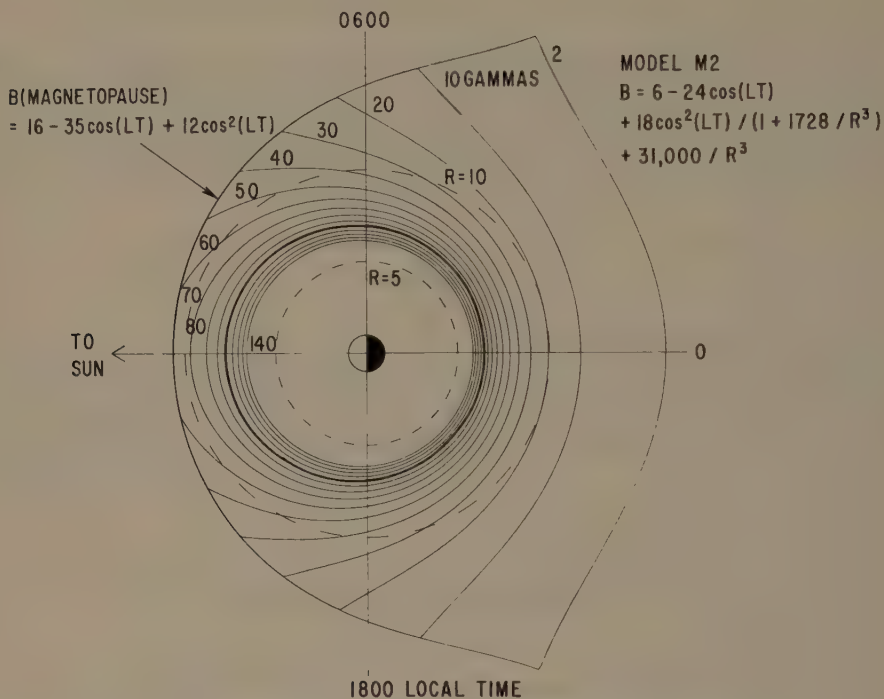


Fig. 1. A Contour plot of Model M2 of the equatorial magnetic field.

Explicitly, the electric potential in a non-rotating reference frame is modeled by choosing the coefficients A_{ij} in the equation

$$\begin{aligned} \Phi(\text{kV}) = & 10 - 92 (B/31000)^{1/3} \\ & + \sum_{i=1}^6 \sum_{j=1}^{20} A_{ij} \exp \{ -a_i (B - B_i)^2 - b_j [1 - \cos(\varphi - \varphi_j)] \}, \quad (3) \end{aligned}$$

where B = magnetic equatorial field and $\varphi = \text{LT}$. The first term is an arbitrary constant set to make the potential vary around zero at the synchronous orbit. The second term gives a corotational-like field at high B values (but does not include the important effects due to the tilt of the magnetic field with respect to the earth's rotational axis). The last term is a set of 120 functions with approximately gaussian forms centered at the B_i and φ_j values and with shapes given by the values of the a_i and b_j coefficients.

The values which were preselected for B_i , $a_i = \ln 2/d_i^2$, φ_j , and $b_j = \ln 2/(1 - \cos C_j)$ are included in Table I where B_i and d_i are in gammas and φ_j and C_j are in hours.

The model electric field has been derived by an iterative process. Initially, the model proposed by Axford and Hines (1961) was studied using graphical procedures to find

TABLE I
Coefficients for electric field Model E3

j	A_{1j}	A_{2j}	A_{3j}	A_{4j}	A_{5j}	A_{6j}	φ_j	c_j
1	2.8	5.4	0.6	2.9	-1.2	0.6	4	2
2	6.0	-1.7	1.7	-1.1	0.9	-0.2	6	2
3	-6.5	3.2	-1.2	1.9	-1.1	0.4	8	2
4	5.7	-2.5	1.1	-0.9	0.5	-0.2	10	2
5	-1.4	1.6	-2.2	1.3	-1.2	-0.1	12	2
6	4.5	-3.3	1.0	-2.1	0.5	-0.7	14	2
7	-5.3	0.7	-3.2	0.6	-1.5	-0.1	16	2
8	3.6	-3.8	0.0	-1.5	-0.2	-0.7	18	2
9	-3.1	-2.0	-2.5	-0.6	-1.3	-0.4	20	2
10	1.7	-1.5	0.2	-0.9	-0.3	-0.2	21	1
11	1.0	-1.5	-1.1	-0.4	-0.6	-0.2	22	1
12	1.7	-0.5	-0.5	-0.6	0.3	-0.2	22.5	0.5
13	2.9	-2.1	1.7	-1.2	0.4	-0.2	23	0.5
14	-0.1	3.6	-4.9	3.5	-2.2	0.7	23.5	0.5
15	2.7	-3.4	5.5	-0.6	0.6	-0.5	0	0.5
16	0.7	5.7	2.1	0.6	0.1	-0.2	0.5	0.5
17	6.0	2.3	2.3	0.3	0.1	-0.1	1	0.5
18	3.5	0.3	2.6	-0.8	0.7	-0.4	1.5	0.5
19	9.5	5.1	1.8	1.7	-0.7	0.3	2	1
20	3.0	-1.9	2.1	-1.3	0.9	-0.4	3	1
i	1	2	3	4	5	6		
B_i	0	40	100	180	280	400		
d_i	30	50	70	90	110	130		

what kinds of particle trajectories might be expected. Previous calculation such as those of Taylor (1966), Kavanaugh *et al.* (1968), and Chen (1970) were also quite helpful in this regard. This work led to two key conclusions:

(1) Most of the intense fluxes correspond to particles which have been convected in from regions of small magnetic field (say less than 40 γ).

(2) The deep minima in the observed proton spectra correspond to protons which penetrate far into the geomagnetic field before coming back out to the synchronous orbit.

The ATS 5 data taken during quiet times were then examined to determine the range of particle charge times energy vs. LT at which intense fluxes were encountered and the energy vs. LT of the minima in the proton spectra. The model field was then repeatedly altered and remolded until the calculated values matched the observed values. Plots of constant LT in the $B-\Phi$ plane were found to be particularly valuable since all trajectories are given by straight lines.

The coefficients for the most recent model (labelled E3) are given in Table I. This potential pattern with $B(\varphi)$ transformed into $R(\varphi)$ according to Equation (1) (model M2) is plotted in Figure 2.

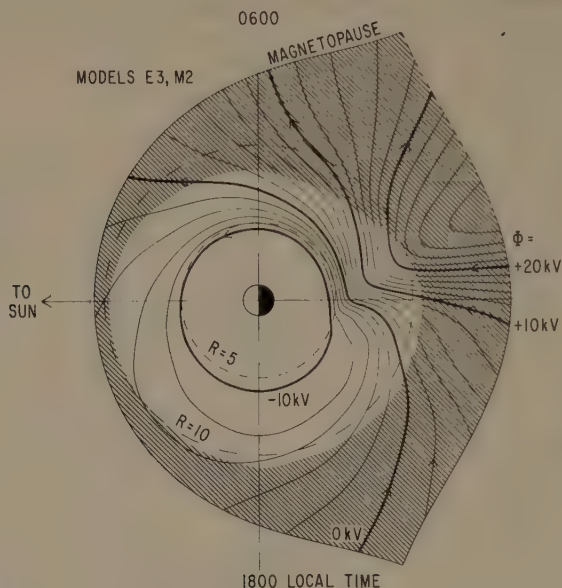


Fig. 2. A contour plot of Model E3 of the electric potential in the magnetic equatorial surface.

4. Particle Trajectories

Since Φ is given as a function B and φ , it is most convenient to compute the trajectories in this coordinate system. The equations of motion are:

$$d\varphi/dt = (\mu + \partial\Phi/\partial B|_{\varphi}) g \quad (4)$$

and

$$dB/dt = -\partial\Phi/\partial\varphi|_B g, \quad (5)$$

where μ = magnetic moment = E_a/qB_a , q = charge (including sign) in units of the electronic charge, E_a = energy when the magnetic field is B_a and

$$g = \frac{1}{RB} \frac{dB}{dR} \bigg|_{\varphi}. \quad (6)$$

Figure 3 is a plot of the trajectories of electrons with $\mu = -0.1$ keV/ γ , i.e., about 10 keV energy at the synchronous orbit. It can be seen that the model indicates that the intense fluxes of these electrons observed by ATS 5 in the midnight to dawn region come from the dusk region of the magnetopause. It should be noted, however, that the model does *not* include the strong fields near the boundary (Freeman *et al.*, 1968) so that these electrons may not cross the magnetopause at the points implied in Figure 3.

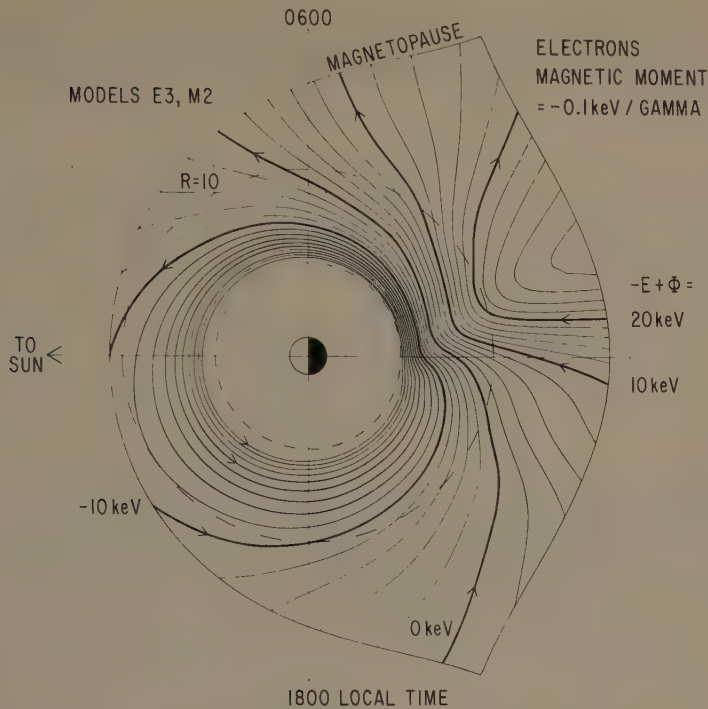


Fig. 3. Trajectories of electrons with magnetic moments of $-0.1 \text{ keV}/\gamma$ in the model fields.

Figure 4 shows that protons with the same magnitude of magnetic moment follow radically different trajectories. The intense fluxes of these protons observed by ATS 5 in the dusk to midnight region also seem to come from the dusk region near the magnetopause and from the dusk side of the magnetotail. It is interesting to note that even this static field model appears to predict an 'asymmetric ring current' and that the expected loss processes should further strengthen the asymmetry.

5. Minima in Proton Spectra

A deep minimum in the proton spectra is probably the most consistent feature to be found in the particle populations observed by ATS 5. It is almost always present over a wide range of LT and the energy at which it is found at a given LT rarely varies more than a factor of 1.7 from its typical value. A graph of the typical energy vs. LT dependence is given by the solid line in Figure 5. Also shown in this Figure are the energies at which the computed trajectories penetrate to the highest magnetic field value (crosses) and which take the longest time (circles). The maximum field values are 300 to 600 γ and the times are 12 to 120 hr; thus the assumption of substantial losses seems quite plausible. The type of trajectory creating the minima in the proton spectra is illustrated by the trajectory in Figure 4 which terminates near the N in MAGNETO-

PAUSE. This trajectory starts in the magnetotail, penetrates to less than 5 earth radii near 21 hr LT, and goes back out to $6.7 R_E$ near 2.5 hr LT (about 12 hr after entering the $R < 10$ region).

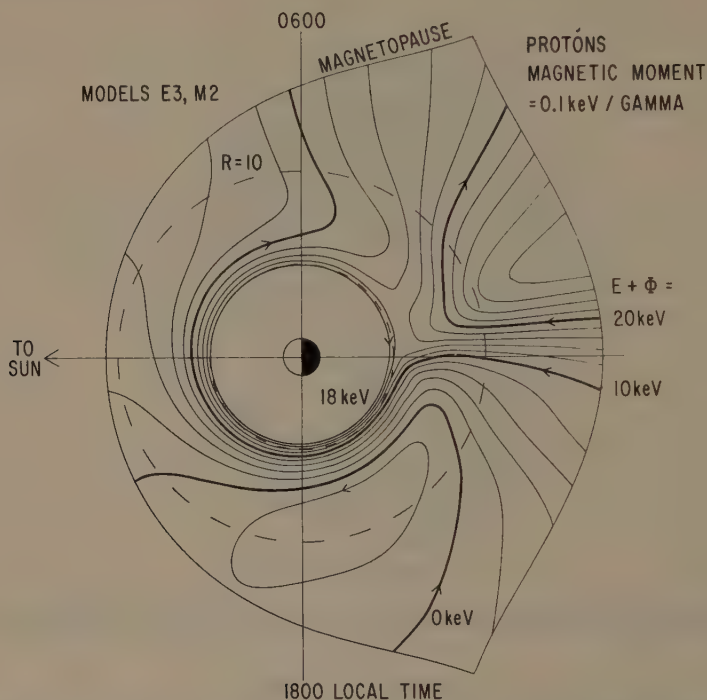


Fig. 4. Trajectories of protons with magnetic moments of $0.1 \text{ keV}/\gamma$.

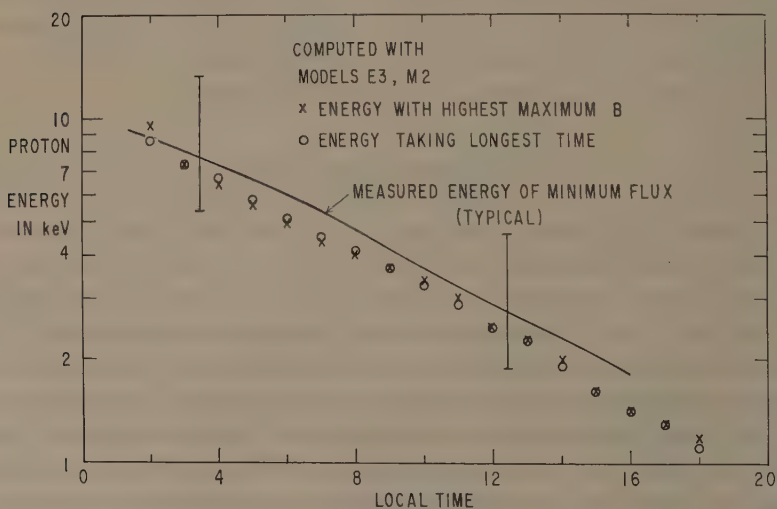


Fig. 5. Comparison of the computed and observed energies of the minima in the proton spectra.

While almost all models of the electric field will predict similar minima in the proton spectra, it is unlikely that any model will show the correspondence with observation exhibited in Figure 5 unless it is carefully tailored to do so.

6. Types of Trajectories

Figure 6 is a spectrogram of data taken by the plasma spectrometers on ATS 5 which are directed perpendicular to the spin axis and thus measure the local mirroring particles. The nonlinear energy scale given by $S = -qE/(3 \text{ keV} + E)$ is employed (see Appendix A, DeForest and McIlwain, 1971). Figures 7 and 8 are drawn with the same scale to simplify comparisons. Figure 7 shows the types of trajectories which the field model gives for the particles encountered by the ATS 5 satellite (or any other syn-

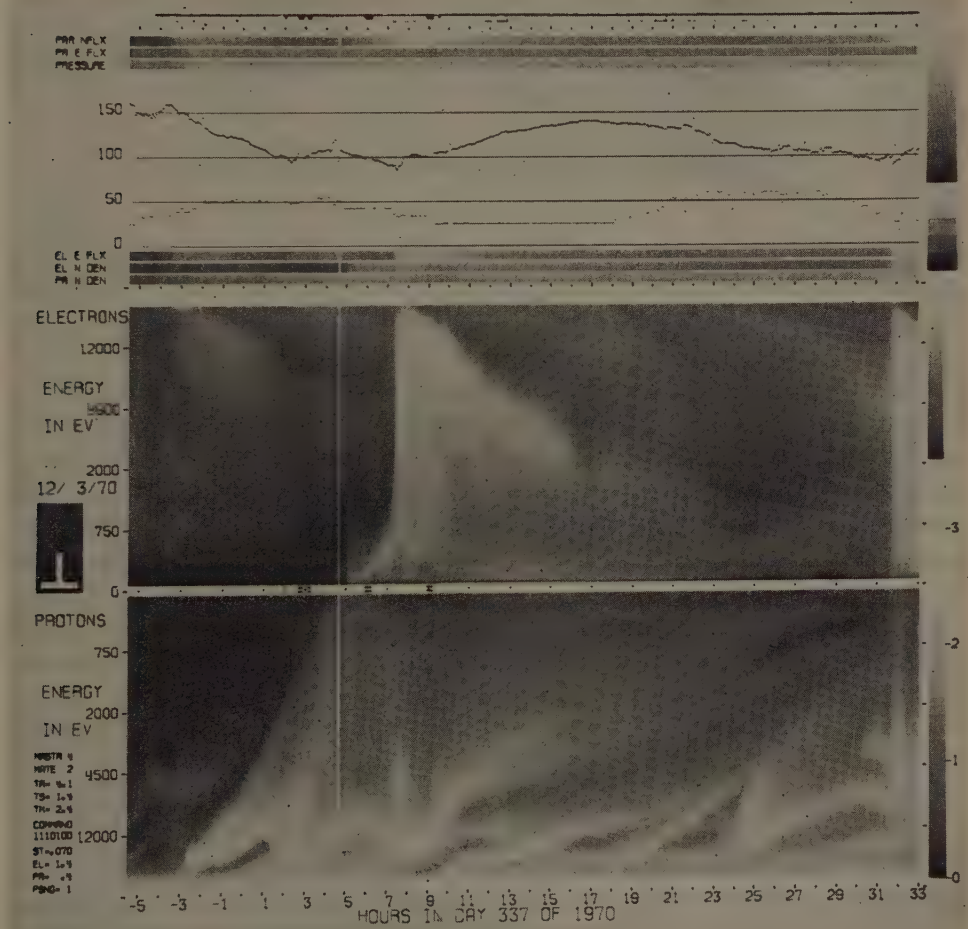


Fig 6. A spectrogram of data from ATS 5 taken during a period in which the average K_p was 1.

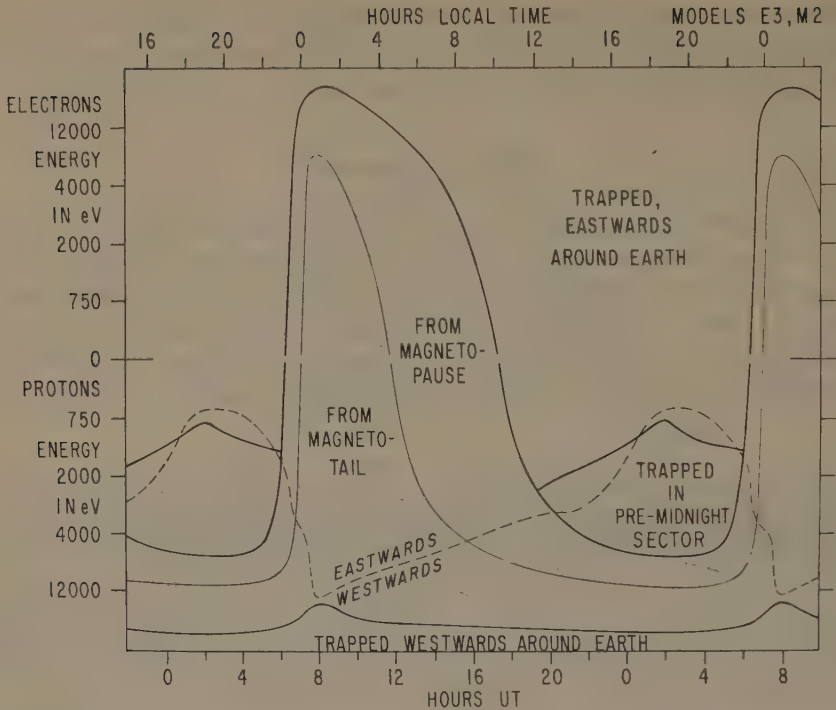


Fig. 7. A plot showing the type of trajectories encountered by the ATS 5 satellite according to the model fields. The scales are the same as in Figure 6.

chronous satellite except for the difference between LT and UT). The open trajectories (quasi-trapped particles) are subdivided into two categories according to whether or not they lead back to the magnetopause before $B=2\gamma$ is reached. As noted before, no prediction of the actual points of entry into the magnetosphere can be made since the boundary fields are not included in the model. The dashed curve is the dividing line between eastward and westward motion (in the non-rotating reference frame) when the particles encounter the satellite.

The trapped trajectories fall into three different categories: (a) energetic protons moving westwards around the earth, (b) medium energy protons which remain in the pre-midnight sector (see Figure 4 for an example), and (c) certain electrons and low energy protons traveling eastwards around the earth.

7. Dispersion Times

As noted previously (DeForest and McIlwain, 1971), each magnetospheric substorm appears to correspond to a sudden intensification of the electric fields such that increases are produced in the vicinity of midnight in the populations of particles on all types of trajectories *including many in the three trapped categories*.

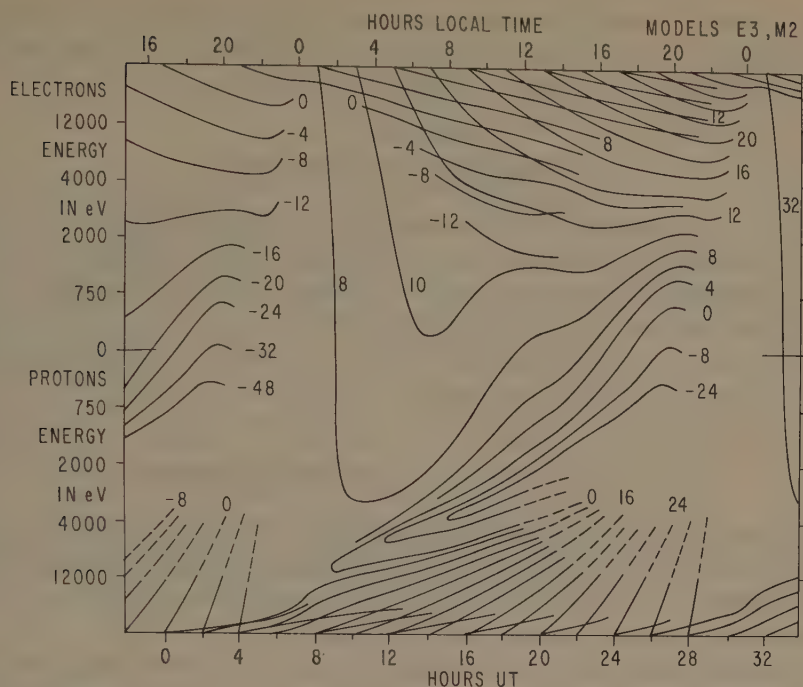


Fig. 8. A plot of the times particles would be detected by the ATS 5 satellite if they were lined up on the 2300 LT meridian at the indicated universal times.

These perturbations are extremely useful in that they provide markers which can be used to determine when a set of particles was in the vicinity of midnight by identifying the substorm causing their enhancement. The spatial extent of the initial enhancements has not yet been determined. Fortunately, the choice of initial location is non-critical because the velocities in the vicinity of midnight are relatively high.

The universal times at which the particles encountered by the ATS 5 satellite were at 23 hr LT are plotted in Figure 8. This starting location was chosen because it is near midnight and is traversed by most of the trajectories. The dashed portions correspond to trajectories which do not meet the 2300 LT meridian so that neighboring starting locations had to be used. The dispersion curves for the energetic trapped particles making between one and two circuits of the earth are also included.

A comparison with Figure 8 reveals that the majority of the 16 or more dispersion traces visible in Figure 6 correspond to substorm enhancements occurring at about -4, 1, 7, and 16 hr UT.

Spectrograms for about 400 days are now available. When those for days in which the daily K_p sum is between 6 and 10 (and no large deviations from $K_p = 1$) are examined, it is found that almost all can be readily interpreted using Figure 7 as the road map, and Figure 8 as the time schedule for the observed particles. The primary

differences between these spectrograms are due to the different times at which substorms occurred, i.e., which traces in Figure 8 were illuminated. Examples of every type of predicted trace can be found in most of these spectrograms.

8. Uniqueness of the Model Field

In common with almost all inverse problems, it is impossible to prove that other quite different solutions do not exist. It seems unlikely, however, that any solution which is substantially different from the present Model E3 can be found which predicts so many of the observed particle characteristics.

It is not possible to test the model for self-consistency since a number of key quantities (Vasyliunas, 1970) remain unmeasured.

9. Comparison with other Models and Measurements

Many previous electric field models have been constructed such as those by Axford and Hines (1961), Taylor and Hones (1965), and by Brice (1967). While some of the previous models are qualitatively similar to the present model, they do not provide the same quantitative explanation of the ATS 5 data.

Unfortunately, almost all of the available electric field measurements were made close to the earth. Accurate comparisons will not be possible until the manner in which high latitude field lines map into the magnetic equator is determined. One exception is the measurement of the E-W component of the field using whistlers (Carpenter and Stone, 1967; Carpenter, 1970). While most of these measurements have been made when K_p was greater than 1, they seem to accurately fit the predictions of the present model when the inward and westward motion of the nightside part of the electric field pattern with increasing activity is considered (this shift in the pattern is clearly exhibited by both the whistler and ATS 5 observations).

It seems possible that many of the previous observations of the magnetospheric plasma, such as those by Vasyliunas (1968) and Frank (1971), could also be interpreted using the model field if computations similar to those made for ATS 5 were performed.

10. Summary

A static electric field model seems to provide a quantitative explanation of many characteristics of the plasma observed by the ATS 5 satellite. The primary exceptions are those which are clearly due to time variations in the magnetic and electric fields. It will be interesting to determine the spatial dependence of the transient electric fields and to find whether they are curl free.

Acknowledgments

I would like to thank Professor Ian Axford, Dr Sherman DeForest, and Dr Robert

LaQuey for their helpful comments. This research is supported in part by NASA Contract NAS 5-10364 and NASA Grant NGL 05-005-007.

References

- Axford, W. I. and Hines, C. O.: 1961, *Can. J. Phys.* **39**, 1433.
Brice, N. M.: 1967, *J. Geophys. Res.* **72**, 5193.
Carpenter, D. L.: 1970, *J. Geophys. Res.* **75**, 3837.
Carpenter, D. L. and Stone, K.: 1967, *Planetary Space Sci.* **15**, 395.
Chen, A. J.: 1970, *J. Geophys. Res.* **75**, 2458.
Cummings, W. D., Coleman, P. J., Jr., and Siscoe, G. L.: 1971, *J. Geophys. Res.* **76**, 926.
De Forest, S. E. and McIlwain, C. E.: 1971, *J. Geophys. Res.* **76**, 3587.
Fairfield, D. H.: 1968, *J. Geophys. Res.* **73**, 7329.
Frank, L. A.: 1971, *J. Geophys. Res.* **76**, 2265.
Freeman, J. W., Jr., Warren, C. S., and Maguire, J. J.: 1968, *J. Geophys. Res.* **73**, 5719.
Kavanagh, L. D., Jr., Freeman, J. W., Jr., and Chen, A. J.: 1968, *J. Geophys. Res.* **73**, 5511.
Taylor, H. E.: 1966, *J. Geophys. Res.* **71**, 5135.
Taylor, H. E. and Hones, E. W., Jr.: 1965, *J. Geophys. Res.* **70**, 3605.
Vasyliunas, V. M.: 1968, *J. Geophys. Res.* **73**, 2839.
Vasyliunas, V. M.: 1970, in B. M. McCormac (ed.), *Particles and Fields in the Magnetosphere*, D. Reidel Publishing Company, Dordrecht, Holland, p. 60.

THERMAL IONS IN THE MAGNETOSPHERE

C. R. CHAPPELL

Lockheed Palo Alto Research Laboratory, Palo Alto, Calif., U.S.A.

Abstract. The distribution and dynamics of thermal (~ 1 eV) plasma are of fundamental importance for understanding many magnetospheric processes. Above the ionosphere the bulk of the thermal plasma is found in the plasmasphere, which displays varying characteristics in the different LT regions. These different characteristics are reviewed herein with specific interest placed on the H^+ ion density profiles since the H^+ ions are the main component of the plasmasphere. Plasmasphere dynamics and morphology can be explained in terms of a time varying convection model of the magnetosphere which incorporates the bulge region as part of the main flow pattern of the plasmasphere.

1. Introduction

As our knowledge of basic magnetospheric processes becomes more complete, the importance of the distribution of low energy (~ 1 eV) thermal plasma becomes increasingly apparent. At altitudes above the ionosphere the bulk of the thermal plasma is found in the plasmasphere whose constantly changing size and shape give important clues to large scale magnetospheric dynamics. The precise size of the plasmasphere is influenced by the magnitude of the convection electric field in the magnetosphere, and a change in this field is reflected in the dynamics of the plasmasphere. Therefore, continual observations of the plasmasphere morphology give an excellent indirect measurement of variations which take place in the convection field.

Wave-particle interactions have become increasingly fashionable as explanations for such magnetospheric phenomena as the asymmetric shape of the ring current, SAR arcs, and others. An important criterion for instability and wave growth is the magnetic energy per particle $B^2/8\pi n$ where B is the magnetic field and n is the total number density. At the plasmopause, the change in the thermal plasma density is the dominant factor influencing this instability criterion. Therefore, the location and motions of the plasmopause are of primary concern in locating regions of plasma turbulence in the magnetosphere.

Finally, it appears that substantial fluxes of ionization can be exchanged between the ionosphere and the plasmasphere. Also, because of infinite conductivity along field lines, $\mathbf{E} \times \mathbf{B}$ drifts of flux tubes in the plasmasphere should produce changes in the F region of the ionosphere. Hence, a thorough knowledge of plasmasphere dynamics and morphology is necessary to fully understand F region phenomena. It is evident therefore that the precise spatial and temporal distribution of thermal particles is of great importance to many magnetospheric processes. It is the purpose of this paper to review the most recent measurements of these particle distributions and to discuss the temporal changes which are observed.

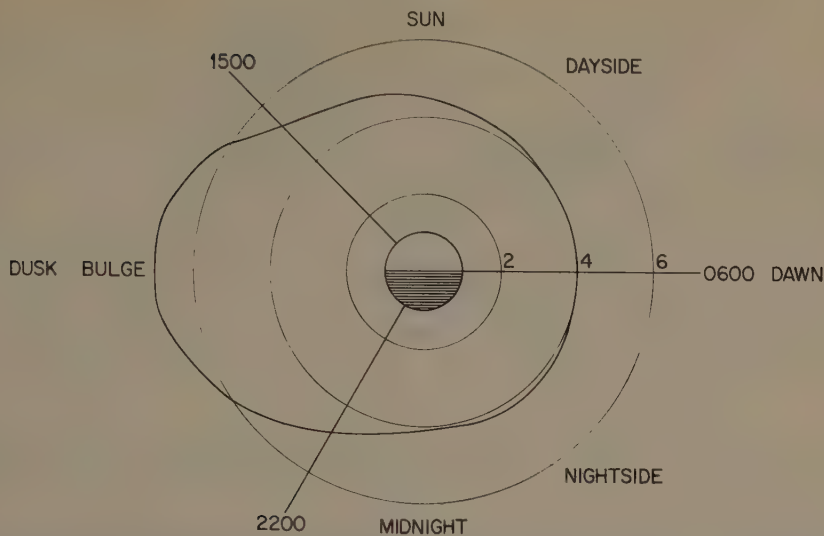


Fig. 1. An L , LT plot showing the different LT sectors of the plasmasphere – dayside, nightside, bulge. The solid line shows the average plasmapause position determined from more than 150 OGO 5 profiles (Chappell *et al.*, 1971a).

2. Morphology of the Plasmasphere

The data for this study were obtained by the Lockheed light ion mass spectrometer flown on the NASA OGO 5 spacecraft. The data cover an altitude range from 300 km to $23 R_E$ over a 1 yr period from March 1968 to February 1969. The instrument sampled the plasmasphere twice each $2\frac{1}{2}$ days at magnetic latitudes of less than 45° covering a density range of greater than 10^4 ion cm^{-3} to less than 0.1 ion cm^{-3} . H^+ ions represent about 99% of the total ion concentration of the plasmasphere and a composite grouping of these H^+ density profiles gives essentially the total picture of plasmasphere morphology. Since the plasmapause appears to be aligned along field lines (Taylor *et al.*, 1965), the L parameter has been used to organize the data.

Plasmasphere morphology is most easily discussed by means of a somewhat artificial division into three LT regions – the nightside region, 2200 to 0600 LT; the dayside region, 0600 to 1500 LT; and the bulge region, 1500 to 2200 LT. The division between the dayside and the bulge regions is by necessity not a rigorous one as we will point out in a later section. These different regions are shown in Figure 1 together with a sketch of the average plasmapause position derived from 150 density profiles by OGO 5 (Chappell *et al.*, 1971a). The spread of the individual plasmapause positions around this sketched average was greatest around the bulge and smallest in the nightside region. This average plasmapause position is in excellent agreement with that derived by Taylor *et al.* (1970) from OGO 3 spectrometer measurements.

A. THE NIGHTSIDE REGION OF THE PLASMASPHERE

In the nightside region the plasmapause position is very closely correlated with the

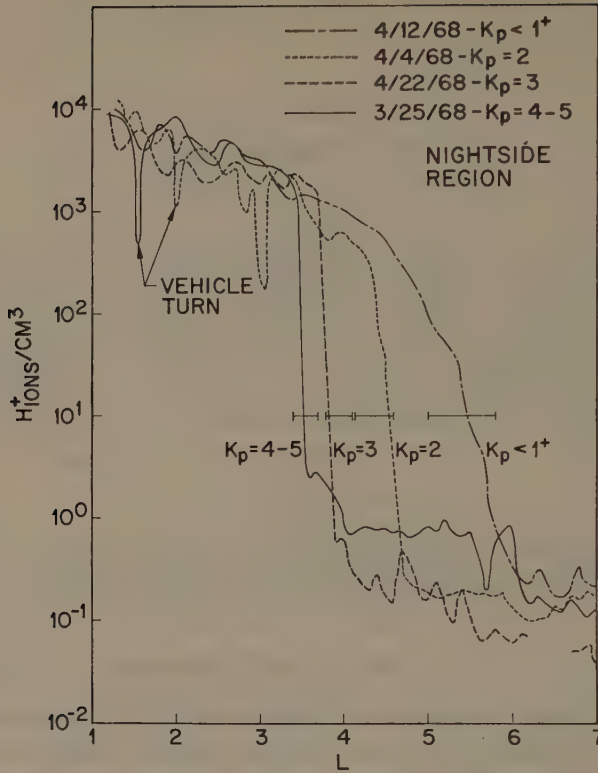


Fig. 2. A composite graph showing the reaction of the plasmasphere in the nightside region to changes in the level of magnetic activity (Chappell *et al.*, 1970a).

average magnetic activity over the preceding 2 to 6 hr period as given by the K_p index (Taylor *et al.*, 1968; Chappell *et al.*, 1970a). The plasmapause decreases in L with increasing magnetic activity in a very well behaved predictable manner; this variation in plasmasphere radius with varying activity is shown in Figure 2 from Chappell *et al.* (1970a). This figure is a composite graph representing more than 40 passes through this LT region. The decrease in plasmasphere radius is accompanied by an increased steepness in the concentration gradient at the plasmapause, with the total concentration levels inside and outside the plasmapause remaining approximately the same at 10^3 ion cm^{-3} and ~ 1 ion cm^{-3} , respectively.

Carpenter and Stone (1967) have shown the presence of flux tube convection events in this nightside region using whistler measurements. These events are characterized by the radially inward motion of the whistler ducts near midnight during a simultaneously observed magnetic bay event in the H component of the local Byrd magnetometer. These convection events, which are found almost exclusively in the nightside region, are probably responsible for the unique ability of this region to react rather quickly (2 to 6 hr) to changes in magnetic activity level.

B. THE DAYSIDE REGION OF THE PLASMASPHERE

1. *Position of the Plasmapause During Varying Magnetic Activity*

This 0600 to 1500 LT region is characterized by a high variability in plasmapause position for a given level of preceding magnetic activity during the 2 to 6 hr prior to the measurement; however, the plasmapause position does show a general decrease in radius with increasing activity.

The work of Carpenter (1970b) and Carpenter *et al.* (1969) has suggested that the characteristics and position of the plasmapause on the dayside are dependent on the sequence of magnetic activity changes which occurred as this dayside sector corotated previously through the nightside region where convection effects are important.

Chappell *et al.* (1971a) examined the idea of nightside determination of the dayside plasmapause position through a study of 41 cases of dayside plasmasphere density profiles. In this study the dayside profiles were divided into two groups where (a) the magnetic activity remained *steady* during the entire corotation of the sector from the nightside to the dayside, and (b) the activity was unsteady, i.e., the level of activity changed in value between the time of the sector corotation through the nightside and the time of corotation from dawn until the measurement was made. In the group measured during steady activity, it was found that the plasmapause was located in the position that would be expected if plasmapause formation had taken place on the nightside, i.e., the plasmapause showed the same predictable decrease with increasing magnetic activity as had been found in the nightside region (Figure 2 above). In the group measured during unsteady activity, with only one exception, the plasmapause was found in the position predicted by the activity level during the nightside transit as opposed to the activity level at the time of the dayside measurement.

This study seems to indicate that the plasmapause position in a particular sector of the dayside plasmasphere is determined not by the magnetic activity level immediately preceding the profile measurement, but by the level of activity which existed during the corotation of this sector through the formative nightside region. It also appears that once the sector has rotated past dawn, it is difficult to change the plasmapause location. This explains why previous attempts to group the dayside profile according to preceding 2 to 6 hr magnetic activity level (Chappell *et al.*, 1970a) were unsuccessful.

2. *Ionospheric Filling of the Plasmasphere on the Dayside*

After the position of the steep gradient in the density profile has been established in the predawn period, the flux tubes rotate into the dayside region where ion production begins in the ionosphere with subsequent flow up the field lines into the plasmasphere. This flow should cause a density increase both in the plasmasphere and in the plasmatrough which should affect the shape of the typical dayside profiles. This increase should be most evident in the plasmatrough where the average density is relatively low (~ 0.1 to 1 ion cm^{-3}). Evidence of density buildup in the trough region was first shown by Angerami and Carpenter (1966) using whistler observations. Their density

profiles showed substantial concentrations of electrons ($> 10 \text{ ion cm}^{-3}$) in the afternoon plasmatrough region outside the plasmopause.

The dayside profiles measured by OGO 5 were examined by Chappell *et al.* (1971a) in light of this expected filling. The density buildup on the dayside should be most apparent immediately following storms during which the plasmopause has been moved to lower L shells and the ambient ion content of the plasmatrough has been greatly reduced by enhanced convection effects. The plasmasphere H^+ density profile during these re-filling periods is characterized by a double plasmopause in the H^+ ion density as shown in Chappell *et al.* (1971a).

Figure 3 shows the H^+ density measured by OGO 5 (Chappell *et al.*, 1971a), at $L=5$ (outside the plasmopause) in the plasmatrough at different LT's following disturbed magnetic periods of one or more days. These densities are plotted vs. LT and show the buildup of ionization during the day following the storm periods. The average K_p during the disturbances was 3^+ . Three theoretical curves were included for purposes of comparison. Curve A shows the expected buildup of ionization in the equatorial plane on a $L=5$ field line. In the calculations for this curve a constant upward flux of $3 \times 10^8 \text{ ion cm}^{-2} \text{ s}^{-1}$ at 1000 km was assumed to fill the flux tube from 0500 to 1900 LT. A diffusive equilibrium distribution of ionization was also assumed to exist along the field line. The upward flux of $3 \times 10^8 \text{ ion cm}^{-2} \text{ s}^{-1}$ was taken from the polar wind estimates of Banks and Holzer (1969). Curve B shows the results using a similar value of constant upward flux with a collisionless distribution

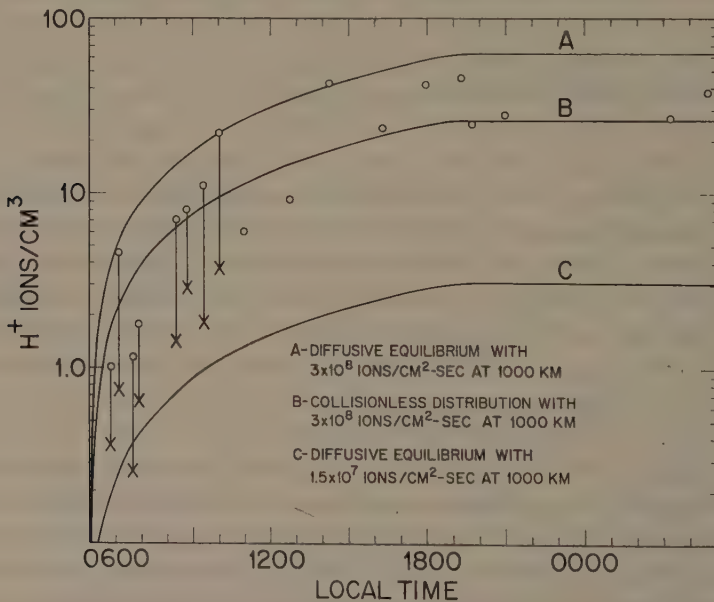


Fig. 3. The measured increase in H^+ ion density at $L=5$ as a function of LT. These data points measured at magnetic latitude of 25 to 49° have been corrected to the equatorial plane. The three curves show the calculated density accumulation for different upward fluxes and ionization distributions along the field line (Chappell *et al.*, 1971a).

of ionization along the field line. In Curve C a diffusive equilibrium distribution has been assumed and a value of $1.5 \times 10^7 \text{ ion cm}^{-2} \text{ s}^{-1}$ used for the upward flux. This value is taken from Hansen and Ortenburger (1961).

The actual data points in Figure 3 have been adjusted in the following way. The OGO 5 measurements at $L=5$ were made at magnetic latitudes between 29 and 49° . Values measured at these latitudes must be adjusted to equatorial densities in order to compare them with the curves shown. To make this adjustment, some assumptions had to be made about the distribution of ionization along the field line. The points between 0500 and 1000 LT have been adjusted for both a diffusive equilibrium (O) and for a collisionless distribution (X) between the measured point and the equator. The time distribution at these early stages of filling is probably some hybrid combination of both. After 1000 LT a diffusive equilibrium distribution has been assumed based on the calculations of Banks (1970).

These data from OGO 5 offer direct evidence of the buildup of ionization in the plasmatrough on the dayside. This density accumulation has a noticeable effect on the dayside plasmasphere profiles. The rate of ionization density buildup is in good agreement with the buildup calculated using a flux of $3 \times 10^8 \text{ ion cm}^{-2} \text{ s}^{-1}$ being bracketed by the collisionless and diffusive equilibrium distribution curves. This value of $3 \times 10^8 \text{ ion cm}^{-2} \text{ s}^{-1}$ at 1000 km is consistent with the fluxes measured indirectly by Park (1970) using whistler data and by Evans (1971) using incoherent backscatter data. It also agrees with the refilling fluxes predicted by Banks *et al.* (1971).

3. Characteristic Profiles in the Afternoon-Dusk Sector

As shown in Figure 3, the flow of ionization from the ionosphere into the plasmasphere on the dayside causes a measurable density increase, particularly in the plasmatrough region, at LT later than about 1200 LT. This density increase should be a repeatable diurnal occurrence and should therefore be reflected in the characteristic afternoon-dusk density profile.

The effects of this density buildup are indeed present in the profiles through this sector. Some 22 density profiles measured by OGO 5 in the afternoon-dusk sector (Chappell *et al.*, 1971a) showed the effect of the upward ionization flow. The effects of upward flow appear either as a smooth filling outside the steep gradient location or as a region of detached plasma which could have accumulated and then been peeled away from the plasmasphere. Two clear examples of these different effects are shown in Figure 4 from Chappell *et al.* (1971a). The September 13, 1968, profile at the top of the Figure shows a region of detached plasma in the afternoon sector (1600 LT) with densities greater than 50 ion cm^{-3} . The occurrence of detached plasma regions is found to be fairly well correlated with enhanced periods of activity.

The October 3, 1968, profile at the bottom of the figure is an excellent example of filling outside the steep gradient location. These smooth filling profiles generally occur following periods of relative magnetic quiet. The examples shown in Figure 4 are typical of this afternoon-dusk region in which all of the measured profiles show some combination of the detachment and filling effects.

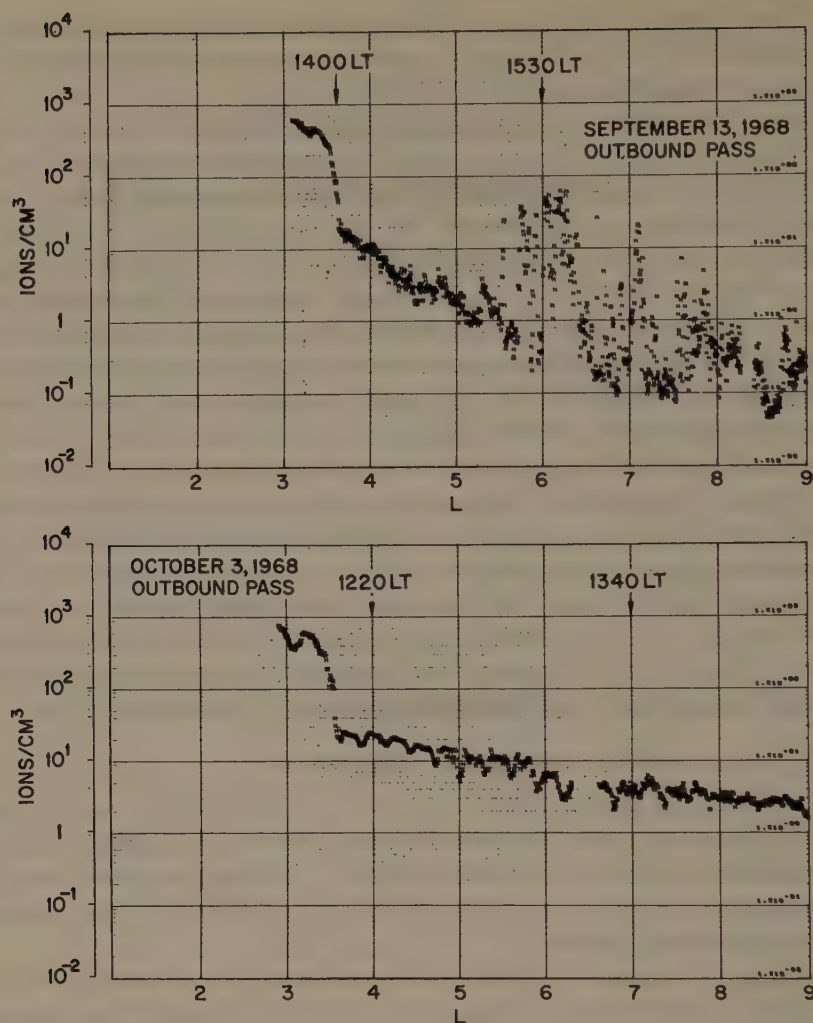


Fig. 4. Two characteristic profiles for the afternoon sector of the plasmasphere. These profiles show the effect of the filling of the plasmasphere and plasmatrough during the day (Chappell *et al.*, 1971a).

4. Regions of Detached Plasma in the Dayside Plasmatrough

As was stated above, detached masses of thermal plasma of enhanced density levels are often found in the afternoon plasmatrough (Chappell *et al.*, 1970b; 1971a; Taylor *et al.*, 1970). To illustrate the complete occurrence pattern of these detached regions an L , LT plot from Chappell *et al.* (1971a) is shown in Figure 5. It covers fluctuation regions out to $L=9$. The figure also contains a sketch of the average plasmopause position (dashed line) for comparison purposes. In this figure only those detached fluctuation regions in which the density level exceeds 10 ion cm^{-3} at some point are considered. The 10 ion cm^{-3} criterion was chosen to delineate between density fluctuations that

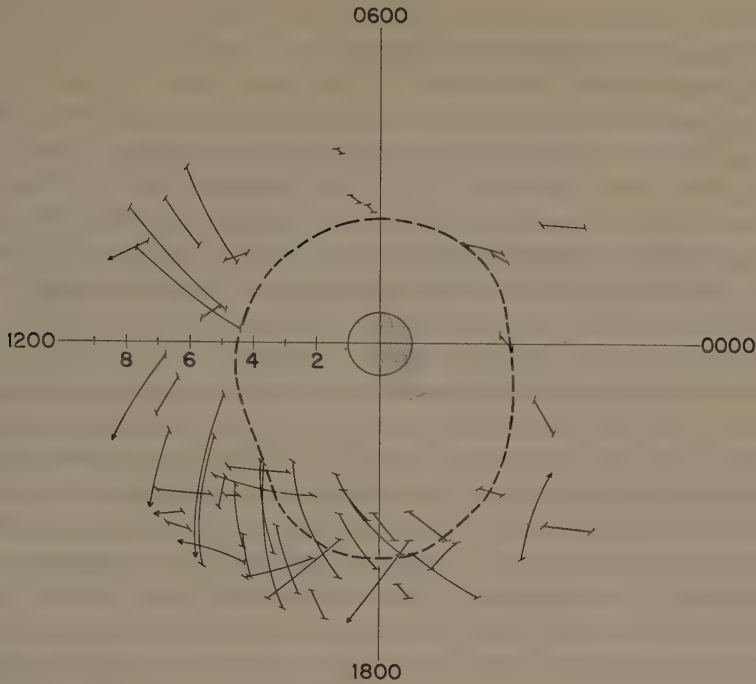


Fig. 5. An L , LT plot showing portions of OGO 5 orbits along which detached regions of plasma with densities greater than 10 ion cm^{-3} were observed. The dashed line shows the average position of the plasmapause for comparison purposes (Chappell *et al.*, 1971a).

represent only small variations in the trough density and fluctuations that represent masses of plasma which probably originated in or near the plasmasphere and then became detached. Out of a total of 202 OGO 5 plasmatrough crossings, there were 49 cases of detached plasma that had densities exceeding 10 ion cm^{-3} . Forty-one cases or 84% of the occurrences were found in the 0600 to 1920 LT region. Of these dayside cases, 31 (or 76%) are located in the afternoon-dusk sector (1240 to 1920 LT). Approximately 70% of the total number of detached plasma cases occurred following periods of moderate to high magnetic activity ($K_p \geq 3^-$ in the previous 24 hr). Therefore, when detached regions of plasma occur they seem to be concentrated in the afternoon-dusk sector with very few detached regions in the nightside sector.

C. THE BULGE REGION OF THE PLASMASPHERE

The bulge region of the plasmasphere covers LT 's from approximately 1500 to 2200 LT . Chappell *et al.* (1970b) have shown that in almost all cases the density profiles through this region exhibit a $1/R^4$ dependence with radial distance (R) and have a steep density gradient at the outer edge of the bulge as shown in the August 12, 1968, profile in Figure 6. (The solid line represents a $1/R^4$ dependence normalized to a typical value of 3×10^3 at $L=2$.) This steep density gradient (plasmapause) can vary

in position from approximately $L=4$ to $L=9$ and is generally found at increasingly larger L values as the magnetic activity decreases.

The bulge region of the plasmasphere is filled out to large L values during quiet magnetic periods. During periods of moderate to high magnetic activity, the plasma appears to be 'peeled away' from the outer parts of the bulge region. Examples of this filling and peeling away measured by OGO 5 are shown in Figure 6 (Chappell *et al.*, 1970b) by a sequence of passes which occurred before, during, and after a magnetic storm. These passes were taken in the LT region 1620 to 1720 LT. A $1/R^4$ profile has been put in as a reference line with which to compare the changing density levels. The first pass (August 12) follows a $2\frac{1}{2}$ day period of generally low activity ($K_p \cong 1^+$). The plasmasphere displays the $1/R^4$ profile inside the steep gradient. The flux tubes making up this profile are relatively full following this quiet period. The second pass (August 15), follows $1\frac{3}{4}$ days of moderate to high activity ($K_p \cong 4$). The plasmapause position has moved inward from about $L=6.8$ to $L \cong 5.5$ and most of the plasma outside of 5.5 appears to have escaped. Note that the part of the profile inside the steep plasma density gradient still follows the $1/R^4$ profile. Note also that there are some regions of detached plasma just outside the plasmapause. The next $2\frac{1}{2}$ days contain high magnetic activity with K_p as high as 6. The pass on August 18 which follows this highly active period shows a depletion of the ions in this LT region. The profile inside the steep gradient still resembles the $1/R^4$ shape but is depleted by roughly an order of

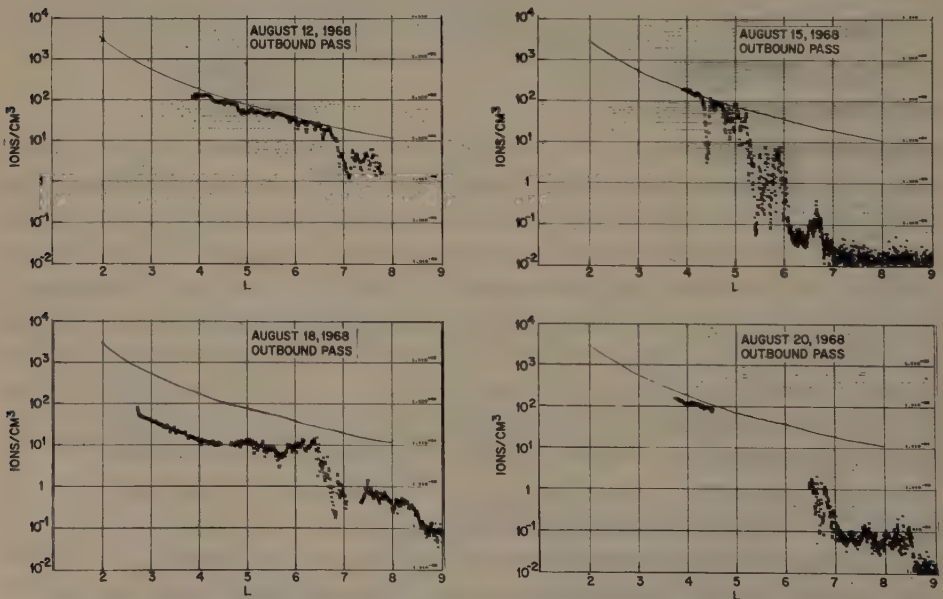


Fig. 6. Four profiles measured in the bulge region before, during, and after a storm occurring on Aug. 14–17, 1968. The Aug. 12 profile is a typical bulge region profile which exhibits a $1/R^4$ decrease in density with increasing R . The subsequent profiles show the depletion of the ion population during the high-activity periods of the storm and the subsequent filling of the plasmasphere in the following quiet period (Chappell *et al.*, 1970b).

magnitude in absolute level. It appears in this pass that the plasmasphere has lost much of its plasma during the period of high activity. The next pass (August 20) follows a $2\frac{1}{2}$ -day period of moderate to low activity. This profile, which contains a data gap, shows the plasmasphere recovery after a storm. This recovery is characterized by a filling of the plasmasphere during the quiet magnetic period with the concentration again approaching the original level.

During certain sequences of magnetic activity, a large portion of the bulge region can become detached and convected sunward toward the magnetopause in one large mass. In these cases, the magnetic activity is initially very low for a period of a day or so and then changes to a steady high activity condition. This sequence of activity changes can greatly reduce the size and plasma content of the plasmasphere and at the same time can move regions of very high thermal plasma density through the afternoon-dusk plasmatrough.

The characteristic profile in the bulge region of the plasmasphere is quite similar to the characteristic profile of the afternoon-dusk sector discussed above, with no apparent sharp transition point evident in the data. Both LT sectors contain detached plasma at or outside of the plasmopause position, and the decrease in density with increasing L values inside the plasmopause is very similar for both sectors. Neither the OGO 3 nor the OGO 5 data show an abrupt outward movement of the plasmopause position in going from the afternoon sector to the bulge region as suggested by the 'shoulder' on the leading edge of the bulge discussed by Carpenter (1966). However, Carpenter (1970a) has shown that the bulge region can move back and forth in LT in response to changes in magnetic activity. This movement of the bulge varies the position of the shoulder and makes its detection difficult in the OGO data, which consist of nearly radial passes through the plasmasphere only once every $2\frac{1}{2}$ days. The OGO 5 profile measurements in the afternoon and bulge regions are not inconsistent with a smooth expansion of flux tubes from the afternoon sector outward into the bulge region.

3. Discussion

The thermal ion density profiles of the plasmasphere display varying characteristics in the different LT regions. These different characteristics as well as the temporal effects which have been discussed can be explained by a time varying convection model of the magnetosphere (Chappell *et al.*, 1970b, 1971a, b) which includes the bulge region as part of the main flow pattern of the plasmasphere. The temporal changes of the plasmasphere size and shape are a result of the variation of the dawn-dusk directed convection electric field in the magnetosphere. The magnitude of this convection field is probably controlled by certain solar wind parameters – in particular, the southward directed component of the interplanetary magnetic field. The excellent agreement of the plasmasphere characteristics with the predictions of this convection model is further evidence in support of the concept of convection in the magnetosphere – a concept which appears to explain a great deal of the large scale magnetospheric dynamics.

Thermal plasma is a very important part of the magnetospheric environment and its distribution and motions must be thoroughly understood if we are to fully comprehend the fundamental physical processes of the magnetosphere.

Acknowledgments

I am indebted to Drs G. W. Sharp and K. K. Harris and to Mr C. W. Gilbreth for the design and development of the light ion mass spectrometer which furnished the data for this study. I would also like to thank Mr A. J. Fernandez for his development of the computer codes used in data reduction.

This work was performed under NASA contract NAS 5-9092.

References

- Angerami, J. J. and Carpenter, D. L.: 1966, *J. Geophys. Res.* **71**, 711.
Banks, P. M.: 1970, private communication.
Banks, P. M. and Holzer, T. E.: 1969, *J. Geophys. Res.* **74**, 6317.
Banks, P. M., Nagy, A. F., and Axford, W. I.: 1971, *Planetary Space Sci.*, in press.
Carpenter, D. L.: 1966, *J. Geophys. Res.* **71**, 693.
Carpenter, D. L.: 1970a, *J. Geophys. Res.* **75**, 3837.
Carpenter, D. L.: 1970b, private communication.
Carpenter, D. L. and Stone, K.: 1967, *Planetary Space Sci.* **15**, 395.
Carpenter, D. L., Park, C. G., Taylor, H. A., Jr., and Brinton, H. C.: 1969, *J. Geophys. Res.* **74**, 1837.
Chappell, C. R., Harris, K. K., and Sharp, G. W.: 1970a, *J. Geophys. Res.* **75**, 50.
Chappell, C. R., Harris, K. K., and Sharp, G. W.: 1970b, *J. Geophys. Res.* **75**, 3848.
Chappell, C. R., Harris, K. K., and Sharp, G. W.: 1971a, *J. Geophys. Res.*, in press.
Chappell, C. R., Harris, K. K., and Sharp, G. W.: 1971b, paper presented at 14th meeting of COSPAR, Seattle, Washington.
Evans, J. E.: 1971, *Trans. Amer. Geophys. Union* **52**, 4.
Hansen, W. B. and Ortenburger, I. B.: 1961, *J. Geophys. Res.* **66**, 1425.
Park, C. G.: 1970, *J. Geophys. Res.* **75**, 4249.
Taylor, H. A., Jr., Brinton, H. C., and Smith, C. R.: 1965, *J. Geophys. Res.* **70**, 5769.
Taylor, H. A., Jr., Brinton, H. C., and Pharo, M. W., III: 1968, *J. Geophys. Res.* **73**, 961.
Taylor, H. A., Jr., Brinton, H. C., and Deshmukh, A. R.: 1970, *J. Geophys. Res.* **75**, 2481.

PART V

ACCELERATION AND DIFFUSION

HIGH ENERGY PROTON MODEL FOR THE INNER RADIATION BELT

MARTIN WALT

Lockheed Palo Alto Research Laboratory, Palo Alto, Calif., U.S.A.

and

THOMAS A. FARLEY

University of California, Los Angeles, Calif., U.S.A.

1. Introduction

The high energy protons of the inner radiation belt offer a unique test for theories of magnetospheric processes. These fluxes are relatively stable, being only slightly affected by magnetic activity, and the very high energy of some of the protons restricts the mechanisms which can be invoked for their acceleration. At the lower edge of the belt the earth's atmosphere provides a calculable loss mechanism and thereby specifies a minimum to the source strength which must exist to maintain the belt. Shortly after the discovery of the inner radiation belt it was suggested (Singer, 1958; Kellogg, 1959; Vernov *et al.*, 1959) that these protons resulted from the decay in flight of albedo neutrons produced by cosmic ray interactions in the atmosphere. The belt was envisioned to represent the equilibrium flux resulting from this source and the losses caused by collisions of the protons with atmospheric constituents. Extensive calculations based on these assumptions were performed, and many of the features of the belt were in agreement with this theory, in particular the spectrum of high energy protons. However, as experimental data on the trapped proton flux, the albedo neutron intensity, and the atmospheric density improved, it became apparent that the theory was deficient in at least two important respects: (a) The energetic proton fluxes predicted by the theory were too small by a factor of 10 to 50, and (b) the spatial distribution of the protons was not in agreement with experiment. There was also a gross discrepancy at low energies where the cosmic ray albedo theory was hopelessly inadequate to supply the observed fluxes.

Recently, it has been well established that fluctuations in magnetospheric electric and magnetic fields cause a radial diffusion of the trapped particles. The magnitude of this diffusion is uncertain, being dependent on the characteristics of the fluctuations. However, on general theoretical grounds it is expected that the diffusion will be more rapid at large L and that the third adiabatic invariant is most likely to be altered by the field changes. The ability of trapped particles to diffuse across magnetic shells radically alters the view of magnetospheric processes and in particular requires a reexamination of the inner belt proton theories. It is therefore desirable to redo the inner belt calculations incorporating the radial diffusion processes and to determine if the gross discrepancies noted earlier have been removed. Since the rate of diffusion

is rather uncertain, the philosophy of the present calculation will be to parameterize the radial diffusion coefficient and to vary the parameters to obtain agreement with experiment. Later the diffusion coefficient obtained in this way will be compared with coefficients derived by other means.

2. Inner Belt Processes

There is no doubt that the following physical processes occur in the inner belt region: proton injection from albedo neutron decay, energy loss by atmospheric collisions, and radial diffusion. Other factors which may affect the proton flux include pitch angle diffusion from wave-particle interactions, solar neutron decay, and direct injection of solar flare protons. However, in the absence of direct evidence for these latter processes they will be neglected in the present paper. A further simplification which will be made is that the radial diffusion proceeds solely by alteration of the third adiabatic invariant. With this assumption the equation describing the equilibrium radiation belt becomes

$$\frac{\partial f}{\partial t} = 0 = \frac{\partial}{\partial L} \left[\frac{D}{L^2} \frac{\partial}{\partial L} (L^2 f) \right] + \text{Sources} - \text{Losses}, \quad (1)$$

where $f d\mu dJ dL$ is the number of protons in the interval $d\mu dJ dL$. The quantities μ , J , and L are, respectively, the magnetic moment, integral invariant, and McIlwain coordinate. In these units the proton source resulting from the decay of albedo neutrons is

$$\text{Source} = 0.044 E^{-1.86} \frac{\pi L}{\gamma \mu \tau} F(L), \quad (2)$$

where E is the proton energy in MeV, γ is the relativistic factor $(1 - \beta^2)^{-1/2}$, and τ is the neutron lifetime. The function $F(L)$ is a geometrical factor containing the injection efficiency. The numerical amplitude factor and energy dependence of the source were taken from Lingenfelter's (1963) neutron leakage intensity at 0° latitude.

The energy loss collisions result in a change of μ and J and will be approximated as a continuous energy degradation. The rate of change in f from energy loss collisions is

$$- \text{Losses} = - \frac{\partial}{\partial \mu} \langle \Delta \mu \rangle f - \frac{\partial}{\partial J} \langle \Delta J \rangle f$$

or since $\Delta \mu$ and ΔJ are related by $\langle \Delta J \rangle = J/2\mu \langle \Delta \mu \rangle$

$$- \text{Losses} = - \frac{\partial}{\partial \mu} \langle \Delta \mu \rangle f - \frac{\langle \Delta \mu \rangle f}{2\mu} - \frac{J}{2\mu} \frac{\partial}{\partial J} \langle \Delta \mu \rangle f. \quad (3)$$

The quantity $\langle \Delta \mu \rangle$ is obtained from the stopping power formula

$$\langle \Delta \mu \rangle = \frac{d\mu}{dt} = \frac{(1 - \eta^2)}{m_p c B} \sqrt{E(E + 2m_p c^2)} \frac{dE}{dx}, \quad (4)$$

where

$$-\frac{dE}{dx} = \frac{4\pi e^4}{mc^2\beta^2} \sum n_i Z_i \left\{ \ln \frac{2mc^2\beta^2}{I_i(1-\beta^2)} - \beta^2 \right\}. \quad (5)$$

In these equations η is the cosine of the equatorial pitch angle, m_p is the proton rest mass, m is the electron rest mass, \bar{n}_i is the average number density of atmospheric constituent i averaged over the proton trajectory, and I_i is the mean excitation energy for the i th constituent. For collisions of protons with free electrons the bracketed term in Equation (5) is replaced by $\ln(\lambda_D mc\beta/h)$, where λ_D is an average Debye length for the atmosphere.

The equilibrium Equation (1) with source and loss terms represented by Equation (2) and (3) can be solved numerically over a region in L, μ space if the values of f are known on the boundaries of the region. The boundary conditions are selected from considerations of the character of the belts and the physical processes occurring near the boundaries. At very high μ , $f=0$. At $L \approx 1.15$ $f=0$ since the dense lower atmosphere reduces the flux to an insignificant value. Since energy loss leads only to a decrease in μ , the value of f in the chosen region is not influenced by the value of f on the lower μ boundary. Hence, the values of f along the $\mu = \mu_{\min}$ boundary need not be specified.

The choice of boundary condition at the upper L boundary and indeed the selection of the L value for this boundary is less straightforward. Our approach is to use as boundary conditions the experimental values of f at the highest L value where Equation (1) can be considered valid. For reasons to be discussed in the next section this boundary is taken to be $L_{\max} = 1.7$.

Equation (1) subject to these boundary conditions can be solved by straightforward numerical techniques and the results compared with experiment. Agreement between theory and experiment can be taken as evidence that the theory contains all processes of importance *within* the region of calculation. All processes above L_{\max} are essentially unknown having been simulated by the selection of the boundary fluxes at L_{\max} .

3. Solutions of Radial Diffusion Equation

The radiation belt which would be produced by albedo neutron decay and atmospheric scattering, but without radial diffusion follows from Equation (1) if D is set equal to zero. Since no cross L motion occurs, the boundary conditions at L_{\min} and L_{\max} are unnecessary. The result of this calculation is shown in Figure 1, where equatorial values of $L^3 j_{\perp}$ for various values of μ are plotted as a function of L . The deficiencies alluded to above are readily apparent in that the theory allows fewer low μ particles than are observed and the theoretical curves rise monotonically with L rather than exhibit the inner belt maximum at $L \approx 1.6$ for high μ . Note, however, that at some μ and L the albedo neutron theory gives too large a flux; for example, at $\mu \approx 1800$ MeV G^{-1} and $L \approx 1.6$. There are, of course, intermediate regions where this theory predicts the flux accurately.

From Equation (1) it is apparent that the algebraic sign of $(\partial/\partial L)(L^2 f)$ determines

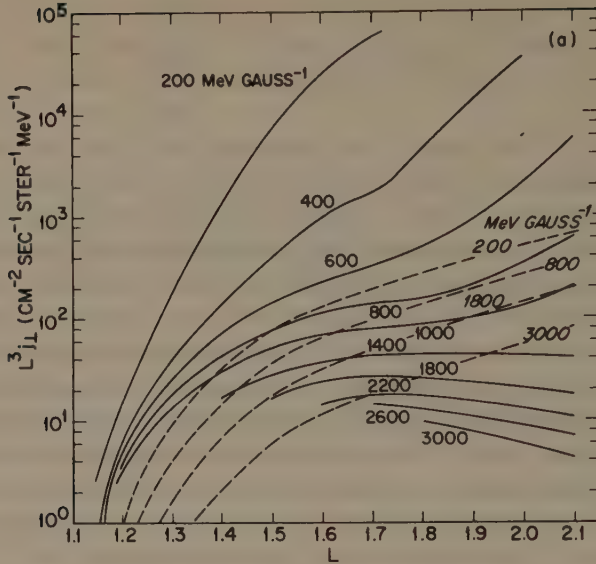


Fig. 1. Comparison of experimental (solid lines) and theoretical (dashed lines) values of $L^3 j_{\perp}$ for equatorial protons at several values of the magnetic moment. Theoretical curves are based on an albedo neutron decay source and atmospheric collision losses.

the direction of net radial flow, a positive value of the derivative indicating inward motion. Since the distribution function $f \propto L j_{\perp}$, plots of $L^3 j_{\perp}$ vs. L readily illustrate the sense of radial flow. In Figure 1 the slopes of the experimental curves for $\mu \lesssim 800$ MeV G^{-1} suggest that inward diffusion is taking place, a process which could explain the existence of large fluxes of low μ protons. On the other hand the diffusion of protons with $\mu \gtrsim 1200$ MeV G^{-1} is inward below $L \approx 1.6$ and outward above that value. Hence in this region radial diffusion constitutes a loss process, which is needed to reduce the flux of neutron decay protons to the observed value. At $L \approx 1.9$ and $\mu \approx 1000$ MeV G^{-1} a dilemma exists. Radial diffusion will add protons to that region; however, the flux from albedo neutron decay alone is already too high. One concludes that an additional loss process not considered thus far must occur in this region and hence Equation (1) with the losses given by Equation (4) is not applicable. The additional loss may be pitch angle scattering by EM waves or perhaps the rapid depletions of particles during magnetic storms. In any case we have selected $L = 1.7$ as the upper boundary to test the adequacy of the present diffusion theory.

4. Experimental Data

Proton flux values in the detail necessary to specify the boundary condition at L_{\max} are not readily available since the differential, directional flux is needed at each point to specify $f(\mu, J, L)$. We have used the fluxes derived by Thede (1969) from a spectrometer flown on OV3-4 as these data gave the most comprehensive coverage of the

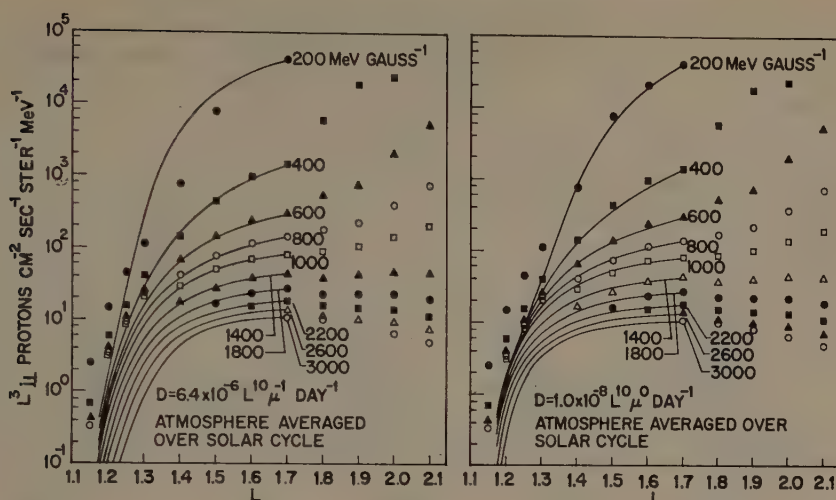


Fig. 2. Comparison of experimental (symbols) and theoretical (lines) values for equatorial trapped protons. Theoretical curves are based on neutron decay source, collisional losses, and radial diffusion with the indicated diffusion coefficients.

inner belt. However, since it was necessary to differentiate integral energy flux values to obtain the differential energy spectra, and the directional flux was in effect obtained from gradients in the omnidirectional flux, the precision of the resulting values of $f(\mu, J, L)$ is not as high as is desired. Comparison of the OV3-4 data with other experiments (Valerio, 1964; McIlwain, 1966) shows good consistency over the common range, although there are discrepancies between OV3-4 and recent Azur results (Hovestadt, 1971) at low L and low energy.

The results of two computations are shown in Figure 2, in which the lines are the theoretical curves and the various symbols denote experimental data. Since the boundary conditions were chosen to fit experiment at $L=1.7$, the curves and points coincide there. The value of D for protons in the inner belt is rather uncertain and various values have been tried. The theory of third invariant diffusion by fluctuating fields predicts that $D \propto L^n \mu^m$. Because of the limited range in L available for the present comparison n could only be determined to lie between 6 and 12. The index m appears to be between zero and -1 . From a variety of trials the values $D=1.0 \times 10^{-8} L^{10} \mu^{-1}$ and $D=6.4 \times 10^{-6} L^{10} \mu^{-1}$ appear to give equally good fits over most of the range. These values of D are quite consistent with those derived from the equilibrium distribution of outer belt protons, the time variations of outer belt protons and electrons, and the measurements of electric and magnetic field variations.

The agreement at $L \approx 1.25$ is not very good, the theoretical values being generally lower than the experimental values. (This discrepancy is not caused by setting $f=0$ at $L=1.15$ since moving L_{\min} to $L=1.1$ has a negligible effect on f at $L=1.2$.) This poor agreement is not considered a serious difficulty at present because the solar cycle variations in atmospheric density, which were neglected in these calculations,

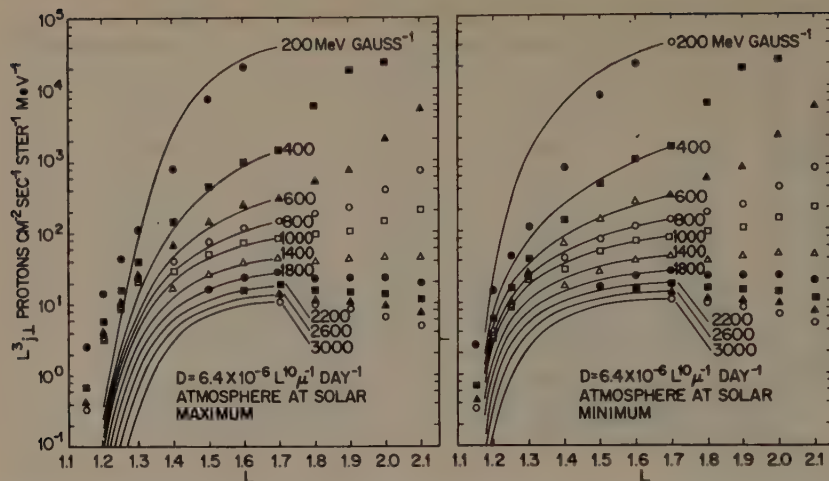


Fig. 3. Same presentation as in Figure 2 but theoretical curves were obtained using an atmosphere appropriate for solar maximum and minimum.

become important at low L . The experimental fluxes of Figure 2 were measured in 1966, a period of low solar activity. While the actual values of f appropriate for checking with experiment should be obtained by solving the time dependent form of Equation (1), an estimate of the effect of atmospheric variations can be obtained readily by computing time independent solutions for solar maximum and solar minimum atmospheres. These results are shown in Figure 3 and it is noted that at solar minimum the computed flux at $L=1.2$ is now adequate. At $L=1.15$ the observed flux is still too high; however, the experimental uncertainties for the very weak fluxes here are severe. Additional experimental data are needed to see if a real discrepancy exists.

5. Characteristics of the Proton Belt

The similarity between the observed inner proton belt and the distributions produced by this simple theory encourages one to use the theory to study characteristics of the belt. From Equation (1) the flow of particles across various boundaries can be calculated to obtain the residence times of protons in regions of L , μ space. Examples of these computations are given in Figure 4 in which the L , μ space studied was divided into nine cells. The residence time in each cell is computed by calculating the net leakage (by energy loss and radial diffusion) out of each cell and dividing the loss rate into the equilibrium population of that cell. Note that in some regions the proton residence times are very long, i.e., several centuries.

6. Other Processes

In this model the decay of solar neutrons was neglected. Although the intensity of

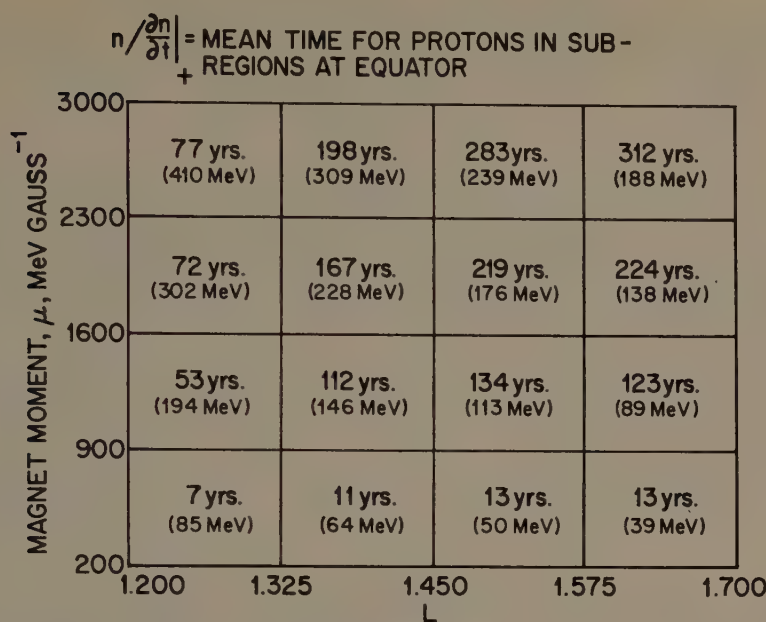


Fig. 4. Theoretical values of the mean residence time of protons in various regions of μ , L space. Average energy of the particles in each region is also given.

solar neutrons has been estimated (Lingenfelter, 1965), and calculations of the resulting trapped proton fluxes have been made, solar neutrons have not been detected experimentally. In view of the gross uncertainties in the magnitude of the solar neutron flux this source has not been included in the present calculation.

The pitch angle scattering of trapped protons by interactions with electromagnetic waves has also been neglected. Although there is much evidence for the importance of this process for outer belt protons, there is at present no direct evidence that it occurs below $L = 1.7$. Calculations were made in which pitch angle scattering was represented by an additional loss term in Equation (3) equal to f/τ where τ is an assumed lifetime taken to be independent of L and μ . In the middle of the inner zone and at high energies the neutron decay source is barely adequate to supply the known losses from atmospheric collisions, and an additional loss process would destroy the present agreement. By adjusting the μ dependence of D some compensation for the additional loss could be obtained; however, the present agreement argues for a pitch angle lifetime of $\lesssim 100$ yr in the inner zone.

The long residence times of inner belt protons raise the question of the effects of the secular variation of the geomagnetic field. Heckman *et al.* (1971) pointed out that the present decay rate of the dipole field causes an inward motion of trapped protons of $\sim 7 \text{ km yr}^{-1}$. More recently Schulz and Paulikas (1972) have also called attention to the secular variation, indicating that it produces an inward current comparable in magnitude to the current from radial diffusion. The slow decay of the earth's dipole can

be simulated in Equation (1) by adding the terms

$$\left(\frac{df}{dt}\right)_d = -\frac{\partial}{\partial L} \left(\left\langle \frac{dL}{dt} \right\rangle f \right) - \frac{\partial}{\partial \mu} \left(\left\langle \frac{d\mu}{dt} \right\rangle f \right), \quad (6)$$

where the bracketed quantities are the rate of changes of the variables due to the decay of the geomagnetic field. In actual fact during dipole decay μ will be invariant. However, as a proton is convected inward, its energy will change relative to that of a proton which diffuses inward, and the second term in Equation (6) compensates for this difference. Since

$$\frac{1}{B} \frac{dB}{dt} \approx \frac{-1}{1933}$$

the dipole decay terms become

$$\left(\frac{df}{dt}\right)_d \approx \frac{\partial}{\partial L} \left(\frac{Lf}{1933} \right) + \frac{\partial}{\partial \mu} \left(\frac{\mu f}{1933} \right). \quad (7)$$

The effect of these terms is apparent in Figure 5 where the dashed curves include the terms of Equation (7) and the solid curves, which are identical to those of Figure 2, do not. The overall nature of the process is to move protons inward thereby reducing

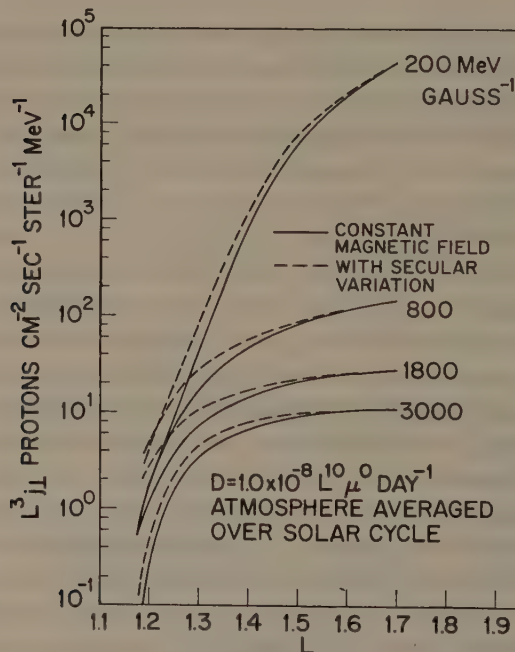


Fig. 5. Effects of secular variation of geomagnetic field on trapped proton fluxes. Solid lines are the same as those in Figure 2; dashed lines include effect of secular variation of magnetic field.

the discrepancy of low L protons noted previously. Quantitatively the magnitude of the effect is uncertain since it is not known whether the dipole decay has occurred at the present rate for more than the past 100 yr.

7. Conclusions

The major features of the equatorially trapped inner belt protons can be explained on the basis of CRAND, atmospheric losses, and radial diffusion through changes in the third adiabatic invariant. The diffusion inward of outer belt protons supplies the vast majority of the inner belt protons between 200 and 1000 MeV G^{-1} , and the diffusion process also redistributes the neutron decay protons in a manner which agrees with experiment. Pitch angle diffusion does not appear to be important for equatorially trapped protons at $L < 1.7$ although it may be necessary to explain off-equatorial particles.

It is desirable to extend these calculations to off-equatorial particles and to include solar cycle variations in atmospheric density.

Acknowledgments

Work supported by Defense Atomic Support Agency Contract No. DA 49-146-XZ-570 at Lockheed and by NASA Grant No. NsG 249-62 at the University of California.

References

- Heckman, H. H., Lindstron, P. J., and Nakano, G. H.: 1971, in *Models of the Trapped Radiation Environment, Volume VII, Long Term Variations*, National Aeronautics and Space Administration Report NASA SP-2034, p. 39.
- Hovestadt, D.: 1971, private communication.
- Kellogg, P. J.: 1959, *Nuovo Cimento* **11**, 48.
- Lingenfelter, R. E.: 1963, *J. Geophys. Res.* **68**, 5633.
- Lingenfelter, R. E.: 1965, *J. Geophys. Res.* **70**, 4077.
- McIlwain, C. E.: 1966, in B. M. McCormac (ed.), *Radiation Trapped in the Earth's Magnetic Field*, D. Reidel Publishing Company, Dordrecht, Holland, p. 593.
- Schulz, M. and Paulikas, G. A.: 1972, *J. Geophys. Res.* **77**, 744.
- Singer, S. F.: 1958, *Phys. Rev. Letters* **1**, 181.
- Thede, A. L.: 1969, *OV3-4 Dose Rate and Proton Spectral Measurements*, Air Force Weapons Laboratory Report AFWL-TR-68-128.
- Valerio, J.: 1964, *J. Geophys. Res.* **69**, 4949.
- Vernov, S. N., Grigorov, N. L., Ivanenko, I. P., Lebedinskii, A. I., Murzin, V. S., and Chudakov, A. E.: 1959, *Soviet Phys-Dokl.* **4**, 154.

MAGNETIC FIELD VARIATIONS AT MICROPULSATION FREQUENCIES

D. J. SOUTHWOOD*

Dept. of Planetary and Space Science, and Institute of Geophysics and Planetary Physics, University of California, Los Angeles, Calif., U.S.A.

1. Introduction

The nature and role of waves at micropulsation frequencies in the magnetosphere are discussed here qualitatively. In particular, generation of such disturbances by extracting energy from the particle distribution is examined.

A useful unperturbed field model is an axisymmetric one and one then takes disturbances to vary in longitude ϕ and time t as $\exp i(m\phi - \omega t)$. Particle motions are naturally described in terms of constants of the unperturbed motion, e.g., the invariants μ , J , and Φ (Northrop and Teller, 1960) or more graphically μ , W and L , where W is particle energy and L the equatorial distance of the field line on which a particle is bouncing. We assume that μ , the magnetic moment is conserved at least approximately, by the disturbances discussed here.

In the absence of a steady applied electric field a steady solution for the distribution will be longitude independent. The distribution in L should be grossly determined by radial diffusion due to quasi-static disturbances (e.g., Fälthammar, 1968). The first two invariants are preserved by all such processes (Southwood, 1971a). Accordingly if particle sources are assumed to be at large L and are steady, one expects:

$$\frac{\partial f}{\partial L_{\mu, J}} > 0.$$

The individual disturbances which result in radial diffusion must be asymmetric and corresponding asymmetries produced in the distribution are only slowly smoothed out (on many drift time scales (Dungey, 1965)). The assumption then of axisymmetry at disturbed times may be weak; however, the disturbances we are interested in are thought to be local in longitude and so this may not be too important.

Theories of micropulsation frequency range disturbances have suggested both fluid-like instabilities and resonant Alfvén or acoustic wave generation may explain the various phenomena observed. Here our aim is to outline such approaches.

2. 'Fluid' Instabilities

Some progress has been made in understanding such instabilities where the bulk of the plasma appears to release energy. A moderately general approach is possible and

* Present address: Physics Department, Imperial College, London.

we outline here arguments presented in more detail by Southwood (1971b). A hydro-magnetic approach is simplest and this involves assuming $E \cdot B$ is small where E is the disturbance electric field and B the ambient magnetic field. Particles move under guiding center motion in the disturbance. A component of the motion shared by all particles is the ' $\mathbf{E} \times \mathbf{B}$ ' drift. This allows us to define a field line displacement by

$$-i\omega\xi = \mathbf{u}_E = \frac{c\mathbf{E} \times \mathbf{B}}{B^2}.$$

One now proceeds to calculate how far the disturbance moves the particle in the L direction and the change in a particle's energy. For a linear theory one simply integrates the disturbance effect back over the unperturbed trajectory. Liouville's theorem then allows one to find an expression for the perturbation in distribution function produced. This then enables one to obtain particle pressure or number density perturbations by taking moments. To get analytic expressions one is forced to approximate since the orbit integrations depend strongly on whether the disturbance frequency is less than or greater than the particle bounce frequency. Furthermore, the resonant particles which satisfy $\omega - m\omega_d = N\omega_b$ (N , integer, or zero), where ω_b = bounce frequency and ω_d = bounce average drift frequency behave in an exceptional manner and must be taken into account. One next inserts the pressure changes into the plasma equation of motion and an instructive next step is to obtain an energy equation by taking the scalar product of this with ξ .

For disturbance frequencies much less than bounce frequencies of particles with significant pressure contributions (thermal particles) one derives an expression for the total plasma energy perturbation, δU :

$$\begin{aligned} \delta U = & \frac{1}{2}Q\omega^2\xi^2 + \left(1 + \frac{4\pi(P_\perp - P_\parallel)}{B^2}\right)\frac{b_\perp^2}{4\pi} + \frac{b_\parallel^2}{4\pi} + \\ & + (\nabla \cdot \xi)_\perp \left(\xi \cdot \nabla P_\perp + \frac{B\hat{e} \cdot \nabla P_\perp}{\hat{e} \cdot \nabla B} (\nabla \cdot \xi)_\perp \right) - \\ & - \xi \cdot \hat{n} \left(\xi \cdot \nabla P_\parallel + \frac{B\hat{e} \cdot \nabla P_\parallel}{\hat{e} \cdot \nabla B} (\nabla \cdot \xi)_\perp \right) - \frac{4\pi(P_\parallel - P_\perp)}{B^2} \text{curl } \mathbf{B} \cdot \xi \times \mathbf{b}_\perp - \\ & - 2\pi \int \frac{Bd\mu dW}{(W - \mu B)^{\frac{1}{2}}} \frac{\omega}{(\omega - m\bar{\omega}_d)} (< \mu B (\nabla \cdot \xi) - \\ & - 2(W - \mu B) \xi \cdot \hat{n} > 0)^2 \frac{df}{dW} - \\ & - 2\pi \int \frac{Bd\mu dW}{(W - \mu B)^{1/2}} i\omega\pi\delta(\omega - m\bar{\omega}_d - N\omega_b) \times \\ & \times \left(\left\langle \mu B (\nabla \cdot \xi)_\perp - 2(W - \mu B) \frac{\xi \cdot \hat{n}}{R} \right\rangle_N \right)^2 \frac{df}{dW}. \end{aligned} \quad (1)$$

In this expression p_\parallel and p_\perp are parallel, perpendicular pressures b_\parallel and b_\perp are parallel,

perpendicular field perturbations \hat{e} and \hat{n} are parallel and ambient field principal normal unit vectors. R is field line radius of curvature and q is plasma density

$$\frac{df}{dW} = \left(\frac{\partial f}{\partial W} \Big|_{\mu, L} - \frac{cm}{qB_{eq}\omega L} \frac{\partial f}{\partial L} \Big|_{\mu, W} \right)$$

and

$$\langle A \rangle_N = \int_{\text{bounce}}^{\tau_b} \omega_b \exp(-iN\omega_b t) A dt.$$

Some terms in the expression are easily identifiable. The first is plasma kinetic energy, δU_K and the remaining is the sum of plasma internal and magnetic energy density ($b^2/4\pi$), $\delta U_T + \delta U_M$. The latter two terms are associated with particle acceleration, the last being the resonant particle contribution.

The expression derived by following the procedure outlined above is very similar to that obtained by Kruskal and Oberman (1958). One splits δU_T into a nonresonant and resonant contribution, $\delta U_{Tres} + \delta U_{Tbulk}$. For small oscillation frequency, ω_r , one hopes to be able to neglect δU_K , the only quadratic term in ω . A more detailed analysis (Southwood, 1971b) shows that stability may be considered by noting that for instability at some point

$$\delta U_{Tbulk} + \delta U_M < 0.$$

From Equation (1) it is clear that if $\beta \ll 1$ (β is the ratio of plasma to magnetic pressure) an electrostatic disturbance will be most likely to be unstable and after some algebra one can obtain Taylor's (1965) condition for interchange instability. A sufficient condition is

$$\frac{\partial f}{\partial W} \Big|_{\mu, J} > 0 \quad \text{which gives} \quad \frac{\partial f}{\partial L} \Big|_{\mu, J} < 0. \quad (2)$$

As pointed out earlier this is not expected on average in the magnetosphere. Interchange motions are furthermore strongly inhibited by the resistive ionosphere and so the instability condition is an underestimate (Chang *et al.*, 1965). Nakada *et al.* (1965) checked explicitly for high energy protons that Equation (2) does not hold.

Any other form of electrostatic instability requires $\mathbf{E} \cdot \mathbf{B} \neq 0$ and such have been investigated further by Liu (1970). When $\beta \sim 1$ as it is in the outer ring current regions, at least near the equator (Frank, 1967), the situation is more complicated and electromagnetic instabilities are more likely. From an observational point of view this is more interesting since magnetic observations are more commonly made. It should be noted, in passing, that electrostatic disturbances should, in principle, be detectable indirectly from the oscillations they produce in particle flux. On an equatorial satellite this would not be an entirely foolproof manner of detection because for instance, the fundamental of a standing transverse Alfvén wave would solely produce flux oscillations at the

equator. However, their presence might be looked for where the situation is unambiguous.

If we assume that field line tying is strong in the ionosphere and look at the possibility of instabilities with

$$\omega_{bT} \gg \omega \gg m\omega_d,$$

the effect of the second from last integral in Equation (1) is now going to be stabilizing but its effect will be minimal for a disturbance that is antisymmetric about the equator (i.e., ξ and b_{\parallel} zero at the equator). As Taylor (1965) noted one can rearrange Equation (1) to

$$\begin{aligned} \delta U = & \left[1 + \frac{(p_{\perp} - p_{\parallel})}{B^2} 4\pi \right] \frac{b_{\perp}^2}{4\pi} + \frac{b_{\parallel}^2}{4\pi} \left[1 + \frac{\hat{e} \cdot \nabla p_{\perp}}{\hat{e} \cdot \nabla \frac{B^2}{8\pi}} \right] - \\ & - \frac{(\xi \cdot \hat{n})^2}{R} \left[\hat{n} \cdot \nabla p_{\parallel} - \frac{\hat{n} \cdot \nabla B}{\hat{e} \cdot \nabla B} \hat{e} \cdot \nabla p_{\parallel} \right] - \\ & - (\xi \cdot \hat{n})^2 \frac{\hat{n} \cdot \nabla B}{B} \left[\hat{n} \cdot \nabla p_{\perp} - \frac{\hat{n} \cdot \nabla B}{\hat{e} \cdot \nabla B} \hat{e} \cdot \nabla p_{\perp} \right] - \\ & - 2b_{\parallel} \frac{\xi \cdot \nabla B}{B} \left[\xi \cdot \nabla p_{\perp} - \frac{\xi \cdot \nabla B}{\hat{e} \cdot \nabla B} \hat{e} \cdot \nabla p_{\perp} \right] \end{aligned} \quad (3)$$

when we neglect field aligned currents.

The condition that the first term be negative is the firehose instability; when the second term is negative we have the mirror instability condition (Dungey, 1972). More interestingly a sufficient condition for the next two terms to be negative is that

$$\left. \frac{\partial f}{\partial L} \right|_{\mu, w} < 0 \quad (4)$$

provided the field is not so distorted that

$$\frac{\hat{n} \cdot \nabla B}{BR} < 0.$$

Equation (4) is almost certainly satisfied in the outer ring current and is a simple consequence of adiabatic injection. The destabilizing influence of these terms is countered normally by the stabilizing magnetic terms as the interchange was by the resistive ionosphere. However, the regular oscillations seen by Barfield *et al.* (1971a) (also similar reports by Sonnerup *et al.* (1969)), Hasegawa (1969), and Barfield and Coleman (1970) are probably due to this cause. These events are, in general, seen near dusk and an example seen on ATS 1 starting at 1750 LT is shown in Figure 1. Anisotropy aids the instability in so far as it decreases the stabilizing effect of the b_{\parallel}^2 term although Lanzerotti *et al.* (1969) and Sonnerup *et al.* (1969) implicitly concluded

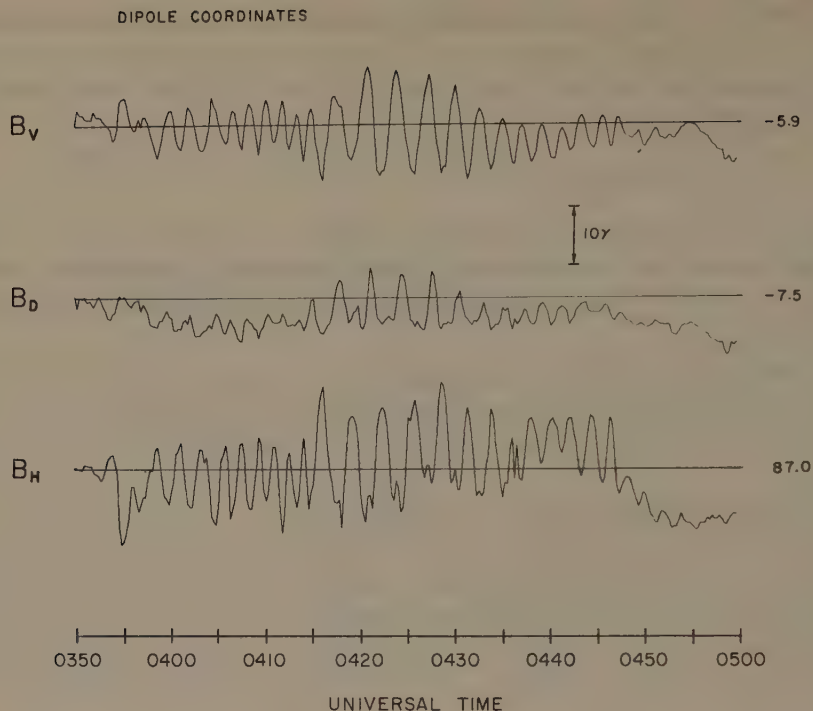


Fig. 1. Large amplitude magnetic oscillations, UCLA ATS 1 magnetometer, May 7, 1967, 03 50-0500 UT. H axis is parallel to dipole axis of earth, D is E-W and V is radial.

the term was not negative for the event observed on Explorer 26. The possibility of the events being due to the mirror instability criterion violation (Hasegawa, 1969) is unlikely particularly since it is observed that $\frac{1}{2}b_{\parallel} \sim b_{\perp}$ and so the system would be stable to disturbances with $\xi \cdot \hat{n} = 0$ (pure mirror effect) even when the simple criterion was violated. Hasegawa, however, made an important contribution by noting that the inhomogeneity of the medium could cause 'fluid' instabilities to appear overstable (oscillatory). This is further discussed by Southwood (1971b). The E-W phase velocity should be of the order of the proton 'diamagnetic drift' velocity for a plasma with a hotter ion distribution than electron. The instability should limit the steepness of the outer ring current gradient and implicitly then limit ring current population.

The occurrence of Barfield-type events is such as to suggest the above is a likely explanation of them. They occur generally near storm main phase near the dusk meridian and appear substorm (and so injection) related. The hottest proton distributions should occur towards dusk (note also the partial ring current attributed to this region, e.g., Frank (1970)). A characteristic decrease of field strength prior to the events might also be interpreted as hot plasma newly arrived at the ATS 1 location. The disturbance magnetic vectors line up quite close to magnetic meridians as one would expect.

Barfield *et al.* (1971a) report that there appears to be no correlation of these events with ground micropulsations. This may be because the instability is localized to the $\beta \gtrsim 1$ equatorial region of the field line.

3. Alfvén and Acoustic Wave Generation

Alfvén waves have been seen in space. The first indication that they might be a regular occurrence was reported by Cummings *et al.* (1969) who observed regular transverse oscillations at quiet times with the UCLA ATS 1 magnetometer. Further reports from a spacecraft at a similar orbit have been made by Dwarkin *et al.* (1971). The means by which Alfvén waves might be generated were outlined by Southwood *et al.* (1969) and Dungey and Southwood (1970). Resonant generation leads one to an interest in waves with large m . This is useful since the transverse mode then is only weakly coupled to the fast mode by plasma inhomogeneity (Dungey, 1968) and energy may remain trapped on local flux tubes, allowing one to envisage steady regular oscillations.

To generate Alfvén oscillations through resonance one requires that the resonant particles experience a net loss of energy which then serves to generate the wave. Particles diffuse both in energy and L and such diffusion could not explain particle spectrums whose characteristic energy decreased with increasing L if an external particle source is assumed. However, the waves may provide fast local diffusion. The diffusion coefficient may be estimated by

$$D_L \sim \left(\frac{b}{B}\right)^2 v^2 \tau_b \sim \left(\frac{b}{B}\right)^2 \frac{mv^2}{\Omega}$$

since $m\omega_b \sim \Omega$ for resonant high energy particles (cf., Southwood *et al.*, 1969) and so Bohm rates might be approached. Fast diffusion rates have been thought necessary at the ring current inner edge (Cornwall *et al.*, 1970; Frank, 1970) and the steep proton gradient here would be conducive to wave generation.

Southwood *et al.*'s (1969) discussion of resonant particle behavior is independent of the actual wave with which the particle resonates in so far as the diffusion curves and the ratio of energy change to L change depend only on disturbance E-W phase velocity and not on wave amplitude. As a result many of the simple ideas put forward by Southwood *et al.* (1969) are not restricted to simply the Alfvén mode. One might investigate the electrostatic acoustic mode as has been done by Kennel and Coroniti (1970). This is most easily understood in low β and where $T_e > T_i$. The electrons are then faster than the wave while the protons behave as cold particles. Whether such modes are important depends on the ability of the plasma to sustain parallel electric fields. This appears strongly dependent on the cold plasma density. For instance in a model with a cold plasma which supports the wave oscillations and a much lower density high energy tail which can provide resonant particles one would not expect acoustic oscillations to be significant. One can briefly note, however, that DeForest (1970) suggests from UCSD ATS 5 particle detector behavior during eclipse that

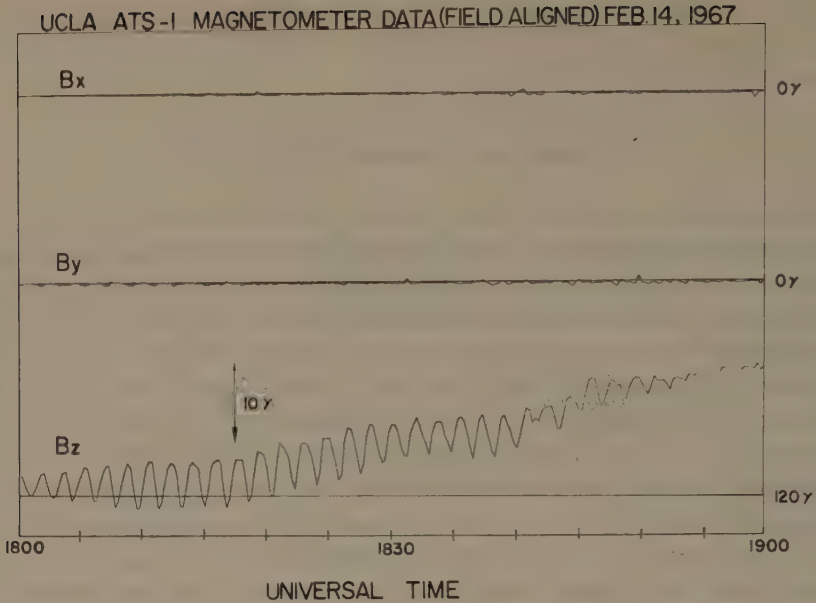


Fig. 2. An example of a regular oscillation observed on ATS 1. Coordinate system is field aligned Z parallel to the field, X in the meridian.

there is essentially no ambient cold plasma outside the plasmasphere. As pointed out previously, micropulsation frequency electrostatic oscillations might be detected indirectly.

There are other ways in which hydromagnetic modes may be affected by the presence of hot plasma. In particular we give a simple possible explanation for the purely 'compressional' oscillation reported by Barfield *et al.* (1971b) shown in Figure 2. As we noted earlier, even in cold plasma, inhomogeneity couples fast and transverse modes. This is only weak when m is large however. Investigating this same limit when the pressure perturbation is finite suggests that (from the E-W fluid equation)

$$\delta p_{\perp} + \frac{B b_{\parallel}}{4\pi} = 0 \quad \text{as } m \rightarrow \infty \quad (5)$$

one can then proceed in a similar manner (Dungey, 1968) to decouple the equations and derive an eigenvalue equation for ξ_n , the displacement in the meridian (alternatively for E_{ϕ} the E-W electric field). The important point is that the eigenvalue equation will only involve the differential operator $\mathbf{B} \cdot \nabla$ as in guided modes for the simplest cases. Equation (5) implies that now the disturbance generally has a change in field strength associated with it where the pressure perturbation is finite. Near the equator in the outer ring current this should be so and since ATS 1 is at the geomagnetic equator the oscillations in Figure 2 may be of the field line fundamental and, ATS 1 being at an expected antinode, only strength changes are observed.

4. Further Remarks

The observations discussed so far have been those thought immediately relevant to the theory outlined here. The variety of waves observed in space at hydromagnetic frequencies is indicated by Heppner *et al.* (1969). A review by McPherron (1971) attempts a more detailed classification of events under observational analysis. Attention has been given to the role of 'band limited pulsations', a dawn side substorm phenomenon. These are probably generated by electrons, once again, by bounce resonance and a theory has been put forward by Kennel and Coroniti (1970). McPherron and Coleman (1971) point out divergences of theory and experiment. Most significantly, waves tilt the field out of the meridian much more than expected. A similar feature is observed in Pc 4 frequency transverse waves observed on OGO 5 near the dawn meridian (Russell and Southwood, 1972). As with many aspects of this subject further study is required.

Acknowledgments

I would like to thank Dr C. T. Russell, Mr J. N. Barfield and Dr R. L. McPherron of the Institute of Geophysics and Planetary Physics, UCLA, for useful comments and discussion during this paper's preparation.

References

- Barfield, J. N. and Coleman, Jr., P. J.: 1970, *J. Geophys. Res.* **75**, 1943.
 Barfield, J. N., McPherron, R. L., Coleman, Jr., P. J., and Southwood D. J.: 1971a, IGPP UCLA preprint.
 Barfield, J. N., Lanzerotti, L. J., MacLennan, C. G., Paulikas, G. A., and Schulz, M.: 1971b, preprint.
 Chang, D. B., Pearlstein, L. D., and Rosenbluth, M. N.: 1965, *J. Geophys. Res.* **70**, 3085, also, 1966.
 Cornwall, J. M., Coroniti, F. V., and Thorne, R. M.: 1970, *J. Geophys. Res.* **75**, 4599.
 Cummings, W. D., O'Sullivan, R. S., and Coleman, P. J., Jr.: 1969, *J. Geophys. Res.* **74**, 778.
 DeForest, S. E.: 1970, *Trans. Amer. Geophys. Union*, **51**, 815.
 Dungey, J. W.: 1965, *Space Sci. Rev.* **4**, 199.
 Dungey, J. W.: 1968, in S. Matsushita and W. H. Campbell (eds.), *Physics of Geomagnetic Phenomena*, Academic Press, New York, p. 913.
 Dungey, J. W.: 1972, E. R. Dyer (General editor), *Solar Terrestrial Physics/1970, Part III*, D. Reidel Publishing Company, Dordrecht, Holland, p. 219.
 Dungey, J. W. and Southwood, D. J.: 1970, *Space Sci. Rev.* **10**, 672.
 Dwarkin, M. L., Zmuda, A. J., and Radford, W. E.: 1971, *J. Geophys. Res.* **76**, 3668.
 Frank, L. A.: 1967, *J. Geophys. Res.* **72**, 3753.
 Frank, L. A.: 1970, *J. Geophys. Res.* **75**, 1263.
 Hasegawa, A.: 1969, *Phys. Fluids* **12**, 2642.
 Heppner, J. P., Ledley, B. G., Skillman, T. L., and Sugiura, M.: 1969, Goddard Space Flight Center Report X-612-69-429.
 Kennel, C. F. and Coroniti, F. V.: 1970, *J. Geophys. Res.* **75**, 1863.
 Kruskal, M. D. and Oberman, C. R.: 1958, *Phys. Fluids* **1**, 275.
 Lanzerotti, L. J., Hasegawa, A., and MacLennan, C. G.: 1969, *J. Geophys. Res.* **74**, 5565.
 Liu, C. S.: 1970, *J. Geophys. Res.* **75**, 3789.
 McPherron, R. L.: 1971, IGPP UCLA, preprint.
 McPherron, R. L. and Coleman, Jr., P. J.: 1971, *J. Geophys. Res.* **76**, 3010.
 Nakada, M. P., Dungey, J. W., and Hess, W. N.: 1965, *J. Geophys. Res.* **70**, 3529.
 Northrop, T. G. and Teller, E.: 1960, *Phys. Rev.* **117**, 215.

- Russell, C. T. and Southwood, D. J.: 1972, in preparation.
- Sonnerup, B. U. O., Cahill, L. J., Jr., and Davis, L. R.: 1969, *J. Geophys. Res.* **74**, 2276.
- Southwood, D. J.: 1971a, preprint.
- Southwood, D. J.: 1971b, IGPP UCLA Publication 964, preprint.
- Southwood, D. J., Dungey, J. W., and Etherington, R. J.: 1969, *Planetary Space Sci.* **7**, 349.
- Taylor, J. B.: 1965, *Plasma Physics*, IAEA, Vienna, p. 449.

CHANGES IN THE DISTRIBUTION FUNCTION OF MAGNETOSPHERIC PARTICLES ASSOCIATED WITH GYRORESONANT INTERACTIONS

R. GENDRIN

Groupe de Recherches Ionosphériques C.N.E.T., Issy-les-Moulineaux, France

1. Introduction

Wave-particle interactions (WPI's) were initially invoked for explaining the origin of natural ELF or VLF electromagnetic emissions. Since the work of Cornwall (1966) and Kennel and Petschek (1966), however, it was recognized that this phenomenon was able to modify the distribution function of the particles themselves. Consequently, and because of the existence of a loss cone, WPI's are responsible for the most part of particle precipitation. But, if one restricts to gyroresonant WPI's, the relative importance of this mechanism with respect to other mechanisms is not yet clearly established. Therefore, it is necessary to improve our theoretical knowledge in this field and to check quantitatively the validity of our conclusions.

We will present here the results of both theoretical and experimental studies which were performed in our laboratory in this field. A special paragraph will be devoted to the most recent results of geophysical importance which were obtained by several authors, by considering the effects of these gyroresonant WPI's in different regions of the magnetosphere.

2. Quasi-Linear Theory

A. BASIC FORMULAS AND CONCEPTS

In order to discuss the different aspects of the QL theory, the following basic formulas will be given without demonstration (for an extensive study of the QL formalism, see for instance Engel (1965) and Matsumoto and Kimura (1971)). These formulas relate the (homogeneous) distribution function $f(\alpha, v, t)$ of the energetic particles, the wave power spectral density per unit wave number b_k or per unit frequency b_f , the diffusion coefficient D and the growth rate γ . One also introduces sources (S) and losses (L).

1. Case $\omega \ll \Omega$

The following expressions are valid

$$\frac{\partial f}{\partial t} = \frac{1}{\sin \alpha} \frac{\partial}{\partial \alpha} \left(D \sin \alpha \frac{\partial f}{\partial \alpha} \right) + S - L \quad (1)$$

$$D = \frac{\pi \Omega^2}{V_r} \left(\frac{b_k}{B_0} \right)^2 = \frac{\Omega^2}{2} \left(\frac{b_f}{B_0} \right)^2 \frac{V_g}{V_r} \quad (2)$$

$$\frac{\partial b_k^2}{\partial t} + V_g \frac{\partial b_k^2}{\partial z} = 2\gamma b_k^2 \quad (\text{plus boundary conditions}) \quad (3)$$

$$\gamma(\omega) = G(\omega) \eta(V_r) [A - \omega/(\Omega - \omega)]. \quad (4)$$

$G(\omega)$ is a slowly varying function (see Table I); ω and k are related by the dispersion relation of cyclotron waves in a cold plasma*

$$F(\omega, k) = 0. \quad (5)$$

TABLE I
Basic formulas

	$x = \omega/ \Omega^\pm $	$V_a^\pm = B_0/(\mu_0 n_0 m^\pm)^{1/2}$	$E_m = (m^\pm V_a^{\pm 2})/2 = B_0^2/(2\mu_0 n_0)$
Type of interaction		e, R	p, L
Wave number $kV_a^\pm/ \Omega^\pm $		$x^{1/2}(1-x)^{-1/2}$	$x(1-x)^{-1/2}$
Phase velocity v_ϕ/V_a^\pm		$x^{1/2}(1-x)^{1/2}$	$(1-x)^{1/2}$
Group velocity V_g/V_a^\pm		$2x^{1/2}(1-x)^{3/2}$	$(1-x)^{3/2}(1-x/2)^{-1}$
Parallel resonant energy E_r/E_m		$x^{-1}(1-x)^3$	$x^{-2}(1-x)^3$
Critical energy E_c/E_m		$A^{-1}(1+A)^{-2}$	$A^{-2}(1+A)^{-1}$
Amplification factor $G(\omega)/ \Omega^\pm V_a^\pm $ (Equation 4)		$2\pi^2 x^{-1/2}(1-x)^{7/2}$	$2\pi^2 x^{-3}(1-x)^{7/2}$
Amplification factor $H(\omega)/ \Omega^\pm $ (Equation 12)		$\pi^2(1-x)^2$	$\pi^2 x^{-2}(1-x)^2$
* Diffusion coefficient $D/(\Omega^\pm)^2$		$x(1+2x)^{-1}(b_t/B_0)^2$	$x(2+x)^{-1}(b_t/B_0)^2$
** Diffusion curve $(v'^2 - v_\perp^2)/V_a^{\pm 2}$		$\frac{2x^2+1}{x} - \text{Ln}x$	$\frac{1-x}{x^2} + \text{Ln}x$

* The correct expression for $D[\pi\Omega^2(b_k/B_0)^2(V_g + |V_r|)^{-1}]$ is taken. Usually, V_g is neglected with respect to V_r , which is true only if $x \ll 1$.

** In these expressions, x is an implicit function of V_r (see the fifth line); v' is the constant defining the diffusion curve in the $v_\perp, v_\parallel = V_r$ plane.

$\alpha, v, v_\perp, v_\parallel$ have their usual meaning, Ω is the relevant cyclotron frequency ($\Omega = \Omega^+$ for (p, L) interactions, $\Omega = |\Omega^-|$ for (e, R) interactions), V_r is the resonant velocity, A is the anisotropy factor of the distribution function, and ηdV_r , the fraction of 'resonant particles' in the frequency range $d\omega$ associated with dV_r **. One has

$$V_r = \frac{\Omega - \omega}{k} \quad (6)$$

* Small changes to this dispersion relation are to be considered when the finite value of the ratio n_1/n_0 of the hot to cold plasma density is taken into account (see for instance Gendrin *et al.*, 1971, Appendix 2; Higuchi and Jacobs, 1970; Matsumoto and Kimura, 1971).

** The definition of η given here differs somewhat from the one of Kennel and Petschek (1966).

$$\eta(V_r) = \eta(\omega) = \int_0^\infty dv_\perp v_\perp f(v, \alpha) \Big|_{v_\parallel = V_r} \quad (7)$$

$$A(V_r) = A(\omega) = \frac{\int_0^\infty dv_\perp v_\perp \operatorname{tg} \alpha \partial f / \partial \alpha}{2 \int_0^\infty dv_\perp v_\perp f} \Big|_{v_\parallel = V_r} \quad (8)$$

The normalization condition for f (Table I) is

$$2\pi \int_0^\pi d\alpha \int_0^\infty dv f v^2 \sin \alpha = n_1/n_0.$$

2. Anisotropy

For simple distribution functions (expressed by a bi-Maxwellian or by an integer power of $\sin \alpha$), the value of A is *independent of V_r* , and due to the zero-order conservation of the first adiabatic invariant, A is *constant along a magnetic line of force*. This is the main advantage of using such a formalism, mainly popularized by Kennel and Petschek (1966).

This formalism also demonstrates that, for a given anisotropy interactions can only take place for frequencies verifying

$$\omega < \omega_c$$

with

$$\omega_c/\Omega = A/(A+1) \quad (9)$$

(see also Liemohn, 1967).

Therefore, the concept of "critical anisotropy"

$$A_c = \omega/(\Omega - \omega) \quad (10)$$

can lead to a misunderstanding because this quantity is not a constant but depends on the frequency which is considered.

3. Critical Energy

The exact meaning of A_c is the following: for a distribution function having a given anisotropy, only those frequencies for which $A > A_c$ can be emitted. Therefore only those particles for which $V_r > V_c$ can participate to the interaction. V_c is defined by solving Equations (5), (6), and (10) with $A = A_c$.

As the total energy is always greater than the parallel energy, one introduces the concept of 'critical energy' $E_c^\pm = (\frac{1}{2}) m^\pm V_c^2$ (see Table I). Particles having an energy smaller than E_c *cannot* participate to the interaction.

However, this does not mean that particles having an energy greater than E_c will *strongly* interact with waves. The growth rate γ is maximum for frequencies much smaller than ω_c (see, for instance, Gendrin *et al.*, 1971, Figure 6). Consequently,

the particles which will diffuse in a very short time are not those whose energy is just slightly above the critical energy, but particles with a much higher energy, which depends both on the mean energy and on the anisotropy of the distribution function that is considered. This remark has to be kept in mind when considering the effects of inward crossing of the plasmopause by streams of energized particles (see Section 5.A).

4. Case $\omega \lesssim \Omega$

The above formulas are valid only for interactions for which

$$V_r \gg |v_\phi|$$

v_ϕ being the phase velocity of the wave. For other interactions, one must use the expressions which were given by Haerendel (1970, 1971). He used, instead of the two independent variables v_\parallel and v_\perp , the two variables v_\parallel and v' , v' being a known function of v_\perp and v_\parallel (see Table I) which remains constant along the diffusion curve that the particle has to follow in the velocity space under the action of the electromagnetic wave (Gendrin, 1968).

Equations (1) and (4) must be replaced by

$$\frac{\partial f(v', v_\parallel)}{\partial t} = \frac{\partial}{\partial v_\parallel} \left(v_\perp^2 D \frac{\partial f}{\partial v_\parallel} \right) + S - L \quad (11)$$

$$\gamma(\omega) = H(\omega) \int dv' v' v_\perp^2 \left. \frac{\partial f}{\partial v_\parallel} \right|_{v_\parallel = V_r} \quad (12)$$

in which v_\perp is to be considered as a function of v' and v_\parallel and in which $H(\omega)$ is a slowly varying function of ω (see Table I).

5. Need for a Self-Consistent Solution

The set of Equations (1) to (4) is self-consistent but it is very difficult to solve. Therefore, in previous solutions, assumptions have been made concerning either the field intensity or the particle distribution function.

Assuming a given distribution function allows oneself to compute the growth rate as a function of frequency (Liemohn, 1967; Criswell, 1969; Gendrin *et al.*, 1971) or the limiting flux of interacting particles (Haerendel, 1970).

Assuming a given field intensity allows oneself to compute the stationary distribution function (Kennel and Petschek, 1966), the diffusion lifetime of particles (Eather and Carovillano, 1971), or the time variation of the distribution function (Gregory, 1971)*.

* Incidentally, in this work, it is shown that the simple expression for the losses which is generally admitted ($L=0$ for $\alpha > \alpha_0$, $L=f/T_e$ for $\alpha < \alpha_0$) is not sufficient. For low energy protons, principally, the charge exchange over the whole trajectory and for every pitch angle must be considered. For 10 keV protons at $L=6$, this effect is approximately of the same importance as the pitch angle diffusion losses under the influence of a realistic wave field.

However, it is obvious that if one of these parameters vary, the other one cannot remain constant. One has to calculate the diffusion of particles under the influence of the waves they are generating. It is toward a solution of this problem that our work was directed.

B. RELAXATION

The hypotheses are the following ones. Let an initially anisotropic distribution function relax towards isotropy under the influence of the waves that such a particle distribution function generates. As time elapses, b_k increases, therefore D , so that $\partial f / \partial t$ is large; then A decreases and also γ . If no losses are introduced, A tends towards zero, and b_k towards a finite value.

1. Wave Spectrum after Isotropization

The medium is assumed to be homogeneous. The assumptions are therefore

$$\partial / \partial z = 0$$

$$f(t=0)(\cdot) \exp[-E/E_0] \sin^m \alpha$$

$$f(t=\infty)(\cdot) \exp[-E/E_0] \text{ (isotropic)}$$

$$b_k^2(t=0) = 0$$

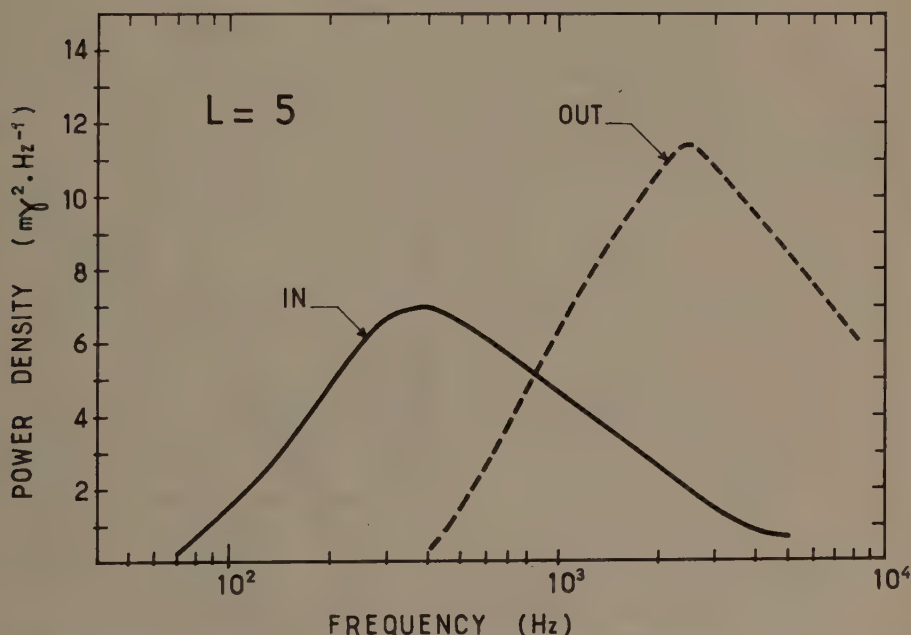


Fig. 1. Limiting spectra of VLF waves inside and outside the plasmasphere. The e -fold energy of the initially anisotropic distribution function is $E_0 \sim 100$ keV and the initial anisotropy $A = m/2 = 0.5$. The ratio n_1/N_0 of the hot to cold plasma density is assumed to be equal to 10^{-3} inside the plasmasphere and 10^{-2} outside. This change is responsible for the change in intensity of the spectrum. Changes of the Alfvén velocity from 3×10^7 ms $^{-1}$ inside to 9×10^7 ms $^{-1}$ outside are responsible for the important change (400 to 2500 Hz) of the frequency of the maximum of the spectrum (after Roux and Solomon, 1971).

and one computes $b_k^2(t=\infty)$. The expression for b_k is the following one (Roux and Solomon, 1971):

$$b_k^2 = K_m \frac{n_1}{n_0} \left(\frac{V_a}{V_0} \right)^3 \left(\frac{\Omega}{\omega} \right)^{5/2} \int_0^{\pi/2} \frac{\sin \alpha}{\cos^4 \alpha} \exp \left[\frac{V_a^2}{V_0^2 \cos^2 \alpha} \left(\frac{\Omega}{\omega} \right) \right] F_m(\alpha) d\alpha \quad (13)$$

in which K_m and $F_m(\alpha)$, respectively, are a constant and a function of α which depend on the value of the source anisotropy, and $V_0 = (2mE_0)^{1/2}$.

Examples of the spectra thus obtained are given in Figure 1, from which one sees that the shape of the spectrum depends primarily upon the cold plasma density. Inside the plasmasphere, the ratio of the mean parallel velocity to the Alfvén velocity is large, and therefore the frequency for which the intensity is maximum is small. Outside the plasmasphere, the reverse situation prevails.

2. Time Variation

It is interesting to follow the time variation of both f and b_k during this process, but this can be achieved only by numerical analysis. This has been done by Etcheto *et al.* (1971c) and their preliminary results are presented in Figure 2. As time proceeds,

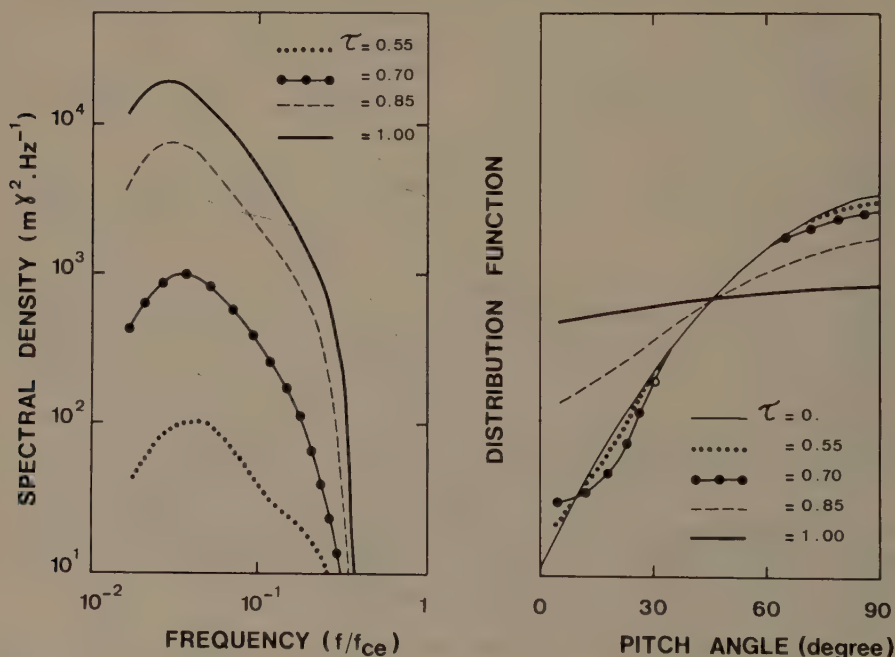


Fig. 2. Time variation of the wave spectrum and of the electron pitch angle distribution function during a relaxation process. The plasma parameters are the ones which are valid inside the plasmasphere (see Figure 1). No losses for the waves are introduced. The frequency of the maximum of the spectrum decreases during the process (Figure 2a) because more and more particles get increased parallel velocity, due to the induced pitch angle diffusion (Figure 2b) (Etcheto *et al.*, 1971c).

the wave intensity grows, and the distribution function tends towards isotropy. However, there is no evidence of a monochromatic phase appearing during this process, as it is usually the case in one dimensional electrostatic interactions (Drummond, 1965), although a small plateau in the distribution function seems to appear in the course of the event (Figure 2b).

A definitive answer to this question is of importance, because if no monochromatic phase appears, and only in this case, then we can apply the QL theory throughout the whole process of relaxation.

3. Self-Consistent Solution

Etcheto *et al.* (1971c) have also obtained a stationary solution of the self-consistent set of Equation (1) to (4) for an interaction between electrons and the whistler mode. The source

$$S(\cdot) \exp[-E/E_0] \sin^m \alpha$$

is supposed to act continuously. Inhomogeneity of the medium is taken into account

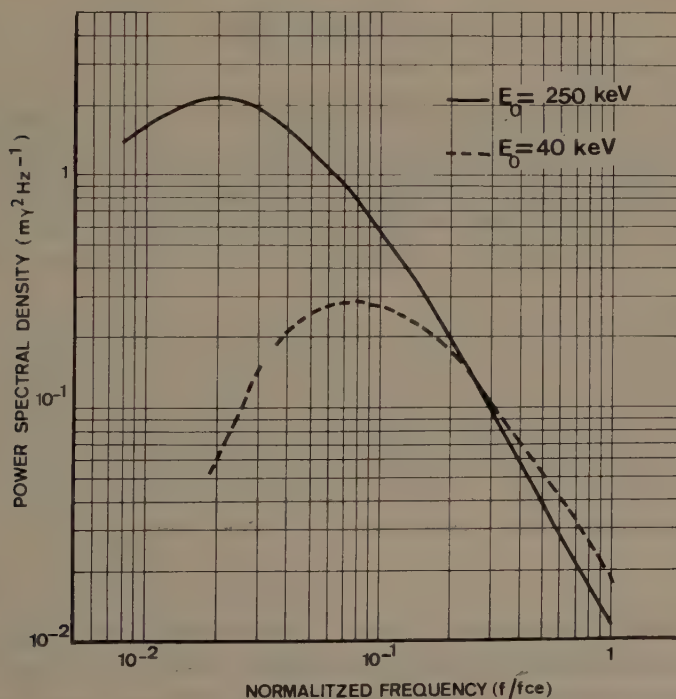


Fig. 3. Steady state spectra computed for $L = 5$. The cold plasma density at the equator is assumed to be equal to 10^8 m^{-3} (i.e., inside the plasmopause); it varies proportionally to B . The source term is proportional to $\exp(-E/E_0) \sin^m \alpha$ with $m = 4$. Its intensity is such that $(1/n_0) (dn_1/dt)$ is equal to 10^{-8} s^{-1} . The ionospheric reflection coefficient for the waves has been assumed to be nearly equal to zero (Etcheto *et al.*, 1971c).

by introducing variations of B and n_0 along the line of force. The existence of a reflexion coefficient R for the waves the ionosphere is also considered.

The field intensity can be expressed analytically as a function of the energy and pitch angle distribution of the source. The amplitude of the source is directly reflected into the amplitude of the flux of precipitated particles, and therefore quantitative estimates of this parameter can be introduced into the computation. An example of the result of such a study is given in Figure 3. One sees that changing the mean energy of the source distribution function produces a change in the central frequency of the spectrum, but not too large a change of its amplitude which is obviously mainly determined by the intensity of the sources. The anisotropy of the source, $m/2$, and the reflexion coefficient of the wave play a less important role provided that $m > 1$ and $R \ll 1$.

The computation of the equilibrium distribution function of the particle flux is now being processed and we will be able to give an exact value of the anisotropy factor as a function of the intensity of the source in the steady state case. (In Kennel and Petschek's work, where a flat spectrum of the waves has been assumed, the anisotropy is independent of the intensity of the source.)

3. Other Nonlinear Effects

A. DISPERSION OF PEARLS

Changes in the distribution function mainly due to the pitch angle diffusion of particles can induce strong changes in the amplification of waves. This amplifying process can compete with the usual dispersive properties of the medium.

For instance it has been demonstrated (Gendrin *et al.*, 1971) that the slope of a pearl element in a frequency-time display was given by the following formula

$$\frac{d\omega}{d\tau} = \frac{vV_g^2}{v^2 + \mu^2} \cdot \frac{1}{t} \quad (14)$$

in which

$$\begin{cases} v = \frac{d^2\omega}{dk^2} = \frac{dV_g}{dk} \\ \mu = -\frac{d^2\gamma}{dk^2} \end{cases} \quad (15)$$

If $\mu \ll v$, this slope is just a consequence of the dispersive properties of the medium; higher frequencies propagate at a smaller velocity. When μ is greater than v , the apparent slope of the pearl element is smaller than the one we would have expected from a usual dispersion theory.

Nonlinear effects will produce a decrease of μ with time. If this decrease is sufficiently fast, then the pearl elements can remain parallel (if $\mu > v$ and $\mu(\cdot) t^{-1/2}$, $d\omega/d\tau = \text{const}$) or even reerect (when $\mu(\cdot) t^{-1}$, $d\omega/d\tau(\cdot) t$).

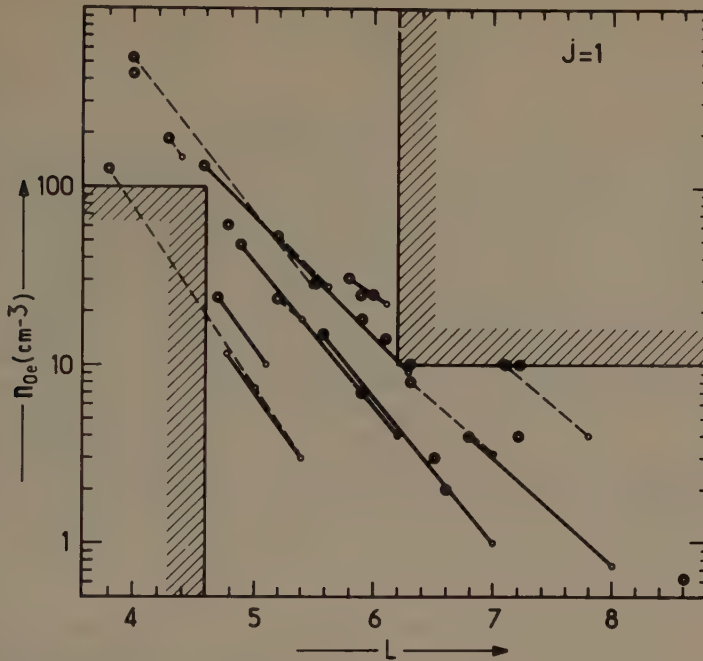


Fig. 4. Determination of the equatorial cold plasma density from the measured pearl dispersion. The lines link the points corresponding to the same emission. One sees that from a given pearl event, one can get large variations both in n_0 and L . The open circles give the most probable values, i.e., the ones for which it is reasonable to assume that the quasi-linear effects have ceased to play a role in the dispersion characteristic of the pearls. The electron density variation along the field line was assumed to follow a law of the type $n_0(\cdot) B^j$ with $j=1$ (Gendrin *et al.*, 1971).

This phenomenon explains why when one computes the L value on which a pearl has been generated by utilizing the usual dispersion theory, one gets large variations depending on the part of the pearl element which has been chosen. Values as large as $\Delta L \sim 1$ and $\Delta n_0/n_0 \sim 2000\%$ can be obtained for this determination (Figure 4). Therefore, the small effect ($\Delta L \sim 0.1$, $\Delta n_0/n_0 \sim 10\%$) which is produced by the finite temperature of the 'cold' plasma (Higuchi and Jacobs, 1970) is negligible as compared with the one which is a consequence of the nonlinear diffusion of interacting protons.

B. ARTIFICIALLY TRIGGERED EMISSIONS

When a wave is monochromatic, the QL formalism cannot be applied. The resonating particles and the wave travel together over a sufficiently long distance so that a coherent action can be exerted. Resonating particles may remain trapped inside the potential well of the wave. The trapping frequency depends upon the intensity of the wave, and is given by

$$\omega_t = 2\pi/f_t = C_1 (kv_\perp \omega_k)^{1/2} \quad (16)$$

for particles having large initial pitch angles, and

$$\omega_t = 2\pi/f_t = C_2 \Omega^{1/3} \omega_k^{2/3} \quad (17)$$

for particles having small initial pitch angles (Roux and Solomon, 1970). In these expressions ω_k is the gyropulsation associated with the magnetic field intensity of the wave ($\omega_k = eb_k/m$), C_1 and C_2 are numerical constants which are of the order of unity.

The trapping of particles inside a monochromatic wave has been studied by Knox (1969), Ashour-Abdalla (1970), Roux and Solomon (1970), and Nunn (1971). On a semi-phenomenological basis, Helliwell (1967) has used this phenomenon to explain the artificially triggered VLF emissions. Laval *et al.* (1971) have worked on a new approach of this mechanism that we will now describe.

Artificial VLF emissions by ground based transmitters provide a unique opportunity for having a wave packet of well defined frequency propagating through the magnetosphere. Particles can be trapped inside such a wave packet, even in an inhomogeneous medium, provided that the following condition is satisfied

$$\mu \frac{\partial B_0}{\partial z} + \frac{m\omega^2}{k^3} \frac{dk}{dz} < \frac{m\omega_t^2}{k}. \quad (18)$$

This condition expresses the fact that the trapping force ($m\omega_t^2/k$) must be larger than the detrapping forces. One of these is the action of converging field lines which tends to increase the particle pitch angle; the other term comes from the change to a non-galilean frame of reference (Laval *et al.*, 1971).

If the inhomogeneity is too large ($\partial B_0/\partial z$ important) or if the wave field intensity is too small (ω_t insignificant) then the detrapping effect can occur before the end of the wave packet. This explains why some triggered emissions start before the end of a morse code dash (~ 150 ms).

By computing the distribution function of particles after they have passed through the wave packet, Laval *et al.* (1971) have been able to deduce the condition for which a new wave of completely different frequency can be generated. They have shown that the amplitude of the triggered emission is larger when the change of the resonant frequency due to the inhomogeneity verifies the following condition

$$\delta\omega/\delta k = v_\phi. \quad (19)$$

In the whistler mode, this condition is fulfilled for frequencies near $\Omega/4\pi$. This could explain why emissions have been observed to be triggered very near to half the equatorial gyrofrequency (Carpenter, 1968; Kimura, 1968; Carpenter and Lasch, 1969).

Nonlinear effects are important, not only in artificially triggered phenomena, but also in the natural ones: for instance, the banded chorus which is observed in the magnetosphere (Coroniti *et al.*, 1971) or the quasi-totality of the Pc 1 oscillations (Roux and Solomon, 1970).

4. Quantitative Verification of the Q.L. Theory

In this section, we will briefly report on a recent experiment by which a quantitative verification of the QL theory has been obtained.

A. RESULTS

The experiment and its most important results have been described elsewhere (Gendrin *et al.*, 1970; Etcheto *et al.*, 1971a, b).

A rocket was fired from Kerguelen Islands ($L=3.7$) including VLF receivers (0.4 to 6 kHz) and particle detectors (30 to 300 keV). During one launch (April, 1, 1968) a periodic modulation (~ 80 s) of both the flux of trapped electrons ($76^\circ < \alpha < 90^\circ$ at 400 km) and the intensity of VLF hiss ($3.5 < f < 4.5$ kHz) was detected. The main results are the following:

(i) By applying Equation (6), it was possible to determine the main region of interaction, i.e., the region in which the most important part of the particle population (the one which has the mean energy ~ 80 keV) is interacting. This region was found to be slightly off the equator ($\lambda \sim 20^\circ$) in agreement with Liemohn's (1967) computation.

(ii) From the measurement of the VLF intensity at 400 km, it is possible to estimate the corresponding intensity in the region of interaction and, by using Equation (2), to deduce the value of the diffusion coefficient D corresponding to the maximum of the modulation. This value amounts to be $\approx 10^{-3} \text{ rd}^2 \text{ s}^{-1}$.

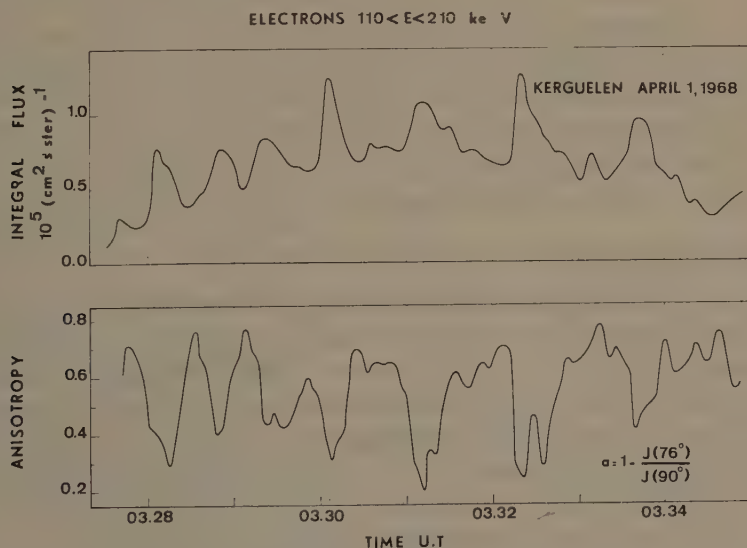


Fig. 5. Simultaneous variation of the mean perpendicular flux of electrons and their partial anisotropy. These measurements were made onboard a rocket (culmination altitude ~ 400 km) launched from Kerguelen Islands ($L \sim 3.7$) on April 1, 1968. Each peak of the flux modulation is associated with a peak in the intensity of the simultaneously detected VLF hiss ($3.5 < f < 4.5$ kHz) (Etcheto *et al.*, 1971b).

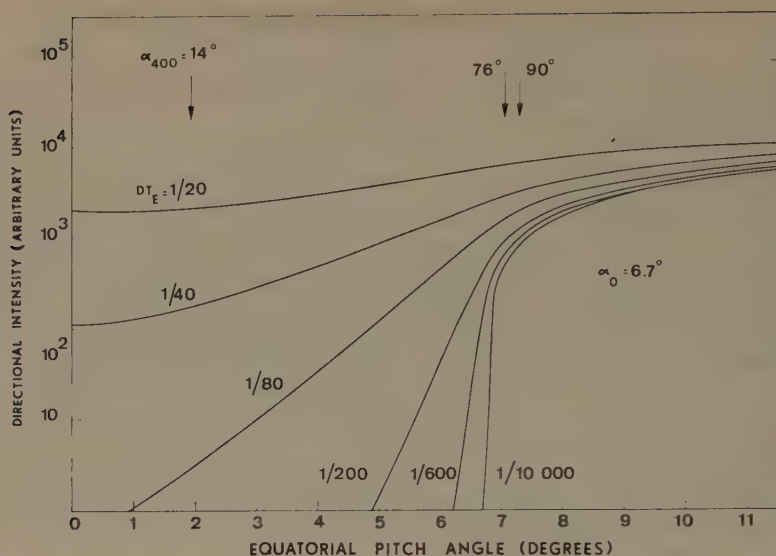


Fig. 6. Equilibrium pitch angle distribution function for different values of the diffusion coefficient D . T is the escape time of particles (roughly 0.15 sec for 100 keV electrons at $L = 3.7$). The arrows indicate the equivalent equatorial pitch angles which were sampled by our detectors (Etcheto *et al.*, 1971b).

(iii) The observed anisotropy decreases when the flux increases (Figure 5) indicating an increase of the diffusion coefficient. By using the steady state solution of Equation (1) (which was computed by Kennel and Petschek (1966) and Theodoridis and Paolini (1967)) it is possible to deduce independently another value of the diffusion coefficient, because, (as it is shown on Figure 6) the anisotropy in the vicinity of the loss cone is very sensitive to the value of D . The measured value agrees well with the one that we can deduce from the measurement of the wave field intensity.

B. DISCUSSION ABOUT THE ORIGIN OF THE 80 s PERIODICITY

In our previous papers (Etcheto *et al.*, 1971a, b), this 80 s modulation was interpreted in the frame of Coroniti and Kennel's (1970) theory. One assumes the existence of a compressional ULF wave ($b_{\parallel} B_0$) of unknown origin. Due to the change of the longitudinal magnetic field, the anisotropy of the electron distribution function varies with time as do the amplification coefficient of the VLF waves and the diffusion coefficient of particles; thus the modulation of the particle flux and the wave intensity are thus explained. A value of the order of 7γ for this ULF wave was necessary quantitatively to interpret the observed ratio of the peak of valley flux of the trapped electrons. Purely compressional waves of this amplitude and this frequency have been recently reported by Barfield *et al.* (1971).

Our interpretation therefore seemed plausible, but we have to explain the origin of the ULF wave.

One can think of another interpretation. Whistler turbulence has been shown to play an important role in the destabilization of drift waves in the presence of pressure and magnetic gradients (Hagege *et al.*, 1971). Once they have been amplified, these drift waves modulate the particle anisotropy and the whistler turbulence itself.

Consequently, the origin of all these modulated or quasi-periodic emissions may be sought in the inward diffusion of particles during substorms by which strong pressure gradients can be generated.

5. Consequences of Geophysical Importance

In a series of recent papers (see Table II), the gyroresonant WPI's have been invoked in order to explain many important geophysical phenomena. One can think of a number of reasons for which this mechanism is favored:

(a) It is symmetric in the sense that both protons and electrons interact (respectively with the ion cyclotron wave and the whistler mode).

(b) Because of the anisotropic properties of the plasma, the waves which are involved are more or less guided by the magnetic field lines; they are not much absorbed by the ionosphere. Therefore they can be detected on the ground and there exists a lot of experimental data concerning them.

(c) This mechanism works in fact by the violation of the first adiabatic invariant, a process much faster than the ones which violate the two other invariants (bounce resonance or radial diffusion, for instance).

TABLE II

Recent interpretations of geophysical phenomena in terms of cyclotron interactions

Phenomena	References
<i>Role of the plasmopause</i>	
– Precipitation of ring current protons	
(a) inside the plasmasphere	Cornwall <i>et al.</i> (1970) Cornwall <i>et al.</i> (1971b)
(b) outside the plasmasphere (in relation with proton auroral arcs)	Eather and Carovillano (1971)
– Generation of VLF and ELF hiss	Burton <i>et al.</i> (1970) McPherson and Koons (1970)
<i>Other induced precipitation by enhancement of the cold plasma density</i>	
– Ionospheric photoelectrons	Brice and Lucas (1971)
– Artificial injection of plasma	Brice (1970, 1971)
– Satellite sunrise	Mozer <i>et al.</i> (1971)
<i>Phenomena involving more than one particle species</i>	
– Proton induced SAR arcs	Cornwall <i>et al.</i> (1971a)
– High energy electron slot	Thorne and Kennel (1971)
– Induced proton precipitation by ELF hiss	Haerendel (1971)

(d) It is very efficient for particles in the 10 to 100 keV energy range; these particles (both electrons and protons) constitute the most important part of the *fluctuating* population of magnetospheric particles.

(e) Finally, its theory is almost fully achieved and presents itself in a coherent fashion, owing principally to the work of Kennel and Petschek (1966).

We will concentrate our discussion on two aspects of the theory: namely, the role of the cold plasma density and the induced interaction of electrons over protons and vice versa.

A. ROLE OF THE COLD PLASMA DENSITY

If the cold plasma density is increased then the Alfvén velocity decreases; therefore, the critical energy is decreased and more particles can interact with the cyclotron waves. This is principally true when the anisotropy of the distribution function is small (see Table I).

In some regions of the magnetosphere, the cold plasma density can increase because of the outward motion of the plasmopause during the recovery phase of storms or substorms. Therefore, low energy ring current protons (~ 10 keV) which have been

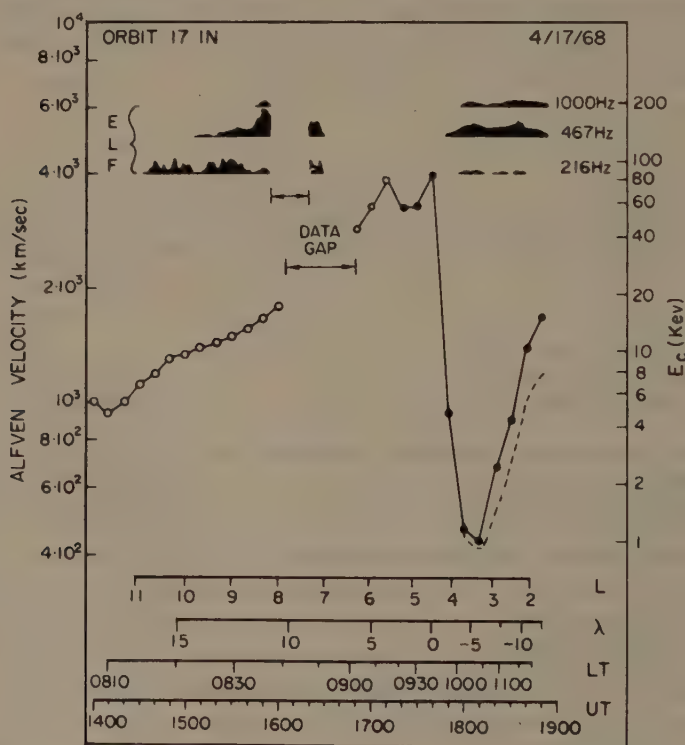


Fig. 7. Variation of the equatorial value of the Alfvén velocity as deduced from measurements onboard OGO 5. One sees that electromagnetic noise (ELF or VLF hiss) is observed only in those regions where the magnetic energy per particle is small, roughly below 20 keV (Burton *et al.*, 1970).

pushed inward during the growth phase of the storm are rapidly precipitated. This could explain the associated displacements of the plasmapause and of the inner edge of the ring current particles (Russell and Thorne, 1970; Frank, 1971) as was proposed by Cornwall *et al.* (1970, 1971b) on the basis of experimental results obtained with both high apogee and low orbiting satellites.

However, even if it is true that just inside the plasmasphere, the magnetic energy per particle can be as low as a few keV (Figure 7), it does not mean that particles having energies just above this limit will strongly interact with cyclotron waves (see Section 2.A.3).

On the contrary, it can be shown that for realistic wave spectrum intensity, the diffusion time to the loss cone increases very much at a given energy when one goes from outside to inside the plasmasphere (see Eather and Carovillano, 1971, Table 3). Of course, estimation of this diffusion lifetime must be made by taking duly into account the energy diffusion which is important for these low energy protons and which can amount to 80% for 10 keV protons (Gendrin, 1968; Eather and Carovillano, 1971). Considering this energy diffusion leads to higher limiting flux of protons inside the plasmapause than outside (Haerendel, 1970), confirming the idea that strong precipitation of low energy protons inside the plasmapause cannot be explained by a simple gyroresonant WPI.

The same arguments apply to theories in which an increase of the cold plasma density is invoked in order to interpret enhanced precipitation of electrons (see Table II). In fact, one has to consider the self-consistent solution in which the self-generated waves are used for computing the new diffusion time in the presence of an enhanced cold plasma density.

B. PROCESSES INVOLVING MORE THAN ONE PARTICLE SPECIES

Once the cyclotron wave has been generated, it can interact with other particles. For instance high frequency cyclotron waves ($\omega \approx \Omega$) are subject to severe Landau damping as soon as they propagate obliquely. This could be at the origin of the precipitation of electrons in the energy range of some eV (Cornwall *et al.*, 1971a).

However, even for waves propagating strictly parallel to the magnetic field secondary effects can be observed on the other category of particles. For instance, let us assume that the proton distribution is such that an ion cyclotron wave can be generated. Usually the anisotropy of electrons is such that they can absorb the ion cyclotron wave. In order to be able to resonate and to fulfill Equation (6) they need to have relativistic energies. This mechanism has been invoked to explain the precipitation of > 1 MeV electrons in the region $3 < L < 5$ during the initial phase of a magnetic storm (Thorne and Kennel, 1971).

A completely symmetric mechanism has been proposed by Haerendel (1971) for explaining the precipitation of protons. Protons, the distribution function of which is insufficiently anisotropic for generating a left hand wave, can absorb a right-hand wave if such a wave is present. This wave can be the result of a gyroresonant WPI between high energy (~ 100 keV electrons) and ELF hiss. For verifying the resonance

conditions in Equation (6), the protons do not need to be relativistic. It is sufficient that their parallel velocity verifies (Gendrin, 1965)

$$V_r \geq \frac{3\sqrt{3}}{2} V_a \quad (20)$$

which does not correspond to a very high energy ($E_r \gtrsim 7 E_m$).

Because they are obliged to follow the diffusion curve in the velocity space, protons will gain very much energy during this process (see Gendrin, 1968, Figure 3), provided that the ELF hiss intensity is sufficiently strong. The details of this mechanism have not yet been completed.

6. Conclusions

From the examination of our data and other theoretical or experimental work, one sees that



Fig. 8. Illustrating the fact that a pitch angle diffusion is always associated with an energy loss (after Schulz and (Sch)Roederer).

(a) Gyroresonant WPI's play an important role in the dynamics of magnetospheric particles;

(b) The QL theory seems to be verified in most of its microscopic aspects and macroscopic consequences;

(c) However, a complete self-consistent solution of the problem has to be found before conclusive remarks can be made about the different loss mechanisms of magnetospheric particles induced by gyroresonant WPI's;

(d) The energy loss of particles during these processes, mainly of protons, must not be forgotten (see Figure 8);

(e) Monochromatic effects are of some importance and must be more considered in the future.

From the experimental point of view, the lack of any precise knowledge of the angular distribution of particles is severely felt. In this respect, work could be done in two directions:

(a) Onboard satellites, at large distances near the equator, a precise determination of the distribution function at large pitch angles will allow a better estimation of the anisotropy factor. Remember that A is weighted by $\tan \alpha$ (see Equation (8)), although $\partial f / \partial \alpha$ is more important for small pitch angles.

(b) Onboard rockets or low altitude orbiting satellites, one could take benefit of the magnifying lense effect which is due to the conservation of μ for getting very fine measurements in the vicinity of the equatorial loss cone (see Figure 6).

Acknowledgments

I am pleased to thank MM. Pellat, Roux, and Solomon for many interesting discussions concerning this subject.

References

- Ashour-Abdalla, A.: 1970, *Planetary Space Sci.* **18**, 1799.
 Barfield, J. N., Lanzerotti, L. J., MacLennan, C. G., Paulikas, G. A., and Schulz, M.: 1971, *J. Geophys. Res.* **76**, 5252.
 Brice, N.: 1970, *J. Geophys. Res.* **75**, 4890.
 Brice, N.: 1971, *J. Geophys. Res.* **76**, 4698.
 Brice, N. and Lucas, C.: 1971, *J. Geophys. Res.* **76**, 900.
 Burton, R. K., Russell, C. T., and Chappell, C. R.: 1970, *J. Geophys. Res.* **75**, 5582.
 Carpenter, D. L.: 1968, *J. Geophys. Res.* **73**, 2919.
 Carpenter, D. L. and Lasch, S.: 1969, *J. Geophys. Res.* **74**, 1859.
 Cornwall, J. M.: 1966, *J. Geophys. Res.* **71**, 2185.
 Cornwall, J. M., Coroniti, F. V., and Thorne, R. M.: 1970, *J. Geophys. Res.* **75**, 4699.
 Cornwall, J. M., Coroniti, F. V., and Thorne, R. M.: 1971a, *J. Geophys. Res.* **76**, 4428.
 Cornwall, J. M., Hilton, H. H., and Mizera, P. F.: 1971b, *J. Geophys. Res.* **76**, 5220.
 Coroniti, F. V. and Kennel, C. F.: 1970, *J. Geophys. Res.* **75**, 1279.
 Coroniti, F. V., Fredricks, P. C., Kennel, C. F., and Scarf, F. L.: 1971, *J. Geophys. Res.* **76**, 2366.
 Criswell, D. R.: 1969, *J. Geophys. Res.* **74**, 205.
 Drummond, W. E.: 1965, in B. B. Kadomtsev, M. N. Rosenbluth, and W. B. Thompson (eds.), *Plasma Physics*, IAEA, Vienna, p. 527.
 Eather, R. H. and Carovillano, R. L.: 1971, *Cosmic Electrodyn.* **2**, 105.

- Engel, R. D.: 1965, *Phys. Fluids* **8**, 939.
- Etcheto, J., Gendrin, R., and Lemaire, D.: 1971a, *J. Geophys. Res.* **76**, 1079.
- Etcheto, J., Gendrin, R., and Lemaire, D.: 1971b, Proceedings of the ESRO Colloquium on Wave Particle Interactions, ESRO/S.P.72, p. 123.
- Etcheto, J., Roux, A., Singh, R. P., and Solomon, J.: 1971c, Paper presented at the XVth IUGG general Assembly, Moscow.
- Frank, L. A.: 1971, *J. Geophys. Res.* **76**, 2265.
- Gendrin, R.: 1965, *J. Geophys. Res.* **70**, 5369.
- Gendrin, R.: 1968, *J. Atmospheric Terrest. Phys.* **30**, 1313.
- Gendrin, R., Etcheto, J., and de la Porte des Vaux, B.: 1970, *J. Geophys. Res.* **75**, 6169.
- Gendrin, R., Lacourly, S., Roux, A., Solomon, J., Feiguin, F. Z., Gokhberg, M. V., Troitskaya, V. A., and Yakimenko, V. L.: 1971, *Planetary Space Sci.* **19**, 165.
- Gregory, C. T.: 1971, *J. Geophys. Res.* **76**, 268.
- Haerendel, G.: 1970, in B. M. McCormac (ed.), *Particles and Fields in the Magnetosphere*, D. Reidel Publishing Company, Dordrecht, Holland, p. 416.
- Haerendel, G.: 1971, Proceedings of the ESRO Colloquium on wave and particle interactions, ESRO/S.P. 72, p. 63.
- Hagege, K., Laval, G., Parks, G., and Pellat, R.: 1971, Paper presented at the XVth IUGG general Assembly, Moscow.
- Helliwell, R. A.: 1967, *J. Geophys. Res.* **72**, 4773.
- Higuchi, Y. and Jacobs, J. A.: 1970, *J. Geophys. Res.* **75**, 7105.
- Kennel, C. F. and Petschek, H. E.: 1966, *J. Geophys. Res.* **71**, 1.
- Kimura, I.: 1968, *J. Geophys. Res.* **73**, 445.
- Knox, F. B.: 1969, *Planetary Space Sci.* **17**, 13.
- Laval, G., Pellat, R., and Roux, A.: 1971, Paper presented at the XVth IUGG general Assembly, Moscow.
- Liemohn, H. B.: 1967, *J. Geophys. Res.* **72**, 39.
- McPherson, D. A. and Koons, H. C.: 1970, *J. Geophys. Res.* **75**, 5559.
- Matsumoto, H. and Kimura, I.: 1971, *Planetary Space Sci.* **19**, 567.
- Mozer, F. S., Bogott, F. H., and Brice, N.: 1971, 'Triggered Acceleration of 50 Kilovolt Protons and Electrons', Preprint, University of California, Berkeley.
- Nunn, D.: 1971, *J. Plasma Phys.* **5**, 199.
- Roux, A. and Solomon, J.: 1970, *Ann. Geophys.* **26**, 279.
- Roux, A. and Solomon, J.: 1971, *J. Atmospheric Terrest. Phys.* **33**, 1457.
- Russell, C. T. and Thorne, R. M.: 1970, *Cosmic Electrodyn.* **1**, 67.
- Theodoridis, G. C. and Paolini, F. R.: 1967, *Ann. Geophys.* **23**, 375.
- Thorne, R. M. and Kennel, C. F.: 1971, *J. Geophys. Res.* **76**, 4446.

ELECTROSTATIC WAVES IN THE MAGNETOSPHERE

F. L. SCARF and R. W. FREDRICKS

Space Sciences Dept. TRW Systems Group, Redondo Beach, Calif., U.S.A.

Abstract. Electric dipole antennas on magnetospheric spacecraft measure E field components of many kinds of electromagnetic waves (lightning whistlers, chorus, triggered emissions, high pass noise). In addition, lower hybrid resonance emissions are frequently observed well above the ionosphere. The OGO 5 plasma wave experiment has also detected new forms of electrostatic emissions that appear to interact very strongly with the local plasma particles. Near the geomagnetic equator, intense waves with $f \simeq (n + \frac{1}{2}) f_c$ are detected on auroral L shells during most passes in the midnight-dawn-noon LT sector. Greatly enhanced wave amplitudes have been found during the expansion phases of substorms, and analysis indicates that these emissions produce strong pitch angle diffusion. Intense broadband electrostatic turbulence is also detected at current layers containing steep magnetic field gradients. This current-driven instability is operative at the bow shock and also at field null regions just within the magnetosheath, and at the magnetopause near the dayside polar cusp. The plasma turbulence appears to involve ion acoustic waves, and the wave particle scattering provides an important collisionless dissipation mechanism for field merging. Another region of unusually intense magnetospheric wave activity occurs at the boundary of the hot cusp plasma and cold plasma-sphere.

1. Introduction

The magnetosphere contains a complex and variable population of charged particles, and it provides an excellent laboratory for the study of non-equilibrium plasma phenomena. On closed field lines, thermal plasma co-exists with a durable but changing population of energetic protons and electrons. The polar cusp provides direct entrance of relatively hot magnetosheath plasma down to the cool ionosphere, and some of these particles migrate to the plasma sheet, although other sources can also contribute to yield the observed plasma sheet and geomagnetic tail particle flux. The large variety of particle sources and sinks leads to complex local distribution functions and, at almost any point in space and time, the overall magnetospheric distributions appear to differ greatly from equilibrium Maxwell-Boltzmann functions. For instance, plasma sheet electrons and ions generally have different temperatures, the closed field line angular distributions are highly anisotropic, and the energy profiles frequently have bumps or significant non-thermal tails.

Extensive laboratory studies and many theoretical analyses show that waves play dominant roles in all non-equilibrium plasma systems. In particular, when the plasma is dilute and cool, ordinary coulomb collisions are unimportant and wave particle interactions provide the scattering and acceleration mechanisms that govern the dynamics. For example, turbulent wave particle scattering leads to an effective conductivity and resistive-type heating; resonant wave particle interactions give rise to acceleration similar to that in a cyclotron; and waves also allow diffusion that can be directly associated with particle energization (i.e., cross L diffusion with conservation of magnetic moment, $\mu = mv_{\perp}^2/B$, gives $v_{\perp} \sim B^{1/2}$). Waves also cause diffusion in pitch angle and particle precipitation.

Historically, the first magnetospheric wave measurements made above the polar

orbit regime were carried out using magnetic antennas, and these instruments gave important information concerning local characteristics of electromagnetic waves. The most extensive theoretical analyses of magnetospheric stability also involved properties of electromagnetic radiation. Several years ago Kennel and Petschek (1966) noted that loss cone distributions on closed field lines would cause electron whistler mode turbulence to grow spontaneously. They estimated the quasi-linear pitch angle diffusion coefficients and showed that the wave particle interactions would limit the electron flux that could be stably trapped in the magnetosphere. Very similar calculations utilizing an electromagnetic proton cyclotron mode instability seem to be capable of accounting for the decay of the ring current (Cornwall *et al.*, 1970), some relativistic electron precipitation phenomena (Thorne and Kennel, 1971), and the appearance of SAR arcs near the plasmapause (Cornwall *et al.*, 1971).

However, this emphasis on electromagnetic instabilities is not a natural one for a collisionless plasma. In most laboratory systems, *electrostatic* wave modes develop more readily, and they interact more strongly with the plasma. The basic reason for this is that most electrostatic waves have phase velocities comparable to the plasma thermal speeds, while electromagnetic oscillations generally have much higher velocities; thus the electrostatic modes are easier to generate (by Čerenkov or two-stream interactions) and many more particles are present in the plasma to interact resonantly with the oscillations.

Since March 1968 the OGO 5 plasma wave experiment has sampled characteristics of electromagnetic and electrostatic waves in the magnetosphere, the magnetosheath, and the upstream solar wind. In this report, we summarize some of the more significant findings, with emphasis on detection of electrostatic wave mode. A general survey is presented first, and we then discuss substorm observations and measurements in the polar cusp region. The final section contains a brief description of certain additional wave measurements.

2. Survey of Magnetospheric Wave Observations

In order to summarize the nature of the various wave observations in the magnetosphere, we display in Figure 1 a sketch of the entire cavity and a number of fairly characteristic but distinct frequency-time diagrams. The dynamic spectrum in the lower left corner of Figure 1 shows the electric dipole response for an INJUN 5 northern hemisphere polar cusp crossing between 2329 and 2333 UT on December 12, 1968 (see Figure 8 of Gurnett and Frank (1971)). This portion contains a number of fairly familiar low altitude waveforms (such as ELF and VLF hiss and electromagnetic chorus), and we will comment on this again in Section 4.

All of the other frequency time diagrams in Figure 1 are made up using high altitude data from the OGO 5 special purpose telemetry. The two panels marked 'B or E' are taken from the output of the JPL-UCLA magnetic search coil sensor and these represent electromagnetic waveforms. The corresponding electric field signals are essentially identical, and both types of sensors detect these waves readily. The narrow

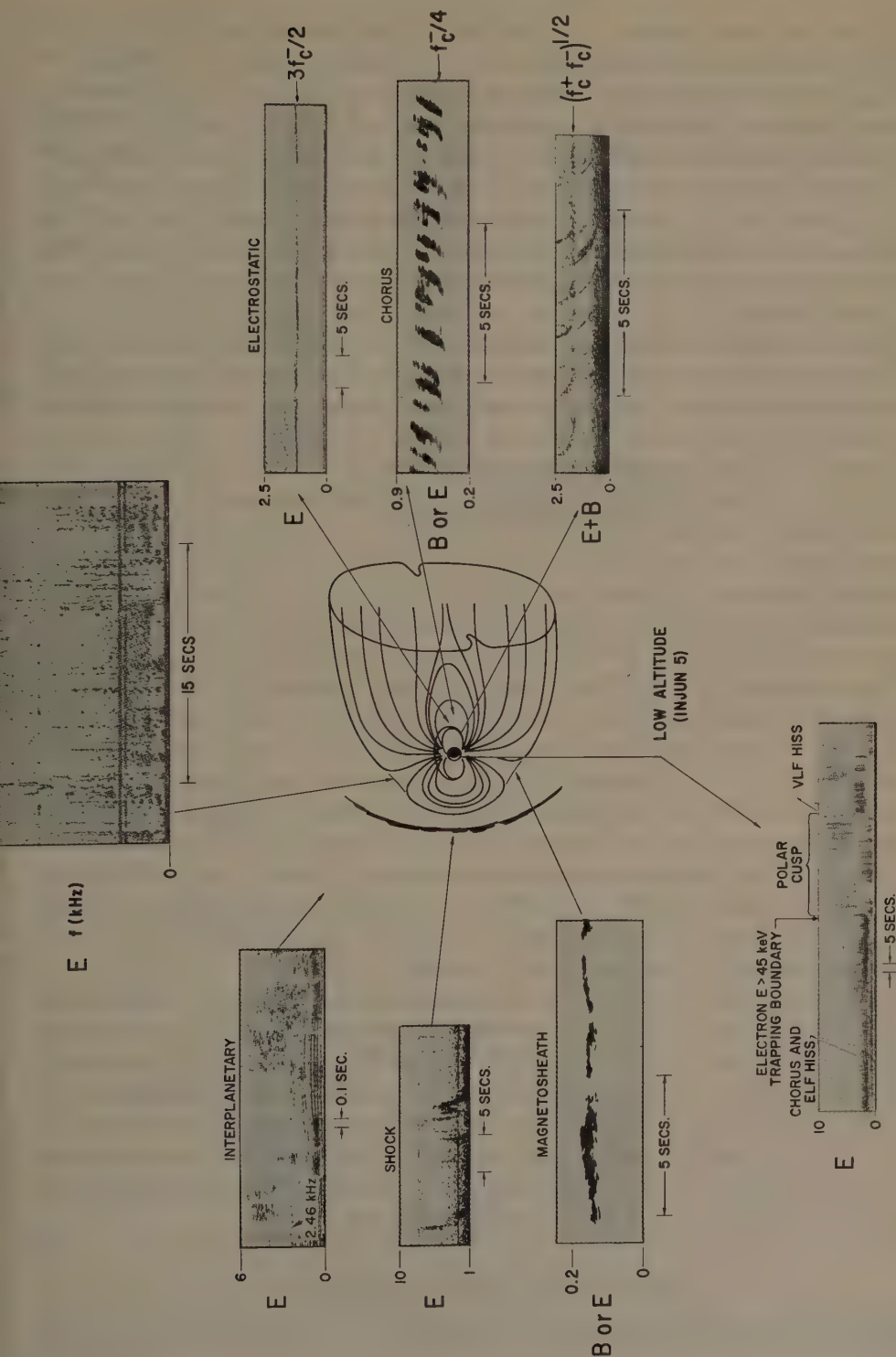


Fig. 1. A survey of the most common intense VLF wave characteristics detected in the earth's plasma environment. Except for the low altitude panel, all frequency time diagrams are based onOGO 5 measurements. The chorus and magnetosheath emissions were recorded by the search coil; the whistler LHR diagram is a superposition of search coil and dipole data; and the other panels contain $f-t$ diagrams from the electric field instrument.

band magnetosheath emission is a 'lion roar' of the type described by Smith *et al.* (1969) and the burst shown here was detected at 1711 UT on March 12, 1968. These strong whistler mode waves are found near magnetic field gradients, and they may be related directly to the low altitude low frequency oscillations detected by INJUN 5 within the polar cusp (Gurnett, 1971). The chorus signal displayed here was recorded by OGO 5 at 0113:19 UT on March 7, 1968 when the spacecraft coordinates were $L=7.9$, $MLAT=-3.7^\circ$, and $LT=1103$. Electric field observations of various chorus elements were recently described by Coroniti *et al.* (1971), and Rosenberg and Helliwell (1971) provided convincing evidence that chorus emissions do precipitate energetic electrons.

The remaining panels of Figure 1 are marked 'E' or 'E+B' and all of these contain frequency time diagrams with electrostatic waves. Only one is familiar from low altitude Alouette measurements. That is, the lowest panel on the right side shows lightning whistlers along with a strong electrostatic lower hybrid resonance emission detected by the OGO 5 wave experiments at 1317 UT on May 15, 1969 ($r=2.4 R_E$, $L=3.1$, $MLAT=-26^\circ$, and $LT=1600$). The data are somewhat unusual in that the E field sensor found no signals below the LHR frequency (~ 1.8 kHz) and the search coil was only sensitive to frequency components below about 1.5 to 1.7 kHz; accordingly, the spectrum shown is a literal superposition of the E and B waveforms, and these continuous lightning whistler curves are actually made up from the output of two separate experiments with quite different characteristics (Scarf *et al.*, 1971a).

The other diagrams describe more important locally generated waves of two types: (a) the narrow band $f \approx 3f_c/2$ E field emissions are detected primarily near the geomagnetic equator on auroral L shells; (b) the strong, impulsive and almost undispersed mid-frequency (1 to 10 kHz) electric field bursts are found near current layers in the upstream solar wind, bow shock region, and magnetosheath. The specific March 10, 1968, interplanetary observations were described by Scarf *et al.* (1970), and general bow shock E field wave measurements were discussed in detail by Fredricks *et al.* (1970) (see Crook *et al.* (1969) for descriptions of the plasma wave instrument and of the particular bow shock data of Figure 1). The panel marked 'polar cusp' contains magnetosheath and/or cusp data from November 1, 1968.

This OGO 5 pictorial survey is actually restricted by instrumental considerations. The TRW instrument has E field waveform data only over the range 1 to 22 kHz and the JPL-UCLA search coil covers $f \approx 10$ Hz to about 1.5 kHz. Moreover, very broad hiss-type spectra do not show up well on the analog telemetry, although their properties can be studied easily using the narrow band spectrum analyzer. With these instrumental considerations in mind, we can state that the OGO 5 waveforms shown in Figure 1 do represent most of the common, or repeatable, intense emissions detected with the broadband OGO 5 telemetry at high altitudes.

3. Electric Field Emissions and Substorms

Kennel *et al.* (1970a) presented the first discussion of 'high frequency', or $f > f_c^-$,

electric field measurements in the magnetosphere, and showed that the OGO 5 dipole frequently detects strong signals at $f \approx 3f_c/2$. Further detailed analysis of all 1968 data (Kennel *et al.*, 1970b) indicated that these waves were clearly detected on more than 60% of the OGO 5 geomagnetic equator crossings between $L=4$ and $L=10$ in the midnight-dawn-noon LT sector. The latter paper also contained a discussion of the large wave amplitudes (up to 10 mV m^{-1}), and the authors noted that $f=3f_c/2$ emissions can provide very efficient scattering of kV energy electrons. In fact, a rough estimate of the velocity space diffusion rate, based on measured wave amplitudes and frequencies, suggested that the high frequency emissions might account for the observed strong diffusion loss rates for soft electrons.

Soon after launch, OGO 5 had no high sensitivity plasma probes covering the 1 to 10 keV range in operation, but it has been possible to use energetic ($E \gtrsim 50 \text{ keV}$) electron detectors to study similar local wave particle interactions during magneto-

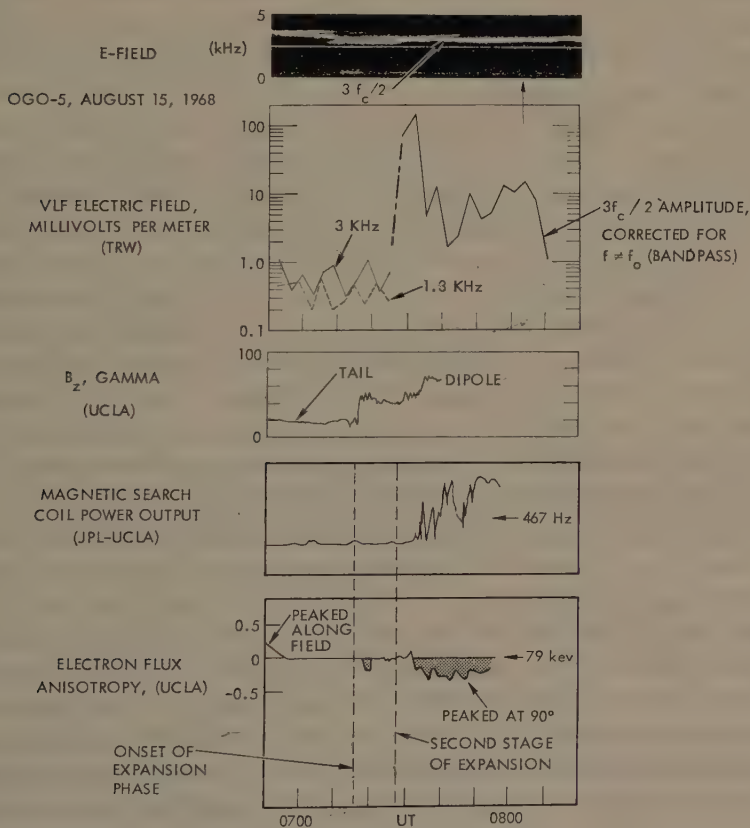


Fig. 2. An OGO 5 example of local wave particle interactions in the nightside equatorial cusp during a substorm. Both electrostatic ($f \approx 3f_c/2$) and electromagnetic (chorus) waves were present after 0733 UT when the loss cone particle distribution developed, but only intense electrostatic waves were detected earlier when the distribution was essentially isotropic. This suggests that the $f \approx 3f_c/2$ waves caused strong diffusion and precipitation. The magnetometer, search coil, and particle flux observations were furnished by C. T. Russell, R. K. Burton, and M. G. Kivelson, respectively.

spheric substorms. An integrated series of detailed reports on the substorms of August 15, 1968, was recently completed, and Figure 2, taken from the report of Scarf *et al.* (1971b), shows some significant correlated wave, particle, and field observations for the period 0650 to 0810 UT on this day. At the onset of the substorm expansion (≈ 0715 UT), OGO 5 was at $7.9 R_E$ and 0045 LT (MLAT = 2.9° and $L = 7.9$), and at this time the local value of B_z (GSM-coordinates) suddenly increased from a typical equatorial cusp-like value ($\sim 10 \gamma$) to one more characteristic of an undistorted dipole ($\sim 20 \gamma$). The second phase of the expansion occurred at about 0727 UT (MLAT = 1.9° , $L = 7.6$) as B_z (GSM) started an even greater increase.

When the field first settled into a dipolar configuration after about 0717, a normal or loss cone distribution of $E \approx 80$ keV electrons was encountered briefly; however the particle distribution soon became quite isotropic, and the loss cone was not detected again until about 0731 to 0733 UT. The search coil output shows that a detectable electromagnetic signal (chorus) was present after the reestablishment of the loss cone, as predicted by the Kennel and Petschek (1966) instability analysis. However, the earlier *isotropic* distribution would appear to involve strong diffusion, and during this period no chorus was present.

The upper panels of Figure 2 describe the high frequency electric field observations, and it is clear that very intense $f \approx 3f_c^-/2$ waves did accompany the particle isotropy. The frequency time diagram in the top panel shows the full E field waveform between 0803:34 UT and 0804:22 UT. Here the strong and diffuse tone with $f \approx 3$ kHz is an $f \approx 3f_c^-/2$ emission, the narrow line with $f = 2.461$ kHz is a spacecraft interference tone, and the sporadic bursts having $f \approx 600$ Hz are chorus emissions. The amplitude trace for the $3f_c^-/2$ emission was obtained by combining the measured instantaneous frequency of the wave (derived from the waveform) with the known response curve for each plasma wave narrow band channel and the measured output level traces in these channels (see Scarf *et al.*, 1971b). It can be seen (second panel from top) that the power in the $3f_c^-/2$ -wave increased by more than five orders of magnitude after the substorm expansion, and this fact suggests that the E field emissions should have produced strong diffusion, local isotropy, and particle precipitation. In fact, Scarf *et al.* (1971b) used the corrected wave amplitude profile and the measured frequency to estimate the variation in the pitch angle diffusion coefficient for 80 keV electrons. They concluded that before 0733 UT the overall diffusion coefficient associated with these waves exceeded $10^{-3}(\text{rad})^2 \text{ s}^{-1}$, and this strongly suggests that E field-wave-particle interactions did control the local angular distributions at the start of the substorm.

It is useful to confirm such a novel result, and Figure 3 shows a very similar sequence of substorm observations in nearly the same spatial location one week earlier. Once again, an intense $f \approx 3f_c^-/2$ emission was detected following the substorm expansion, and this wave could have produced the particle isotropy and attendant precipitation. However, when the August 7 substorm was first detected by OGO 5 before 1130 UT, the special purpose telemetry was of poor quality and it was not possible to evaluate the corrected $3f_c^-/2$ amplitude with sufficient precision to compute the overall diffusion coefficient. Moreover, the University of Minnesota balloon was not on the same

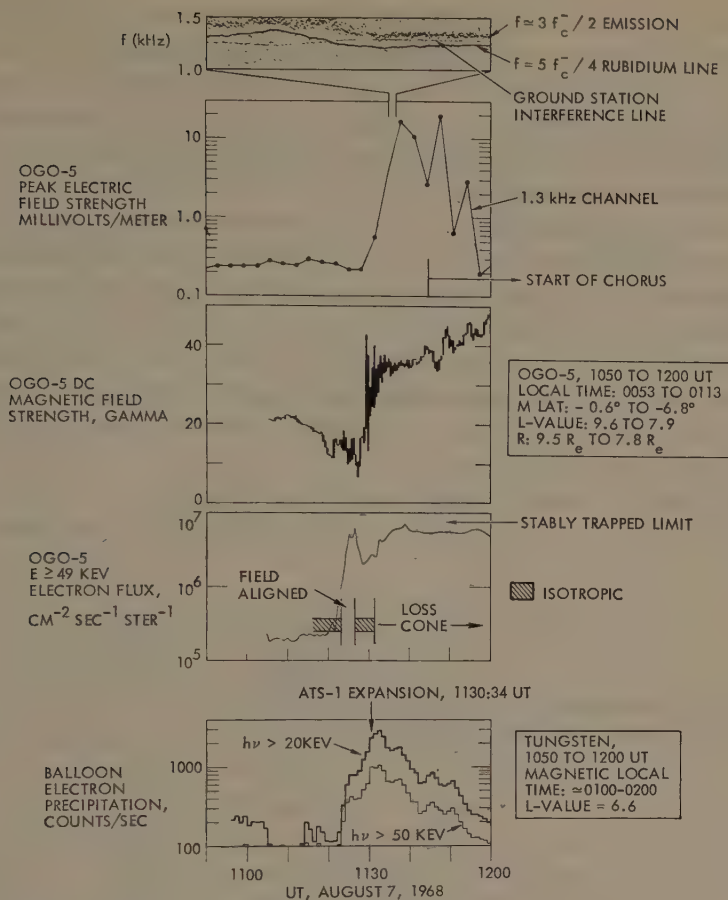


Fig. 3. Another example of local wave particle interactions in the nightside equatorial cusp during a substorm. C. T. Russell, M. G. Kivelson, and G. K. Parks generously provided the unpublished magnetometer, electron flux, and balloon X-ray results shown here, and R. L. McPherron examined the ATS 1 magnetometer data to determine the $L = 6.6$ expansion time.

L shell as OGO 5 during this storm, but clearly the substorm did have an associated precipitation event, and intense local E field wave levels did develop here also.

Several additional substorms have been analyzed (in lesser detail) and it appears that the high frequency electric field oscillations have enhanced amplitudes during substorms, and that they locally interact with energetic electrons to produce strong diffusion. In general, strong chorus also develops, but much later in time.

4. Waves in the Polar Cusp

During the large magnetic storm of November 1, 1968, K_p was 8^+ , Dst was $\approx -200 \gamma$, and strong field-aligned currents were detected at INV Lat as low as 63.9° (Armstrong

and Zmuda, 1970). At this time OGO 5 was outbound near local noon at high latitudes ($MLAT \approx 40$ to 44°) and magnetosheath plasma was encountered very close to earth (e.g., $r \approx 3.1 R_E$ at 1221 UT). Russell *et al.* (1971) showed that OGO 5 made repeated penetrations of the storm time polar cusp (see Frank (1971) for a discussion of quiet-time observations), and here we briefly present highlights of some highly unusual wave observations in the cusp region.

The lower panels in Figure 4 show the density and mean energy of the hot electrons detected by the JPL plasma probe, along with the electric field amplitude ranges in the 1.3 kHz bandpass channel. The Lockheed light ion spectrometer detected the plasmopause at 1137 UT when L was equal to 2, but low fluxes of cold protons were seen out to 1221 ($L=5$, $LT \approx 1100$, $MLAT \approx 43^\circ$) when the hot electrons first appeared. There were additional intermittent cusp encounters until 1427, when the magnetosheath was entered ($r \approx 7.5 R_E$), and another type of wave disturbance was detected at the very end of this plot.

The lower panels of Figure 4 show extremely large 1.3 kHz wave level enhancements near steep gradients in plasma density. Actually, this type of display does not fully

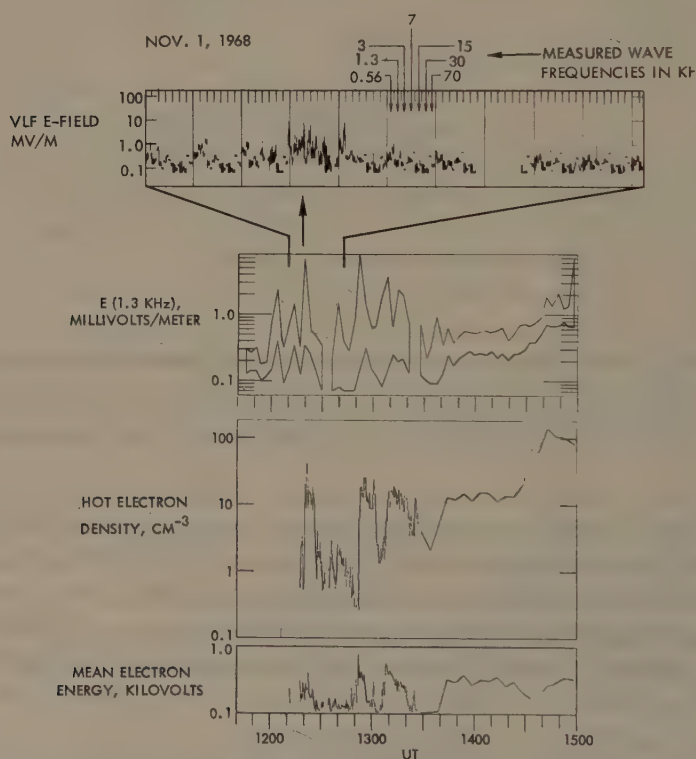


Fig. 4. Outbound high latitude wave and particle measurements near local noon on November 1, 1968, when OGO 5 encountered the dayside polar cusp during a large magnetic storm. The compressed plasmopause was crossed at 1137 UT ($L=2$), the cusp was first encountered at 1221 ($L=5$, $r=3.1 R_E$), and the magnetosheath was entered at 1427 ($r=7.2 R_E$).

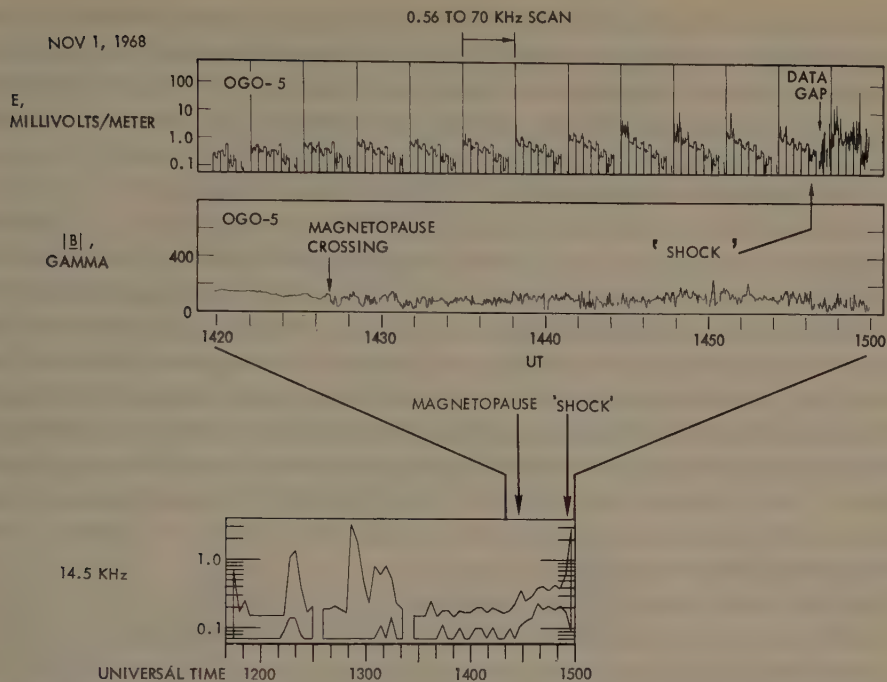


Fig. 5. Details of the wave and field measurements in the polar cusp-magnetosheath coupling region on November 1, 1968. The 'shock' at 1456 UT is not the detached bow shock, and possible interpretations are discussed in the text.

indicate how rapidly the wave amplitudes change because the plasma wave detector on OGO 5 scans slowly in frequency (27.6 s at 560 Hz, then 27.6 s at 1.3 kHz, etc.; see Crook *et al.* (1969) for details). Better indicators of the wave modes and their rapid changes at the cusp boundary come from examination of the actual E vs. f scan sequence, and at the top of Figure 4 we display an expanded view of the full temporal scan for the interval between 1210 UT ($r=2.8 R_E$, $L=4.7$) and 1243 UT ($r=4.0 R_E$, $L=7.5$). It can be seen that the spectrum did change very rapidly near the cusp boundary, and that many modes were strongly excited. A detailed analysis was recently carried out (Scarf *et al.*, 1971c), and it was determined that the November 1, 1968, cusp boundary was 'maximally turbulent' in the sense that almost every possible local wave mode was excited. It would appear that the low altitude polar cusp plasmasphere boundary is a highly unstable region and that many significant collisionless plasma phenomena (such as cross L diffusion, particle acceleration, field merging, etc.) develop here because of the strong wave particle interactions.

Complex and rapid changes in the E field wave spectrum were also seen in the polar cusp magnetosheath coupling region, and the upper part of Figure 5 shows the November 1, 1968, amplitude scan and the magnetic field profile between 1420 UT ($r=7.0 R_E$, LT=1406) and 1500 UT ($r=8.1 R_E$, LT=1434), when MLAT was still 43° . The bottom panel gives the 14.5 kHz electric field amplitude range for the entire

period (compare with Figure 4). Near 1427 UT the magnetometer indicated that the magnetopause was crossed, but this was not marked by any dramatic shift in E field wave levels. However, sporadic noise bursts were detected in the E and B channels at 560 Hz (magnetosheath 'lion roars') while, between 1427 and 1456 UT, the high frequency noise levels merely rose in a very steady fashion, as indicated.

The wave spectrum changed abruptly at 1446 UT, and we use the term 'shock' to describe this change. After 1456 the plasma was turbulent (Neugebauer, 1970) and the dc magnetic field had huge fluctuations (such as 300 to 20 γ in 2 s), indicating that large current layers were present (Scarf *et al.*, 1971c). The broadband electric field spectrum showed impulsive undispersed noise 'spikes' extending up to about 10 kHz, and the top panel in Figure 1 displays the actual E field dynamic spectrum from 1505 UT on November 1, 1968. There were no shocks in the incident solar wind at this time, and Dessler (1971) suggested that OGO 5 had passed behind the demarcation shock expected to be attached to the magnetosphere south of the neutral point (Walters, 1966). Whatever the detailed explanation, it appears that the polar cusp magnetosheath interface is a region in which intense electric field wave activity causes particle heating, field merging, etc.

It is worth noting that within the polar cusp both OGO 5 and INJUN 5 detected very similar electric field waveforms (see Figure 1). The 2 to 10 kHz range, for instance, has impulsive vertical bursts in both cases. However, at the INJUN 5 altitude the waves are electromagnetic, and they are identified as downgoing auroral hiss (Gurnett and Frank, 1971). The INJUN 5 experimenters estimated that the electromagnetic hiss is generated at an altitude at least (1 to 2) R_E above the ionosphere, and they noted that a natural limit (such as 5 R_E for 10 kHz) is largely set by the need to have $f(\text{hiss}) < < f_c^-$ (local) in order for the waves to propagate in the whistler mode. Nevertheless, the simplest hiss analysis is not satisfactory because the observed VLF intensities cannot be accounted for by incoherent Cerenkov radiation from the observed electron fluxes, and this indicates that some coherent plasma instability mechanism is somehow involved in the hiss generation. The OGO 5 polar cusp data suggest a possible connection between distant electrostatic waves and low altitude electromagnetic waves; mode coupling in the non-uniform polar cusp could contribute to the observed high intensity levels.

5. Conclusion

The present analysis has centered on VLF electric field wave observations in the dayside polar cusp and the nightside equatorial cusp, and during disturbed periods we find evidence for very significant wave particle interactions in both regions. However, many other types of signals have been detected with the OGO 5 electric dipole antenna (high frequency narrow band emissions, $3f_c/2$ waves away from the magnetic equator, LHR emissions and hiss bands at high altitudes, MR whistlers, and triggered emissions, etc.), and the material discussed above certainly does not exhaust the interesting phenomena. Moreover, since October 1970, the TRW experiment has had sole use of the OGO 5 special purpose telemetry on alternate orbits, and this provides

a greatly enhanced effective sensitivity for more recent observations. Finally, it should be kept in mind that all of the substorm measurements reported here refer to electrons and electron wave modes. We should expect a variety of proton mode emissions perhaps as intense and as varied as the corresponding electron mode waves already observed.

Acknowledgments

We are indebted to our colleagues, R. K. Burton, A. M. A. Frandsen, D. A. Gurnett, M. G. Kivelson, M. Neugebauer, G. K. Parks, C. T. Russell, and E. J. Smith for providing us with the data needed to construct the figures. We are especially grateful to Drs Parks, Kivelson, and Russell for allowing us to display and discuss their unpublished August 7 observations in Figure 3, and we thank Dr A. J. Dessler for suggesting the possible explanation of the distant polar cusp measurements. This work was supported by the OGO Project of the National Aeronautics and Space Administration under Contract NAS5-9278.

References

- Armstrong, J. C. and Zmuda, A. J.: 1970, *J. Geophys. Res.* **75**, 7122.
 Cornwall, J. M., Coroniti, F. V., and Thorne, R. M.: 1970, *J. Geophys. Res.* **75**, 4699.
 Cornwall, J. M., Coroniti, F. V., and Thorne, R. M.: 1971, *J. Geophys. Res.* **76**, 4428.
 Coroniti, F. V., Fredricks, R. W., Kennel, C. F., and Scarf, F. L.: 1971, *J. Geophys. Res.* **76**, 2366.
 Crook, G. M., Scarf, F. L., Fredricks, R. W., Green, I. M., and Lukas, P.: 1969, *IEEE Trans. Geosci. Electron.*, **GE-7**, 2, 120.
 Dessler, A. J.: 1971, private communication.
 Frank, L. A.: 1971, *J. Geophys. Res.*, in press.
 Fredricks, R. W., Crook, G. M., Kennel, C. F., Green, I. M., Scarf, F. L., Coleman, P. J., and Russell, C. T.: 1970, *J. Geophys. Res.* **75**, 3751.
 Gurnett, D. A.: 1971, private communication.
 Gurnett, D. A., and Frank, L. A.: University of Iowa Report 71-19, May 1971.
 Kennel, C. F. and Petschek, H. E.: 1966, *J. Geophys. Res.* **71**, 1.
 Kennel, C. F., Fredricks, R. W., and Scarf, F. L.: 1970a, in B. M. McCormac (ed.), *Particles and Fields in the Magnetosphere*, D. Reidel Publishing Company, Dordrecht, Holland, p. 257.
 Kennel, C. F., Scarf, F. L., Fredricks, R. W., McGehee, J. H., and Coroniti, F. V.: 1970b, *J. Geophys. Res.* **75**, 6136.
 Neugebauer, H.: 1970, private communication.
 Rosenberg, T. J. and Helliwell, R. A.: 1971, *EOS* **52**, 535.
 Russell, C. T., Chappell, C. R., Montgomery, M. D., Neugebauer, M., and Scarf, F. L.: 1971, *J. Geophys. Res.*, in press.
 Scarf, F. L., Fredricks, R. W., Frank, L. A., Russell, C. T., Coleman, P. J., and Neugebauer, M.: 1970, *J. Geophys. Res.* **75**, 7316.
 Scarf, F. L., Fredricks, R. W., Smith, E. J., Frandsen, A. M. A., and Serbu, G. P.: 1971a, *J. Geophys. Res.*, submitted.
 Scarf, F. L., Fredricks, R. W., Kennel, C. F., and Coroniti, F. V.: 1971b, *J. Geophys. Res.*, submitted.
 Scarf, F. L., Fredricks, R. W., Green, I. M., and Russell, C. T.: 1971c, to be published.
 Smith, E. J., Holzer, R. E., and Russell, C. T.: 1969, *J. Geophys. Res.* **74**, 3027.
 Thorne, R. M. and Kennel, C. F.: 1971, *J. Geophys. Res.* **76**, 4446.
 Walters, G. K.: 1966, *J. Geophys. Res.* **71**, 1341.

VLF PHENOMENA

T. R. KAISER

Dept. of Physics, University of Sheffield, Sheffield, England

1. Introduction

Wave-particle interactions play an important part in the dynamics of the magnetosphere, hence studies of VLF emissions contribute to the knowledge of magnetospheric structure and behavior. Until relatively recently, most available data have been from ground based observations and these continue to be of importance, especially if direction finding (goniometer) techniques can be used to locate the ionospheric exit regions of the signals. Satellite measurements have the advantage that they are not affected by varying ionospheric transparency and a low altitude polar orbiting vehicle can give world coverage.

A particularly important mechanism by which energetic electrons produce VLF electromagnetic waves is the transverse resonance instability generating radiation which propagates in the whistler mode at frequencies below the electron gyrofrequency f_H . Kennel and Petschek (1966) have shown that the wave generation, which takes place near the equator, causes diffusion of trapped particles into the loss cone and hence particle precipitation. The VLF emissions tend to travel along field lines by weak guiding (the permitted ray vectors for propagating waves form a cone of finite half angle about the magnetic field direction) and ducting due to field aligned electron density structure. In the latter case the upper frequency limit is of the order of $f_H/2$. For a given ratio of wave frequency f to gyrofrequency the particle parallel resonant energy E_R is proportional to a characteristic energy $E_c = B^2/(2\mu_0 N)$, where B is the steady magnetic field and N is the ambient plasma particle density. It is appropriate to take equatorial values for B and N and E_c and is clearly the magnetic energy per particle. It follows that, if azimuthally drifting charged particles encounter an enhanced electron density, E_R is decreased and enhanced wave generation and precipitation will result.

In the whistler mode ($f < f_H$, $f < f_p$, where f_p is the plasma frequency) the refractive index is greater than unity and hence Cerenkov radiation can be produced by particles having a component of velocity in the direction of the wave normal which is equal to the wave phase velocity. Cerenkov radiation can also occur at frequencies above both f_H and f_p , namely between the plasma and upper hybrid frequency, $f_{UH} = (f_p^2 + f_H^2)^{1/2}$.

VLF noise emissions are observed, on low altitude polar orbiting satellites, primarily in two regions: (a) at high IN Lat between 70 and 80° Λ , and (b) at medium latitudes between 50 and 60° Λ .

The medium latitude emissions are primarily due to the transverse resonance instability and have a strong storm time dependence with intensity consistent with the weak pitch angle diffusion theory of Kennel and Petschek (1966). Strong evidence

exists for marked longitudinal structure in electron tube content which corotates with the earth. High latitude emissions are an auroral oval type of phenomenon and are probably produced on open field lines by Cerenkov radiation from precipitating soft electrons from the magnetosheath through the cusp regions on the solar side and from the plasma sheet on the nightside.

New types of magnetospheric electric field emissions have been detected near the equator on L shells between $4 < L < 10$ (Kennel *et al.*, 1970). The most common emissions occur between the lowest electron cyclotron harmonics ($f \approx 3f_H/2$) with large field amplitudes (1 to 10 mV m⁻¹) which suggests that they may also be sources of pitch angle diffusion and turbulent energization of auroral zone electrons.

2. High Latitude Emissions

High latitude emissions ($A > 60^\circ$) have been detected on Injun 3 (Gurnett, 1966) and

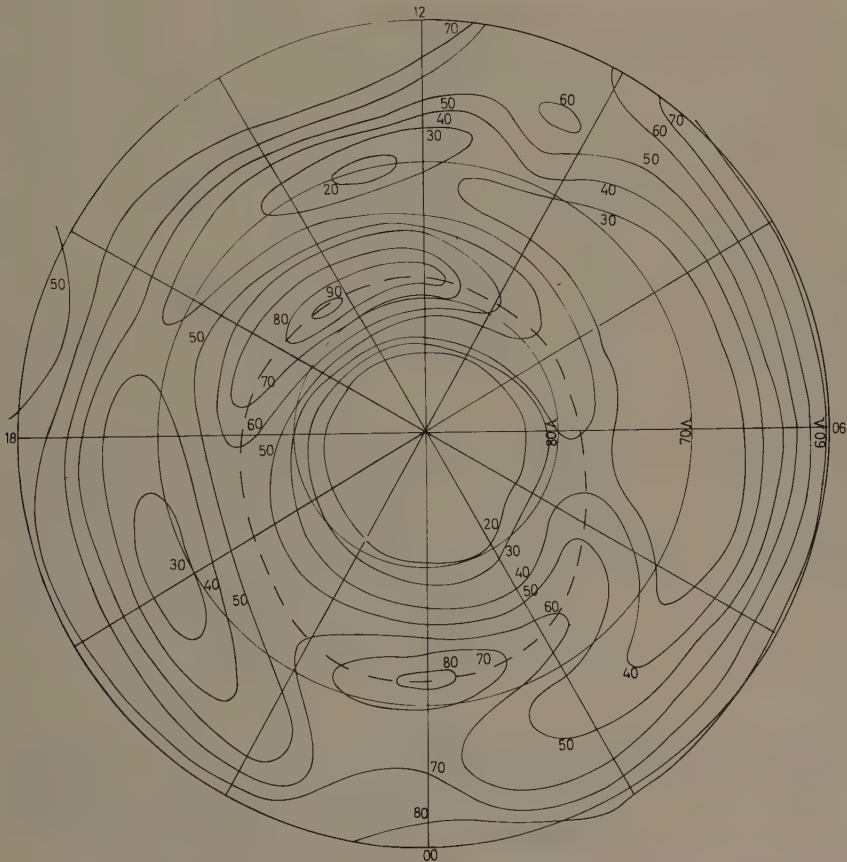


Fig. 1. Percentage frequency of occurrence of VLF emissions at 3.2 kHz (mean intensity $> 10^{-12}$ γ^2 Hz⁻¹ f.s.e.) in the northern hemisphere for May 5–July 24, 1967. The coordinates are IN Lat and MLT (centred dipole).

Ariel 3 (Bullough *et al.*, 1969b; Hughes and Kaiser, 1971; Hughes *et al.*, 1971). At the Ariel 3 sensitivity levels, emissions are identifiable on the majority of high latitude passes and neither their occurrence nor intensity correlate strongly with world-wide magnetic activity, although there is a tendency for more intense emissions ($> 10^{-9} \gamma^2 \text{ Hz}^{-1}$) to be relatively less frequent when K_p exceeds 4.

The Ariel 3 satellite, which was in a high inclination (80°) near circular (mean altitude $\approx 550 \text{ km}$) orbit, provided tape recorded data of the magnetic component of the VLF wavefield for approximately 10 months from launch on May 5, 1967. The morphology of the emissions is illustrated in Figure 1 which shows the percentage frequency of occurrence at 3.2 kHz of emissions with mean intensity greater than $10^{-12} \gamma^2 \text{ Hz}^{-1}$ free space equivalent (f.s.e.) as a function of λ and MLT (centred dipole). Measurements of local electron density were used to convert measured field intensities to f.s.e. assuming quasi-longitudinal wave propagation: $10^{-12} \gamma^2 \text{ Hz}^{-1}$, for

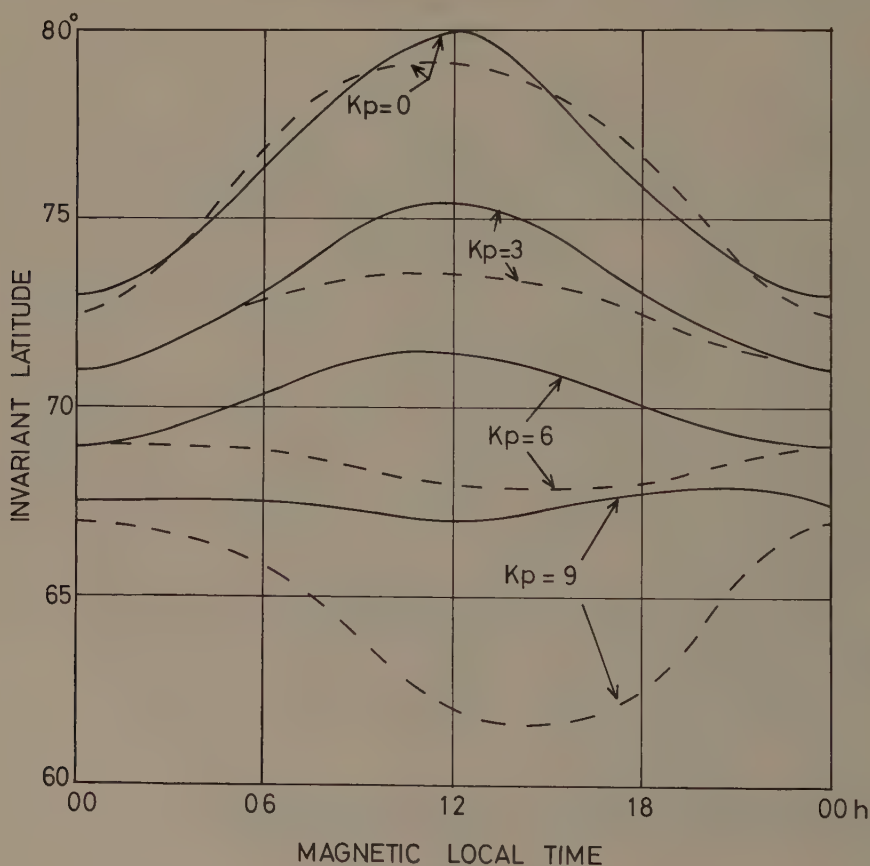


Fig. 2. Location of the VLF high latitude oval for various K_p (May 5–July 24, 1967).
 — Northern hemisphere
 ---- Southern hemisphere

a circularly polarized wave, corresponds to $4.8 \times 10^{-16} \text{ w m}^{-2} \text{ Hz}^{-1}$. Figure 1 refers to the northern hemisphere during summer; a similar pattern is found during the same period in the southern hemisphere (winter) but, whereas at midnight the occurrence frequency was nearly the same (80%), the early afternoon maximum is 90% in the north compared with 50% in the south.

The emissions have maxima in occurrence at or before magnetic midnight and at 14 to 15 hr MLT, at 72° and 78° IN Lat, respectively, with minima between 05 to 06 hr and 19 to 21 hr separating the active regions. A band of minimum occurrence at about $\lambda = 68^\circ$ separates the high and medium latitude emissions. The dashed curve in Figure 1 defines an oval locus of maximum occurrence which varies in latitude between $79^\circ \lambda$ at noon and $72^\circ \lambda$ at midnight. This oval lies just poleward of Feldstein's auroral oval (Feldstein, 1966) and of the boundary of the closed magnetic field lines given by McDiarmid and Burrows (1968). Emissions are also observed over the polar cap with a maximum in occurrence in the vicinity of the pole of about 15% at 3.2 kHz with intensity above $10^{-12} \gamma^2 \text{ Hz}^{-1}$.

Both the shape and location of this VLF oval (as defined above) change systematically with magnetic activity. This is illustrated in Figure 2 which gives the latitude, λ , of the oval as a function of MLT at various levels of K_p for both northern and southern hemispheres during May 5 to July 24, 1967. In the quietest conditions both ovals are the same (within limits of error) and λ varies between 73° at midnight and 79° at noon. With increasing K_p , there is a general equatorwards movement which is most marked near noon. Thus the oval first becomes circular and then, at the highest K_p levels, develops its greatest equatorwards extension near noon. In Figure 2, this behavior seems more pronounced in the southern hemisphere. The significance of this must, however, be treated with some caution since, for any given MLT, the northern and southern hemisphere data refer to different times during the extended observing period.

The Ariel 3 measurements at 3.2 and 9.6 kHz give some information on the spectrum of the emissions. These data are illustrated in Figure 3 which gives the median ratio of the intensities (f.s.e.) at the two frequencies as a function of MLT for both hemispheres. In the north there is a systematic variation, with the 3.2 kHz emissions being ~ 5 dB more intense at midnight and ~ 1 dB less intense at noon than those at 9.6 kHz. In the south the 3.2 kHz emissions are generally a few dB less than those at 9.6 kHz. Ariel 3 also observed emissions at 16 kHz; these have not been fully reduced but indicate that, on the average, the power spectrum remains fairly flat between 9.6 and 16 kHz.

The picture that emerges from the above is that the postnoon activity is produced by soft (~ 150 eV) electrons entering the dayside cusp regions from the magnetosheath. The displacement to post-noon is consistent with the similar predicted displacement of the region of reconnection of field lines on the dayside due to convection from the magnetotail with the effect of the earth's rotation superimposed upon a dawn-dusk electric field. The midnight activity is attributed to precipitation of soft electrons from the plasma sheet with energies $\lesssim 1$ keV. These conclusions are in good accord with

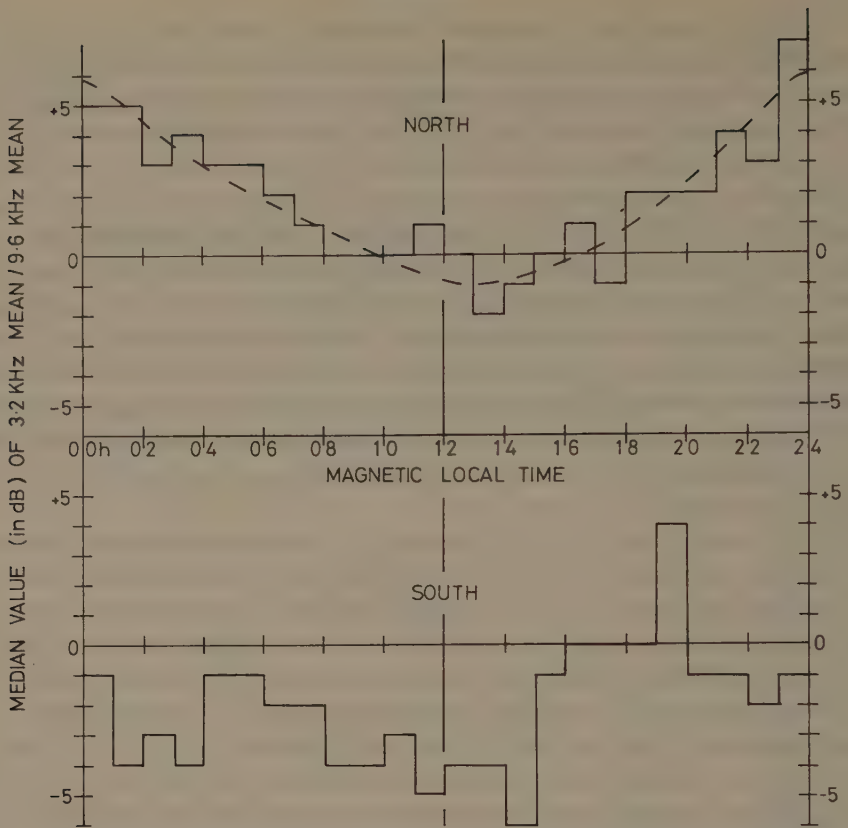


Fig. 3. High latitude emissions. The ordinate gives the median ratio of the mean signal at 3.2 kHz to that at 9.6 kHz as a function of MLT (centered dipole) in the two hemispheres, for May 5–July 24, 1967.

those of Eather and Mende (1971) who have derived similar zones of soft electron precipitation from photometric auroral observations.

These high latitude VLF emissions are most likely generated at altitudes up to twenty thousand km above the Ariel 3 satellite by the Čerenkov process. Jørgensen (1968) has shown that the observed intensities could just be produced in this way, by precipitating electrons with energies in excess of 1 keV. Since the bulk of the soft electrons (both on the day and nightside) has lower energy than this (Frank and Ackerson, 1971), Jørgensen's calculations will err on the conservative side. Hughes and English (1971) have extended these computations to include energies down to 100 eV and find that the predicted intensities are increased by more than thirty times. There is also some discrepancy between the Ariel 3 spectra and Jørgensen's prediction of a maximum in intensity at about 10 kHz. Hughes and English have shown that by modifying the pitch angle distribution from isotropic, the spectrum can be made fairly flat above 10 kHz but they still predict the intensity to drop at lower frequencies.

The Ariel 3 satellite also incorporated a receiver with a loop aerial which swept

in frequency between 1.95 and 4.24 MHz. The observed emissions clearly were generated locally, almost certainly by the Čerenkov mechanism, since they were restricted to the frequency range between the local plasma and upper hybrid frequencies (Gregory, 1971). The location of the most intense emissions in the midnight-dawn sector of the auroral zone corresponds closely with the pattern of precipitation of >5 keV electrons reported by Vette (1972). Rocket observations at 7.35 kHz reported by Ungstrup (1971) indicate that VLF hiss can also be generated in auroral arcs at altitudes of 105 to 110 km with wave normal directions approaching an angle of 90° to the magnetic field.

3. Emissions at Medium Latitudes

Unlike the high latitude phenomena described in Section 2 the medium latitude emissions, occurring on closed field lines, exhibit strong dependence on magnetic disturbance. The evolution of the emissions during the great magnetic storm of 1967 May 25 to 26 has been described in detail by Bullough *et al.* (1969a). During this period the Ariel 3 satellite was in a favorable dawn-dusk orbit and, before the SSC, the mean intensity* at zone maximum on 3.2 and 9.6 kHz was typically 10^{-11} to $10^{-9} \gamma^2 \text{ Hz}^{-1}$. The effect of the solar wind enhancement is first observed at 3.2 kHz on the morning side and shortly afterwards the SSC occurs and enhanced 9.6 kHz morning emission appears. These morning emissions reach a relatively steady mean intensity* of about $10^{-7} \gamma^2 \text{ Hz}^{-1}$ and $10^{-6} \gamma^2 \text{ Hz}^{-1}$ on 9.6 and 3.2 kHz, respectively, which is maintained until, during the initial recovery phase of the storm, the solar wind pressure drops when the morning emissions fall to the pre-storm level. The evening emissions remain low until the initial recovery period when they rise to comparable intensities to those observed in the morning. This accords with the establishment of the symmetrical ring current. The evening emissions decay, following the drop in solar wind pressure, somewhat more slowly than those in the morning. During this period of decay of the ring current there is some recovery of the 3.2 kHz emissions from their sharp drop to background level and moderately strong emissions continue in both morning and evening at 3.2 kHz and to a lesser extent at 9.6 kHz.

During intense emissions the high latitude boundary is usually well defined with a decrease in intensity of 5 to 15 dB per observing interval ($\sim 2^\circ$ along the orbit) towards the pole. In the pre-storm period the 3.2 kHz boundary (defined as 10 dB down on the zone maximum) was typically at 64 to $65^\circ A$, while that for 9.6 kHz was centered around 57 to $59^\circ A$. During the main phase both boundaries moved to a lower latitude of about $52^\circ A$ ($L=2.6$). The first displacement and final recovery of the morning boundary appears to be associated with the onset and termination of the solar wind enhancement. The evening boundary moves to lower latitudes approximately in phase with the decrease in Dst.

Bullough *et al.* (1969a) have shown that the emissions on a given shell are limited

* The figures given for these intensities have not been corrected to the free space equivalent value.

to frequencies somewhat below the minimum gyrofrequency encountered on the field line; thus the source must lie close to the geomagnetic equator. From this we conclude that the mechanism is that of cyclotron resonance, since Kennel and Petschek (1966) have shown that the wave growth in this case is restricted to the vicinity of the equator. Their weak diffusion theory also predicts a limiting trapped particle flux associated with a wide-band whistler mode field of the order of $10^{-2} \gamma$ at the equator. The equivalent field at low altitudes is of the order of 0.1γ . If we take the saturation levels stated above and assume that, because of the minimum gyrofrequency cutoff, the bandwidth is approximately that of the observing frequency we find that the mean signals at zone maximum obtained during the May 25 to 26 storm correspond to a wave field strength at the satellite of about 0.05γ . Having regard for the uncertainties involved, this is in good agreement with Kennel and Petschek.

From the observations on frequencies f , of 3.2, 9.6 and 16 kHz it appears that the emissions during this disturbed period have a spectrum such that the wave field in $\gamma^2 \text{ Hz}^{-1}$ varies as f^{-n} where $n \sim 2$. When corrected for the variation of local refractive index with frequency, this would indicate a power spectral index $n \sim 1.5$.

Thorne and Kennel (1967) have shown that, in the absence of duct guiding, emis-

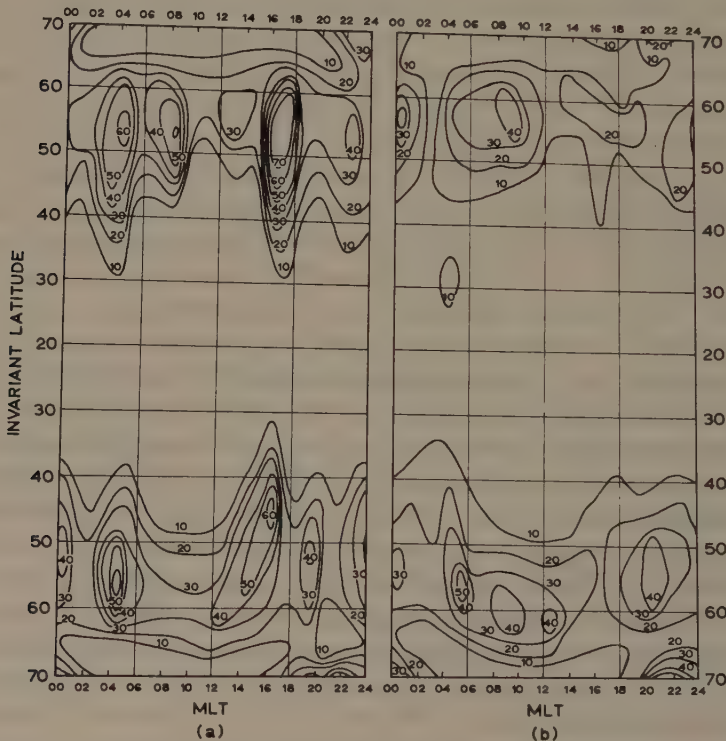


Fig. 4. Percentage frequency of occurrence of VLF emissions at 3.2 kHz (mean intensity $> 10^{-11} \gamma^2 \text{ Hz}^{-1}$ f.s.e.) in the IN Lat interval 20 to 70° for quiet magnetic conditions ($K_p \leq 2+$). (a) May 5 to July 24, 1967. (b) August 13 to October 31, 1967.

sions will be largely reflected at an altitude where the wave frequency equals the lower hybrid frequency. This would usually occur at altitudes above the satellite for the Ariel 3, 3.2 kHz channel. Bullough *et al.* (1969a) have concluded from this and other evidence that these emissions have been duct-guided down to an altitude close to the satellite. During quiet periods ($K_p \leq 2+$) the 3.2 kHz signal is often weaker than that at 9.6 kHz, suggesting non-ducted propagation on these occasions.

Hughes (1971) has analyzed Ariel 3 data for two extended periods (May 5 to July 24, 1967 and August 13 to October 31, 1967) and produced maps of occurrence of emissions as a function of IN Lat and MLT (centered dipole). An example is given in Figure 4 which refers to emissions at 3.2 kHz with intensity greater than $10^{-11} \gamma^2 \text{ Hz}^{-1}$ f.s.e. for magnetically quiet periods ($K_p \leq 2+$). The occurrence is greatest in the latitude range 50 to 60° with, especially in the data of Figure 4a, pronounced maxima in the dawn and evening sectors. The morning emissions are clearly related to the 'chorus' observed at the ground but the evening ones seem much better defined at the satellite than on the ground. Although Figure 4 suggests somewhat dissimilar distributions in the two hemispheres, this could be misleading since a given time zone in the south will have been sampled during a different period of the extended observing interval than the same time zone in the north. The differences between Figures 4a and 4b may in part be seasonal but it is important to note that the earlier period was generally more magnetically disturbed than the later one.

A most significant feature of the medium latitude behavior is the discovery on Ariel 3 of strong emissions at particular longitudes, which may persist for a day or so and which corotate with the earth. Their intensity frequently approaches the saturation level observed during the great storm of May 1967 (see above) i.e., they approach the limit predicted by the weak diffusion theory. On occasions when Ariel 3 closely

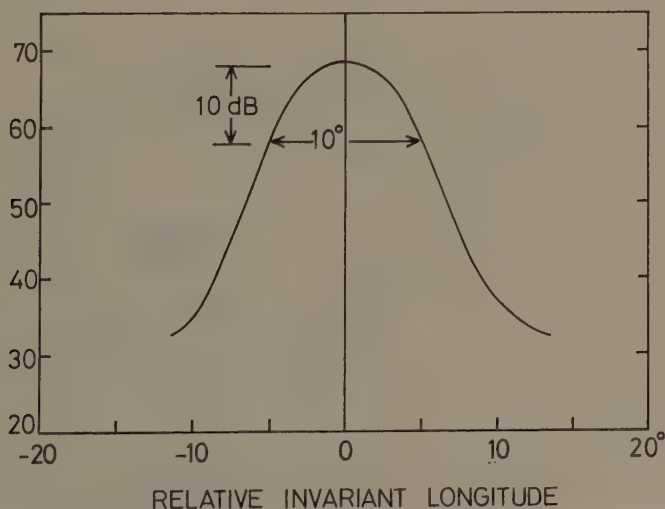


Fig. 5. Representative profile of a localized (in longitude) zone of mid-latitude emissions. The ordinate gives signal intensity in $\text{dB} > 10^{-15} \gamma^2 \text{ Hz}^{-1}$ (f.s.e.).

followed a magnetic meridian, conjugate peaks were observed in both hemispheres. These events tend to occur some 5 to 10° polewards of the more normal zones of emission shown in Figure 4 and have a width in invariant longitude of the order of 10° to 10 dB below the maximum intensity; for this reason they frequently appear on a single pass and not on adjacent ones. From a number of events studied by Bulough and Lefeuve (1971) a representative longitude profile (shown in Figure 5) has been obtained.

If the Kennel-Petschek mechanism is responsible for these enhanced emissions then we require that energetic trapped electrons drifting eastward encounter a region of increasing plasma tube content so that the resonant energy (see Section 1) decreases, causing precipitation and enhanced wave turbulence. Noting that they occur in the outer plasmasphere the following explanation is proposed. In Figure 6, the broken curves (a) and (b) represent, in the equatorial plane, the limiting closed electric equipotential (and hence the equilibrium plasmopause) for a rotating dipole magnetic field and a uniform dusk-dawn electric field. The difference is that (b) refers to an electric field which is double in intensity that for (a). Inside this closed equipotential plasma corotates with the earth while outside it convects to the dayside magnetopause. If the plasmasphere is initially defined by curve (a) and the electric field is then

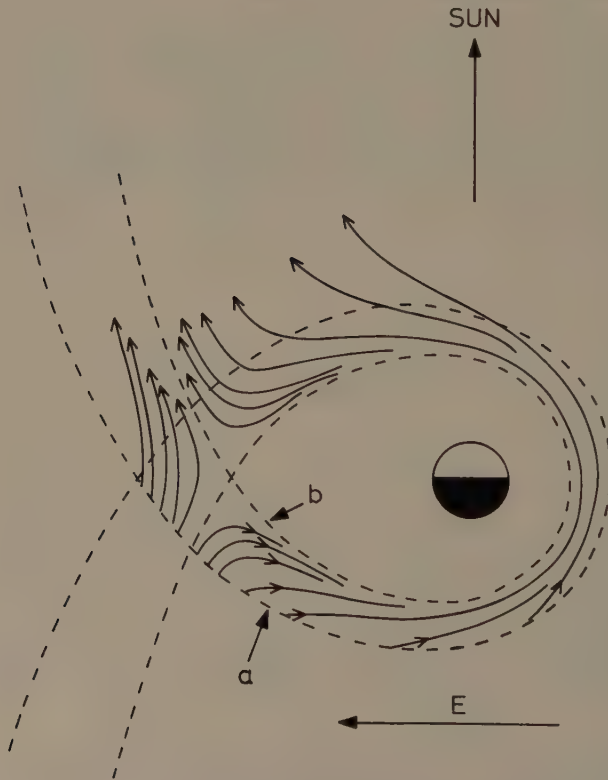


Fig. 6. For explanation, see text.

increased to the value corresponding to curve (b), the subsequent flow of plasma outside (b) is as indicated by the full curves with arrows. It is thus clear that fluctuations in the dawn-dusk E field (associated with substorm activity) will produce the required corotating modulation (in longitude) of the outer plasmasphere, originating in the dusk sector, together with plasma clouds which migrate from this sector towards the dayside magnetopause.

Hargreaves and Bullough (1971) have shown that daytime ionospheric radio wave absorption at 30 MHz, measured with a riometer at Byrd, Antarctica, correlates well with the mid-latitude VLF emissions received on Ariel 3. The upper limit to the absorption (~ 10 dB at 30 MHz) corresponds to the saturation level of VLF intensity observed on Ariel 3. In addition, 10 dB of absorption corresponds to $6.10^6 \text{ cm}^{-2} \text{ s}^{-1} \text{ sr}^{-1}$ of >40 keV electrons which is close to the weak diffusion limit ($3.10^7 \text{ cm}^{-2} \text{ s}^{-1}$ omnidirectional) predicted by Kennel and Petschek for the latitude concerned. These results give further support to the conclusion that equatorial transverse gyroresonance is the primary mechanism for wave generation.

A further feature in the Ariel 3 data is the occurrence, on a significant number of occasions, of a zone of emission localized near 250° east geographic longitude in the southern hemisphere between 40 and 50° IN Lat (Lefevre, 1971). Somewhat less pronounced emissions are also observed in the conjugate region. The zone seems to be associated with the precipitation of eastward drifting trapped electrons as they approach the South Atlantic anomaly; it is also possible that the Čerenkov process plays a role in the generation of these emissions. Enhanced VLF emissions are also observed on Ariel 3 at and near the equator. These are a nighttime phenomenon with a sharp boundary at dawn and dusk; it is therefore suggested that they are initiated by thunder storm activity, the daytime intensities being greatly reduced through D region absorption.

4. Recent Developments in Ground Based Observations

The purpose of this brief section is to draw attention to the successful application of a goniometer technique to ground based studies (Bullough and Sagredo, 1970; Sagredo and Bullough, 1971). It should be recalled that Carpenter originally identified the plasmopause from whistler studies. By employing a goniometer, Bullough and Sagredo (1970) have been able to determine, from observations made at Halley Bay (Antarctica), the magnetospheric plasma tube content as a function of both IN Lat and IN Long and have demonstrated the existence of pronounced longitudinal structure. They report a variation of up to 3:1 over 10° of longitude on L shells external to the plasmopause. On a particular occasion Sagredo and Bullough (1971) were able to identify a clearly defined locus of whistler exit points which persisted for some 16 hr. This appears to be associated with a well defined structure in the plasmasphere which was created in the dusk sector at the time of a substorm. This is further evidence that persistent longitudinally localized enhancements in plasma density are an important feature of the magnetosphere.

By using spaced goniometers it is also possible by triangulation to determine the location of the exit regions through the ionosphere of chorus and hiss (when these are sufficiently localized). This provides a considerable improvement over conventional ground based observations when the emissions are received after propagating a considerable distance in the earth-ionosphere wave guide.

Acknowledgments

I am indebted to Drs M. Rycroft, D. Southwood and colleagues in the Sheffield Space Physics Group for stimulating discussions, also to Drs K. Bullough, H. English, J. K. Hargreaves, A. R. W. Hughes, F. Lefevre and J. L. Sagredo for permission to refer to unpublished work.

References

- Bullough, K. and Lefevre, F.: 1971, private communication.
 Bullough, K. and Sagredo, J. L.: 1970, *Nature* **225**, 1038.
 Bullough, K., Hughes, A. R. W., and Kaiser, T. R.: 1969a, *Planetary Space Sci.* **17**, 363.
 Bullough, K., Hughes, A. R. W., and Kaiser, T. R.: 1969b, *Proc. Roy. Soc. A.* **311**, 563.
 Eather, R. H. and Mende, S. B.: 1971, in B. M. McCormac (ed.), *The Radiating Atmosphere*, D. Reidel Publishing Company, Dordrecht, Holland, p. 255.
 Feldstein, Y. I.: 1966, *Planetary Space Sci.* **14**, 121.
 Frank, L. A. and Ackerson, K. L.: 1971, *J. Geophys. Res.* **76**, 3612.
 Gregory, P. C.: 1971, *Planetary Space Sci.* **19**, 813.
 Gurnett, D. A.: 1966, *J. Geophys. Res.* **71**, 5399.
 Hargreaves, J. K. and Bullough, K.: 1971, *Planetary Space Sci.*, in press.
 Hughes, A. R. W.: 1971, private communication.
 Hughes, A. R. W. and English, H.: 1971, private communication.
 Hughes, A. R. W. and Kaiser, T. R.: 1971, in B. M. McCormac (ed.), *The Radiating Atmosphere*, D. Reidel Publishing Company, Dordrecht, Holland, p. 336.
 Hughes, A. R. W., Kaiser, T. R., and Bullough, K.: 1971, in *Space Res.* **11**, Akademie-Verlag, Berlin, p. 1323.
 Jørgensen, T. S.: 1968, *J. Geophys. Res.* **73**, 1055.
 Kennel, C. F. and Petschek, H. E.: 1966, *J. Geophys. Res.* **71**, 1.
 Kennel, C. F., Scarf, F. L., Fredricks, R. W., McGehee, J. H., and Coroniti, F. V.: 1970, *J. Geophys. Res.* **75**, 6136.
 Lefevre, F.: 1971, private communication.
 McDiarmid, I. B. and Burrows, J. R.: 1968, *Can. J. Phys.* **46**, 49.
 Sagredo, J. L. and Bullough, K.: 1971, *Planetary Space Sci.*, in press.
 Thorne, R. M. and Kennel, C. F.: 1967, *J. Geophys. Res.* **72**, 857.
 Ungstrup, E.: 1971, *Planetary Space Sci.* **19**, 1475.
 Vette, J. I.: 1972, this volume, p. 53.

A THEORY ON THE LATITUDE AND LOCAL TIME DISTRIBUTION OF PRECIPITATING ELECTRONS DURING A SUDDEN COMMENCEMENT

GIOVANNI E. PERONA

Istituto di Elettronica e Telecomunicazioni, Politecnico di Torino, Torino, Italy

Abstract. The magnetic field compression during an SC excites VLF waves. In turn the wave turbulence drives the pitch angle diffusion of energetic electrons trapped in the magnetosphere, causing them to be precipitated into the lower ionosphere.

Electron precipitation during an SC shows a very pronounced maximum at geomagnetic latitude 68° and at 12 hr LT (Anderson, 1958; Ortner *et al.*, 1962; Hartz, 1963; Keppler *et al.*, 1962; Leinbach *et al.*, 1970). Estimates of electron precipitation fluxes were presented by Brown *et al.* (1961) and Hofmann and Winckler (1963) and they agree with the fluxes that are predicted by the current theory when a regime of strong pitch angle diffusion occurs in the magnetosphere (Kennel and Petschek, 1966).

In this paper, following a suggestion by Axford (1967), a theory is briefly presented whereby VLF waves in the magnetosphere at the time of an SC, cause pitch angle diffusion of local electrons, which in turn explains the precipitation that is observed in the lower ionosphere. More precisely, it will be shown that in the sunlit hemisphere between 65 and 70° geomagnetic latitude, the compression of the magnetic field during an SC is often strong enough to increase the VLF level up to the point where strong pitch angle diffusion will take place.

The pitch angle diffusion of electrons by VLF waves is controlled by the diffusion coefficient D (Kennel and Petschek, 1966). When D is larger than a critical value D_c , the so-called strong diffusion regime is reached. It can be shown that on a particular field line, D obeys the following equation (Coroniti and Kennel, 1970):

$$dD/dt = 2(\gamma - \nu) D. \quad (1)$$

The VLF growth rate γ , is proportional to $\Omega^- A \eta$, where Ω^- is the electron cyclotron frequency, A is the anisotropy of the electron distribution, and η is the 'fraction' of the total distribution near resonance with whistlers (Kennel and Petschek, 1966). In what follows η will be assumed to be constant on a particular field line. The quantity, the VLF loss rate, is very difficult to evaluate. However its relative latitude dependence will be estimated in an extremely simplified way with the assumption that ν is proportional to $K_M L s$. Quantity s is of the order of the group velocity divided by the length of the growth region (Coroniti and Kennel, 1970). L is the length of the magnetic field line and K_M is the maximum of the difference between the magnetic field curvature over the ray curvature at VLF (Booker, 1962).

TABLE I
Parameters of interest for the numerical analysis

Γ	$\delta(\Gamma), \text{s}^{-1}$	$\nu_0(\Gamma), \text{s}^{-1}$	$\eta(\Gamma)/\eta(68^\circ)$	$\gamma_0(\Gamma), \text{s}^{-1}$
<i>Noon</i>				
60°	0.0015	1.67	0.1	0.15
68°	0.005	0.5	1	0.5
75°	0.0087	0.5	0.2	0.047
<i>Midnight</i>				
68°	0.0006	0.5	1	0.25

The anisotropy A satisfies the following equation:

$$\frac{dA}{dt} = \frac{1+A}{B} \frac{dB}{dt} - 2DA, \quad (2)$$

which is a modified version of the equation used by Coroniti and Kennel (1970). The magnetic field B will be assumed to increase linearly in time during the SC:

$$B = B_0(1 + \delta t), \quad (3)$$

where B_0 is the initial value and δ is a coefficient function of the magnetic latitude Γ and LT.

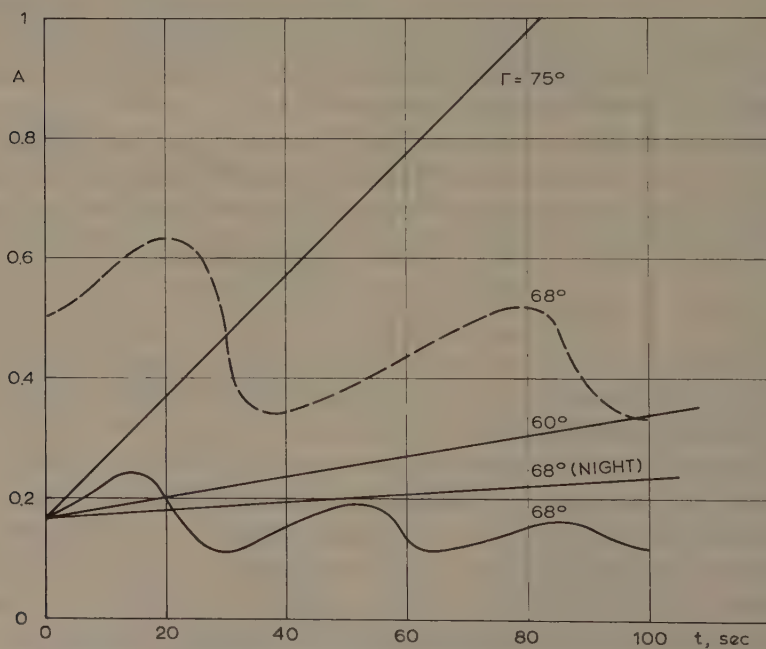


Fig. 1. A as a function of time for different values of Γ , LT (noon and midnight), and initial values.

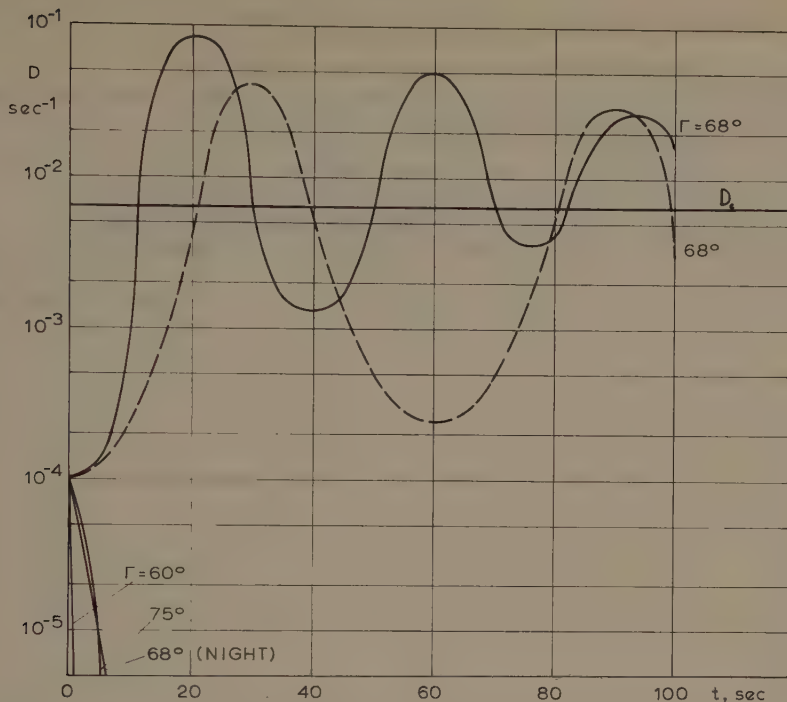


Fig. 2. D as a function of time for different values of Γ , LT (noon and midnight), and initial values.

At $\Gamma = 68^\circ$, Kennel and Petschek (1966) give $A = \frac{1}{6}$ and $D = 10^{-4} \text{ s}^{-1}$ under quiet conditions. These two values will be used as initial values A_0 and D_0 of the unknowns in Equations (1) and (2) at all latitudes, since the general behavior of the solution is not strongly dependent on them. Table I shows the estimated initial values of the parameters appearing in Equations (1), (2) and (3), namely $\gamma_0(\Gamma)$, $\nu_0(\Gamma)$ and $\delta(\Gamma)$.

Graphs of the numerical solutions of Equations (1) and (2) for few geomagnetic latitudes and LT appear in Figure 1 and 2, where diagrams of A and D have been plotted as functions of time. The full lines correspond to the initial value of A and D introduced above; the dashed lines have been obtained starting with $A = \frac{1}{2}$.

From Figures 1 and 2 it appears that strong pitch angle diffusion, that is $D > D_c$, is reached only in the noon sector at $\Gamma = 68^\circ$, in agreement with experimental results. Furthermore, it is important to note the oscillating character of such a solution. The oscillations may be related to the slow quasi-periodical changes in electron precipitation that were observed by Ullaland *et al.* (1970).

References

- Anderson, K. A.: 1958, *Phys. Rev.* **111**, 1397.
 Axford, W. I.: 1967, in B. M. McCormac (ed.), *Aurora and Airglow*, Reinhold Publishing Corporation, New York, p. 499.
 Booker, H. G.: 1962, *J. Geophys. Res.* **67**, 4135.

- Brown, R. R., Hartz, T. R., Landmark, B., Leinbach, H., and Ortner, J.: 1961, *J. Geophys. Res.* **66**, 1035.
- Coroniti, P. V. and Kennel C. F.: 1970, *J. Geophys. Res.* **75**, 1279.
- Hartz, T. R.: 1963, in J. Aarons (ed.), *Radio Astronomical and Satellite Studies of the Atmosphere*, North-Holland Publishing Company, Amsterdam, Holland, p. 220.
- Hofmann, D. J. and Winckler, J. R.: 1963, *J. Geophys. Res.* **67**, 5001.
- Kennel, C. F. and Petschek, H. E.: 1966, *J. Geophys. Res.* **71**, 1.
- Keppler, E., Ehmert, A., Plotzer, G., and Ortner, J.: 1962, *J. Geophys. Res.* **67**, 5343.
- Leinbach, H., Schmidt, R. J., and Brown, R. R.: 1970, *J. Geophys. Res.* **75**, 7099.
- Ortner, J., Hultquist, B., Brown, R. R., Hartz, T. R., Holt, O., and Landmark, B.: 1962, *J. Geophys. Res.* **67**, 4169.
- Ullaland, S. L., Wilhelm, K., Kangas, J., and Riedler, W.: 1970, *J. Atmospheric Terrestr. Phys.* **32**, 1545.

PART VI

MAGNETOSPHERIC SUBSTORMS

A SHORT REVIEW OF MAGNETOSPHERIC SUBSTORMS

MICHEL P. AUBRY*

Institute of Geophysics and Planetary Physics, University of California, Los Angeles, U.S.A.

1. Introduction

Due to the great number of papers on magnetospheric substorms published in the recent years I will give only a short account of the main progress realized since the publication of Akasofu's (1968) book. The purpose of Figure 1 is to place the substorm phenomena in the general frame of the solar wind magnetosphere interaction. When this interaction increases as a consequence of a southward interplanetary field, energy is stored in the magnetosphere (substorm growth phase). Beyond a certain limit the resultant configuration is unstable and the energy stored is suddenly released producing the substorm expansion phase. A recovery phase ends this explosive part of the substorm; the process repeats as long as the strong interaction is maintained. A reversal of the interplanetary magnetic field northward switches off the strong interaction.

After an account of the difficulties involved in the timing and definition of a 'standard substorm' I will try to give an overall view of the magnetospheric changes involved in the growth phase and the onset of the expansion phase of the substorm and to specify some of the questions which must be answered in order to allow further progress.

2. Definition and Timing of Substorms

Until recently the study of geomagnetic activity was essentially performed from the ground and thus used generally well behaved events. This led to major breakthroughs such as the definition of substorms as the constituent elements of magnetic storms (see references in Akasofu (1968)) and the discovery that a substorm growth phase precedes the expansion phase (McPherron, 1970). In contrast present studies attempt to reach an overall view of the magnetospheric mechanism by primarily using satellite observations of perturbations in space. An attempt to find the ground counterpart of these perturbations leads to several difficulties. First, these ground counterparts include a continuous spectrum of events from the large isolated substorms recorded throughout the whole nightside auroral zone to the 'wiggle' recorded by only one magnetic observatory. They also include events with various combinations of negative and positive bays at two or more magnetic stations. The substorm label has been generously applied to all of these events, and this is the source of some confusion. For instance, the division into three phases which is not always obvious even for a large isolated substorm becomes meaningless for the 'wiggle' and so are the conclusions

* Present address: CNET, Dept. RSR, Issy les Moulineaux, 92, France.

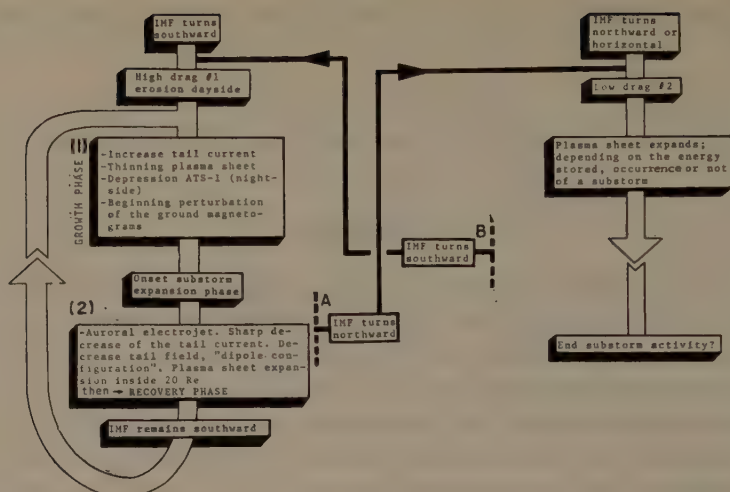


Fig. 1. Diagram of the two different time sequences of events in the magnetosphere associated with the southward or northward orientations of the solar wind magnetic field. The double lines correspond to purely magnetospheric regimes when the solar wind magnetic field does not change. The bold lines show how the reversals of the vertical component of this solar wind magnetic field allow the magnetosphere to switch randomly from one regime to the other (the vertical positions of the points A and B are arbitrary). Except for the vertical component of the interplanetary magnetic field it is assumed that everything remains constant in the solar wind ($V \sim 400 \text{ km s}^{-1}$, $N \sim 5 \text{ cm}^{-3}$, $B \sim 5 \gamma$, and oriented away from the sun).

drawn from their study. Second, the timing of even a large substorm can lead to controversy. The techniques presently used to determine the onset of the expansion phase (generally taken to be $t=0$, the growth phase time being negative) are the:

- (a) onset of a negative bay at an auroral ground station near midnight (Akasofu, 1968);
- (b) burst of Pi 2 close to this onset (Camidge and Rostoker, 1970);
- (c) sudden brightening and northward motions of the auroral arcs (Akasofu, 1968);
- (d) onset of a positive bay at a mid-latitude ground station near midnight (McPherron, 1971b).

Although for a 'standard substorm' all these methods should lead to the same $t=0$ within a few minutes, it appears that for complex events they can lead to completely different timing.

This probably explains some of the contradictory ground satellite correlations published in the recent literature. Another comment could be made about the timing; the emphasis which several years ago was put on ground observations has now shifted to satellite observations. This reflects the fact that we now study magnetospheric substorms as a whole, the auroral (ionospheric) substorm being only one of its consequences. The timing procedure should take account of this new point of view and should accordingly use features related to the magnetosphere (technique (d) above, for instance) and not to the ionosphere alone.

One way to minimize the timing difficulties is to limit when possible the correlation studies to 'standard substorms', namely *substorms isolated in time and space* and with a clear transition from the growth phase to the expansion phase, and to time these substorms by as many techniques as possible. In the next two paragraphs it will be my basic assumption that such a 'standard substorm' exists and that partial and sometimes ambiguous observations made at different times and places can be assembled in order to create a composite picture of it.

3. Growth Phase

Since the substorm growth phase or development phase (Ivliyev *et al.*, 1970; McPherron, 1970; Hones *et al.*, 1971) is the interval during which the solar wind energy is stored in the magnetosphere the first problem is to determine how this energy storage changes the magnetospheric configuration. Aubry *et al.* (1970) observed an inward motion of the dayside magnetopause following a reversal of the interplanetary magnetic field from northward to southward, the solar wind momentum flux remaining constant. This was interpreted as an erosion of the dayside, and was followed by an increase of the tail magnetic field and then a substorm expansion phase. This sequence of events allows one to link together the observations published recently by many authors and summarized in Figure 2.

A. INFLUENCE OF THE SOLAR WIND MAGNETIC FIELD ORIENTATION ON THE OCCURENCE OF A SUBSTORM

This influence is well known (see Nishida, 1970). Unfortunately, as shown by Hirshberg and Colburn (1969), the issue has been confused because the geomagnetic activity was often determined from K_p , which was apparently correlated with all the

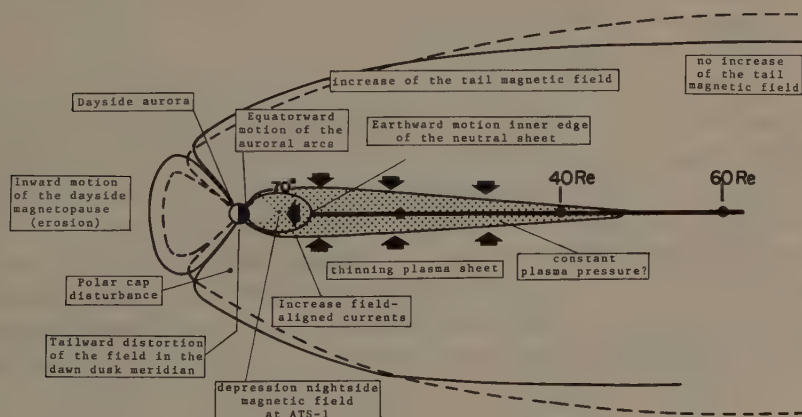


Fig. 2. Diagram of the magnetospheric changes during the substorm growth phase (Box #1 in Figure 1). The solar wind momentum flux is assumed constant. The dashed line represents the shape of the magnetopause at the end of the growth phase (model of Kennel and Coroniti (1971)). The plasma sheet (shading) is assumed to be limited by a closed field line.

solar wind parameters. Moreover it seems that some substorm activity can be triggered directly by changes of the solar wind pressure. The direct influence of the solar wind magnetic field orientation on substorms activity was shown by Pudovkin *et al.* (1970a) and finally established firmly by Arnoldy (1971). The latter study proved that the solar wind parameter best correlated with the hourly AE index is the integral over time of the southward component of the interplanetary field (in GSM) for the hour preceding the AE hourly average.

B. INWARD MOTION OF THE DAYSIDE MAGNETOPAUSE

Meng (1970) and Rudneva and Feldstein (1970) have shown that the dayside magnetopause is closer to the earth at the time of substorm activity and the latter authors further showed that this could not be due to an increase of the solar wind pressure. Fairfield (1970) confirmed that with the solar wind momentum flux being constant, the magnetosphere boundary is closer to the earth when the interplanetary magnetic field is southward.

C. GROUND GEOMAGNETIC OBSERVATIONS

Geomagnetic variations during the growth phase were analyzed by Ijima *et al.* (1968) and McPherron (1970). Oguti (1969) studied the dayside variations and Pudovkin *et al.* (1970b) the polar cap variations.

D. INCREASE OF THE TAIL MAGNETIC FIELD

This increase occurring as precursor of magnetic activity was observed at about $30 R_E$ by Lazarus *et al.* (1968) and Fairfield and Ness (1970) and from 17 to $8 R_E$ by Russell *et al.* (1971) and McPherron *et al.* (1971). The increased tail magnetic field implies a larger tail current whose influence is felt in the tail cusp (Aubry *et al.*, 1971; McPherron *et al.*, 1971) and which produces the well known depressed field at ATS 1 (Coleman and McPherron, 1970).

E. EARTHWARD MOTION OF THE PLASMA SHEET

The increased drag on the magnetopause during the growth phase must be balanced by an earthward motion of the tail current sheet and of the plasma sheet (Siscoe and Cummings, 1969). This general earthward motion before $t=0$ has been observed by Carpenter (1970) and Shelley *et al.* (1970). It can be associated with a westward electric field of a few tenth of a mV m^{-1} . Mozer and Manka (1971) confirmed that this westward electric field appears roughly 1 hr before the substorm expansion phase. During this same time interval auroral arcs are observed to move equatorward (Ivliyev *et al.*, 1970), and a weak westward electrojet is observed to grow in strength and move equatorward (Kisabeth and Rostoker, 1971).

F. THINNING OF THE PLASMA SHEET

The decisive observations were made at $20 R_E$ by using simultaneous measurements from VELA 3A and VELA 4A on both sides of the neutral sheet (Hones *et al.*, 1970a

and references therein). Hones *et al.* (1970b) reported that this thinning occurs at constant plasma pressure. The plasma sheet thinning was also observed at $30 R_E$ by Fairfield and Ness (1970) and from 12 to $8 R_E$ by McPherron *et al.* (1971) and Aubry *et al.* (1971).

Many problems remain to be solved; for instance, the exact influence of the southward interplanetary field on the drag at the magnetopause is not quantitatively understood. It must be emphasized however that Kennel and Coroniti (1971) have already presented quantitative studies of some features of the growth phase. They investigated more specifically the source and consequence of a pressure unbalance at the dayside magnetopause and the field increase in the near tail.

4. Onset of the Expansion Phase

Figure 3 summarizes the main magnetospheric phenomenon associated with this onset. Immediately coincident with the breakup on the ground, a plasma sheet expansion is observed to start in the tail cusp (McPherron *et al.*, 1971). This expansion begins with a rapid motion of the cusp boundary followed several minutes later by a sharp decrease of a portion of the tail current sheet (Aubry *et al.*, 1971). This is equivalent to field line reconnection at the cusp, a basic element of many substorm models (Akasofu, 1968; Unti and Atkinson, 1968; Axford, 1969; Rostoker, 1970; Mozer and Manka, 1971). A perturbation is observed moving inward from the cusp producing the well known recovery of the field at ATS 1 (McPherron and Coleman, 1970); another perturbation moves tailward associated with a sharp decrease of the tail current sheet and the expansion of a plasma sheet filled with energetic electrons (Oguti and Kokubun, 1969; McPherron *et al.*, 1971; Aubry *et al.*, 1971). At $20 R_E$

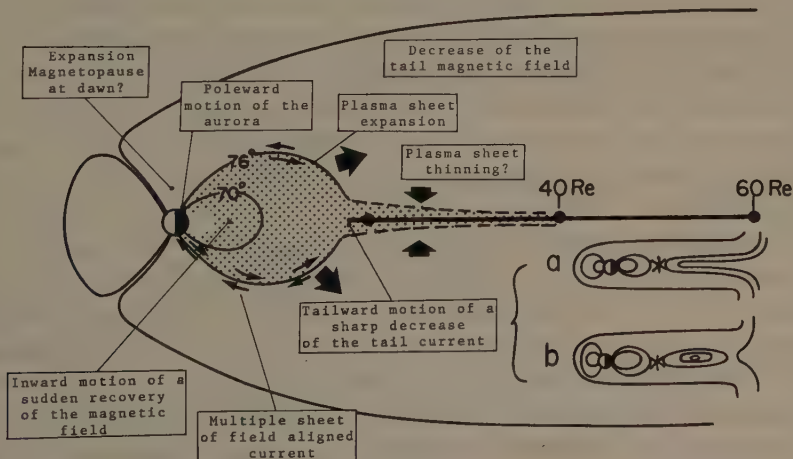


Fig. 3. Diagram of the magnetospheric changes at the beginning of the substorm expansion phase (Box #2 in Figure 1). The two small models at right show two possible structures associated with the reconnection in the tail cusp.

the plasma sheet appears to expand at 5 to 20 km s^{-1} away from the neutral sheet (Hones *et al.*, 1970a). Within $15 R_E$ Aubry *et al.* (1971) observed on the border of the expanding plasma sheet, multiple sheets of field aligned currents similar to those observed in the auroral arcs by Armstrong and Zmuda (1970) and Cloutier *et al.* (1970). This coincidence shows that the expansion of the plasma sheet is the tail counterpart of the northward expansion of the aurora as was previously suggested by Hones *et al.* (1970a). At the same time the total field begins to decrease in the main lobe of the tail (Fairfield and Ness, 1970; Aubry and McPherron, 1971). Inside the magnetosphere the pattern of convection and precipitation of particles produced by the substorm have been extensively studied (McIlwain, 1972).

Many questions still need to be answered. For instance, the current system leading to the auroral electrojet is not precisely known. This current system is quite probably made of a Pedersen current which is essentially the model of Akasofu (1969) and double sheets of field aligned current (Hall current) (Fukushima, 1968). It is also probable that the triggering mechanism for the expansion phase involves some instability of this field aligned current. Carlqvist and Bostrom (1970) claim that the instability switches off the current while Kindel and Kennel (1971) consider that the instability limits only the current amplitude. Both conclude that the instability should first appear in the topside ionosphere producing field aligned electrostatic fields which in turn accelerate particles to the auroral energy level. O'Brien (1970) disagrees with this acceleration scheme. Decisive observations of this most important step of the substorm are still missing.

The perturbation moving tailward from the cusp is not clearly understood. Indeed, if as a consequence of field line reconnection, an x neutral point appears at $10 R_E$ then we do not know what could prevent the plasma sheet particles from escaping beyond this point. One could invoke one of the two models a and b in Figure 3; in (b) a 0 neutral point is associated with the x neutral point (McPherron, 1971a) in (a) particles could be prevented from escaping by the turbulence (Hill and Dessler, 1971). Relevant to this question is the problem of tearing mode instability (Schindler, 1970). Moreover, the observations of the plasma sheet expansion beyond $15 R_E$ in the tail, after $t=0$ the onset of the substorm expansion phase, are rather contradictory; the plasma sheet has been seen to expand (Hones *et al.*, 1970a) to continue to shrink (Hones *et al.*, 1970b), or to begin to shrink (Akasofu *et al.*, 1970). The same kind of discrepancies appears between the results reported by Meng and Akasofu (1971) and Oguti and Kokubun (1969). Although the substorm timing is probably responsible for some of these contradictions, the changes in the tail geometry associated with the return to the 'dipole configuration' could be an alternative explanation (Hones *et al.*, 1970a; Aubry *et al.*, 1971). Finally, at such distances from the earth, some of the plasma sheet expansions are probably triggered by a reversal of the solar wind magnetic field from southward to northward (Aubry and McPherron, 1971). As a final comment, let us emphasize that we observe thinning and expansion of the plasma sheet, but there is still no agreement on the source of the plasma sheet particles and the nature of its boundary.

5. Conclusions

The study of substorms has reached a turning point. There seems to be a general agreement about the main sequence of events taking place during the growth phase and expansion phase, and about the place of the substorm in the overall magnetospheric machinery. This is reflected from a theoretical point of view in the more and more convergent set of qualitative substorm models presently available and in the presentation of the first quantitative model (Kennel and Coroniti, 1971). From an experimental point of view once we agree on some rational ways to define and time the magnetospheric substorm, more extensive correlation of the presently available satellite data should allow us to resolve some of the remaining major problems such as the substorm triggering mechanism, the plasma sheet behavior and the substorm recovery phase.

Acknowledgments

This study was performed while I enjoyed the kind hospitality of Dr Paul J. Coleman, Jr. at the Planetary and Space Science Department of UCLA, and is mainly the result of many helpful discussions with my colleagues in this department.

References

- Akasofu, S. I.: 1968, *Polar and Magnetospheric Substorms*, D. Reidel Publishing Company, Dordrecht, Holland.
- Akasofu, S. I.: 1969, *Nature* **221**, 1020.
- Akasofu, S. I., Hones, E. W., Montgomery, M. D., Bame, S. J., and Singer, S.: 1970, Preprint LA-DC 12267, Los Alamos Scientific Laboratory.
- Armstrong, J. C. and Zmuda, A. J.: 1970, *J. Geophys. Res.* **75**, 34, 7122.
- Arnoldy, R. L.: 1971, Preprint UNH-71-1, University of New Hampshire.
- Aubry, M. P. and McPherron, R. L.: 1971, *J. Geophys. Res.* **76**, 4381.
- Aubry, M. P., Russell, C. T., and Kivelson, M. G.: 1970, *J. Geophys. Res.* **75**, 7018.
- Aubry, M. P., Kivelson, M. G., McPherron, R. L., Russell, C. T., and Colburn, D. S.: 1971, 'Changes in the Magnetotail Cusp Associated with Magnetospheric Substorms', Preprint IGPP-UCLA.
- Axford, W. I.: 1969, *Rev. Geophys.* **7**, 421.
- Camidge, F. P. and Rostoker, G.: 1970, *Can. J. Phys.* **48**, 2002.
- Carlqvist, P. and Bostrom, R.: 1970, *J. Geophys. Res.* **75**, 7140.
- Carpenter, D. L.: 1970, *Ann. Geophys.* **26**, 363.
- Cloutier, P. A., Anderson, H. R., Park, R. J., Vondrak, R. R., Spiger, R. J., and Sandel, B. R.: 1970, *J. Geophys. Res.* **75**, 2595.
- Coleman, P. J., Jr. and McPherron, R. L.: 1970, in B. M. McCormac (ed.), *Particles and Fields in the Magnetosphere*, D. Reidel Publishing Company, Dordrecht, Holland, p. 171.
- Fairfield, D. H.: 1970, Preprint X 692-70-452 NASA-Goddard.
- Fairfield, D. H. and Ness, N. F.: 1970, *J. Geophys. Res.* **75**, 7032.
- Fukushima, N.: 1968, *Rep. Ionosph. Space Res. Japan* **22**, 173.
- Hill, T. W. and Dessler, A. J.: 1971, 'Plasma-Sheet Structure and the Onset of Magnetospheric Substorms', Preprint Rice University.
- Hirshberg, J. and Colburn, D. S.: 1969, *Planetary Space Sci.* **17**, 1183.
- Hones, E. W., Jr., Akasofu, S. I., Perreault, P., Bame, S. J., and Singer, S.: 1970a, *J. Geophys. Res.* **75**, 34, 7060.
- Hones, E. W., Jr., Asbridge, J. R., and Bame, S. J.: 1970b, Preprint LA-DC 12176, Los Alamos.
- Hones, E. W., Jr., Singer, S., Lanzerotti, L. J., Pierson, J. D., and Rosenberg, T. J.: 1971, *J. Geophys. Res.* **76**, 2977.

- Ijima, T., Fukushima, N., and Kamide, Y.: 1968, *Rep. Ionosph. Space Res. Japan* **22**, 161.
- Ivliyev, D. Ya., Pudovkin, M. I., and Zaytseva, S. A.: 1970, *Geomagnetizm i Aeronomiya* **10**, 231.
- Kennel, C. F. and Coroniti, F. V.: 1971, 'A Model of Magnetospheric Substorms', Paper presented at the IUGG Meeting, Moscow.
- Kindel, J. M. and Kennel, C. F.: 1971, *J. Geophys. Res.* **76**, 13, 3055.
- Lazarus, A. J., Siscoe, G. L., and Ness, N. F.: 1968, *J. Geophys. Res.* **73**, 7, 2399.
- McIlwain, C. E.: 1972, this volume, p. 268.
- McPherron, R. L.: 1970, *J. Geophys. Res.* **75**, 28, 5592.
- McPherron, R. L.: 1971a, private communication.
- McPherron, R. L.: 1971b, Preprint IGPP UCLA-940.
- McPherron, R. L. and Coleman, P. J., Jr.: 1970, (abstract), *Trans. Amer. Geophys. Union* **51**, 4, 402.
- McPherron, R. L., Aubry, M. P., Russell, C. T., and Coleman, P. J., Jr.: 1971, Preprint IGPP UCLA-947.
- Meng, C. I.: 1970, *J. Geophys. Res.* **75**, 16, 3252.
- Meng, C. I. and Akasofu, S. I.: 1971, 'Magnetospheric Substorm Observations Near the Neutral Sheet', Preprint, Berkeley.
- Mozer, F. S. and Manka, R. H.: 1971, *J. Geophys. Res.* **76**, 7, 1697.
- Nishida, A.: 1970, *Ann. Geophys.* **26**, 2, 401.
- O'Brien, B. J.: 1970, *Planetary Space Sci.* **18**, 1821.
- Oguti, T.: 1969, *Rep. Ionosph. Space Res. Japan* **23**, 175.
- Oguti, T. and Kokubun, S.: 1969, *Rep. Ionosph. Space Res. Japan* **23**, 151.
- Pudovkin, M. I., Raspopov, O. M., Dmitrieva, L. A., Troitskaya, V. A., and Shepetnov, R. V.: 1970a, *Ann. Geophys.* **26**, 389.
- Pudovkin, M. I., Isaev, S. I., and Zaitzeva, S. A.: 1970b, *Ann. Geophys.* **26**, 761.
- Rostoker, G.: 1970, 'Polar Substorms and the Dynamics of the Magnetosphere', Preprint University of Alberta Edmonton, Canada.
- Rudneva, N. M. and Feldstein, Ya. I.: 1970, *Geomagnetizm i Aeronomiya* **10**, 635.
- Russell, C. T., McPherron, R. L., and Coleman, P. J., Jr.: 1971, *J. Geophys. Res.* **76**, 7, 1823.
- Schindler, K.: 1970, in V. Manno and D. E. Page (eds.), *Intercorrelated Satellite Observations Related to Solar Events*, D. Reidel Publishing Company, Dordrecht, Holland, p. 309.
- Shelley, E. G., Johnson, R. G., and Sharp, R. D.: 1970, 'Plasma Sheet Convection Velocities Inferred from Electron Flux Measurements at Synchronous Altitude', Preprint, Lockheed Palo Alto Research Laboratories.
- Siscoe, G. L. and Cummings, W. D.: 1969, *Planetary Space Sci.* **17**, 1795.
- Unti, T. and Atkinson, G.: 1968, *J. Geophys. Res.* **73**, 7319.

SUBSTORM BEHAVIOR OF PLASMA SHEET PARTICLES

EDWARD W. HONES, JR.

University of California, Los Alamos Scientific Laboratory, Los Alamos, N.M., U.S.A.

1. Introduction

The earth's magnetotail plays an important role in the production of magnetospheric substorms. It evidently serves as a storehouse of magnetic energy (and also, perhaps, of particle kinetic energy) which is replenished by action of the solar wind. Accumulated energy is periodically released into the auroral regions of the earth in the form of kinetic energy of precipitating particles and joule heating of the upper atmosphere by intense electric currents. The release of most of the stored energy is often triggered quite suddenly by some as yet unknown process interior to the magnetosphere, resulting in the 'breakup' and the expansive phase of the substorm.

A striking feature of the magnetotail's behavior during a substorm is the 'thinning' and subsequent thickening or 'recovery' of the plasma sheet. This phenomenon was discovered in particle measurements made by the Vela satellites (at $r \approx 18 R_E$) and has subsequently been confirmed both by particle and magnetic field measurements made by other satellites at other distances. In the initial report of this phenomenon Hones *et al.* (1967) suggested that the thinning of the plasma sheet was caused by displacement of magnetotail plasma toward the earth, possibly as a result of merging of the interplanetary and magnetospheric magnetic fields, as suggested by Dungey (1961), and the consequent buildup of the tail magnetic field intensity. They suggested that the subsequent thickening of the plasma sheet might then result when merging of magnetic field across the neutral sheet in the tail starts, allowing stretched-out field lines to contract rapidly earthward as proposed by Axford (1966, 1967).

That interpretation of the plasma sheet thinning and recovery phenomena seems now to be supported in its essential features by several pieces of observational evidence which have since been reported: (a) erosion of magnetic field from the front of the magnetosphere before the expansive phase of a substorm (Aubry *et al.*, 1970), (b) buildup of tail magnetic field strength early in substorms (Fairfield and Ness, 1970; Meng *et al.*, 1971; Russell *et al.*, 1971); (c) magnetic field line contraction or 'collapse' toward the earth during the expansive phase of substorms (Cummings *et al.*, 1968; Fairfield and Ness, 1970; Lezniak and Winckler, 1970) and (d) movement of the inner edge of the plasma sheet toward the earth during substorms (Vasyliunas, 1968). Many questions remain to be answered, however, before a full understanding of these characteristic plasma sheet variations and of their relation to other features of magnetospheric substorms is reached. For example, the source of the plasma sheet particles and the means of energization to their characteristic energies of several keV are not agreed upon. The relationship of the plasma sheet particles to auroral particles is unclear. The nature and location in the magnetotail of the 'trigger'

mechanism which initiates the expansive phase of a substorm and the thickening of the plasma sheet are not known.

In this paper I shall recount briefly the general features of plasma sheet substorm behavior which had been established by about 1 yr ago and then I shall describe in more detail some of the most recent results of our studies done with the Vela satellites.

2. General Features of Plasma Sheet Substorm Variations

It is essential in studying the behavior of the plasma sheet (or of any other region of the magnetosphere) during substorms, to relate measurements made far from the earth to the features of substorms derived from the more traditional observations of magnetic activity, auroral luminosity, etc., made from the earth. It has been

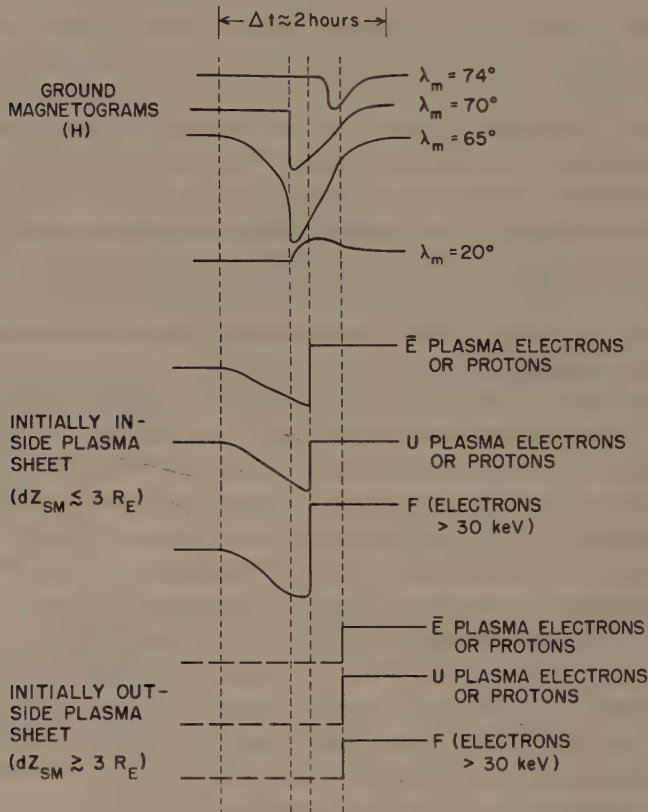


Fig. 1. Idealized representation of substorm phenomena. Top four curves are traces of the horizontal component of magnetograms from ground stations at various magnetic latitudes (λ_m) in the midnight sector. Middle three curves are variations of average energy, \bar{E} , and energy density, U , of 'plasma' electrons (and/or) protons and of the energetic electron flux, F , at a Vela satellite initially inside the plasma sheet. Bottom three curves are same quantities for a Vela satellite initially outside the plasma sheet.

customary to speak of the 'onset' of a substorm (Akasofu, 1968) as being evidenced by the nearly simultaneous occurrence (in the midnight sector) of:

- (a) brightening of auroral arcs near the equatorward edge of the auroral oval;
- (b) beginning of rapid poleward expansion of auroral brightness,
- (c) rapid deepening of a negative bay in the auroral zone, and
- (d) onset of a positive bay at low latitudes.

Here we shall refer to these as four criteria indicating the 'classical onset' ($T=0$ in Akasofu's notation) of a substorm. There is now evidence that the complete set of causally-related phenomena which constitute a magnetospheric substorm may sometimes start before $T=0$.

At the top of Figure 1 is a schematic representation of magnetic records which might be obtained at several magnetic latitudes during a substorm. The second vertical dashed line from the left is drawn through the sharp deepening of the negative bay at $\lambda_m = 65^\circ$ and the beginning of the positive bay at $\lambda_m = 20^\circ$ (i.e., criteria (c) and (d) above) and thus marks $T=0$, the time of the substorm's 'classical onset.' The bay at $\lambda_m = 65^\circ$ is depicted as deepening gradually starting about 1 hr before $T=0$.

The three curves at the middle of Figure 1 represent variations of the plasma sheet particle population that would be observed by a Vela satellite which is near the neutral sheet when the substorm events begin. The average energy, \bar{E} , and energy density, U of the 'plasma' electrons or protons (i.e., those with energies from ~ 100 eV to ~ 20 keV measured with the Vela electrostatic analyzers) are shown by the first two curves and the flux F , of energetic (e.g., $E_e \gtrsim 30$ keV) electrons is shown by the third curve. These three quantities typically decrease as the auroral zone bay (at $\lambda_m \approx 65^\circ$) deepens. This is the 'thinning' of the plasma sheet and we shall illustrate later that it typically starts within minutes of the beginning of the auroral zone (i.e., $\lambda_m \approx 65^\circ$) bay associated with a substorm. That the decrease of \bar{E} , U , and F typically seen by the Vela satellites results from a 'thinning' rather than a 'flapping' of the plasma sheet has been conclusively shown by means of simultaneous observations from a pair of Vela satellites situated at different distances from the neutral sheet (Hones, 1970; Hones *et al.*, 1971c).

No indication of the substorms 'classical onset' is observed at the satellite; the thinning of the plasma sheet often simply continues.

Some time after $T=0$ the three quantities, \bar{E} , U and F rise again. This is the thickening or recovery of the plasma sheet. The delay in its occurrence after $T=0$ increases with increasing distance, dZ_{SM} , of a satellite from the neutral sheet but does not seem to be a simple linear function of dZ_{SM} . In particular the delay from $T=0$ does not vanish even when the satellite (at $r \approx 18 R_E$) is very near the neutral sheet (Akasofu *et al.*, 1970; Hones *et al.*, 1970; Meng and Akasofu, 1971). The plasma sheet recovery often is much more rapid than was the preceding thinning in a given substorm. As indicated by the curves in Figure 1, \bar{E} and F are significantly higher after plasma sheet recover at a satellite than they were before thinning began. The quantity U , however, seems simply to regain approximately its initial value.

The bottom three curves in Figure 1 represent the variations of \bar{E} , U , and F at a

satellite that was initially outside the plasma sheet. Here the thinning cannot, of course, be observed; the recovery is then evidenced by a relatively sudden appearance of the plasma and energetic electrons. Recovery would typically occur later at this satellite than at one initially inside the plasma sheet and thus, presumably, closer to the neutral sheet.

Figure 2 illustrates the change of energy density profile of the plasma sheet that occurs during thinning. The energy density of the plasma electrons is plotted vs. a satellite's estimated distance from the neutral sheet. (The neutral sheet's position is estimated by the formula of Russell and Brody (1967).) The dots are values taken before the onset of thinning of the plasma sheet and the triangles are values taken just after plasma sheet recovery. The squares are values recorded at the maximum epoch of thinning. This figure (taken from Hones *et al.*, 1971c) reveals several important aspects of plasma sheet thinning:

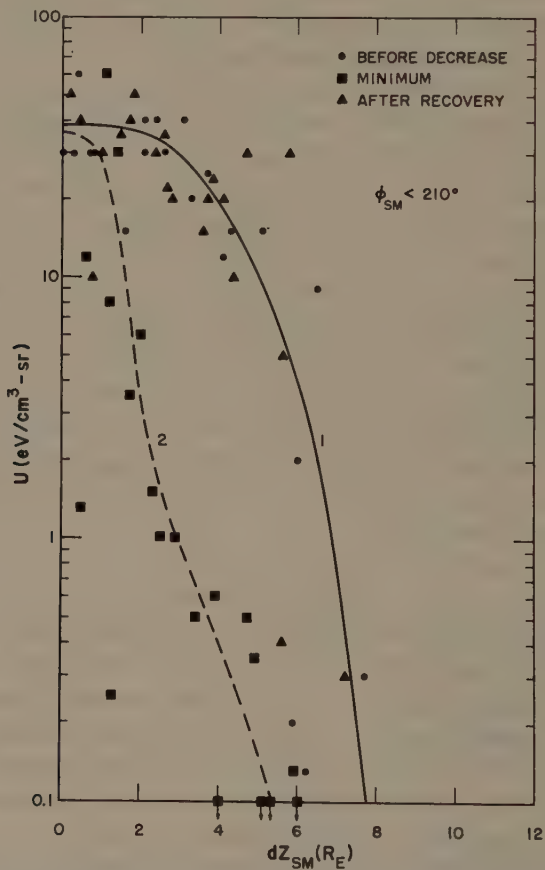


Fig. 2. Energy density, U , of plasma electrons vs distance, dZ_{SM} , from the neutral sheet. The dots are values taken just before plasma sheet thinning began; the squares are values at the maximum epoch of thinning; the triangles are values shortly after plasma sheet recovery. All points shown were obtained at solar magnetospheric longitudes ϕ_{SM} between ~ 150 and $\sim 210^\circ$ (Hones *et al.*, 1971c).

(a) The energy density profiles before thinning and after recovery are roughly similar.

(b) The plasma sheet's thickness is reduced by a factor of ~ 3 or more during thinning but it evidently does not go to zero.

(c) The plasma intensity very near the center of the plasma sheet (i.e., near the neutral sheet) does not increase by a large factor, if at all, during thinning. This indicates, of course, that the plasma is not all compressed into a thin more intense plasma sheet but most of it leaves the region of the tail at $18 R_E$.

The data in Figure 2 were taken by Vela satellites near the midnight sector of the tail. Other data, taken near the dawn edge of the tail where the plasma sheet is normally thicker, showed that the plasma sheet there does not thin down by a factor as great as that observed in the midnight sector (Hones *et al.*, 1971c).

3. Do Substorms Have a Development Phase?

The magnetic features (i.e., criteria (c) and (d)) of a 'classical onset' of a substorm occurred at 23 14 UT, August 25, 1967 (Hones *et al.*, 1971b). Negative bays at auroral zone stations deepened sharply then and a positive bay started at the low latitude station, M'Bour (see Figure 3). For more than 1 hr before this (starting at ~ 2200 UT), however, negative bays at Kiruna and Dixon Island deepened gradually. Vela satellite 3A (at solar magnetospheric longitude (ϕ_{SM}) $\approx 211^\circ$ and $dZ_{SM} \approx 3.8 R_E$) detected a thinning of the plasma sheet starting at ~ 2200 UT and Vela 4A (at $\phi_{SM} \approx 199^\circ$ and $dZ_{SM} \approx -2.1 R_E$) sensed this thinning starting at ~ 2220 UT (see Figure 4). Recovery of the plasma sheet was detected by Vela 4A at ~ 2330 UT, 16 min after $T=0$. It was detected by Vela 3A, $\sim 1.3 R_E$ farther from the neutral sheet ~ 20 min later.

It is well established that plasma sheet thinning typically accompanies the development phase of auroral zone negative bays (Hones *et al.*, 1967, 1968). Since in this event on August 25, 1967, the thinning and gradual bay development went on together for 1 hr before the eventual 'classical onset' of the substorm at 23 14 UT, it is natural to believe that both were causally related to the classical onset and may thus be regarded as features of a 'development phase' of the substorm. Magnetic field measurements obtained for this period in the solar wind by Ness reveal that the interplanetary field took a sharp southward turn at ~ 2150 UT on August 25, ~ 10 min before plasma sheet thinning began, and maintained a southward direction until ~ 2343 UT (Hones *et al.*, 1971b). The observations in this event are thus consistent with the idea that plasma sheet thinning results from an enhanced rate of merging of magnetospheric and interplanetary magnetic field and consequent buildup of the magnetotail field strength (Hones *et al.*, 1967). The 'development phase' of a substorm is thus a period preceding the 'classical onset' during which the particle kinetic energy in the distant magnetotail decreases and the magnetic energy increases. It seems likely that the plasma particles are mostly driven toward the earth during the development phase (Hones *et al.*, 1967). This earthward convection of the plasma and its enhanced inter-

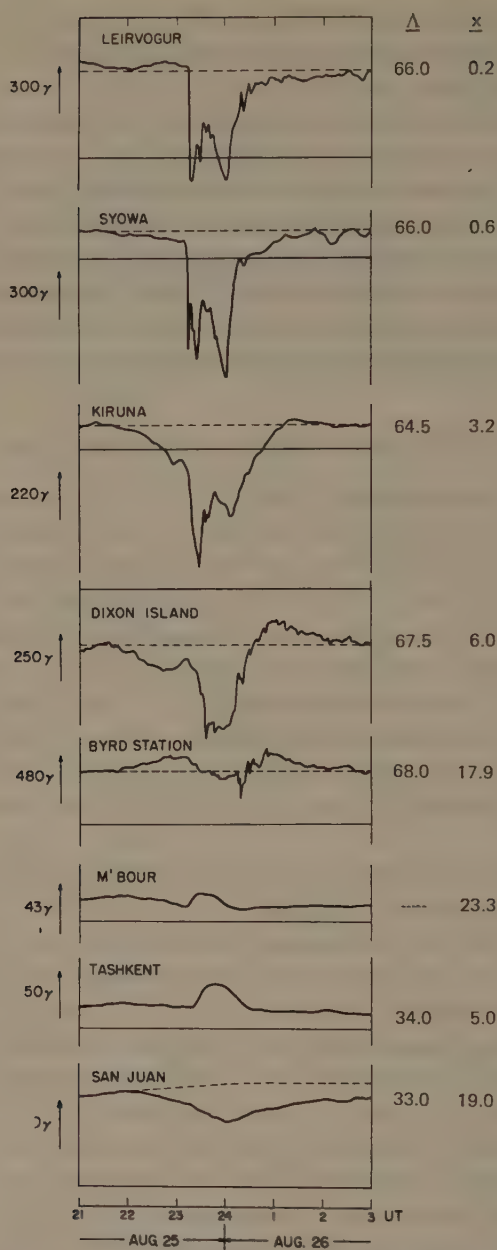


Fig. 3. Magnetograms from selected ground stations showing the development of the August 25-26, 1967, substorm. To the right of each trace is the IN Lat, Λ , of the station and the number of hours, x , that must be added to UT to obtain the approximate (MLT) at the station (Hones *et al.*, 1971b).

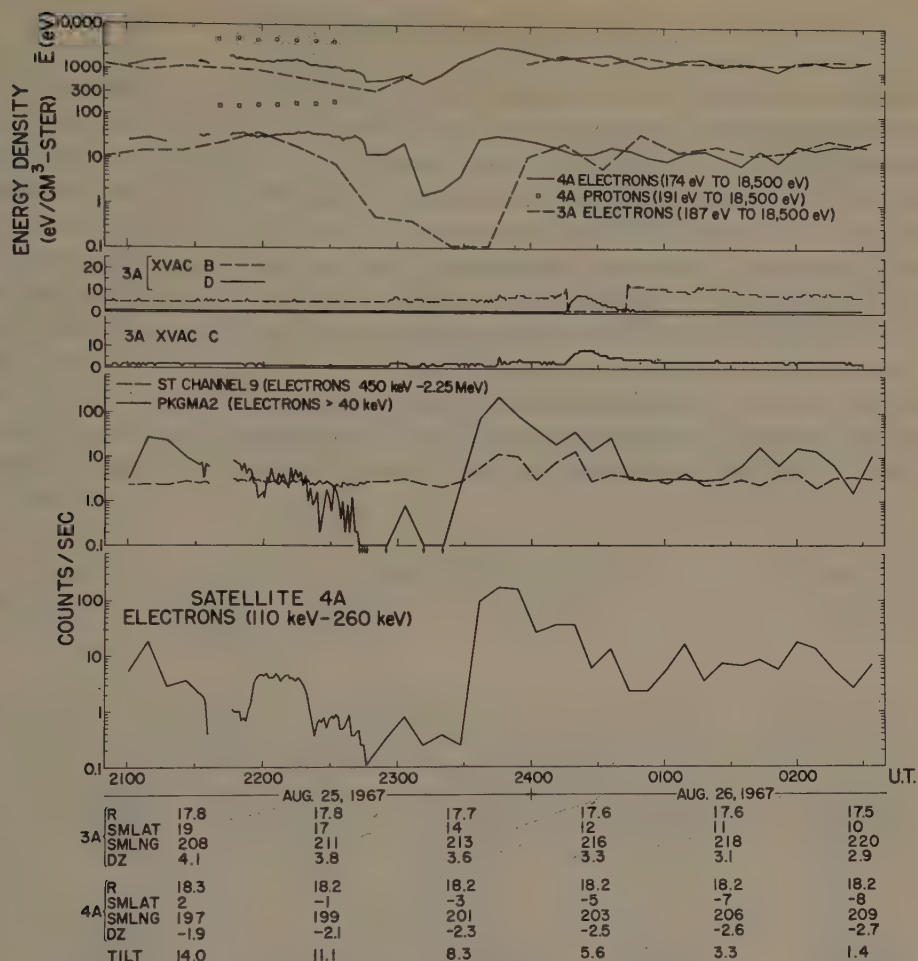


Fig. 4. Data from Vela 3A and 4A during the Aug. 25-26, 1967, substorm. Top box shows the average energy, \bar{E} , and the energy density of electrons and protons measured by electrostatic analyzers. The bottom two boxes show responses of energetic detectors on Vela 4A. The locations of the two satellites are indicated at the bottom (Hones *et al.*, 1971b).

action with the auroral ionosphere cause the gradual deepening of bays (McPherron, 1970) and equatorward motion of auroral arcs (Ivliev *et al.*, 1970; Feldstein, 1971) which are manifestations of the development phase sometimes observed at ground stations.

Thinning of the plasma sheet and other manifestations of a development phase are not always so evident as in the substorm of August 25 to 26, 1967, just discussed. I shall now describe measurements from another event which will illustrate this point and some other points which I wish to make regarding substorm onset and the expansion phase.

4. Substorms on September 18, 1969

Figure 5 shows data from a solid state detector on Vela 4B and ground magnetic records on September 18, 1969. Figures 6a and 6b show all-sky camera pictures from Fort Churchill for the same period. A substorm started at ~ 0515 UT. Its onset was signaled by brightening of the aurora over Great Whale River (i.e., on the southern horizon of Fort Churchill), by the sharp onset of a negative bay at Great Whale River and by the onset of a positive bay at San Juan. Note that a weak bay started gradually at Fort Churchill at the same time. The energetic electron intensity at Vela 4B (at $r=19.1 R_E$, $\phi_{SM}=162^\circ$, $dZ_{SM}=-1.3 R_E$) increased briefly at *this same time* (within ~ 1 min) and then decreased rapidly. The intensities of the plasma electrons and protons, measured with the electrostatic analyzer on Vela, decreased rapidly also starting ~ 0515 UT. This substorm did not satisfy completely the criteria given above for the 'classical onset' of a substorm because the auroras did not advance poleward

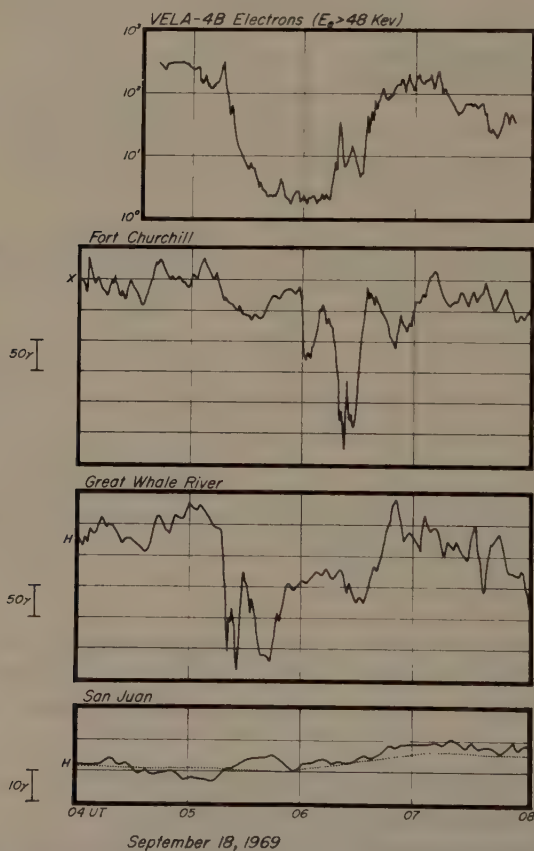


Fig. 5. Vela 4B energetic electron data and corresponding ground magnetic records on September 18, 1969 (Hones *et al.*, 1971e).

appreciably after their brightening but remained bright over Great Whale River. Nevertheless, criteria (a), (c) and (d) *were* satisfied.

It would be difficult to identify a development phase (prior to 0515 UT) from the ground magnetic records for this substorm. The substorm thus began with a (nearly) 'classical onset' at 0515 UT and plasma sheet thinning began at the same time. The brief 'spike' in the energetic electron flux at Vela precisely at the onset of the substorm is significant and we shall discuss it later.

A second substorm started at 0557 UT. Its onset was signaled by all four of the onset criteria adopted above, i.e., by brightening of the auroras near Fort Churchill's southern horizon, by rapid poleward advance of the aurora, by onset of a sharp negative bay at Fort Churchill and by onset of a weak positive bay at San Juan. Vela 4B (at $\phi_{SM}=165^\circ$; $dZ_{SM}=-1.9 R_E$) detected no immediate effect of this substorm. It could not have detected a further thinning of the plasma sheet (if that occurred) since its instruments were already counting at their background rates, (i.e., the satellite was outside the plasma sheet). The energetic electron flux rose above background in a brief burst at 0615 UT coincident with a further sharp deepening of the bay at Fort Churchill. Final recovery of the energetic electron flux and of the plasma sheet began at Vela ($\phi_{SM}=166^\circ$; $dZ_{SM}=-2.3 R_E$) at 0630 as the bays at

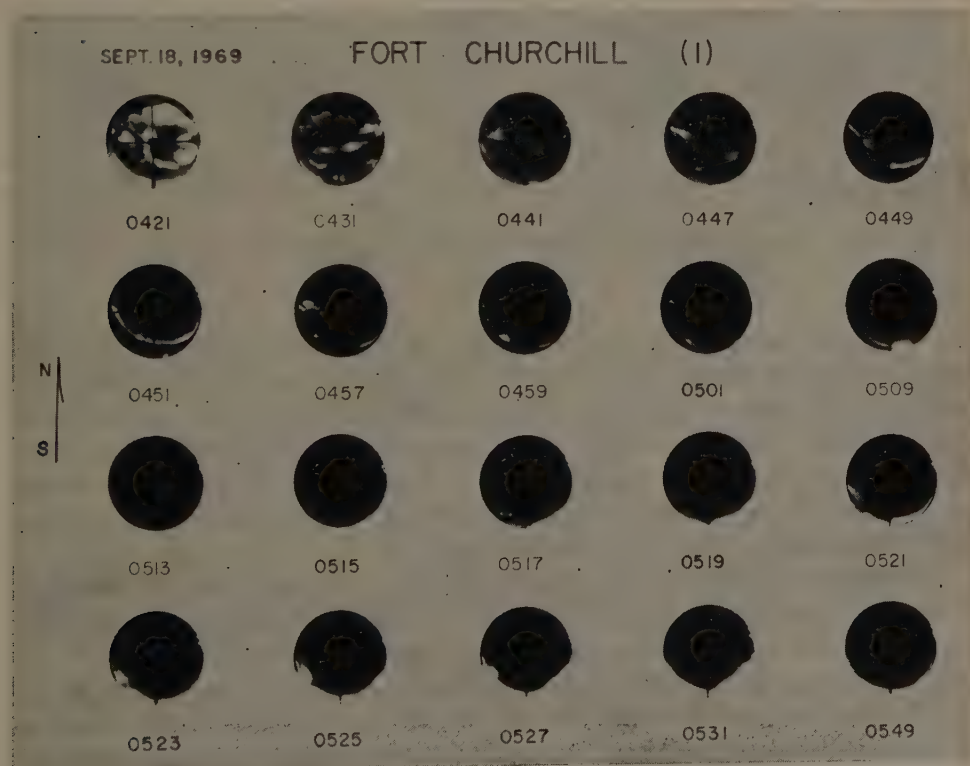


Fig. 6a.



Fig. 6a-b. All-sky camera pictures from Fort Churchill, September 18, 1969 (Hones *et al.*, 1971e).

Fort Churchill and Great Whale River were recovering. There was little magnetic activity at Baker Lake ($\lambda_m \approx 74^\circ$), about 5° north of Fort Churchill, until 0642 UT. At that time a negative bay started to develop (data not shown). It reached a peak intensity of 200γ at 0700 at which time the electrojet passed overhead moving northward (indicated by the Z-component record). Note in Figure 6b that the aurora started to advance far poleward of Fort Churchill at ~ 0643 to 0646 and at 0650 to 0700 it extended nearly to the norther horizon.

These events on September 18, 1969, illustrate the following points: (a) The onset of thinning quite near the neutral sheet ($dZ_{SM} = -1.3 R_E$) coincident with the 'classical onset' features of a substorm for which there was no obvious development phase. (Hones *et al.* (1971e) have reported other such events.) (b) Absence of any particle effects of a substorm onset (at 0557 UT) at a satellite outside the plasma sheet (at $dZ_{SM} = -1.9 R_E$). (c) Final recovery of the plasma sheet starting (at ~ 0630 UT) at a satellite fairly near the neutral sheet ($dZ_{SM} = -2.3 R_E$) coincident with the *recovery*

of negative bays at auroral latitudes (Great Whale River at $\lambda_m \approx 67^\circ$ and Fort Churchill at $\lambda_m \approx 69^\circ$) and a few minutes before the *onset* of a negative bay (arrival of the electro-jet) at low polar cap latitudes (Baker Lake at $\lambda_m \approx 74^\circ$). (This last point is consistent with conclusions reached by Hones *et al.* (1970).) (d) A brief impulse of energetic

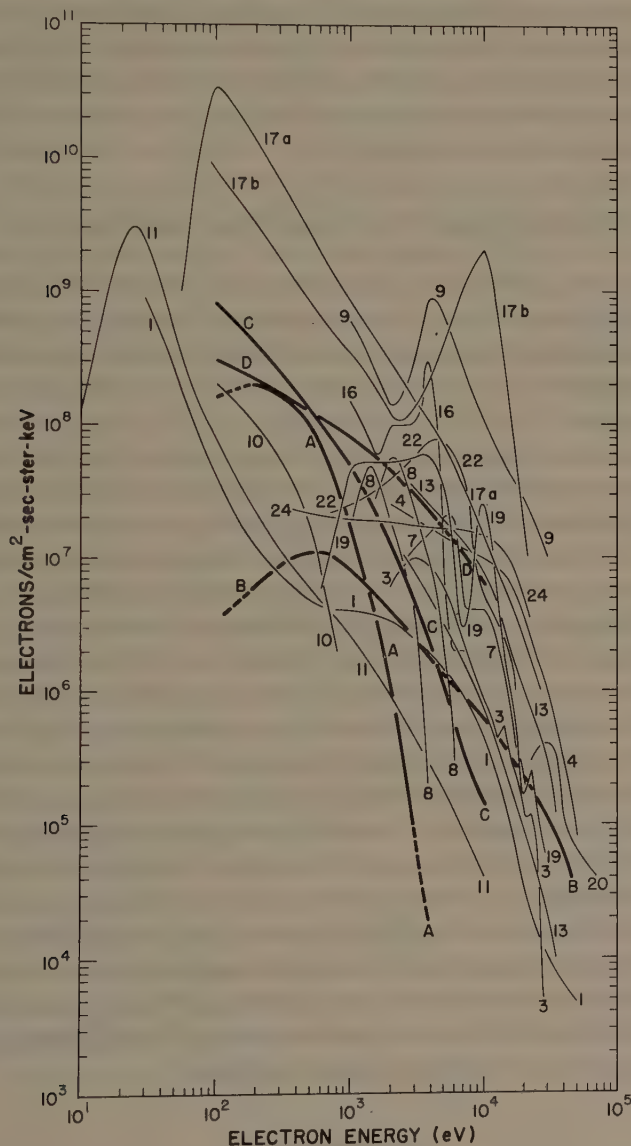


Fig. 7. Auroral electron spectra measured by rockets and by a polar orbiting satellite and plasma sheet electron spectra measured by Vela satellites. The numbers on the rocket spectra are for identification (see original paper). A is a Vela 'cool' spectrum obtained near the center of the plasma sheet during very quiet geomagnetic conditions. B is a Vela 'hot' spectrum obtained shortly after plasma sheet recovery late in a substorm (Hones *et al.*, 1971a).

electron flux occurring coincident with the classical onset of a substorm (0515 UT). Akasofu *et al.* (1971) have reported that this latter phenomenon is observed by Vela satellites in a significant fraction of substorms. Hones *et al.* (1971d) have suggested that phenomenon (d) occurs because magnetic field lines from auroral latitudes are stretched far (sometimes $> 18 R_E$) into the tail before the classical onset of a substorm. At substorm onset energetic auroral electrons are generated in a limited region containing such lines and if a Vela satellite is in the region it detects the electron flux immediately. The lines then contract rapidly earthward, usually faster than the electron containing region builds outward, so the Vela satellite is soon outside it and no longer detects the electron flux.

5. Particle Spectra in the Plasma Sheet and in the Aurora

The nightside of the auroral oval is thought to be magnetically connected to the plasma sheet; thus, auroral particles are related to those in the plasma sheet. The geometry of the magnetic linkage is not known, however, and must vary greatly with geomagnetic conditions as I have indicated just above. However, it seems reasonable to suppose, because of the findings of Hones *et al.* (1970), that the boundary of the thickening plasma sheet late in a substorm is magnetically connected to the poleward edge of the poleward moving auroras. On the basis of this supposition electron and proton spectra measured by the Vela satellites in the newly recovering plasma sheet were compared with published auroral particle spectra measured with rockets and satellites. Many of the rocket spectra have been made in "break-up auroras" and thus the particles at the two locations should be quite directly related. Some results of the comparison are shown in Figure 7 (Hones *et al.*, 1971a). The many *numbered* curves are electron spectra measured by rockets. The numbers identify the particular rocket flights in the original paper. Curve B, a spectrum typical of the newly recovered plasma sheet, was measured by Vela 3B at $\phi_{SM} \approx 203^\circ$, $dZ_{SM} \approx -2.9 R_E$ just after plasma sheet recovery at the satellite late in a substorm that occurred on October 22, 1965. Most of the rocket spectra are seen to be much more intense and to have more complex structure than the plasma sheet spectrum. Hones *et al.* (1971a) found experimental evidence for a very strong peaking of the plasma electrons *along* the magnetic field lines in the plasma sheet. They suggested that the particles constituting this peak at very small pitch angles in the plasma sheet were the auroral particles. These particles might be accelerated by electric fields in or just above the ionosphere or by some mechanism (e.g., the Fermi mechanism) acting deep in the magnetotail which accelerates particles preferentially along the field lines.

6. Conclusions

The magnetotail plasma sheet becomes thin during magnetospheric substorms starting at the same time (within a few minutes or less) that auroral zone negative bays start develop. Often this coincides with other auroral and magnetic phenomena which

constitute the features of auroral 'breakup' or the classical onset of a substorm. Sometimes, however, these other features do not occur at the start of the thinning but much later (many minutes to an hour). In such a sequence of events, the gradual plasma sheet thinning and bay development may be indicative that a 'development phase' precedes the onset and expansive phase of the substorm.

A brief impulsive enhancement of energetic electron flux sometimes occurs at the Vela satellites coincident with the onset of thinning at substorm onset and then rapidly dies away as plasma sheet thinning continues. This suggests that magnetic field lines from auroral latitudes may reach farther than $18 R_E$ into the tail at substorm onset and contract rapidly earthward during the substorm's expansive phase.

During thinning the plasma sheet's total thickness may be reduced from the 'normal' value of ~ 6 to $8 R_E$ to ~ 1 to $2 R_E$ or less. The plasma sheet does not disappear completely at these times. The plasma intensity throughout the plasma sheet (even very near the neutral sheet) usually starts decreasing at the onset of thinning. There is little or no indication of a 'compression' of all of the plasma into a thinner more intense plasma sheet. There are Vela satellite observations (not described here) which suggest that plasma leaks out of the plasma sheet into the magnetosheath during substorms.

There is evidence that plasma sheet thinning starts in quick response (10 to 15 min delay) to southward turning of the interplanetary magnetic field. Thus the thinning probably is caused by a buildup of the magnetic tail field and enhanced sunward convection of plasma due to increased magnetic merging at the sunward magnetopause.

The classical onset of a substorm probably marks the beginning of very rapid contraction of tail magnetic field lines toward the earth. Some of these contracting lines, just prior to onset, extend beyond $18 R_E$ into the tail. The contraction may result from merging of field lines across the neutral sheet at distances beyond the Vela satellites.

Recovery of the plasma sheet at a Vela satellite ~ 1 to $2 R_E$ from the neutral sheet typically occurs when the auroral electrojet reaches low polar cap latitudes (e.g., $\lambda_m \approx 74^\circ$) and often coincides with rapid relaxation of bays at auroral zone latitudes ($\lambda_m \approx 65^\circ$ to 70°). If the thickening of the plasma sheet during recovery is due to piling up of contracting merged field lines from far out in the tail, the merging process must proceed in a rather irregular fashion.

The intensity and particle energy of auroral particle fluxes are considerably greater than those in the plasma sheet. There is evidence that the particle fluxes in the plasma sheet are very strongly peaked along the magnetic field lines. This suggests that auroral particles are accelerated by electric fields along the magnetic field lines quite close to the earth, or perhaps by the Fermi mechanism acting deep in the magnetotail.

Acknowledgments

It is a pleasure to thank Drs J. R. Asbridge, S. J. Bame, and Sidney Singer for the use of data obtained from their experiments on the Vela satellites. Extended periods of continuous tracking of the Vela satellites are important for the success of the plasma

sheet studies described here. For such periods of tracking I thank the many people who operate the U.S. Air Force satellite tracking network and particularly Mr Harry Hallman and Major Richard Corya, USAF, of the Satellite Test Center, Sunnyvale, California.

Magnetograms used in these studies have been obtained through the services of Mr William Paulishak, World Data Center A, NOAA, Rockville, Maryland.

The Vela nuclear test detection satellites have been designed, developed and flown as part of a joint program of the Advanced Research Projects Agency of the U.S. Department of Defense and the U.S. Atomic Energy Commission. The program is managed by the U.S. Air Force.

References

- Akasofu, S.-I.: 1968, *Polar and Magnetospheric Substorms*, D. Reidel, Publishing Company, Dordrecht, Holland.
- Akasofu, S.-I., Hones, E. W., Jr., and Meng, C.-I.: 1970, *J. Geophys. Res.* **75**, 7296.
- Akasofu, S.-I., Hones, E. W., Jr., and Singer, S.: 1971, *J. Geophys. Res.* **76**, 6976.
- Aubry, M. P., Russell, C. T., and Kivelson, M. G.: 1970, *J. Geophys. Res.* **75**, 7018.
- Axford, W. I.: 1966, in *Auroral and Associated Magnetospheric Phenomena at Very High Latitudes*, Proceedings of the ESRO Colloquium, Stockholm, 16–18 November 1965, ESRO SP-8, p. 15.
- Axford, W. I.: 1967, in B. M. McCormac (ed.), *Aurora and Airglow*, Reinhold Publishing Corporation, New York, p. 499.
- Cummings, W. D., Barfield, J. N., and Coleman, P. J., Jr.: 1968, *J. Geophys. Res.* **73**, 6687.
- Dungey, J. W.: 1961, *Phys. Rev. Letters* **6**, 47.
- Fairfield, D. H. and Ness, N. F.: 1970, *J. Geophys. Res.* **75**, 7032.
- Feldstein, Y. I.: 1971, in E. R. Dyer (General editor), *Solar Terrestrial Physics/1970, Part III*, D. Reidel Publishing Company, Dordrecht, Holland, p. 152.
- Hones, E. W., Jr.: 1970, in B. M. McCormac (ed.), *Particles and Fields in the Magnetosphere*, D. Reidel Publishing Company, Dordrecht, Holland, p. 24.
- Hones, E. W., Jr., Asbridge, J. R., Bame, S. J., and Strong, I. B.: 1967, *J. Geophys. Res.* **72**, 5879.
- Hones, E. W. Jr., Singer, S., and Rao, C. S. R.: 1968, *J. Geophys. Res.* **73**, 7339.
- Hones, E. W., Jr., Akasofu, S.-I., Perreault, P., Bame, S. J., and Singer, S.: 1970, *J. Geophys. Res.* **75**, 7060.
- Hones, E. W., Jr., Asbridge, J. R., Bame, S. J., and Singer, S.: 1971a, *J. Geophys. Res.* **76**, 63.
- Hones, E. W., Jr., Singer, S., Lanzerotti, L. J., Pierson, J. D., and Rosenberg, T. J.: 1971b, *J. Geophys. Res.* **76**, 2977.
- Hones, E. W., Jr., Asbridge, J. R., and Bame, S. J.: 1971c, *J. Geophys. Res.* **76**, 4402.
- Hones, E. W., Jr., Karas, R. H., Lanzerotti, L. J., and Akasofu, S.-I.: 1971d, *J. Geophys. Res.* **76**, 6765.
- Hones, E. W., Jr., Akasofu, S.-I., Bame, S. J., and Singer, S.: 1971e, *J. Geophys. Res.* **76**, 8241.
- Ivliev, D. Ya., Pudovkin, M. I., and Zaitseva, S. A.: 1970, *Geomagnetizm i Aeronomiya* **10**, 300.
- Lezniak, T. W. and Winckler, J. R.: 1970, *J. Geophys. Res.* **75**, 7075.
- McPherron, R. L.: 1970, *J. Geophys. Res.* **75**, 5592.
- Meng, C.-I. and Akasofu, S.-I.: 1971, *J. Geophys. Res.* **76**, 4679.
- Meng, C.-I., Akasofu, S.-I., Hones, E. W., Jr. and Kawasaki, K.: 1971, *J. Geophys. Res.*, to be published.
- Russell, C. T. and Brody, K. I.: 1967, *J. Geophys. Res.* **72**, 6104.
- Russell, C. T., McPherron, R. L., and Coleman, P. J., Jr.: 1971, *J. Geophys. Res.* **76**, 1823.
- Vasyliunas, V. M.: 1968, *J. Geophys. Res.* **73**, 2839.

INTERPRETATION OF MAGNETIC FIELD VARIATIONS DURING SUBSTORMS

GORDON ROSTOKER

Institute of Earth and Planetary Physics, University of Alberta, Edmonton, Canada

1. Introduction

Over the last decade there has been considerable interest in the problem of how energy is transferred from the interplanetary medium to the interior of the earth's magnetosphere. The most spectacular result of this interaction is the so-called *magnetospheric substorm*. During this period of intense disturbance, regions of the nighttime magnetosphere become violently distorted and large amounts of energy are dissipated in various fashions, viz. ionospheric current systems, visual radiation or auroras, wave-particle interactions, etc. The most dominant magnetic field perturbation associated with the magnetospheric substorm is termed the *polar magnetic substorm*, although other types of magnetic perturbations may be generated during periods of large scale magnetospheric activity.

At the present time much effort is being devoted to studying magnetospheric substorms through the correlation of satellite data and data recorded at ground based observatories. Historically, magnetometers have provided the most comprehensive coverage of magnetospheric activity, so that polar magnetic substorms are generally used as a ground based indicator of magnetospheric substorms. In order to appreciate the significance of the correlation of satellite data with ground based magnetometer data, one must first realize the limitations of such studies. The major difficulty centers around the fact that the ground based magnetometer measures the integrated effect of all magnetospheric and ionospheric current systems, while satellite probes generally measure the characteristics of their immediate environment. The importance of this problem can be understood when one realizes that polar magnetic substorms represent relatively localized intensifications of the PEJ typically ranging from 20° to 90° in longitudinal extent. Unless the position of this intensified portion of the PEJ can be localized, there will always be a question of the position of the satellite with respect to the disturbed region of the magnetosphere. In this paper I shall attempt to outline how space physicists have attempted to meet this problem.

2. Presentation of Ground Based Magnetometer Data

Scientists working with ground based magnetometer data have continually been faced with the problem that data are only generally available from magnetic observatories distributed globally in a loose network. The arbitrary spacing of the observatories has also contributed to the difficulty in presentation of data. The most commonly used form of presentation to date is the *equivalent current system* introduced by Birkeland

(1908). Here the direction and magnitude of the horizontal magnetic perturbation vector are noted at all available observatories. Based on the assumption that the total perturbation at each station is caused by a uniform overhead sheet current flowing in the ionosphere, equivalent current lines are drawn normal to the magnetic perturbation vectors so that the distance between current lines is inversely proportional to the strength of the horizontal component of the magnetic field perturbation. An example of an equivalent current system recorded at an instant during magnetic substorm activity is shown in Figure 1. It should be emphasized that such current patterns do not necessarily represent purely ionospheric current systems. Although Chapman (1935) suggested that this was the case, the original interpretation by Birkeland (1908) that the equivalent current system was merely the potential pattern from a three dimensional current system has now come back into favor (Bonnevier *et al.*, 1970). The major difficulty with equivalent current system representation is the low density of observatories over the earth's surface, coupled with the fact that auroral zone and

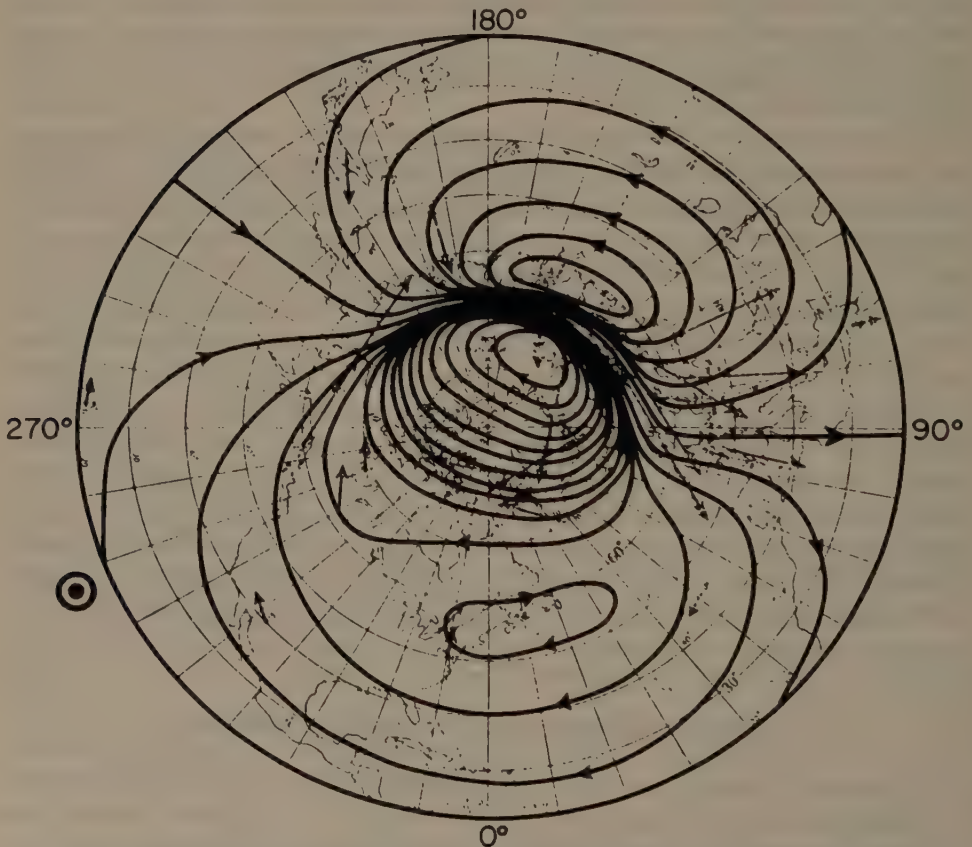


Fig. 1. Equivalent current system recorded at an instant during substorm activity on April 30, 1933. Regions where equivalent current lines are close together indicate regions of intense current flow (Fukushima, 1953).

polar cap coverage is anomalously sparse. Thus equivalent current systems are synthesized through the use of extrapolation in a situation where the rate of falloff of perturbation field strength moving away from the source is not really known.

A second technique for portraying magnetic perturbation patterns is the use of the *latitude profile*. Birkeland (1908) used this technique to provide information about the Z component perturbation, and Vestine and Chapman (1938) used it to portray all three components of the magnetic field perturbation. In this technique the magnitudes of the three components (H, D, and Z) are plotted as a function of the latitude of the observing station, assuming all stations to lie on a common meridian. An example of such a profile is shown in Figure 2, assuming a line current to flow westward in the ionosphere at a latitude of 70° N. It is useful to keep this simple model in mind when trying to interpret the actual observed perturbation pattern. The latitude profile technique suffers from the deficiency that it only provides information about the perturbation pattern along a single meridian (as compared to the equivalent current system which presents a global picture of magnetic perturbation pattern). On the other hand it presents easily readable quantitative information on all three components of the perturbation field, and lends itself to easy comparison of observed data and data synthesized from model current systems.

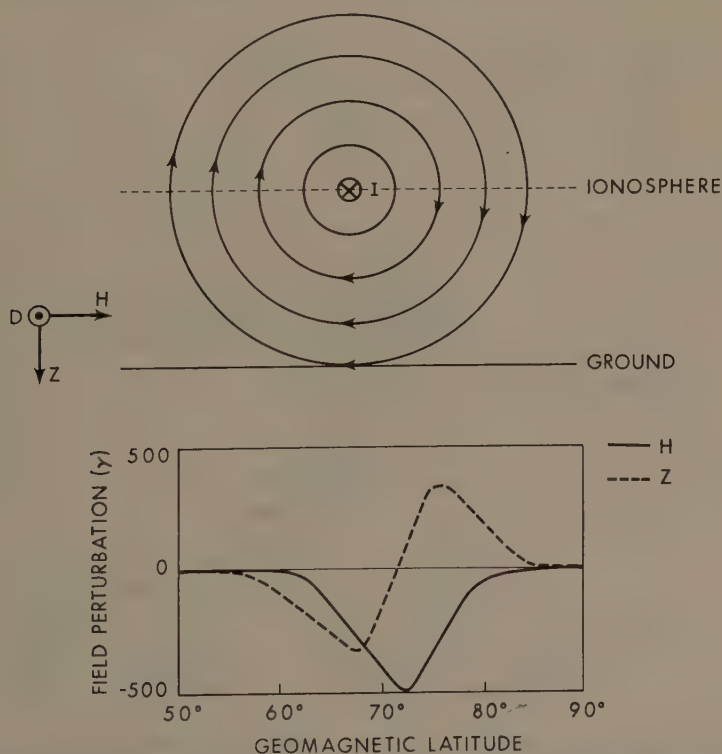


Fig. 2. Schematic representation of latitude profile representation of magnetic perturbation pattern from a line current of infinite extent flowing westward through the ionosphere.

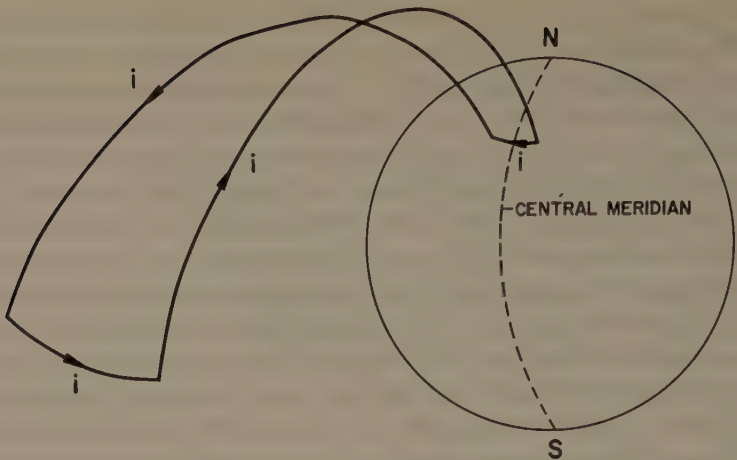


Fig. 3. Model current system thought to be responsible for polar magnetic substorm perturbation (Kisabeth and Rostoker, 1971).

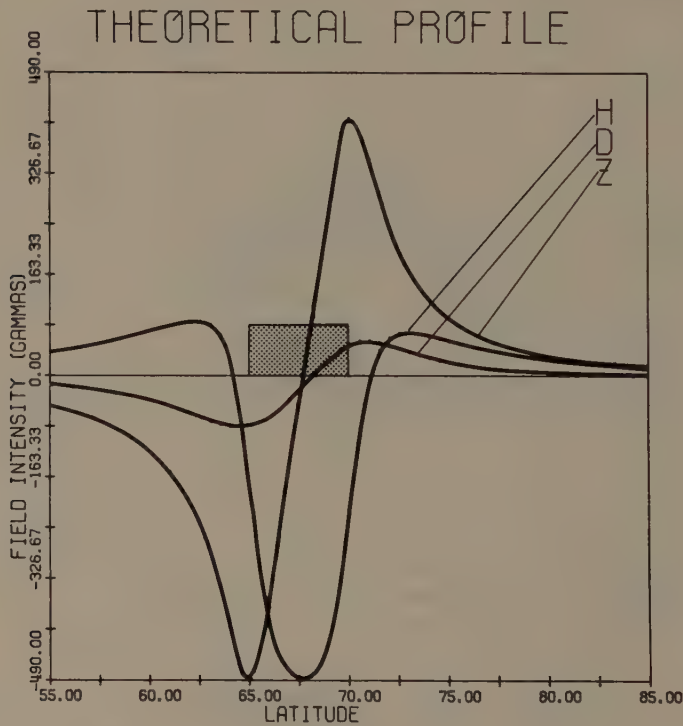


Fig. 4. Latitude profile of magnetic perturbation pattern from three dimensional current system shown in Figure 3. The integrated current of 10^6 amp is uniformly distributed across the latitudinal regime $65^\circ < \lambda < 70^\circ$ (indicated by the shaded box). The E-W extent of the electrojet is 20° and the meridian of observation is 4° east of the central meridian (Kisabeth and Rostoker, 1971).

3. Modeling of Substorm Magnetic Field Perturbation Pattern

Within the last few years, it has become apparent that field aligned currents flow during magnetospheric substorm activity. The recent studies of Meng and Akasofu (1969) and Bonnevier *et al.* (1970) suggest that a three dimensional current system of the type proposed by Boström (1964) is responsible for the polar magnetic substorm perturbation pattern. This model current system (Figure 3) features a current flowing down field lines into the ionosphere, westward through the ionosphere in the form of the westward electrojet, and back up the field lines into the magnetosphere. The interpretation of the magnetic perturbation pattern associated with substorms which I shall present, will be based on this model current system. In Figure 4 a sample latitude profile computed from the theoretical model is presented for a meridian 4° east of the central meridian. For this model the E-W extent of the ionospheric portion of the current is 20° , the current is uniformly distributed across the 5° width of the electrojet, and the electrojet itself is centered at 67° N. In the context of present day terminology we would say that there are negative H bays in the latitude range $64 < \lambda < 71^\circ$ with positive H bays north and south of that latitude regime. South of the center of the electrojet negative Z bays are observed, while positive Z bays occur to the north. The



Fig. 5. Line of magnetometers through western Canada from which data were taken. Digital data were obtained from stations Calgary (58.5° N) to Cambridge Bay (77° N) with normal magnetograms available from Newport (55° N) and Resolute Bay (84.5° N).

D bay configuration is determined by whether the latitude profile pertains to a meridian east or west of the central meridian. Comparing the profile shown in Figure 4 with the profile associated with a purely westward ionospheric electrojet (shown in Figure 2), it is apparent that the positive H bay regime is generated by the field aligned

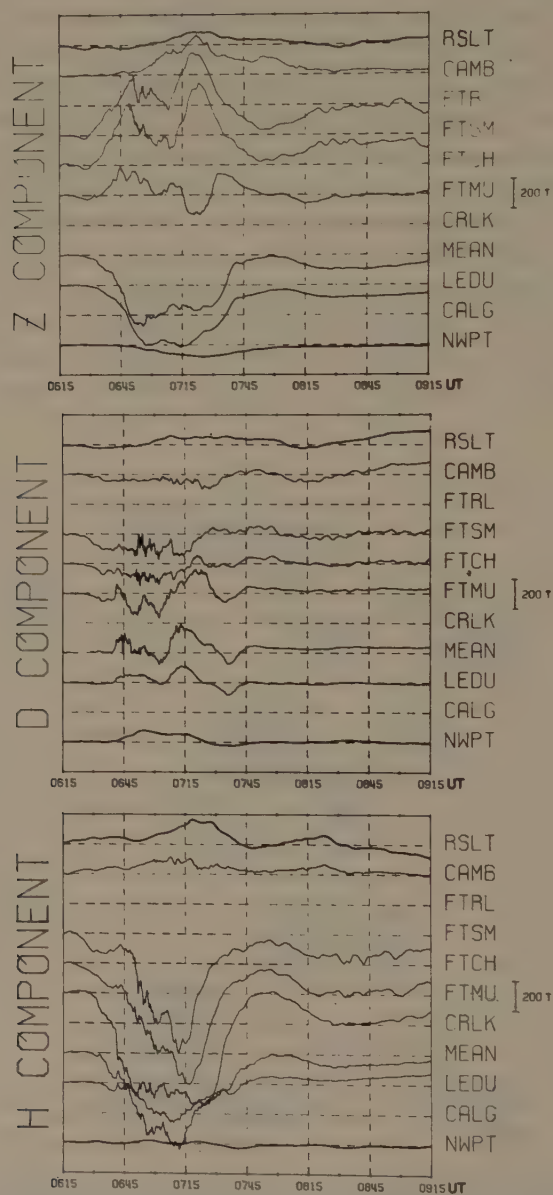


Fig. 6a. Normal magnetograms for polar magnetic substorm of July 2, 1970 (Day 183).

currents, as is the D bay perturbation pattern (neglecting end effects). On the other hand the Z component perturbation pattern is dominated by the ionospheric portion of the current system. We shall now attempt to explain observational data in the context of the model discussed above.

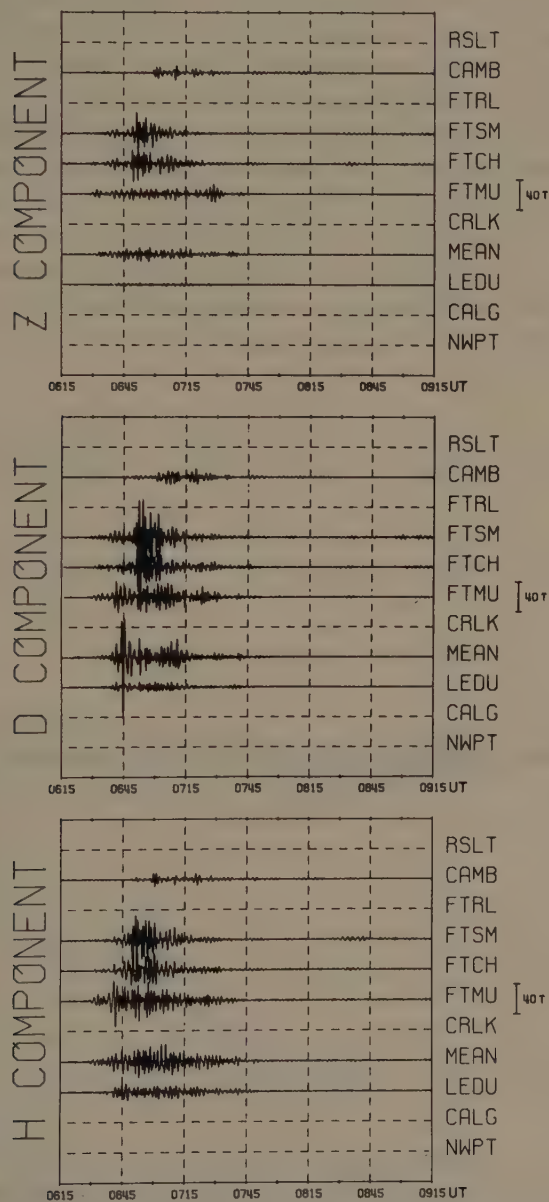


Fig. 6b. Rapid run micropulsation records for polar magnetic substorm of July 2, 1970. The filter used in the processing of the data band passed the period range of 40–150 s.

4. Development of the Polar Magnetic Substorm Perturbation Pattern

To demonstrate the use of the latitude profile technique we shall analyze data from a substorm recorded on July 2, 1970. The data were recorded at a line of magnetometer stations set up along a corrected geomagnetic meridian $\sim 302^\circ$ E through western Canada (Figure 5). The normal magnetograms and filtered, micropulsation records are shown in Figures 6a and 6b respectively. The substorm onset occurred at 0632 UT as identified by the Pi2 micropulsation onset. However, approximately 10 min prior to the substorm onset, a small westward electrojet was observed to grow near 70° N and move slightly southward. By 0631 UT (Figure 7a) the magnetic perturbation was close to 100γ ; the development of this perturbation is probably related to the growth phase reported by McPherron (1970). The substorm onset shown in Figure 7b featured the intensification of the current at the southern border of the westward electrojet near 65° N. The intensified portion of the electrojet grew in magnitude until 0648 UT (see Figure 7c) at which time the system was centered at $\sim 65^\circ$ N and produced a maximum perturbation of $\sim 450 \gamma$. (At this point it is useful to note that if the station

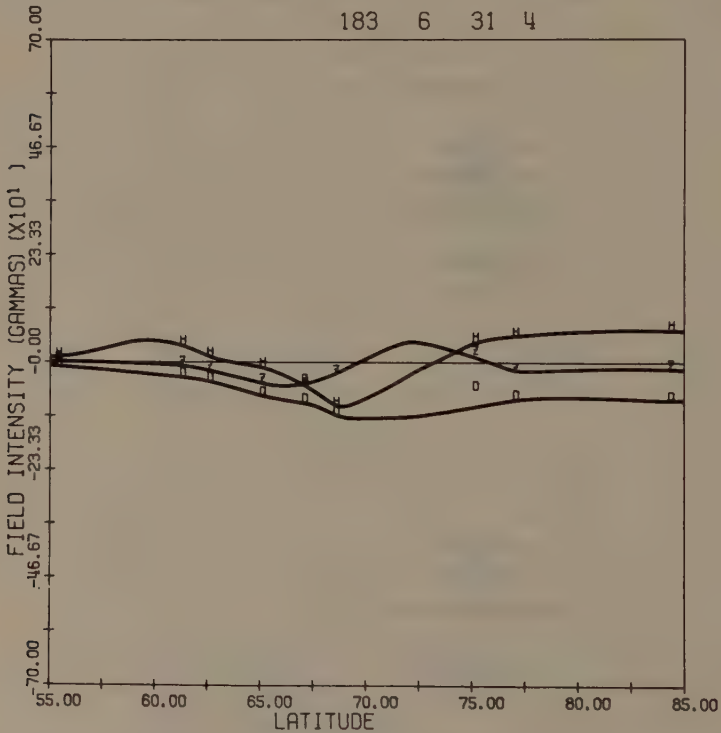


Fig. 7a. Latitude profile of magnetic perturbation pattern 1 min prior to the onset of the substorm expansive phase. Numbers at top of figure are the day of the year, hour, minute and second, respectively, for which the data pertain. Data at 75° N are from Baker Lake and do not necessarily lie on the curves as that station is $\sim 18^\circ$ east of the station line's average meridian (Kisabeth and Rostoker, 1971).

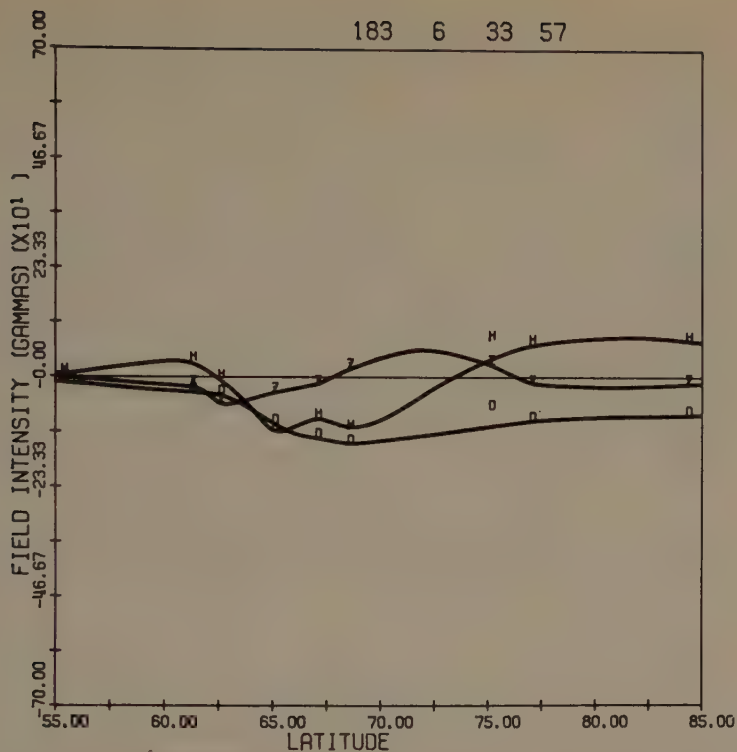


Fig. 7b. Latitude profile showing the intensification of current at the southern border of the westward electrojet associated with the onset of the substorms expansive phase at 0632 UT.

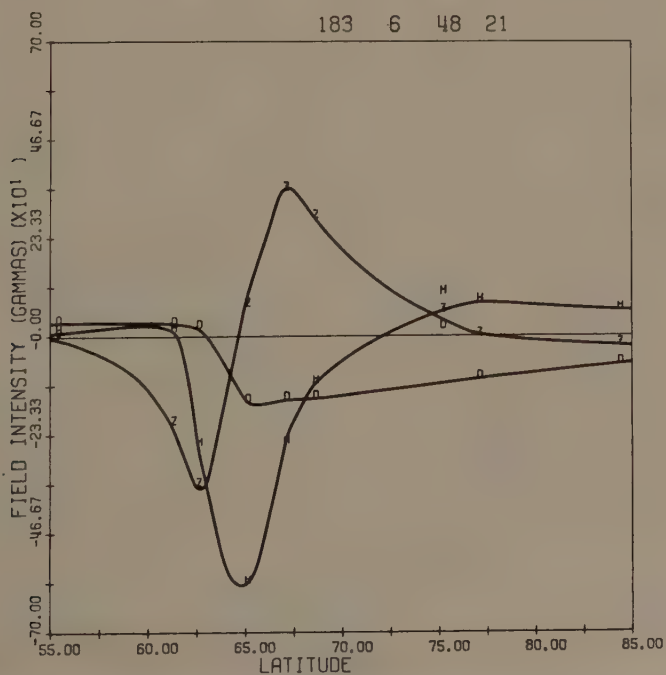


Fig. 7c. Latitude profile showing magnetic perturbation pattern associated with the substorm just prior to the development of the westward traveling surge.

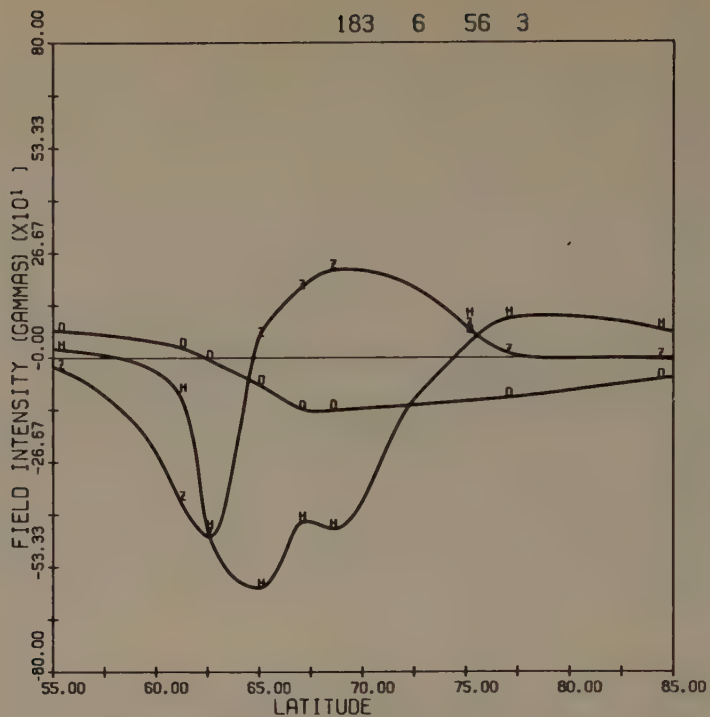


Fig. 7d. Latitude profile showing magnetic perturbation pattern associated with the intensification of current at the northern border of the westward electrojet.

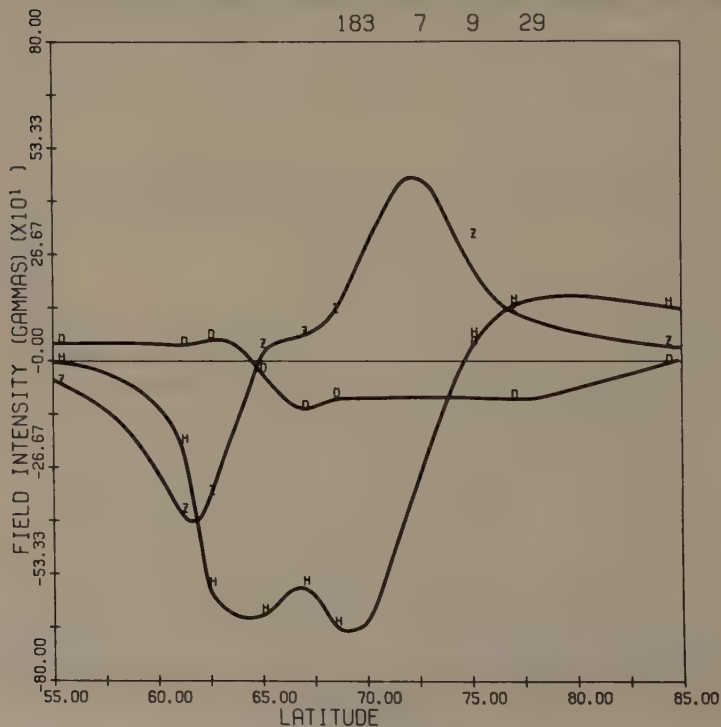


Fig. 7e. Latitude profile showing the magnetic perturbation pattern associated with the intensification of the current at the northern border of the westward electrojet.

at 65° N was not present, one could easily underestimate the maximum magnetic perturbation produced by the current system. This illustrates the importance of having data from a closely spaced network of stations to describe the characteristics of the substorm current system). Around 0648 UT there was a sharp intensification of the current at the northern border of the electrojet, and by 0656 UT (see Figure 7d) the double peak in the H component profile is readily apparent. Approximately 19 min after this effect started, the current at the northern border of the electrojet again intensified producing a double peak in the magnetic perturbation pattern as shown in Figure 7e. After this time the substorm decayed.

It is useful to briefly note some of the facts which we may infer from latitude profiles such as those presented above. Choosing the substorm magnetic perturbation pattern at 0648 UT as an example, we can say

- (a) The electrojet is centered around 65° N.
- (b) The maximum magnetic perturbation is greater than $\sim 500 \gamma$.
- (c) The center of the intensified portion of the electrojet lies to the east of the line of stations.
- (d) From the distance between the peaks in the Z component profile, the width of the electrojet is $\sim 5^{\circ}$ of latitude.

By fitting model current system perturbation patterns to such observed profiles, it is possible to comment more exactly on the strength of the current system, and the latitude and longitude of the center of the intensified portion of the westward electrojet.

5. Conclusions on Substorm Development Obtained from Latitude Profiles

The morphology of substorm development based on this type of data has been discussed in detail by Kisabeth and Rostoker (1971). The pattern is as follows:

(a) Prior to the onset of the substorm's expansive phase, the westward electrojet *may* intensify. There are no Pi2 micropulsations associated with this intensification.

(b) In general, at the onset of the substorm's expansive phase the current at the southern border of the westward electrojet intensifies (although on occasion the whole electrojet intensifies). At the same time a Pi2 micropulsation burst occurs, and the auroral arcs break up and begin to expand northward.

(c) Approximately 15 to 20 min after the onset of the substorm's expansive phase, the current at the northern border of the electrojet intensifies accompanied by a Pi2 micropulsation burst and the generation of a westward traveling surge.

(d) The substorm further develops through quasi-periodic intensifications of the current at the northern border of the electrojet. The intensifications are about 15 to 20 min apart, and each is thought to be associated with the development of a westward traveling surge or loop.

Acknowledgments

The work described in this paper has been carried out in association with J. L. Kisabeth.

This research was supported (in part) by the Defense Research Board of Canada, Grant number 9510-82 and by the National Research Council of Canada.

References

- Birkeland, K.: 1908, *The Norwegian Aurora Polaris Expedition 1902-1903*, Vol. I, First Section, Aschhoug and Co., Christiania.
- Bonnevier, B., Boström, R., and Rostoker, G.: 1970, *J. Geophys. Res.* **75**, 107.
- Boström, R.: 1964, *J. Geophys. Res.* **69**, 4983.
- Chapman, S.: 1935, *Terrest. Mag. Atmosph. Elec.* **40**, 349.
- Fukushima, N.: 1953, *J. Fac. Sci. Tokyo Univ.* **8**, 293.
- Kisabeth, J. L. and Rostoker, G.: 1971, *J. Geophys. Res.*, 6815
- McPherron, R. L.: 1970, *J. Geophys. Res.* **75**, 5592.
- Meng, C.-I. and Akasofu, S.-I.: 1969, *J. Geophys. Res.* **74**, 4035.
- Vestine, E. H. and Chapman, S.: 1938, *Terrest. Mag. Atmosph. Elec.* **43**, 351.

X-RAY OBSERVATIONS AND INTERPRETATIONS

G. R. PILKINGTON

Max-Planck-Institut für Aeronomie, Institut für Stratosphärenphysik, Lindau, Germany

1. Introduction

The presence of soft X-rays in the stratosphere at high latitudes was first reported in 1956, and correctly identified as due to Bremsstrahlung from energetic auroral electrons entering the atmosphere. Balloon X-ray measurements provide the most direct means of monitoring auroral electron precipitation both day and night from a relatively fixed location, and for long periods of time. Further, no time constants are involved in the Bremsstrahlung process, and the approximate electron spectrum and flux can be obtained quite readily. X-ray measurements however, do suffer severe limitations. The Bremsstrahlung process is very inefficient and this, plus atmospheric attenuation of the X-rays, makes the method useful only in the energy range 20 to 200 keV. Further, due to the isotropic emission of X-rays by the source and subsequent scattering in the atmosphere, detectors at balloon altitudes provide only a spatially averaged picture of the electron precipitation.

In this paper the LT aspects of the X-ray substorm are reviewed. A calculation on the passage of X-rays through the atmosphere and recent high resolution energy spectrum measurements are presented. Finally temporal variations are discussed.

2. X-Ray Substorm

X-ray precipitation shows quite distinct characteristics during the substorm at different LT's and to a certain extent different latitudes. Figure 1 summarizes the main features of the X-ray substorm for an auroral zone station. The Figure shows typical precipitation observed at about the indicated LT's when a substorm occurs every 4 hr (starting at 00 LT). Shown are local magnetic activity, X-ray activity, approximate electrojet location relative to balloon, e -fold energy of electron spectrum (assumed exponential), and characteristics of temporal variations.

Evidence of *growth phase* precipitation has been observed (Pytte and Trefall, 1971) in the midnight sector (Figure 2). This precipitation occurs up to $1\frac{1}{2}$ hr prior to isolated bays at high latitudes ($L \gtrsim 6$), and consists of slowly varying activity with an energy spectrum which is well represented by an exponential function with e -fold energy of about 50 keV.

In the *midnight sector* impulsive X-ray events are observed (Pytte and Trefall, 1971) at the onset of bay activity as shown in Figure 2 at 2130. These events start abruptly and are closely associated with the Pi2 magnetic pulsations which are a common feature at bay onset (Rostoker, 1967). Considerable softening of the X-ray spectrum is noted during these events. Pytte and Trefall interpreted these pulsations as due to

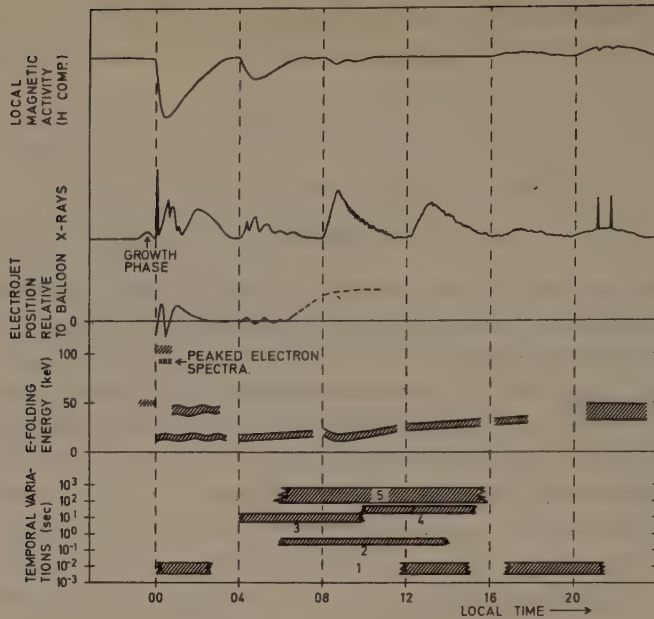


Fig. 1. Schematic diagram summarizing the X-ray substorm and associated magnetic activity at an auroral zone station. Diagram shows events observed at each 4 hr LT, when bays occur in the midnight sector.

standing Alfvén waves on closed magnetic field lines near the inner edge of the plasma sheet.

Immediately following the above, X-ray precipitation is impulsive with no fast time structure of less than minutes, at L values between about 5 and 7 (Kremser, 1969), although impulsive precipitation over times of 5 to 30 s is observed at higher L values ($L \approx 8$). This is similar to the latitude dependence of CNA measurements (Jelly, 1970).

In the midnight sector X-ray source regions are of limited N-S extent, but of considerable E-W extent, and are aligned along and move with the electrojet when the latter can be well defined (Clark and Anger, 1967; Bjordal *et al.*, 1971).

During the expansion phase both equatorward and poleward motions of the electrojet and X-ray source regions were found to be equally likely, probably due to the general expansion of the oval. During the recovery phase poleward motions of the electrojet predominated, possibly due to the northward relative movement of the oval in the early morning hours.

Jentsch (1970) carried out an investigation of X-ray energy spectra. He found that in many cases the X-ray (and hence electron) spectrum could be well represented by an exponential function, during midnight activity, with sometimes a high (about 60 keV) and sometimes low (15 keV) e -fold energy. During midnight events the spectrum e -fold energy was often constant for over 1 hr, despite considerable variations in the X-ray flux. Occasionally extremely hard spectra were observed (e -fold energy

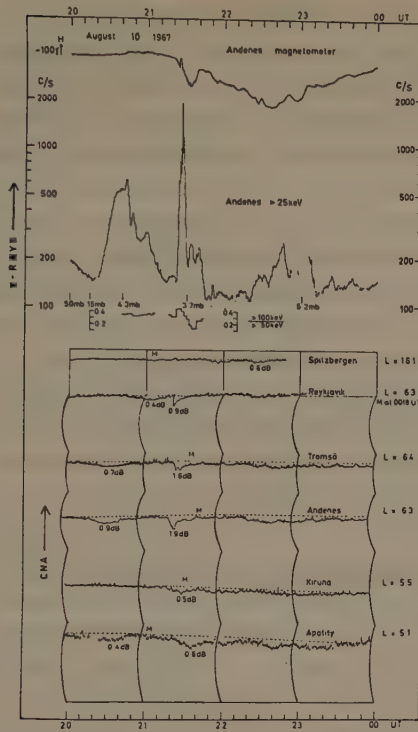


Fig. 2. Example of a growth phase X-ray event. X-ray precipitation and CNA are observed well before the bay. Also indicated are balloon altitude in mb (millibar) and X-ray energy spectrum index – the ratio of X-ray flux with energy $E > 100$ keV to that with $E > 50$ keV (Pytte and Trefall, 1971).

> 150 keV) but at these times an exponential representation of the spectrum over a wide energy range was not valid. These spectra were observed between 2200 and 0200 LT. They occurred predominantly during count rate increases and sometimes during bay onset.

As pointed out above, during midnight activity X-ray source regions have a considerable E-W extent along the electrojet. Measurements in the *early morning sector* between Iceland and Scandinavia indicate that this activity may extend over 2000 km along the electrojet. Further, there is evidence that this activity spreads very rapidly eastward from the midnight sector at typically 10 km s^{-1} (similar to the eastward traveling surge; Akasofu, 1968) resulting in electron enhancements in the morning hours occurring with no significant delay from the midnight events. This appears to be followed by a slower eastward movement (about 1 km s^{-1}) of this entire elongated region (Kremser, 1969).

X-ray events in the *later morning sector* are most intense in the auroral zone and are accompanied by little or no magnetic activity (0800 in Figure 1) (Bewersdorff *et al.*, 1968). The precipitation region is widespread but there is evidence of a southward

movement of its southern edge of 500 m s^{-1} during the initial increasing phase, and at the same time a significant softening of the X-ray (and electron) (Parks *et al.*, 1968) spectrum. This southward motion could be caused by differential L shell drifting, as electrons on higher L shells drift faster. The spectrum softening is also consistent with gradient drifting, but the subsequent spectrum hardening cannot be explained by this mechanism.

Around *noon* the gross features of X-ray precipitation are more extended than those observed earlier and fluxes are usually weaker (Kremser, 1969). X-ray spectra show no large variations, except for a slight hardening during the event (see Figure 1).

In the *afternoon* hours, X-ray events are rare but what measurements there are show weak unstructured activity (McPherron *et al.*, 1968).

Evening events often consist of impulsive bursts (Trefall, 1970), which are probably associated with the westward traveling surge. X-ray energy spectra at this time are typically hard and exponential like with an e -folding energy of 30 to 50 keV (Barcus and Rosenberg, 1966).

3. Discussion of X-Ray Substorm Activity

Considerable similarity is evident between the X-ray substorm and the auroral substorm described in detail by Akasofu (1968). Growth phase activity occurs prior to magnetic bay activity when quiet arcs are observed in the auroral oval. Various other phenomena occur in the magnetosphere at this time, for example, thinning of the plasma sheet and development of an asymmetric ring current.

During the substorm expansion and recovery phases X-ray events in the midnight sector of the oval are closely associated with the electrojet responsible for magnetic bay activity. Trefall (1970) suggests that the associated precipitating electrons are coming directly from some primary source. Such bay associated events are observed from the midnight sector up to about 0400 LT, which is approximately the same LT region over which Pfitzer and Winckler (1970) found evidence of adiabatic acceleration of electrons from ATS 1 measurements.

During the day time X-ray events are observed in the absence of local magnetic activity. Electron gradient drifting from the midnight sector is believed in some way responsible for these events. A study (Sletten *et al.*, 1971) of the delay times between bays in the midnight sector and associated X-ray events in the morning sector did indicate an increasing delay with increasing LT as expected from electron drifting. However, the study found that zero delays were observed up to 0600 LT and the delay times were too short for electrons corresponding to the measured X-ray energies. Both these problems could be overcome by assuming an elongated primary source region from about midnight to 0600 LT and gradient drifting from all along this region. This assumption in fact is consistent with observations (Kremser, 1969).

Electron gradient drifting from near midnight is also indicated by ATS 1 measurements (Arnoldy and Chan, 1969) of energetic electrons. However, comparison of ATS 1 electrons and simultaneous X-ray measurements at the near conjugate point

in the auroral zone indicates that simple gradient drifting of electrons cannot be responsible for the morning events (Parks, 1970). These measurements indicate strong to weak pitch angle diffusion of electrons, with corresponding electron lifetimes of 200 to 1000 s, which are much shorter than the duration of day time events.

The diurnal variation of the electron energy spectrum is also shown in Figure 1. This amounts to an increase throughout the day time of about 1 keV hr^{-1} in e -fold energy. Maximum hardness is usually observed about 1700 LT (Bewersdorff *et al.*, 1966), although Anderson (1967) reported one event in which maximum spectrum hardness was observed around noon. The latter results can be interpreted in terms of the known zones of hard and soft electron precipitation (Kremser, 1969).

4. Passage of X-Rays Through the Atmosphere

Balloon measurements are usually conducted at atmospheric depths of 2 to 10 gm cm^{-1} and so the observed X-ray spectrum is affected by photoelectric absorption and Compton scattering. Recently the Monte Carlo method (Pilkington and Anger, 1971a) has been employed to study the passage of X-rays through the atmosphere and in particular the effects on the observed spectrum of different source geometries and locations relative to the detector, and different detector types (collimated or omnidirectional).

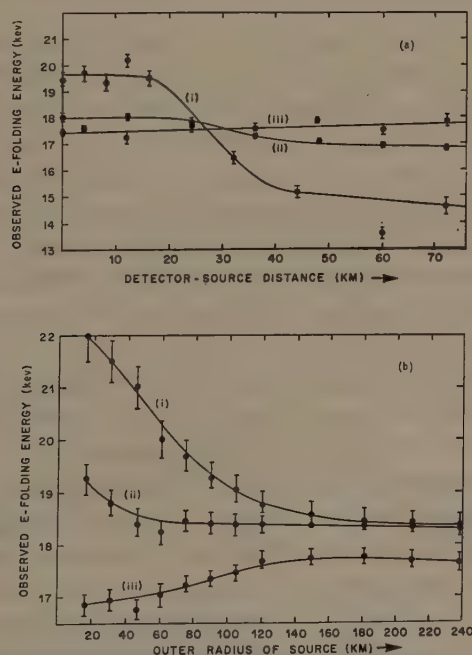


Fig. 3. The variation of e -folding energy of X-ray spectrum observed at 5 gm cm^{-2} vs. horizontal distance of line source from detector (a), and radius of circular source above detector (b). An exponential X-ray source spectrum with e -fold energy of 20 keV is considered and the different curves are for (i) collimated, (ii) flat, and (iii) omnidirectional detectors.

The results show that above 40 keV the observed X-ray spectrum is similar in shape to the source spectrum. Below 40 keV photoelectric absorption is dominant and the observed spectrum falls steeply (see inserts in Figure 4 for examples of X-ray spectra). Figure 3 shows an example of the effects of different source geometries, locations and detector types on the observed X-ray spectrum for a source with an exponential X-ray spectrum and e -fold energy of 20 keV. Data are given for an atmospheric depth of 5 gm cm^2 . The e -fold energy (for energies above 40 keV) is indicated as a function of the horizontal distance of a line source from the detector (a) and radius of a circular source over the detector (b). Results for (i) a collimated detector (30° half angle), (ii) a flat and (iii) an omnidirectional detector are presented. It can be seen that the e -fold energy of the observed spectrum is very dependent on source location and size for the collimated detector, but not for the omnidirectional or flat detector.

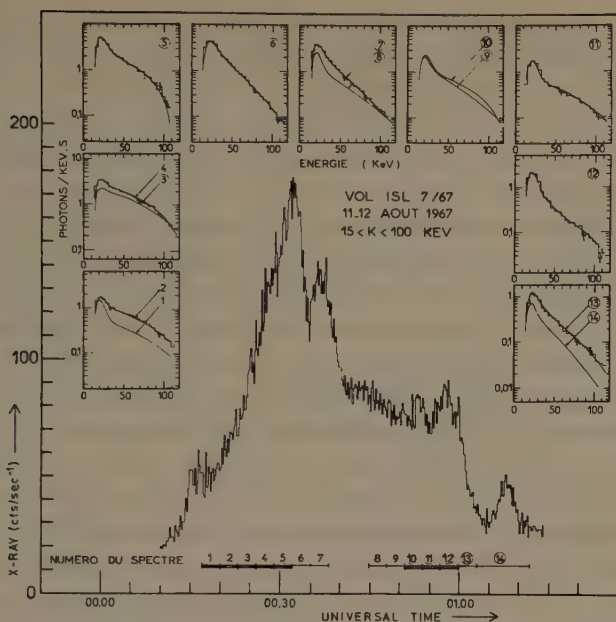
The results presented here are quite typical of different source spectra and indicate that X-ray measurements made by omnidirectional or flat detectors can be converted to a source X-ray and hence electron spectrum (albeit spatially averaged) provided some simple form for the electron spectrum can be assumed. For a collimated detector, however, evaluation of the source X-ray spectrum is not simple without knowledge of the source size and location; also spectrum variations must be viewed with considerable caution.

5. High Resolution Energy Spectrum Measurements

Balloon instruments are usually designed to provide only a rough indication of the X-ray spectrum with typically between 2 to 8 integral or differential energy channels. Recently, high resolution measurements have been conducted using 32 (Pilkington and Anger, 1971b) and 128 (Maral, 1970) differential energy channels. These measurements indicated the occurrence of electron spectra peaked at energies between 70 and 150 keV. Up to now only three such measurements have been reported all occurring during the expansion phase of substorms in the midnight sector. Similar peaked electron spectra were reported from early morning rocket measurements by Riedler (1966) and the extremely hard spectra observed by Jentsch (1970) from integral measurements may also be of this type.

The X-ray spectra corresponding to peaked electron spectra are identified by a distinct curvature at energies above 50 keV, when the spectra are plotted in semi-logarithmic representation (Figure 4). In the figure observed X-ray spectra are shown at the top. The indicated electron energy spectrum was assumed and the corresponding X-ray spectrum at balloon altitudes calculated. For each X-ray spectrum observed, the best fit e -fold energies and/or E peak values of the electron spectrum were obtained and these are tabulated on Figure 4.

Electric fields may be responsible for such spectra. Vertical electric fields of sufficient magnitude have been observed (mV m^{-1}), but in the wrong direction to accelerate electrons into the atmosphere (Fahleson, 1972). Another possible explanation is wave-particle interactions. Scarf and Fredricks (1972) reported observing electrostatic waves of about 3 kHz (the gyrofrequency of about 80 keV electrons), near the equatorial



$$\frac{dn(E)}{dE} = Ae^{-E/E_{01}} + B\delta(E_{\text{peak}} - E) + Ce^{-E/E_{02}}$$

Spectrum number	1	2	3	4	5	6	7	8	9	10	11	12	13	14
$E_{01}(\text{keV})$	4	4	4	4	4	4	4	4	4	4	4	4	4	4
$E_{\text{peak}}(\text{keV})$	150	150	150	130	110					130	150	130		
$E_{02}(\text{keV})$						35	40	70	70				40	30

Fig. 4. Examples of peaked electron spectra. Differential electron spectra of the form given were calculated to correspond to the observed X-ray spectra (insets). E -fold energies and/or peak values of the electron spectra are given in the table (Maral, 1970).

plane during a substorm. These waves were of sufficient intensity to cause pitch angle diffusion of kilovolt electrons.

6. Temporal Variations

So far we have considered only gross variations of the X-ray precipitation. A wide range of temporal variations from 5 ms to 300 s (Anderson, 1968) has been observed by X-ray measurements. As shown in Figure 1, these variations occur at particular LT during the substorm.

The fastest time variations (fast impulses and microbursts; 1 and 2 in Figure 1) have millisecond rise times which are equal to or less than electron bounce times. Little is known of fast impulses but microbursts (2) are associated with magnetic impulses and VLF. These phenomena are probably produced near or in the ionosphere, as is

indicated from rocket measurements, possibly by microscopic plasma instabilities.

The fast irregular pulsations (3 and 4) occur during the recovery phase of the sub-storm and are associated with auroral pulsations (Rosenberg *et al.*, 1971) and magnetic pulsations of similar period (McPherron *et al.*, 1968). The 5 to 15 s pulsations occur when the electrojet is in the vicinity of the balloon and the electron spectrum is soft, possibly indicating an association with early morning oval precipitation.

The 5 to 15 s period pulsations have been found to persist also in the trapped equatorial electrons at $L=6.6$ but with peak-to-valley ratios of only a few percent, compared to a factor of 2 in the X-ray flux (Parks and Winckler, 1969). The source mechanism for such pulsations is thought to involve wave-particle coupling, plasma instabilities, or a combination of both. Coroniti and Kennel (1970) investigated the effects of a drift wave instability at the inner edge of the plasma sheet and found that such a model fits many of the features of these X-ray pulsations.

Long period pulsations (5) are generally observed over considerable longitudinal and limited latitudinal extent. This spatial extent and association with similar magnetic pulsations suggest hydromagnetic waves as the most probable origin. Influence of the solar wind on the magnetosphere has been suggested as the source of these waves, as, in fact, waves of 1 to 5 min period are commonly observed near the magnetopause. Cladis (1971) considers magnetic field oscillations caused by sudden particle injection into the magnetic flux tubes. Such oscillations would be of the required period and could be triggered by drifting particles.

In the above the temporal variations have been accredited to several different processes. D'Angelo (1969) points out that many of the features of these pulsations, including relationship between pulsation period and size, can be explained by a drift wave instability.

Acknowledgments

The author is grateful to Dr G. Kremser for discussions, and to Professor H. Trefall for permission to use his results prior to their publication. This work was carried out while the author was a stipendiate at the Max-Planck-Institut für Aeronomie, Lindau. Thanks are due to the Max-Planck-Gesellschaft for this financial assistance.

References

- Akasofu, S.-I.: 1968, *Polar and Magnetospheric Substorms*, D. Reidel Publishing Company, Dordrecht, Holland.
- Anderson, K. A.: 1967, in B. M. McCormac (ed.), *Airglow and Aurora*, Van Nostrand Reinhold Publishing Company, New York, p. 249.
- Anderson, K. A.: 1968, in B. M. McCormac (ed.), in *Earth's Particles and Fields*, Van Nostrand Reinhold Company, New York, p. 429.
- Arnoldy, R. L. and Chan, K. W.: 1969, *J. Geophys. Res.* **74**, 5019.
- Barcus, J. R. and Rosenberg, T. J.: 1966, *J. Geophys. Res.* **71**, 803.
- Bewersdorff, A., Dion, J., Kremser, G., Keppler, E., Legrand, J. P., and Riedler, W.: 1966, *Ann. Geophys.* **22**, 23.
- Bewersdorff, A., Kremser, G., Stadsnes, J., Trefall, H., and Ullaland, S. L.: 1968, *J. Atmospheric Terrest. Phys.* **30**, 591.

- Bjordan, J., Trefall, H., Ullaland, S. L., Bewersdorff, A., Kangas, J., Tanskanen, P., Kremser, G., Saeger, K. H., and Specht, H.: 1971, *J. Atmospheric Terrest. Phys.* **33**, 605.
- Cladis, J. B.: 1971, *J. Geophys. Res.* **76**, 2345.
- Clark, T. A. and Anger, C. D.: 1967, *Planetary Space Sci.* **15**, 1287.
- Coroniti, F. V. and Kennel, C. F.: 1970, *J. Geophys. Res.* **75**, 1863.
- D'Angelo, N.: 1969, *J. Geophys. Res.* **74**, 909.
- Fahleson, U. V.: 1972, this volume, p. 223.
- Jelly, D. H.: 1970, *Can. J. Phys.* **48**, 335.
- Jentsch, V.: 1970, Diplomarbeit, Technische Universität Clausthal, W. Germany.
- Kremser, G.: 1969, in B. M. McCormac and A. Omholt (eds.), *Atmospheric Emissions*, Van Nostrand Reinhold Company, New York, p. 181.
- Maral, G.: 1970, Thèse Docteur des Sciences Physiques, Université de Toulouse, France.
- McPherron, R. L., Parks, G. K., Coroniti, F. V., and Ward, S. H.: 1968, *J. Geophys. Res.* **73**, 1697.
- Parks, G. K.: 1970, *J. Geophys. Res.* **75**, 3802.
- Parks, G. K. and Winckler, J. R.: 1969, *J. Geophys. Res.* **74**, 4003.
- Parks, G. K., Arnoldy, R. L., Lezniak, T. W., and Winckler, J. R.: 1968, *Radio Sci.* **3**, 715.
- Pfitzer, K. A. and Winckler, J. R.: 1970, *J. Geophys. Res.* **74**, 5005.
- Pilkington, G. R. and Anger, C. D.: 1971a, *Planetary Space Sci.* **19**, 1069.
- Pilkington, G. R. and Anger, C. D.: 1971b, *Planetary Space Sci.*, to be published.
- Pytte, T. and Trefall, H.: 1971, *J. Atmospheric Terrest. Phys.* **34**, 315.
- Riedler, W.: 1966, North-Holland Publishing Company, Amsterdam, Holland. *Space Res.* **8**, 195.
- Rosenberg, T. J., Bjordan, J., Trefall, H., Kvifte, G. J., Omholt, A., and Egeland, A.: 1971, *J. Geophys. Res.* **76**, 122.
- Rostoker, G.: 1967, *J. Geophys. Res.* **72**, 2032.
- Scarf, F. L. and Fredricks, R. W.: 1972, this volume, p. 329.
- Sletten, A., Stadsnes, J., and Trefall, H.: 1971, *J. Atmospheric Terrest. Phys.* **33**, 589.
- Trefall, H.: 1970, *SPARMO-Bulletin* **4**, No. 3.

EXCITATION OF POLAR SUBSTORMS BY NORTHWARD INTERPLANETARY MAGNETIC FIELD

ATSUHIRO NISHIDA

*Institute of Space and Aeronautical Science, University of Tokyo,
Komaba, Meguro-Ku, Tokyo, Japan*

1. Introduction

It has been generally recognized that the activity of the polar substorm is strongly influenced by the N-S component B_z of the interplanetary magnetic field. The relation between B_z and the substorm activity is usually expressed as 'substorms occur when B_z is southward' or 'substorms follow north-to-south changes in B_z '. However, we can find cases of substorms during intervals of the northward B_z , and these cases appear to form exceptions if the relation is expressed as the above. In order to resolve this difficulty some suggestions have been made. The first is that substorms may appear to result from the northward B_z because of the time delay between B_z and the corresponding substorm activity, but the time delay has been found to be 1 to 2 hr and is not likely to explain the occurrence of substorms during intervals of prolonged (5 hr or more) northward B_z . The other suggestion has been that interplanetary parameters other than B_z may also be important, but we have not yet seen convincing evidence, either theoretical or observational, in favor of that view.

Thus the B_z -substorm relation during the intervals of northward B_z has not yet been established. If B_z is indeed the most significant parameter that governs the substorm activity, then it should be possible to express the B_z -substorm relation in a way that applies to both southward and northward B_z intervals. Hence we have repeated the comparison between the records of B_z and AE selecting the prolonged intervals of northward B_z . The interplanetary magnetic field data used are 5.46 min averages of the Explorer 28 (IMP C) observation and the substorm activity is expressed by AE (defined by Davis and Sugiura (1966)) given at 2.5 min intervals.

2. Analysis

Before examining the effect of the B_z decrease within the northward range, we shall briefly review the effect of the N-S change in B_z . Such change has been reported as a necessary but not sufficient condition for the excitation of a substorm (Fairfield and Cahill, 1966; Rostoker and Fälthammar, 1967), and we wish to find what additional conditions are required. In Figure 1 the records of B_z (top panel) and AE (bottom panel) are compared for seven well defined cases of the N-S change. (The B_z record is labeled as Z_{SE} since B_z in this figure refers to the solar ecliptic coordinate system.) Figures are aligned by the time (taken as time zero) when the southward B_z is first observed, and each record covers an interval of 5 hr of which 2 are before and 3 are

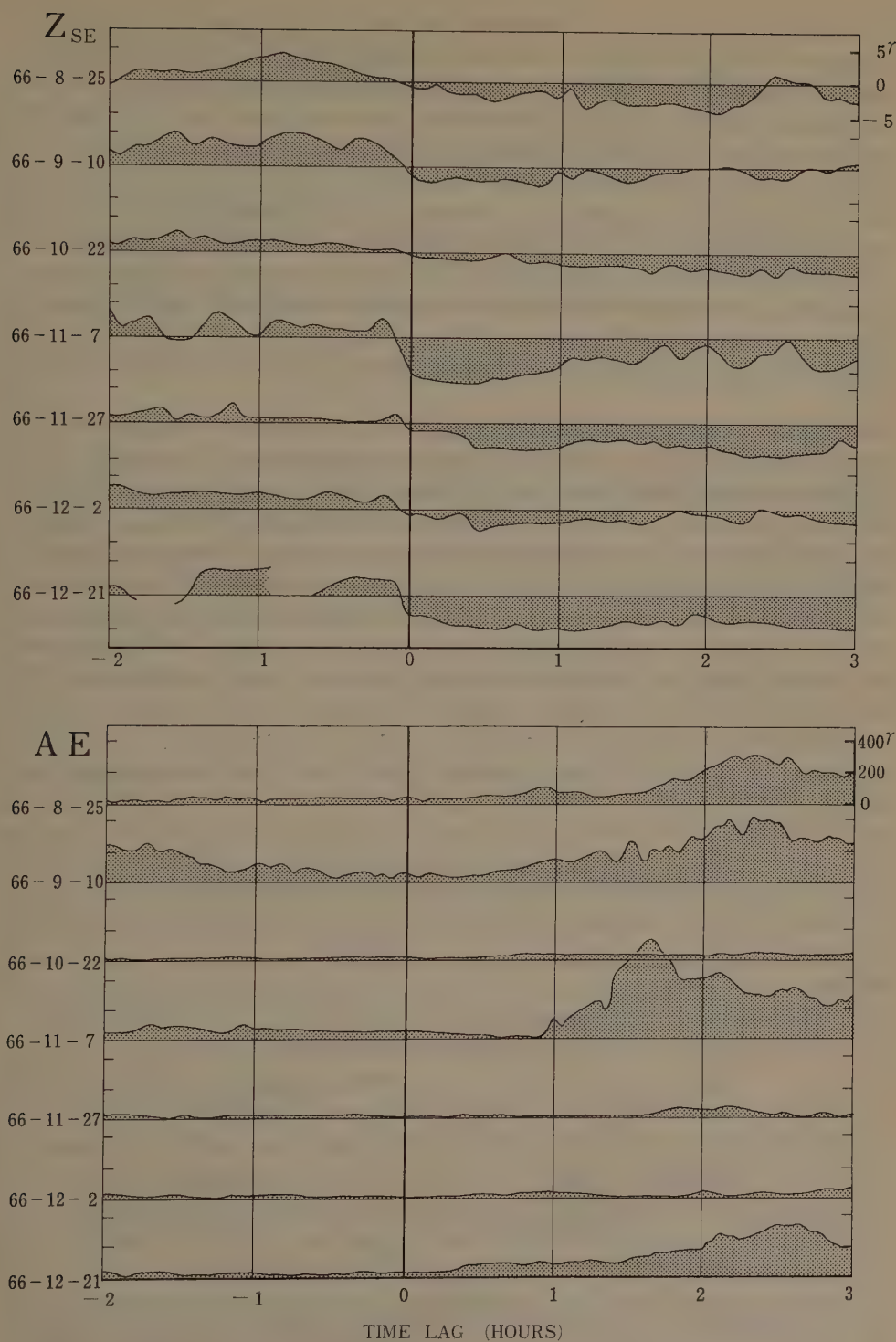


Fig. 1. Influence of the N-S change in Z_{SM} (northward component of the interplanetary magnetic field in the solar ecliptic coordinate system) on AE.

after time zero. In 4 out of 7 examples a peak in AE exceeding 200γ is observed between 1.5 and 2.5 hr after time zero but in the remaining 3 instances the increase in AE is very small or absent. From the corresponding B_z records we can see that the above discrimination originates from the difference in the amount of the decrement in B_z ; appreciable AE increase identifiable as the breakup of a substorm follows only when the B_z decrease exceeds a threshold of approximately 6γ . This seems to be the first requirement for the excitation of a substorm by the N-S change in B_z . The second requirement seems to be the one recently reported by Tsurutani and Meng (1971). They have noted that for a substorm to occur the N-S change in B_z should not be followed by a S-N change of a comparable magnitude within about 1 hr. By analyzing a greater amount of IMP C data in 1965 and 1966 we have confirmed that a N-S change satisfying the above two requirements indeed leads to a substorm (Nishida, 1971).

Hence we have looked for the instances of the northward B_z decreases that are greater than 6γ and are not followed by a comparable increase within 1 hr. As it happens such instances are rare, since B_z decreases which satisfy the above requirements tend to bring B_z to the southward range. Examples shown in Figures 2 and 3 thus, are selected by slightly relaxing the requirements. Figure 2 compares three sets of B_z and AE records for those B_z decreases that may be slightly less than 6γ and may slightly touch the southward range. (In Figures 2 and 3 where the sign of B_z is important, B_z in the solar magnetospheric coordinate is shown as Z_{SM} .) In the examples presented in Figure 3 B_z enters the southward range still further. Nevertheless, B_z is predominantly northward in all the examples, and the hourly average of B_z is positive everywhere.

In all sets of B_z and AE records shown in Figures 2 and 3 it can be seen that B_z and

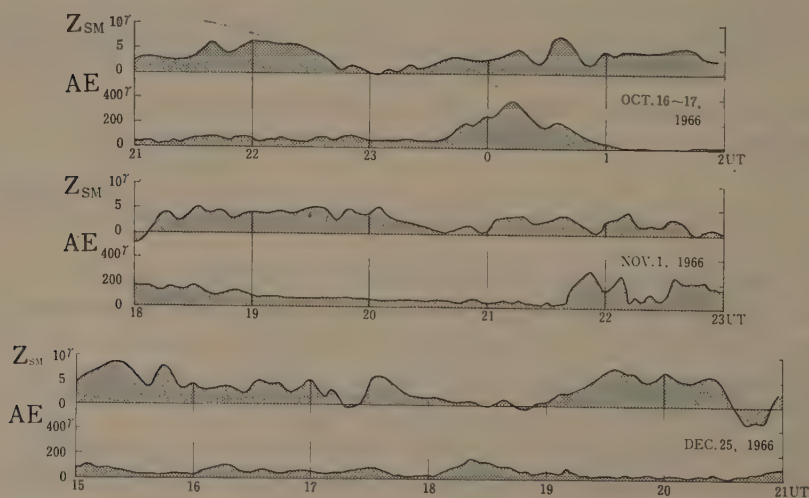


Fig. 2. Comparison of Z_{SM} (northward component of the interplanetary magnetic field in the solar magnetospheric coordinate) and AE for three cases where Z_{SM} is predominantly positive.

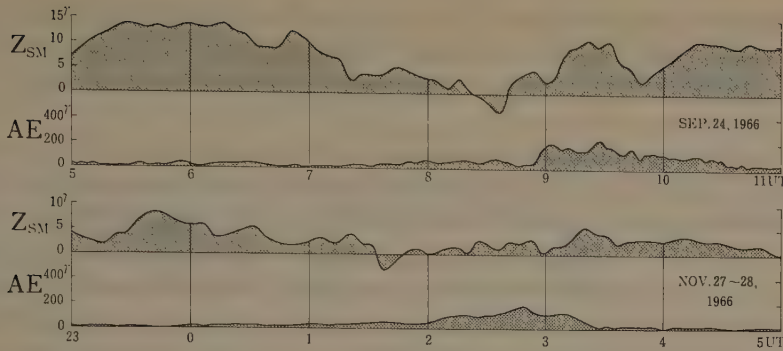


Fig. 3. Comparison of Z_{SM} and AE for two cases where Z_{SM} enters slightly the southward range.

AE are related in the expected way: maximum AE is observed a couple of hours after the B_z decrease. In the first example of Figure 2 a maximum AE is observed around 0015 and the B_z decrease is seen around 2240. In the second example maxima in AE observed at 2150 and 2210 would be related to the B_z decrease around 2030; another AE maximum seen in the second example around 2240 would correspond to the B_z decrease around 2150. In the third example a maximum in AE is observed around 1820 following the B_z decrease that starts from around 1700, terminates briefly, but resumes and lasts until the time of maximum AE; in the third example there is also a slight AE enhancement after 1615 and this may be related to the B_z decrease starting from 1530. Other B_z decreases seen in the records are smaller in magnitude or shorter in duration (or both) when compared with the decreases which lead to the enhancement in AE.

The relation between B_z and AE observed in Figure 3 is essentially the same as above. In the first example of Figure 3 there is a maximum around 0905 following a B_z decrease that lasts from 0630. In the second example the AE maximum around 0250 would be related to the B_z decrease that has started around 2340. Although in these examples B_z briefly enters the southward range, the duration of the southward polarity is much less than the critical value of about 1 hr (noted earlier) so that the brief occurrences of the southward B_z do not seem to play a vital role in the B_z -AE relation examined above. By the same reason the negative B_z which might have occurred within a 5.46 min interval over which the average B_z is positive does not seem to be the cause of the AE increase.

In the 6 mo interplanetary field data of the Explorer 28 covering July through December 1966, there are 26 intervals during which B_z is kept predominantly northward for more than 5 hr. Among these, 7 intervals contain the case(s) of B_z decrease that is greater than 5γ and is not followed by a comparable B_z increase within 1 hr. Five intervals out of these are already presented in Figures 2 and 3, and the same B_z -AE relation is seen in the remaining 2 intervals. Among the 19 intervals which do not contain significant B_z decreases (as defined above) 18 can be said to have no significant substorm activity in the sense that AE stays below 100γ except during sporadic

spikes that last less than 10 min. The only interval that does not follow the expected trend is found on November 15, 1966. On this date $B_z(Z_{SM})$ is kept within $0.5 \pm 1.5 \gamma$ from 0700 to 1100 but AE shows a peak which lasts about 1.5 hr and attains a maximum of 136 γ at 1105.

Thus there is a significant correlation between the decrease in B_z and the activation of the polar substorm, regardless of whether the decrease occurs in the northward or the southward range. In this way it seems possible to extend the B_z -substorm relation (reported previously) and accomodate the cases of substorms associated with the northward B_z . The association between northward B_z and substorm has been overlooked probably because B_z tends to be quiet when northward (as noted above) and, moreover, after a large decrease B_z tends to touch the southward range which is apt to be chosen as the signature of the substorm.

3. Discussion

It is generally thought that a substorm breaks up when the field lines extended to the tail return to a more dipolar configuration. The process is believed to follow the build-up of the magnetic flux content in the tail. In terms of this model the present observations can be interpreted to suggest the following.

The flux content in the tail is a function of B_z in the interplanetary space, and more flux is contained in the tail when B_z is lower. Thus the decrease in B_z is followed by the increase in the amount of the tail flux and sets the condition for the substorm break-up. The interplanetary magnetic field influences the magnetospheric structure under all conditions of the B_z polarity, and a decrease in B_z leads to an increase in the tail flux regardless of whether it occurs when B_z is northward or southward, provided that requirements on the magnitude and the duration of the decrease are fulfilled.

The reconnection model of the magnetosphere has been discussed almost exclusively for cases of the purely southward B_z . However, for the model to be applicable to the real magnetosphere, the reconnection should be possible for a wide range of the polarity of the interplanetary magnetic field. In order to produce large scale topological changes in the magnetospheric configuration, the presence of neutral points at several limited locations of the magnetopause would not suffice, and it seems necessary to have a reconnection line of a finite length on the magnetopause. This requires that the reconnection can proceed when the field directions on both sides of the interface are not exactly antiparallel, but it would be achieved by placing a pair of Alfvén shocks at the interface to rotate the original field directions to the antiparallel positions. In this way it may be possible to extend the reconnection model to include the interaction during the intervals of northward B_z .

In addition to the change in the magnetospheric configuration in response to the change in B_z , there is another conceivable way to increase the flux content of the tail. Even when the interplanetary magnetic condition is kept steady the accumulation of the flux to the tail can occur if there is an imbalance between the flux transport rates to and from the tail. The presence of the high β plasma in the plasma sheet may well

modify the flow and produce such imbalance. This would explain the occurrence of substorms during the intervals of relatively steady B_z .

References

- Davis, T. N. and Sugiura, M.: 1966, *J. Geophys. Res.* **71**, 785.
Fairfield, D. H. and L. J. Cahill, Jr.: 1966, *J. Geophys. Res.* **71**, 155.
Nishida, A.: 1971, *Cosmic Electrodyn.* **2**, 350.
Rostoker, G. and Fälthammar, C.-G.: 1967, *J. Geophys. Res.* **72**, 5853.
Tsurutani, B. and Meng, C.-I.: 1971, *Trans. Amer. Geophys. Union* **52**, 325.

PART VII

SUMMARY AND CONCLUSIONS

SUMMARY AND CONCLUSIONS

BILLY M. McCORMAC

Lockheed Palo Alto Research Laboratory, Palo Alto, Calif., U.S.A.

The behavior of the magnetosphere is a plasma physics problem for which the basic physics is poorly understood. Much more theoretical work is needed. In many cases the experimental observations have outstripped theories. Instabilities play an important role; however, there are very many potential types from which to select. The balance of particle density energy and momentum is needed throughout the magnetosphere (Schindler). Progress depends on combining many different types of observations.

1. Magnetospheric Structure

Two major developments in the past year in magnetospheric physics were summarized by Vasyliunas. These are the polar cusp and reconnection.

The polar cusp drastically modifies many ideas about the magnetosphere. The data examined at the Institute are extremely convincing so far as the general character of the polar cusp and its connection to the magnetosheath; however, there are many details to be determined. In general, measurements of magnetosheath spectra are not helpful in determining what regions can be mapped where because the magnetosheath plasma has very large spatial and temporal variations.

Another major development in magnetospheric physics highlighted in this Institute is the conclusive evidence that there is some kind of reconnection of field lines across the magnetopause. The evidence is the influence of the southward interplanetary magnetic field on portions of the magnetosphere. How or where reconnection occurs is still to be determined.

There has been a long controversy over open vs. closed magnetospheric models which used to be a fixed feature of all the previous Institutes but it finally seems to be resolved in favor of some type of an open model. The direct access of the magnetosheath plasma also fits this concept qualitatively. Although it is agreed that there is an open magnetosphere, it is still drawn with the magnetic field lines closed. The magnetosphere was originally closed for such basic concepts as the magnetopause which was derived on the basis of continuity. It is still impossible to specify the basic factors for an open model. We do not understand how the magnetospheric plasma enters that easily into the polar cusp, how it turns sharp corners in the field lines, etc. It is now necessary to commence with an open magnetosphere and make it quantitative.

2. Substorms

The status of magnetospheric substorms was summarized by Vasyliunas and Hones.

Much experimental data are now available and were presented at this conference.

There seems to be a fairly consistent picture for what happens during a substorm in terms of observables such as magnetic fields and particle fluxes. The overall concept seems to more or less fit some of the qualitative ideas of substorms under consideration for many years. However, the observations still do not give a positive fit to the available theory. There is no longer any need to argue whether there is an increase in the flux in the tail or whether some sort of reconnection is occurring in the tail as now there is good evidence that these indeed are occurring. It is now necessary to try to understand what has happened, i.e., where do all the particles go and where do they come from.

Although there is still some disagreement on the morphology of substorms, it is now mainly a question of terms and definitions. The evidence indicates that there is something called the growth phase preceding each substorm; however, the growth and expansion phases may be of the same phenomena but with different intensities.

There is no understanding at all either of the theory of the mechanism or of the triggering mechanism for substorms. There are no direct data on triggering except that it is agreed that the triggering starts in the magnetosphere at maybe 5, 10, or 20 R_E but not out at 100 R_E . Now satellite data are perhaps much more useful than ground data because correlated observations of the particles and fields out in the magnetosphere are obtained from the satellite. There should be much progress in the next few years in developing detailed theoretical descriptions for the behavior of particles and fields during substorms. More data are needed to be able to explain the triggering mechanism and more plasma flow measurements are needed at a number of locations.

3. E Fields and Convection

The experimenters who measure E fields seem to present their data in terms of convection and those who measure convection present their data as E fields.

Measurement of E fields in the ionosphere does not help to provide the E fields in the rest of the magnetosphere. The E fields must be measured deep in the magnetosphere. When the E_{\parallel} fields are also determined, it should be possible to map between the ionosphere and the magnetosphere. An important question is the destination of lines $> 65^\circ$ IN Lat.

Care must be taken about physical interpretations connecting the magnetosphere and ionosphere.

4. Particle Populations

The developments in magnetospheric particle populations were summarized by Elliot and Burrows.

The only really new addition to the magnetospheric particle populations since the Santa Barbara meeting seems to be that in the polar cusp observed by Winningham and others. The penetration of magnetosheath plasma through the magnetosphere down into the ionosphere is clearly of major importance in relation to polar auroral

phenomena and we can look forward to developments in this connection in the next few years.

The question of the source of the stably trapped particles is still an issue to be resolved. In principle, the charge spectrum of the radiation could provide a decision as between a solar and a terrestrial origin since the charge composition in the solar wind is different from that in the terrestrial atmosphere. However, the processes whereby the particles diffuse across L shells and the associated loss processes are likely to be so complicated that it is difficult to be sure that they do not distort the charge composition beyond recognition. The presence of particles with $Z > 3$ in the stable trapping zone has now been established and a direct comparison of the O:C abundance ratio has been made. The observed ratio strongly favors a solar origin. In this case it seems that there is unlikely to be any significant difference in the transport path characteristics (unlike H and He) and that the observed ratio correctly indicates that existing in the source. There is now good evidence for direct injection of α -particles with $1 < E < 8$ MeV at times of magnetic disturbance.

The problem of the origin of the high energy protons with $E < 50$ MeV is still obscure. In particular, we cannot yet be sure whether CRAND is or is not a dominant source for this part of the spectrum. The treatment by Walt was limited to $L < 1.7$ because of significant impulsive fluctuations at higher L values.

Paschmann presented data on the inner belt protons with $1.5 < E < 204$ MeV. His data appear to be consistent with a spatially constant source and atmospheric losses. This would be characteristic of the CRAND source but there are other observed intensity variations in the literature that point the other way.

5. Future Institute

It was concluded that the rapid evolution of earth's particles and fields justified another two-week Advanced Study Institute in 1973. England is a likely site for the next Institute. The 'Earth's Particles and Fields, 1973' Institute Program Committee members are: Drs J. Ronald Burrows, James Dungey, Carl-Gunne Fälthammar, Roger Gendrin, Thomas R. Kaiser, Reimar Lüst, Bernt Maehlum, J. Ortner, J. R. U. Page, Atsuhiko Nishida, and Martin Walt.

GLOSSARY

Most of the abbreviations and terms utilized in this book are obvious. Several whose meaning may not be apparent are listed below.

AA. Auroral absorption. Measure of cosmic noise absorption through the ionosphere in the auroral oval.

AEJ. Auroral electrojet. Current system in the ionosphere of the auroral region.

AU. Astronomical unit.

Auroral Oval. Locus of auroras in latitude as a function of time, which has an oval shape.

Bow Shock. Collisionless shock set up by the interaction of the solar wind and the earth's magnetosphere.

Closed Magnetic Field Line. Earth's magnetic field line which is continuous through space from one hemisphere to the other.

CNA. Cosmic noise absorption. Surface measurement of the absorption of cosmic noise, usually about 30 MHz, passing through the ionosphere.

Conjugate. Used herein for magnetic conjugacy and refers to the opposite ends of the same closed magnetic field line.

EDT. Eccentric dipole time.

ELF. Extremely low frequency and extends from 3 to 10^3 Hz.

Equatorial Electrojet. A current system in the ionosphere, flowing generally along the earth's equator.

FD. Forbush decrease.

FP. Fabry-Pérot.

FWHM. Full width half maximum.

Geomagnetic Micropulsation. Magnetic field fluctuations in the period range of 0.2 s to 10 min.

Hall Currents. Current flow perpendicular to both the electric and magnetic fields.

IGY. International Geophysical Year.

IN Lat. Invariant latitude, Φ .

IN LT. Invariant local time.

IN Pole. Invariant pole, where $\Phi = 90^\circ$.

Invariant Coordinate System. McIlwain's B, L space magnetic coordinates.

IQSY. International Year of the Quiet Sun.

IR. Infrared radiation covering from about 7800 Å to 1000 μm .

K_p. Quasi-logarithmic scale, from 0 to 9, measuring the range of activity of the most active component of the magnetic field within a 3 hr interval.

L. McIlwain's invariant shell parameter, whose units are expressed in R_E at the magnetic equator.

LT. Local time.

Magnetic Bay. Positive or negative deviations from the normal magnetograms, having a characteristic shape of the shore line of a bay.

Magnetopause. Boundary of the earth's magnetosphere.

Magnetosheath. Region between the magnetopause and the bow shock.

Magnetosphere. Region inside the magnetopause.

Magnetotail. Region of the magnetosphere extending in the antisolar direction beyond the trapping region.

MHD. Magnetohydrodynamics.

MLT. Magnetic local time.

M Substorm. Magnetospheric substorm.

Neutral Sheet. Narrow region about 1000 km thick in the middle of the tail of the plasma sheet where the magnetic field falls to a very low value.

Open Magnetic Field Line. One of the earth's magnetic field lines which is connected to the interplanetary magnetic field.

PCA Event. Polar cap absorption event. High energy proton precipitation in the polar cap producing high cosmic noise absorption.

Pedersen Current. Current flow along electric field which is perpendicular to the magnetic field.

PEJ. Polar electrojet. See auroral electrojet.

Pitch Angle. Angle between the instantaneous velocity vector of a charged particle and the direction of the magnetic field.

Plasmapause. Boundary at about L of 3.5 to 4 inside of which the plasma density is much higher.

Plasma Sheet. Thick slab of hot plasma in the magnetosphere.

Polar Cap. Region inside the auroral oval.

Pre-dawn Enhancement. Enhanced optical emission produced before normal sunrise behavior as a result of charge particles from the sunlit conjugate region.

QL. Quasi-linear.

R_E . Earth radius.

Ring Current. Current of trapped low energy protons at $L=3$ to 6.

rms. Root mean square.

SAR Arc. Stable auroral red arc.

SC. Sudden commencement.

SCA. Sudden commencement absorption.

SCNA. Sudden cosmic noise absorption.

SI. Sudden impulse.

Solar Wind. Electron, proton, α -particle and other charged particle emissions from the sun.

Trapping Region. Region of closed lines wherein charged particles can bounce from one hemisphere to the other and can drift all of the way around the earth.

ULF. Ultra low frequency and is from 10^{-2} to 3 Hz.

UT. Universal time.

UV. Ultraviolet radiation and extends from 100 to 3800 Å.

VK. Vegard-Kaplan band system.

VLf. Very low frequency and is from 3 to 30 kHz.

VLf Chorus. Radiation consisting of a multiple of overlapping rising tones, usually in the band of 2 to 4 kHz, which peaks in the morning hours, sounding like those of a distant bird colony.

Whistler. Radio signals in the audio-frequency that 'whistle'.

WPI. Wave particle interaction.

INDEX OF SUBJECTS

- Alfvén waves 5, 7, 307–308
- Acoustic waves 307–308
- Alpha particles
 - solar wind 54, 64
 - trapped 13–14, 64–66
- Auroral particles
 - acceleration 258–267
 - electrons 58–59, 133–139, 141–152, 179–186
 - protons 59, 95–100, 133–139
- Auroral zone 53
 - electric field 228, 246–251
 - ionosphere 246–256
 - mantle 163–166
 - plasma drift 246–256
- Barium ion clouds 225–230
 - aurora 246–256
- Bow shock 3–6, 42–44, 53–54
 - boundary 189–193
 - electric field 4
 - electrons 42
 - magnetic field 189–193
 - protons 3–4, 42–44
- Bremsstrahlung 391–398
- Carbon ions 65–66
- Cerenkov radiation 340–345
- Charged particles, *see* Alpha particles, Electrons, and Protons
- Collisionless shock 4
- Conductivity
 - Hall 19, 31–38, 248–249
 - Pedersen 19, 32, 248–249
- Convection, magnetospheric 3, 12, 17, 23–24, 29–38, 164–166, 235–245, 247–251, 268–278
- CRAND 61
- Currents
 - Birkeland 22, 26
 - field aligned 22, 26, 29–33
 - line 19
 - magnetospheric 29–38
 - ring 17, 21, 30–38, 49, 54–60
- Cyclotron wave turbulence 60
- Diffusion 17
 - pitch angle 83–86
- Drift 61
 - gradient 17, 24, 34–35, 38, 61
 - inertial 17
 - plasma 246–256
- Electric double layers 229, 258–267
- Electric field
 - auroral 228, 246–251
 - bow shock 4
 - convection 3, 12, 17, 23–24, 29–38, 164–166, 235–245, 247–251, 268–278
 - ionospheric 227, 246–251
 - magnetopause 8–9, 227
 - magnetosheath 68–80
 - magnetospheric 11–12, 29–32, 226, 233–245, 268–278, 332–333, 410
 - magnetotail 210–216, 227
 - measurement methods 223–226, 233–235
 - plasmopause 226
 - plasmasphere 226
 - polar cap 226, 235
 - polar cusp 68–80, 165–166
- Electric waves 39, 44–46
- Electrojet 19
- Electromagnetic waves
 - VLF 340
- Electrons
 - auroral 58–59, 133–139, 141–152, 179–186
 - bow shock 42
 - magnetopause 8–9
 - magnetosheath 55
 - magnetosphere 68–80, 272–278
 - neutral sheet 213–216
 - pitch angle scattering 164
 - plasma sheet 11, 57–59, 366–377
 - polar cusp 55–56, 68–80, 165–166, 335–338
 - precipitation 23, 59, 133–139, 141–164, 168–173, 351–353
 - solar wind 54
 - trapped 13, 58–63, 147–164, 175–177
- Electrostatic waves 5, 329–339
- ELF emissions 45–46, 311, 323–326
- Hall conductivity 19, 31–38, 238–249
- Hydromagnetic waves 5, 302–309
- Interplanetary magnetic field 40, 101–111, 192–193
- Instabilities 18, 21
 - current driven 5
 - fluid 302–307
 - magnetospheric 302–307

- neutral sheet 216–219
- two-stream 5
- Ionosphere
 - aurora 246–256
 - conductivity 19, 31–38, 248–249
 - convection 227, 246–251
 - electric field 227, 246–251
 - plasma 19–23
 - plasma drift 246–256
- Ions, thermal 280–290
- Magnetic field
 - bow shock 189–193
 - interplanetary 40, 101–111, 192–193
 - magnetopause 189–193
 - magnetosheath 42–45, 89
 - magnetosphere 3–14, 16–26, 30, 81–82, 189, 193–194, 269
 - micropulsations 302–309
 - neutral sheet 196–198, 210–216
 - plasma sheet 45–46, 189
 - polar cusp 189, 196
 - reconnection 210–216
- Magnetic substorms 18–19, 22, 60–61, 147–152, 276–277, 357–363, 365–377, 379–389, 400–404, 409
- X-Ray 391–395
- Magnetic waves 39–49
- Magnetohydrodynamics 5, 16
- Magnetopause 3, 6–10, 12, 17–18, 53–56, 360
 - electric field 8–9, 227
 - electrons 8–9
 - magnetic field 189–193
 - protons 8–9
- Magnetosheath 3–7, 10–11, 53
 - electric field 68–80
 - electrons 55
 - magnetic field 42–45, 189
 - protons 55–57, 68–80
- Magnetosphere
 - auroral zone 53
 - alpha particles 64–66
 - convection 3, 12, 17, 23–24, 29–38, 164–166, 235–245, 247–251, 268–278
 - electric fields 11–12, 29–32, 226, 233–245, 268–278, 332–333, 410
 - electrons 68–80, 272–278
 - electrostatic waves 329–339
 - instabilities 302–307
 - magnetic field 3–14, 16–26, 81–82, 189, 193–194, 269
 - magnetotail 17, 19, 46–47, 56–57, 200–216, 272–278, 360
 - neutral sheet 18, 53, 196–198, 210–219, 368, 374
 - particles 53–66, 311–327
 - plasma 19–23, 227–228, 360
 - plasmopause 18, 36, 226, 281–290
 - plasmasheet 3, 11, 17–18, 30, 45–47, 53–56, 189, 360–361, 366–377
 - plasmasphere 20–21, 53–54, 226, 280–290
 - polar cap 53, 81–87, 95–97, 101–106, 111–114, 226, 235
 - polar cusp 3, 9–11, 17, 47–48, 53, 55–56, 68–80, 165–166, 189, 196, 335–338, 410
 - processes 16–26, 29–38
 - protons 30–37, 68–80, 293–301
 - structure 3–14, 53–54, 200–209, 409
 - thermal ions 280–290
- Magnetotail 17, 19, 46–47, 200–210, 360
 - electric field 210–216, 227
 - protons 56–57, 272–278
- Micropulsations 302–309
- Neutral sheet 18, 53, 210–219, 368, 374
 - electrons 213–216
 - instabilities 216–219
 - magnetic field 196–198, 210–216
 - protons 213–216
 - reconnection 210–216
- Nitrogen ions 65–66
- Oxygen ions 65–66
- Pedersen conductivity 19, 32, 248–249
- Plasma
 - ionospheric 19–23
 - magnetospheric 19–23
- Plasma sheet 3, 17–18, 47, 53–56, 360–361
 - electric field 227
 - electrons 11, 57–59, 366–377
 - magnetic field 45–46, 189
 - protons 11, 30, 57–59, 366–371
- Plasma waves 4
- Plasmopause 18, 36, 226, 281–290
 - electric field 226
- Plasmasphere 20–21, 53–54
 - electric field 226
 - ions 281–290
- Polar cap 53
 - electric field 226, 235
 - protons 81–87, 95–106, 111–114
- Polar cusp 3, 9–11, 17, 53, 410
 - electric field 68–80, 165–166
 - electrons 55–56, 68–80, 165–166, 335–338
 - magnetic field 189, 196
 - protons 56, 68–80
 - VLF waves 335–338
 - waves 47–48
- Protons
 - auroral 59, 95–100, 133–139
 - bow shock 3–4, 42–44
 - drift 82–86
 - injection 81–86

- loss 82–86
 - L* shell diffusion 86
 - magnetopause 8–9
 - magnetosheath 55–57, 68–80
 - magnetosphere 30–37, 272–278
 - magnetotail 56–57, 272–278
 - model 393–401
 - neutral sheet 213–216
 - pitch angle scattering 83–86
 - plasma sheet 11, 30, 57–59, 366–371
 - polar cap 81–87, 95–106, 111–114
 - polar cusp 56, 68–80
 - precipitation 23, 59, 120–139, 153–154, 160–163
 - radial diffusion 393–401
 - solar wind 54–55, 81, 95–114
 - trapped 13, 58–61, 115–132, 160–163, 293–301, 411
- Ring current 17, 21, 30–38, 49, 54–60
- SAR arc 21, 48, 133, 139
- Satellites
- Ariel 3: 342–349
 - ATS 1: 8, 60–62, 195–196, 227
 - ATS 5: 8–9, 12, 223, 268–278
 - AZUR: 60, 115–119, 147–152
 - ESRO 1: 107–108, 111–113, 120–139
 - ESRO 2: 81, 86, 90, 95–106
 - Explorer 12: 8
 - Explorer 35: 108–109, 111
 - HEOS 1: 107–108
 - Injun 3: 341
 - Injun 4: 13, 56, 82
 - Injun 5: 13–14, 60–65, 78–79, 223, 226, 229, 233–245, 248
 - ISIS 1: 55–56, 68–80, 154–166
 - OGO 1: 4
 - OGO 3: 60–62, 195
 - OGO 4: 13, 64, 108
 - OGO 5: 4, 11, 43–49, 56, 78, 195, 252, 281, 324
 - OGO 6: 223
 - OV1-10: 223
 - OV1-18: 168–173
 - OV1-17: 223
- VELA 3: 6–7
 - VELA 4: 55, 372–377
 - 1966-70A: 13, 64
 - 1968-26B: 13, 62–64
- Solar wind 3–7, 39–40, 44, 53–55, 359
- access to magnetosphere 3–7, 17–18, 25, 64, 81, 86–93, 95–100
 - Alfvén waves 39–40
 - alpha particles 13, 14, 54, 64
 - electrons 54
 - protons 54–55, 81, 95–114
- Substorm
- expansion phase 361–362
 - growth phase 361–362
 - magnetospheric 18–19, 22, 60–61, 147–152, 276–277, 357–363, 365–377, 379–389, 400–404, 409
 - photon 122–126
 - X-ray 391–395
- Sudden commencement 351–353
- Spacecraft
- IMP 5: 6, 10–11, 70, 76–79, 165, 189–191, 196–197
 - Mariner 5: 40, 64
- Trapped radiation. *See* Alpha particles, Electrons, and Protons.
- VLF emissions 311 315, 320–325, 330–331, 335–338, 340–353
- Waves
- Alfvén 5, 7, 307–308
 - acoustic 307–308
 - electric 39, 44–46
 - electrostatic 5, 329–339
 - ELF 45–46, 311, 323–326
 - hydromagnetic 5, 302–309
 - magnetic 39–49
 - pearls 318–319
 - VLF 40–42, 46, 329–340
 - Whistler 320
- Wave-particle interactions 40, 60–61, 311–327, 329–339, 340
- Whistlers 5, 7, 320
- X-rays 391–398

ASTROPHYSICS AND SPACE SCIENCE LIBRARY

Edited by

J. E. Blamont, R. L. F. Boyd, L. Goldberg, C. de Jager, Z. Kopal, G. H. Ludwig, R. Lüst,
B. M. McCormac, H. E. Newell, L. I. Sedov, Z. Švestka, and W. de Graaff

1. C. de Jager (ed.), *The Solar Spectrum. Proceedings of the Symposium held at the University of Utrecht, 26–31 August, 1963*. 1965, XIV + 417 pp.
2. J. Ortner and H. Maseland (eds.), *Introduction to Solar Terrestrial Relations. Proceedings of the Summer School in Space Physics held in Alpbach, Austria, July 15–August 10, 1963 and Organized by the European Preparatory Commission for Space Research*. 1965, IX + 506 pp.
3. C. C. Chang and S. S. Huang (eds.), *Proceedings of the Plasma Space Science Symposium, held at the Catholic University of America, Washington, D.C., June 11–14, 1963*. 1965, IX + 377 pp.
4. Zdeněk Kopal, *An Introduction to the Study of the Moon*. 1966, XII + 464 pp.
5. Billy M. McCormac (ed.), *Radiation Trapped in the Earth's Magnetic Field. Proceedings of the Advanced Study Institute, held at the Chr. Michelsen Institute, Bergen, Norway, August 16–September 3, 1965*. 1966, XII + 901 pp.
6. A. B. Underhill, *The Early Type Stars*. 1966, XIII + 282 pp.
7. Jean Kovalevsky, *Introduction to Celestial Mechanics*. 1967, VIII + 427 pp.
8. Zdeněk Kopal and Constantine L. Goudas (eds.), *Measure of the Moon. Proceedings of the Second International Conference on Selenodesy and Lunar Topography held in the University of Manchester, England, May 30–June 4, 1966*. 1967, XVIII + 479 pp.
9. J. G. Emming (ed.), *Electromagnetic Radiation in Space. Proceedings of the Third ESRO Summer School in Space Physics, held in Alpbach, Austria, from 19 July to 13 August, 1965*. 1968, VIII + 307 pp.
10. R. L. Carovillano, John F. McClay, and Henry R. Radoski (eds.), *Physics of the Magnetosphere. Based upon the Proceedings of the Conference held at Boston College, June 19–28, 1967*. 1968, X + 686 pp.
11. Syun-Ichi Akasofu, *Polar and Magnetospheric Substorms*. 1968, XVIII + 280 pp.
12. Peter M. Millman (ed.), *Meteorite Research. Proceedings of a Symposium on Meteorite Research held in Vienna, Austria, 7–13 August, 1968*. 1969, XV + 941 pp.
13. Margherita Hack (ed.), *Mass Loss from Stars. Proceedings of the Second Trieste Colloquium on Astrophysics, 12–17 September, 1968*. 1969, XII + 345 pp.
14. N. D'Angelo (ed.), *Low-Frequency Waves and Irregularities in the Ionosphere. Proceedings of the 2nd ESRIN-ESLAB Symposium, held in Frascati, Italy, 23–27 September, 1968*. 1969, VII + 218 pp.
15. G. A. Partel (ed.), *Space Engineering. Proceedings of the Second International Conference on Space Engineering, held at the Fondazione Giorgio Cini, Isola di San Giorgio, Venice, Italy, May 7–10, 1969*. 1970, XI + 728 pp.

16. S. Fred Singer (ed.), *Manned Laboratories in Space. Second International Orbital Laboratory Symposium*. 1969, XIII + 133 pp.
17. B. M. McCormac (ed.), *Particles and Fields in the Magnetosphere. Symposium Organized by the Summer Advanced Study Institute, held at the University of California, Santa Barbara, Calif., August 4-15, 1969*. 1970, XI + 450 pp.
18. Jean-Claude Pecker, *Experimental Astronomy*. 1970, X + 105 pp.
19. V. Manno and D. E. Page (eds.), *Intercorrelated Satellite Observations related to Solar Events. Proceedings of the Third ESLAB/ESRIN Symposium held in Noordwijk, The Netherlands, September 16-19, 1969*. 1970, XVI + 627 pp.
20. L. Mansinha, D. E. Smylie and A. E. Beck, *Earthquake Displacement Fields and the Rotation of the Earth. A NATO Advanced Study Institute Conference Organized by the Department of Geophysics, University of Western Ontario, London, Canada, June 22-28, 1969*. 1970, XI + 308 pp.
21. Jean-Claude Pecker, *Space Observatories*. 1970, XI + 120 pp.
22. L. N. Mavridis (ed.), *Structure and Evolution of the Galaxy. Proceedings of the NATO Advanced Study Institute, held in Athens, September 8-19, 1969*. 1971, VII + 312 pp.
23. A. Muller (ed.), *The Magellanic Clouds. A European Southern Observatory Presentation: Principal Prospects, Current Observational and Theoretical Approaches, and Prospects for Future Research. Based on the Symposium on the Magellanic Clouds, held in Santiago de Chile, March 1969, on the Occasion of the Dedication of the European Southern Observatory*. 1971, XII + 189 pp.
24. B. M. McCormac (ed.), *The Radiating Atmosphere. Proceedings of a Symposium Organized by the Summer Advanced Study Institute, held at Queen's University, Kingston, Ontario, August 3-14, 1970*. 1971, XI + 455 pp.
25. G. Fiocco (ed.), *Mesospheric Models and Related Experiments. Proceedings of the 4th ESRIN-ESLAB Symposium, held at Frascati, Italy, July 6-10, 1970*. 1971, VIII + 298 pp.
26. I. Atanasijević, *Selected Exercises in Galactic Astronomy*. 1971, XII + 144 pp.
27. C. J. Macris (ed.), *Physics of the Solar Corona. Proceedings of NATO Advanced Study Institute on Physics of the Solar Corona, held at Cavouri-Vouliagmeni, Athens, Greece, 6-17 September 1970*. 1971, XII + 345 pp.
28. F. Delobbeau, *The Environment of the Earth*. 1971, IX + 113 pp.
29. E. R. Dyer (general ed.), *Solar-Terrestrial Physics/1970. Proceedings of the International Symposium on Solar-Terrestrial Physics, held in Leningrad, U.S.S.R., 12-19 May 1970*. 1972, VIII + 938 pp.
30. V. Manno and J. Ring (eds.), *Infrared Detection Techniques for Space Research, Proceedings of the Fifth ESLAB-ESRIN Symposium, held in Noordwijk, The Netherlands, June 8-11, 1971*. 1972, XII + 344 pp.
31. M. Lecar (ed.), *Gravitational N-Body Problem, Proceedings of IAU Colloquium No. 10, held in Cambridge, England, August 12-15, 1970*. 1972, XI + 441 pp.

SOLE DISTRIBUTORS FOR U.S.A. AND CANADA :

Vols. 2-6, and 8: Gordon & Breach Inc., 150 Fifth Ave., New York, N.Y. 10011
 Vols. 7 and 9-28: Springer Verlag New York, Inc., 175 Fifth Ave., New York, N.Y. 10011

MICHIGAN STATE UNIV. LIBRARIES



31293002483083